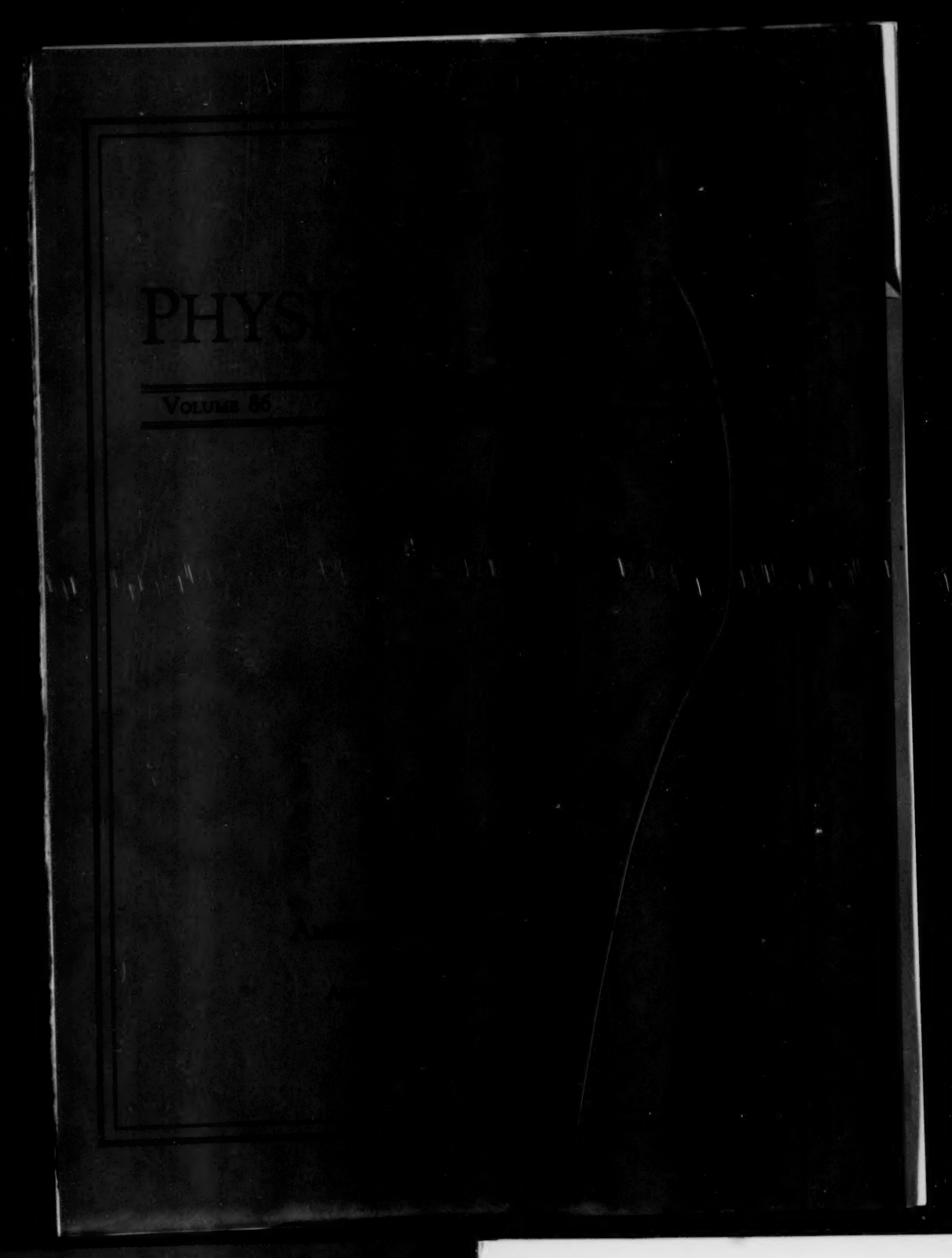
PHYS
VOLUME 86

THE PHYSICAL REVIEW

A journal of experimental and theoretical physics established by E. L. Nichols in 1893

Published by the American Institute of Physics for the

AMERICAN PHYSICAL SOCIETY

Officers

President

J. H. Van Vleck
Harvard University
Cambridge, Massachusetts

Vice-President

Enrico Fermi
Institute for Nuclear Studies
University of Chicago
Chicago 37, Illinois

Secretary

K. K. Darrow
Bell Telephone Laboratories
Office:
Columbia University
New York 27, New York

Treasurer

G. B. Pegram
Columbia University
New York 27, New York

Local Secretary for the Pacific Coast

J. Kaplan
University of California at Los Angeles
Los Angeles, California

Managing Editor

S. A. Goudsmit
Brookhaven National Laboratory
Upton, Long Island
New York

BOARD OF EDITORS

Editor

S. A. Goudsmit

Associate Editors

Harvey Brooks	M. Goldhaber	W. F. Arendt
R. F. Christy	R. Hofstadter	F. G. Brickwedde
C. L. Critchfield	A. W. Lawson	W. R. Fuller
M. Deutsch	A. Pais	*Circular Manager*
T. H. Johnson	R. Serber	H. W. Lewispaul
Bruno Rossi	C. H. Townes	*Associate Manager*

Manuscripts for publication should be submitted to S. A. Goudsmit, Brookhaven National Laboratory, Upton, Long Island, New York. The authors' institutions are requested to pay a publication charge of $8 per page which, if honored, entitles them to 100 free reprints. Instructions will be sent with galley proofs.

Proofs and all correspondence concerning papers in the process of publication should be addressed to the Publication Manager, American Institute of Physics, 57 East 55 Street, New York 22, New York.

Subscription Price

United States and Canada $20.00
Elsewhere $25.00

Back Numbers[1]

Yearly back number rate when complete year is available
Prior to 1949: $20.00
Thereafter: $27.00

Single copies: $2.00 each, prior to July, 1929;
$2.50 each, July, 1929–December, 1941;
$2.00 each, January, 1942–December, 1946;
$2.00 each, January, 1947–December, 1948;
$2.25 each, thereafter.

General Index, 1893–1929: $4.00.

Subscriptions, renewals, and orders for back numbers should be addressed to the American Institute of Physics, 57 East 55 Street, New York 22, New York.

Changes of address in the case of members of the American Physical Society should be addressed to the Treasurer; in the case of other subscribers to the American Institute of Physics.

[1] For Series I, Index of Physical Department, Cornell University, Ithaca, New York.

The Physical Review is published semi-monthly at Prince and Lemon Streets, Lancaster, Pennsylvania.

Entered as second-class matter March 6, 1942, at the Post Office at Lancaster, Pennsylvania, under the Act of March 3, 1879.

Acceptance for mailing at special rate of postage provided for in paragraph (d-2), section 34.40, P. L. & R. of 1948, authorized January 27, 1942.

CONTENTS

APRIL 1, 1952

Forward Scattering of Light by a Coulomb Field . . . F. ROHRLICH AND R. L. GLUCKSTERN 1
Small Angle Scattering of Light by a Coulomb Field . . . . H. A. BETHE AND F. ROHRLICH 10
Scattering and Absorption of Pi-Mesons in Carbon . . . . . H. BYFIELD, J. KESSLER, AND L. M. LEDERMAN 17
Spontaneous Fission . . . . . EMILIO SEGRÈ 21
Nuclear Elastic Scattering of High Energy Protons . . . . . R. E. RICHARDSON, W. P. BALL, C. E. LEITH, JR., AND B. J. MOYER 29
Nuclear Photodissociation by High Energy Synchroton Gamma-Rays . . . SEISHI KIKUCHI 41
Nature of Work-Hardening . . . . . J. S. KOEHLER 52
High Energy Electron-Electron Scattering . . . . . WALTER H. BARKAS, ROBERT W. DEUTSCH, F. C. GILBERT, AND CHARLES E. VIOLET 59
First-Forbidden Beta-Decay Matrix Elements . . . . . T. AHRENS AND E. FEENBERG 64
Nonlinear Meson Theory for Heavy Nuclei . . . . . BERTRAM J. MALENKA 68
Magnetic Moment of K^{40} and the Hyperfine Structure Anomaly of the Potassium Isotopes . . . . . J. T. EISINGER, B. BEDERSON, AND B. T. FELD 73
Average Energy of Beta-Ray Spectra . . . . . RANDALL S. CASWELL 82
Shape of Cosmic-Ray Star-Size Distributions in Nuclear Emulsions . . . . . M. BIRNBAUM, M. M. SHAPIRO, B. STILLER, AND F. W. O'DELL 86
Condensations in Expanding Cosmologic Models . . . . . AMALKUMAR RAYCHAUDHURI 90
Convergence of Intermolecular Force Series . . . . . FRANKLIN C. BROOKS 92
Nuclear Spectrum of Ge^{77} . . . . . ALAN B. SMITH 98
Positive Ions in the Afterglow of a Low Pressure Helium Discharge . . . . . ARTHUR V. PHELPS AND SANBORN C. BROWN 102
Meson-Nucleon Scattering and Nucleon Isobars . . . . . KEITH A. BRUECKNER 106
Fast Protons from 270-Mev *n-d* Collisions . . . J. B. CLADIS, J. HADLEY, AND W. N. HESS 110
Dielectric Constant in Perovskite Type Crystals . . . . . JOHN H. BARRETT 118

Letters to the Editor:

Spin-Wave Treatment of the Saturation Magnetization of Ferrites . . . . . HARVEY KAPLAN 121
Angular Distribution of π^+ Production in n-p Collisions . . . . . H. A. BETHE AND N. AUSTERN 121
Faraday Rotation of Guided Waves . . . . . H. SUHL AND L. R. WALKER 122
Radiation from an Electron in a Magnetic Field . . . . . D. L. JUDD, J. V. LEPORE, M. RUDERMAN, AND P. WOLFF 123
Radiation Loss of Electrons in the Synchroton . . . . . H. OLSEN AND H. WERGELAND 123
Electrical Properties of the Sodium Tungsten Bronzes . . . . . HELLMUT J. JURETSCHKE 124
Photodisintegration by Meson Reabsorption . . . . . ROBERT R. WILSON 125
Condensation Phenomenon of an Ideal Einstein-Bose Gas . . . . . OTTO HALPERN 126
Photodissociation of the Helium Nucleus by High Energy Gamma-Rays . . . . SEISHI KIKUCHI 126
V^0 Particles and Isotopic Spin . . . . . D. C. PEASLEE 127
Absorption Rate of Cosmic-Ray Neutrons Producing C^{14} in the Atmosphere . RUDOLF LADENBURG 128
Production Rate of Cosmic-Ray Neutrons and C^{14} . . HERBERT J. KOUTS AND LUKE C. L. YUAN 128
Search for New Mesons by Means of a Cloud Chamber . M. INOKI, T. YASAKI, AND Y. MATSUKAWA 129
Dark Current in the Intermittent Glow Discharge in Hydrogen . . . . . HERMAN RITOW 130
Dispersion of Permittivity and Conductivity of Semiconductors . . . . . R. E. BURGESS 131
Inelastic Scattering of Fast Neutrons from Iron . . . . . P. H. STELSON AND W. M. PRESTON 132
Domain Patterns on FeSi Crystals . . . . . C. F. YING, S. LEVY, AND R. TRUELL 133
Formative Time Lags of Positive Point Corona in Air . . . . . M. MENES AND L. H. FISHER 134
Behavior of the Heat Capacity of Superconducting Niobium below 4.5°K . . . . . A. BROWN, M. W. ZEMANSKY, AND H. A. BOORSE 134
Total Collision Cross Sections of Negative Atomic Iodine Ions in Nitrogen and Argon . . . . . FRANK L. MCCRACKIN 135
Diffusion of Donor and Acceptor Elements into Germanium . . . . . CALVIN S. FULLER 136
Measurement of Diffusion in Semiconductors by a Capacitance Method . . . . . K. B. MCAFEE, W. SHOCKLEY, AND M. SPARKS 137
Pressure Broadening of Absorption Lines . . . . . GILBERT N. PLASS AND DOUGLAS WARNER 138
Interferometric Measurements of the Hyperfine Structure of the Mercury Green Line . JOHN STERNER 139

APRIL 15, 1952

New Kind of Radio Propagation at Very High Frequencies Observable over Long Distances . . . . . D. K. BAILEY, R. BATEMAN, L. V. BERKNER, H. G. BOOKER, G. F. MONTGOMERY, E. M. PURCELL, W. W. SALISBURY, AND J. B. WIESNER 141
Magnetic Resonance in a System Containing Two Magnetic Sublattices . . . . . ROALD K. WANGSNESS 146
Effects of Configuration Interaction on the Atomic Hyperfine Structure of Gallium . . . . . G. F. KOSTER 148
Angular Distribution of Neutrons Scattered by Helium . . . . . ROBERT K. ADAIR 155
Isotope Effect in Superconductivity. II. Tin and Lead . . . . . B. SERIN, C. A. REYNOLDS, AND C. LOHMAN 162
Beta- and Gamma-Radiation of Al^{28} . . . . . HENRY T. MOTZ AND DAVID E. ALBURGER 165

Stars Initiated by High Energy Protons and Neutrons . . . HERBERT FISHMAN AND ALFRED MORRIS PERRY, JR. 167
Production of Positive Mesons by Photons . . . J. STEINBERGER AND A. S. BISHOP 171
Further Results on the Production of Neutral Mesons by Photons . . . W. K. H. PANOFSKY, J. N. STEINBERGER, AND J. STELLER 180
Measurement of the In^{115*} Conversion Coefficient with a Scintillation Spectrometer . . . THOMAS B. COOK, JR., AND SHERWOOD K. HAYNES 190
Shapes of Negative Beta-Spectra at the Low Energy End . . . HERMAN M. SCHWARTZ 195
Application of the Fermi Model to Cosmic-Ray Events of Primary Energy Greater than 10^{13} ev . . . W. E. HAZEN, R. E. HEINEMAN, AND E. S. LENNOX 198
Solubility of He^3 in Liquid He^4 . . . J. G. DAUNT AND C. V. HEER 205
High Energy Collisions with the Production of Meson Showers . S. BISWAS AND V. D. HOPPER 209
Disintegration Scheme of I^{131} . . . R. E. BELL AND R. L. GRAHAM 212
Ferroelectricity and Antiferroelectricity in Ceramic $PbZrO_3$ Containing Ba or Sr . . . GEN SHIRANE 219
Theoretical Estimate of the Effect of Radiation on the Elastic Constants of Simple Metals . . . G. J. DIENES 228
Superconductivity of the Isotopes of Tin . . . E. MAXWELL 235
Chemical Effects in Nuclear Magnetic Resonance and in Diamagnetic Susceptibility . . . NORMAN F. RAMSEY 243

Letters to the Editor:

Size Effects and Diamagnetism in Finite Systems . . . M. F. M. OSBORNE AND M. C. STEELE 247
Hyperfine Structure of the Spectra of Gadolinium and Zirconium . . . S. SUWA 247
Radiations from Ne^{19} and Na^{21} . . . G. SCHRANK AND J. R. RICHARDSON 248
Crystal Structure of the Ferroelectric Phase in $PbZrO_3$ Containing Ba or Ti . . . GEN SHIRANE AND SADAO HOSHINO 248
$\beta-\gamma$ Polarization Correlation in Sb^{124} . . . ROBERT STUMP 249
New Technique for the Determination of Photonuclear Cross Sections . . LESTER L. NEWKIRK 249
Role of Turbulence in the Evolution of the Universe . . . G. GAMOW 251
Thermal Conductivity of Carbons and Graphite . . . S. MROZOWSKI 251
Radiation Characteristics of Cm^{240} and Cm^{242} . . . G. H. HIGGINS AND K. STREET, JR. 252
Short-Range Protons from the Deuteron Bombardment of Li^6 . R. W. GELINAS AND S. S. HANNA 253
Spectroscopic Isotope Shift and Nuclear Shell Structure . . . G. BREIT 254
jj-Coupling in Nuclei . . . B. H. FLOWERS 254
Color-Center Formation in NaCl Containing Ag^+ . . . E. BURSTEIN, J. J. OBERLY, B. W. HENVIS, AND MARGARET WHITE 255
Mechanism of the Trichel Pulses of Short Time Duration in Air . . . LEONARD B. LOEB 256
Electrodynamic Corrections to the Fine Structure of Positronium . . . ROBERT KARPLUS AND ABRAHAM KLEIN 257
Emission of the Atmospheric Oxygen Bands in Discharges and Afterglows . LEWIS N. BRANSCOMB 258
Bardeen's Theory of Superconductivity and the f-Sum Rule . . . EDWARD N. ADAMS, II 258
Magnetic Moment of Se^{77} . . . S. S. DHARMATTI AND H. E. WEAVER, JR. 259
Mass Difference $Mg^{23}-Na^{23}$ . . . H. B. WILLARD, J. D. KINGTON, AND J. K. BAIR 259
Unified Description of Leptons . . . V. VOTRUBA AND M. LOKAJÍČEK 260

MAY 1, 1952

Monte Carlo Study of Shower Production . . . ROBERT R. WILSON 261
Comparative Models in Nuclear Scattering . . . D. C. PEASLEE 269
Extinction Effects in Neutron Transmission of Polycrystalline Media . . . R. J. WEISS 271
Evidence for K-Shell Ionization Accompanying the Alpha-Decay of Po^{210} . . . W. C. BARBER AND R. H. HELM 275
Sign of the Quadrupole Interaction Energy in Diatomic Molecules . . . R. A. LOGAN, R. E. COTÉ, AND P. KUSCH 280
Electrodynamic Displacement of Atomic Energy Levels. II. Lamb Shift . . . ROBERT KARPLUS, ABRAHAM KLEIN, AND JULIAN SCHWINGER 288
Energy Levels of C^{11} and C^{12} from Photographic Plate Observation of Neutron Spectra . . . VIRGIL R. JOHNSON 302
New "Double Resonance" Method for Investigating Atomic Energy Levels. Application to Hg $^3P_1$ . . . JEAN BROSSEL AND FRANCIS BITTER 308
Effect of the Atomic Core on the Magnetic Hyperfine Structure . . . R. STERNHEIMER 316
Interpretation of Experiments on the Photonuclear Effect in Heavy Elements . . L. EYGES 325
Nuclear Phenomena Deducible from μ-Pair Theory with Pseudoscalar Coupling . . . L. M. TANNENWALD 332
Second-Quantized Theory of Spin-$\frac{1}{2}$ Particles in the Nonrelativistic Limit . RICHARD K. OSBORN 340
Radioisotopes of Bromine . . . S. C. FULTZ AND M. L. POOL 347
Dynamic Characteristics of a Low Pressure Discharge . . . B. T. BARNES 351
Photodisintegration of the Deuteron at Intermediate Energies. I. . . . C. A. BARNES, J. H. CARVER, G. H. STAFFORD, AND D. H. WILKINSON 359
Photodisintegration of the Deuteron at Intermediate Energies. II. . . . D. H. WILKINSON 373
Scattering of Neutrons by Systems of Heavy Nuclei . . . G. PLACZEK 377
Triton Binding Energy by a Randomized Net-Point Method . . . S. I. RUBINOW 388
Photodisintegration of the Deuteron . . . V. E. KROHN, JR., AND E. F. SHRADER 391
Covariant Theory of Radiation Damping . . . JEAN PIRENNE 395

Neutron-Proton Scattering with Spin-Orbit Coupling. I. General Expressions . . . . . JOHN M. BLATT AND L. C. BIEDENHARN 399
Yield of F^{18} from Medium and Heavy Elements with 420-Mev Protons . . . LUIS MARQUEZ 405
Atomic Masses from Titanium through Zinc . . . . . THOMAS L. COLLINS, ALFRED O. NIER, AND WALTER H. JOHNSON, JR. 408

Letters to the Editor:

Deuterium Total Cross Sections for Positive and Negative Pions . . . . . H. L. ANDERSON, E. FERMI, D. E. NAGLE, AND G. B. YODH 413
Gamma-Gamma Angular Correlation in Pd^{106} . G. B. ARFKEN, E. D. KLEMA, AND F. K. MCGOWAN 413
Helium II Transfer Rates on Lucite and Perspex Surfaces . . . . . B. S. CHANDRASEKHAR 414
Radioactivity in Neutron Activated Platinum . . . . . J. M. CORK, J. M. LEBLANC, F. B. STUMPF, AND W. H. NESTER 415
Electrolysis of Thorium Oxide . . . . . W. E. DANFORTH 416
Alpha-Particles from the Li^7+T Reactions . . . . . J. T. DEWAN, T. P. PEPPER, K. W. ALLEN, AND E. ALMQVIST 416
$p-n$ Junction Method for Measuring Diffusion in Germanium . . . . . W. C. DUNLAP, JR., AND D. E. BROWN 417
Unusual $\pi-\mu$ Decays in Photographic Emulsions . . . . . W. F. FRY 418
Polarization of $D-D$ Neutrons . . . . . H. J. LONGLEY, R. N. LITTLE, JR., AND J. M. SLYE 419
Decay of Rubidium 87 . . . . . M. H. MACGREGOR AND M. L. WIEDENBECK 420
Transmission of X-Rays through Calcite near the Bragg Angle . . . . . GUENTER SCHWARZ AND GEORGE L. ROGOSA 421
Gamma-Radiations from V^{48} and Nb^{93} . . . . . HAROLD K. TICHO, DAVID GREEN, AND J. REGINALD RICHARDSON 422
Disintegration Scheme of K^{40} . . . . . M. PAGANELLI AND G. QUARENI 423
Detection of Millimeter Wave Solar Radiation . . . . . WILLIAM M. SINTON 424
Hexagonal Iron-Oxide Compounds as Permanent-Magnet Materials . . . . . J. J. WENT, G. W. RATHENAU, E. W. GORTER, AND G. W. VAN OOSTERHOUT 424
Magnetic Domains on Silicon Iron by the Longitudinal Kerr Effect . . . . . C. A. FOWLER, JR., AND E. M. FRYER 426
Occurrence of Heavy Mesons in Penetrating Showers . . . R. B. LEIGHTON AND S. D. WANLASS 426
Motion of an Electron in a Perturbed Periodic Potential . . . . . EDWARD N. ADAMS, II 427
Saturation Property of Nuclear Forces . . . . . HIDEO KANAZAWA 428
β-Decay of Mirror Nuclei and the Shell Model . . . . O. KOFOED-HANSEN AND AAGE WINTHER 428
Tests of Charge Independence from Pion Production in Nuclear Collisions . . A. M. L. MESSIAH 430
Regularities in the Total Cross Sections for Fast Neutrons . . . . . H. H. BARSCHALL 431
Investigation of the Magnetic Properties of Liquid He^3 . . . . . E. F. HAMMEL, H. L. LAQUER, S. G. SYDORIAK, AND W. E. MCGEE 432
Virial Theorem for a Dirac Particle . . . . . M. E. ROSE AND T. A. WELTON 432
Soft and Hard F-Centers . . . . . JORDAN J. MARKHAM 433
Optical Focusing in Constant Radius Accelerators . . . . . DAVID C. DEPACKH 433
Electron Neutron Interaction . . . . . BURTON D. FRIED 434
Spin and Parity of the First (603-kev) Excited State of Te^{124} . . . . . FRANZ R. METZGER 435
Emission of Deuterons from the Nucleus . . . . . A. G. W. CAMERON 435

MAY 15, 1952

Pion-Proton Scattering and the Strong Coupling Meson Theory . . . . . G. WENTZEL 437
Microwave Spectrum of BrCN at Six Millimeters . . . . . S. J. TETENBAUM 440
Neutrino Recoils Following the Capture of Orbital Electrons in A^{37} . . . . . GEORGE W. RODEBACK AND JAMES S. ALLEN 446
Re-Investigation of the Double Beta-Decay from Sn^{124} . . E. L. FIREMAN AND D. SCHWARZER 451
Association of Bursts and Penetrating Showers . . . . . DONALD E. HUDSON 453
Production of Neutrons by μ-Meson Capture in Lead, Magnesium, and Calcium . . . . . ANNA MARIA CONFORTO AND R. D. SARD 465
Exchange Current Effects in the Deuteron . . . . . FELIX VILLARS 476
Total Neutron Cross Section of Nitrogen . J. H. HINCHEY, P. H. STELSON, AND W. M. PRESTON 483
Electron Spectra Produced by a Co^{60} Source in Water . . . . . EVANS HAYWARD 493
Radial Distribution Function in Liquid Helium . . . . . P. J. PRICE 495
Second-Order Acoustic Fields: Streaming with Viscosity and Relaxation . JORDAN J. MARKHAM 497
Excited States of P^{32} from the $P^{31}(d,p)P^{32}$ Reaction . . . . . D. M. VAN PATTER, P. M. ENDT, A. SPERDUTO, AND W. W. BUECHNER 502
Interpretation of Image Transitions in Beta-Decay Theory . . . . . GEORGE L. TRIGG 506
Mean Life of the Positive π-Meson . . . . . WILLIAM L. KRAUSHAAR 513
Magnetic Analysis of the $Mg^{25}(d,p)Mg^{26}$, $Mg^{26}(d,p)Mg^{27}$, and $Mg^{25}(d,\alpha)Na^{23}$ Reactions. . . . . P. M. ENDT, J. W. HAFFNER, AND D. M. VAN PATTER 518
Cloud-Chamber Identification of Photodeuterons from Copper . . . . . WARREN H. SMITH AND L. JACKSON LASLETT 523
Multiple Scattering of Protons in Gases . . . . . EUGENE H. GERBER 525
Disintegration of N^{15} by Protons . . . . . ALOIS SCHARDT, WILLIAM A. FOWLER, AND CHARLES C. LAURITSEN 527
Primary Cosmic Radiation at High Latitudes . . . . . MARTIN A. POMERANTZ AND GORDON W. MCCLURE 536
Emission of L X-Rays of Lead in Po^{210} Decay . WILLIAM RUBINSON AND WILLIAM BERNSTEIN 545
Electronic Energy Bands in Crystals . . . . . R. H. PARMENTER 552

Letters to the Editor:

Third-Order Elastic Coefficients in Trigonal and Hexagonal Crystals . . . . . FAUSTO G. FUMI 561
Decay Energy of Si^{31} . . . . . A. H. WAPSTRA 561

Decay Energy of Pb^{209} . . . A. H. Wapstra 562
Stopping Power of Polystyrene and Acetylene for Alpha-Particles . . . R. H. Ellis, Jr., H. H. Rossi, and G. Failla 562
Scattering of Protons by the Loosely Bound Neutron in Beryllium . K. Strauch and J. A. Hoffmann 563
Argument Against the Majorana Theory of Neutral Particles . . . E. R. Caianiello 564
Experimental Search for Self-Trapped Electrons in the Alkali Halides . . . William H. Duerig 565
Energy Dependence of $(n,2n)$ Reactions in Ni^{58}, Cu^{63}, and Tl^{203} from 11 to 19 Mev . . . H. C. Martin and B. C. Diven 565
Neutron-Electron Interaction . . . Sidney Borowitz 567
Energy Available for Double Beta-Decay of Sn^{124} . Benjamin G. Hogg and Henry E. Duckworth 567
Theory of Antiferromagnetic Resonance in a Crystal of Rhombic Symmetry at the Absolute Zero . . . J. Ubbink 567
Scintillation Response of Organic Crystals to Low Energy Alpha-Particles . . . J. W. King and J. B. Birks 568
Theory of the Response of Organic Scintillation Crystals to Short-Range Particles . . . J. B. Birks 569
Composition and Time Variation of Primary Cosmic Radiation . . . D. Lal, Yash Pal, M. F. Kaplon, and B. Peters 569
Internal Conversion of the 0.411-Mev Gamma-Ray of Hg^{198} . . . Lennart Simons 570
Thermal Conductivity of Germanium . . . A. Grieco and H. C. Montgomery 570
Short Duration Afterglow of Nitrogen in the Photographic Infrared . . . R. Herman, L. Herman, and G. Hepner 570
498-kev Gamma-Ray of Ru^{100} . . . Arthur W. Knudsen 571
Pion Production and Charge Independence . . . J. M. Luttinger 571
Angular Distributions of Inelastically Scattered Protons from C^{12} and Mg^{24} . . . H. E. Gove and H. F. Stoddard 572
Nuclear Resonance and the Electronic Structure of Transition Metals . W. D. Knight and C. Kittel 573
Thermal Conductivity in the Intermediate State of Pure Superconductors . . . D. P. Detwiler and Henry A. Fairbank 574
Angular Correlation between Gamma-Rays and Inelastically Scattered Protons from Mg^{24} . . . H. E. Gove and A. Hedgran 574
Radioactive Decay of Ruthenium 103 . . . J. M. Cork, J. M. LeBlanc, F. B. Stumpf, and W. H. Nester 575
Co-Existence of Liquid Helium I and II . . . Philip Closmann and Richard T. Swim 576
High Latitude North-South Asymmetry of Cosmic Rays . . . D. W. P. Burbury 577
Gamma-Radiations from 36.5-hr Rh^{105g} . . . G. E. Boyd 578

Proceedings of the American Physical Society:

Minutes of the Meeting of the New England Section on November 3, 1951 . . . 579
Minutes of the Meeting at New York City, January 31, 1951 through February 2, 1952 (Bull. Am. Phys. Soc. 27, No. 1 (1952)) . . . 579
Minutes of the Meeting at Columbus, Ohio, March 20 through 22, 1952 (Bull. Am. Phys. Soc. 27, No. 2 (1952)) . . . 637

June 1, 1952

Some Remarks on the *V*-Particles . . . A. Pais 663
High Frequency Resistance of Metals in the Normal and Superconducting State . . . C. J. Grebenkemper and John P. Hagen 673
Low Energy *n-d* Scattering: Comparison of Experiment with Theory . . . M. M. Gordon and W. D. Barfield 679
Particle Counting by Čerenkov Radiation . . . John Marshall 685
Approximate Quantum Theory of the Antiferromagnetic Ground State . . . P. W. Anderson 694
On a Theorem of Irreversible Thermodynamics . . . Herbert B. Callen and Richard F. Greene 702
Second-Order Acoustic Fields: Relations between Density and Pressure . . . Jordan J. Markham 710
Second-Order Acoustic Fields: Energy Relations . . . Jordan J. Markham 712
Intermediate Coupling Theory of the Pseudoscalar Meson-Nucleon Interaction . . . P. T. Mathews and Abdus Salam 715
Phase Shift Analysis of Neutron-Deuteron Scattering . . . A. L. Latter and R. Latter 727
Renormalized *S*-Matrix for Scalar Electrodynamics . . . Abdus Salam 731
Nuclear Magnetic Resonance of Hydrogen Absorbed into Palladium Wires . R. E. Norberg 745
Gamma-Ray Spectra of the Los Alamos Reactors . . . J. W. Motz 753
Theory of the Production of Secondary Electrons in Solids . . . A. J. Dekker and A. van der Ziel 755
Angular Correlation of First and Third Gamma-Rays . . . G. B. Arfken, L. C. Biedenharn, and M. E. Rose 761
Production of High Energy Secondaries by Cosmic Rays Underground . . . W. E. Hazen 764
Neutron Diffraction Study of the Crystal Structure of Ammonium Chloride . . . Henri A. Levy and S. W. Peterson 766
Scattering of Electrons in Metals by Dislocations . . . D. L. Dexter 770
Gamma-Rays Associated with Selected Neutron-Induced Radioactivities . . . W. C. Rutledge, J. M. Cork, and S. B. Burson 775
Critical Shear Stresses in Body-Centered Cubic Lattices . . . R. Smoluchowski 787

Letters to the Editor:

Parities of the Ground States of N^{14} and C^{14} . . . D. A. Bromley and L. M. Goldman 790
Rotational Temperatures of Vegard-Kaplan Auroral Bands . . . W. Petrie 790
Nuclear Emulsion and Scintillation Crystal Processes . . . J. B. Birks 791
Third Forbidden Beta-Spectrum from Rb^{87} . . . Y. Tomozawa, M. Umezawa, and S. Nakamura 791
Possible Influence of K-Mesons on the Underground Cosmic Radiation . . . Loup Verlet 792

Ferroelectric Ammonium Metaphosphate . . . . . R. Pepinsky, C. M. McCarty, E. Zemyan, and K. Drenck 793
Angular Distribution of Pions Scattered by Hydrogen . . . . . H. L. Anderson, E. Fermi, D. E. Nagle, and G. B. Yodh 793
Scattering and Capture of Pions by Hydrogen . . . . . H. L. Anderson and E. Fermi 794
Half-Life of Tantalum-182 . . . . . G. G. Eichholz and L. A. Ficko 794
Collective Description of Electron Interactions . . . . . R. Kronig 795
Experimental Evidence for Classical Electron Radiation at 300 Mev . . . . . Joseph W. Mather 795
Associated Pairs of Particles in Cosmic-Ray Showers in Photographic Emulsions . . . . . J. Y. Mei and E. Pickup 796
Structure of Ammonium Chloride by Neutron Diffraction . G. H. Goldschmidt and D. G. Hurst 797
Soft Radiations from Am^{241} . . . . . J. K. Beling, J. O. Newton, and B. Rose 797
Microwave Spectrum and Molecular Constants of Hydrogen Cyanide . . . . . A. H. Nethercot, Jr., J. A. Klein, and C. H. Townes 798
Velocity of Light Determined by the Band Spectrum Method . . . . . D. H. Rank, R. P. Ruth, and K. L. Vander Sluis 799
Photoconductivity of Trapped Electrons in KCl Crystals between 24°C and −190°C . J. J. Oberly 799
Spectrum of L X-Rays from RaD and the Possibility of $L_I \rightarrow L_{II}N$ Auger Transitions . . . . . S. G. Cohen and A. A. Jaffe 800
Plastic Flow in Alkali Halide Crystals . . . . . W. W. Tyler 801
Pseudoscalar Coupling in Pseudoscalar Meson Theory . . . . . G. Wentzel 802
Low Temperature Thermal Expansion of Uranium . . Adam F. Schuch and Henry L. Laquer 803
Calorimetric Determination of the Relationship between the Half-Life and Average Beta-Energy of C^{14} . . . . . G. H. Jenks and F. H. Sweeton 803
Formation and Annulment of Space Charges in Glass and Their Influence on Electric Breakdown . . . . . H. J. Keller 804
Recent Studies of the Isotopes of Emanation, Francium, and Radium . . . . . F. F. Momyer, E. K. Hyde, A. Ghiorso, and W. E. Glenn 805
Symmetrical Pseudoscalar Meson Theory of Nuclear Forces . . . . . Maurice M. Levy 806
Isolated and Adiabatic Susceptibilities . . . . . Martin J. Klein 807
Neutron Groups from Protons on Cr^{50}, Co^{59}, and Cl^{37} . . . . . P. H. Stelson and W. M. Preston 807
Numerical Work on the Fluctuation Problem in Cascade Shower Theory . . . . . J. W. Gardner and H. Messel 808
Method of Synthesis of the Statistical and Impact Theories of Pressure Broadening . . . . . P. W. Anderson 809
Quadrupole Coupling Ratio of the Chlorine Isotopes . . . . . T. C. Wang, C. H. Townes, A. I. Schawlow, and A. N. Holden 809
Hyperfine Structure of $p_{3/2}$ States . . . . . W. W. Clendenin 810
Half-Life and Mass Assignment of Argon 39 . . . . . H. Zeldes, B. H. Ketelle, A. R. Brosi, C. R. Fults, and R. F. Hibbs 811
Broadening of Microwave Absorption Lines by Collisions with the Cell Walls . . . . . R. H. Johnson and M. W. P. Strandberg 811
Stability of Plane Poiseuille Flow . . . . . L. H. Thomas 812
Radiations from Nb^{97} . . . . . C. E. Mandeville, E. Shapiro, R. I. Mendenhall, E. R. Zucker, and G. L. Conklin 813
Microwave Spectroscopy at High Temperature-Spectra of CsCl and NaCl . . . . . M. L. Stitch, A. Honig, and C. H. Townes 813
μ-Meson Decay and β-Radioactivity . . . . . Louis Michel 814

Proceedings of the American Physical Society:

Minutes of the 1952 Spring Meeting of the New York State Section in Corning, New York, April 18 and 19, 1952 816
Minutes of the 1952 Spring Meeting of the Ohio Section at Kent State University, Kent, Ohio, April 18 and 19, 1952 818

June 15, 1952

Spherical Model of a Ferromagnet . . . . . T. H. Berlin and M. Kac 821
Theory of the Impulse Approximation . . . . . Saul T. Epstein 836
Charged Photomesons from Various Nuclei . Raphael M. Littauer and Darcy Walker 838
Solution of the Fluctuation Problem in Electron-Photon Shower Theory . . . . . H. Messel and R. B. Potts 847
Possibility of Frequency Multiplication and Wave Amplification by Means of Some Relativistic Effects . . . . . K. Landecker 852
Nonlinear Meson Theory of Nuclear Forces. III. Quantization of the Neutral Scalar Case with Nonlinear Coupling . . . . . L. I. Schiff 856
Nuclear Energy Levels of Al^{27} . . . . . E. M. Reilley, A. J. Allen, J. S. Arthur, R. S. Bender, R. L. Ely, and H. J. Hausman 857
Inelastic Scattering of Protons from Nickel . . . . . Ralph Ely, Jr., A. J. Allen, J. S. Arthur, R. S. Bender, H. J. Hausman, and E. M. Reilley 859
Scattering of Fast Neutrons by Wolfram . . . . . C. E. Mandeville, C. P. Swann, and F. J. Seymour 861
Internal Conversion in I^{131} . . . . . D. Rose, G. Hinman, and L. G. Lang 863
Comparison of Penetrating Showers in Light and Heavy Elements. I . . . . . W. D. Walker, N. M. Duller, and J. D. Sorrels 865
Liquid-Solid Transformation in Helium from 1.6° to 4°K . . . . . C. A. Swenson 870
Second-Order Radiative Corrections to Hyperfine Structure . . . . . Norman M. Kroll and Franklin Pollock 876
Scattering of Plane Waves by Soft Obstacles. III. Scattering by Obstacles with Spherical and Circular Cylindrical Symmetry . . Elliott W. Montroll and J. Mayo Greenberg 889
Magnetostrictive Vibration of Prolate Spheroids. Ni-Fe and Ni-Cu Alloys . . . . . J. S. Kouvelites and L. W. McKeehan 898

Gyromagnetic Effect in a Superconductor . R. H. Pry, A. L. Lathrop, and W. V. Houston 905
Angular Momentum Distributions in the Thomas-Fermi Model . . . . . J. H. D. Jensen and J. M. Luttinger 907
Further Considerations Regarding the Theory of Bose-Einstein Liquids . . . . . J. G. Daunt, T. P. Tseng, and C. V. Heer 911
Note on Wooldridge's Theory of Secondary Emission . . . . . E. M. Baroody 915
Analysis of the Nucleonic Component Based on Neutron Latitude Variations . S. B. Treiman 917
Phenomenological Relationships between Photomeson Production and Meson-Nucleon Scattering . . . . . K. A. Brueckner and K. M. Watson 923
Thermal Ionization of Trapped Electrons . . . . . Ryogo Kubo 929
Measurement of Neutron Densities with Crystals of NaI(Tl) . . . . Bertel Grimeland 937
Momentum Spectra of Cosmic-Ray Mesons and Protons at Sea Level and 3.4-km Altitude . . . . . W. L. Whittemore and R. P. Shutt 940
Radioactivities of Platinum and Iridium from Photonuclear Reactions in Platinum . . . . . Darleane Christian, Russell F. Mitchell, and Don S. Martin, Jr. 946
Q Values of the $C^{13}(d,p)C^{13}$, $Be^{9}(d,p)Be^{10}$, and $O^{16}(d,p)O^{17}$ Reactions . . . . . E. D. Klema and G. C. Phillips 951
Impedance Measurements on PbS Photoconductive Cells . . E. S. Rittner and F. Grace 955
Comparison of Magnetoelastic Energy Losses and Magnetic Hysteresis in Ferromagnetic Materials . . . . . G. Bonfiglioli, A. Ferro, and G. Montalenti 959
Hysteresis Effect in the Transmission of Electrons through Thin Dielectric Foils . . . . . Paul H. Owen and C. Sharp Cook 961
Effects of Dislocations on Mobilities in Semiconductors . . . D. L. Dexter and F. Seitz 964
Search for Alpha-Particles from the $O^{16}(d,\alpha)N^{14*}$ Reaction . . . . . R. J. Van de Graaff, A. Sperduto, W. W. Buechner, and H. A. Enge 966
Molecular Field Treatment of Ferromagnetism and Antiferromagnetism . J. Samuel Smart 968
Note on the Absorber Theory of Radiation . . . . . Peter Havas 974
Nuclear Recoil Following Neutrino Emission from Beryllium 7 . . . . Raymond Davis, Jr. 976
On the Stress Tensor of the Electron . . . . . Sidney Borowitz and Walter Kohn 985
Nuclear Matrix Elements in the Theory of Beta-Decay . . . . . Henry Brysk 996
Hyperfine Structure Anomalies in the $^2P_1$ State of Tl^{205} and Tl^{203} . . . . . Alan Berman 1005
Ferromagnetic Resonance in Nickel Ferrite as a Function of Temperature . . . . . D. W. Healy, Jr. 1009
Fine Structure of the Hydrogen Atom. IV . . . . . Willis E. Lamb, Jr., and Robert C. Retherford 1014
Decay of Sr^{85} and Sr^{85m} . . . . . A. W. Sunyar, J. W. Mihelich, G. Scharff-Goldhaber, M. Goldhaber, N. S. Wall, and M. Deutsch 1023
Relative Pair Production Cross Sections in the Energy Region 50 to 300 Mev . C. R. Emigh 1028
Investigation into the Nuclear Scattering of High Energy Protons . . . . . Kantilal M. Gatha and R. J. Riddell, Jr. 1035

Letters to the Editor:

Thermal and Electrical Conductivities of Carbon Materials . . . . . S. Mizushima 1040
Ferromagnetic Resonance in Copper Ferrite . . . . . Tosihiko Okamura and Yuzo Kojima 1040
β-Spectra of RaD . . . . . A. A. Jaffe and S. G. Cohen 1041
Excitation in High Energy Nuclear Reactions . . . . . Norton M. Hintz 1042
(γ,α) Reactions on Li^7, O^{16}, and $Br^{79,81}$ . . . . . H. Nabholz, P. Stoll, and H. Wäffler 1043
Fast Neutron Spectrometer . . . L. E. Beghian, R. A. Allen, J. M. Calvert, and H. Halban 1044
Collision of Heavy Primary Cosmic-Ray Nucleus . . . . . N. L. Allen, J. Y. Mei, E. Pickup, and L. Voyvodic 1045
Possible Charged *V*-Particle or Kappa-Meson Event Observed in a Photographic Emulsion . . . . . L. Voyvodic 1046
Magnetic Effect in Magnesium Titanate . . . . . E. K. Weise and H. Katz 1046
Secondary Electron Spectrum of Pr^{142} . . . . . Erling N. Jensen, L. Jackson Laslett, and D. J. Zaffarano 1047
Nature of Cosmic-Ray Bursts Underground . . . . . C. N. Chou 1048
Double Beta-Decay of Sn^{124} . . . . . R. M. Pearce and E. K. Darby 1049
Method of Interpreting the Distribution in Multiplicity of Shower Secondaries . . John Linsley 1050
Half-Life and Radiations of Te^{100} . . . . . G. E. Boyd, Q. V. Larson, and G. W. Parker 1051
High Energy Photodisintegration of the Deuteron . . . . Raphael Littauer and James Keck 1051
Radiation Loss by Electrons in Large Orbits . . . . . Dale R. Corson 1052
Angular Distribution of 53-Mev Positive Pions Scattered by Protons . . . . . E. C. Fowler, W. B. Fowler, R. P. Shutt, A. M. Thorndike, and W. L. Whittemore 1053
Photodisintegration of the Deuteron at High Energies . . . . . B. Bruno and S. Depken 1054
Internal Conversion in Cu^{64} and Fe^{59} . D. Brower, G. Hinman, G. Lang, R. Leamer, and D. Rose 1054
Lattice Imperfections of Diamond . . . . . P. G. Klemens 1055

Errata 1055
Author Index to Volume 86 1056
Analytic Subject Index to Volume 86 1072
Volume Table of Contents iii

THE
PHYSICAL REVIEW

A journal of experimental and theoretical physics established by E. L. Nichols in 1893

SECOND SERIES, VOL. 86, No. 6 JUNE 15, 1952

The Spherical Model of a Ferromagnet*†

T. H. BERLIN
Department of Physics, The Johns Hopkins University, Baltimore, Maryland

AND

M. KAC
Department of Mathematics, Cornell University, Ithaca, New York

(Received February 28, 1952)

A mathematical model, the spherical model, of a ferromagnet is described. The model is a generalization of the Ising model; and one-, two-, and three-dimensional lattices of infinite extent can be extensively discussed. A three-dimensional lattice shows ferromagnetic behavior and provides a statistical model of the Weiss phenomenological theory. The limiting free energy appears in a form which contains two of the essential features of the exactly known Ising model results in one and two dimensions. This suggests the probable form of the limiting free energy for the three-dimensional Ising model. A simplified model, the Gaussian model, is briefly discussed because this model also contains some of the significant features of the Ising model. However, the Gaussian model, unlike the spherical model, is not defined for all temperatures.

INTRODUCTION

THE subtlety and difficulty of the theoretical problem of the phase transition of a ferromagnet has been well established by the work of Bloch, Kramers, Heisenberg, and Onsager. In fact, the only nontrivial systems exhibiting a phase transition which can be exactly discussed are the Bose-Einstein gas and the two-dimensional Ising model of a ferromagnet. One may also include the work on the condensation of a non-ideal gas by Mayer and by Kahn and Uhlenbeck.

The problems are purely statistical mechanical, and the idealizations of the underlying physical problems are readily formulated. All that remains is the explicit evaluation of the partition function (even if only in the limiting case of an infinite number of particles). This evaluation is, of course, the difficulty.

There does not appear to be any single technique of sufficient generality which can be applied to the evaluation of partition functions. This lack of a general technique is very apparent now because of the work of Onsager on the Ising model. Onsager evaluated the partition function of the two-dimensional Ising model by an algebraic technique [1] This method, a magnificent achievement, is apparently restricted to the two-dimensional case. Nevertheless, the situation that presents itself is that no analytical method is available for the Ising model, whereas the Bose-Einstein condensation is demonstrated by a purely analytical method and the appropriate algebra is not available.

The partition function is the result of a generally complicated interplay between the Boltzmann factor and the weighting factor. One can expect that the characteristics of either factor may be responsible for a transition or the characteristics of both factors may be required. It is difficult to separate the relative importance of these factors with respect to their influence for a transition and also to discover the derivation of particular features of a transition. For the Bose-Einstein gas, condensation occurs in three dimensions but not in one or two dimensions. In this case, the transition can be ascribed to the weighting of the momentum states for the given Boltzmann factor.

We agree with Onsager that it is desirable to investigate models which yield to exact analysis and show transition phenomena. It is irrelevant that the models may be far removed from physical reality if they can illuminate some of the complexities of the transition phenomena.

We shall analyze two mathematical models: the Gaussian model, and the spherical model. These models

* This work was supported in part by the ONR.

† An outline of this paper was presented at the New York Meeting of the American Physical Society, January 26–29, 1949 [Phys. Rev. 75, 1298(A), (1949)].

[1] L. Onsager, Phys. Rev. 65, 117 (1944).

are continuum modifications of the Ising model of a ferromagnet. Montroll[2] has formulated more general continuum models in the hope that they will converge on the Ising model. The low temperature features of continuum models are obviously spurious. Nevertheless, we do not consider this aspect as detrimental to the discussion of possible transition phenomena. The Gaussian model becomes invalid for temperatures below a certain critical temperature (the partition function becomes complex). The reason for this behavior will become apparent, but it is surprising that the Gaussian model exhibits some of the general features of the exactly calculated one- and two-dimensional Ising models. The spherical model is a valid model for all temperatures. The one- and two-dimensional models do not exhibit transitions, whereas the three-dimensional model does. This model, in fact, can be regarded as a model for the Weiss phenomenological theory of ferromagnetism.

THE ISING MODEL

It is assumed that there is a spin at each site of a regular lattice of N sites. The interaction energy between neighboring spins may be written as $-J\epsilon_i\epsilon_j$, where J is the interaction energy and each spin can take on the discrete values ± 1. The partition function, normalized to unity, is

$$Q_N(I)=2^{-N}\sum_{\{\epsilon_j=\pm 1\}}\exp[(J/kT)\sum{}'\epsilon_i\epsilon_j], \tag{1}$$

where $\{\epsilon_j\}$ denotes a given configuration of spins and $\sum'$ denotes the sum over nearest neighbors. If we write $K=J/2kT$,

$$Q_N(I)=2^{-N}\sum_{\{\epsilon_j=\pm 1\}}\exp[K\sum{}'_{i,j}\epsilon_i\epsilon_j], \tag{2}$$

with $\sum_{i,j}'$ counting a given i, j twice, that is, the matrix of the quadratic form is symmetric.

We are essentially interested in the limiting free energy per particle which means that

$$-\psi/kT=\lim_{N\to\infty}N^{-1}\ln Q_N(I). \tag{3}$$

THE GAUSSIAN MODEL

This model assumes that the probability of finding a given spin ϵ_j between ϵ_j and $\epsilon_j+d\epsilon_j$ is given by

$$(2\pi)^{-\frac{1}{2}}\exp[-\epsilon_j^2/2]d\epsilon_j. \tag{4}$$

The model simulates the Ising model insofar as $\langle\epsilon_j\rangle=0$ and $\langle\epsilon_j^2\rangle=1$.

The normalized partition function is

$$Q_N(G)=(2\pi)^{-N/2}\int_{-\infty}^{\infty}\cdots\int d\epsilon_1\cdots d\epsilon_N \times\exp[-\tfrac{1}{2}\sum_{j=1}^{N}\epsilon_j^2+K\sum_{i,j}{}'\epsilon_i\epsilon_j]. \tag{5}$$

[2] E. W. Montroll, Nuovo cimento VI, 264 (1949).

Assuming that the quadratic form is negative definite,

$$Q_N(G)=\prod_{p=1}^{N}(1-2K\lambda_p)^{-\frac{1}{2}} =\exp[-\tfrac{1}{2}\sum_{p=1}^{N}\ln(1-2K\lambda_p)], \tag{6}$$

where λ_p is given in Appendix A for the several simple lattices. The free energy per particle is then, in the limit,

$$-\frac{\psi}{kT}=\lim_{N\to\infty}\left[-\frac{1}{2N}\sum_{p=1}^{N}\ln(1-2K\lambda_p)\right]. \tag{7}$$

The limit of the above sum over the characteristic values is discussed in Appendix B. The following results are obtained.

One-dimensional lattice:

$$-\frac{\psi}{kT}=-\frac{1}{2}\cdot\frac{1}{2\pi}\int_0^{2\pi}d\omega_1\ln[1-4K\cos\omega_1]; \tag{8a}$$

Two-dimensional square lattice:

$$-\frac{\psi}{kT}=-\frac{1}{2}\cdot\frac{1}{(2\pi)^2}\int_0^{2\pi}\int d\omega_1 d\omega_2 \times\ln[1-4K(\cos\omega_1+\cos\omega_2)]; \tag{8b}$$

Three-dimensional cubic lattice:

$$-\frac{\psi}{kT}=-\frac{1}{2}\cdot\frac{1}{(2\pi)^3}\int_0^{2\pi}\int\int d\omega_1 d\omega_2 d\omega_3 \times\ln[1-4K(\cos\omega_1+\cos\omega_2+\cos\omega_3)]. \tag{8c}$$

It is to be noticed that these results break down at a critical K which is $K_c=1/4n$, where n is the dimensionality of the lattice. For temperatures smaller than the critical temperature, the model is not defined since the free energy becomes complex. The source of this difficulty is obvious. Inspection of the characteristic values of the quadratic form shows that the form is not definite. Consequently, $Q_N(G)$ diverges for $T<T_c$.

This failure of the Gaussian model is trivial and is not the point. What is of interest is the comparison with the known results for the one- and two-dimensional Ising models.

One-dimensional Ising:

$$-\frac{\psi}{kT}=\frac{1}{2}\cdot\frac{1}{2\pi}\int_0^{2\pi}d\omega_1\ln[\cosh 4K-\sinh 4K\cos\omega_1]; \tag{9a}$$

Two-dimensional Ising:

$$-\frac{\psi}{kT}=\frac{1}{2}\cdot\frac{1}{(2\pi)^2}\int_0^{2\pi}\int d\omega_1 d\omega_2 \times\ln[\cosh^2 4K-\sinh 4K(\cos\omega_1+\cos\omega_2)]. \tag{9b}$$

The comparison is striking in the closeness in the formal structure of the expressions for ψ. The two features are the appearance of the logarithmic form and the structure of the cosines. The source of the formal appearance of the Ising model results is not clear. But the source is clear in the Gaussian model. The number and structure of the cosine terms arise from the "periodicity" in the interaction matrix. This periodicity is not simply due to the number of nearest neighbors because, for example, a doubly periodic interaction matrix is obtained for a plane regardless of the number of nearest neighbor interactions. Furthermore, we note that for a two-dimensional hexagonal lattice the structure of the cosine terms, easily obtained for the Gaussian and spherical models, is precisely that obtained by use of Onsager's method.

We shall now proceed to discuss the spherical model which retains the important formal features of the Gaussian model, but which also has the advantage of being valid for all temperatures.

THE SPHERICAL MODEL

A way of geometrically describing this model is the following. Let us suppose that we have N spins ϵ_j with $j=1, 2, \cdots, N$. Construct an N-dimensional cartesian space. A point P in this space is represented by the set of N coordinates $\{\epsilon_j\}$. The point P represents a spin configuration of the Ising model if $\epsilon_j=\pm 1$ for all j. The 2^N configurations in the Ising model are the vertices of an N-dimensional cube. Suppose that an N-dimensional sphere is circumscribed about the hypercube. The radius of this sphere is $N^{\frac{1}{2}}$, and the points on the sphere are given by the equation

$$\epsilon_1^2+\epsilon_2^2+\cdots+\epsilon_N^2=N. \tag{10}$$

The spherical model allows every point on this sphere to be an acceptable configuration. The model is a step closer to the Ising model than was the Gaussian model in that not only is $\langle\epsilon_j^2\rangle=1$, but also

$$\sum_{j=1}^{N}\epsilon_j^2=N$$

for every configuration. Furthermore, the interaction energy can now be replaced by a definite quadratic form so that a partition function valid for all temperatures is obtainable.

There are obvious defects in a continuum model. The entropy at absolute zero is infinite and the specific heat per particle is finite rather than zero. These defects, however, should not distract one's interest from the transition mechanism.

One can also raise the question that the spherical condition (10) allows configurations wherein a small number of spins can be very large, since $|\epsilon_j|\leq N^{\frac{1}{2}}$, so that these configurations could contribute a large magnetic moment to the system. It will be shown later that such states are not responsible for the behavior of the model. In fact, condition (10) implies that fluctuations are small.

The partition function for the spherical model is

$$Q_N(S)=A_N^{-1}\int\cdots\int_{\sum_{j=1}^{N}\epsilon_j^2=N} d\epsilon_1\cdots d\epsilon_N \exp[K\sum_{i,j}{}' \epsilon_i\epsilon_j], \tag{11}$$

where

$$A_N=\int\cdots\int_{\sum_{j=1}^{N}\epsilon_j^2=N} d\epsilon_1\cdots d\epsilon_N=2\pi^{N/2}N^{\frac{1}{2}(N-1)}/\Gamma(N/2). \tag{12}$$

There are various ways of evaluating the multiple integral. One can use the method of von Neumann,[3] one can use the Dirichlet factor[2] to remove the condition on the variables, or one can most conveniently use the delta function to evaluate the integral. The integral is evaluated using the delta function technique in Appendix C, where the details are also discussed.

If we let n denote the dimensionality of the simple lattices, then the result of the evaluation in the limit of $N\to\infty$ is that

$$-\psi_n/kT=-\tfrac{1}{2}-\tfrac{1}{2}\ln 4K+2Kz_s-\tfrac{1}{2}f_n(z_s), \tag{13}$$

where ψ_n is the limiting free energy per particle. The parameter z_s is the saddle point of the steepest descent evaluation of the partition function. It is the solution of

$$4K=[df_n(z)/dz]_{z=z_s}. \tag{14}$$

A solution $z_s(K)$ is possible for all temperatures for $n=1$ and 2. The reason for this is that the right side of Eq. (14) approaches infinity as z_s approaches the branch point of $f_1(z)$ and $f_2(z)$. Therefore ψ_1 and ψ_2 are regular functions of T and no transitions are obtained. In the three-dimensional lattice, the right side of Eq. (14) has a finite value, called $4K_c$, when $z_s=3$, the branch point of $f_3(z)$. For $T<T_c$, or $K>K_c$, the new path of steepest descent has a cusp at $z=3$. Then for $T<T_c$, ψ_3 is given by Eq. (13) when we put $z_s=3$. This "sticking" of the saddle point corresponds to a phase transition. The phase transition corresponds thermodynamically to a discontinuity in the temperature coefficient of the specific heat.

If we let U_n, C_n denote the internal energy per particle and specific heat per particle, respectively, for an n-dimensional simple lattice, $n=1, 2, 3$, then

$$U_n=\tfrac{1}{2}J\frac{d}{dK}(\psi_n/kT);\quad C_n=-kK^2\frac{d^2}{dK^2}(\psi_n/kT). \tag{15}$$

[3] J. von Neumann, Ann. Math. Stat. 12, 367 (1941), in particular pp. 372–374.

Now

$$\frac{d}{dK}(\psi_n/kT)=\frac{\partial}{\partial K}(\psi_n/kT)+\frac{dz_s}{dK}\frac{\partial}{\partial z_s}(\psi_n/kT)=\frac{\partial}{\partial K}(\psi_n/kT). \quad (16)$$

The last equality is true since $(\partial/\partial z_s)(\psi_n/kT)$ vanishes when the saddle point exists. In the case $n=3$, $T<T_c$, then $z_s=3$ and is independent of K so that dz_s/dK vanishes. We then have

$$\frac{d}{dK}(\psi_n/kT)=\frac{1}{2K}-2z_s, \quad \frac{d^2}{dK^2}(\psi_n/kT)=-\frac{1}{2K^2}-2\frac{dz_s}{dK}. \quad (17)$$

Consequently,

$$U_n=J[(1/4K)-z_s], \quad (18)$$

and

$$C_n=\tfrac{1}{2}k[1+4K^2dz_s/dK]. \quad (19)$$

It is clear from the analysis that z_s is a continuous function of T so that U_n is continuous. It is shown in Appendix C that dz_s/dK is a continuous function of T and vanishes at T_c when $n=3$. Hence, C_n is a continuous function of T approaching $\frac{1}{2}k$ as T approaches absolute 0. However, for $n=3$, $C_3=\frac{1}{2}k$, for $T<T_c$, and it is shown in Appendix C that d^2z_s/dK^2 is discontinuous at $T=T_c$. Thus, C_3 has a break in slope at the critical temperature. A sketch of the behavior is shown in Fig. 1.

The mechanical nature of the transition may be elucidated without difficulty. We shall show that the transition corresponds to spontaneous magnetization.

If μ_0 denotes the magnetic moment associated with a single spin, then the magnetic moment per particle of a given spin configuration, μ, is given by

$$\mu=(\mu_0/N)\sum_{j=1}^{N}\epsilon_j. \quad (20)$$

The magnetic susceptibility is given by

$$\chi=(N/kT)\langle\mu^2\rangle. \quad (21)$$

We now compute $\langle\mu^2\rangle$. Using the orthogonal transformation of the variables $\{\epsilon_j\}$ to the variables $\{y_j\}$ discussed in Appendix A, we note that

$$y_1=N^{-\frac{1}{2}}\sum_{j=1}^{N}\epsilon_j.$$

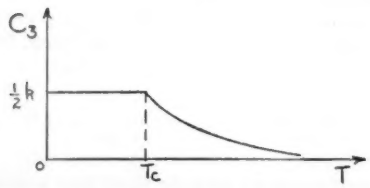

FIG. 1. The specific heat per particle *versus* temperature.

Therefore, using $Q_N(S)$ as given in Appendix C, Eqs. (C3) and (C4), we have

$$\mu=N^{-\frac{1}{2}}\mu_0 y_1, \quad \chi=(\mu_0^2/kT)\langle y_1^2\rangle,$$

$$\langle y_1^2\rangle=Q_N^{-1}(S)A_N^{-1}\frac{1}{2\pi i}\int_{z_0-i\infty}^{z_0+i\infty}ds\times\exp[Ns]\int_{-\infty}^{\infty}\cdots\int dy_1\cdots dy_N y_1^2\times\exp[-\sum_{j=1}^{N}(s-K\lambda_j)y_j^2]. \quad (22)$$

Hence,

$$\langle y_1^2\rangle\frac{1}{2\pi i}\int_{z_0-i\infty}^{z_0+i\infty}dz(z-\tfrac{1}{2}\lambda_1)^{-\frac{1}{2}}e^{Ng(z)}=\frac{1}{2\pi i}\int_{z_0-i\infty}^{z_0+i\infty}dz(4K)^{-1}(z-\tfrac{1}{2}\lambda_1)^{-\frac{1}{2}}e^{Ng(z)}. \quad (23)$$

Whenever a normal saddle point z_s exists, then

$$\langle y_1^2\rangle=1/[4K(z_s-\tfrac{1}{2}\lambda_1)]; \quad \chi=\mu_0^2/[2J(z_s-\tfrac{1}{2}\lambda_1)]. \quad (24)$$

We see that $\chi\to\infty$ when $z_s\to\frac{1}{2}\lambda_1$. In the one- and two-dimensional lattices, $T=0$ corresponds to $z_s=\frac{1}{2}\lambda_1$. In the three-dimensional lattice,

$$\chi=\mu_0^2/[2J(z_s-3)], \quad (25)$$

for $T>T_c$, and χ is infinite at the transition temperature. This result implies the finiteness of μ for $T<T_c$. We shall compute this magnetic moment. Because of the directional symmetry of the model $\langle\mu\rangle=0$, we therefore calculate

$$\langle|\mu|\rangle=N^{-\frac{1}{2}}\mu_0\langle|y_1|\rangle. \quad (26)$$

With the procedure used above,

$$\langle|y_1|\rangle\frac{1}{2\pi i}\int_{z_0-i\infty}^{z_0+i\infty}dz(z-\tfrac{1}{2}\lambda_1)^{-\frac{1}{2}}e^{Ng(z)}=\frac{1}{2\pi i}\int_{z_0-i\infty}^{z_0+i\infty}dz(2\pi K)^{-\frac{1}{2}}(z-\tfrac{1}{2}\lambda_1)^{-\frac{1}{2}}e^{Ng(z)}. \quad (27)$$

When the normal saddle point exists, then

$$\langle|y_1|\rangle=[2\pi K(z_s-\tfrac{1}{2}\lambda_1)]^{-\frac{1}{2}}, \quad \langle|\mu|\rangle=\mu_0[N2\pi K(z_s-\tfrac{1}{2}\lambda_1)]^{-\frac{1}{2}}\to 0, \quad (28)$$

in the limit $N\to\infty$. Hence, in the limit $N\to\infty$, $\langle|\mu|\rangle=0$ for the one- and two-dimensional models and also in the three-dimensional model for $T>T_c$.

For $T<T_c$, the numerator of Eq. (27) must be reconsidered. In the numerator, we note that the branch point, $z=3$, of the integrand is also a pole. Consequently, the contribution to the integral is obtained

from the infinitesimally small circle about the pole. The path of integration is shown in Fig. 2. We then find that for $T<T_c$,

$$\frac{1}{2\pi i}\int_{a-i\infty}^{a+i\infty} dz(z-3)^{-\frac{1}{2}}e^{Ng(z)}\simeq e^{Ng(3)}, \tag{29}$$

and

$$\frac{1}{2\pi i}\int_{a-i\infty}^{a+i\infty} dz(z-3)^{-\frac{1}{2}}e^{Ng(z)}\simeq[N2\pi(K-K_c)]^{-\frac{1}{2}}e^{Ng(3)}.$$

Therefore,

$$\begin{aligned}&\langle|y_1|\rangle=N^{\frac{1}{2}}[1-K_c/K]^{\frac{1}{2}};\\ &\langle|\mu|\rangle=\mu_0[1-K_c/K]^{\frac{1}{2}}=\mu_0[1-T/T_c]^{\frac{1}{2}}.\end{aligned} \tag{30}$$

This result proves the onset of spontaneous magnetization at the transition temperature T_c.

The possibility remains that the magnetization is due to a few spins taking on abnormally large values of the order $N^{\frac{1}{2}}$. We now show this possibility is not real by means of a calculation of the correlation between two spins.

The correlation C_{jk} between two spins ϵ_j, ϵ_k situated at the jth and kth lattice sites, respectively, is defined as

$$C_{jk}=\langle\epsilon_j\epsilon_k\rangle/\langle\epsilon_j^2\rangle^{\frac{1}{2}}\langle\epsilon_k^2\rangle^{\frac{1}{2}}. \tag{31}$$

Since the spherical condition, Eq. (10), requires $\langle\epsilon_j^2\rangle=1$ for all j, $C_{jk}=\langle\epsilon_j\epsilon_k\rangle$. In terms of the variables $\{y_j\}$,

$$\epsilon_j\epsilon_k=\left(\sum_{s=1}^{N}V_{js}y_s\right)\left(\sum_{t=1}^{N}V_{kt}y_t\right),$$

so that

$$C_{jk}=\sum_{s,t}V_{js}V_{kt}\langle y_sy_t\rangle.$$

However, $\langle y_sy_t\rangle=0$ unless $s=t$ because of the symmetry of the model. Thus,

$$C_{jk}=\sum_{s=1}^{N}V_{js}V_{ks}\langle y_s^2\rangle. \tag{32}$$

It is clear from Eq. (22) that

$$\begin{aligned}&\langle y_s^2\rangle\frac{1}{2\pi i}\int_{a-i\infty}^{a+i\infty} dz(z-\tfrac{1}{2}\lambda_1)^{-\frac{1}{2}}e^{Ng(z)}\\ &=\frac{1}{2\pi i}\int_{a-i\infty}^{a+i\infty} dz[4K(z-\tfrac{1}{2}\lambda_s)]^{-1}(z-\tfrac{1}{2}\lambda_1)^{-\frac{1}{2}}e^{Ng(z)}.\end{aligned} \tag{33}$$

Consequently,

$$\begin{aligned}&C_{jk}\frac{1}{2\pi i}\int_{a-i\infty}^{a+i\infty} dz(z-\tfrac{1}{2}\lambda_1)^{-\frac{1}{2}}e^{Ng(z)}\\ &=\frac{(4K)^{-1}}{2\pi i}\int_{a-i\infty}^{a+i\infty} dzF_{jk}(z)(z-\tfrac{1}{2}\lambda_1)^{-\frac{1}{2}}e^{Ng(z)},\end{aligned} \tag{34}$$

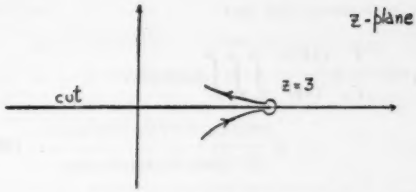

FIG. 2. The path of integration for $T<T_c$.

where

$$F_{jk}(z)=\sum_{s=1}^{N}V_{js}V_{ks}/(z-\tfrac{1}{2}\lambda_s).$$

The evaluation of a function such as F_{jk} as N becomes very large is described in Appendix B. We may write that

$$\begin{aligned}F_{jk}(z)=&\frac{1}{N(z-3)}+\frac{1}{(2\pi)^3}\int_0^{2\pi}\int_0^{2\pi}\int_0^{2\pi}d\omega_1d\omega_2d\omega_3\\ &\times\frac{\cos(x'\omega_1/a+y'\omega_2/a+z'\omega_3/a)}{z-(\cos\omega_1+\cos\omega_2+\cos\omega_3)}.\end{aligned} \tag{35}$$

We now see that for $T>T_c$,

$$\begin{aligned}C_{jk}=&\frac{(4K)^{-1}}{(2\pi)^3}\int_0^{2\pi}\int_0^{2\pi}\int_0^{2\pi}d\omega_1d\omega_2d\omega_3\\ &\times\frac{\cos(x'\omega_1/a+y'\omega_2/a+z'\omega_3/a)}{z_s-(\cos\omega_1+\cos\omega_2+\cos\omega_3)}.\end{aligned} \tag{36}$$

Note that $C_{jj}=\langle\epsilon_j^2\rangle=1$ and from the above equation, putting $x'=y'=z'=0$,

$$C_{jj}=\frac{(4K)^{-1}}{(2\pi)^3}\int_0^{2\pi}\int_0^{2\pi}\int_0^{2\pi}\frac{d\omega_1d\omega_2d\omega_3}{z_s-(\cos\omega_1+\cos\omega_2+\cos\omega_3)}=1,$$

because this is the equation determining z_s.

It is also apparent that as (x', y', z') increase, C_{jk} decreases so that the correlation monotonically approaches zero as the distance between spins increases.

For $T<T_c$ a closer examination is required because the first term in $F_{jk}(z)$ is a pole at $z=3$. However, since the integral part converges at $z=3$, this part is the same as Eq. (36) with $z_s=3$. A straightforward evaluation yields

$$\begin{aligned}&\frac{1}{2\pi i}\int_{a-i\infty}^{a+i\infty} dz[N(z-3)]^{-1}(z-3)^{-\frac{1}{2}}e^{Ng(z)}\\ &\simeq 4\left[\frac{(K-K_c)}{2\pi N}\right]^{\frac{1}{2}}e^{Ng(3)}.\end{aligned} \tag{37}$$

We consequently find that

$$C_{jk}=1-\frac{T}{T_c}+\frac{(4K)^{-1}}{(2\pi)^3}\int\int\int_0^{2\pi}d\omega_1 d\omega_2 d\omega_3 \times\frac{\cos(x'\omega_1/a+y'\omega_2/a+z'\omega_3/a)}{3-(\cos\omega_1+\cos\omega_2+\cos\omega_3)}. \quad (38)$$

This result demonstrates that below the transition temperature an extended correlation exists of magnitude $1-T/T_c$. Superimposed on the correlation extending over the whole lattice is a correlation monotonically decreasing with increasing distance.

As a check on this result we note that

$$C_{jj}=1-\frac{T}{T_c}+\frac{(4K)^{-1}}{(2\pi)^3}\int\int\int_0^{2\pi}\frac{d\omega_1 d\omega_2 d\omega_3}{3-(\cos\omega_1+\cos\omega_2+\cos\omega_3)}.$$

However, we have defined K_c so that

$$4K_c\equiv\frac{1}{(2\pi)^3}\int\int\int_0^{2\pi}\frac{d\omega_1 d\omega_2 d\omega_3}{3-(\cos\omega_1+\cos\omega_2+\cos\omega_3)}.$$

Hence,

$$C_{jj}=1-T/T_c+4K_c/4K=1.$$

The integrals are readily evaluated in the case of the one-dimensional lattice. We have then for all T,

$$C_{jk}=\frac{(4K)^{-1}}{2\pi}\int_0^{2\pi}d\omega_1\frac{\cos(x'\omega_1/a)}{z_s-\cos\omega_1}.$$

This gives

$$C_{jk}=[z_s-(z_s^2-1)^{\frac{1}{2}}]^{x'/a}/4K(z_s^2-1)^{\frac{1}{2}} =[z_s-(z_s^2-1)^{\frac{1}{2}}]^{x'/a}, \quad (39)$$

since $4K(z_s^2-1)^{\frac{1}{2}}=1$. Thus the correlation falls off with distance exponentially.

The connection between the spherical and Gaussian models is rather transparent. In the spherical model, if we ask for the distribution of a finite number of spins, that is, a number independent of N for large N, then this distribution is Gaussian, at least above the transition temperature. The spherical condition forces a cooperation among the spins which does not exist in the Gaussian model. Therefore, deviations from a Gaussian distribution are obtained when the cooperation sets in, that is, below the transition temperature. We can see this by means of a calculation of $\langle\epsilon_j^4\rangle$.

A Gaussian distribution of ϵ_j with $\langle\epsilon_j\rangle=0$, $\langle\epsilon_j^2\rangle=1$, yields $\langle\epsilon_j^4\rangle=3$. In the spherical model,

$$\langle\epsilon_j^4\rangle=\left\langle\left[\sum_{s=1}^N V_{js}y_s\right]^4\right\rangle =\sum_{s=1}^N V_{js}^4\langle y_s^4\rangle+3\sum_{r\neq s}V_{js}^2V_{jr}^2\langle y_s^2y_r^2\rangle, \quad (40)$$

because the average of odd powers of the y's vanishes. Then

$$\langle\epsilon_j^4\rangle\frac{1}{2\pi i}\int_{\alpha-i\infty}^{\alpha+i\infty}dz(z-3)^{-\frac{1}{2}}e^{Ng(z)}=\frac{3}{16K^2}\frac{1}{2\pi i}\int_{\alpha-i\infty}^{\alpha+i\infty}dz \times\left[\sum_{s=1}^N V_{js}^2(z-\tfrac{1}{2}\lambda_s)^{-1}\right]^2(z-3)^{-\frac{1}{2}}e^{Ng(z)}. \quad (41)$$

However,

$$\sum_{s=1}^N V_{js}^2(z-\tfrac{1}{2}\lambda_s)^{-1}=\frac{1}{N(z-3)} +\frac{1}{(2\pi)^3}\int\int\int_0^{2\pi}\frac{d\omega_1 d\omega_2 d\omega_3}{z-(\cos\omega_1+\cos\omega_2+\cos\omega_3)} \quad (42)$$

for the simple three-dimensional lattice.

When $T>T_c$, $(K<K_c)$, a normal saddle point exists and we may use

$$\sum_{s=1}^N V_{js}^2(z_s-\tfrac{1}{2}\lambda_s)^{-1}=4K. \quad (43)$$

Consequently $\langle\epsilon_j^4\rangle=3$ for $T>T_c$. (44)

Below the transition temperature the integral in Eq. (42) is finite and we may use

$$\sum_{s=1}^N V_{js}^2(z-\tfrac{1}{2}\lambda_s)^{-1}=\frac{1}{N(z-3)}+4K_c. \quad (45)$$

It is then found that

$$\langle\epsilon_j^4\rangle=3-2(1-T/T_c)^2 \quad \text{for} \quad T<T_c. \quad (46)$$

Note that at $T=0$, $\langle\epsilon_j^4\rangle=1$, which is as it should be because all the spins are lined up. Equation (46), by showing that $\langle\epsilon_j^4\rangle$ is finite, proves (along with the correlation) that configurations in which a small number of spins have moments of the order $N^{\frac{1}{2}}$ are not responsible for the behavior of the spherical model.

In concluding this section we wish to point out that we may write the limiting free energy per particle for the spherical model in the form

$$-\frac{\psi_n}{kT}=-\frac{1}{2}\cdot\frac{1}{(2\pi)^n}\int_0^{2\pi}\cdots\int d\omega_1\cdots d\omega_n \times[F(T)-G(T)\sum_{j=1}^n\cos\omega_j], \quad (47)$$

where $F=z_sG$, $G=4Ke^{1-4kz_s}$, and n is the dimensionality of the simple lattice.

The analogy with the Ising model solutions is close. Furthermore, we have noted that the structure of the

cosine terms in the integrand is simply determined from the cyclized interaction energy matrix of the Boltzmann factor. If we consider a two-dimensional hexagonal lattice with six nearest neighbors, then we easily find that, with $n=2$, the cosine terms $[\cos\omega_1+\cos\omega_2]$ for the square lattice are replaced by $[\cos\omega_1+\cos\omega_2+\cos(\omega_2-\omega_1)]$.

These same cosine terms were found by Onsager in his solution of the corresponding Ising model. It may then be conjectured that the solution of the three-dimensional simple cubic Ising model is of the form

$$-\frac{\psi_3}{kT}=\frac{1}{2}\cdot\frac{1}{(2\pi)^3}\int_0^{2\pi}\int\int d\omega_1 d\omega_2 d\omega_3 \times\ln[F(T)-G(T)(\cos\omega_1+\cos\omega_2+\cos\omega_3)], \quad (48)$$

where $F(T)$, $G(T)$ are the appropriate functions of temperature.

THE SPHERICAL MODEL IN AN HOMOGENEOUS MAGNETIC FIELD

Let us assume that the lattice is in an homogeneous magnetic field of strength H and that the direction of the spins is in the direction of the magnetic field. Then the additional energy of the system is

$$-H\mu_0\sum_{j=1}^{N}\epsilon_j=-N^{\frac{1}{2}}H\mu_0 y_1. \quad (49)$$

This then yields for the partition function

$$Q_{NH}(S)=\frac{A_N^{-1}}{2\pi i}\int_{\omega-i\infty}^{\omega+i\infty}ds\exp[Ns]\int_{-\infty}^{\infty}\cdots\int dy_1\cdots dy_N \times\exp\left[-\sum_{j=1}^{N}(s-K\lambda_j)y_j^2+2N^{\frac{1}{2}}My_1\right], \quad (50)$$

with $M=\mu_0 H/2kT$.

The integration of y_1 introduces a new factor $\exp[NM^2/(s-K\lambda_1)]$. This then gives

$$-\psi_n(H)/kT=-\tfrac{1}{2}-\tfrac{1}{2}\ln 4K+2Kz_s -\tfrac{1}{2}f_n(z_s)+M^2/2K(z_s-\tfrac{1}{2}\lambda_1), \quad (51)$$

where the saddle point $z_s(K, H)$ is given by

$$4K=[df_n(z)/dz]_{z=z_s}+M^2/[K(z_s-\tfrac{1}{2}\lambda_1)^2]. \quad (52)$$

We see immediately that for $M\neq 0$, a normal saddle point always exists because the M dependent term approaches ∞ as z_s approaches $\frac{1}{2}\lambda_1=n$. This means that a magnetic field destroys the transition to a spontaneously magnetized state for the three-dimensional lattice.

The mean magnetic moment per particle is $\langle\mu\rangle=\mu_0 N^{-1}\langle y_1\rangle$. Since a normal saddle point always exists, we easily find that

$$\langle y_1\rangle=\frac{N^{\frac{1}{2}}M}{2K(z_s-\tfrac{1}{2}\lambda_1)}=\tfrac{1}{2}N^{\frac{1}{2}}\frac{\partial}{\partial M}(-\psi_n/kT), \quad (53)$$

so that

$$\langle\mu\rangle=\mu_0 M/[2K(z_s-n)]=H\mu_0^2/[2J(z_s-n)], \quad (54)$$

and we have the magnetic equation of state for the model through Eqs. (51), (52), and (54). The magnetic susceptibility per particle is

$$\chi=\langle\mu\rangle/H=\mu_0^2/[2J(z_s-n)]. \quad (55)$$

The high temperature and saturation behavior of $\langle\mu\rangle$, χ, is precisely as expected. In fact, this model provides a mechanism for and essentially the formulas of the Curie-Weiss phenomenological theory of ferromagnetism.

In the Curie-Weiss theory,

$$\chi=T_c^*/[\alpha^*(T-T_c^*)], \quad (56)$$

where T_c^* is the transition temperature and α^* is a parameter controlling the strength of the local field. (α^* is chosen to enable the theory to fit the experimental data.)

Putting Eq. (55) in a form similar to that of Eq. (56), we find that, with $n=3$,

$$\chi=T_c/\alpha[h(T)T-T_c], \quad (57)$$

where

$$\alpha=6J/\mu_0^2, \quad h(T)=Tz_s/3T.$$

The quantity α is to be identified with α^*. According to the Curie-Weiss theory, $T_c^*=6J/k$. The present model yields $T_c\simeq 6J/1.5k$. If we set $T_c^*=\gamma T_c$, then

$$\chi=T_c^*/\alpha[\gamma h(T)T-T_c^*]. \quad (58)$$

We find that for $T_c\leqslant T<\infty$, $3/2\geqslant\gamma h(T)\geqslant 1$, so that the spherical model yields a slightly modified Curie-Weiss formula for the case of zero magnetic field strength. Equation (57) holds for all field strengths when z_s is determined by Eq. (52).

DISCUSSION

The virtue of the spherical model of a ferromagnet is that its properties can be rather extensively discussed and that a three-dimensional lattice has ferromagnetic properties. It is of further interest that the model provides a classical mechanism for the Weiss phenomenological theory.

With respect to the physical ferromagnet, the model has nothing to say positively. We may briefly consider, however, the bearing of our results on the nature of the transition.

The Bloch spin wave theory, which is valid near saturation or low temperature, has the result that a two-dimensional net is nonferromagnetic and a three-dimensional lattice is ferromagnetic. The spherical model yields the same result. On the other hand, the two-dimensional Ising model is ferromagnetic.

A recent paper by Herring and Kittel[4] illuminates the Ising model transition. These authors discussed a phenomenological theory based on the spin-wave treatment

[4] C. Herring and C. Kittel, Phys. Rev. **81**, 869 (1951).

and they demonstrate that ferromagnetism may be induced in a two-dimensional lattice by the presence of anisotropic interactions. This they suggest, lies behind the Ising transition. The spherical model weakens the anisotropy of the Ising model, and, in fact, has destroyed the transition in the two-dimensional lattice.

One might now infer that although the three-dimensional Ising model certainly will provide a transition, this transition may still be more descriptive of the anisotropy of the Ising model rather than descriptive of the transition in an ideal isotropic ferromagnet. It is more likely that the spherical model transition is closer to the actual transition behavior.

There is a further feature of the spherical model which is probably of significance. The point in question is also shown by the Gaussian model. Comparing, say, Eq. (8) with (11), note that the Gaussian model (and the spherical model) have a minus sign before the integral representation, whereas the Ising model has a plus sign. Although the minus sign can be converted into a plus sign by an appropriate transformation, it is true that the conversion is not unique. We cannot throw any light on this point, but it may be indicative of an essential difference between the transition mechanisms of the two models (spherical and Ising).

The authors wish to express their sincere appreciation to Professors G. E. Uhlenbeck and E. W. Montroll for their several helpful discussions. One of us (T. H. B.) wishes to thank Professor L. P. Smith for extending to him the hospitality of the Physics Department of Cornell University for the summer of 1948.

APPENDIX A. ON THE QUADRATIC FORM $\sum_{i,j} c_i a_j$

It will be convenient to set down here properties associated with the quadratic form describing the interaction energy which will be useful in the body of the paper. The properties are all connected with the diagonalization of the quadratic form. Since the form is symmetric, its diagonalization is always possible by means of an orthogonal transformation.

It is also particularly convenient to make the matrix of the coefficients of the form cyclic. Cyclization is achieved by postulating an appropriate periodicity. In a one-dimensional lattice, the chain is bent into a ring so that the Nth site is a nearest neighbor of the 1st site. In two dimensions, the simple lattice is constructed on a torus. These are the obvious geometrical representations.

Consider first the cyclic matrix $M(c_1, c_2, \cdots, c_N)$.

$$M \equiv \begin{pmatrix} c_1 & c_2 & c_3 & \cdots & c_{N-1} & c_N \\ c_N & c_1 & c_2 & \cdots & c_{N-2} & c_{N-1} \\ c_{N-1} & c_N & c_1 & \cdots & c_{N-3} & c_{N-2} \\ \cdot & \cdot & \cdot & \cdots & \cdot & \cdot \\ \cdot & \cdot & \cdot & \cdots & \cdot & \cdot \\ c_2 & c_3 & c_4 & \cdots & c_N & c_1 \end{pmatrix}. \tag{A1}$$

We wish to find the characteristic values and vectors associated with M, that is

$$MV = \lambda V. \tag{A2}$$

For the characteristic values we must solve the equation

$$|M(c_1 - \lambda c_2 \cdots, c_N)| = 0. \tag{A3}$$

Following Kowaleski,[5] let $r_1, r_2, \cdots, r_N$ denote the N roots of unity and we shall choose

$$r_k = \exp[2\pi i(k-1)/N].$$

Construct the determinant

$$\Delta \equiv \begin{vmatrix} 1 & 1 & \cdots & 1 \\ r_1 & r_2 & \cdots & r_N \\ r_1^2 & r_2^2 & \cdots & r_N^2 \\ \cdot & \cdot & \cdots & \cdot \\ \cdot & \cdot & \cdots & \cdot \\ r_1^{N-1} & r_2^{N-1} & \cdots & r_N^{N-1} \end{vmatrix} \neq 0. \tag{A4}$$

We next form the product $|M|\Delta \equiv |P_{jk}|$. Now

$$P_{jk} = \sum_{s=1}^{N} M_{js} r_k^{s-1}.$$

But $M_{js} = c_{N-j+1+s}$, where we define $c_{N+s} \equiv c_s$. Hence, if we define

$$f(r_k) = \sum_{s=1}^{N} c_s r_k^{s-1}, \tag{A5}$$

then

$$P_{jk} = \sum_{s=1}^{N} c_{N-j+1+s} r_k^{s-1} = r_k^{j-1} f(r_k). \tag{A6}$$

It is apparent that

$$|P_{jk}| = \Delta \prod_{k=1}^{N} f(r_k),$$

so that

$$|M| = \prod_{k=1}^{N} f(r_k). \tag{A7}$$

This immediately yields the result that

$$\lambda_k = f(r_k). \tag{A8}$$

Let V_{ks} denote the sth component of the characteristic vector belonging to λ_k. Then, from (A2),

$$\sum_{s=1}^{N} c_{N-j+1+s} V_{ks} = \lambda_k V_{kj}. \tag{A9}$$

If we set $V_{ks} = \alpha r_k^{s-1}$, then

$$\alpha \sum_{s=1}^{N} c_{N-j+1+s} r_k^{s-1} = \alpha \lambda_k r_k^{j-1}.$$

Since the left sum is $r_k^{j-1} f(r_k) = r_k^{j-1} \lambda_k$, we have deter-

[5] G. Kowaleski, *Determinantentheorie* (Chelsea Publishing Company, New York, 1948), 3rd edition, p. 105.

mined the characteristic vector up to a multiplicative constant.

Now suppose that the matrix M is also symmetric. This requires that $M_{jk}=M_{kj}$ or $c_{N-j+1+k}=c_{N-k+1+j}$. Setting $j=1$,

$$c_{N+k}\equiv c_k=c_{N-k+2}. \tag{A10}$$

This implies that $\lambda_k=\lambda_{N-k+2}$, because

$$\lambda_k=\sum_{s=1}^{N} c_s r_k^{s-1}=\sum_{s=1}^{N} c_{N-s+2} r_k^{s-1}=\sum_{p=1}^{N} c_p r_k^{N-p+1},$$

and since

$$r_k^{N-p+1}=r_{N-k+2}^{p-1},$$

$$\lambda_k=\sum_{p=1}^{N} c_p r_{N-k+2}^{p-1}=\lambda_{N-k+2}. \tag{A11}$$

Consequently, the characteristic values of a symmetric, cyclic matrix are twofold except for λ_1, and $\lambda_{\frac{1}{2}N+1}$ if N is even.

The corresponding real, orthogonal characteristic vectors, normalized to unity, are given by

$$V_{ks}=N^{-\frac{1}{2}}\left[\cos\frac{2\pi}{N}(k-1)(s-1)+\sin\frac{2\pi}{N}(k-1)(s-1)\right]. \tag{A12}$$

Now consider the quadratic forms of immediate interest.

Let ϵ denote the column matrix with components $\epsilon_1, \epsilon_2, \cdots, \epsilon_N$. Then

$$\sum_{i,j}' \epsilon_i\epsilon_j=\epsilon' M\epsilon,$$

with M symmetric and cyclic. We make an orthogonal transformation $\epsilon=Vy$ with Jacobian unity. Thus

$$\epsilon' M\epsilon=\sum_{p=1}^{N}\lambda_p y_p^2 \quad\text{and}\quad \sum_{p=1}^{N}\epsilon_p^2=\sum_{p=1}^{N} y_p^2. \tag{A13}$$

The elements of V, V_{ks}, are given by (A12).

One-dimensional lattice:

$$\begin{aligned} &c_2=c_N=1. \text{ All other } c\text{'s}=0.\\ &\lambda_p=2\cos(2\pi/N)(p-1). \end{aligned} \tag{A14}$$

Two-dimensional lattice:

We shall take a rectangular lattice with n_1 sites in a row, n_2 rows, so that $N=n_1n_2$. The ith site may be represented by the number pair (p, q) and by the space coordinates (x, y). If a is the spacing, we set

$$\begin{aligned} &x=(p-1)a, \quad y=qa,\\ &i=p+qn_1, \end{aligned} \tag{A15}$$

where

$$p=1, 2, \cdots, n_1; \quad q=0, 1, \cdots, n_2-1.$$

We then choose

$$c_2=c_{n_1+1}=c_{N-n_1+1}=c_N=1, \tag{A16}$$

and all other c's$=0$. Then,

$$\lambda_p=2\cos\frac{2\pi}{N}(p-1)+2\cos\frac{2\pi n_1}{N}(p-1). \tag{A17}$$

Three-dimensional lattice:

We shall take a lattice with n_1 sites in a row, n_2 rows in a plane, and n_3 planes so that the total number of sites $N=n_1n_2n_3$. The ith site may be represented by the number triple (p, q, s) and by the space coordinates (x, y, z). If a is the spacing, we set

$$x=(p-1)a, \quad y=qa, \quad z=sa, \quad i=p+qn_1+sn_1n_2, \tag{A18}$$

where

$$p=1, 2, \cdots, n_1: \ q=0, 1, \cdots, n_2-1: \ s=0, 1, \cdots, n_3-1.$$

We choose

$$\begin{aligned} c_2=c_{n_1+1}=c_{n_1n_2+1}&=c_{N-n_1n_2+1}\\ &=c_{N-n_1+1}=c_N=1, \end{aligned} \tag{A19}$$

and all other c's$=0$. Then,

$$\lambda_p=2\cos\frac{2\pi}{N}(p-1)+2\cos\frac{2\pi n_1}{N}(p-1)+2\cos\frac{2\pi n_1n_2}{N}(p-1). \tag{A20}$$

APPENDIX B. ON THE $\lim_{N\to\infty} N^{-1}\sum_{p=1}^{N}\ln[1-2K\lambda_p]$

Consider the general sum

$$S(f)=\lim_{N\to\infty} N^{-1}\sum_{p=1}^{N} f(\lambda_p/2). \tag{B1}$$

The largest characteristic value occurs for $p=1$. We will then assume that the function $f(z)$ is regular when $z>\lambda_1/2$. Consequently, if we write

$$N^{-1}\sum_{p=1}^{N} f(\lambda_p/2)=N^{-1}f(\lambda_1/2)+N^{-1}\sum_{p=2}^{N} f(\lambda_p/2),$$

then

$$S(f)=\lim_{N\to\infty} N^{-1}\sum_{p=2}^{N} f(\lambda_p/2),$$

if $f(\lambda_1/2)$ is finite. This point is mentioned because the significant singularity of the functions to be considered depends on λ_1.

One-dimensional lattice:

From Eq. (A14), we have

$$\frac{\lambda_p}{2}=\cos\frac{2\pi}{N}(p-1).$$

Subdivide the interval $0-2\pi$ into N equal intervals of length $2\pi/N=\Delta\omega_1$. Then set $\omega_1=(p-1)\Delta\omega_1$. Consequently,

$$N^{-1}\sum_{p=2}^{N} f(\lambda_p/2)=\frac{1}{2\pi}\sum_{\omega_1=\Delta\omega_1}^{2\pi-\Delta\omega_1} f(\cos\omega_1)\Delta\omega_1, \quad \text{(B2)}$$

and

$$S(f)=\lim_{\Delta\omega_1\to 0}\frac{1}{2\pi}\sum_{\omega_1=\Delta\omega_1}^{2\pi-\Delta\omega_1} f(\cos\omega_1)\Delta\omega_1 = \frac{1}{2\pi}\int_0^{2\pi} f(\cos\omega_1)d\omega_1. \quad \text{(B3)}$$

It then follows that for $f(\lambda_p/2)=\ln[1-4K(\lambda_p/2)]$,

$$\lim_{N\to\infty} N^{-1}\sum_{p=1}^{N}\ln[1-2K\lambda_p] = \frac{1}{2\pi}\int_0^{2\pi} d\omega_1 \ln[1-4K\cos\omega_1]. \quad \text{(B4)}$$

Two-dimensional lattice:

For this lattice,

$$\frac{\lambda_p}{2}=\cos\frac{2\pi}{N}(p-1)+\cos\frac{2\pi n_1}{N}(p-1), \quad \text{(B5)}$$

with $N=n_1n_2$.

Let us write

$$p-1=p_2+p_1n_2, \qquad p_1=0,1,\cdots,n_1-1; \quad p_2=0,1,\cdots,n_2-1. \quad \text{(B6)}$$

Then

$$\frac{2\pi}{N}(p-1)=\frac{2\pi}{n_1n_2}p_2+\frac{2\pi}{n_1}p_1, \quad \frac{2\pi n_1}{N}(p-1)=\frac{2\pi}{n_2}p_2+2\pi p_1,$$

and

$$\frac{\lambda_p}{2}=\cos\left(\frac{2\pi}{n_1n_2}p_2+\frac{2\pi}{n_1}p_1\right)+\cos\left(\frac{2\pi}{n_2}p_2\right), \quad \text{(B7)}$$

since p_1 is an integer.

Hence,

$$N^{-1}\sum_{p=2}^{N} f(\lambda_p/2)=N^{-1}\sum_{\substack{p_1=1\\ p_2=0}}^{n_1-1} f(\lambda_{p_1+1/2}) + N^{-1}\sum_{p_1=1}^{n_1-1}\sum_{p_2=0}^{n_2-1} f(\lambda_{p_2+p_1n_2+1/2}). \quad \text{(B8)}$$

Now let

$$\Delta\omega_2=2\pi/n_2, \quad \omega_2=(2\pi/n_2)p_2.$$

$$\frac{\lambda_{p_2+p_1n_2+1}}{2}=\cos\left(\frac{\omega_2}{n_1}+\frac{2\pi}{n_1}p_1\right)+\cos\omega_2. \quad \text{(B9)}$$

Since ω_2 always ranges between 0 and 2π, ω_1/n_1 vanishes in the limit n_1. We then may write, as $n_2\to\infty$,

$$\sum_{p_1=0}^{n_1-1} f\left(\frac{\lambda_{p_2+p_1n_2+1}}{2}\right)\to\frac{n_2}{2\pi}\int_0^{2\pi} d\omega_2 f \times\left(\cos\frac{2\pi}{n_1}p_1+\cos\omega_2\right), \quad \text{(B10)}$$

and

$$N^{-1}\sum_{p=2}^{N} f\left(\frac{\lambda_p}{2}\right)\to\frac{1}{2\pi n_1}\int_0^{2\pi} d\omega_2 f(1+\cos\omega_2) + \frac{n_2}{2\pi N}\sum_{p_1=1}^{n_1-1}\int_0^{2\pi} d\omega_2 f\left(\cos\frac{2\pi}{n_1}p_1+\cos\omega_2\right). \quad \text{(B11)}$$

The summation over p_1 leads to a second independent integral. Letting $\Delta\omega_1=2\pi/n_1$, $\omega_1=(2\pi/n_1)p_1$, then

$$S(f)=\frac{1}{(2\pi)^2}\int_0^{2\pi}\int_0^{2\pi} d\omega_1 d\omega_2 f(\cos\omega_1+\cos\omega_2). \quad \text{(B12)}$$

In the case that $f(\lambda_p/2)=\ln[1-4K(\lambda_p/2)]$,

$$\lim_{N\to\infty} N^{-1}\sum_{p=1}^{N}\ln[1-2K\lambda_p]=\frac{1}{(2\pi)^2}\int_0^{2\pi}\int_0^{2\pi} d\omega_1 d\omega_2 \times\ln[1-4K(\cos\omega_1+\cos\omega_2)]. \quad \text{(B13)}$$

Three-dimensional lattice:

For this lattice

$$\frac{\lambda_p}{2}=\cos\frac{2\pi}{N}(p-1)+\cos\frac{2\pi n_1}{N}(p-1)+\cos\frac{2\pi n_1n_2}{N}(p-1)$$

with $N=n_1n_2n_3$.

There is no need to repeat the analysis, as it follows the two-dimensional analysis closely. The result is that

$$S(f)=\frac{1}{(2\pi)^3}\int_0^{2\pi}\int\int d\omega_1 d\omega_2 d\omega_3 \times f(\cos\omega_1+\cos\omega_2+\cos\omega_3). \quad \text{(B14)}$$

If $f(\lambda_p/2)=\ln[1-4K(\lambda_p/2)]$, then

$$\lim_{N\to\infty} N^{-1}\sum_{p=1}^{N}\ln[1-2K\lambda_p]=\frac{1}{(2\pi)^3}\int_0^{2\pi}\int\int d\omega_1 d\omega_2 d\omega_3 \times\ln[1-4K(\cos\omega_1+\cos\omega_2+\cos\omega_3)]. \quad \text{(B15)}$$

Consider now a function

$$F_{jk}(f)=\sum_{p=1}^{N} V_{jp}V_{kp}f(\lambda_p/2), \quad \text{(B16)}$$

with

$$V_{jp}V_{kp}=N^{-1}\left[\cos\frac{2\pi}{N}(j-k)(p-1)+\sin\frac{2\pi}{N}(j+k-2)(p-1)\right].$$

$$F_{jk}(f)=N^{-1}f\left(\frac{\lambda_1}{2}\right)+N^{-1}\sum_{p=2}^{N}f\left(\frac{\lambda_p}{2}\right)\times\left[\cos\frac{2\pi}{N}(j-k)(p-1)+\sin\frac{2\pi}{N}(j+k-2)(p-1)\right].$$

Therefore, let us consider

$$G_{jk}(f)=N^{-1}\sum_{p=2}^{N}f(\lambda_p/2)\exp\left[in_{jk}\frac{2\pi}{N}(p-1)\right], \quad \text{(B17)}$$

where n_{jk} is an integer depending linearly on j and k, that is,

$$n_{jk}=A+Bj+Ck,$$

with A, B, C as integers.

From before,

$$\frac{\lambda_p}{2}=\cos\frac{2\pi}{N}(p-1)+\cos\frac{2\pi n_1}{N}(p-1)+\cos\frac{2\pi n_1n_2}{N}(p-1),$$

$N=n_1n_2n_3$, where we are supposing the three-dimensional lattice.

Let us now write

$$p-1=rn_3+q;\ r=0,1,\cdots,n_1n_2-1;\ q=0,1,\cdots,n_3-1.$$

Now

$$\sum_{p=2}^{N}=\sum_{r=0}^{n_1n_2-1}\sum_{q=1}^{n_3-1},$$

so that

$$G_{jk}(f)=N^{-1}\sum_{r=0}^{n_1n_2-1}\sum_{q=1}^{n_3-1}f(\lambda_p/2)\times\exp\left[in_{jk}\left(\frac{2\pi r}{n_1n_2}+\frac{2\pi q}{n_1n_2n_3}\right)\right],$$

and

$$\frac{\lambda_p}{2}=\cos\left(\frac{2\pi r}{n_1n_2}+\frac{2\pi q}{n_1n_2n_3}\right)+\cos\left(\frac{2\pi r}{n_2}+\frac{2\pi q}{n_2n_3}\right)+\cos\left(2\pi r+\frac{2\pi q}{n_3}\right).$$

Let

$$\Delta\omega_3=2\pi/n_3,\quad \omega_3=(2\pi/n_3)q.$$

Since r is an integer, $\cos(2\pi r+2\pi q/n_3)=\cos\omega_3$. Also as n_1, n_2, n_3 become large,

$$\lambda_p/2=\cos\frac{2\pi r}{n_1n_2}+\cos\frac{2\pi r}{n_2}+\cos\omega_3.$$

Furthermore,

$$\sum_{q=1}^{n_3-1}=\frac{n_3}{2\pi}\sum_{2\pi/n_3}^{2\pi-2\pi/n_3}\Delta\omega_3\to\frac{n_3}{2\pi}\int_0^{2\pi}d\omega_3.$$

Hence,

$$G_{jk}(f)=\frac{n_3}{2\pi N}\int_0^{2\pi}d\omega_3\sum_{r=0}^{n_1n_2-1}f(\lambda_p/2)\times\exp\left[in_{jk}\left(\frac{2\pi r}{n_1n_2}+\frac{\omega_3}{n_1n_2}\right)\right].$$

Now let

$$r=ln_2+U,\quad l=0,1,\cdots,n_1-1;\quad U=0,1,\cdots,n_2-1.$$

$$\frac{\lambda_p}{2}=\cos\left(\frac{2\pi l}{n_1}+\frac{2\pi u}{n_1n_2}\right)+\cos\left(2\pi l+\frac{2\pi u}{n_2}\right)+\cos\omega_3.$$

Let $\Delta\omega_2=2\pi/n_2$, $\omega_2=(2\pi/n_2)U$. Then

$$\sum_{r=0}^{n_1n_2-1}=\sum_{l=0}^{n_1-1}\sum_{u=0}^{n_2-1}=\sum_{l=0}^{n_1-1}\frac{n_2}{2\pi}\sum_{0}^{2\pi-2\pi/n_2}\Delta\omega_2\to\sum_{l=0}^{n_1-1}\frac{n_2}{2\pi}\int_0^{2\pi}d\omega_2.$$

Then $\cos(2\pi l+2\pi U/n_2)=\cos\omega_2$, and

$$\lambda_p/2=\cos(2\pi l/n_1)+\cos\omega_2+\cos\omega_3,$$

$$G_{jk}(f)\to\frac{n_2n_3}{(2\pi)^2N}\int_0^{2\pi}\int d\omega_2d\omega_3\sum_{l=0}^{n_1-1}f\left(\frac{\lambda_p}{2}\right)\times\exp\left[in_{jk}\left(\frac{2\pi l}{n_1}+\frac{\omega_2}{n_1}+\frac{\omega_3}{n_1n_2}\right)\right].$$

Now set $\Delta\omega_1=2\pi/n_1$, $\omega_1=2\pi l/n_1$. Hence,

$$G_{jk}(f)\to\frac{1}{(2\pi)^3}\int_0^{2\pi}\int\int d\omega_1d\omega_2d\omega_3f\left(\frac{\lambda}{2}\right)\times\exp\left[in_{jk}\left(\omega_1+\frac{\omega_2}{n_1}+\frac{\omega_3}{n_1n_2}\right)\right], \quad \text{(B18)}$$

with $\lambda/2=\cos\omega_1+\cos\omega_2+\cos\omega_3$.

The numbers j, k denote lattice sites, and these numbers will change as N changes. We must now use the one invariant property of the lattice site—its distance from a fixed origin. Let $j=p_1+q_1n_1+s_1n_1n_2$ as

defined in Appendix A, Eq. (A18). Then $x_1=(p_1-1)a$, $y_1=q_1a$, $z_1=s_1a$. Thus, we write

$$n_{jk}=A+B(p_1+q_1n_1+s_1n_1n_2)+C(p_2+q_2n_1+s_2n_1n_2),$$

or

$$n_{jk}=(A+Bp_1+Cp_2)+(Bq_1+Cq_2)n_1+(Bs_1+Cs_2)n_1n_2, \tag{B19}$$

where only n_1, n_2, n_3 change as N changes.

Consequently,

$$\begin{aligned}n_{jk}(\omega_1+\omega_2/n_1+\omega_3/n_1n_2)&=(A+Bp_1+Cp_2)\omega_1\\&+(Bq_1+Cq_2)n_1\omega_1+(Bs_1+Cs_2)n_1n_2\omega_1\\&+(Bq_1+Cq_2)\omega_2+(Bs_1+Cs_2)n_1n_2\omega_2\\&+(Bs_1+Cs_2)\omega_3.\end{aligned}$$

We now note that

$$\begin{aligned}(Bq_1+Cq_2)n_1\omega_1&=(Bq_1+Cq_2)2\pi l;\\(Bs_1+Cs_2)n_1n_2\omega_1&=(Bs_1+Cs_2)n_2 2\pi l;\\(Bs_1+Cs_2)n_1n_2\omega_2&=(Bs_1+Cs_2)n_1 2\pi U;\end{aligned}$$

that is, these quantities are integral multiples of 2π, and they can be neglected in the exponential. Thus,

$$\begin{aligned}n_{jk}\left(\omega_1+\frac{\omega_2}{n_1}+\frac{\omega_3}{n_1n_2}\right)&\simeq(A+Bp_1+Cp_2)\omega_1\\&+(Bq_1+Cq_2)\omega_2+(Bs_1+Cs_2)\omega_3\\&=\left[A+B\left(\frac{x_1}{a}+1\right)+C\left(\frac{x_2}{a}+1\right)\right]\omega_1\\&+\left[B\frac{y_1}{a}+C\frac{y_2}{a}\right]\omega_2+\left[B\frac{z_1}{a}+C\frac{z_2}{a}\right]\omega_3\equiv\theta.\end{aligned} \tag{B20}$$

Finally,

$$G_{jk}(f)=\frac{1}{(2\pi)^3}\int_0^{2\pi}\!\!\int\!\!\int d\omega_1d\omega_2d\omega_3 f(\lambda/2)\exp[i\theta], \tag{B21}$$

with θ defined in Eq. (B20).

If we assume that one of the spins is located at the origin, it is very easy to see that

$$\begin{aligned}\lim_{N\to\infty}N^{-1}\sum_{p=2}^{N}f(\lambda_p/2)\cos\frac{2\pi}{N}(j-k)(p-1)&\\=\frac{1}{(2\pi)^3}\int_0^{2\pi}\!\!\int\!\!\int d\omega_1d\omega_2d\omega_3 f(\lambda/2)&\\\times\cos\left(\frac{x_1\omega_1}{a}+\frac{y_1\omega_2}{a}+\frac{z_1\omega_3}{a}\right),&\end{aligned}$$

$$\begin{aligned}\lim_{N\to\infty}N^{-1}\sum_{p=2}^{N}f(\lambda_p/2)\sin\frac{2\pi}{N}(j+k-2)(p-1)&\\=\frac{1}{(2\pi)^3}\int_0^{2\pi}\!\!\int\!\!\int d\omega_1d\omega_2d\omega_3 f(\lambda/2)&\\\times\sin\left(\frac{x_1\omega_1}{a}+\frac{y_1\omega_2}{a}+\frac{z_1\omega_3}{a}\right),&\end{aligned}$$

where it is understood that x_1, y_1, z_1 are multiples of a.

Hence, we have

$$\begin{aligned}F_{jk}(f)=\frac{f(3)}{N}+\frac{1}{(2\pi)^3}\int_0^{2\pi}\!\!\int\!\!\int d\omega_1d\omega_2d\omega_3 f\left(\sum_{j=1}^{3}\cos\omega_j\right)&\\\times\cos\left(\frac{x_1\omega_1}{a}+\frac{y_1\omega_2}{a}+\frac{z_1\omega_3}{a}\right),&\end{aligned} \tag{B22}$$

because the integral having the sine in the integrand is zero since λ is an even function of ω_1, ω_2, ω_3.

APPENDIX C. THE EVALUATION OF THE PARTITION FUNCTION OF THE SPHERICAL MODEL

$$Q_N(S)=A_N^{-1}\int\cdots\int_{\sum_{j=1}^{N}\epsilon_j^2=N}d\epsilon_1\cdots d\epsilon_N\exp[K\sum_{i,j}{}'\epsilon_i\epsilon_j]. \tag{C1}$$

We may also write

$$\begin{aligned}Q_N(S)=A_N^{-1}\int_{-\infty}^{\infty}\cdots\int d\epsilon_1\cdots d\epsilon_N&\\\times\exp[K\sum_{i,j}{}'\epsilon_i\epsilon_j]\delta(N-\sum_{j=1}^{N}\epsilon_j^2),&\end{aligned}$$

or

$$\begin{aligned}Q_N(S)=A_N^{-1}\int_{-\infty}^{\infty}\cdots\int d\epsilon_1\cdots d\epsilon_N&\\\times\exp[K\sum_{i,j}{}'\epsilon_i\epsilon_j]\frac{1}{2\pi i}\int_{-i\infty}^{+i\infty}ds&\\\times\exp[s(N-\sum_{j=1}^{N}\epsilon_j^2)].&\end{aligned} \tag{C2}$$

For our next step, we wish to interchange the integration over the $\{\epsilon_j\}$ with the integration over s. This can not be done because the form $K\sum_{i,j}{}'\epsilon_i\epsilon_j$ is not negative definite. However, we may write

$$\begin{aligned}K\sum_{i,j}{}'\epsilon_i\epsilon_j&=N\alpha_0-N\alpha_0+K\sum_{i,j}{}'\epsilon_i\epsilon_j\\&=N\alpha_0-\alpha_0\sum_{j=1}^{N}\epsilon_j^2+K\sum_{i,j}{}'\epsilon_i\epsilon_j,\end{aligned}$$

because of the spherical condition. By choosing α_0 real,

positive, and sufficiently large, the form can be made negative definite. Then we have

$$Q_N(S)=\frac{A_N^{-1}}{2\pi i}\int_{\alpha_0-i\infty}^{\alpha_0+i\infty} ds\exp[Ns]\int_{-\infty}^{\infty}\cdots\int d\epsilon_1\cdots d\epsilon_N$$

$$\times\exp[-s\sum_{j=1}^{N}\epsilon_j^2+K\sum_{i,j}{}'\epsilon_i\epsilon_j], \quad \text{(C3)}$$

where $s=\alpha_0$ is a line to the right of the singularities of the integrand as a function of s.

Making use of the orthogonal transformation of the variables $\{\epsilon_j\}$ discussed in Appendix A, the integration over the $\{\epsilon_j\}$ may be written

$$\int_{-\infty}^{\infty}\cdots\int dy_1\cdots dy_N\exp[-s\sum_{j=1}^{N}y_j^2+K\sum_{j=1}^{N}\lambda_j y_j^2]$$

$$=\pi^{N/2}[\prod_{j=1}^{N}(s-K\lambda_j)]^{-\frac{1}{2}}$$

$$=\pi^{N/2}\exp[-\tfrac{1}{2}\sum_{j=1}^{N}\ln(s-K\lambda_j)], \quad \text{(C4)}$$

and

$$Q_N(S)=\frac{A_N^{-1}\pi^{N/2}}{2\pi i}\int_{\alpha_0-i\infty}^{\alpha_0+i\infty} ds$$

$$\times\exp[Ns-\tfrac{1}{2}\sum_{j=1}^{N}\ln(s-K\lambda_i)]. \quad \text{(C5)}$$

It is clear that we require $\alpha_0>K|\lambda_{\max}|$.

It is somewhat convenient to let $s=2Kz$. Then

$$Q_N(S)=A_N^{-1}\pi^{N/2}2Ke^{-\frac{1}{2}N\ln 2K}\frac{1}{2\pi i}\int_{z_0-i\infty}^{z_0+i\infty} dz$$

$$\times\exp[N2Kz-\tfrac{1}{2}\sum_{j=1}^{N}\ln(z-\tfrac{1}{2}\lambda_j)], \quad \text{(C6)}$$

where $z_0>\frac{1}{2}|\lambda_{\max}|=\frac{1}{2}\lambda_1$.

Since we are interested in the limit $N\to\infty$, let

$$f(z)=\lim_{N\to\infty}N^{-1}\sum_{j=0}^{N}\ln(z-\tfrac{1}{2}\lambda_j), \quad \text{(C7)}$$

$$g(z)=2Kz-\tfrac{1}{2}f(z).$$

Therefore,

$$Q_N(S)=A_N^{-1}\pi^{N/2}2Ke^{-\frac{1}{2}N\ln 2K}\frac{1}{2\pi i}$$

$$\times\int_{z_0-i\infty}^{z_0+i\infty} dz(z-\tfrac{1}{2}\lambda_1)^{-\frac{1}{2}}e^{+Ng(z)}. \quad \text{(C8)}$$

Evaluating the complex integral by the method of steepest descent,

$$Q_N(S)\cong\frac{2K\pi^{N/2}e^{-\frac{1}{2}N\ln 2K+Ng(z_s)}}{A_N(z_s-\frac{1}{2}\lambda_1)^{\frac{1}{2}}[2\pi N(\partial^2 g/\partial z^2)_{z_s}]^{\frac{1}{2}}}, \quad \text{(C9)}$$

where the saddle point z_s is determined by

$$(\partial g/\partial z)_{z_s}=0, \quad \text{and} \quad (\partial^2 g/\partial z^2)_{z_s}>0. \quad \text{(C10)}$$

If the saddle point exists, then, with

$$A_N=2\pi^{N/2}N^{\frac{1}{2}(N-1)}/\Gamma(N/2),$$

$$-\psi/kT=\lim_{N\to\infty}N^{-1}\ln Q_N(S)=-\tfrac{1}{2}-\tfrac{1}{2}\ln 4K+g(z_s),$$

or

$$-\psi/kT=-\tfrac{1}{2}-\tfrac{1}{2}\ln 4K+2Kz_s-\tfrac{1}{2}f(z_s). \quad \text{(C11)}$$

We now proceed to investigate the existence of a saddle point.

If we let n denote the dimensionality of the simple lattices, let us denote $f(z)$ by $f_n(z)$. From Appendix B we have

$$f_n(z)=\frac{1}{(2\pi)^n}\int_0^{2\pi}\cdots\int d\omega_1\cdots d\omega_n\ln[z-\sum_{j=1}^{n}\cos\omega_j]. \quad \text{(C12)}$$

Then

$$\frac{\partial g_n}{\partial z}=2K-\frac{1}{2}\frac{\partial f_n}{\partial z}=2K-\frac{1}{2}\cdot\frac{1}{(2\pi)^n}\int_0^{2\pi}\cdots\int d\omega_1\cdots d\omega_n$$

$$\times[z-\sum_{j=1}^{n}\cos\omega_j]^{-1}, \quad \text{(C13)}$$

and

$$\frac{\partial^2 g_n}{\partial z^2}=-\frac{1}{2}\frac{\partial^2 f_n}{\partial z^2}=\frac{1}{2}\cdot\frac{1}{(2\pi)^n}\int_0^{2\pi}\cdots\int d\omega_1\cdots d\omega_n$$

$$\times\left[z-\sum_{j=1}^{n}\cos\omega_j\right]^{-2}. \quad \text{(C14)}$$

The equation for the saddle point is

$$4K=\frac{1}{(2\pi)^n}\int_0^{2\pi}\cdots\int d\omega_1\cdots d\omega_n[z_s-\sum_{j=1}^{n}\cos\omega_j]^{-1}. \quad \text{(C15)}$$

The only possible value for z_s is real and positive. If z_s exists, then Eq. (C14) shows that $(\partial^2 g_n/\partial z^2)_{z_s}>0$.

If T is very large, K is very small. Therefore, z_s must be large, and in first approximation $4Kz_s=1$. As T decreases, z_s decreases.

Let us consider the one-dimensional lattice.

The saddle point equation is

$$4K=\frac{1}{2\pi}\int_0^{2\pi}d\omega_1[z_s-\cos\omega_1]^{-1}=(z_s^2-1)^{-\frac{1}{2}}, \quad \text{(C16)}$$

and

$$z_s=[1+(4K)^{-2}]^{\frac{1}{2}}.$$

Furthermore,

$$f_1(z_s)=\frac{1}{2\pi}\int_0^{2\pi} d\omega_1 \ln[z_s-\cos\omega_1] = \ln\tfrac{1}{2}[z_s+(z_s^2-1)^{\frac{1}{2}}]. \quad \text{(C17)}$$

Hence,

$$-\psi_1/kT=-\tfrac{1}{2}+\tfrac{1}{2}[1+(4K)^2]^{\frac{1}{2}} -\tfrac{1}{2}\ln\tfrac{1}{2}\{1+[1+(4K)^2]^{\frac{1}{2}}\}. \quad \text{(C18)}$$

In this case, as $T\to 0$, $K\to\infty$ so that $z_s\to 1$. The singularity of $f_1(z)$, $z=1$, is never reached. The steepest descent technique improves in accuracy insofar as $(\partial^2 g_1/\partial z^2)_{z_s}$ approaches ∞ as z_s approaches 1. The conclusion is that ψ_1 is a regular function of T in the range $0<T<\infty$.

Continuing with the two-dimensional lattice, the saddle point equation is

$$4K=\frac{1}{(2\pi)^2}\int_0^{2\pi}\int d\omega_1 d\omega_2[z_s-\cos\omega_1-\cos\omega_2]^{-1}. \quad \text{(C19)}$$

This equation may be written

$$4K=(2/\pi z_s)K(2/z_s), \quad \text{(C20)}$$

with $K(u)$ the complete elliptic integral

$$K(u)=\int_0^1 dt[(1-t^2)(1-u^2t^2)]^{-\frac{1}{2}}. \quad \text{(C21)}$$

As T decreases, z_s decreases and approaches the singularity $z=2$ of $f_2(z)$. In the neighborhood of $z=2$ we can use the expansion[6]

$$K\left(\frac{2}{z}\right)=-\frac{1}{2\pi}\sum_{n=0}^{\infty}\left\{\frac{\Gamma(\frac{1}{2}+n)}{n!}\right\}^2\left(1-\frac{4}{z^2}\right)^n \times\left\{\ln\left(1-\frac{4}{z^2}\right)-4\ln 2+\left(\frac{1}{1}+\frac{1}{2}+\cdots+\frac{1}{2n}\right)\right\}. \quad \text{(C22)}$$

Consequently, we see that $K(2/z_s)$ approaches infinity as $z_s\to 2$, and so z_s will exist for all allowed K. The singularity is not reached for a finite temperature. For this lattice, ψ_2 is again a regular function of T in the range $0<T<\infty$.

Finally, we take up the three-dimensional lattice for which the saddle point equation is

$$4K=\frac{1}{(2\pi)^3}\int_0^{2\pi}\int\int d\omega_1 d\omega_2 d\omega_3 \times[z_s-\cos\omega_1-\cos\omega_2-\cos\omega_3]^{-1}. \quad \text{(C23)}$$

[6] E. T. Whittaker and G. N. Watson, *Modern Analysis* (Cambridge University Press, London, England, 1927), fourth edition, p. 299.

The singularity of $f_3(z)$ occurs at $z=3$. As T decreases, z_s decreases and approaches the value 3. It is easy to show that for $z_s=3$ the integral converges. In fact, the integral has been evaluated by Watson[7] with the result that

$$4K_c\equiv\frac{1}{(2\pi)^3}\int_0^{2\pi}\int\int d\omega_1 d\omega_2 d\omega_3 \times[3-\cos\omega_1-\cos\omega_2-\cos\omega_3]^{-1}=0.50546. \quad \text{(C24)}$$

This means that a saddle point exists down to a critical temperature $T_c=(3.9568)J/k$. Therefore, we have:

$T>T_c(K<K_c)$

$$-\psi_3/kT=-\tfrac{1}{2}-(\tfrac{1}{2})\ln(4K)+2Kz_s-(\tfrac{1}{2})f_3(z_s), \quad \text{(C25)}$$

where z_s is defined through Eq. (C23).

Since the partition function is defined for all positive T, we must investigate the range $T<T_c$. This requires consideration of the complex integral in the neighborhood of the branch point, $z=3$, of $f_3(z)$. The integral to consider is

$$\frac{1}{2\pi i}\int_{z_0-i\infty}^{z_0+i\infty} dz(z-3)^{-\frac{1}{2}}e^{+Ng_3(z)}. \quad \text{(C26)}$$

If we cut the z-plane from $z=3$ to $z=-\infty$ along the real axis, then the integrand is analytic in the cut plane. Since $f_3(z)$ is analytic in the cut plane, we shall consider the behavior of df_3/dz in the neighborhood of $z=3$ and obtain $f_3(z)$ by integration. Now

$$\frac{df_3}{dz}=\frac{1}{(2\pi)^3}\int_0^{2\pi}\int\int d\omega_1 d\omega_2 d\omega_3 \times[z-\cos\omega_1-\cos\omega_2-\cos\omega_3]^{-1} =\frac{1}{\pi^2}\int_0^{\pi} d\omega_3 \frac{2}{q}K\left(\frac{2}{q}\right), \quad \text{(C27)}$$

where $q=z-\cos\omega_3$. Using the expansion for $K(2/q)$ given in Eq. (C22), it is found by analytic continuation that

$$df_3/dz=4K_c-(2\pi^2)^{-1}(z-3)^{\frac{1}{2}}+O(z-3), \quad \text{(C28)}$$

and, therefore,

$$f_3(z)=f_3(3)+4K_c(z-3) -(2^{\frac{1}{2}}/3\pi)(z-3)^{\frac{1}{2}}+O([z-3]^2). \quad \text{(C29)}$$

We then have

$$g_3(z)=g_3(3)+2(K-K_c)(z-3) +(2^{-\frac{1}{2}}/3\pi)(z-3)^{\frac{1}{2}}+O([z-3]^2). \quad \text{(C30)}$$

Consequently, the integrand always has a saddle point

[7] G. N. Watson, Quart. J. Math. **10**, 266 (1939).

at $z=3$ if $K>K_c$ ($T<T_c$).[8] The path of steepest descent has a cusp at $z=3$ and the path is shown in Fig. 3.

Evaluating the complex integral, we find that

$$\frac{1}{2\pi i}\int_{\omega-i\infty}^{\omega+i\infty} dz(z-3)^{-\frac{1}{2}}e^{+N\psi_3(z)} \cong[N2\pi(K-K_c)]^{-\frac{1}{2}}e^{+N\psi_3(z)}. \quad \text{(C31)}$$

Hence, for $T<T_c(K>K_c)$

$$-\psi_3/kT=-\tfrac{1}{2}-(\tfrac{1}{2})\ln(4K)+6K-(\tfrac{1}{2})f_3(3). \quad \text{(C32)}$$

The discontinuity that is involved can also be seen from the following consideration. Dropping the subscript s, the saddle point is the solution of the equation

$$4K=df_3(z)/dz,$$

which defines z as a function of K. From this equation, it follows that for $T>T_c$,

$$\frac{dz}{dK}=4\Big/\frac{d^2f_3}{dz^2}, \quad \text{(C33)}$$

and

$$\frac{d^2z}{dK^2}=-\left(\frac{dz}{dK}\right)^2\frac{d^3f_3}{dz^3}\Big/\frac{d^2f_3}{dz^2}. \quad \text{(C34)}$$

[8] The mathematical reason for the transition in the three-dimensional lattice is the "sticking" of the saddle point. This same phenomenon has been found by Kramers. [H. A. Kramers, Commun. Kamerlingh Onnes Lab., Leiden, Suppl. No. 83 (1936).]

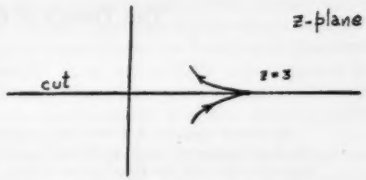

FIG. 3. Path of steepest descent for $T<T_c$.

In the neighborhood of the branch point $z=3$, we have from Eq. (C29)

$$\begin{aligned} d^2f_3/dz^2&\simeq-(2^{-\frac{1}{2}}/\pi)(z-3)^{-\frac{1}{2}};\\ d^3f_3/dz^3&\simeq(2^{-5/2}/\pi)(z-3)^{-1}. \end{aligned} \quad \text{(C35)}$$

Consequently,

$$\lim_{z\to3}\frac{dz}{dK}=\lim_{z\to3}\{-\pi2^{7/2}(z-3)^{\frac{1}{2}}\}=0,$$

and

$$\lim_{z\to3}\frac{d^2z}{dK^2}=64\pi^2.$$

On the other hand, for $T<T_c$, $z=$constant, so that $dz/dK=d^2z/dK^2=0$. The discontinuity occurs in the second derivative, and this causes a discontinuity in slope of the specific heat *vs* temperature curve at T_c.

The Theory of the Impulse Approximation

SAUL T. EPSTEIN
New York, New York
(Received February 4, 1952)

An integral equation is derived for the scattering of a neutron by a bound proton. This equation has the impulse approximation as the first approximation to its solution. The connection between the impulse approximation and the Fermi approximation is discussed and clarified.

I. INTRODUCTION

RECENTLY, Chew[1] has proposed a method, the impulse approximation, for treating problems in which a free particle collides with bound particles. An essential feature of the method is the neglect of binding forces during the collision. However, this simplification alone is, in general, not enough to enable one to solve the problem. If there are N bound scatterers, then one has reduced the problem to an $N+1$ body problem with N interactions, and this reduced problem is itself not susceptible to exact treatment unless $N=1$. In this paper we will not be concerned with the further approximations which are necessary if $N\neq 1$, but will confine ourselves to $N=1$. For this case we will derive the impulse approximation as a well-defined first approximation to the exact solution and will have available an iteration scheme for improving this approximation.

In particular we shall consider a system consisting of a neutron and a proton. The neutron-proton potential will be denoted by V, and the proton will be assumed to be bound by a potential U due to a fixed center of force.[2] The form into which we shall put the solution to this problem will be dictated by our desire to describe the scattering of the neutron by the bound proton in terms of the free neutron-proton scattering. Guided by this we shall in the next section relate the solution of our problem to the solution of a certain integral equation. The impulse approximation will then appear naturally as a first approximation to the solution of this equation. In the final section the connection between the impulse approximation and the Fermi approximation is discussed and clarified.

II. DERIVATION OF THE INTEGRAL EQUATION

Let $\Psi(E)$ be the wave function describing the scattering of the neutron by the bound proton. E is the total energy. $\Psi(E)$ satisfies an integral equation which we can write symbolically[3] as

$$\Psi(E)=\Phi_0(E)+(E^+-T-U)^{-1}V\Psi(E). \tag{1}$$

Here T is the kinetic energy operator and $\Phi_0(E)$ is the incident wave. $\Phi_0(E)$ is therefore the product of a plane wave for the neutron and a bound state wave function for the proton. To compute the differential scattering cross section one needs[3] the matrix element

$$W=(\Phi_F(E),\, V\Psi(E)), \tag{2}$$

where $\Phi_F(E)$ is the wave function of the final state.

In order to relate the bound scattering to the free scattering it seems natural to write[4]

$$\Psi(E)=\textstyle\sum_{E'}\psi(E')\alpha(E',E), \tag{3}$$

where the $\alpha(E',E)$ are to be determined and where the $\psi(E')$ describe free neutron-proton scattering at an energy E'.[5] $\psi(E')$ thus satisfies the integral equation

$$\psi(E')=\varphi(E')+(E'^+-T)^{-1}V\psi(E'), \tag{4}$$

where, of course, $\varphi(E')$ is simply the product of two plane waves, one for the neutron and one for the proton. To find the integral equation which determines $\alpha(E',E)$ we insert the expansion (3) into the second term on the right-hand side of (1). We then get

$$\Psi(E)=\Phi_0(E)+\textstyle\sum_{E'}(E^+-T-U)^{-1}V\psi(E')\alpha(E',E)$$

which we rewrite as

$$\Psi(E)=\Phi_0(E)+\textstyle\sum_{E'}(E'^+-T)^{-1}V\psi(E')\alpha(E',E)$$
$$+\textstyle\sum_{E'}[(E^+-T-U)^{-1}-(E'^+-T)^{-1}]V\psi(E')\alpha(E',E).$$

But from (4) we can write this as

$$\Psi(E)=\Phi_0(E)+\textstyle\sum_{E'}(\psi(E')-\varphi(E'))\alpha(E',E)$$
$$+\textstyle\sum_{E'}[(E^+-T-U)^{-1}-(E'^+-T)^{-1}]V\psi(E')\alpha(E',E),$$

which from (3) is just

$$\textstyle\sum_{E'}\varphi(E')\alpha(E',E)=\Phi_0(E)+\sum_{E'}[(E^+-T-U)^{-1}$$
$$-(E'^+-T)^{-1}]V\psi(E')\alpha(E',E).$$

Finally, we derive the integral equation[6]

$$\alpha(E',E)=\alpha_i(E',E)+\textstyle\sum_{E''}\mathcal{G}(E,E',E'')\alpha(E'',E). \tag{5}$$

Here

$$\alpha_i(E',E)=(\varphi(E'),\Phi_0(E)), \tag{6}$$

[1] G. F. Chew, Phys. Rev. **80**, 196 (1950); G. F. Chew and G. C. Wick, Phys. Rev. **85**, 636 (1952).
[2] This same problem is discussed in the papers of reference 1.
[3] B. A. Lippmann and J. Schwinger, Phys. Rev. **79**, 469 (1950).
[4] By the symbol $\Sigma_{E'}$ we mean integration over the two momenta involved in $\psi(E')$.
[5] For simplicity of presentation we have omitted any "pick-up" terms [M. Goldberger and G. F. Chew, Phys. Rev. **77**, 470 (1950)].
[6] Had we included "pick-up" terms this one integral equation would be replaced by two integral equations coupling the simple scattering amplitudes with the "pick-up" amplitudes.

represents a first approximation to $\alpha(E', E)$ which we may hope to improve by iteration. When inserted into (2) and (3), $\alpha_i(E', E)$ gives just the impulse approximation to W. The kernel of our integral equation is given by

$$\mathcal{G}(E, E', E'') = (\varphi(E'), [(E^+ - T - U)^{-1} - (E''^+ - T)^{-1}] V\psi(E'')), \quad (7)$$

and, in principle, is a known function. $(E''^+ - T)^{-1}$ is, of course, just the familiar Green's function for two free particles while $(E^+ - T - U)^{-1}$ is the Green's function for a free neutron and a bound proton. Both are readily expressible in terms of one-particle eigenfunctions.

In connection with the solution of (5) by iteration, it is of interest to note that this corresponds to the solution of (1) by successive impulse approximations. That is, let us write

$$\Psi(E) = \sum_{E'} \psi(E')(\varphi(E'), \Phi_0(E)) + \Psi_1(E),$$

then in a manner analogous to our derivation of (5) one finds that $\Psi_1(E)$ satisfies

$$\Psi_1(E) = \Phi_1(E) + (E^+ - T - U)^{-1} V \Psi_1(E),$$

where

$$\Phi_1(E) = \sum_{E'} [(E^+ - T - U)^{-1} - (E'^+ - T)^{-1}] V\psi(E')(\varphi(E'), \Phi_0(E)).$$

Now put

$$\Psi_1(E) = \sum_{E'} \psi(E')(\varphi(E'), \Phi_1(E)) + \Psi_2(E),$$

and one finds

$$\Psi_2(E) = \Phi_2(E) + (E^+ - T - U)^{-1} V \Psi_2(E).$$

Continuing the process one finds after n steps

$$\Psi(E) = \sum_{E'} \psi(E') \alpha^{(n)}(E', E) + \Psi_{n+1}(E),$$
$$\Psi_{n+1}(E) = \Phi_{n+1}(E) + (E^+ - T - U)^{-1} V \Psi_{n+1}(E),$$

and one readily verifies that, not unexpectedly, $\alpha^{(n)}(E', E)$ is identical with the result of n iterations of (5).

III. CONNECTION WITH THE FERMI APPROXIMATION

Chew has shown that the impulse approximation yields a good approximation in the problem of the scattering of slow neutrons by protons bound in molecules. However, the only proof of this which has been offered is simply the demonstration that in the slow neutron limit the impulse approximation to W becomes identical with the Fermi approximation which is known[7] to be an excellent approximation in such problems. No real reason has been given as to why the impulse approximation is such a good approximation for this case.

By use of the integral equation (5)[8] we are now able to clarify this situation. Indeed (5) is very closely related to the integral equation used by Lippmann and Schwinger[3] in their discussion of slow neutron scattering by molecules; their equation in turn being a generalization of the equation used by Breit.[7] Following Lippmann and Schwinger, we will now make it plausible that the term in (5) which involves $\mathcal{G}$ will make only a small contribution to $\alpha(E', E)$ for this problem. To do this we note that (i) $\mathcal{G}$, because it has V as a factor, is concerned only with happenings during the collision; (ii) the significant values of E'' differ from E by something of the order of the proton's binding energy; and (iii) the proton's binding energy, the potential energy of the proton in the molecule, and E are all very small when compared with V. This means that during the collision the kinetic energy of the neutron-proton system will become so large that one may very nearly replace each Green's function in $\mathcal{G}$ by T^{-1}, thus making the contribution of the $\mathcal{G}$ term essentially zero.

This completes our discussion of the impulse approximation. The one major point which we have not considered is the problem of determining the error in the impulse approximation at high energies. This problem has been discussed already by Wick and Chew, and at this time we shall remark only that the expression on which they base their estimate of the error is easily shown to be identical with the result of a first iteration of (5).

I would especially like to thank Professor G. F. Chew of the University of Illinois for valuable correspondence on the subject of the impulse approximation. It is a pleasure also to acknowledge helpful discussions with Professor N. M. Kroll and Professor R. Serber of Columbia University, and Professor G. J. Yevick of the Stevens Institute of Technology.

[7] G. Breit, Phys. Rev. **71**, 215 (1947).

[8] Quite apart from the question of the validity of the impulse approximation, the probability of "pick-up" is obviously negligible for molecular problems so that (5) provides a suitable basis for the discussion of the applicability of the impulse approximation to these problems.

Charged Photomesons from Various Nuclei*

RAPHAEL M. LITTAUER AND DARCY WALKER†
Cornell University, Ithaca, New York
(Received January 31, 1952)

The yield of π^- and π^+ photomesons from a wide range of nuclei has been measured. The irradiating photon flux was 310-Mev bremsstrahlung and the mesons were selected magnetically at 135° with an energy of 65±15 Mev. The experimental results include the following features: (1) the π^-/π^+ ratio from deuterium is close to unity; (2) the charged meson cross sections for deuterium are close to that for hydrogen; (3) the total charged meson cross section per nucleus varies as $A^{\frac{1}{3}}$; (4) the π^-/π^+ ratios show a remarkable correlation with the masses of the isobars adjacent in Z to the target nucleus; (5) the π^-/π^+ ratio from beryllium is energy sensitive. The implications of these results are discussed.

I. INTRODUCTION

THE production of charged π-mesons by high energy gamma-rays incident on nuclei was first observed by McMillan, Peterson and White,[1] and has since been studied by a number of workers. The elementary particle interactions which presumably give rise to the production can be written

$$\gamma+p\rightarrow n+\pi^+ \quad (1)$$

and

$$\gamma+n\rightarrow p+\pi^-. \quad (2)$$

A complete experimental investigation of these reactions should be of great interest in view of their bearing on the nature of the coupling of the π-meson, the nucleons, and the electromagnetic field. In particular, it is of interest whether the coupling with the electromagnetic field is via the electric interaction only, or whether the magnetic moment of the nucleons plays an important role.

Reaction (1) can of course be studied directly by irradiating a hydrogenous material, or preferably liquid or compressed hydrogen, with high energy gamma-rays; a fairly detailed study of this case has already been made.[2,3] The complementary reaction (2) is not as easily accessible, since free neutrons are not available in sufficient density. Now one of the chief points of interest lies in the comparison between reactions (1) and (2), since this will give some information about the importance of the coupling with the nucleon magnetic moment. Thus, in the absence of a direct comparison between (1) and (2), one must be content with an investigation of the relative production rates of negative and positive mesons from more complex nuclei. In this case, however, factors other than the elementary interactions will enter into consideration. Most important among them are the following: (a) the nucleons in a complex nucleus are not at rest; (b) the proximity of a nucleon may affect the meson cloud surrounding another nucleon and thus alter its interaction with the gamma-ray; (c) the presence of the other nucleons will limit the number of states available to the recoiling nucleon after the interaction, and will affect the energy balance of the reaction; and (d) mesons produced in the interior of the nucleus may be reabsorbed before they can escape.

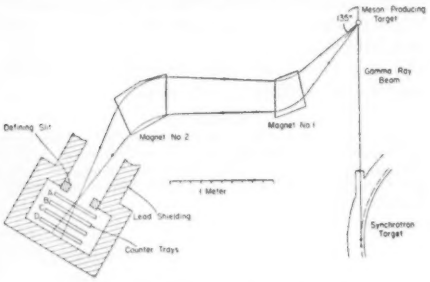

FIG. 1. Diagrammatic view of apparatus.

These effects should be least important in the case of the deuteron, which is a very loosely bound structure. Thus, the photoproduction of mesons from deuterium is the nearest approach we have for a comparison between reactions (1) and (2). Even here, however, the effects mentioned above may not be negligible.

Experimentally, the most easily accessible quantity is the relative yield of negative and positive mesons from nuclei considerably heavier than the deuteron. (Alone, deuterium must be used in the form of either compressed gas or low temperature targets, while deuterium in a chemical compound necessitates a subtraction method.) Accordingly, most of the early measurements were made with carbon as target material.

The mesons may be detected in a photographic emulsion, or some form of electronic counting technique may be employed. In the former case, uncertainty in the relative detection efficiencies for positive and negative mesons may arise from the fact that different criteria are used for the identification of the π^- and π^+ mesons. This point is well illustrated by the wide discrepancies among the first estimates of the π^-/π^+

* Work supported by the ONR.
† Commonwealth Fund Fellow, now at Birmingham University, Birmingham, England.
[1] McMillan, Peterson, and White, Science **110**, 579 (1949).
[2] J. Steinberger and A. S. Bishop, Phys. Rev. **78**, 494 (1950).
[3] Bishop, Steinberger, and Cook, Phys. Rev. **80**, 291 (1950).

ratio from carbon. The emulsion technique has now been much improved, however.

The electronic counting methods usually require a rather complex arrangement for the identification of a particle as a meson; frequently magnetic fields are employed as an aid for this purpose, the magnetic field at the same time determining the sign of the charge. In the case of the positive meson, which decays at rest before it undergoes nuclear interaction, the $\pi^+ \rightarrow \mu^+ \rightarrow \beta^+$ decay can be utilized to give an unambiguous identification without the use of a magnetic field. Unfortunately, no such unique process is available in the case of the negative meson.

The present work was undertaken when relatively little was yet known in this field. The estimates of the π^-/π^+ ratio from carbon had converged towards the value of about 1.3; the energy spectrum and angular distribution of π^+ mesons from hydrogen had been measured, and a measurement of the relative yield of π^+ mesons from various elements had been made.[4] The aim of the present investigation was to make a preliminary survey of the relative yields of mesons of both signs from a wide range of nuclei, using essentially the same method of detection for both π^- and π^+ mesons. The apparatus used for the work was to a large extent available from a previous experiment;[5] it consisted of a pair of electromagnets so arranged that mesons from a target bombarded by high energy bremsstrahlung from the Cornell 310-Mev electron synchrotron could be focused into a region relatively free from other radiations. The previous experiments with a cloud chamber had already established the fact that the flux of mesons from the magnets was almost entirely uncontaminated by other particles; it therefore seemed desirable to use the apparatus in its existing form for a preliminary survey, accepting its limitations for the time being and reserving a more detailed inquiry for the time when the general character of the results should become apparent.

During the course of the work a number of surprising features were observed, notably the wide variation of the π^-/π^+ ratio from nucleus to nucleus. The investigation was thus extended to include as large a number of nuclei as possible, in the hope of finding regularities which would permit some conclusions to be drawn. It became clear that, beyond some general features, a detailed interpretation of the results would require far greater knowledge of the effects concerned than is at present available. Thus the work has evolved into a compromise between the generality of a first survey and the particular conditions of experiment as dictated by the existing apparatus.

II. EXPERIMENTAL METHOD

The experimental arrangement is shown diagrammatically in Fig. 1. The gamma-rays used to bombard the targets were produced in the Cornell 310-Mev electron synchrotron. The circulating electron beam of this machine strikes an internal target, consisting of a 0.040-inch diameter tungsten wire, and produces a sharply collimated beam of bremsstrahlung which differs only slightly in energy distribution from the theoretically predicted distributions for infinitely thin targets. The maximum energy is 315±3 Mev.[6] The gamma-flux is delivered in 30 bursts per second, the duration of the bursts being adjustable between a few microseconds and about 2 milliseconds.

The target materials for photomeson production were placed, for the most part, in thin-walled glass containers. These consisted of the envelopes of 60-watt electric light bulbs onto which a thin-walled filling tube, 1 inch in diameter, had been sealed. These bulbs have been found to be very uniform in diameter (6 cm) and wall thickness (0.5 mm).

The density of the fillings was adjusted, as far as possible, so that the mean energy loss (~5 Mev) of the escaping mesons was roughly the same for all the targets. This was arranged by choosing the mode of subdivision and packing of the material; the standard energy loss was that in the water target. In the case of some materials, however, it was found impossible to obtain the correct stopping power. The details for all the targets will be found in Table I.

TABLE I. Details of photomeson targets.

Element	A	Isotopic abundance %	Target material used	Weight of target (grams)	Notes
H	1	99.98	H_2O	118.7+120.6	
D	2	a	D_2O	132.4+132.6	f, g
			C	118.7+120.9	
C	12	98.9	$CH_{1.96}$ [b]	105.8+106.0	
O	16	99.8	$CD_{1.72}$ [c]	57.54	f, h
Li	7	92.5	Li	67.7	i, j
Be	9	100	Be	111.7	k, l
F	19	100	$(CF_2)_n$ [d]	127.8+126.3	f, g
Al	27	100	Al	138.1	
P	31	100	P	137.2	
S	32	95.1	S	156.7	
K	39	93.4	K [e]	100.9	i
Ca	40	97.0	CaF_2	128.9+127.8	f, g
Mn	55	100	MnO_2	228.0	f, k
Co	59	100	Co	216.4	h, k
As	75	100	As_2O_3	284.6	f, k
I	127	100	I	201.9	
Bi	209	100	Bi	236.3	

[a] D_2O purity >99.8 percent; $CD_{1.72}$ deuterated >96 percent.
[b] Commercial white petrolatum, combustion analysis.
[c] >96 percent deuterated oil, chemical analysis by combustion.
[d] Teflon.
[e] Fused under kerosene.
[f] Subtraction method.
[g] Two-bulb target (see text).
[h] Smaller glass bulb.
[i] Stopping power too low.
[j] No glass envelope, thin coating of paraffin wax.
[k] Stopping power too high.
[l] No glass envelope.

[4] R. F. Mozley, Phys. Rev. **80**, 493 (1950).
[5] Camac, Corson, Littauer, Shapiro, Silverman, Wilson, and Woodward, Phys. Rev. **82**, 745 (1951).
[6] J. W. DeWire and L. A. Beach, Phys. Rev. **83**, 476 (1951). The figure 315 Mev gives the maximum photon energy if the circulating electron beam strikes the internal target at exactly peak magnetic field, a condition which was not quite realized during the calibrating experiments, nor during the present experiment.

For the investigation we selected mono-isotopic elements, or those in which one isotope predominates overwhelmingly. It was also required that the elemental form, or a simple compound suitable for subtraction measurements, be readily available in a sufficient degree of chemical purity.

The particles emerging from the target were analyzed as to momentum and charge by an arrangement of two magnets which has been described previously.[7] This arrangement provides rather crude refocusing of the selected mesons in both horizontal and vertical planes; the aberration is largely due to the presence of fringe fields in the wide pole gaps which it was found necessary to employ. Owing to these field inhomogeneities, the energy of the mesons leaving the magnets was not very well defined. From absorption measurements and an investigation with a stretched current-carrying wire we estimate the energy to cover the range from 45–75 Mev, which corresponds to an energy of 65 ± 15 Mev for the mesons, at creation.[8]

It is possible, of course, to vary the energy of the mesons accepted by changing the field settings of the two magnets; unfortunately, however, the detection efficiency will vary in an unknown manner at the same time, owing to the fact that the fringing fields and focusing properties will not remain constant. Moreover, the coincidence array used to detect the mesons imposes a lower limit on the energy that can be used without loss of geometrical efficiency, on account of the fact that the cylindrical walls of the counters present a non-uniform absorber to the mesons. For these reasons it is not possible to make a meaningful measurement of the energy spectrum of the mesons in this way. The mean energy of mesons accepted was lowered on one occasion in order to find out how the π^-/π^+ ratios varied (see Sec. IV); no significance can however be attached to the relative counting rates for the two magnet settings.

Fortunately it appears from the above experiment as well as from other measurements, since published, that the π^-/π^+ ratios do not depend critically on the energy, at least in the case of carbon,[9] beryllium,[10] and deuterium.[11] This means that the energy spread in the present work will not prove too great an obstacle to its interpretation. To reduce the energy spread significantly, it would have been necessary to sacrifice geometrical efficiency and thus statistical accuracy in a reasonable time of counting. It seemed preferable to obtain better statistics under less well defined conditions, since it was possible to maintain these conditions accurately constant for relative measurements.

The mesons emerging from the magnets were detected by coincidence in three trays of Geiger counters, each consisting of four 1 in.$\times$18 in. brass counters with 0.030 in. brass walls. The four counters were slightly staggered and so arranged that there were no insensitive gaps between them. The fact that the counters had cylindrical walls meant that the amount of absorber in the path of a particle varied with the exact position of its trajectory. Mesons of energy above about 40 Mev, however, could penetrate over essentially the whole area of the trays, so that the geometrical efficiency above this energy approached unity. The sensitive length of the trays was restricted to 10 in. by lead stops which were kept in a fixed position relative to the magnet system. The counters and magnet gaps were enclosed in a lead shield of about 9 in. wall thickness.

As an over-all check on the method of detecting mesons, the triple coincidence counting rate was measured as a function of (a) target position both along and perpendicular to the gamma-ray beam; (b) magnet currents; (c) Geiger counter overvoltages; (d) absorbers placed between the trays of counters. Satisfactory plateaux in the counting rate could be obtained as a function of each of these variables. This, together with the high degree of internal consistency of the various runs, indicates a high "resetting accuracy" in the experiment. Since subtractions were involved in most of the determinations, this fact is very important.

A previous investigation with a cloud chamber[5] had shown that the contamination of the mexon flux by other particles, especially by electrons, did not exceed 2 percent. The time of flight of the mesons through the system is about one-half mean life, so that some π-mesons decay into μ-mesons before they reach the detector. In most cases, however, the decay will throw the particles out of the region of acceptance of the magnets. For the interpretation of the present experiment, we have assumed that the decay characteristics of positive and negative π-mesons are identical.[12]

Although the magnets and counters were heavily shielded, a certain background single counting rate could not be eliminated. This background is important because of the dead-time losses it produces in the Geiger counters. With the best shielding conveniently possible, each Geiger tray was fired about once in three bursts of the synchrotron. A careful examination disclosed that about 70 percent of the background counts occurred after the time of the gamma-ray burst, with delays ranging up to several hundred microseconds.[13] By working with a short gamma-ray burst, and by suitable electronic gating, it was thus possible to reduce the background counting rate to about one count in ten bursts. Working with a short gamma-burst has the additional advantage that the exact dead-time of the counters becomes unimportant: once a counter is fired,

[7] M. Camac, Rev. Sci. Instr. **22**, 197 (1951).

[8] The mean energy of "about 50 Mev" quoted in the earlier reports was in error owing to an inaccurate analysis of the absorption curves.

[9] Peterson, Gilbert, and White, Phys. Rev. **81**, 1003 (1951).

[10] H. A. Medicus, Phys. Rev. **83**, 662 (1951).

[11] R. S. White, Ph.D. thesis, University of California, 1951.

[12] See the work of C. E. Wiegand, Phys. Rev. **83**, 1085 (1951); and of Lederman, Booth, Byfield, and Kessler, Phys. Rev. **83**, 685 (1951).

[13] Presumably this delayed background is due to capture gamma-rays from neutrons, whose slowing-down time is of the right order of magnitude.

it remains dead for the whole of the burst, but certainly recovers for the next burst. The dead-time losses are still relatively high in this mode of operation, however: about 5 percent for each tray, or 15 percent of the triple coincidence rate (the background counts in the trays were uncorrelated).

An experimental method of measuring over-all losses in one representative tray was devised as follows: behind the three trays A, B, and C used for counting the mesons, a fourth tray D was placed (see Fig. 1). Together with the triple rate ABC, the two rates $ABCD$ and ACD were also measured. Their difference gives the loss in tray B from all causes. Since the losses in A, B, and C are identical (the background rates are the same, the trays are physically similar) it is then possible to deduce the over-all loss in triple coincidences for the particular run and make the necessary correction.

The random triple coincidence rate was negligible. Background coincidences due to mesons from the glass envelope of the target and possibly due to penetrating particles from other sources in the system were determined by running with an unfilled glass bulb, and subtracted out. This background was usually about 10 percent of the total coincidence rate, and was not the same for positive and negative magnet settings. It therefore had to be determined separately for the two polarities. Target and background runs, the two polarities, and various target materials used in the subtraction measurements were alternated throughout the course of the experiment to avoid the danger of any unknown, and possibly progressive, systematic errors. The internal consistency of the various runs was as good as their statistical accuracy.

The gamma-ray flux was standardized by means of a thin ionization chamber placed in front of the meson target, and a current integrator. In the case of the heavy target materials, correction had to be made for the absorption of the gamma-rays in traversing the target: here it was assumed that the daughter products of a gamma ray, once it had initiated a shower, were degraded in energy sufficiently so that they gave no further contribution to the meson production in the energy range accepted.

The nuclear absorption of mesons leaving the target was very small, and nearly equal for all the materials used. No correction has thus been made for this effect.

Owing to a number of uncertain factors, such as the effective solid angle of acceptance of the magnet system and the effective energy interval of the mesons, no attempt has been made here to obtain yields in absolute value. Instead, all yields are given relative to that of π^+ mesons from hydrogen.

III. RESULTS[14]

Table I gives a list of the various targets which were used in the investigation. The measured counting rates from these targets were reduced as follows: each run was corrected for the measured dead-time loss (~15 percent), and then all runs from a given target and with a given magnet polarity were pooled. The result was then corrected by subtracting the empty bulb background count (~10 percent) and by allowing for the absorption of the gamma-rays in traversing the targets (usually 1–3 percent, but reaching 30 percent for Bi). In the case of compound targets, the appropriate subtractions were then carried out in order to obtain the yield per nucleus for each of the elements. For deuterium, two independent methods were employed, one involving the direct difference between a deuterated hydrocarbon and a carbon target, the other a chain of subtractions between water, heavy water, a hydrocarbon, and carbon. The former, despite its merit of directness, contributed very little to the statistical information on account of the small quantity of deuterated oil (60 cc) available. The use of heavy water allowed a more accurate determination; for this purpose, two bulbs were filled with each of the target materials and irradiated simultaneously, one behind the other. Since the magnet system accepted particles from a wide region, this procedure almost doubled the counting rates. A separate check was made to determine the exact ratio of the counting efficiencies with one bulb and with two bulbs, and it was also verified that the measured π^-/π^+ ratios remained unaffected by the modification.

A further advantage of the method using heavy water is that the exact composition of the targets is known; in the case of the deuterated oil,[15] the chemical composition was determined by means of a combustion analysis, and the results of this were slightly uncertain owing to the presence of a volatile component. Within the statistical accuracy achieved, the two methods gave the same result, and in what follows a suitably weighted mean has been taken as the best estimate.

In Table II we have collected all the results. The yields have been normalized arbitrarily in such a

TABLE II. Yields Y of π^- and π^+ mesons per nucleus. Meson energy = 65±15 Mev, angle of emission = 135°. Maximum photon energy = 310±10 Mev.

Element	A	Z	$Y(\pi^+)$	$Y(\pi^-)$	$Y(\pi^+)+Y(\pi^-)$	$Y(\pi^-)/Y(\pi^+)$
H	1	1	1.00 ±0.05	0.04 ±0.05	1.04 ±0.07	–
D	2	1	0.87 ±0.07	1.04 ±0.07	1.91 ±0.10	1.19 ±0.12
Li	7	3	2.25 ±0.14	4.65 ±0.28	6.90 ±0.31	2.06 ±0.18
Be	9	4	2.39 ±0.01	5.39 ±0.02	7.78 ±0.03	2.25 ±0.11
C	12	6	3.54 ±0.05	3.77 ±0.06	7.31 ±0.08	1.06 ±0.02
O	16	8	4.08 ±0.13	4.25 ±0.13	8.33 ±0.18	1.04 ±0.05
F	19	9	4.26 ±0.13	6.04 ±0.14	10.3 ±0.18	1.42 ±0.05
Al	27	13	6.01 ±0.20	7.18 ±0.21	13.2 ±0.29	1.20 ±0.05
P	31	15	7.25 ±0.28	7.54 ±0.28	14.8 ±0.4	1.04 ±0.06
S	32	16	7.76 ±0.18	6.63 ±0.16	14.4 ±0.24	0.85 ±0.03
K	39	19	9.37 ±0.42	9.58 ±0.42	19.0 ±0.6	1.02 ±0.1
Ca	40	20	9.01 ±0.46	5.20 ±0.46	14.2 ±0.7	0.58 ±0.06
Mn	55	25	9.08 ±0.56	10.9 ±0.7	20.0 ±0.9	1.20 ±0.11
Co	59	27	9.79 ±0.35	13.1 ±0.35	22.9 ±0.5	1.34 ±0.07
As	75	33	9.72 ±0.49	13.9 ±0.7	23.6 ±0.9	1.43 ±0.1
I	127	53	15.8 ±0.7	23.2 ±0.8	39.0 ±1.1	1.46 ±0.08
Bi	209	83	19.2 ±1.4	25.3 ±1.4	44.5 ±2.0	1.32 ±0.12

[14] Some of the results of this work have already been published [R. M. Littauer and D. Walker, Phys. Rev. **83**, 206 (1951); **82**, 746 (1951)] and are here included for completeness.

[15] This oil is a residue in the manufacture of deuterated paraffin, and is thus presumably deuterated to the same extent as the final product, the quoted figure for which was >96 percent.

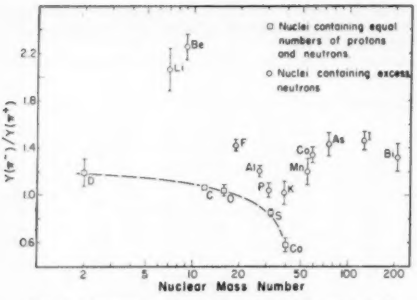

FIG. 2. Measured π^-/π^+ ratios. Errors are statistical standard deviations.

manner that the best estimate for the yield of π^+ mesons from hydrogen is 1.00. The errors associated with each measurement are kept separate, and are not compounded during the normalization. The quoted errors are statistical standard deviations in all cases. From internal consistency and a number of other checks (see Sec. II) it is believed that any systematic errors are smaller than the smallest statistical deviations quoted.

Table II contains, in addition to the relative yields of negative and positive mesons from the various elements, the π^-/π^+ ratios computed from these yields, and the total yields of charged mesons, independent of sign.

The π^-/π^+ ratios are exhibited also in Fig. 2. The dashed curve in this figure connects the points for the nuclei containing equal numbers of protons and neutrons, ranging from deuterium to calcium. The remaining nuclei contain excess neutrons, one each for all those below and including potassium, more for those above. In the case of bismuth, the neutron excess amounts to over 50 percent.

The total yield of charged mesons is plotted logarithmically against nuclear mass number in Fig. 3. It is seen that this yield is very closely represented by a law of the form

$$Y = kA^{\frac{2}{3}}.$$

It is interesting to note from Table II that, within statistical error, no π^- mesons were observed from hydrogen. The accuracy of the determination limits the π^- cross section for hydrogen to about 7 percent of the π^+ cross section.

All the results quoted above apply to a maximum gamma-ray energy of 310±10 Mev,[16] a meson energy of 65±15 Mev (extreme limits), and an angle of emission of 135°. It is interesting to compare some of them with the results of other workers, where possible.

Peterson, Gilbert, and White[9] have used a photographic emulsion method for examining mesons of both signs produced by 322-Mev bremsstrahlung on carbon. They have measured the π^-/π^+ ratio both as a function of meson energy and of angle; unfortunately the statistical errors in the individual determinations do not allow one to see any significant variation of the ratio with these variables. The authors take an average to arrive at a figure of 1.34±0.20 for the π^-/π^+ ratio at 135°, with a median energy around 60 Mev. This ratio is slightly higher than the one reported in the present work; however, if one takes into account only those points which correspond strictly to the conditions of our experiment, there is agreement within statistical error.

Medicus,[10] using the same apparatus as Peterson, Gilbert and White,[9] has investigated the π^-/π^+ ratio for Be at 90°. He finds no significant change over the energy region 30–70 Mev within an accuracy of about 20 percent, and quotes an over-all value of 2.2±0.25, which is in excellent agreement with our value measured at 135°.

White[11] has measured the π^-/π^+ ratio from deuterium at 45° and 90° for mesons of energy 45–85 Mev, using a gas target and photographic detection. His values are 0.96±0.11 and 0.98±0.18, respectively.

Mozley[4] has measured the relative yield of π^+ mesons from a number of elements and finds that the yield per nucleus follows approximately an $A^{\frac{1}{3}}$ dependence. The same result has been demonstrated in the present work, and holds most accurately for the total yield of charged mesons of both signs (see Fig. 3).

IV. ENERGY DEPENDENCE OF THE π^-/π^+ RATIO FROM BERYLLIUM

Since the photons used for these experiments are not monochromatic, any variation in the energy balance of the reactions will alter the amount of the bremsstrahlung spectrum which can be utilized, and thus affect the over-all yield. It is of interest, therefore, to find out whether the observed π^-/π^+ ratios depend on the meson energy and on the maximum energy of the bremsstrahlung. In particular, the dependence should

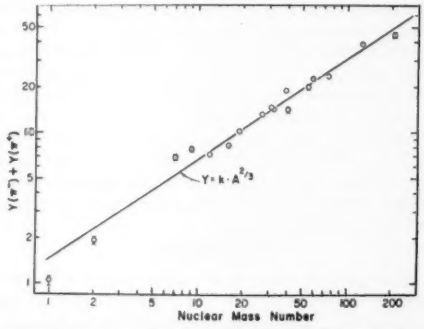

FIG. 3. Total charged meson yield plotted logarithmically against mass number.

[16] The limits of error on the beam energy have been increased slightly to allow for a small error that was made by not extracting the beam at exactly the peak magnetic field of the synchrotron.

be greatest for those nuclei which have π^-/π^+ ratios deviating strongly from unity (see Sec. V).

The dependence of the π^- and π^+ yields from beryllium on energy was investigated by changing both the maximum energy of the bremsstrahlung spectrum and the mean energy of mesons accepted by the magnet system. The meson energy was lowered to approximately 50 Mev by reducing the magnetic fields of the two magnets in the same ratio. The uncertainties connected with our knowledge of the meson energy have already been discussed in Sec. II, and it was also pointed out there that the relative counting rates at the two magnet settings could not be compared. Thus only the variation of the π^-/π^+ ratio is significant as far as dependence on meson energy is concerned.

More detailed information can be gained by varying the maximum energy of the photon spectrum, keeping the magnet settings unchanged. Here even the variation of the single π^- or π^+ counting rates is significant and may give evidence as to the energy of the photon which was responsible for the production.

The maximum photon energy was varied by contracting the circulating electron beam of the synchrotron onto the internal target at different times during the magnetic cycle. The two energies here employed were 310±10 Mev (as during the main body of the work) and 256±10 Mev. At both these photon energies the yields were measured for the two magnet settings corresponding to mean meson energies of about 65 and 50 Mev. The results, normalized to a constant number of effective quanta‡ in the irradiation, are displayed in Tables III and IV. In Table III, for the single π^- and π^+ counting rates at the two meson energies, the yields have been normalized in each case so that at the higher photon energy the π^- yield is 1.00.

It is evident from these results that the π^- and π^+ yields as well as their ratio depends on the energy balance of the reaction. The π^-/π^+ ratio deviates further from unity the stricter the energy requirements of the reaction are made, whether this is done by lowering the photon energy or by increasing the required meson energy. The variation with meson energy over the range here covered, however, is not very steep; since the meson energy ranges overlap in the two cases, no quantitative deductions can be made from this variation in any case.

TABLE III. Yield of photomesons from beryllium as a function of energy (arbitrary normalization at the two meson energies).

E_{max} (Mev)	E_π = 65±15 Mev		E_π = 50±10 Mev	
	$Y(\pi^-)$	$Y(\pi^+)$	$Y(\pi^-)$	$Y(\pi^+)$
310±10	1.00±0.02	0.44 ±0.01	1.00±0.02	0.47±0.01
256±10	0.24±0.01	0.064±0.004	0.33±0.01	0.13±0.01

TABLE IV. Variation of the π^-/π^+ ratio from beryllium with energy.

E_{max} (Mev)	E_π = 65±15 Mev	E_π = 50±10 Mev
310±10	2.27±0.07	2.12±0.06
256±10	3.7 ±0.3	2.56±0.16

V. DISCUSSION

(a) The $A^{2/3}$ Dependence

The simplest assumption that can be made to explain the variation of meson yield with nuclear mass is that the elementary cross section per nucleon is roughly constant, and that the mesons are observed only from the surface of the nucleus. To explain the suppression of mesons from the interior of the nucleus, one can postulate a strong reabsorption as they traverse nuclear matter;[4] it is known from direct absorption experiments[17] that the mean free path of mesons of about 50 Mev in nuclear matter is of the order of $2-3a_0$ (a_0 = standard nuclear radius 1.4×10^{-13} cm). However, for reabsorption to give an $A^{\frac{2}{3}}$ dependence valid down to the lightest nuclei, it would be necessary to assume a mean free path shorter than consistent with the absorption experiments; it appears, therefore, that either some additional mechanism for the suppression of meson production inside a nucleus must contribute, or else the validity of the $A^{\frac{2}{3}}$ law down to the lightest nuclei is a chance combination of other effects. There can be little doubt, however, that in the heavier nuclei reabsorption plays an important role; we shall return to this point below in connection with the variation of the π^-/π^+ ratios. In displaying the $A^{\frac{2}{3}}$ dependence, we have chosen the total charged meson production as our variable, since the relative concentration of protons and neutrons on the surface of a nucleus may be materially affected by the Coulomb repulsion and by the relative binding of the individual particles.

(b) The π^-/π^+ Ratios

An interesting result of the present work, and probably the most fundamentally significant, is the fact that the π^-/π^+ ratio from deuterium does not depart significantly from unity (this result has since been independently confirmed by White[11]). One would expect the effects of nuclear binding on meson production to be very small in deuterium; moreover they would presumably be the same for π^- as for π^+ production, apart from the small effects of the Coulomb interaction. Thus a measurement of the π^-/π^+ ratio from deuterium comes as close as is possible to a direct comparison between the elementary reactions (1) and (2) defined in Sec. I. Brueckner[18] has shown that the ratio of the cross sections for these reactions should vary strongly with energy and angle if the interaction of the electro-

‡ The number of effective quanta is defined as

$$Q=(\int EN(E)dE)/E_{max},$$

where $N(E)dE$ is the well-known bremsstrahlung spectrum of upper energy E_{max}.

[17] H. A. Bethe and R. R. Wilson, Phys. Rev. **83**, 690 (1951).
[18] K. A. Brueckner, Phys. Rev. **79**, 641 (1950).

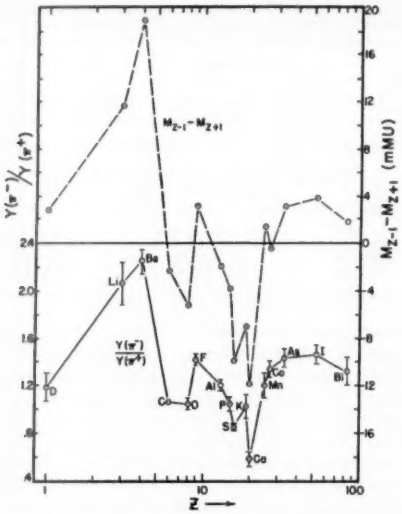

FIG. 4. π^-/π^+ ratios and mass differences (see text) plotted against Z.

magnetic field with only the currents of the particles is considered. If in addition the interaction with the magnetic moments is taken into account, the ratio becomes very close to unity and insensitive to both energy and angle. The predicted value for 135° and 65-Mev mesons is about 1.1, which would have to be corrected for the slight effect of the Coulomb barrier before comparison with the experimental figure of 1.19 ± 0.12. It appears established, then, that the interaction of the electromagnetic field with the nucleon magnetic moments plays an important role.

From Table II it can be seen that the production cross sections for mesons from deuterium are very close to that of π^+ from hydrogen, a result which is to be expected from the loosely bound nature of the deuteron.

The wide variations of the π^-/π^+ ratios from element to element suggest that they are connected with some detailed feature of nuclear structure rather than with a variation of the elementary production process itself. In an effort to find some empirical correlation that would give a clue to the nature of this nuclear factor, we have plotted the mass differences $M_{Z-1}-M_{Z+1}$ side by side with the π^-/π^+ ratios. M_{Z-1} and M_{Z+1} are the masses of the ground states of the final isobars $Z-1$ and $Z+1$ produced by removing or adding one charge to the initial target nucleus Z.[19] The resulting curves are displayed in Fig. 4. It is at once apparent that a strong correlation between the mass differences and the π^-/π^+ ratios exists. The same fact is brought out in Fig. 5, where a direct linear plot of the two variables has been made. The points fall remarkably close to a straight line, extending over a range of more than 3:1 in the π^-/π^+ ratio and from -12 to $+19$ mMU in the mass differences (1 mMU=0.93 Mev). There can thus be no doubt that a functional relationship, direct or indirect, exists between the two variables. It must be remembered, however, that there are many nuclear features which vary sympathetically with the masses of the ground states, and thus the functional dependence displayed above may be quite indirect. The fact that the plot of Fig. 5 is so nearly linear might also be fortuitous.

The factors which may modify the meson production from a complex nucleus have been mentioned in Sec. I; we shall regroup them here in a slightly different way, and attempt a very elementary discussion of their effects. These factors may be listed under the following three heads: (a) specifically mesonic factors, i.e., the effect of the overlap of meson clouds within the nucleus on the elementary production process; (b) effects of nuclear structure, including the initial momentum distribution of the nucleons, the absorption of outgoing mesons, and the limitation of momentum space available to recoil particles; (c) effects concerned with energy balance in the reaction and the fact that the primary photon spectrum is not monochromatic.

The results of the present experiment are of course not cross sections for meson production in the usual sense of the word, but rather meson yields integrated over the relevant part of the bremsstrahlung spectrum. To account for this fact, one might write the yields in the form

$$Y\sim(\text{Number of nucleons of relevent sign})\times\int N(E)\sigma(E)\eta(E)\rho(E)dE.$$

Here $N(E)$ is the number of photons of energy E; $\sigma(E)$ is the elementary production cross section; $\eta(E)$ is the nuclear modification factor mentioned in (a) above, averaged over the nucleus while taking account of reabsorption; and $\rho(E)$ is a weighting factor to account for the number of initial and final states possible in the reaction, always keeping the meson angle and energy fixed as dictated by the conditions of experiment. The above separation of variables is, of course, quite arbitrary and is intended solely as a basis for discussion.

If the production of mesons is from a free nucleon at rest, the factor $\rho(E)$ will be zero everywhere except at $E=E_0$ corresponding to the correct energy and momentum relationships. The effect of nuclear structure on $\rho(E)$ is to smear out the delta-function into a more or less broad curve, whose width will be primarily determined by the initial momenta of the target nucleons within the nucleus. The center of gravity of the curve

[19] Above and including O^{16}, the nuclear masses have been taken from a semi-empirical formula (E. Fermi, *Nuclear Physics*, revised edition (University of Chicago Press, Chicago, 1950). For the mass of He^7 we have used He^6+n; for Li^9, Li^8+n.

may be shifted in energy: the fact that during charged meson production the isotopic spin of a nucleon is changed implies a potential energy "opposition" ΔE from the rest of the nucleus, which will lead to the subtraction of some 20–40 Mev from the energy available in the reaction.

In a complex nucleus there is also the possibility that the elementary reaction takes place involving more than one nucleon. In this case, the energy of the photon required to produce a given meson would be lowered, and incidentally the nucleon recoil energy reduced. During the present discussion, we shall restrict ourselves to the case in which only one nucleon takes part in the primary production process, a condition which is likely to be satisfied in view of the high energies involved in the reaction.

The effect of $\rho(E)$ on the integral for Y can be visualized as a weighting function imposed on the other variables $N(E)\sigma(E)\eta(E)$. Since little is known about $\eta(E)$, we will leave this factor out of consideration for the moment. For $\sigma(E)$ we can assume as a first approximation the cross section for meson production from hydrogen as measured by Bishop, Steinberger and Cook.[3] In Fig. 6 we have plotted the product $N(E)\sigma(E)$ as a function of E, using for $N(E)$ the well-known bremsstrahlung spectrum with an upper limit of 310 Mev. The arrow at 290 Mev marks the value E_0 for which the 65-Mev mesons can be produced at 135° from free nucleons. For production of mesons from single nucleons in a complex nucleus, $\rho(E)$ will presumably be centered about the somewhat higher gamma-ray energy $E_0+\Delta E$.

$\rho(E)$ thus covers a very steep part of the curve, suggesting that slight changes in the energy balance of the reaction would affect the yield considerably. To determine the exact extent of this energy sensitivity, we would need to know the shape of $\rho(E)$ and its placing on the energy scale. Owing to the wide range of internal momenta for the nucleons in a complex nucleus, $\rho(E)$ will be a very broad curve, thus offsetting in part the steepness of the function $N(E)\sigma(E)$.

It is possible that the observed variations of the π^-/π^+ ratios from nucleus to nucleus are produced largely by the energy sensitivity of the individual yield

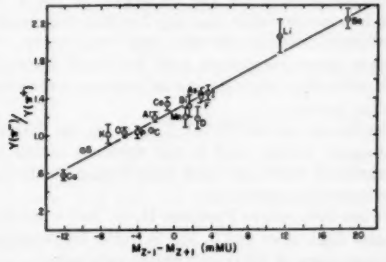

FIG. 5. π^-/π^+ ratios plotted against mass differences.

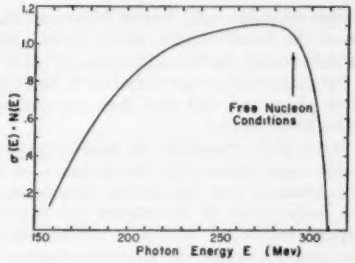

FIG. 6. $\sigma(E)N(E)$ as a function of E (see text).

functions. If there is a difference in the energy balance of the reaction according to whether a positive or a negative meson is produced, then the π^-/π^+ ratio will be altered correspondingly. Such an energy difference might be due to the Coulomb potential, or specifically nuclear factors may also contribute.[20]

If the variation of the π^-/π^+ ratios is governed by these energy considerations, one would expect the ratios to be energy sensitive, deviating further from unity the tighter the energy requirements are made. In Sec. IV we have described an experiment to investigate the variation of the π^-/π^+ ratio for beryllium with energy. From the results it is evident that there is a fairly strong energy dependence, so that the above arguments are borne out at least qualitatively. A quantitative interpretation would require, as has been pointed out above, an exact knowledge of the shape of $\rho(E)$ and of the energy balance of the reaction.

Apart from the energy dependence of $\rho(E)$, this factor influences the production rates through the density of initial and final states it contains. The exclusion principle will limit the number of states available for a recoiling nucleon, and in a rough way one would say that all energies below the Fermi surface for the residual nuclear core will be excluded.[21] The number of final

[20] A plausible way of analyzing the production process would be to consider first the creation of a meson by the impact of a photon on a single nucleon, then the fate of the particles as they recoil through the remainder of the nucleus. In the first instance, creation of a meson does not alter the local charge density in the nucleus, and will thus not give rise to an electrostatic potential energy. The change of the isotopic spin of the nucleon, however, causes an opposing potential ΔE of some 20–40 Mev. ΔE need not necessarily be the same when a proton is changed into a neutron as for the inverse process, and this difference $\Delta E_+ - \Delta E_-$ is the first factor which may distinguish positive from negative meson production. Although no Coulomb energy is required at the instant of creation, positive and negative mesons will behave differently upon escaping from the nucleus, the ones experiencing an acceleration on crossing the potential barrier, the others a retardation. When we observe mesons of a given energy in the laboratory, therefore, their energy at creation will not be the same, differing for the two signs by approximately 2.4 times the height of the potential barrier of the nucleus (the average potential inside the nucleus is 1.2 times the potential barrier). This is, in a way, equivalent to a difference between the energy balances of the reaction for the two cases.

[21] If the recoiling nucleons tended to be of relatively low energy, as would be the case if there were more than one nucleon involved

states thus excluded will depend of course on the position of the Fermi surface, which varies with the ground state energy. Bethe and Hayakawa[22] have estimated the magnitude of the variations to be expected from this effect, and find that they account for no more than 10–20 percent.

The factor $\eta(E)$ represents the modification of the production cross section by the presence of other nucleons, averaged over the nucleus while taking into account reabsorption of the mesons produced. The reabsorption makes the surface of the nucleus more effective for producing mesons externally observed than the interior; one will thus expect the relative concentration of neutrons and protons on the surface to have an important effect on the π^-/π^+ ratio. If there are other factors which reduce $\eta(E)$ in the interior of the nucleus, one might, following Butler,[23] consider the extreme case in which mesons are produced from only that part of a nucleon's wave function which exists outside the nuclear radius $a_0A^{\frac{1}{3}}$. This means that the binding of a nucleon becomes an important factor in its availability for meson production, since the more loosely bound nucleons spend more time outside the nuclear potential well than the more tightly bound particles. Thus, on a nuclear shell model, the last-added "odd" particle has the largest meson yield. Although this line of argument depends on somewhat extreme assumptions about the factor $\eta(E)$, there are certain experimental features which bear it out in a qualitative way. Consider first the variation of the π^-/π^+ ratio among the elements containing equal numbers of protons and neutrons. In Fig. 2 the relevant points have been connected by a smooth curve, which decreases steadily with increasing A. This decrease is paralleled by a progressively looser binding of the protons in these nuclei. The elements with one excess neutron in this region all have π^-/π^+ ratios lying above the curve. One can make the formal assumption[14] that the increased π^- yield is due entirely to the odd neutron, which will be more loosely bound than the other particles. On this basis one can work out the meson cross section from the odd neutron in terms of the cross sections from the paired neutrons in the same nucleus, and finds in all cases that the cross section is larger by a factor of about 4. This formal line of approach meets with difficulties, however, since it would attribute to the odd neutron a meson yield greater than that from the free proton (more than twice the free proton yield in the case of Be^9) which is not a very plausible conclusion. Moreover, an indirect measurement of the π^- production from the loose neutron in Be^9 has been made in this laboratory,[24] which indicates the cross section to be of the same order as that from the free proton.

With less extreme assumptions about the suppression of mesons from the interior of the nucleus, there will remain nevertheless an effect on the π^-/π^+ ratios which varies in the correct sense from nucleus to nucleus, although it will probably not be sufficiently large to account by itself for the observed deviations from unity.

VI. CONCLUSION

The most important features of the experimental results presented in this paper are:

(1) that the π^-/π^+ ratio from deuterium is close to unity, showing that the electromagnetic field interacts with the magnetic moments of the nucleons during charged meson production;

(2) that the charged meson cross sections for deuterium are close to that for π^+ from hydrogen;

(3) that the total charged meson cross section per nucleus varies as $A^{\frac{1}{3}}$, showing that the production is largely a surface effect, as is to be expected in the case of the heavier nuclei from the known absorption of mesons in nuclear matter;

(4) that the π^-/π^+ ratios vary widely from nucleus to nucleus, showing a remarkable correlation with the masses of the isobars adjacent in Z to the target nucleus; and

(5) that the π^-/π^+ ratio from beryllium is energy sensitive, bearing out qualitatively an argument concerning the effect of the bremsstrahlung distribution on the observed meson yields.

A detailed theory of the variations of the π^-/π^+ ratio has not yet been given, but a number of effects are suggested, each of which would contribute in the right sense to modifying the production of mesons according to their sign. The effects mentioned in the discussion are (1) the variation of the amount of bremsstrahlung spectrum utilized in the production because of the energy requirements of the reaction; (2) the relative proportion of neutrons and protons on the surface of the nuclei; and (3) the limitations of recoil momentum imposed on the nucleons by the residual nuclear core through the exclusion principle.

Although none of these effects appears by itself large enough to account for the variations of the π^-/π^+ ratio, it seems probable that together they will produce a sufficient deviation of this ratio from unity. The accurate linear correlation with the mass differences displayed in Figs. 4 and 5 remains, however, a somewhat puzzling feature.

Thanks are due to Mr. M. Camac for the design of the magnet system, and to the members of the first experimental team[5] for their contribution to the construction of the apparatus.

We are indebted to Professor H. A. Bethe for many valuable discussions and to Mr. S. Butler for permission to discuss some of his results before publication.

in the interaction, we might have to consider the density of states in the whole excited product nucleus.

[22] H. A. Bethe and S. Hayakawa (private communication).

[23] S. Butler (private communication).

[24] J. C. Keck and R. M. Littauer (to be published).

The Solution of the Fluctuation Problem in Electron-Photon Shower Theory

H. MESSEL AND R. B. POTTS
University of Adelaide, Adelaide, South Australia
(Received February 25, 1952)

The analytical solution is given for the fluctuation problem arising in electron-photon shower theory under approximation A. The diffusion equations for two fundamental distribution functions are derived, and by transforming them into matrix recurrence relations their solution is obtained directly. From one of these distribution functions follows the analytical solution for the (n, m)th moments. The method of solution is similar to that previously employed by Messel and Potts to solve the fluctuation problems in nucleon shower theory. The G-equations used by Janossy and Scott play no role in the solution of the problem.

I. INTRODUCTION

ALTHOUGH the fluctuation problem in electron-photon shower theory has received much attention in the last fifteen years, little progress has been made towards its solution. Furry,[1] Arley,[2] Euler,[3] Nordsieck *et al.*,[4] and Scott and Uhlenbeck,[5] who were among the first to discuss the problem, were mainly concerned with the simplified "Furry" model of the shower. More recently the problem has been investigated by Arley,[6] Bhabha,[7] Bhabha and Ramakrishnan,[8] Janossy,[9] Janossy and Messel,[10] Messel[11] and Scott.[12] Even when ionization loss has been neglected (approximation A) explicit analytical solutions have been obtained for only the first and second moments of the distribution function;[5,8,10] for these, Janossy and Messel[10] have given extensive numerical results, and using them Messel[11] has calculated the probability function, assuming it to be a Polya distribution.

It is the purpose of the present paper to give the analytical solution of the fluctuation problem in approximation A. We have previously[13–16] given the solutions of similar problems in nucleon cascade theory and the present work is a further application of the methods developed there. In the present problem, the method consists essentially in transforming the "last-collision" diffusion equation for the distribution function into a matrix recurrence relation, the solution of which follows immediately. A similar procedure is used for obtaining the nth moments.

II. DEFINITIONS

Let $p_{n,m}^{(j)}(\eta_1, \cdots, \eta_n; \eta_{n+1}, \cdots, \eta_{n+m}; x)d\eta_1 \cdots d\eta_{n+m}$ be the differential probability that after a depth x cascade units a primary (j) of unit energy has given rise to n electrons with energies in the ranges $\eta_k, \eta_k+d\eta_k$, $k=1, \cdots, n$ in any order, and m photons with energies in the ranges $\eta_{n+l}, \eta_{n+l}+d\eta_{n+l}$, $l=1, \cdots, m$ in any order. When $j=1$, the primary is an electron and when $j=2$, a photon. Further, let $q_{n,m}^{(j)}(\eta_1, \cdots, \eta_n; \eta_{n+1}, \cdots, \eta_{n+m}; x)d\eta_1 \cdots d\eta_{n+m}$ be the differential probability that that after a depth x a primary (j) of unit energy has given rise to n electrons with energies in the intervals $d\eta_k$, $k=1, \cdots, n$ and to m photons with energies in the intervals $d\eta_{n+l}$, $l=1, \cdots, m$ and to any numbers of electrons and photons with arbitrary energies.

The relation between $q_{n,m}^{(j)}$ and $p_{n,m}^{(j)}$ is expressed by

$$q_{n,m}^{(j)} = \sum_{a=0}^{\infty}\sum_{b=0}^{\infty} \frac{1}{a!b!} \int_0^1 d\eta_{n+1} \cdots \int_0^1 d\eta_{n+a} \times \int_0^1 d\eta_{n+a+m+1} \cdots \int_0^1 d\eta_{n+a+m+b} p_{n+a,m+b}^{(j)}, \quad (1)$$

and the inverse relation

$$p_{n,m}^{(j)} = \sum_{a=0}^{\infty}\sum_{b=0}^{\infty} \frac{(-1)^{a+b}}{a!b!} \int_0^1 d\eta_{n+1} \cdots \int_0^1 d\eta_{n+a} \times \int_0^1 d\eta_{n+a+m+1} \cdots \int_0^1 d\eta_{n+a+m+b} q_{n+a,m+b}^{(j)}. \quad (2)$$

Hence, if either $p_{n,m}^{(j)}$ or $q_{n,m}^{(j)}$ is known the other may in theory be determined. It is found, however, to be more expedient to derive diffusion equations for each of the $p_{n,m}^{(j)}$ and $q_{n,m}^{(j)}$ and to solve them directly.

The (n, m)th factorial moment $T_{n,m}^{(j)}(\eta; x)$ is defined by

$$T_{n,m}^{(j)}(\eta; x) = \sum_{a=0}^{\infty}\sum_{b=0}^{\infty} \frac{(n+a)!}{a!} \frac{(m+b)!}{b!} \varphi_{n+a,m+b}^{(j)}(\eta; x), \quad (3)$$

[1] W. H. Furry, Phys. Rev. **52**, 569 (1937).
[2] N. Arley, Proc. Roy. Soc. (London) **A168**, 519 (1938).
[3] H. Euler, Z. Physik **110**, 450 (1938).
[4] Nordsieck, Lamb, and Uhlenbeck, Physica **7**, 344 (1940).
[5] W. T. Scott and G. E. Uhlenbeck, Phys. Rev. **62**, 497 (1942).
[6] N. Arley, *On the Theory of Stochastic Processes* (John Wiley & Sons, Inc., New York, 1949).
[7] H. J. Bhabha, Proc. Roy. Soc. (London) **A202**, 301 (1950).
[8] H. J. Bhabha and A. Ramakrishnan, Proc. Indian Acad. Sci. **32**, 141 (1950).
[9] L. Janossy, Proc. Phys. Soc. (London) **A63**, 241 (1950).
[10] L. Janossy and H. Messel, Proc. Phys. Soc. (London) **A63**, 1101 (1950).
[11] H. Messel, Proc. Phys. Soc. (London) **A64**, 807 (1951).
[12] W. T. Scott, Phys. Rev. **82**, 893 (1951).
[13] H. Messel, Proc. Phys. Soc. (London) (to be published, 1952).
[14] H. Messel and R. B. Potts, Proc. Phys. Soc. (London) (to be published, 1952).
[15] H. Messel and R. B. Potts, Proc. Phys. Soc. (London) (to be published, 1952).
[16] H. Messel and J. W. Gardner, Phys. Rev. **84**, 1256 (1951).

where $\varphi_{n+a,m+b}^{(j)}(\eta;x)$ is the probability that after a depth x a primary (j) of unit energy has given rise to $n+a$ electrons and $m+b$ photons with energies $>\eta$ and any numbers of electrons and photons with energies $<\eta$. The inverse relation is expressed by

$$\varphi_{n,m}^{(j)}(\eta;x)=\sum_{a=0}^{\infty}\sum_{b=0}^{\infty}\frac{(-1)^{a+b}}{a!b!n!m!}T_{n+a,m+b}^{(j)}(\eta;x). \quad (4)$$

Here again, if either $\varphi_{n,m}^{(j)}$ or $T_{n,m}^{(j)}$ is known the other can be found by a double summation, but this may be exceedingly difficult to perform.

The function $\varphi_{n,m}^{(j)}$ is related to the $p_{n,m}^{(j)}$ by

$$\varphi_{n,m}^{(j)}=\sum_{a=0}^{\infty}\sum_{b=0}^{\infty}\frac{1}{a!b!n!m!}\int_{\eta}^{1}d\eta_1\cdots\int_{\eta}^{1}d\eta_n\int_{0}^{\eta}d\eta_{n+1}\cdots$$
$$\times\int_{0}^{\eta}d\eta_{n+a}\int_{\eta}^{1}d\eta_{n+a+1}\cdots$$
$$\times\int_{\eta}^{1}d\eta_{n+a+m}\int_{0}^{\eta}d\eta_{n+a+m+1}\cdots$$
$$\times\int_{0}^{\eta}d\eta_{n+a+m+b}p_{n+a,m+b}^{(j)}. \quad (5)$$

The moments $T_{n,m}^{(j)}$ may be expressed in terms of the distribution function $q_{n,m}^{(j)}$ by means of the simple relation (see reference 15),

$$T_{n,m}^{(j)}(\eta;x)=\int_{\eta}^{1}d\eta_1\cdots\int_{\eta}^{1}d\eta_{n+m}q_{n,m}^{(j)}$$
$$\times(\eta_1,\cdots,\eta_n;\eta_{n+1},\cdots,\eta_{n+m};x). \quad (6)$$

It is this relation which will be used for obtaining the $T_{n,m}^{(j)}$. Once the solution for $q_{n,m}^{(j)}$ is known, the moments are obtained by an elementary integration over the energy variables.

For the cross sections, the Bethe-Heitler expressions in the full-screening approximation will be used; $w^{(1)}(\eta_k,\eta_l)d\eta_l dx$ will denote the probability that an electron of energy $\eta_k+\eta_l$ emits in a distance dx a photon of energy in the range η_l, $\eta_l+d\eta_l$ and $w^{(2)}(\eta_k,\eta_l)d\eta_l dx$ the probability for pair production. For the total cross sections we write

$$\alpha^{(j)}=\int_{0}^{1}w^{(j)}(\eta_k,\eta_l)d\eta_l. \quad (7)$$

For $j=1$, this integral diverges (the infrared catastrophe) and to obtain numerical results for the $p_{n,m}^{(j)}$ it is necessary to impose a cutoff at the lower limit of integration. In the solutions for the $q_{n,m}^{(j)}$ and the $T_{n,m}^{(j)}$ the divergences cancel out.

III. THE SOLUTION FOR $p_{n,m}^{(j)}$

By considering all possible last collisions, the diffusion equation satisfied by the $p_{n,m}^{(j)}$ is obtained in the form

$$(\partial/\partial x+n\alpha^{(1)}+m\alpha^{(2)})p_{n,m}^{(j)}$$
$$=\sum_{C_1^n}\sum_{C_1^m}p_{n,m-1}^{(j)}(\eta_1',\cdots,\eta_{n-1}',\eta_n'+\eta_{n+m}';$$
$$\eta_{n+1}',\cdots,\eta_{n+m-1}';x)w^{(1)}(\eta_n',\eta_{n+m}')$$
$$+\sum_{C_2^n}p_{n-2,m+1}^{(j)}(\eta_1',\cdots,\eta_{n-2}';\eta_{n+1},\cdots,$$
$$\eta_{n+m},\eta_{n-1}'+\eta_n';x)w^{(2)}(\eta_{n-1}',\eta_n'), \quad (8)$$

with the initial conditions

$$p_{n,m}^{(j)}(x=0)=\delta_{n+j,2}\delta_{m+1,j}\delta(1-\eta_1). \quad (9)$$

In (4), the sum over C_1^n and C_2^n signify summations over all possible choices of η_n' and η_{n-1}', η_n' respectively from the η_k, $k=1,\cdots,n$ and the sum over C_1^m signifies summation over all possible choices of η_{n+m}' from the η_{n+l}, $l=1,\cdots,m$.

If we define the Laplace transform of $p_{n,m}^{(j)}$ as

$$P_{n,m}^{(j)}(\lambda)=\int_{0}^{\infty}e^{-\lambda x}p_{n,m}^{(j)}(x)dx, \quad (10)$$

then (8) may be transformed into the matrix equations

$$\left[\lambda\mathbf{E}_N+\sum_{k=1}^{N}\boldsymbol{\alpha}_N(k)\right]\mathbf{P}_N(\eta_1,\cdots,\eta_N;\lambda)$$
$$=\sum_{C_2^N}\mathbf{w}_{N-1}(\eta_{N-1},\eta_N)\mathbf{P}_{N-1}(\eta_1,\cdots,$$
$$\eta_{N-2},\eta_{N-1}+\eta_N;\lambda), \quad N>1 \quad (11)$$

and

$$[\lambda\mathbf{E}_1+\boldsymbol{\alpha}_1(1)]\mathbf{P}_1(\eta_1;\lambda)=\mathbf{E}_1\delta(1-\eta_1), \quad N=1. \quad (12)$$

$\mathbf{E}_N$ is the unit matrix of order 2^N. The $\boldsymbol{\alpha}_N(k)$ are given by the direct product of N matrices

$$\boldsymbol{\alpha}_N(k)=\mathbf{E}_1\times\cdots\times\underset{k\text{th place}}{\begin{bmatrix}\alpha^{(1)} & 0\\ 0 & \alpha^{(2)}\end{bmatrix}}\times\cdots\times\mathbf{E}_1. \quad (13)$$

The $\mathbf{P}_N$ is a $2^N\times 2$ matrix the columns of which correspond to $P^{(1)}$ and $P^{(2)}$ and the rows are ordered by writing $\eta_1\cdots\eta_N$ as a binary number with digits 1 and 2, standing for an electron and photon respectively. The $\mathbf{w}_{N-1}$ is a $2^N\times 2^{N-1}$ matrix in which the nonzero elements $w^{(j)}(\eta_k,\eta_l)$ are ordered according to the following rules:

(1) If in the binary number $\eta_1\cdots\eta_N$, $\eta_k=1$ and $\eta_l=1$, then all the elements of the row corresponding to this number are zero except for the term $2w^{(2)}(\eta_k,\eta_l)$, which is placed in the first even-numbered column in which this term has not already appeared.

(2) If $\eta_k=1$ and $\eta_l=2$, then all the elements of the row are zero except for the term $w^{(1)}(\eta_k, \eta_l)$, which is placed in the first odd-numbered column in which this term has not already appeared.

(3) If $\eta_k=2$ and $\eta_l=1$, then all the elements of the row are zero except for the term $w^{(1)}(\eta_l, \eta_k)$, which is placed in the first odd-numbered column in which this term has not already appeared.

(4) If $\eta_k=2$ and $\eta_l=2$, all the elements of the row are zero.

According to these rules there will be two non-zero elements in each odd-numbered column and one in each even-numbered column.

Equation (11) is a simple matrix recurrence relation, the solution of which is immediately given by[17]

$$\mathbf{P}_N(\eta_1, \cdots, \eta_N; \lambda)=\left\{\prod_{l=N-1}^{1}\sum_{C_2^{l+1}}\left[\lambda\mathbf{E}_{l+1}+\sum_{k=1}^{l+1}\boldsymbol{\alpha}_{l+1}(k)\right]^{-1}\mathbf{w}_l(\eta_l, \eta_{l+1}+\cdots+\eta_N)\right\}\times[\lambda\mathbf{E}_1+\boldsymbol{\alpha}_1(1)]^{-1}\delta(1-\eta_1-\cdots-\eta_N), \quad (14)$$

where the sum over C_2^{l+1} signifies summation over all possible choices of η_l, $\eta_{l+1}+\cdots+\eta_N$ from $\eta_1, \eta_2, \cdots, \eta_l, \eta_{l+1}+\cdots+\eta_N$. The $p_{n,m}{}^{(l)}$ are now obtained by taking an inverse Laplace transform.

The solution given in (14) should be compared with that given for the corresponding functions appearing in nucleon cascade theory.[13,14] The delta function in (14) merely ensures the conservation of energy in the shower, which is a consequence of the full-screening cross sections used and the neglect of ionization losses.

In order to illustrate our notation, the case $N=3$ will now be discussed in detail.

From (14)

$$\begin{aligned}\mathbf{P}_3(\eta_1, \eta_2, \eta_3; \lambda)&=\left\{\prod_{l=2}^{1}\sum_{C_2^{l+1}}\left[\lambda\mathbf{E}_{l+1}+\sum_{k=1}^{l+1}\boldsymbol{\alpha}_{l+1}(k)\right]^{-1}\times\mathbf{w}_l(\eta_l, \eta_{l+1}+\cdots+\eta_3)\right\}\times[\lambda\mathbf{E}_1+\boldsymbol{\alpha}_1(1)]^{-1}\delta(1-\eta_1-\eta_2-\eta_3)\\&=\sum_{C_3^4}[\lambda\mathbf{E}_3+\boldsymbol{\alpha}_3(1)+\boldsymbol{\alpha}_3(2)+\boldsymbol{\alpha}_3(3)]^{-1}\mathbf{w}_2(\eta_2, \eta_3)\times[\lambda\mathbf{E}_2+\boldsymbol{\alpha}_2(1)+\boldsymbol{\alpha}_2(2)]^{-1}\mathbf{w}_1(\eta_1, \eta_2+\eta_3)\times[\lambda\mathbf{E}_1+\boldsymbol{\alpha}_1(1)]^{-1}\delta(1-\eta_1-\eta_2-\eta_3).\end{aligned}$$

From the binary numbers

$$\eta_1\eta_2\eta_3=111, 112, 121, 122, 211, 212, 221, 222,$$

the explicit form for $\mathbf{P}_3(\eta_1, \eta_2, \eta_3; \lambda)$ is

$$\mathbf{P}_3=\begin{bmatrix}P_{3,0}{}^{(1)}(\eta_1, \eta_2, \eta_3; \lambda) & P_{3,0}{}^{(2)}(\eta_1, \eta_2, \eta_3; \lambda)\\ P_{2,1}{}^{(1)}(\eta_1, \eta_2; \eta_3; \lambda) & P_{2,1}{}^{(2)}(\eta_1, \eta_2; \eta_3; \lambda)\\ P_{2,1}{}^{(1)}(\eta_1, \eta_3; \eta_2; \lambda) & P_{2,1}{}^{(2)}(\eta_1, \eta_3; \eta_2; \lambda)\\ P_{1,2}{}^{(1)}(\eta_1; \eta_2, \eta_3; \lambda) & P_{1,2}{}^{(2)}(\eta_1; \eta_2, \eta_3; \lambda)\\ P_{2,1}{}^{(1)}(\eta_2, \eta_3; \eta_1; \lambda) & P_{2,1}{}^{(2)}(\eta_2, \eta_3; \eta_1; \lambda)\\ P_{1,2}{}^{(1)}(\eta_2; \eta_1, \eta_3; \lambda) & P_{1,2}{}^{(2)}(\eta_2; \eta_1, \eta_3; \lambda)\\ P_{1,2}{}^{(1)}(\eta_3; \eta_1, \eta_2; \lambda) & P_{1,2}{}^{(2)}(\eta_3; \eta_1, \eta_2; \lambda)\\ P_{0,3}{}^{(1)}(\eta_1, \eta_2, \eta_3; \lambda) & P_{0,3}{}^{(2)}(\eta_1, \eta_2, \eta_3; \lambda)\end{bmatrix}.$$

From the rules (1)–(4) above and the binary numbers $\eta_1, \eta_2+\eta_3=11, 12, 21, 22$ the matrix $\mathbf{w}_1(\eta_1, \eta_2+\eta_3)$ is

$$\mathbf{w}_1(\eta_1, \eta_2+\eta_3)=\begin{bmatrix}0 & 2w^{(2)}(\eta_1, \eta_2+\eta_3)\\ w^{(1)}(\eta_1, \eta_2+\eta_3) & 0\\ w^{(1)}(\eta_2+\eta_3, \eta_1) & 0\\ 0 & 0\end{bmatrix}$$

and from the binary number $\eta_1\eta_2\eta_3$

$$\mathbf{w}_2(\eta_2, \eta_3)=\begin{bmatrix}0 & 2w^{(2)}(\eta_2, \eta_3) & 0 & 0\\ w^{(1)}(\eta_2, \eta_3) & 0 & 0 & 0\\ w^{(1)}(\eta_3, \eta_2) & 0 & 0 & 0\\ 0 & 0 & 0 & 0\\ 0 & 0 & 0 & 2w^{(2)}(\eta_2, \eta_3)\\ 0 & 0 & w^{(1)}(\eta_2, \eta_3) & 0\\ 0 & 0 & w^{(1)}(\eta_3, \eta_2) & 0\\ 0 & 0 & 0 & 0\end{bmatrix}$$

and

$$\mathbf{w}_2(\eta_1, \eta_2)=\begin{bmatrix}0 & 2w^{(2)}(\eta_1, \eta_2) & 0 & 0\\ 0 & 0 & 0 & 2w^{(2)}(\eta_1, \eta_2)\\ w^{(1)}(\eta_1, \eta_2) & 0 & 0 & 0\\ 0 & 0 & w^{(1)}(\eta_1, \eta_2) & 0\\ w^{(1)}(\eta_2, \eta_1) & 0 & 0 & 0\\ 0 & 0 & w^{(1)}(\eta_2, \eta_1) & 0\\ 0 & 0 & 0 & 0\\ 0 & 0 & 0 & 0\end{bmatrix}.$$

[17] Scott (see reference 12) has recently considered the fluctuation problem for a simplified model of the electron-photon shower. Although he was able to obtain a recurrence relation for the distribution function he was unable to solve it. His recurrence relation is a very special case of (11) and its solution is (in his notation)

$$r_N=\prod_{l=N-1}^{1}\sum_{C_2^{l+1}}(E_l+E_{l+1}+\cdots+E_N)^{-1},$$

where the sum over C_2^{l+1} signifies summation over all possible ways of choosing $E_l, E_{l+1}+\cdots+E_N$ from $E_1, \cdots, E_l, E_{l+1}+\cdots+E_N$.

In a similar way one obtains $\mathbf{w}_2(\eta_1, \eta_3)$. It should be noted that $\mathbf{w}_2(\eta_1, \eta_2)$ cannot be obtained from $\mathbf{w}_2(\eta_2, \eta_3)$ by merely changing the variables in the elements of the matrix.

From (13) $\lambda\mathbf{E}_3+\boldsymbol{\alpha}_3(1)+\boldsymbol{\alpha}_3(2)+\boldsymbol{\alpha}_3(3)$ is the diagonal matrix

$$\begin{bmatrix}
\lambda+3\alpha^{(1)} & 0 & 0 & 0 & 0 & 0 & 0 & 0 \\
0 & \lambda+2\alpha^{(1)}+\alpha^{(2)} & 0 & 0 & 0 & 0 & 0 & 0 \\
0 & 0 & \lambda+2\alpha^{(1)}+\alpha^{(2)} & 0 & 0 & 0 & 0 & 0 \\
0 & 0 & 0 & \lambda+\alpha^{(1)}+2\alpha^{(2)} & 0 & 0 & 0 & 0 \\
0 & 0 & 0 & 0 & \lambda+2\alpha^{(1)}+\alpha^{(2)} & 0 & 0 & 0 \\
0 & 0 & 0 & 0 & 0 & \lambda+\alpha^{(1)}+2\alpha^{(2)} & 0 & 0 \\
0 & 0 & 0 & 0 & 0 & 0 & \lambda+\alpha^{(1)}+2\alpha^{(2)} & 0 \\
0 & 0 & 0 & 0 & 0 & 0 & 0 & \lambda+3\alpha^{(2)}
\end{bmatrix}$$

and similarly one obtains $\lambda\mathbf{E}_2+\boldsymbol{\alpha}_2(1)+\boldsymbol{\alpha}_2(2)$ and $\lambda\mathbf{E}_1+\boldsymbol{\alpha}_1(1)$. The inverses of these matrices are obtained by replacing the diagonal elements by their reciprocals.

By carrying out the matrix product one obtains, for instance,

$$P_{3,0}{}^{(1)}(\eta_1, \eta_2, \eta_3; \lambda)=\frac{\sum_{C_3^2} 2w^{(2)}(\eta_2, \eta_3)w^{(1)}(\eta_1, \eta_2+\eta_3)}{(p+3\alpha^{(1)})(p+\alpha^{(1)}+\alpha^{(2)})(p+\alpha^{(1)})} \times\delta(1-\eta_1-\eta_2-\eta_3).$$

Similar expressions are obtained for $P_{2,1}{}^{(2)}(\eta_1, \eta_2; \eta_3; \lambda)$ and $P_{1,2}{}^{(1)}(\eta_1; \eta_2, \eta_3; \lambda)$. The solution for $p_{2,0}{}^{(1)}(\eta_1, \eta_2, \eta_3; x)$ follows by taking the inverse Laplace transform of $P_{2,0}{}^{(1)}(\eta_1, \eta_2, \eta_3; \lambda)$.

IV. THE SOLUTION FOR $q_{n,m}{}^{(j)}$ AND $T_{n,m}{}^{(j)}$

The "last-collision" diffusion equation satisfied by $q_{n,m}{}^{(j)}$ is given by

$$\begin{aligned}
&(\partial/\partial x+n\alpha^{(1)}+m\alpha^{(2)})q_{n,m}{}^{(j)}(\eta_1, \cdots, \eta_n; \\
&\qquad \eta_{n+1}, \cdots, \eta_{n+m}; x) \\
&=\sum_{C_1^n}\sum_{C_1^m} q_{n,m-1}{}^{(j)}(\eta_1', \cdots, \eta_{n-1}', \eta_n'+\eta_{n+m}'; \\
&\qquad \eta_{n+1}', \cdots, \eta_{n+m-1}'; x)w^{(1)}(\eta_n', \eta_{n+m}') \\
&\quad+\sum_{C_2^n} q_{n-2,m+1}{}^{(j)}(\eta_1', \cdots, \eta_{n-2}'; \eta_{n+1}, \cdots, \\
&\qquad \eta_{n+m}, \eta_{n-1}'+\eta_n'; x)w^{(2)}(\eta_{n-1}', \eta_n') \\
&\quad+\sum_{C_1^n}\int_0^1 q_{n-1,m+1}{}^{(j)}(\eta_1', \cdots, \eta_{n-1}'; \eta_{n+1}, \cdots, \\
&\qquad \eta_{n+m}, u; x)2w^{(2)}(u-\eta_n', \eta_n')du \\
&\quad+\sum_{C_1^m}\int_0^1 q_{n,m}{}^{(j)}(\eta_1', \cdots, \eta_{n-1}', u; \eta_{n+1}, \cdots, \\
&\qquad \eta_{n+m}; x)w^{(1)}(\eta_n', u-\eta_n')du \\
&\quad+\sum_{C_1^m}\int_0^1 q_{n+1,m-1}{}^{(j)}(\eta_1, \cdots, \eta_n, u; \eta_{n+1}', \cdots, \\
&\qquad \eta_{n+m-1}'; x)w^{(1)}(u-\eta_{n+m}', \eta_{n+m}')du \quad (15)
\end{aligned}$$

where $q_{0,0}{}^{(j)}(x)=1$. The initial conditions for $q_{n,m}{}^{(j)}$ are given by

$$\begin{aligned}
&q_{n,m}{}^{(j)}(x=0)=\delta_{n+j,2}\delta_{m+1,j}\delta(1-\eta_1) \\
&\text{and} \qquad (16) \\
&q_{0,0}{}^{(j)}(x=0)=1.
\end{aligned}$$

We define the n-fold Mellin and single Laplace transform of $q_{n,m}{}^{(j)}$ by

$$\begin{aligned}
&Q_{n,m}{}^{(j)}(s_1, \cdots, s_n; s_{n+1}, \cdots, s_{n+m}; \lambda) \\
&\quad=\int_0^1 d\eta_1 \cdots \int_0^1 d\eta_{n+m}\int_0^\infty dx\eta_1^{s_1-1}\cdots \\
&\qquad \times\eta_{n+m}^{s_{n+m}-1}e^{-\lambda x}q_{n,m}{}^{(j)} \quad (17)
\end{aligned}$$

and

$$\begin{aligned}
&W^{(j)}(s_1, s_2) \\
&\quad=\int_0^1\left(\frac{\eta_1}{\eta_1+\eta_2}\right)^{s_1-1}\left(\frac{\eta_2}{\eta_1+\eta_2}\right)^{s_2-1}w^{(j)}(\eta_1, \eta_2)d\eta_2. \quad (18)
\end{aligned}$$

By taking the Mellin-Laplace transform of (15) we get

$$\begin{aligned}
&(\lambda+n\alpha^{(1)}+m\alpha^{(2)})Q_{n,m}{}^{(j)}(s_1, \cdots, s_n; \\
&\qquad s_{n+1}, \cdots, s_{n+m}; \lambda)-\delta_{n+j,2}\delta_{m+1,j} \\
&=\sum_{C_1^n}\sum_{C_1^m} Q_{n,m-1}{}^{(j)}(s_1', \cdots, s_{n-1}', s_n'+s_{n+m}'; \\
&\qquad s_{n+1}', \cdots, s_{n+m-1}'; \lambda)W^{(1)}(s_n', s_{n+m}') \\
&\quad+\sum_{C_2^n} Q_{n-2,m+1}{}^{(j)}(s_1', \cdots, s_{n-2}'; s_{n+1}, \cdots, \\
&\qquad s_{n+m}, s_{n-1}'+s_n'; \lambda)W^{(2)}(s_{n-1}', s_n') \\
&\quad+\sum_{C_1^n} Q_{n-1,m+1}{}^{(j)}(s_1', \cdots, s_{n-1}'; \\
&\qquad s_{n+1}, \cdots, s_{n+m}, s_n'; \lambda)2W^{(2)}(s_n', 0) \\
&\quad+\sum_{C_1^m} Q_{n,m}{}^{(j)}(s_1, \cdots, s_n; \\
&\qquad s_{n+1}, \cdots, s_{n+m}; \lambda)W^{(1)}(s_n', 0) \\
&\quad+\sum_{C_1^m} Q_{n+1,m-1}{}^{(j)}(s_1, \cdots, s_n, s_{n+m}'; \\
&\qquad s_{n+1}', \cdots, s_{n+m-1}'; \lambda)W^{(1)}(0, s_{n+m}'). \quad (19)
\end{aligned}$$

The first two terms on the right hand side of (19) are similar in form to those in (8) and may be expressed in matrix notation as before. By transferring the last three terms of the right hand side of (19) to the left hand side, the equation may be written in the following

matrix form:

$$\left[\lambda\mathbf{E}_N+\sum_{k=1}^{N}\mathbf{A}_N(s_k)\right]\mathbf{Q}_N(s_1,\cdots,s_N;\lambda)=\sum_{C_2^N}\mathbf{W}_{N-1}(s_{N-1},s_N)\mathbf{Q}_{N-1}(s_1,\cdots,s_{N-2},s_{N-1}+s_N;\lambda),\quad N>1 \tag{20}$$

and

$$[\lambda\mathbf{E}_1+\mathbf{A}_1(s_1)]\mathbf{Q}_1(s_1;\lambda)=\mathbf{E}_1,\quad N=1. \tag{21}$$

The matrices $\mathbf{Q}_N$ and $\mathbf{W}_{N-1}$ are constructed in a manner identical to that used for $\mathbf{P}_N$ and $\mathbf{w}_{N-1}$ in (11). The $\mathbf{A}_N(s_k)$ are given by the direct product of N matrices:

$$\mathbf{A}_N(s_k)=\mathbf{E}_1\times\cdots\times\underset{k\text{th place}}{\begin{bmatrix}A_1(s_k) & A_2(s_k)\\ A_3(s_k) & A_4(s_k)\end{bmatrix}}\times\cdots\times\mathbf{E}_1, \tag{22}$$

where, as in reference 10,

$$\begin{aligned}A_1(s)&=A(s+1)=\alpha^{(1)}-W^{(1)}(s,0)\\ A_2(s)&=-B(s+1)=-2W^{(2)}(s,0)\\ A_3(s)&=-C(s+1)=-W^{(1)}(0,s)\\ A_4(s)&=D=\alpha^{(2)}.\end{aligned} \tag{23}$$

Note that the divergent term $\alpha^{(1)}$ has cancelled out in $A_1(s)$ above.

The solution of Eq. (20) is

$$\mathbf{Q}_N(s_1,\cdots,s_N;\lambda)=\left\{\prod_{l=N-1}^{1}\sum_{C_2^{l+1}}\left[\lambda\mathbf{E}_{l+1}+\sum_{k=1}^{l+1}\mathbf{A}_{l+1}(s_k)\right]^{-1}\mathbf{W}_l(s_l,s_{l+1}+\cdots+s_N)\right\}\times[\lambda\mathbf{E}_1+\mathbf{A}_1(s_1+\cdots+s_N)]^{-1}, \tag{24}$$

where the sum over C_2^{l+1} signifies summation over all possible choices of s_l, $s_{l+1}+\cdots+s_N$ from $s_1,\cdots,s_l$, $s_{l+1}+\cdots+s_N$, and where for $k=l+1$, the matrix $\mathbf{A}_{l+1}(s_k)$ stands for $\mathbf{A}_{l+1}(s_{l+1}+\cdots+s_N)$. For example, when $l=2$, the expression inside the brackets in (24) is

$$[\lambda\mathbf{E}_2+\mathbf{A}_2(s_1)+\mathbf{A}_2(s_2)+\mathbf{A}_2(s_3+\cdots+s_N)]^{-1}\times\{\mathbf{W}_2(s_2,s_3+\cdots+s_N)+\mathbf{W}_2(s_1,s_3+\cdots+s_N)+\mathbf{W}_2(s_1,s_2)\}.$$

By taking the inverse transform of (17) we immediately obtain the solution for the $q_{n,m}^{(j)}$

$$q_{n,m}^{(j)}(\eta_1,\cdots,\eta_n;\eta_{n+1},\cdots,\eta_{n+m};x)=\frac{1}{(2\pi i)^{n+m+1}}\int_{u_1-i\infty}^{u_1+i\infty}ds_1\cdots\times\int_{u_{n+m}-i\infty}^{u_{n+m}+i\infty}ds_{n+m}\int_{\lambda_0-i\infty}^{\lambda_0+i\infty}d\lambda e^{\lambda x}\times\eta_1^{-(a_1+1)}\cdots\eta_{n+m}^{-(a_{n+m}+1)}Q_{n,m}^{(j)}; \tag{25}$$

and from (6) the analytical solution for the moments is

$$T_{n,m}^{(j)}(\eta;x)=\frac{1}{(2\pi i)^{n+m+1}}\int_{u_1-i\infty}^{u_1+i\infty}\frac{ds_1}{s_1}\cdots\times\int_{u_{n+m}-i\infty}^{u_{n+m}-i\infty}\frac{ds_{n+m}}{s_{n+m}}\int_{0-i\infty}^{\lambda_0+i\infty}d\lambda e^{\lambda x}\times\eta^{-(a_1+\cdots+a_{n+m})}Q_{n,m}^{(j)}. \tag{26}$$

This completes the analytical solution of the fluctuation problem in approximation A; as all functions of interest may be obtained from the $p_{n,m}^{(j)}$, $q_{n,m}^{(j)}$ and $T_{n,m}^{(j)}$ we have complete knowledge of the number behavior of the shower.

IV. DISCUSSION

In the solution (14) for $\mathbf{P}_N$, the elements of the inverse diagonal matrices are reciprocals of linear functions of λ; and as these are independent of the summations over the energy variables, the inverse Laplace transform may be easily taken. Apart from the depth-dependent factor, the solution for $p_{n,m}^{(j)}$ is a sum of products of various combinations of the cross-sections $w^{(1)}$ and $w^{(2)}$. The complexity of this result reduces its usefulness for numerical calculations, especially as the physically interesting distribution function $\varphi^{(j)}$ is obtained from the $p^{(j)}$ by a difficult double summation.

The solution (24) for $\mathbf{Q}_N$ is of direct physical interest because it leads to the general analytical solution for all the moments, including the correlations between electrons and photons. The diffusion equation for the moments as previously derived[10] from the Janossy G-equation was not in a form amenable to direct solution. The relation (6), however, enabled us to by-pass the G-equation and obtain the solution for the moments by a simple integration over the energy variables of $q_{n,m}^{(j)}$. The solution (26) for the moments contains the special cases $n=1$, $m=0$ and $n=1$, $m=1$ already calculated by Janossy and Messel.[10] Bhabha[18] has recently given a recurrence equation for his correlation functions similar to (19) without, however, obtaining a solution.

In this paper only the fluctuation problem neglecting ionization loss (approximation A) has been discussed. Any results which can be obtained for the problem including ionization losses (approximation B) will be even more complicated in nature and less amenable to numerical calculations than those obtained above. The numerical evaluations in approximation A for $p^{(j)}$, $q^{(j)}$, $\varphi^{(j)}$ and the moments $T^{(j)}$ will be discussed in a later publication together with those for the nucleon cascades.

[18] H. J. Bhabha, Proc. Indian Acad. Sci. **32**, 154 (1950).

Possibility of Frequency Multiplication and Wave Amplification by Means of Some Relativistic Effects

K. LANDECKER
School of Physics, University of Sydney, Sydney, Australia
(Received July 27, 1951)

A method is proposed of converting the frequency of an electromagnetic wave to a higher frequency by reflection from an electron cloud moving with relativistic velocity. Such an electron cloud can be realized by compressing all or part of the electron beam of an electron accelerator into one or more groups. It is shown that there is a gain of wave energy arising from the relativistic law of reflection of a wave which is reflected from such a cloud. It is also shown on the basis of Bailey's relativistic electro-magneto-ionic theory that under certain circumstances the reflection from a moving slab of electrons may be increased considerably if the slab moves through a longitudinal or transverse magnetic field. It is estimated that a wave of length 1 mm and of a power at least one milliwatt can be generated by reflecting a wave of length 3 cm from the beam of a small betatron. Equipment is being designed to test this prediction experimentally.

THE purpose of this note is to point out that through the development of electron accelerators (such as the van de Graaff machine and the betatron) the generation of very short electromagnetic waves by means of some relativistic effects has come within the range of possibility.[1]

I. RELATIVISTIC DOPPLER EFFECT

Consider first the expression for the relativistic Doppler effect in the form

$$\nu' = \nu[1+(u/c)\cos\phi](1-u^2/c^2)^{-\frac{1}{2}}, \tag{1}$$

where u = velocity of an electron in the beam of an accelerator, c = velocity of light in vacuum, ν' = frequency of an electromagnetic wave in a coordinate system S' at rest with respect to the observer, ν = frequency of an electromagnetic wave in a coordinate system S moving with an electron in the beam, and ϕ is the angle between the wave normal in the system S of a spherical wave originating at the electron and the direction of the relative velocity u.

Thus,

$$\nu' = \nu F \quad \text{for} \quad \phi = 0, \tag{2}$$

$$\nu' = \nu f \quad \text{for} \quad \phi = \pi, \tag{3}$$

where

$$F = \{(1+u/c)/(1-u/c)\}^{\frac{1}{2}} = f^{-1}. \tag{4}$$

TABLE I. Conversion factor F for typical accelerating voltages.

V(Mev)	0.1	1	2	5	10	25	100
F	1.85	5.75	9.7	21.5	41.1	97.7	394
$K=F^2$	3.44	33	94	463	1690	9570	154800

F and f in (2) and (3) may be termed "conversion factors" because the frequency of an electromagnetic wave radiated by the moving electron appears to a stationary observer F times greater [in the case of Eq. (2)] and F times less [in the case of Eq. (3)], i.e., the observed frequency depends on the "direction of observation" as specified by ϕ. Also F and f interchange when u changes its sign.

It may easily be seen that as $(u/c)\to 1$, $F\to\infty$ in (2) and $f\to 0$ in (3). The first case is of course the one of interest for the present purpose.

In Table I the values of F are given for a selection of accelerating voltages typical of present day machines. As may be seen from this table, a large frequency multiplication is theoretically possible even for accelerating voltages of 5 Mev, e.g., electrons radiating a wavelength of 3 cm in the system S would appear to radiate a wavelength of about 1.5 mm in the laboratory frame.

The question naturally arises how the electrons in the beam of an accelerator, linear or circular, can be made to oscillate at a desired frequency. Several schemes seem feasible, but that which appears to be most practicable is better discussed in terms of the motion of a mirror moving with relativistic velocity.

II. MIRROR MOVING WITH RELATIVISTIC VELOCITY

Consider an electromagnetic wave originating in the laboratory frame S' and traveling towards the oncoming electron stream of an accelerator and also a slab, cut out of this stream by planes perpendicular to the direction of the beam, in which the wave is absorbed by imparting energy of oscillation to the electrons and then re-radiated.

It will be recognized that the situation is then analogous to reflection by a mirror moving with relativistic velocity.

An electromagnetic wave of frequency ν incident at an angle θ on such a mirror is reflected back with the increased frequency ν' if the mirror moves towards

[1] Since this paper was submitted for publication an article by H. Motz entitled "Applications of the radiation from fast electron beams" [J. Appl. Phys. **22**, 527 (1951)], which deals with a similar problem, has become available in this country. We agree with this author on the importance of coherence of the radiation from the electron beam. However, a large increase of intensity above incoherent radiation will be obtained even if grouping or bunching of the electrons is not perfect (see Secs. IV and V of this paper).

the observer with the velocity u. This frequency is known to be given by

$$\nu' = \nu[1+2(u/c)\cos\theta+u^2/c^2]/(1-u^2/c^2). \quad (5)$$

In the present case where the directions of incidence and reflection are perpendicular to the surface of the slab (the "mirror") $\theta=0$ and the expression reduces to

$$\nu' = \nu K, \quad (6)$$

where

$$K=(1+u/c)/(1-u/c)=F^2. \quad (7)$$

Clearly, when u approaches c, then

$$K\sim 2/(1-u/c).$$

The values of K are also given in Table I. It will be observed that if this mechanism can be used, a notable multiplication of frequency ($K\sim 30$) will occur even at velocities corresponding to 1 Mev.

III. RELATIVISTIC WAVE AMPLIFICATION

Before attempting to obtain at least an approximate estimate of the efficiency of such a scheme, it may be pointed out that another relativistic theorem greatly increases the chances of observing the present mode of frequency conversion. As is well known, the theory of relativity shows[2] that the field amplitudes A and A' measured by two observers in two different systems of coordinates S and S' are in the ratios of the frequencies measured by these observers, i.e., the amplitudes transform as follows:

$$A/\nu = A'/\nu'. \quad (8)$$

Applied to the present case this means that if the conversion factors F or K are large, the electrons in the slab will experience a field amplitude much larger than that originally measured in the laboratory frame, and an observer in the laboratory frame will observe a field amplitude much larger than the amplitude of the wave re-radiated from the electrons and, *a fortiori*, much larger (by the factor K) than the amplitude of the wave originally sent out from the laboratory frame. In fact, we should expect a total increase of wave energy by the factor K^2.

IV. A NUMERICAL EXAMPLE

For the purpose of a first estimate of the conversion efficiency of such an arrangement [corresponding to Eq. (6)] we take as a concrete example a wave in the laboratory (S') frame of 3 cm wavelength, i.e., 10,000 Mc/sec frequency and an amplitude of 100 v/cm at the position of the slab. This can be provided by a standard magnetron radar transmitter. We disregard initially the effect described by Eq. (8) and also assume that in the electron beam of the accelerator there is no restoring force on the electrons at right angles to the beam. Although in most machines there exists a small radial magnetic field for focusing purposes, this will be allowable because under these assumptions the amplitude a of the electron vibrations created by the wave is given by

$$a=(e/m)(E/\omega^2) \text{ cm}, \quad (9)$$

where E = field strength in esu and $\omega/2\pi$ = frequency of the incident wave. For the present numerical example this yields $a\sim 4.5\times 10^{-5}$ cm. We may therefore restrict our considerations, if necessary, to regions where the transverse magnetic field is small or even zero, e.g., with a betatron to the immediate neighborhood of the median plane. We shall return to this aspect of the problem in Sec. V, where it will be shown that this restriction on the magnetic field may be removed by using the results of Bailey's relativistic electro-magneto-ionic theory ("E.M.I." theory).[3]

We will now consider the electron density in the beam of the machine. Data published for the original betatron built at the University of Illinois[4] yield $\sim 10^9$ as the total number of electrons in the orbit of this machine.

The final answer to our problem depends on how many of these electrons can be made to oscillate coherently as a group. If by suitable means it is possible for the wave to excite all the 10^9 electrons as a group then, by the classical radiation theory, the energy S radiated per second is given by

$$S=\tfrac{1}{3}(q^2/c^3)(e^2/m^2)E^2$$

or

$$S=\tfrac{1}{3}[(Ne)^2/c^3](e/m)^2E^2 \text{ erg/sec}, \quad (10)$$

where N is the electron density and $q=Ne$ is the total charge in the group of electrons. For our numerical example this expression yields $S\sim 10^2$ erg/sec $=10^{-2}$ mw. In practice it may not be possible to group all the electrons in the beam together in the manner indicated. In the betatron being designed in this laboratory to test the generation of short waves by the present method (see Sec. VI) the electrons are compressed into regions about 30 wavelengths apart.

V. THE PROCESS OF WAVE AMPLIFICATION AND FREQUENCY CONVERSION ON THE BASIS OF BAILEY'S RELATIVISTIC E.M.I. THEORY

Professor V. A. Bailey has kindly drawn the writer's attention to the fact that a more detailed analysis of the wave conversion process considered may be carried out by using the results of his relativistic E.M.I. theory.[3] In fact, this theory makes it possible to take into account the effect of any transverse or longitudinal magnetic field pervading the electron beam which introduces an electronic gyrofrequency and which we were forced to exclude in our above approximation. Professor Bailey has carried out an analysis of the

[2] Abraham-Becker, *Theorie der Elektrizitaet* (Leipzig-Berlin 1933), p. 314, Vol. 2.

[3] V. A. Bailey, Phys. Rev. **78**, 428 (1950) and earlier communications.

[4] D. W. Kerst, Phys. Rev. **60**, 47 (1941).

reflection of a circularly polarized wave by a uniform semi-infinite slab of electrons moving with the velocity U along or transverse to a uniform magnetic field H. Clearly this is the configuration that exists in most electron accelerators. The calculations are here reproduced with Professor Bailey's permission.

Let S be a frame of reference in which the slab is at rest and S' a parallel frame moving relatively to K with a velocity $-U$ along the axis $0x$.

In S let $\mathbf{E}_i$, $\mathbf{E}_r$, and $\mathbf{E}_n$ be the electric vectors, near the face of the slab, of the incident, reflected, and transmitted waves, respectively. The corresponding magnetic vectors are proportional to $-\mathbf{E}_i$, $\mathbf{E}_r$, and $-M\mathbf{E}_n$, where the refractive index M is given by the relevant dispersion equation.

The boundary conditions at the face of the slab yield the following relations between parallel tangential components:

$$E_r+E_i=E_n, \quad E_r-E_i=-ME_n,$$

and so

$$E_r/E_i=(1-M)/(1+M). \tag{11}$$

If P_i and P_r are the incident and reflected Poynting fluxes, then the coefficient of reflection ρ is given by

$$\rho=P_r/P_i=|1-M|^2/|1+M|^2. \tag{12}$$

The phases of the three waves are, respectively, ϕ_i, ϕ_r, ϕ_n, where

$$\begin{aligned}\phi_i&=\omega t+(\omega/c)x, \quad \phi_r=\omega t-(\omega/c)x,\\ \phi_n&=\omega t+(M\omega/c)x.\end{aligned} \tag{13}$$

Since the phase $\phi=\omega t-lx$ of any wave is invariant to a Lorentz transformation, it follows that $(l, 0, 0, i\omega/c)$ is a four-vector and so transforms like $(x, 0, 0, ict)$. Hence, in the frame S' we have

$$\left.\begin{aligned}l'&=\beta(l+\omega U/c^2)\\ \omega'&=\beta(\omega+Ul)\end{aligned}\right\}, \tag{14}$$

where

$$\beta=(1-U^2/c^2)^{-\frac{1}{2}}.$$

Also the field components of this wave are given by

$$\left.\begin{aligned}E_2'&=\beta(E_2+UH_3/c), \quad H_2'=\beta(H_2-UE_3/c)\\ E_3'&=\beta(E_3-UH_2/c), \quad H_3'=\beta(H_3+UE_2/c)\end{aligned}\right\}. \tag{15}$$

The Poynting flux in S is

$$P=(E_2H_3-E_3H_2)/4\pi,$$

and so, by (15), the flux in S' is

$$P'=\beta^2(1+U/c)^2P/4\pi.$$

i.e.,

$$P'=KP, \tag{16}$$

where

$$K=(1+U/c)/(1-U/c). \tag{17}$$

For the three waves considered we have from (13)

$$\begin{aligned}\omega_i&=\omega, \quad l_i=-\omega/c,\\ \omega_r&=\omega, \quad l_r=\omega/c,\\ \omega_n&=\omega, \quad l_n=-M\omega/c,\end{aligned}$$

and so by (14) we have in S'

$$\left.\begin{aligned}\omega_i'&=\beta(1-U/c)\omega, \quad l_i'=\beta(1-U/c)\omega/c\\ \omega_r'&=\beta(1+U/c)\omega, \quad l_r'=\beta(1+U/c)\omega/c\\ \omega_n'&=\beta(1-MU/c)\omega, \quad l_n'=\beta(-M+U/c)\omega/c.\end{aligned}\right\} \tag{18}$$

Hence,

$$\omega_r'/\omega_i'=K, \tag{19}$$

$$\omega_n'/\omega_i'=(1-MU/c)/(1-U/c). \tag{20}$$

Also by (16) and (17) we have

$$P_i'=K^{-1}P_i, \quad P_r'=KP_r,$$

and so, on using (12) we find

$$\rho'=\frac{P_r'}{P_i'}=\left(\frac{1+U/c}{1-U/c}\right)^2\left|\frac{1-M}{1+M}\right|^2=K^2\rho. \tag{21}$$

We now consider in turn the two important cases in which the magnetic field is, respectively, longitudinal and transverse to the electron beam.

In the first case, where the magnetic field is parallel to the electron beam, the refractive index M in the frame S is given by

$$M=\{1-p_0^2/\omega(\omega-k_n\Omega)\}^{\frac{1}{2}}, \tag{22}$$

where $p_0^2=4\pi Ne^2/m_0$, $\Omega=-He/m_0c$, $k_n=\pm1$, and ω is the wave angular frequency in S.

Since by (21) ρ' is the coefficient of reflection in S' of a wave of frequency ω_i', M is now given by (22) with $\omega=\omega_i'\sqrt{K}$, i.e., by

$$M=\{1-p_0^2/\omega_i'K^{\frac{1}{2}}(\omega_i'K^{\frac{1}{2}}-k_n\Omega)\}^{\frac{1}{2}}. \tag{23}$$

To an observer at rest in S', (19) and (21) give the frequency multiplication $\mu=\omega_r'/\omega_i'$ and intensity amplification $\alpha=P_r'/P_i'$, which are caused by reflection from the moving slab of electrons. Since $\mu=K$ and $\alpha=K^2$, it follows that only α depends on ρ.

When M is real and $\ll1$ or $\gg1$, or when M is purely imaginary, then $\alpha=K^2$ and the slab behaves like a perfect mirror in motion.

It is interesting to note that when $M=U/c$ then $\rho'=1$, i.e., the moving slab reflects like a perfect mirror at rest (i.e., without amplification) but multiplies the frequency by K. So when $U\sim c$ we have $M\sim1$ and may use a beam of low density for frequency multiplication. However, since there is no amplification this case will probably not be important in practice.

A low density can also be used with amplification ($\alpha=K^2$) when $|M|\gg1$, i.e., by (23) when $k_n\Omega>0$ and

$$\omega_i'\sim|\Omega|/\sqrt{K}=1.77\times10^7H/\sqrt{K}. \tag{24}$$

This requires the proper choice of the direction of the

magnetic field H, and a value of H which is $\sqrt{K}$ times larger than that corresponding to a gyrofrequency equal to the frequency of the incident wave. For example, for an incident 3-cm wave the magnetic field would need to be about $3300\sqrt{K}$ gauss; hence, K could easily be as high as 25. If H_m and K_m are the practically maximum possible values of H and K, respectively, then

$$\left.\begin{aligned}\omega_i' &= 1.77\times 10^7 H_m/\sqrt{K_m},\\ \omega_r' &= 1.77\times 10^7 H_m\sqrt{K_m}.\end{aligned}\right\} \tag{25}$$

Thus, if $H_m=20{,}000$ gauss and $K_m=94$ (corresponding to 2-Mev electrons), we have $\lambda_i'=5.2$ cm, $\lambda_r'=0.55$ mm and an amplification $\alpha=8900$. The resonance required here is the less critical the higher the electron density.

Equation (20) suggests also that the wave inside the medium will have a multiplied frequency when $|M|U \ll c$ or $\gg c$. But the observable wave intensity is then very much diminished.

For the other case of interest, where the magnetic field is transverse to the electron beam, the equation of dispersion (22) is replaced by the equations

$$M=(1-p_0^2/\omega^2)^{\frac{1}{2}} \tag{26}$$

and

$$M=\{1-p_0^2(\omega^2-p_0^2)/\omega^2(\omega^2-p_0^2-\Omega^2)\}^{\frac{1}{2}}, \tag{27}$$

which relate to linearly polarized waves in the frame S with their electric vectors, respectively, parallel and perpendicular to the magnetic field.

Transforming to the frame S' by replacing ω in (26) and (27) by $\omega_i'\sqrt{K}$, we find, as before, that the frequency multiplication $\mu=K$ is independent of the coefficient of reflection ρ, but the intensity amplification $\alpha=K^2\rho$ depends on ρ. Also, as before, when M is real and $\ll 1$ or $\gg 1$, or when M is pure imaginary, then $\alpha=K^2$. When $M=U/c$ and $U\sim c$ we may again use a beam of low intensity for frequency multiplication, but again we lose the advantage of amplification.

A low density can also be used with amplification of intensity ($\alpha=K^2$) when the wave's electric vector is perpendicular to the magnetic field and $|M|\gg 1$, i.e., by (27), when

$$\omega_i'\sim\{(\Omega^2+p_0^2)/K\}^{\frac{1}{2}}.$$

If $p_0^2\ll\Omega^2$, i.e., $(4\pi Nec)^2\ll H^2$, this last condition reduces to (24), and we are led to the same formulas (25) and conclusions as in the case in which the magnetic field is parallel to the electron beam.

It thus appears that simultaneous frequency multiplication and wave amplification is possible both with and without a magnetic field; but the presence of a longitudinal or transverse magnetic field of suitable strength allows this to be done with beams of lower electron density.

VI. CONCLUSION. EXPERIMENTS PLANNED

Irrespective of how one may visualize the reflection process, it is not possible to state in simple terms how much of the energy is reflected in such a direction as to be detected at a higher frequency in the laboratory frame, since this also depends amongst other factors on the band width of the detecting device. However, certain simple considerations lead one to believe that the useful part of the radiation differs from the total radiation by a factor not very different from $\frac{1}{2}$.[5] This factor has not been taken into account in the following discussion.

Referring to the numerical example of Sec. IV, we may now introduce the relativistic increase of intensity and select a suitable value of K from Table I. If we aim at the very moderate value $K\sim 30$, which requires only about 1 Mev, the total radiation from the beam at the frequency 3×10^5 Mc/sec ($\lambda=1$ mm) should be about 10 mw.

From this estimate we conclude that, by using the frequency conversion and wave amplification indicated by the foregoing theory, it should be possible to generate waves of wavelength equal to a small fraction of a millimeter and of useful intensity. It is hoped to verify the theoretical conclusions and produce such short waves in this laboratory with the help of a small betatron at present under construction. It is clear that a van de Graaff machine or linear accelerator of corresponding energy would make the experimental work easier because the electron density in the beams of these machines is much higher than in a betatron. But such instruments are not available in this laboratory. On the other hand, a betatron has the advantage that the disturbing γ-radiation may be largely eliminated by omitting the target. It is also hoped that by a slight elaboration of the method of observation planned for these experiments it may be possible to investigate the transverse Doppler effect which, as far as we are aware, has not hitherto been observed.

This problem arose out of work on wave amplification in ionized media carried out by the writer in association with Professor Bailey.

[5] From more accurate calculations carried out by Motz (reference 1) it appears that this factor is 1/20 for a 10 percent spread of frequency. However, the value of the field strength assumed in our numerical example for the "original" wave (100 volts/cm) was purposely chosen very small. There is no difficulty in increasing this value at least one hundredfold.

Nonlinear Meson Theory of Nuclear Forces. III. Quantization of the Neutral Scalar Case with Nonlinear Coupling

L. I. SCHIFF
Stanford University, Stanford, California
(Received March 3, 1952)

The problem of a number of infinitely massive point nucleons interacting according to the neutral scalar meson theory with a nonlinear coupling of the power-law type was considered classically in an earlier paper. It was found there that the interaction is the same as with the usual linear coupling. This system is now quantized, and it is shown that the same conclusion is valid in quantum theory. The case of exponential coupling, considered by Glauber, lies outside the scope of the present investigation.

IN two earlier papers, a classical nonlinear meson theory of nuclear forces was presented.[1] The neutral scalar theory with nonlinearity in the field was discussed in I, and the similar theory with nonlinearity in the coupling was considered in II. The quantization of the latter case with infinitely massive point nucleons can easily be carried through with the help of a simple canonical transformation. When this is done it is found that the earlier conclusion, that the interaction of a number of nucleons is the sum of Yukawa terms regardless of whether the coupling is linear or nonlinear, still holds in quantum theory provided the coupling is of the power-law form.

The field Hamiltonian is

$$H=\int[\tfrac{1}{2}\pi^2+\tfrac{1}{2}(\nabla\phi)^2+\tfrac{1}{2}\phi^2-f(\mathbf{r})F(\phi)]d\tau,$$

where ϕ and π are the meson field amplitude and canonically conjugate momentum, f is the nucleon source density, F is the nonlinear coupling function, and units are chosen such that $\hbar$, c, and the meson mass are equal to unity. The quantum condition on the field is

$$[\phi(\mathbf{r},t),\pi(\mathbf{r}',t)]=i\delta(\mathbf{r}-\mathbf{r}').$$

The canonical transformation[2]

$$S=\exp\left[i\int\phi_0(\mathbf{r})\pi(\mathbf{r})d\tau\right],$$

where ϕ_0 is a c-number function that commutes with ϕ and π, has the following effects:

$$S\phi S^*=\phi+\phi_0,\quad S\pi S^*=\pi,$$

$$SHS^*=\int[\tfrac{1}{2}\pi^2+\tfrac{1}{2}(\nabla\phi+\nabla\phi_0)^2+\tfrac{1}{2}(\phi+\phi_0)^2-f(\mathbf{r})F(\phi+\phi_0)]d\tau$$

$$=\int[\tfrac{1}{2}(\nabla\phi_0)^2+\tfrac{1}{2}\phi_0^2-f(\mathbf{r})F(\phi_0)]d\tau$$

$$+\int[\tfrac{1}{2}\pi^2+\tfrac{1}{2}(\nabla\phi)^2+\tfrac{1}{2}\phi^2]d\tau$$

$$+\int\phi[-\nabla^2\phi_0+\phi_0-f(\mathbf{r})F'(\phi_0)]d\tau$$

$$-\int f(\mathbf{r})[\tfrac{1}{2}\phi^2F''(\phi_0)+\cdots]d\tau.$$

If now ϕ_0 is chosen to be the solution of the classical field equation given in II, Eq. (1), the third line of the last expression for the transformed Hamiltonian given above is identically zero, and the first line is just the classical Hamiltonian treated in II. The second line is the quantum Hamiltonian for free mesons and need not be discussed further. We now show that the fourth line, which contains the rest of the terms in the Taylor's series expansion of $F(\phi+\phi_0)$, vanishes if f represents a number of point nucleons and if F has the power-law form $F(\phi)=b\phi^m$.

Consider the contribution to the nth derivative term that arises from one of the nucleons. The factor ϕ^n can be evaluated at the nucleon and taken outside the integral, and the rest is proportional to the limit as a approaches zero of $g(d^nF/d\phi_0^n)$, where g is the single nucleon source strength and a is the radius of the source. Now the nth derivative of F is proportional to ϕ_0^{m-n}; from II, Eq. (5), ϕ_0 is proportional to $1/a$, and from II, Eq. (7), g is proportional to a^{m-1}. Thus, the term in question is proportional to a^{n-1} and approaches zero in the limit $a\to 0$ if $n\geqq 2$, as it is for all the terms in the fourth line of the expression for the transformed Hamiltonian.

The foregoing development shows that the quantum interaction energy is the same as that calculated classically in II and, hence, does not lead to saturation. The case in which the nonlinear function F has an exponential dependence on ϕ, considered recently by Glauber,[3] cannot be handled as simply as the power-law case, since the F derivative terms do not then vanish in the point source limit.

It should be noted, as pointed out in II, that the conclusions reached here are valid only for point nucleons and, hence, will not be expected to hold, for example, when nucleon recoil is taken into account.

[1] L. I. Schiff, Phys. Rev. **84**, 1, 10 (1951); referred to here as I and II, respectively. The notation of the present paper is the same as that used in these references.

[2] This transformation was also applied independently to the nonlinear field case considered classically in I, by D. R. Yennie and M. Gell-Mann (private communication).

[3] R. J. Glauber, Phys. Rev. **84**, 395 (1951).

Nuclear Energy Levels of Al^{27}†

E. M. Reilley,* A. J. Allen, J. S. Arthur, R. S. Bender, R. L. Ely,‡ and H. J. Hausman
University of Pittsburgh, Pittsburgh 13, Pennsylvania

(Received February 18, 1952)

Twenty energy levels in Al^{27} have been found by the magnetic analysis of inelastically scattered protons at 90° from thin targets of aluminum. An analyzed beam of 8.0-Mev protons was utilized for the bombardment. Tentative values for the levels found are 0.844, 1.016, 2.259, 2.782, 3.046, 3.736, 4.018, 4.115, 4.473, 4.575, 4.647, 4.875, 4.996, 5.107, 5.220, 5.341, 5.501, 5.565, 5.620, 5.736 Mev. A broad alpha-particle group from the $Al^{27}(p,\alpha)Mg^{24}$ reaction corresponding to an excited state of Mg^{24} was also observed and is believed to be complex.

INTRODUCTION

WILKENS and Kuerti[1,2] were the first to report on the measurement of the energy levels of aluminum by observation of inelastic scattering of protons. Since then, additional studies of this same nucleus have been made by several observers both by inelastic scattering experiments[3–8] and by other nuclear reactions.[9,10] In the experiment to be described, a large magnetic spectrometer was utilized for the measurement of energy of charged particles emitted from an aluminum foil target bombarded with a beam of magnetically analyzed 8-Mev protons.

APPARATUS

Details of the apparatus have been published elsewhere.[11] The proton beam was produced by the 47-inch University of Pittsburgh cyclotron. A large focusing magnet, placed about seven feet from the cyclotron vacuum tank, focused the beam on the entrance slits of a beam analyzer magnet which was located in an adjacent room. An eight-foot thick shielding wall separated this room from the cyclotron chamber. After traversing the beam analyzer field the beam was limited by stops to an angular extent of ±3 degrees horizontally and passed through a final analyzer slit, $\frac{1}{16}$ inch wide and $\frac{7}{8}$ inch high which limited the beam energy spread to 20 kev. Targets were placed at the center of a large scattering chamber at a distance of 1.75 inches from the final beam analyzer slit.

A large 60°-sector magnetic spectrometer was positioned at an angle of 90° with respect to the beam center. Charged particles emitted from the target were focused by this magnetic lens on a scintillation screen mounted external to the vacuum system. A 0.1-mil nickel foil served as the window. Stops were provided to limit the angular aperture to ±2° with respect to the center line of the system.

Field excitation currents for the three magnets were obtained from motor-generator sets which were electronically stabilized. The magnetic field of the beam focusing magnet was adjusted so as to yield maximum beam on the entrance slit of the beam analyzer. The magnetic fields in the beam and particle analyzers were measured by means of the proton magnetic resonance method[12] to one part in 10,000 and were continuously monitored during the experiment. Target beam currents of 0.5 to 1.0 microamperes were obtained.

In order to provide uniform bombardments, an insulated Faraday cup was placed behind the target so as to collect the beam. This cup was connected to a precharged polystyrene condenser, the potential of which was monitored by means of a Lindeman-Ryerson electrometer. A switching arrangement was provided so as to permit termination of the counting period when the electrometer indicated zero potential.

Scintillation counters consisting of a phosphor screen and either an RCA type 5819 or an EMI 5311 photomultiplier tube were used as particle detectors. Rather thick layers of silver-activated zinc sulfide deposited on glass slides from alcohol-water suspensions were found to be satisfactory for initial survey work. These had adequate sensitivity for both alpha-particles and protons and yet were comparatively insensitive to the gamma-ray background. Thin deposits of this same phosphor were found to be useful in obtaining discrimination in counting alpha-particles in the presence of undesired protons. A selsyn-controlled absorption-foil shutter was mounted immediately in front of the scintillation screen so that alpha-particles could be stopped when desired. This shutter carried a number of aluminum foils of different thickness. Pulses from the photomultiplier tube were fed by a cathode follower through a long matched coaxial line to a separate room and further amplified by a Jordan and Bell type linear

† Work done in the Sarah Mellon Scaife Radiation Laboratory and assisted by the joint program of the ONR, AEC, and the Research Corporation.

* Now at Camp Evans Signal Laboratories, Belmar, New Jersey.
‡ Now at Westinghouse Atomic Power Division, Bettis Field, Pittsburgh, Pennsylvania.

[1] T. R. Wilkens, and G. Kuerti, Phys. Rev. **57**, 1082 (1940).
[2] T. R. Wilkens, Phys. Rev. **60**, 365 (1941).
[3] R. H. Dicke and J. Marshall, Phys. Rev. **59**, 914 (1941).
[4] E. M. Hafner, Ph.D. thesis, University of Rochester (1948).
[5] E. H. Rhoderick, Proc. Roy. Soc. (London) **201**, 348 (1950).
[6] Brolley, Sampson, and Mitchell, Phys. Rev. **76**, 624 (1949).
[7] H. W. Fulbright and R. R. Bush, Phys. Rev. **74**, 1323 (1948).
[8] K. K. Keller, Phys. Rev. **84**, 884 (1951).
[9] Swann, Mandeville, and Whitehead, Phys. Rev. **79**, 598 (1950).
[10] VanPatter, Sperduto, and Enge, Phys. Rev. **83**, 212 (1951).
[11] Bender, Reilley, Allen, Ely, Arthur, and Hausman, Rev. Sci. Instr. (to be published).
[12] R. V. Pound and W. D. Knight, Rev .Sci. Instr. **21**, 219 (1950).

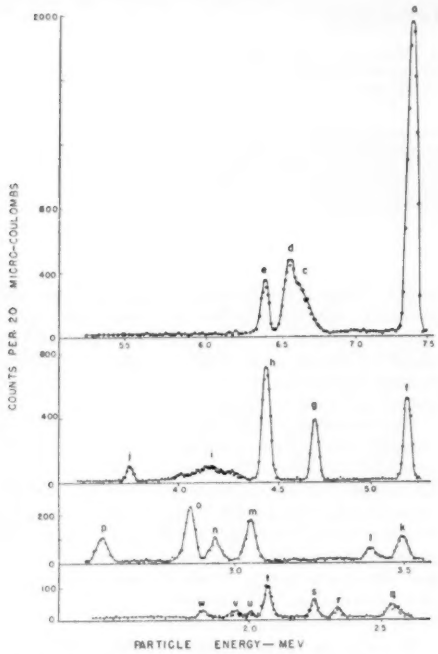

FIG. 1. Spectrum of magnetically analyzed particles obtained at 90° and Al^{27} bombarded by 8-Mev protons.

amplifier. The amplified pulses were fed into three pulse-height discriminators, each set at a different level and each connected to a separate scaling circuit. This counting arrangement permitted crude pulse-height analysis to be made and indicated whether protons, deuterons, or alpha-particles were being counted during initial searches for charged particle groups.

CALIBRATION

The spectrometer was calibrated by using alpha-particles from a polonium deposit on a nickel plate which was inserted in the normal target position. The $B\rho$ value assumed for these particles was 3.3159×10^5 gauss-cm[13] which corresponds to an energy of 5.298 $\pm$0.002 Mev. Since the magnetic fields were always measured in terms of the frequency of proton magnetic resonance, the spectrometer constants were calculated in terms of frequency. The spectrometer constant[11] for alpha-particles (C_α) was found to be $(1.0363\pm0.002)\times10^{-14}$ Mev-sec^2, and the constant for protons (C_p) was found to be $(1.0292\pm0.002)\times10^{-14}$ Mev-sec^2. Group energies calculated from these constants and from the magnetic resonance frequencies corresponding to the centers of the groups were corrected for energy loss in the target and for relativistic shift.

RESULTS

A spectrum obtained from the bombardment of a 0.14 mg/cm^2 foil target is shown in Fig. 1. Spectroscopic analysis showed that there was less than 0.1 percent of Na, Cu, and Fe in the target. Twenty inelastic proton groups were observed, nineteen appearing in this particular run. Two alpha-particle groups from the $Al^{27}(p,\alpha)Mg^{24}$ reaction corresponding to excitation of the 1.38-Mev and 4.14-Mev levels in Mg^{24} were found. These two are labelled "*c*" and "*i*"§ in the figure. Carbon deposits which formed during bombardment contributed another proton group which does not appear in Fig. 1 since these data were obtained immediately after a clean target was inserted. The proton group "*d*" was superimposed on the alpha-group "*c*" and was isolated by insertion of a 10 mg/cm^2 absorbing foil between the spectrometer exit-slit and scintillation detector.

The energy resolution obtained for these groups was about one percent. The width of the groups was attributed to several sources: (1) the proton beam had a half-width of 20 kev; (2) the angular acceptance of the spectrometer plus the angular divergence of the beam contributed 45 kev to the width of 6 Mev; (3) the finite resolution of the spectrometer ($\frac{1}{16}$-in. source and exit slit widths) contributed 31 kev to the width at 6 Mev.

The measured line shapes were quite good fits to a normal distribution function and exhibited little asymmetry. Application of Pearson's chi-square test to the data for five of the most intense inelastic groups resulted in an average probability of 0.5 for the normal dis-

TABLE I. Energy levels of aluminum.

Present work	Alburger and Hafner	Keller	Shoemaker *et al.*	VanPatter
0.844	0.84		0.82	0.86
1.016	1.02	0.97	1.045	1.02
	1.85			
2.259	2.15	2.39	2.225	2.12
2.782	2.78		2.75	2.72
3.046	3.04	3.17		
3.736	3.7			
4.018				
4.115				
4.473	4.3			
4.575				
4.647		4.74		
4.875				
4.996				
5.107				
5.220				
5.341	5.3			
5.501				
5.565				
5.620				
5.736	5.8	5.76		

[13] VanPatter, Sperduto, Huang, Strait, and Buechner, Phys. Rev. **81**, 233 (1951).

§ *Note added in proof:* Subsequent investigations have shown peak "*i*" to be a doublet, corresponding to levels in Mg^{24} at 4.11 and 4.21 Mev.

tribution. Since a chi-square probability of 0.01 is considered satisfactory,[14] the lines were assumed to be normal in shape, and line centers were determined from the computed "best-fit" curves.

The energy levels determined for Al^{27} are shown in Table I and Fig. 2. The probable errors in these have been estimated as being 0.020 Mev from the uncertainty in determination of the group centers and from the uncertainty in the calibration constant. In Table I the levels listed by Alburger and Hafner,[15] which were the result of a literature survey covering the work reported before 1950, are given, along with more recent data reported by Keller,[8] by Van Patter, Sperduto, and Enge,[10] and by Shoemaker, Faulkner, Bouricius, Kaufmann, and Mooring.[16] It will be noted that in this experiment no scattering was observed corresponding to excitation of the 1.85-Mev level. Ten levels which were not previously reported were found.

We wish to acknowledge the help received from Dr. D. Halliday, Dr. L. Page, Dr. P. Stehle, from Mr. E. Perkins, Mr. R. Weise, Mr. J. Kane, as well as from the many other members of the Laboratory who have taken an interest in this project.

FIG. 2. Energy level scheme for Al^{27}.

[14] A. G. Worthing and J. Geffner, *Treatment of Experimental Data* (John Wiley & Sons, Inc., New York, 1946), pp. 183–184.
[15] D. E. Alburger and E. M. Hafner, Revs. Modern Phys. **22**, 373 (1950).
[16] Shoemaker, Faulkner, Bouricius, Kaufmann, and Mooring, Phys. Rev. **83**, 1011 (1951).

PHYSICAL REVIEW VOLUME 86, NUMBER 6 JUNE 15, 1952

Inelastic Scattering of Protons from Nickel*

RALPH ELY, JR.,† A. J. ALLEN, J. S. ARTHUR, R. S. BENDER, H. J. HAUSMAN, AND E. M. REILLEY‡
University of Pittsburgh, Pittsburgh 13, Pennsylvania
(Received February 18, 1952)

By use of the equipment developed for the precision scattering project at the University of Pittsburgh, inelastic scattering of 8-Mev protons from a thin nickel target has been observed at 90°. The energy levels obtained for natural nickel are 1.344, 1.479, 2.186, 2.326, 2.501, 2.660, 2.814, 2.946, 3.081, 3.161, 3.226, 3.308, 3.462, 3.575,3 .646, 3.773, 3.823, 3.944, 3.979, and 4.066 Mev. At present, only the three levels 1.344, 1.479, 2.501 Mev can be assigned to nickel 60 from comparison with beta-decay of cobalt 60.

INTRODUCTION

ENERGY levels in nickel have been observed by the inelastic scattering of protons from a nickel foil. The apparatus and method of analysis of the data are the same as that of the preceding paper.[1] Dicke and Marshall,[2] with incident protons of 6.9 Mev, were unable to observe any levels in nickel. Fulbright and Bush,[3] using 5–17 Mev protons from the Princeton cyclotron, reported one weak level in nickel at 3.8 Mev as well as a broad band of tracks in the photographic emulsion used for detection. This broad band suggests either that a three-particle disintegration is occurring or that the levels are too close to be resolved with their equipment. In the present study, twenty energy levels have been observed.

The target (obtained from the Chromium Corporation of America) was a nickel foil of areal density 0.592 ± 2.5 percent mg/cm^2. Spectroscopic analysis showed less than 0.01 percent of copper in the target. The source and analyzer slits were $\frac{1}{4}$-inch wide. In all other respects the experimental details were essentially as reported in the preceding paper.

* Work done in the Sarah Mellon Scaife Radiation Laboratory and assisted by the joint program of the ONR and AEC and the Research Corporation.
† Now at Westinghouse Atomic Power Division, Bettis Field, Pittsburgh, Pennsylvania.
‡ Now at Camp Evans Signal Laboratories, Belmar, New Jersey.
[1] Reilley, Allen, Arthur, Bender, Ely, and Hausman, Phys. Rev. **86**, 857 (1952).
[2] R. H. Dicke and J. Marshall, Phys. Rev. **63**, 86 (1943).
[3] H. W. Fulbright and R. R. Bush, Phys. Rev. **74**, 1323 (1948).

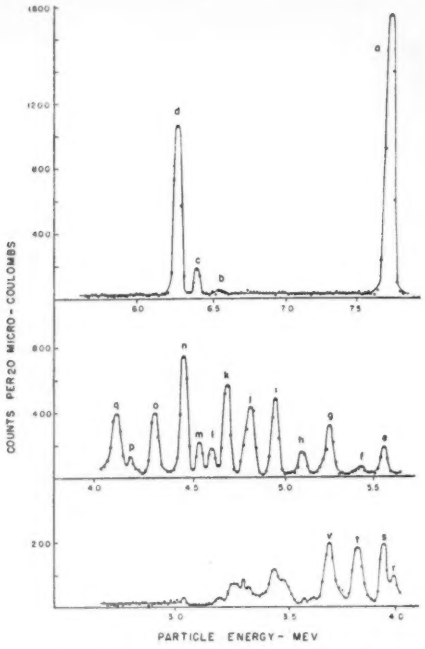

FIG. 1. Spectrum of protons scattered from nickel at 90°.

RESULTS

Figure 1 shows the energy spectrum obtained for 8-Mev protons scattered from nickel at 90°. Inserting absorption foils in front of the detector shows that all are proton peaks. Peak "*a*" is the nickel elastic peak, while "*b*" is the elastic peak caused by a thin carbon deposit which formed during bombardment. Table I shows the energies of the resultant levels; they are corrected for recoil nucleus, relativistic, and target energy loss effects. A probable error of the order of 20 kev seems reasonable. Below 3.6 Mev in Fig. 1 are several partially resolved peaks. Tentative but questionable assignment of these peaks are: 4.29, 4.33, 4.44, 4.47, and 4.50 Mev.

Figure 2 shows the energy level scheme for nickel. Brady and Deutsch,[4] from beta-decay of Co^{60}, report levels of 1.33 Mev and 2.50 Mev in Ni^{60}. The third level is at 1.5 Mev in Ni^{60} as reported by Leith, Bratenahl, and Moyer[5] from positron decay of Cu^{60}. The remaining levels are as yet unassigned to a particular isotope. The level obtained by Fulbright and Bush[3] is shown at 3.8 Mev.

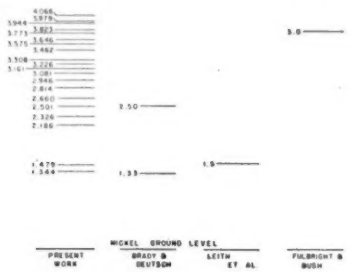

FIG. 2. Energy level scheme for nickel.

TABLE I. Energy levels of nickel.

Level	Energy Mev	Brady and Deutsch Mev	Leith *et al.* Mev	Fulbright and Bush Mev
c	1.344	1.33		
d	1.479		1.5	
e	2.186			
f	2.326			
g	2.501	2.50		
h	2.660			
i	2.814			
j	2.946			
k	3.081			
l	3.161			
m	3.226			
n	3.308			
o	3.462			
p	3.575			
q	3.646			
r	3.773			
s	3.823			3.8
t	3.944			
u	3.979			
v	4.066			

We wish to acknowledge the help received from Dr. D. Halliday, Dr. L. Page, Dr. P. Stehle, Mr. E. Perkins, Mr. R. Weise, and Mr. J. Kane, as well as from the many other members of the Laboratory who have taken an interest in this project.

[4] E. L. Brady and M. Deutsch, Phys. Rev. **74**, 154 (1948).
[5] Leith, Bratenahl, and Moyer, Phys. Rev. **72**, 732 (1947).

The Scattering of Fast Neutrons by Wolfram*

C. E. MANDEVILLE, C. P. SWANN, AND F. J. SEYMOUR
Bartol Research Foundation, Franklin Institute, Swarthmore, Pennsylvania
(Received December 31, 1951)

Employing good geometry, homogeneous fast neutrons of energy 4.3 Mev, supplied by the *d-d* reaction in the Bartol Van de Graaff statitron, have been scattered in wolfram. Using binocular microscopes and Eastman NTA plates, twenty-four thousand fields of view were examined to obtain 2700 acceptable recoil proton tracks. The distribution in energy of the inelastically scattered neutrons is obtained. It is roughly estimated that the inelastic scattering cross section at 4.3 Mev is less than three-fourths as great as the elastic one.

INTRODUCTION

EMPLOYING several different primary neutron energies the maximum of which was 3 Mev, Barschall *et al.*[1] have investigated the inelastic scattering of fast neutrons in wolfram and other elements. Their measurements have been subsequently interpreted by Feld.[2] The measurements of the present paper were carried out with a geometry and general method which have been previously described[3] in their application to the particular cases of the scattering of fast neutrons by bismuth and lead. In these previously reported measurements[3] unfavorable conditions of background were encountered, and it was found to be impossible to give an accurate estimate of the cross section for inelastic scattering. Many months of plate reading and analysis were required to establish the undesirable features of the method, and during that time the exposure for wolfram had been carried out. Consequently, it has been decided to present the results, recognizing that certain difficulties are inherent in the analysis and interpretation.

THE MEASUREMENTS

Monochromatic fast neutrons of energy 4.3 Mev, produced in the deuteron-deuterium reaction, were scattered in a scatterer of metallic wolfram, having an average length of 4 cm. The bombarding deuterons were supplied by the Bartol Van de Graaff statitron. With no scatterer present the curve of Fig. 1(A) was obtained. With scatterer in position, the curve of Fig. 1(B) resulted. These curves have been normalized to take into account bombarding time and plate area scanned. The principal group of particles in Fig. 1(B) is composed of primary neutrons, those which passed through the scatterer without suffering a scattering collision of any kind, and neutrons which have been elastically scattered. The broken line of Fig. 1(B) is a plot of the principal group using the shape of Fig. 1(A). From Fig. 1(B) it is clear that insertion of the scatterer has shifted the peak of the curve slightly and broadened it somewhat, giving evidence of elastic scattering. As in the previous paper the energy interval 0.2 Mev$\leq E_n \leq$3.7 Mev has been designated as the region of inelasticity. A detail of the results of this region is shown in Fig. 2. The data without scatterer are represented by the open circles, whereas those obtained with scatterer in position are indicated by the closed circles. These data have been plotted in energy intervals of 0.2 Mev. The open circles are not, however, taken to be the true background. It was demonstrated in the case of neutron scattering by bismuth[3] that the background without scatterer is greatly reduced by scattering of the background neutrons with scatterer in position. To obtain the appropriate background with scatterer in position, the open circles of Fig. 2 have been reduced by the factor $\exp(-n_w\sigma_w x)$, where n_w is the number of wolfram atoms per cc, σ_w the total scattering cross section for wolfram, and $x=4$ cm, the average length of the wolfram scatterer. The product $n_w\sigma_w$ was, of course, evaluated as a function of energy, on each energy

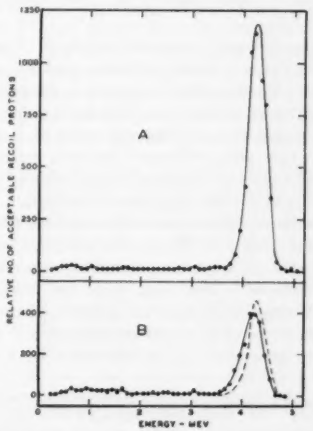

FIG. 1. Curve *A* is the "background run" or energy distributions of neutrons with no scatterer. Curve *B* was observed with the wolfram scatterer in position. The two curves were "normalized" to take into account irradiation time and plate area scanned.

* Assisted by the joint program of the ONR and AEC.
[1] Barschall, Battat, Bright, Graves, Jorgensen, and Manley, Phys. Rev. **72**, 881 (1947); Barschall, Manley, and Weisskopf, Phys. Rev. **72**, 875 (1947).
[2] B. T. Feld, Phys. Rev. **75**, 1115 (1949).
[3] C. E. Mandeville and C. P. Swann, Phys. Rev. **84**, 214 (1951).

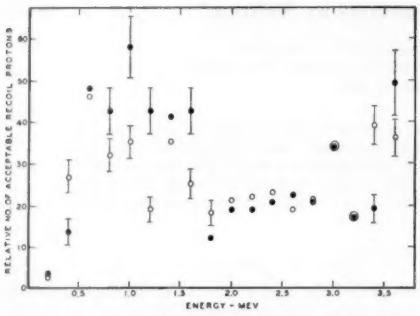

FIG. 2. Distribution of neutron energies less than or equal to 3.7 Mev collected with and without the wolfram scatterer in position. The data are plotted in energy intervals of 0.20 Mev. The open circles refer to the "background run" with no scatterer, and the closed circles to data obtained with scatterer in position.

interval of width 0.2 Mev. Thus, letting I_{0j} be the number of tracks on the jth interval of the "background run," and letting I_j be the background with scatterer in position, I_j can be calculated. The total number of background tracks on the large interval, 0.2 Mev$\leq E_n \leq$3.7 Mev, is given by

$$I_0=\sum_1^N I_{0j},$$

and the total number of background tracks in the region of inelasticity with scatterer in position may be calculated from

$$I=\sum_1^N I_j=\sum_1^N I_{0j}\exp[-n_w(\sigma_w)_j x].$$

The observed and calculated values of I and I_0 are given in Table I, where it is seen that I calculated is 95±3 tracks, the actual observed I_0 without scatterer being 471±15 tracks. This calculated value of I is to be compared with an observed value of I of 524±21 tracks. This great difference between calculated and observed values of I is taken to be evidence for inelastic scattering of 4.3-Mev neutrons in wolfram.

Considerable debate has centered about the fact that the open circles of Fig. 2, the observed background tracks with no scatterer present, show an increase in the vicinity of 1 Mev, just as do the closed circles of data obtained with scatterer present. These tracks in the case of the open circles are presumed to arise from neutrons generated in the reaction $C^{12}(d,n)N^{13}$, since carbon may be present as a contaminant on the target of D_2O. If these neutrons originate at the target and proceed to the photographic plates without having been first scattered about the observation room, they will certainly be reduced in intensity when the scatterer is placed in position. From Fig. 2 it is evident that considerably more neutrons are encountered in the vicinity of 1 Mev with scatterer in position. Most of these are evidently inelastically scattered ones, since those of any carbon contamination would be reduced in each energy interval by the factor $\exp(-n_w\sigma_w x)$. It has been argued that perhaps the neutrons from $C^{12}(d,n)N^{13}$ are room scattered to give the tracks of the closed circles in the vicinity of 1 Mev with scatterer in position, and that the assumption that the background emanates primarily from the direction of the target is incorrect, contrary to the findings of the bismuth measurements.[3] Further evidence that the background neutrons do emanate from the target area may be cited as follows. Many targets of light nuclei have been irradiated by deuterons supplied by the Bartol Van de

TABLE I. Number of tracks calculated and observed in the inelastic region, for W.

Observed I_0	Observed I	Calculated I
471±15	524±21	95±3

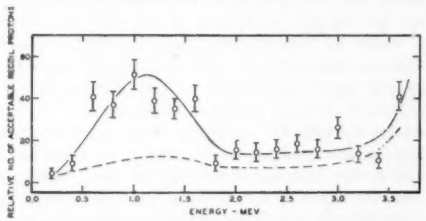

FIG. 3. Distribution in energy of 4.3-Mev neutrons inelastically scattered in wolfram. The broken line is the distribution after correction for variation with energy of n-p scattering cross section and acceptance probability.

Graaff statitron. The neutrons from $C^{12}(d,n)N^{13}$ have often appeared in spectra observed in photographic plates placed at angles of zero and ninety degrees with the incident beam in the laboratory system of coordinate axes. These plates have always given evidence of a sharply defined group from $C^{12}(d,n)N^{13}$, exhibiting the proper energy shift with the angle of observation. This would not be the case were "room scattering" of the carbon neutrons an important factor. These irradiations were often of the same length in time as those of the scattering experiments and were carried out in a much less advantageous geometry from the standpoint of the reduction of background. The removal of the target of the scattering experiments to a point at a great distance from scattering materials has been previously described.[3]

CONCLUSIONS

As described above, the data of the open circles of Fig. 2 were reduced in each energy interval by the factor $\exp(-n_w\sigma_w x)$ and subtracted from the appropriate closed circle. After properly combining the sta-

tistical probable errors the curve of Fig. 3 was obtained. The broken line of Fig. 3 represents the distribution in energy of fast neutrons inelastically scattered in wolfram, corrected for variation with energy of the n-p scattering cross section and acceptance probability. The distribution appears to be for the most part constant with energy, rising somewhat in the region of lower energies. Using Fig. 1(B) and a method of analysis previously described,[3] it is estimated that at 4.3 Mev the inelastic scattering cross section is less than three-fourths as large as the elastic one for W.

The writers wish to acknowledge the continued interest of Dr. W. F. G. Swann, Director of the Bartol Research Foundation.

PHYSICAL REVIEW VOLUME 86, NUMBER 6 JUNE 15, 1952

Internal Conversion in I^{131}†

D. Rose,* G. Hinman, and L. G. Lang
Carnegie Institute of Technology, Pittsburgh, Pennsylvania
(Received February 27, 1952)

The β-radiations from the decay of I^{131} to Xe^{131} have been investigated in a large ($\rho=50$ cm) double-focusing β-ray spectrometer to determine the internal conversion coefficients for the 284-, 364-, 638-, and 724-kev γ-rays. The continuous β-spectrum is resolved into 3 components with end points of 338, 606, and 807 kev. Conclusions about the multipole character of the γ-ray transitions are made.

THE β-radiations from the decay of I^{131} to Xe^{131} have been investigated in a large ($\rho=50$ cm) double-focusing β-ray spectrometer[1] to determine the internal conversion coefficients for the 284-, 364-, 638-, and 724-kev γ-rays. Earlier work, prior to the time this investigation was started, on internal conversion coefficients in I^{131} due to Metzger and Deutsch,[2] Kern *et al.*,[3] and Feister,[4] is summarized in *Nuclear Data*.[5] For the 284- and 364-kev γ-rays, the results of references 2 and 4 are in agreement while both disagree with those of reference 3. The conversion coefficients for the 638- and 724-kev γ-rays had not been measured previously and the present investigation was undertaken to determine them. Conversion coefficients for the 284- and 364-kev γ-rays were also determined in an attempt to resolve the disagreement mentioned above, where possible, and as a check on our experimental method.

Three essentially weightless sources of I^{131} were prepared from solutions of "carrier-free" NaI (obtained from the Oak Ridge National Laboratory over a period of several months) by depositing the solution on 0.1 mg/cm² Ag foil on which a narrow line of Insulin solution had previously been deposited, and drying under a heat lamp. The Ag foil was backed with a zapon film of approximately 0.03 mg/cm² and covered over with another zapon film of about the same thickness. The strengths of the three sources were about 4 mc, 6 mc, and 10 mc, respectively; the second source was used in two runs.

Analysis of the Kurie plots resulted in the resolution of three β-components with endpoints of 338.6 ± 9.7, 605.9 ± 1.2, and 806.7 ± 10.0 kev, and relative intensities of (13.3 ± 0.3) percent, (84.7 ± 0.3) percent, and 1.4 percent, respectively. These results are the weighted means of three runs for the softest component and four runs for the other two components. The errors listed are probable errors. Until recently only two components of the β-spectra had been resolved[2,3,6,7] with the endpoint of the softer component varying from about 250 to 315 kev. While the present work was being carried out Verster *et al.*[8] reported the results of their investigation of I^{131}, in which they also resolved three β-components. Our results above generally agree with theirs, except for the intensity of the hard component, for which they report (0.56 ± 0.10) percent. The results of others, for example, Emery,[9] who gives the value (0.8 ± 0.1) percent as determined by means of a cavity

TABLE I. Results of internal conversion measurements in I^{131}. α_K is the K-shell internal conversion coefficient, N_K/N_L the ratio of K-shell to L-shell conversion electrons, and $N_K/(N_L+N_M)$ the ratio of K-shell to L- plus M-shell conversion electrons.

γ-ray energy (kev)	α_K	N_K/N_L	$\frac{N_K}{(N_L+N_M)}$
284	$0.036\ \pm0.002$	5.4 ± 1.2	5.2 ± 2.1
364	0.0174 ± 0.0001	6.6 ± 0.2	4.7 ± 0.3
638	0.0021 ± 0.0001		5.2 ± 0.9
724	0.0037 ± 0.0005		

* Now at Argonne National Laboratory, Chicago, Illinois.
† This work was partially supported by the AEC.
[1] G. W. Hinman, Atomic Energy Commission, New York Operations Report No. 912.
[2] F. Metzger and M. Deutsch, Phys. Rev. **74**, 1640 (1948).
[3] Kern, Mitchell, and Zaffarano, Phys. Rev. **76**, 94 (1949).
[4] I. Feister, private communication to *Nuclear Data* (National Bureau of Standards Circular 499, 1949), ref. 5.
[5] K. Way *et al.*, *Nuclear Data* (Natl. Bur. Standards Circular 499, 1949), p. 151.
[6] Cork, Keller, Sazynski, Ruthledge, and Stoddard, Phys. Rev. **75**, 1621 (1949).
[7] I. Fesiter and L. F. Curtiss, Phys. Rev. **78**, 179 (1950).
[8] N. F. Verster *et al.*, Physica **17**, 637 (1951).
[9] E. W. Emery, Phys. Rev. **83**, 679 (1951).

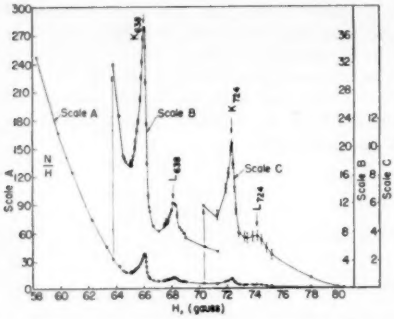

FIG. 1. Upper end of the momentum distribution of the negatrons from I^{131}. N is the intensity in counts per min, H the field strength in gauss. Scales for the ordinates of the magnified conversion peaks are shown at the right of the figure as scales B and C.

ionization chamber, substantiate their value for this component. We attribute the discrepancy to the effect of the background subtracted, which is larger than this weak β-component in the region beyond the 606 β-component. Inasmuch as the error in this hard component resulting from the background is larger than the errors computed on the basis of counting statistics, no error has been shown for the percentage of this component above. In any case, the effect of this component on the remainder of the spectrum is small and does not affect the values of the internal conversion coefficients. More recently Ketelle *et al.*,[10] by means of beta-gamma-coincidences, succeeded in resolving four components in the β-spectrum. We were unable to resolve this low intensity fourth component because of the large uncertainties in the least energetic component arising from successive subtraction of the β-components in the Kurie plot analysis.

For the calculation of the internal conversion coefficients, the number of conversion electrons arising from each γ-ray was determined from the area under the conversion peak after subtraction of the underlying continuous spectrum. The number of unconverted γ-rays was not measured directly. The total number of γ-rays, converted and unconverted, arising from each excited level was determined from the intensity of the β-decay branch leading to that level in those cases where the excited level was known to decay by emission of a single γ-ray, and, in addition, by the known branching ratio for the 364-kev level which is known to decay through two γ-rays in parallel. The ratio of the number, for example, of K-shell conversion electrons to the total number of γ-rays gives the quantity C_K related to the K-shell conversion coefficient, α_K, by the simple relation $C_K/(1-C_K)=N_e/N_\gamma$, where N_e = number of K-shell conversion electrons, and N_γ = number of unconverted γ-rays. These calculations of conversion coefficients are seen to be dependent on the decay scheme.

TABLE II. Comparison of calculated and experimental values of α_K. The last column lists the possible types of transitions.

γ-ray energy (kev)	Calculated values				Experimental values	Transition type
	E1	*E2*	*M1*	*E3*		
284.1	0.0107	0.0423	0.0446	0.147	0.036 ±0.002	*E2*, *M1*
364.2	0.00578	0.0201	0.0239	0.0625	0.0174 ±0.0001	*E2*
638	0.00152	0.00417	0.00588	0.0102	0.0021 ±0.0001	*E1*
724	0.00116	0.00305	0.00436	0.00713	0.0037 ±0.0005	*E2*, *M1*

[10] B. H. Ketelle *et al.*, Phys. Rev. **84**, 585 (1951).

Two different decay schemes for I^{131} have been proposed recently which are modifications of the earlier decay schemes of references 2 and 3 to include the additional β-branches. The difference lies in considering the 638-kev γ-ray as a cross-over transition from a level at about 720 kev to the 80-kev level, or as a transition directly to the ground state of Xe^{131} with the higher energy γ-ray arising from a separate excited level. The work of Thulin,[11] in which he determined an energy difference of 85.7±0.4 kev for these two γ-rays from the photoelectric doublet of the K_{724} and L_{638} lines from a uranium converter, instead of an energy difference of 80.1 kev (which would give twice the measured doublet separation), excludes the possibility of a cross-over transition. Further convincing evidence excluding the cross-over transition is presented by Ketelle *et al.*[10] by their resolution of the two softer components leading to separate excited energy levels for the 724- and 638-kev γ-rays. Thulin also estimated the relative intensities of the 638- and 724-kev γ-rays to be 7.8:1 as determined from the heights of the K photoelectric lines from a uranium radiator, with the energies 638.0±0.6 kev and 723.9±0.7 kev. Our result of 13.3 percent for the two unresolved soft components, using this ratio of 7.8:1 yields 11.8 percent and 1.5 percent for these two γ-rays, respectively. These percentages and the branching ratio of 8:100 of Metzger and Deutsch[2] for the 284- and 364-kev γ-rays were used in determining the values of the K-shell internal conversion coefficients listed in Table I.

Figure 1, the upper end of the momentum distribution of the negatrons from I^{131}, shows the conversion peaks of the 638- and 724-kev γ-rays. Calibration of the spectrometer with the well-known values 284.1±0.1; 364.2±0.1 of Lind *et al.*[12] for these two γ-rays gives the following energies: for the 638-kev γ-ray, 638.8, 637.8 from the K- and L-peaks, respectively; for the 724-kev γ-ray, 723.7-kev from the K-peak. The L_{724} peak is shown resolved in Fig. 1, but the uncertainties in the points resulting from subtraction of the underlying continuous spectrum are too large for the measurement to be meaningful.

Table II shows a comparison of the interpolated values for the K-shell internal conversion coefficients

[11] Sigvard Thulin, Phys. Rev. **83**, 860 (1951).

[12] Lind, Brown, Klein, Muller, and DuMond, Phys. Rev. **75**, 1544 (1949).

taken from the calculations of M. E. Rose *et al.*,[13] from which conclusions may be drawn concerning the types of transitions involved. The probable types of transitions are listed in the last column. The N_K/N_L ratios in Table I give some additional information with regard to transition types on comparison with the empirical curves of Goldhaber and Sunyar.[14] From the K/L ratios for $E2$ transitions (Fig. 11 of reference 13) we have the following: for the 284-kev transition, the empirical value $K/L \simeq 5$, which is in agreement with the experimental value of 5.4 ± 1.2; for the 364-kev transition, the empirical value $K/L \simeq 6.5$ (on extrapolation of their empirical curve), which is in agreement with the experimental value of 6.6 ± 0.2. These do not definitely exclude admixtures of $M1$ for both these transitions. However, a self-consistent assignment of spin and parity for the 364-kev level and the level for the 80-kev γ-ray[15] (which is in cascade with the 284-kev γ-ray forming the parallel branch with the 364-kev γ-ray) appears to require that the 284 transition be pure $E2$ while permitting the 364 transition to be a mixture of $E2$ and $M1$.

We wish to thank Mr. R. Leamer and Mr. David Brower for assistance in taking some of the experimental data, and the NBS Computation Laboratory for calculations of the Fermi distribution function.

[13] Rose, Goertzel, and Perry, Oak Ridge National Laboratory Report No. 1023 (1951).
[14] M. Goldhaber and A. W. Sunyar, Phys. Rev. **83**, 906 (1951).

[15] Verster *et al.* (see reference 8) term the 80-kev level an $s_{\frac{1}{2}}$ level. Our results are generally in agreement with theirs where results are obtained in common. Our conclusions on level assignments are also in agreement with theirs so that they are not repeated here. In addition we conclude that the 724-kev level should be even with spin $\frac{3}{2}$ or $\frac{1}{2}$, it not being apparent which spin value is to be preferred; also this level is probably not a single-nucleon state.

PHYSICAL REVIEW VOLUME 86, NUMBER 6 JUNE 15, 1952

A Comparison of Penetrating Showers in Light and Heavy Elements. I*

W. D. WALKER,† N. M. DULLER, AND J. D. SORRELS‡
Rice Institute, Houston, Texas
(Received March 3, 1952)

A comparison of the multiplicity of penetrating particles has been made for penetrating showers originating in C and Pb, and for showers starting in Fe and paraffin. The comparison is made by observing the rates of different sized showers per mean free path of the generating material. Large differences are found in the comparison of Pb and C. The comparison of Fe and paraffin essentially gives a comparison of Fe and C as the showers originating in hydrogen were not recorded efficiently. The difference between showers starting in Fe and C is smaller than in the comparison of Pb and C.

The ratio of neutral to charged primaries is determined to be 0.5 ± 0.15. The collision mean free path of charged primaries in paraffin is measured to be 56^{+12}_{-7} g/cm², and the mean free path of charged primaries in carbon is measured to be 76 ± 8 g/cm². A search was made for elastic scatterings of penetrating shower primary particles in which only a small amount of energy is transferred to a target nucleon. Only one example of such scattering was observed in the traversal of 11,960 g/cm² of carbon.

I. INTRODUCTION

IN the past few years much effort has been directed toward gaining a qualitative understanding of the processes involved in high energy π-meson production. Two of the extreme models which have been used to describe the process are the plural model and the multiple model. The plural model proposed by Heitler and Janossy[1] supposes that the primary particle loses its energy by making several collisions in one nucleus with only one meson produced in each collision. The multiple model originally proposed by Heisenberg[2] is based on the assumption that several π-mesons are produced in a single nucleon-nucleon encounter. This model has been used by Fermi in his statistical theory.[3]

The problem has been attacked by experimenters by comparing the multiplicities of the lightly ionizing or penetrating particles generated in penetrating showers in light and heavy elements. Investigators using photographic plates have found a strong correlation for primary energies of greater than 5 Bev between the number of heavy prongs and the number of shower particles.[4,5] Cloud-chamber investigations have given conflicting results.[6–9]

Gregory and Tinlot[8] found that for the production of

* Supported in part by grants from the Research Corporation and R.E.S.A.
† Presently on leave of absence at the University of California, Berkeley, California.
‡ Now at California Institute of Technology, Pasadena, California.
[1] W. Heitler and L. Janossy, Proc. Phys. Soc. (London) **A62**, 669 (1949).
[2] W. Heisenberg, Z. Physik **126**, 569 (1949).
[3] E. Fermi, Prog. Theoret. Phys. **5**, 570 (1950).
[4] Salant, Hornbostel, Fisk, and Smith, Phys. Rev. **79**, 184 (1950).
[5] Camerini, Davies, Fowler, Franzinetti, Lock, Perkins, and Yekutieli, Phil. Mag. **42**, 1241, 1261 (1951).
[6] Lovati, Mura, Salvini, and Tagliaferri, Phys. Rev. **77**, 284 (1950).
[7] J. R. Green, Phys. Rev. **80**, 832 (1950).
[8] B. P. Gregory and J. H. Tinlot, Phys. Rev. **81**, 675 (1951).
[9] W. Y. Chang and G. del Castillo, Phys. Rev. **84**, 582 (1951).

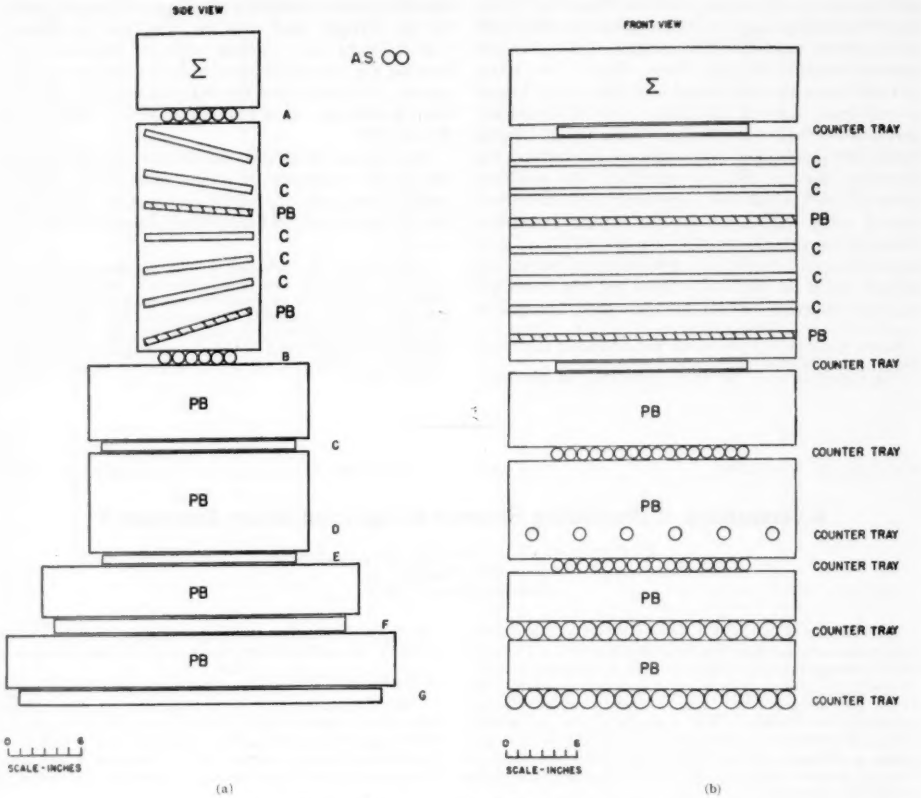

FIG. 1. Diagram of counter and cloud-chamber arrangement.

large penetrating showers, the cross section in Pb was more than a factor of $(208/27)^{\frac{1}{2}}$ greater than the cross section in Al. This agreed qualitatively with the earlier experiments of Lovati[6] *et al.* Green[7] and Chang[9] have concluded that lead and carbon are about equivalent as generators for penetrating showers.

II. EXPERIMENTAL APPARATUS

The apparatus used in this experiment consisted of a large rectangular cloud chamber (illuminated volume 8 in.×17 in.×20 in.) in conjunction with a hodoscope arrangement of counters. The chamber was filled with argon saturated with a 70–30 percent water-ethyl alcohol mixture. The chamber contained five carbon plates and two lead plates. The plates were covered with thin glass mirrors to increase the illumination in the center of the chamber. The chamber was illuminated by means of 4 flash tubes behind Lucite lenses, and photographed by a stereoscopic camera whose lenses were covered with polaroid. The polaroid cut down the effect of the polarized light scattered off the back velvet. A drawing of the apparatus is shown in Fig. 1.

An anticoincidence tray of two 16-in. by 1-in. counters was placed one meter from the top of the chamber to prevent triggering on dense air showers. Either coincidences $A^{>0}B^{>1}C^{>1}-AS$ or $A^{>0}B^{>0}D^{>1}-AS$ could trigger the apparatus. Most of the useful pictures were of the first type. In order to have made such a coincidence a shower must have had at least two particles capable of traversing 195 g/cm² of lead. A picture of a shower is shown in Fig. 2. The apparatus was operated at Echo Lake, Colorado, elevation 3250 meters.

III. COMPARISON OF MULTIPLICITY IN LIGHT AND HEAVY ELEMENTS

The rates of production of penetrating showers with two, three, four, etc., penetrating secondaries were compared for different producing materials. The rates

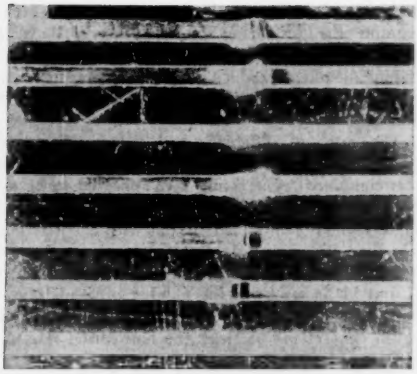

FIG. 2. A charged primary interacts in carbon or glass producing a shower of 5 penetrating particles and one heavy particle. There is no cascade multiplication in the lead plate immediately below the point of origin.

TABLE I. A comparison of showers from lead and carbon.

No. of penetrating secondary particles	No. of showers observed	R Rate[a] of showers observed, hr^{-1}	R_0 normalized rate, hr^{-1}	
A. Carbon				
2	100	0.231	1.041	2.08±0.14[b]
3	100	0.231	1.041	
4	81	0.186	0.836	1.57±0.12
5	70	0.162	0.731	
6	44	0.103	0.468	0.72±0.08
7	24	0.055	0.250	
8	10	0.023	0.104	0.14±0.04
9	3	0.0069	0.032	
10	3	0.0069	0.032	
11	3	0.0069	0.032	
12	2	0.0047	0.021	
13	0	...	...	0.14±0.04
14	2	0.0047	0.021	
15	2	0.0047	0.021	
16	1	0.0024	0.011	
	445	1.025	4.63	4.63±0.22
B. Lead				
2	19	0.0455	0.536	1.24±0.18
3	25	0.0598	0.706	
4	30	0.0718	0.846	1.64±0.20
5	28	0.0671	0.790	
6	32	0.0765	0.900	1.13±0.18
7	8	0.0192	0.226	
8	14	0.0334	0.395	0.57±0.13
9	6	0.0144	0.170	
10	6	0.0144	0.170	
11	1	0.0024	0.028	
12	2	0.0048	0.056	
13	0	...	...	
14	3	0.0072	0.084	0.47±0.12
15	2	0.0048	0.056	
16	1	0.0024	0.028	
17	1	0.0024	0.028	
20	1	0.0024	0.028	
	179	0.428	5.05	5.05±0.35

[a] Corrected for chamber dead-time.
[b] All errors indicated are standard statistical errors calculated from the number of counts.

in lead were compared with those in carbon, and a similar comparison was made between paraffin and iron. For each producing material a histogram of the rate of showers with N penetrating secondaries *versus* N has been plotted (see Figs. 3, 4). In order to compare the rates in different materials, the rates for each material have been divided by the probability that a primary will interact while traversing it. For Pb, C, and Fe this probability is simply $(1-e^{-x/\lambda})$, where x is the thickness of material and λ the mean free path in it. As pointed out in Sec. V, it appears that few of the showers produced in paraffin and recorded by this apparatus originated in the hydrogen. The probability that a primary will interact in the carbon while traversing the paraffin is

$$\frac{6\lambda_{\text{para}}}{7\lambda_{\text{C}}}[1-e^{-x/\lambda_{\text{para}}}].$$

It should be noticed that for $x/\lambda_{\text{para}} \leq \frac{1}{2}$ this expression is nearly independent of the λ_{para}.

The values of λ used in calculating the probabilities were $\lambda_{\text{C}}=65$ g/cm^2,[10,11] $\lambda_{\text{Pb}}=160$ g/cm^2,[12] $\lambda_{\text{Fe}}=115$ g/cm^2,[10] and $\lambda_{\text{para}}=56$ g/cm^2 (see Sec. V).

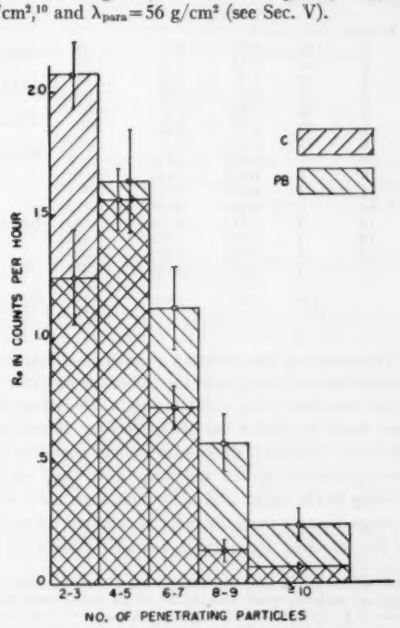

FIG. 3. A comparison of multiplicity of penetrating particles for showers originating in carbon and lead.

[10] R. R. Brown, Phys. Rev. **85**, 773(A) (1952).
[11] It is apparent from other experiments [W. D. Walker, Phys. Rev. **77**, 686 (1950); K. Sitte, Phys. Rev. **77**, 714 (1950)] that the m.f.p. for shower production decreases with increasing energy of the primary until the m.f.p. corresponding to the geometric

TABLE II. A comparison of showers from iron and paraffin.

No. of penetrating secondary particles	No. of showers observed	R Rate of showers observed, hr^{-1}	R_s Normalized rate, hr^{-1}	
A. Iron				
2	100	0.605	2.08	3.54±0.25
3	70	0.424	1.46	
4	68	0.411	1.41	2.91±0.24
5	72	0.436	1.50	
6	55	0.333	1.14	1.74±0.18
7	29	0.176	0.60	
8	34	0.206	0.71	1.08±0.15
9	18	0.109	0.374	
10	20	0.121	0.42	
11	17	0.103	0.35	
12	9	0.054	0.187	
13	3	0.018	0.062	1.21±0.16
14	2	0.012	0.041	
15	5	0.030	0.104	
~22	1	0.006	0.020	
~30	1	0.006	0.020	
	504	3.05	10.50	10.50±0.51

No. of penetrating secondary particles	No. of showers observed	R Rate of showers observed hr^{-1}	R_s normalized rate hr^{-1}	$R_s\frac{7\lambda_C}{6\lambda_{para}}$ hr^{-1}	
B. Paraffin					
2	150	1.00	2.72	3.68	5.25±0.37
3	64	0.43	1.16	1.57	
4	70	0.47	1.27	1.72	2.72±0.27
5	41	0.27	0.74	1.00	
6	36	0.24	0.65	0.87	1.59±0.20
7	29	0.19	0.53	0.72	
8	15	0.10	0.27	0.365	0.54±0.11
9	7	0.047	0.127	0.172	
10	8	0.053	0.145	0.196	
11	3	0.020	0.055	0.075	
12	7	0.047	0.127	0.172	
13	2	0.013	0.036	0.049	0.64±0.13
14	1	0.007	0.018	0.024	
15	4	0.027	0.073	0.099	
~22	1	0.007	0.018	0.024	
	438	2.93	7.95	10.75	10.75±0.51

The efficiency for detecting a shower is a function of the number and energies of the secondary particles, and of the location of the point of origin. No attempt has been made to correct the histograms for differences in efficiency. However, differences due to geometry have been minimized in the following way. Only showers starting in the upper lead plate have been used, so the average distance from the point of origin of the showers to the detecting apparatus is almost the same for lead and carbon (see Fig. 1). In the comparison of Fe with paraffin the producing materials were above the chamber. With Fe above the chamber the distance from the middle of the producing layer to the bottom row of triggering counters was 34 inches; with paraffin it was 38.5 inches.

The rates of different sized penetrating showers produced in Pb and C are given in Table I. A secondary was considered penetrating if it appeared to be minimum ionizing and went through at least one ½-inch lead plate without multiplication and with a scattering of less than 20°. These data are plotted in a histogram shown in Fig. 3. It is seen that the difference between C and Pb increases as the number of secondaries becomes larger and that for showers with more than seven penetrating particles the normalized rate in Pb is 4 times that in C.

For showers produced in Fe and paraffin, minimum ionizing tracks which traversed the upper lead plate without multiplication or scattering and appeared to converge to a common point in the producing layer were called penetrating secondaries. Undoubtedly some of these penetrating secondaries were missed. However, since the showers are fairly well collimated, it is thought that the number missed is a small fraction of the number observed. The results for this part of the experiment are given in Table II and Fig. 4. As explained in

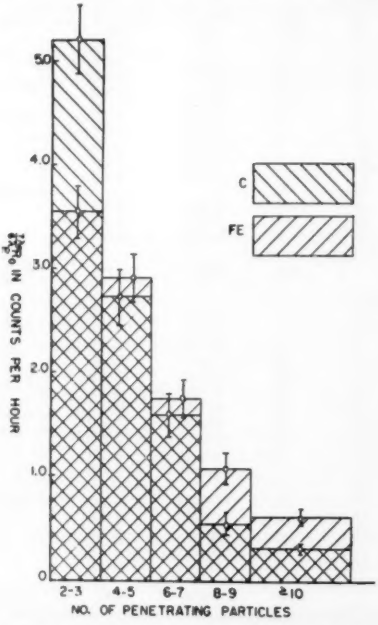

FIG. 4. A comparison of multiplicity of penetrating particles for showers originating in carbon and iron.

cross section is reached. The comparison of multiplicities of the large or more energetic showers are of particular interest. The value 65 g/cm² from Brown's experiments has been chosen because his apparatus selected higher energy primaries than the experiment of Walker, Walker, and Greisen (reference 12). From a comparison of the rate of showers in this experiment with the rate in the experiment of Walker, Walker, and Greisen, the average energy of the primaries is estimated to be 2 to 3 times as great in the former as in the latter. The rate of charged primary particles capable of producing showers recorded by this apparatus is estimated to be 1.2×10^{-6} cm^{-2} sec^{-1} steradian^{-1}.

[12] Walker, Walker, and Greisen, Phys. Rev. **80**, 546 (1950).

TABLE III. Results of search for elastic scattering of penetrating shower primaries.

	No. of plates traversed	Grams/cm² traversed	No. of heavy particles observed
C. (3.46 g/cm² thick)	3458	11,960	1
Pb (15.5 g/cm² thick)	845	13,100	0

Sec. V, this is probably a comparison of showers produced in Fe with those produced in C. The difference in the normalized rates for showers with more than seven penetrating particles is about a factor of 2 which is less than in the comparison of Pb and C.

For showers starting in the absorber above the chamber, the primaries can be either charged or neutral. For showers inside of the chamber most of the primaries will be charged because of the requirement that tray A be struck. Thus a comparison of the total normalized rates in Tables I and II should give a measure of the ratio of neutral to charged primaries. After a correction for the absorption in Σ the ratio of neutral to charged primaries is equal to 0.5 ± 0.15.

IV. ELASTIC COLLISIONS BY PENETRATING SHOWER PRIMARIES

According to Fermi's statistical theory of meson production,[3] the probability of elastic nucleon-nucleon scattering is very small at high energy. It was therefore of interest to look for elastic scatterings in the chamber of particles capable of producing a large penetrating shower. The paths of primaries which produced penetrating showers in the lower part of the chamber or in the hodoscope were studied, and each plate traversal was examined for accompanying heavily ionizing particles which would indicate an elastic collision in a carbon or lead nucleus. If an elastic collision in which a few hundred Mev is transferred occurs in a plate then there is a fair probability[13] of seeing a heavy track.

The data in Table III indicate that a high energy nucleon very seldom makes a collision in which only a small fraction of its energy is transferred.

During this investigation, no cases of charge exchange were observed. This agrees with the results of Gregory and Tinlot.[5]

V. MEAN FREE PATH IN PARAFFIN

The rate of showers produced inside the chamber was measured first with paraffin and then with iron placed above the chamber in position Σ. The mean free path in paraffin was obtained by comparing the absorption of primaries in paraffin with that in iron. The data are given in Table IV.

By taking the mean free path in iron to be 115 ± 10 g/cm² and considering the ratio of the rates R_{Fe}/R_{para}, the mean free path in paraffin is determined to be 56^{+12}_{-7} g/cm². From this, using a mean free path in carbon of 65^{+5}_{-2} g/cm², a mean free path of 31^{+35}_{-7} g/cm² in hydrogen is obtained.

From consideration of Table IV and the (unnormalized) rates in Table II it is seen that the paraffin is a better absorber than the iron but that the iron is a better generating material than the paraffin. This means that many of the showers by which the primaries have been absorbed in paraffin have not been recorded. If we assume that all the showers produced in paraffin are recorded then

$$R_0 = R_{para}/(1-e^{x/\lambda_{para}}),$$

where R_0 is the rate of primaries, R the observed rate of showers produced in paraffin. The same formula holds for iron and the values of R_0 for iron and paraffin should agree if the efficiencies for detecting the showers are not too different. We see from Table II that R_0 for paraffin is only about three-quarters of that for iron.

If, on the other hand, we assume that only showers produced in the carbon of the paraffin are recorded in the apparatus, an elementary calculation gives

$$R_0' = R_{para}\Big/\left[\frac{6}{7}\cdot\frac{\lambda_{para}}{\lambda_C}(1-e^{-x/\lambda_{para}})\right].$$

This rate, it is seen in Table II, agrees very well with R_0(Fe). Consequently it appears that a large fraction of the showers originating in the hydrogen are missed by this triggering arrangement.

VI. MEAN FREE PATH FOR SHOWER PRODUCTION IN CARBON

From the relative number of showers starting in the carbon and lead plates it is possible to calculate the mean free path in carbon assuming that the mean free path in lead is known and that the detection efficiency is the same for carbon and lead. The number of showers originating in the different plates of the cloud chamber are given in Table V. In order to minimize geometrical effects we use only showers starting in the top lead plate and the carbon plates above and below the lead plate.

The mean free path in lead was assumed to be 160 g/cm², as this apparatus selected mainly rather large showers. After a small correction for the fact that some of the plates act as absorbers for lower plates this gives

TABLE IV. Comparison of rates of showers occurring inside the chamber.

Σ = 39.5 g/cm² Fe	Σ = 25.7 g/cm² paraffin
$R_{Fe}=1.95\pm0.11$ counts per sensitive hour	$R_{para}=1.74\pm0.12$ counts per sensitive hour

[13] If too little energy is transferred the chance of observing a star particle is very small, whereas if too much is transferred the interaction might be misclassified as a penetrating shower.

TABLE V. Location of showers within the chamber.

Plate No.	Material	Thickness g/cm²	No. showers
1 (top)	C	3.67	132
2	C	3.47	113
3	Pb	15.5	204
4	C	3.29	78
5	C	3.40	64
6	C	3.46	55
7	Pb	19.0	191

a mean free path for production of 76 ± 8 g/cm². This value is probably slightly too high because showers in lead have more secondaries and are possibly recorded with greater efficiency.

DISCUSSION

From the comparison of showers starting in carbon, iron, and lead it seems apparent that in the more energetic showers secondary multiplication occurs inside of the struck nucleus. Not many of the details of the multiplication process can be derived from these experiments. The number of particles formed in the initial encounter of the primary with the nucleus is not known. However, the fact that a large fraction of the showers starting in hydrogen were missed would indicate that the average number of fast particles produced in a single nucleon-nucleon encounter must be smaller than the number observed in the average shower from carbon in this experiment (about 5). The ratio of the normalized rates for large showers of eight or more penetrating particles is 4:1 for lead as compared to carbon and is 2:1 for iron as compared with carbon. This indicates that in a large fraction of the showers in iron the cascade process has not gone to completion. This fact seems to indicate that the secondary particles which produce the later multiplication have a long mean free path in nuclear matter for doing so.

Practically no elastic collisions occurred in carbon in which a small amount of energy was transferred. This would seem to indicate that whenever a primary particle encounters a nucleus a shower is produced with high probability and there is only very small probability of a collision with small energy transfer.

ACKNOWLEDGMENTS

The authors wish to thank Professors T. W. Bonner and W. V. Houston for their interest and support in these experiments. They also wish to thank Professors Iona and Cohn of the University of Denver for their aid in making the facilities of the Inter-University Laboratory available. The cooperation and aid of Dr. H. S. Bridge at Echo Lake is acknowledged. The authors wish to thank Mr. Raymond Orr of the Athletic Mining and Smelting Company for a loan of part of the lead used in the experiment. The authors gratefully acknowledge the financial support in the form of a grant from the Research Corporation. Part of the lead used was purchased by means of a grant in aid from R.E.S.A.

PHYSICAL REVIEW VOLUME 86, NUMBER 6 JUNE 15, 1952

The Liquid-Solid Transformation in Helium from 1.6° to 4°K

C. A. SWENSON
Jefferson Physical Laboratory, Harvard University, Cambridge, Massachusetts
(Received January 30, 1952)

The transformation from liquid to solid helium behaves quite differently above and below the intersection of the λ-point-pressure curve with the melting pressure curve. The experimental data given here extend previous work from below 1.8° to about 4°, and show the effect of the λ-transformation on the latent heat of melting, the change in molar volume on melting, and the melting pressure curve. When these data are combined with a new determination of the λ-point-pressure curve, the indication seems to be that the λ-transformation is not truly of second order; that is, that it does not obey the Ehrenfest equations.

I. INTRODUCTION

THE phase diagram for the liquid and solid phases of helium, shown in Fig. 1, is quite unique in its general characteristics. Helium normally remains a liquid to absolute zero, with the vapor and solid phases never coexisting. However, upon the application of moderate pressures to the liquid helium at these very low temperatures, solid helium is formed, and the liquid-solid equilibrium curve is shown in Fig. 1. At higher temperatures, a "triple point" is found between solid helium, liquid helium I, and liquid helium II. It is not a triple point in the usual sense of the word, since the helium I–helium II transformation (called the λ-transformation) is believed to be of the second order, and, as a consequence, the slope of the melting pressure curve should be continuous, with a discontinuous second derivative.

Since the properties of solid helium are quite regular, the changes in the properties of liquid helium at the λ-point should be reflected quantitatively in the experimental values of the molar change in volume on melting ($\Delta V = V_L - V_S$), the heat of melting [$\rho = T(S_L - S_S)$], and the melting pressure curve. A detailed study of these quantities in the region of the "triple point"

should give a bit more insight as to the nature of the λ-transformation in liquid helium, and also should furnish additional opportunity to check the applicability of the Ehrenfest equations, which, presumably, are obeyed in this case.

The liquid-solid transformation in helium has been investigated in some detail below 1.8°,[1,2] with the emphasis placed on the region near 1°K. The thermodynamics of the "triple point" were also discussed qualitatively in this work, although the only available melting data for the region above 1.8° were doubtful, since they had to be extrapolated from 2.2°, and showed deviations from the Clausius-Clapeyron equation above 3°. Thus, it seemed worth while to extend the work from below 1.8° to higher temperatures, both to investigate the effect of the λ-transformation on the melting phenomenon, and also to investigate the inconsistencies in the data above 3°.

The techniques used were similar to those described previously and will be outlined in the section on experimental details. In the past, melting pressure curves at low temperatures have been determined almost invariably through the use of the blocked capillary technique.[3] This technique has been open to criticism, mostly owing to the fact that pressure gradients exist across the sample and could give melting pressures that are too low.[4] In addition to these objections, preliminary experiments showed that in this work, at any rate, supercooling effects became very troublesome, so that it was hard to reproduce points accurately. A version of the piston displacement method used by Bridgman and others was found to be more satisfactory and was adopted for these experiments.[5]

In essence, this method consisted of determining the temperature at which the liquid-solid transformation took place under constant pressure in an isolated cryostat. The helium in the cryostat was connected directly to a pressure balance (dead-weight piston gauge) by means of an oil transmitter,[6] and the temperature of the cryostat was slowly decreased. At the melting point the increase in the density of the helium on solidification caused the pressure balance piston to drop slowly, while the temperature of the cryostat remained constant. Thus, supercooling effects were avoided, and by cooling very slowly, readings could be taken in a leisurely manner. The response of the temperature of the isolated cryostat to changes in pressure was very rapid.

The ΔV and ρ measurements were performed in exactly the same manner, except that they involved warming up a vessel full of solid helium, rather than cooling liquid helium. One run could in principle give

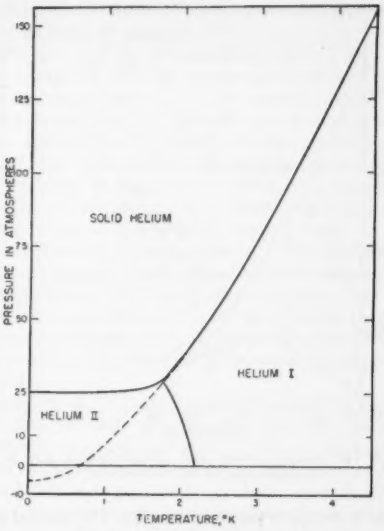

FIG. 1. The phase diagram of helium below 4°K.

all three pieces of data, but, in fact, the experimental difficulties increased markedly from P *vs* T to ΔV *vs* T to ρ *vs* T, and the number of points taken decreased in this order.

The above measurements cast some doubt as to the coordinates of the "triple point" as given by earlier workers,[7] so the λ-point-pressure curve was redeter-

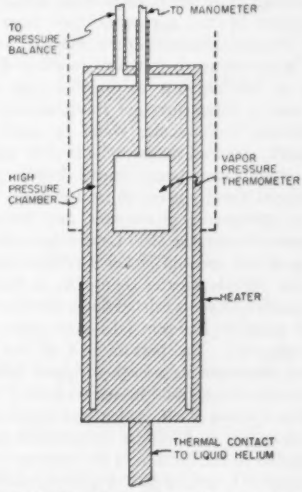

FIG. 2. A schematic diagram of the cryostat used.

[1] F. E. Simon and C. A. Swenson, Nature **165**, 829 (1950).
[2] C. A. Swenson, Phys. Rev. **79**, 626 (1950).
[3] W. H. Keesom, *Helium* (Elsevier, Amsterdam, 1942), p. 180.
[4] P. W. Bridgman, Revs. Modern Phys. **18**, 28 (1946).
[5] P. W. Bridgman, *The Physics of High Pressure* (G. Bell, London, England, 1949), p. 190.
[6] C. A. Swenson, Rev. Sci. Instr. **21**, 22 (1950).
[7] Reference 3, p. 225.

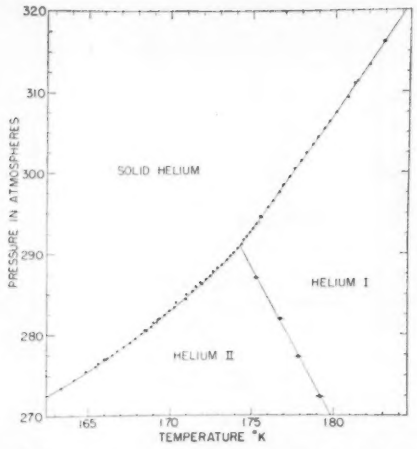

FIG. 3. The melting pressure and λ-point-pressure data in the neighborhood of the "triple point."

mined to complete the phase diagram. The method used was essentially the determination of the temperature at which the thermal conductivity of liquid helium under constant pressure increased suddenly as the temperature was decreased. This information was necessary to determine the slope of the λ-line at the upper "triple point," and to check the other data for their consistency.

II. EXPERIMENTAL DETAILS

The cryostat used for these measurements was unusual enough to be described in some detail, whereas the remainder of the apparatus was more or less standard. The main features of the cryostat, which was mounted in a vacuum jacket, are shown in Fig. 2. It consisted of two separate sections: a high pressure chamber and a vapor pressure thermometer bulb. A vapor pressure thermometer could be used directly for this work, since all measurements were made at a constant equilibrium temperature. Vapor pressures were measured directly using either a mercury manometer or an Apiezon oil manometer, and temperatures were calculated using the 1949 Cambridge scale.

The top of the vacuum jacket was maintained at a temperature slightly greater than 4°K, so that a temperature gradient always existed down the thin stainless steel high pressure (0.3-mm i.d.) and vapor pressure tubes (2-mm i.d.). The bottom half of the vacuum jacket was immersed in a bath of liquid helium, the temperature of which could be varied from 4° to about 1.4°K. The cryostat itself, which was constructed entirely from copper to minimize temperature gradients, was connected to the bottom of the vacuum jacket by a thin copper rod, and its rate of cooling could be controlled by varying the temperature of the helium bath.

The annular high pressure space was 1 mm wide and 15 cm long, with a total volume of about 6 cc. The object of this type of construction was twofold: first, to have as large a ratio of surface area to volume as possible, since solid helium is a relatively poor heat conductor; and secondly, to surround the vapor pressure thermometer completely with a relatively constant temperature. The actual success of this design is shown in Fig. 3, where points taken at about 30-atmos pressure are shown, reproducible (but not accurate) to 0.01 atmos and 0.001°K. These points represent several runs made with different diameter high pressure capillaries, two different size copper connections to the helium bath, and various rates of cooling.

The relative values of melting pressures are accurate to within about 0.01 atmos, since the pressure balance was able to reproduce pressures this well from run to run. Two different pistons were used: one of 0.9828 sq cm area for pressures up to 45 atmos, and the other, 0.3296 sq cm area, for pressures up to 145 atmos. The pressures were calculated from the weights used and the areas of the pistons, and the calibrations were checked against the vapor pressure of carbon dioxide at 0°C.[8] The agreement was closer than one tenth of one percent.

The heater on the outer surface of the cryostat was used to ascertain that a reversible freezing process was being observed. If the temperature of the cryostat remained constant with the pressure balance piston dropping slowly, then, presumably, solidification was taking place. To verify this, the addition of heat to the helium should cause only a reversal of the piston motion and have no effect on the temperature. This was checked in each case.

For the ΔV measurements, the cryostat was first filled with solid helium, after which heat was applied and the piston kept at constant height by bleeding gas through a needle valve at room temperature into a calibrated volume. The two main sources of error here were incomplete filling of the cryostat, which could be checked as above, and the natural leak rate of the oil past the pressure balance piston. The annular shape of the high pressure space and the fact that all the cooling was from the bottom helped to reduce the filling factor error. The second error depended directly on the time needed for melting, and, fortunately, ΔV depends so slightly on pressure that rather rapid rates of warming could be used. These two sources of error are perhaps equal in magnitude, and set the limit of accuracy.

The heat-of-melting measurements involved a modification of the cryostat shown in Fig. 2. The copper connection to the helium bath was removed, and a second vacuum jacket was added inside the original one (see the dotted lines in Fig. 2). The heat of solidification was removed from the cryostat by a few mm pressure of helium gas in the outer vacuum jacket, while a good vacuum in the inner one kept the high pressure tube from being blocked. This exchange gas

[8] O. C. Bridgeman, J. Am. Chem. Soc. **49**, 1174 (1927).

TABLE I. The smoothed thermodynamic functions for the liquid-solid transformation in helium between 1.6° and 4.0°K. For data below 1.6°, see reference 2, and for data above 4.0°, see reference 13.

T (°K)	P(atmos)	dP/dT (atmos/°K)	ΔV (cc/mol)	ρ(calc. cal/mol)
4.0	128.6	56.0	1.03	5.56
3.5	102.0	51.0	1.10	4.75
3.0	78.1	46.5	1.19	4.02
2.5	56.3	41.6	1.29	3.26
2.0	37.10	34.15	1.41	2.35
1.9	33.90	...	...	...
1.8	30.76	30.0	1.45	1.80
1.75	29.31	29.0	1.48	1.82
1.72[a]	28.75	18.7	1.52[a]	1.19
1.70	28.30	16.6	1.60	1.09
1.6	27.01	10.2	1.89	0.75

was then pumped out, and, with the outer bath at roughly the melting temperature, the amount of heat needed to melt the solid at constant pressure was measured. A ΔV measurement, as outlined above, was made simultaneously. The oil leak past the piston does not affect the accuracy of the heat of melting measurement, so the main error here is in the filling factor. It cannot be eliminated completely.

III. RESULTS

The melting pressure data fall roughly into two groups, above and below 2.1°K, and the agreement with earlier and less precise work is, in general, satisfactory.[2] The 22 experimental points in the high temperature group could be represented within 0.1 percent by the equation,

$$p+5.6=13.458T^{1.66074} \text{ atmos.} \qquad (1)$$

This curve is shown in Fig. 1, together with its extrapolation to absolute zero.

Figure 1 shows that below 2.1° the melting pressures begin to fall off less rapidly, and the data did not fit an empirical curve of the above type. These data, representing about 65 separate points, are tabulated in column 2 of Table I as a smooth curve. The reproducibility of these measurements is shown in Fig. 3, where the vicinity of the upper "triple point" is shown in some detail. Whereas a gradual change in curvature begins at about 2.1°, an abrupt change takes place at 1.743°, and this temperature corresponds almost exactly with the termination of the λ-point-pressure curve on the melting pressure curve.

The complete λ-point-pressure curve, as redetermined in these experiments, is given in Fig. 4. The agreement with earlier measurements is quite good, except for the point of intersection, which was, according to Professor Clusius, obtained by extrapolation from the other points. These data are summarized in the smoothed curve of Table II, and the coordinates of the upper triple point can be given as

$$P_\lambda=29.12(\pm0.05) \text{ atmos}, \quad T_\lambda=1.743(\pm0.003)°\text{K}.$$

The less accurate values given in reference 2 were based almost entirely on the ΔV data, and were weighted by the data given by Keesom.

The results of the ΔV measurements are shown in Fig. 5, together with the previously determined curve for temperatures below 1.75°. The agreement above 2.2° with previous work by Keesom[9] (not shown) is quite good, although fundamentally different methods were used.[10] Since the experimental error involved in these measurements is about three percent, it is impossible to make any decision as to whether or not a discontinuity exists in the slope of the ΔV curve at the λ-point. Possibly the easiest check of this point would be to redetermine the density or thermal expansion of liquid helium in the vicinity of the λ-point, since the rapid increase of ΔV is due to the change in the thermal expansion coefficient of liquid helium from positive to negative as its temperature is decreased through the λ-point.[11]

The slope of the melting pressure curve (dP/dT) was then combined with the ΔV data using the Clausius-Clapeyron equation to obtain the heat of melting, ρ. These calculations are shown in the solid curve of Fig. 6, and they are tabulated in column 5 of Table I. Previous experimental determinations of the heat of melting are also shown in Fig. 6, and the agreement between 3° and 4° is very poor.[12,13]

Using the technique outlined previously, ρ was remeasured, and the data are indicated in Fig. 6 also.

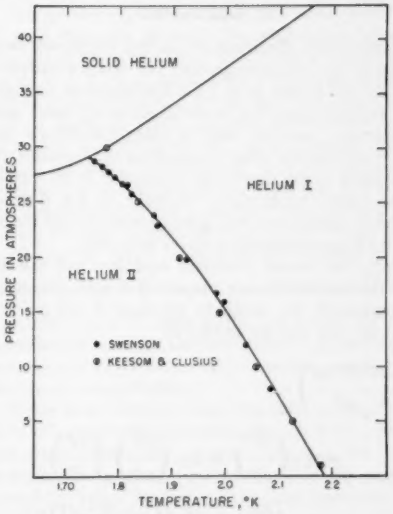

FIG. 4. The λ-point-pressure curve.

[9] Reference 3, p. 210.
[10] See Table I, column 4 of reference 2.
[11] Reference 3, pages 206 and 245.
[12] W. H. Keesom and A. P. Keesom, Leiden comm. **240b** (1936).
[13] R. Kaischew and F. E. Simon, Nature **113**, 460 (1934).

TABLE II. Smoothed values for the coordinates of the λ-point-pressure curve.

T_λ (°K)	P_λ (atmos)
1.743	29.12
1.750	28.78
1.85	24.4
1.95	18.8
2.05	11.3
2.15	3.0

The agreement is well within experimental error. No effort was made to obtain extreme accuracy, and the possible error of these measurements is of the order of five percent. The calculated values for ρ are probably the more reliable.

The reason for these discrepancies with earlier work is not obvious. The results quoted by Keesom rely on two values for the absolute entropy of solid helium, and one of these might have been in error due to an incorrect extrapolation. The data due to Kaischew and Simon were essentially preliminary in nature, although the deviation at 4° seems high. It is unlikely that these deviations have any significance, since the melting pressure measurements have been so easily reproducible, with no points significantly off the curve. These data, both ΔV and ρ, agree well with recent work at higher temperatures and pressures by Dugdale and Simon at Oxford.[14]

IV. DISCUSSION

Qualitatively, these results confirm the second-order nature of the λ-transformation. The first derivatives of both ΔV and ρ seem to be, if not discontinuous, changing very rapidly. Quantitative verifications are much more satisfactory, however, and by using Ehrenfest's relations[15] and certain other thermodynamic formulas, the consistency of the results can be checked in the vicinity of the upper "triple point." Actually, as Fig. 6 shows, the heats of melting are in good agreement with the ΔV and melting pressure data above this point.

Using the second Ehrenfest equation, and the fact that the thermodynamic properties of solid helium are well-behaved, the change in the slope of the ΔV *vs* T curve at 1.74° can be written as

$$\Delta_{\mathrm{I,II}}\left(\frac{d(\Delta V)_M}{dT}\right)_M = \Delta_{\mathrm{I,II}}\left(\frac{\partial V}{\partial T}\right)_P + \Delta_{\mathrm{I,II}}\left(\frac{\partial V}{\partial P}\right)_T\left(\frac{dP}{dT}\right)_M = \Delta_{\mathrm{I,II}}\left(\frac{\partial V}{\partial T}\right)_P\left[\frac{(dP/dT)_\lambda - (dP/dT)_M}{(dP/dT)_\lambda}\right]. \quad (2)$$

Here, $\Delta_{\mathrm{I,II}}(\partial V/\partial T)_P$ is the difference in the thermal expansions of helium I and helium II at the upper triple point, and $(dP/dT)_\lambda$ and $(dP/dT)_M$ are the slopes of the λ-point-pressure and melting pressure curves, respectively, at this point.

Using $(\partial V_{\mathrm{I}}/\partial T)_P \doteq 0$, $(\partial V_{\mathrm{II}}/\partial T)_P = -2.5$ cc/mol-deg, $(dP/dT)_\lambda = -37.5$ atmos/deg, $(dP/dT)_M = 29$ atmos/deg, calculation gives $\Delta_{\mathrm{I,II}}(d\Delta V_M/dT)_M = -4.5$ cc/mol-deg. This agrees well with an experimental value of $-4(\pm 1)$ cc/mol-deg, obtained from Fig. 5.

A second relationship can be derived in much the same way for the difference in the slope of the dP/dT curve on the two sides of the "triple point," $\Delta_{\mathrm{I,II}}(d^2P/dT^2)_M$. This derivation involves using the Clausius-Clapeyron equation, the first Ehrenfest equation, the above relationship, and

$$c_{PL} - c_{PS} = \frac{d\rho}{dT} - \frac{\rho}{T} + \frac{\rho}{\pi V}\left[\left(\frac{\partial V_L}{\partial T}\right)_P - \left(\frac{\partial V_S}{\partial T}\right)_P\right].^{16}$$

The result is

$$\Delta_{\mathrm{I,II}}\left(\frac{d^2P}{dT^2}\right)_M = \frac{1}{(\Delta V)_M}\Delta_{\mathrm{I,II}}\left(\frac{d(\Delta V)_M}{dT}\right)_M\left[\left(\frac{dP}{dT}\right)_\lambda - \left(\frac{dP}{dT}\right)_M\right]. \quad (3)$$

The data from the previous paragraph, and $\Delta V = 1.48$ cc/mol from this equation, gives $\Delta_{\mathrm{I,II}}(d^2P/dT^2)_M = -180$ atmos/deg^2.

The experimental dP/dT curve, obtained by a graphical differentiation of Fig. 3 and confirmed by differencing the data and obtaining average slopes by least square straight lines, is shown in Fig. 7. The gist of the evidence is that dP/dT at 1.74° is about 20 atmos/deg and that it rises to about 29 atmos/deg at 1.75°. The shape of the curve is doubtful in this interval and is indicated by a dotted curve, The

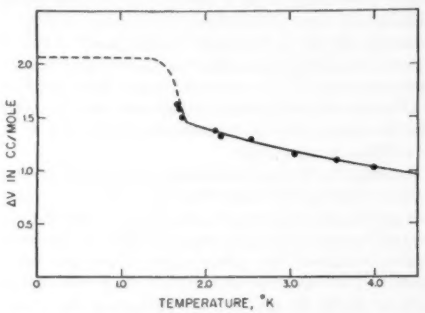

FIG. 5. The change in molar volume of helium on melting ($\Delta V = V_L - V_S$).

[14] J. S. Dugdale and F. E. Simon, Proceedings of the International Conference on Low Temperature Physics, Oxford, 1951, p. 25.

[15] Reference 3, p. 255.

[16] See, for instance, E. A. Guggenheim, *Thermodynamics* (Interscience Publishers, Inc., New York, 1949), p. 126.

average value of $\Delta_{I,II}(d^2P/dT^2)_M$ over this interval is about -900 atmos/deg^2, and the actual value just below 1.743° is most likely two or three times this figure. The predicted slope is also shown in Fig. 7 for comparison.

The discrepancy between the calculated and experimental values is very large and cannot be explained readily by experimental error in any of the quantities involved, especially in view of the good agreement with the ΔV curve. When these melting pressure data are compared with earlier data, the deviations are always in such a direction so as to decrease the slope of the dP/dT curve below the λ-point, although the discrepancies in melting pressures are of the order a few tenths of a percent. Further experiments are planned, using the blocked capillary technique, to check the accuracy of these melting pressure data by an independent method.

An alternative suggestion is that there is something incorrect in the application of second-order phase transition theory to liquid helium, although Eq. (2) seems to hold quite well. The usual "proof" of the second-order nature of the λ-transformation uses the first Ehrenfest equation,[15]

$$\left(\frac{dP}{dT}\right)_\lambda = \frac{\Delta C_P}{T\Delta(\partial V/\partial T)_P}, \tag{4}$$

and the experimental values of $(dP/dT)_\lambda$ and ΔC_P to calculate $\Delta(\partial V/\partial T)_P$. The agreement with experiment, usually quoted as "good," is of the order of fifty percent or less, if the original calculation is checked. Since it is doubtful that the accuracy of the melting pressure measurements can be pushed any farther, it would seem that a new and much more accurate determination

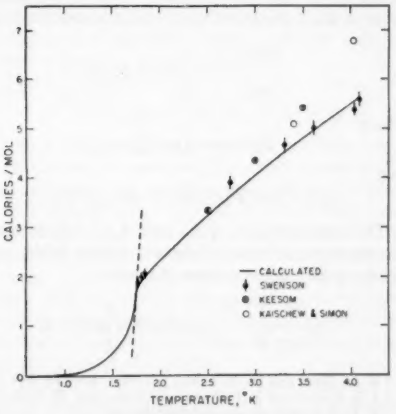

FIG. 6. The latent heat of fusion of helium, as calculated from the Clausius-Clapeyron equation and as determined experimentally.

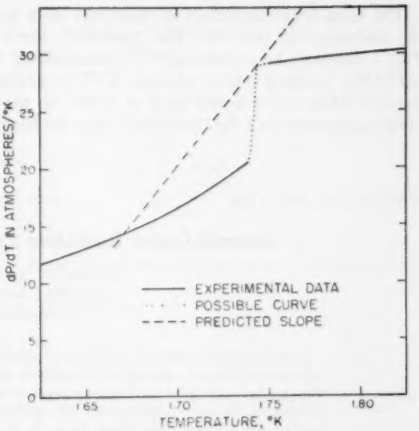

FIG. 7. Experimental values for the slope of the melting pressure curve in the vicinity of the "triple point."

of $\Delta(\partial V/\partial T)_P$ would be of value to help decide whether or not the Ehrenfest relations apply to liquid helium. It is obviously quite important that the Ehrenfest equations should be checked closely in the one case in which they are believed to apply accurately.

The greater part of this work was made possible by a grant from the Harvard Foundation for Advanced Study and Research. I wish to express my appreciation to Mr. J. A. Stewart for his help in taking the data and to Mr. Gösta Bjorklund for his technical assistance.

Note added in proof:—Recent experiments at this laboratory cast doubt on the λ-point-pressure curve of Fig. 4, and it was redetermined using a more accurate technique. These measurements show that below 1.85° the λ-temperatures are appreciably higher than given above, and the coordinates of the upper "triple point" on the helium phase diagram should be given as

$$P_\lambda = 29.64(\pm.03) \text{ atmos}, \quad T_\lambda = 1.764(\pm.003)\ ^\circ\text{K}.$$

The discrepancy is most likely due to the rather insensitive method used previously, which, it would seem, gave a point of high thermal conductivity, rather than the onset of superfluidity.

There is no evidence from the data of Fig. 3 that $(dP/dT)_M$ begins to decrease until below 1.75°, although one would expect the change to occur at the "triple point." New melting pressure data, which were obtained by using the blocked capillary technique, confirm this curve to within ±.001° below 1.75° but indicate that the melting temperatures of Fig. 3 are low (by 0.001° to 0.002°) above this point. Thus, it is suggested that this obvious break in the curve is due to the onset of the high thermal conductivity of helium II, the maximum value of which occurs a few hundredths of a degree below the λ-point.

The most important effect of these new data is on the discussion in Sec. IV. The "possible" curve in Fig. 7 can now be constructed by extrapolating the $(dP/dT)_M$ curve in helium II from 1.74° to intersect the $(dP/dT)_M$ curve in helium I at 1.764°, so that a better agreement with the "predicted" slope is obtained (using a new $(dP/dT)_\lambda = 54.5$ atmos/deg). A difference of a factor of three or more still exists in the slopes, however, and this seems to be outside experimental error.

Details of the capillary blocking and λ-point-pressure experiments will be published elsewhere.

PHYSICAL REVIEW VOLUME 86, NUMBER 6 JUNE 15, 1952

Second-Order Radiative Corrections to Hyperfine Structure*

NORMAN M. KROLL AND FRANKLIN POLLOCK
Columbia University, New York, New York

(Received February 18, 1952)

In this paper the effect of second-order radiative displacements of the energy levels of a bound electron on hyperfine structure separation is examined, and a correction to the Fermi formula for s levels is obtained. The treatment is based on an approximate evaluation of a finite, completely renormalized, and exact expression for the second order energy. The correction, which is restricted to atoms of small αZ, is found to be $[\alpha/2\pi - \alpha^2 Z(5/2 - \ln 2)]E_H$, where E_H is the Fermi energy. The effect of this and other corrections to the Fermi formula on the presently accepted value of the fine structure constant is discussed.

INTRODUCTION

THE interaction of the quantized electromagnetic field with the electron field modifies the properties of the electron and thus causes displacement of the energy levels of electrons bound in atomic or prescribed external fields. The existence of electromagnetic displacements was first recognized through observation of energy level separations, and it is through precise measurement of these separations that the various predictions of quantum electrodynamics are accessible to detailed experimental investigation. Previous theoretical treatments of this problem have been limited by the fact that weak field approximations are made in the process of recognizing and removing charge and mass renormalizations. In the case of the hyperfine structure, the radiative corrections have never been calculated directly, previously obtained results having been inferred from the anomalous magnetic moment of the electron.[1] It has long been realized, however, that a direct evaluation of the second order radiative displacement might yield, in addition to the effect of the second order moment, corrections to the hyperfine structure frequency of order $\alpha^2 Z$. As such corrections arise from the high momentum parts of the external field and electron wave function, their evaluation and comparison with experiment may serve to extend the domain in which the theory has been investigated. Furthermore, in view of the important role played by the hyperfine structure formula in recent determinations of the fine structure constant, it is clear that such corrections may significantly affect the numerical value which one obtains.[2-4]

* Work supported in part by the Signal Corps and ONR.
[1] J. Schwinger, Phys. Rev. **73**, 416 (1948).
[2] H. A. Bethe and C. Longmire, Phys. Rev. **75**, 306 (1949).
[3] J. A. Bearden and H. M. Watts, Phys. Rev. **81**, 73 (1951).
[4] J. W. M. DuMond and E. R. Cohen, Phys. Rev. **82**, 555 (1951).

THE SELF-ENERGY FORMULA

In order to deal systematically with the energy level displacement problem it is desirable to begin with an exact expression for the second order correction. Such expressions in noncovariant form were in fact the starting point of the earliest calculations of the level shift[5,6] and have been given in covariant form by Feynman[7] and Schwinger.[8] We shall briefly derive these here following the methods of Dyson.[9]

As a starting point we consider our theory to be cast in a modified interaction representation in which the effects of the external potential appear in the equations of motion for the field variables, while that of the interaction between the electron and photon fields appears in the interaction Hamiltonian.[10] That is, the development of the wave functional in time is described by

$$\frac{\delta\Psi[\sigma]}{\delta\sigma(x)} = -\frac{i}{\hbar c}H_i(x)\Psi[\sigma], \tag{1}$$

where

$$H_i(x) = -j_\mu(x)A_\mu(x)/c, \tag{2}$$

and

$$j_\mu(x) = \tfrac{1}{2}iec[\bar{\psi}(x)\gamma_\mu\psi(x) - \psi(x)\gamma_\mu{}^T\bar{\psi}(x)]. \tag{3}$$

The operators $\psi(x)$, $\bar{\psi}(x)$, and $A_\mu(x)$, which describe the electron-positron and electromagnetic fields, respectively, satisfy the equations of motion

$$\gamma_\mu\frac{\partial\psi}{\partial x_\mu} + \left[-\frac{ie}{\hbar c}\gamma_\mu A_\mu{}^e(x) + \kappa_0\right]\psi(x) = 0, \tag{4}$$

[5] N. M. Kroll and W. E. Lamb, Jr., Phys. Rev. **75**, 388 (1949).
[6] J. B. French and V. F. Weisskopf, Phys. Rev. **75**, 1240 (1949).
[7] R. P. Feynman, private communication.
[8] J. Schwinger, Proc. Nat. Acad. **7**, 452, 455 (1951).
[9] F. J. Dyson, Phys. Rev. **75**, 486 (1949).
[10] W. H. Furry, Phys. Rev. **81**, 115 (1951).

$$-\frac{\partial\bar{\psi}}{\partial x_\mu}\gamma_\mu+\bar{\psi}(x)\left[-\frac{ie}{\hbar c}\gamma_\mu A_\mu^e(x)+\kappa_0\right]=0, \quad (5)$$

$$\Box^2 A_\mu(x)=0, \quad (6)$$

and the usual commutation relations. $A_\mu^e(x)$ is a specified external potential.

Mass renormalization can be formally inserted into these equations by means of a unitary transformation which takes (2), (4), and (5) into

$$H_I(x)=c^{-1}j_\mu(x)A_\mu(x)-[(\kappa-\kappa_0)/\kappa_0]mc^2\bar{\psi}(x)\psi(x) \quad (2')$$
$$=H_1(x)+H_2(x),$$

$$\gamma_\mu\frac{\partial\psi}{\partial x_\mu}+\left[-\frac{ie}{\hbar c}\gamma_\mu A_\mu^e(x)+\kappa\right]\psi(x)=0, \quad (4')$$

$$-\frac{\partial\bar{\psi}}{\partial x_\mu}\gamma_\mu+\bar{\psi}(x)\left[-\frac{ie}{\hbar c}\gamma_\mu A_\mu^e(x)+\kappa\right]=0. \quad (5')$$

Equation (1) has the well-known solution

$$\Psi[t_+]=U(t_+,t_-)\Psi[t_-],$$

where

$$U(t_+,t_-)=\sum_{n=0}^{\infty}\frac{1}{n!}\left(\frac{-i}{\hbar c}\right)^n\int_{t_-}^{t_+}$$
$$\times P[H_I(x_1),\cdots,H_I(x_n)]d_4x_1\cdots d_4x_n.$$

Second-order radiative corrections are contained in

$$U^{(2)}(t_+,t_-)=\frac{1}{2}\left(\frac{-i}{\hbar c}\right)^2\int_{t_-}^{t_+}d_4x_1d_4x_2$$
$$\times P[H_1(x_1),H_1(x_2)]+\frac{-i}{\hbar c}\int_{t_-}^{t_+}H_2(x_1)d_4x_1,$$

since H_2 is already of second order in the coupling constant. The second-order correction to the energy of an electron in a stationary state a of the external potential is given by the relation

$$-(i/\hbar)(t_+-t_-)\Delta E^{(2)}$$
$$=\text{imaginary part }(\Psi_a,U(t_+,t_-)\Psi_a), \quad (7)$$

where Ψ_a is the wave functional of the uncoupled electron photon system corresponding to the presence of a single electron in the specified state and no photons. The time difference (t_+-t_-) is to be taken large, and any oscillating dependence on the limits t_+ and t_- is to be ignored. Equation (7) simply states that a change in the energy of the state Ψ_a manifests itself by a change in phase. The real part of the expression on the right side of (7) corresponds to the decay of the state Ψ_a arising from a transition to a lower energy state accompanied by emission of a photon.

The expression (7) can be conveniently analyzed by means of Feynman diagrams in a manner entirely analogous to the corresponding problem for a free

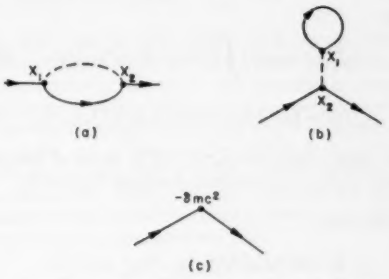

FIG. 1. Feynman diagrams for the self-energy of a bound electron.

electron. One obtains

$$-(i/\hbar)(t_+-t_-)\Delta E=$$
$$-\left(\frac{-i}{\hbar c}\right)^2(-ie)^2\frac{\hbar c}{4}\int_{t_-}^{t_+}\bar{\phi}_a(x_2)\gamma_\mu S_F^e(x_2,x_1)\gamma_\mu$$
$$\times\phi_a(x_1)D_F(x_2-x_1)d_4x_1d_4x_2$$
$$+\left(\frac{-i}{\hbar c}\right)^2(-ie)^2\frac{\hbar c}{4}\int_{t_-}^{t_+}\bar{\phi}_a(x_2)\gamma_\mu\phi(x_2)D_F(x_2-x_1)$$
$$\times\mathrm{Tr}[\gamma_\mu S_F^e(x_1,x_1)]d_4x_2d_4x_1$$
$$+\frac{i}{\hbar c}\frac{\kappa-\kappa_0}{\kappa_0}mc^2\int_{t_-}^{t_+}\bar{\phi}_a(x_1)\phi_a(x_1)d_4x_1, \quad (8)$$

corresponding to the diagrams in Fig. 1. $\phi_a(x)$ and $\bar{\phi}_a(x)$ are the normalized c-number solutions of the Dirac equation and its adjoint (4′ and 5′) corresponding to a designated stationary state. $D_F(x_2-x_1)$ is the photon propagation function defined by Feynman and Dyson (the notation and normalization are Dyson's), while $S_F^e(x_2,x_1)$ is defined in a manner analogous to the free electron propagation function by

$$\tfrac{1}{2}S_F^e(x_2,x_1)_{\alpha\beta}=\langle P[\bar{\psi}_\alpha(x_2),\bar{\psi}_\beta(x_1)]\rangle_0\epsilon(x_1,x_2),$$

where $\langle\ \rangle_0$ denotes the vacuum expectation value.[11]

We shall refer to the energy represented by diagram (a) as the fluctuation energy, $\Delta E_F^{(a)}$. It contains a mass-like part which is to be just canceled by the energy corresponding to diagram (c).

The energy corresponding to diagram (b) will be referred to as the polarization energy. It can be written as[12]

$$\Delta E_P=\frac{-ie}{c(t_+-t_-)}\int_{t_-}^{t_+}\bar{\phi}_a(x_1)\gamma_\mu A_\mu^P(x_1)\phi_a(x_1)d_4x_1, \quad (9)$$

[11] Note that the vacuum state with respect to the matter field is defined by the condition $\psi^+(x)\Psi_0=0$ and $\bar{\psi}^-(x)\Psi_0=0$ and differs from the vacuum state used in the free particle interaction representation.

[12] $S_F^e(x_2,x_2)$ is to be understood as $\frac{1}{2}\lim_{x_2',x_2''\to x_2}[S_F^e(x_2',x_2'')+S_F^e(x_2'',x_2')]$ where x_2' is earlier, x_2'' is later than x_2. [See Schwinger, Phys. Rev. 82, 664 (1951).] This definition insures

where

$$A_\mu^P(x_1)=(i/2c)\int D_F(x_1-x_2)j_\mu^P(x_2)d_4x_2, \quad (10)$$

and

$$j_\mu^P(x_2)=\tfrac{1}{2}iec\ \mathrm{Tr}[\gamma_\mu S_F^e(x_2,x_2)]=\langle j_\mu(x_2)\rangle_0. \quad (11)$$

An explicit form for $S_F^e(x_2,x_1)$ in terms of the stationary states of the external potential is given by

$$\begin{aligned}\tfrac{1}{2}S_F^e(x_2,x_1)_{\alpha\beta}&=\sum_{E_r^P>0}(\phi_r(x_2))_\alpha(\bar{\phi}_r(x_1))_\beta; \quad (x_2-x_1)_0>0,\\ &=-\sum_{E_\rho^P<0}(\phi_\rho(x_2))_\alpha(\bar{\phi}_\rho(x_1))_\beta; \quad (x_2-x_1)_0<0. \quad (12)\end{aligned}$$

Use of this form in (8) followed by integration over the time variables in d_4x_1 and d_4x_2 reduces the above formula for ΔE to the possibly more familiar form used by Kroll and Lamb[5] and French and Weisskopf.[6]

We shall, in fact, find it convenient to carry out one time integration at this time. In view of (12), $S_F^e(x_2,x_1)$ depends upon the time-like components of x_1 and x_2 only through their difference $x_0=(x_2-x_1)_0$. This same remark applies, therefore, to the entire integrands of 8(*a*) and 8(*b*), while the integrand of 8(*c*) is independent of the time-like component. Thus in the limit $t_+\to\infty$, $t_-\to-\infty$ one time integration may be performed immediately, yielding

$$\begin{aligned}\Delta E=\text{real part}\Big\{&-i\alpha\pi\hbar c\int\bar{\phi}_a(x_2)\gamma_\mu S_F^e(x_2,x_1)\gamma_\mu\\ &\times\phi_a(x_1)D_F(x_2-x_1)d\mathbf{x}_1d\mathbf{x}_2dx_0\\ &-ie\int\bar{\phi}_a(x_1)\gamma_\mu A_\mu^P(x_1)\phi_a(x_1)d\mathbf{x}_1\\ &-\frac{\kappa-\kappa_0}{\kappa_0}mc^2\int\bar{\phi}_a(x_1)\phi_a(x_1)d\mathbf{x}_1\Big\}. \quad (13)\end{aligned}$$

REDUCTION OF THE SELF-ENERGY FORMULA

Although the expression (13) is exact, $\Delta E^{(a)}$ contains an infinite mass term which must be isolated and canceled against $\Delta E^{(c)}$, while $\Delta E^{(b)}$ contains an infinite term corresponding to a charge renormalization which must be recognized and removed. The renormalization program will be carried through in such a way as to yield an expression which is still exact and whose individual terms are finite and well defined.

We first rewrite our expressions in momentum space by introducing the appropriate Fourier transforms defined by[13]

$$\begin{aligned}\phi_a(x)&=\int\phi_a(\mathbf{p})\delta(p_0-p_a)e^{ip\cdot x}d_4p,\\ \bar{\phi}_a(x)&=\int\bar{\phi}_a(\mathbf{p})\delta(p_0-p_a)e^{-ip\cdot x}d_4p,\\ S_F^e(x_2,x_1)&=\int S_F^e(p_2,p_1)\delta[(p_2-p_1)_0]\\ &\qquad\times e^{i(p_2\cdot x_2-p_1\cdot x_1)}d_4p_1d_4p_2, \quad (14)\\ D_F(x)&=\int D_F(k)e^{ik\cdot x}d_4k=\frac{-2i}{(2\pi)^4}\int\frac{e^{ik\cdot x}}{k^2}d_4k,\\ A_\mu^e(x)&=\int A_\mu^e(\mathbf{q})\delta(q_0)e^{iq\cdot x}d_4q,\\ A_\mu^P(x)&=\int A_\mu^P(\mathbf{q})\delta(q_0)e^{iq\cdot x}d_4q.\end{aligned}$$

Inserting these in (13), carrying out the coordinate space integrations, and the trivial momentum space integrations, we find

$$\begin{aligned}\Delta E=\mathrm{Re}\Big\{&-\alpha\hbar c(2\pi)^4\int\bar{\phi}_a(\mathbf{p}_2)\gamma_\mu S_F^e(p_2-k,p_1-k)\\ &\times\gamma_\mu\phi_a(\mathbf{p}_1)\frac{d_4k}{k^2}d\mathbf{p}_1d\mathbf{p}_2\\ &-ie(2\pi)^3\int\bar{\phi}_a(\mathbf{p}_2)\gamma_\mu A_\mu^P(p_2-p_1)\phi_a(\mathbf{p}_1)d\mathbf{p}_1d\mathbf{p}_2\\ &-\frac{\kappa-\kappa_0}{\kappa}mc^2(2\pi)^3\int\bar{\phi}_a(\mathbf{p})\phi_a(\mathbf{p})d\mathbf{p}\Big\}. \quad (15)\end{aligned}$$

(a) Renormalization of the Polarization Energy

We first note that as a consequence of its definition and the equations of motion (4′) and (5′), $S_F^e(x_2,x_1)$ satisfies

$$\gamma_\mu\frac{\partial S_F^e}{\partial x_{2\mu}}+\left[-\frac{ie}{\hbar c}\gamma_\mu A_\mu^e(x_2)+\kappa\right]S_F^e(x_2,x_1)=2i\delta_4(x_2-x_1),$$

and (16)

$$-\frac{\partial S_F^e}{\partial x_{1\mu}}\gamma_\mu+S_F^e(x_2,x_1)\left[-\frac{ie}{\hbar c}\gamma_\mu A_\mu^e(x_1)+\kappa\right]=2i\delta_4(x_2-x_1),$$

that $\langle j_\mu(x_2)\rangle_0=\frac{1}{2}iec\ \mathrm{Tr}(\gamma_\mu S_F(x_2,x_2)]=0$ for zero external field. It is for this reason that diagrams like (*b*) are omitted from the usual Feynman rules, which apply for a representation in which the matter field operators obey a free particle equation of motion.

[13] The following remarks concerning the notation may be useful. Four vectors will be denoted by ordinary type (p, k, etc.) while boldface type ($\mathbf{p}$, $\mathbf{k}$, etc.) will be used to denote their respective space parts. The notations $p_\mu k_\mu$ and $p\cdot k$ will be used interchangeably to denote the four dimensional scalar product, so that $p_\mu k_\mu=p\cdot k=\mathbf{p}\cdot\mathbf{k}-p_0k_0$. It is hoped that the use of the same symbol for a function and its Fourier transform will not be a source of confusion. They are, of course, not the same functions of their respective arguments.

which in momentum space take the form

$$(i\gamma\cdot p_2+\kappa)S_F^e(p_2,p_1)$$
$$=\frac{ie}{\hbar c}\int\gamma\cdot A^e(p_2-p_3)S_F^e(p_3,p_1)d\mathbf{p}_3+\frac{2i}{(2\pi)^4}\delta_3(\mathbf{p}_2-\mathbf{p}_1),$$

and (17)

$$S_F^e(p_2,p_1)(i\gamma\cdot p_1+\kappa)$$
$$=\frac{ie}{\hbar c}\int S_F^e(p_2,p_3)\gamma\cdot A^e(p_3-p_1)d\mathbf{p}_3+\frac{2i}{(2\pi)^4}\delta_3(\mathbf{p}_2-\mathbf{p}_1).$$

Iteration of these equations in combination then yields

$$S_F^e(p_2,p_1)$$
$$=\frac{-2i}{(2\pi)^4}\Big[\frac{i\gamma\cdot p_2-\kappa}{p_2^2+\kappa^2}\delta_3(\mathbf{p}_2-\mathbf{p}_1)-\Big(\frac{ie}{\hbar c}\Big)\frac{i\gamma\cdot p_2-\kappa}{p_2^2+\kappa^2}$$
$$\times\gamma\cdot A^e(p_2-p_1)\frac{i\gamma\cdot p_1-\kappa}{p_1^2+\kappa^2}\Big]$$
$$+\Big(\frac{ie}{\hbar c}\Big)^2\frac{i\gamma\cdot p_2-\kappa}{p_2^2+\kappa^2}\Big[\int\gamma\cdot A^e(\mathbf{q})$$
$$\times S_F^e(p_2-q,p_1+q')\gamma\cdot A^e(q')d\mathbf{q}d\mathbf{q}'\Big]\frac{i\gamma\cdot p_1-\kappa}{p_1^2+\kappa^2}$$
$$=S_F(p_2)\delta_3(\mathbf{p}_2-\mathbf{p}_1)-\Big(\frac{(2\pi)^4}{-2i}\Big)\Big(\frac{ie}{\hbar c}\Big)S_F(p_2)$$
$$\times\gamma\cdot A^e(p_2-p_1)S_F(p_1)$$
$$+\Big(\frac{ie}{\hbar c}\Big)^2\Big(\frac{(2\pi)^4}{-2i}\Big)^2S_F(p_2)\Big[\int\gamma\cdot A^e(\mathbf{q})$$
$$\times S_F^e(p_2-q,p_1+q')\gamma\cdot A^e(\mathbf{q}')d\mathbf{q}d\mathbf{q}'\Big]S_F(p_1). \quad (18)$$

The definition of $A_\mu^P(x)$ given by (10) and (11) yields for $A_\mu^P(\mathbf{q})$,

$$A_\mu^P(\mathbf{q})=-e(2\pi)^4D_F(q)\int\mathrm{Tr}[\gamma_\mu S_F^e(p,p-q)]d_4p. \quad (19)$$

On inserting the expression (18) for S_F^e in (19) one finds that the contribution from the first term vanishes, while that of the second is identical to the weak field polarization potential which has been computed many times before. Using this result in the form quoted by Karplus and Kroll[14] we have

$$A_\mu^P(\mathbf{q})=\frac{\alpha}{2\pi}AA_\mu^e(\mathbf{q})+\frac{\alpha}{2\pi}q^2\int_0^1dv\frac{2v^2(1-\frac{1}{3}v^2)}{4\kappa^2+q^2(1-v^2)}$$
$$\times A_\mu^e(\mathbf{q})+\delta A_\mu^P(\mathbf{q}). \quad (20)$$

[14] R. Karplus and N. M. Kroll, Phys. Rev. **77**, 540 (1950). Equation (14).

The first term of (20), which contains the infinite constant factor A, is the well-known charge renormalization term and is to be henceforth ignored. $\delta A_\mu^P(q)$ is the part of the polarization potential which arises from the third term of (18) and is of importance only in the case of a strong external field. It is, however, finite and entirely free of effects to be attributed to renormalization. Using (20) but omitting the renormalization term we find for the second-order polarization energy, the finite exact expression,

$$\Delta E_P=-ie(2\pi)^2\alpha\int_0^1dv\int\bar{\phi}_a(\mathbf{p}_2)$$
$$\times\frac{2v^2(1-\frac{1}{3}v^2)(p_2-p_1)^2\gamma\cdot A^e(p_2-p_1)}{4\kappa^2+(p_2-p_1)^2(1-v^2)}\phi_a(\mathbf{p}_1)d\mathbf{p}_1d\mathbf{p}_2$$
$$-ie(2\pi)^3\int\bar{\phi}_a(p_2)\gamma\cdot\delta A^P(p_2-p_1)\phi_a(p_1)d\mathbf{p}_1d\mathbf{p}_2. \quad (21)$$

(b) Rearrangement of the Fluctuation Energy

The fluctuation energy can be treated in a manner entirely analogous to our treatment of the polarization energy. That is, $S_F^e(p_2,p_1)$ appearing in $\Delta E^{(a)}$ can be replaced by the right side of (18). The first term then contains the mass term which one cancels with $\Delta E^{(c)}$, while the first and second terms each contain an infinite charge term which can be isolated and are found to just cancel. The remaining expression is then finite and exact. This particular separation of terms, while straightforward, turns out to be unsuited to the approximations which we shall subsequently make. We use instead a separation of terms which is due to Feynman[15] and is based on the pair of identities,[16]

$$\gamma_\mu=-[i\gamma\cdot(p_1-k)+\kappa]\frac{2ip_{1\mu}-i\gamma\cdot k\gamma_\mu}{k^2-2p_1\cdot k}$$
$$+\frac{2ip_{1\mu}-i\gamma\cdot k\gamma_\mu}{k^2-2p_1\cdot k}[i\gamma\cdot p_1+\kappa], \quad (22a)$$

$$\gamma_\mu=[i\gamma\cdot p_2+\kappa]\frac{2ip_{2\mu}-i\gamma_\mu\gamma\cdot k}{k^2-2p_2\cdot k}$$
$$-\frac{2ip_{2\mu}-i\gamma_\mu\gamma\cdot k}{k^2-2p_2\cdot k}[i\gamma\cdot(p_2-k)+\kappa]. \quad (22b)$$

[15] R. P. Feynman, private communication. The authors are indebted to Professor Feynman for describing this method to them.

[16] It is to be noted that each of the two terms appearing in these identities are singular at the zeros of the denominator. It is convenient to displace this singularity from the real axis by replacing $k^2-2p\cdot k$ by $k^2-2p\cdot k-i\epsilon$, where ϵ is a small positive quantity. It is then possible to treat these denominators on the same footing as those arising from $D_F(k)$ and $S_F(p)$ and thus to apply Feynman's contour integral method to the evaluation of the k-space integrals. While ϵ will not be explicitly displayed in any of our formulas, it is to be tacitly understood that these quantities are to be set equal to zero only after the entire calculation is completed.

We insert these in expression (15) for $\Delta E_F^{(a)}$, the form (a) for the γ_μ on the right, the form (b) for the γ_μ on the left. Each free electron operator, $i\gamma\cdot p+\kappa$, then appears with the appropriate momentum and adjacent to a wave function or the propagation function S_F^e. Now in addition to Eq. (17) for S_F^e we have

$$(i\gamma\cdot p_1+\kappa)\phi_a(\mathbf{p}_1)=\frac{ie}{\hbar c}\int\gamma\cdot A^e(\mathbf{p}_1-\mathbf{p}_1')\phi_a(\mathbf{p}_1')d\mathbf{p}_1',$$
$$\bar\phi_a(\mathbf{p}_2)(i\gamma\cdot p_2+\kappa)=\frac{ie}{\hbar c}\int\bar\phi_a(\mathbf{p}_2')\gamma\cdot A^e(\mathbf{p}_2-\mathbf{p}_2')d\mathbf{p}_2'. \tag{23}$$

Applying these as well as (17) we obtain[17]

$$\Delta E^{(a)}=C+L+Q, \tag{24}$$

where

$$C=4i\hbar c\alpha\int\bar\phi_a(\mathbf{p})\frac{i\gamma\cdot(p+k)}{k^2-2p\cdot k}\phi_a(\mathbf{p})\frac{d_4k}{k^2}d\mathbf{p}, \tag{25}$$

$$L=-2i\hbar c\alpha\left(\frac{ie}{\hbar c}\right)\Big[\int\bar\phi_a(\mathbf{p}_2)\frac{2ip_{2\mu}-i\gamma_\mu\gamma\cdot k}{k^2-2p_2\cdot k}\times\gamma\cdot A^e(\mathbf{p}_2-\mathbf{p}_1)\frac{2ip_{1\mu}-i\gamma\cdot k\gamma_\mu}{k^2-2p_1\cdot k}\phi_a(p_1)\frac{d_4k}{k^2}d\mathbf{p}_1d\mathbf{p}_2$$
$$+4\int\bar\phi_a(\mathbf{p}_2)\frac{k^2-p_2\cdot k+p_2^2}{(k^2-2p_2\cdot k)^2}\times\gamma\cdot A^e(\mathbf{p}_2-\mathbf{p}_1)\phi_a(\mathbf{p}_1)\frac{d_4k}{k^2}d\mathbf{p}_1d\mathbf{p}_2\Big], \tag{26}$$

$$Q=-\hbar c\alpha(2\pi)^4\left(\frac{ie}{\hbar c}\right)^2\int\bar\phi_a(\mathbf{p}_2)\mathfrak{A}_\mu'(q_2,p_2,k)\times S_F^e(p_2-k-q_2,p_1-k+q_1)\mathfrak{A}_\mu(q_1,p_1,k)\times\phi_a(\mathbf{p}_1)\frac{d_4k}{k^2}d\mathbf{p}_1d\mathbf{p}_2d\mathbf{q}_1d\mathbf{q}_2, \tag{27}$$

where,

$$\mathfrak{A}_\mu(q_1,p_1,k)=-\gamma\cdot A^e(\mathbf{q}_1)\frac{2ip_{1\mu}-i\gamma\cdot k\gamma_\mu}{k^2-2p_1\cdot k}+\frac{2i(p_1+q_1)_\mu-i\gamma\cdot k\gamma_\mu}{k^2-2(p_1+q_1)\cdot k}\gamma\cdot A^e(\mathbf{q}_1), \tag{28}$$

$$\mathfrak{A}_\mu'(q_2,p_2,k)=-\gamma\cdot A^e(q_2)\frac{2ip_{2\mu}-i\gamma_\mu\gamma\cdot k}{k^2-2p_2\cdot k}+\frac{2i(p_2-q_2)_\mu-i\gamma_\mu\gamma\cdot k}{k^2-2(p_2-q_2)\cdot k}\gamma\cdot A^e(\mathbf{q}_2). \tag{29}$$

We now proceed to a rearrangement of (24) with the objective of isolating and removing renormalizations.

From (25),

$$C=4i\hbar c\alpha\int\bar\phi_a(\mathbf{p})I(p)\phi_a(\mathbf{p})d\mathbf{p},$$

with

$$I(p)=\int\frac{i\gamma\cdot(p+k)}{(k^2-2p\cdot k)}\frac{d_4k}{k^2}.$$

Following the procedure of Karplus and Kroll,[18] we find

$$I(p)=\int dxd_4k\left[\frac{i\gamma\cdot p(1+x)}{(k^2-p^2x^2)^2}+xi\gamma\cdot p\frac{x^2p^2}{(k^2-p^2x^2)^3}\right]$$
$$=-\kappa_0\left[\frac{9i\pi^2}{4}+\frac{3}{2}\int\frac{d_4k}{(k^2+\kappa^2)^2}\right]+(i\gamma\cdot p+\kappa)\left[-\frac{3}{4}i\pi^2+\frac{3}{2}\int\frac{d_4k}{(k^2+\kappa^2)^2}\right]$$
$$-\frac{3}{2}i\pi^2\int_0^1\frac{[i\gamma\cdot p+\kappa][i\gamma\cdot p(1-2z)-2\kappa(1-z)][i\gamma\cdot p+\kappa]}{\kappa^2-(p^2+\kappa^2)z}dz. \tag{30}$$

Inserting (30) into (25) and applying (23) we find

$$C=\frac{\kappa-\kappa_0}{k_0}mc^2\int\bar\phi_a(\mathbf{p})\phi_a(\mathbf{p})d\mathbf{p}+4\hbar c\alpha\left[\frac{3}{4}\pi^2+\frac{3}{2}i\int\frac{d_4k}{[k^2+\kappa^2]^2}\right]\left(\frac{ie}{\hbar c}\right)\int\bar\phi_a(\mathbf{p}_2)\gamma\cdot A^e(\mathbf{p}_2-\mathbf{p}_1)\phi_a(\mathbf{p}_1)d\mathbf{p}_2d\mathbf{p}_1$$
$$+6\pi^2\hbar c\alpha\left(\frac{ie}{\hbar c}\right)^2\int\bar\phi_a(\mathbf{p}_2)\gamma\cdot A^e(\mathbf{p}_2-\mathbf{p}_3)\frac{[i\gamma\cdot p_3(1-2z)-2\kappa(1-z)]}{\kappa^2-(p_3^2+\kappa^2)z}\gamma\cdot A^e(\mathbf{p}_3-\mathbf{p}_1)\phi_a(\mathbf{p}_1)d\mathbf{p}_1d\mathbf{p}_2d\mathbf{p}_3dz, \tag{31}$$

$$\frac{\kappa-\kappa_0}{\kappa_0}=\frac{\alpha}{(2\pi)^3}\left[\frac{9\pi^2}{4}-\frac{3i}{2}\int\frac{d_4k}{[k^2+\kappa^2]^2}\right].$$

[17] It is worth noting that the form of (24) is very similar to that of the expression which would have been obtained had (18) been substituted for $S_F^e(p_2,p_1)$ in $\Delta E^{(a)}$. The essential difference is the appearance of the factors $\mathfrak{A}$, $\mathfrak{A}'$ in Q in place of $i\gamma\cdot A^e(\mathbf{q}_1)\times S_F(p_1-k)\gamma_\mu$ and $\gamma_\mu S_F(p_2-k)i\gamma\cdot A^e(\mathbf{q}_2)$. The significance of this difference will be discussed later.

[18] See reference 14, Eqs. (16) to (23). The expression $I(p)$ above is very similar to $I(i\gamma\cdot p+\kappa)$ there evaluated.

The first term is the well-known divergent mass term and is just canceled by $\Delta E^{(c)}$. The second term is also divergent and corresponds to a modification of the electron's charge. It will be canceled by a similar term in L.

Applying similar methods to (26) we find

$$L=-4\hbar c\alpha\left[\frac{3}{4}\pi^2+\frac{3}{2}i\int\frac{d_4k}{[k^2+\kappa^2]^2}\right]\left(\frac{ie}{\hbar c}\right)\times\int\bar{\phi}_a(\mathbf{p}_2)\gamma\cdot A^e(\mathbf{p}_2-\mathbf{p}_1)\phi_a(\mathbf{p}_1)d\mathbf{p}_1d\mathbf{p}_2$$
$$-6\pi^2\hbar c\alpha\left(\frac{ie}{\hbar c}\right)^2\int\bar{\phi}_a(\mathbf{p}_2)\gamma\cdot A^e(\mathbf{p}_2-\mathbf{p}_3)\times\frac{[i\gamma\cdot p_3-\kappa]}{\kappa^2-(p_3^2+\kappa^2)z}\gamma\cdot A^e(\mathbf{p}_3-\mathbf{p}_1)\phi_a(\mathbf{p}_1)d\mathbf{p}_1d\mathbf{p}_2d\mathbf{p}_3dz$$
$$+2\pi^2\hbar c\alpha\left(\frac{ie}{\hbar c}\right)\int\bar{\phi}_a(\mathbf{p}_2)A_\mu^e(\mathbf{p}_2-\mathbf{p}_1)\times K_\mu(p_2,\,p_1)\phi_a(\mathbf{p}_1)d\mathbf{p}_1d\mathbf{p}_2+L_D,\quad(32)$$

where[19]

$$K_\mu(p_2,\,p_1)=\frac{(p_2-p_1)^2}{\kappa^2}\gamma_\mu\int_0^1\left(\frac{2-6y(1-y)}{\Lambda_1{}^2}-\frac{y(1-y)}{\Lambda_2{}^2}\right)dydz$$
$$+\frac{i(p_2-p_1)_\nu\sigma_{\mu\nu}}{\kappa}\int_0^1\frac{dy}{\Lambda_1{}^2}$$
$$+\int_0^1\frac{dy}{\kappa^2\Lambda_1{}^2}\{(5/2)(1-2y)(p_2{}^2-p_1{}^2)\gamma_\mu$$
$$+(i\gamma\cdot p_2+\kappa)\gamma_\mu(i\gamma\cdot p_1+\kappa)$$
$$-\tfrac{1}{2}(i\gamma\cdot p_2+\kappa)^2\gamma_\mu-\tfrac{1}{2}\gamma_\mu(i\gamma\cdot p_1+\kappa)^2$$
$$-iy(p_2-p_1)_\nu\sigma_{\mu\nu}(i\gamma\cdot p_1+\kappa)$$
$$+i(1-y)(i\gamma\cdot p_2+\kappa)(p_2-p_1)_\nu\sigma_{\mu\nu}\}$$
$$+\int_0^1\frac{dydz}{\kappa^2\Lambda_2{}^2}y(p_2{}^2-p_1{}^2)\gamma_\mu,\quad(33)$$

with

$$\Lambda_1{}^2=1-\kappa^{-2}[(p_1{}^2+\kappa^2)y+(p_2{}^2+\kappa^2)(1-y)-(p_2-p_1)^2y(1-y)],$$
$$\Lambda_2{}^2=1-\kappa^{-2}[(p_1{}^2+\kappa^2)yz+(p_2{}^2+\kappa^2)(1-yz)-(p_2-p_1)^2yz(1-y)].$$

[19] In writing out (33) we have omitted terms of the form $q\cdot A^e(\mathbf{q})$. We are at liberty to choose our gauge so that this quantity vanishes and shall do so.

L_D is that part of L which diverges in the infrared. It is given by

$$L_D=-8i\hbar c\alpha\left(\frac{ie}{\hbar c}\right)\int\bar{\phi}_a(\mathbf{p}_2)\frac{p_{2\mu}}{k^2-2p_2\cdot k}\times\left(\frac{p_{2\mu}}{k^2-2p_2\cdot k}-\frac{p_{1\mu}}{k^2-2p_1\cdot k}\right)\gamma\cdot A^e(p_2-p_1)\times\phi_a(\mathbf{p}_1)\frac{d_4k}{k^2}d\mathbf{p}_2d\mathbf{p}_1.\quad(34)$$

There is, of course, a compensating divergence in Q. In order to make evident the fact that $Q+L_D$ is finite, we note that L_D may also be written

$$L_D=\hbar c\alpha(2\pi)^4\left(\frac{ie}{\hbar c}\right)^2\int\bar{\phi}_a(\mathbf{p}_2)\left[\frac{2i(p_2-q_2)_\mu}{k^2-2(p_2-q_2)\cdot k}-\frac{2ip_{2\mu}}{k^2-2p_2\cdot k}\right]\gamma\cdot A^e(\mathbf{q}_2)S_F{}^e(p_2-q_2,\,p_1+q_1)\times\left[\frac{2i(p_1+q_1)_\mu}{k^2-2(p_1+q_1)\cdot k}-\frac{2ip_{1\mu}}{k^2-2p_1\cdot k}\right]\times\gamma\cdot A^e(\mathbf{q}_1)\phi_a(\mathbf{p}_1)\frac{d_4k}{k}d\mathbf{p}_1d\mathbf{p}_2d\mathbf{q}_1d\mathbf{q}_2.\quad(35)$$

In order to verify the identity of (34) and (35) one need merely note that (17) and (22) imply

$$(ie/\hbar c)\int\bar{\phi}(\mathbf{p}_2)[f(p_2)-f(p_3)]\gamma\cdot A^e(\mathbf{p}_2-\mathbf{p}_3)\times S_F{}^e(p_3,\,p)d\mathbf{p}_2d\mathbf{p}_3=-[2i/(2\pi)^4]\bar{\phi}(\mathbf{p})f(p),$$

where $f(p)$ is any function of momentum which is diagonal in the spinor indices. The coefficient of (35) is equal in magnitude and opposite in sign to that of Q, while it is apparent that in the limit of low k_μ, the two integrands become identical.

We obtain finally for the fluctuation energy

$$\Delta E_F=\Delta E^{(a)}+\Delta E^{(c)}=2\pi^2\hbar c\alpha\left(\frac{ie}{\hbar c}\right)\int\bar{\phi}_a(\mathbf{p}_2)\times A_\mu{}^e(\mathbf{p}_2-\mathbf{p}_1)K_\mu(p_2,\,p_1)\phi_a(\mathbf{p}_1)d\mathbf{p}_1d\mathbf{p}_2$$
$$-6\pi^2\hbar c\alpha\left(\frac{ie}{\hbar c}\right)^2\int\bar{\phi}_a(\mathbf{p}_2)\gamma\cdot A^e(\mathbf{p}_2-\mathbf{p}_3)\times\frac{[2i\gamma\cdot p_3z+\kappa(1-2z)]}{\kappa^2-(p_3{}^2+\kappa^2)z}\gamma\cdot A^e(\mathbf{p}_3-\mathbf{p}_1)\times\phi_a(\mathbf{p}_1)d\mathbf{p}_1d\mathbf{p}_2d\mathbf{p}_3dz+(L_D+Q).\quad(36)$$

THE FORM OF THE EXTERNAL POTENTIAL

In order to apply the general expressions derived above to the problem of hyperfine structure it is necessary to specify the form of the external potential. We shall confine our attention to hydrogenic atoms; for these the potential is given by

$$\frac{e}{\hbar c}A_\mu^e(r)=-\frac{i\alpha Z}{r}\delta_{\mu 4}-\frac{e}{\hbar c}\frac{\boldsymbol{\mu}}{4\pi}\times\boldsymbol{\nabla}\left(\frac{1}{r}\right),$$

where α is the fine structure constant, Z the atomic number, and $\boldsymbol{\mu}$ the nuclear magnetic moment operator. The first term is simply the Coulomb potential produced by the nuclear charge, while the second is the magnetic dipole potential produced by the nuclear magnetic moment. $\boldsymbol{\mu}$ can be conveniently expressed in terms of the gyromagnetic ratio, g, the nuclear magneton, $|e|\hbar/2Mc$, and the nuclear spin operator, $\boldsymbol{\Sigma}$, by $\boldsymbol{\mu}=g(|e|\hbar/2Mc)\boldsymbol{\Sigma}$, yielding

$$\frac{e}{\hbar c}A_\mu^e(\mathbf{r})=-\frac{i\alpha Z}{r}\delta_{\mu 4}+\frac{\alpha}{2\kappa}\frac{m}{M}g\boldsymbol{\Sigma}\times\boldsymbol{\nabla}\left(\frac{1}{r}\right). \quad (37)$$

From (14) one easily finds

$$\frac{e}{\hbar c}A_\mu^e(\mathbf{q})=-\frac{i\alpha Z}{2\pi^2q^2}\delta_{\mu 4}+\frac{\alpha}{2\kappa}\frac{m}{M}g\frac{i\boldsymbol{\Sigma}\times\mathbf{q}}{2\pi^2q^2}$$

$$=\frac{e}{\hbar c}A_\mu^{(E)}(\mathbf{q})+\frac{e}{\hbar c}A_\mu^{(H)}(\mathbf{q}), \quad (38)$$

where the superscripts (E) and (H) refer to the electric and magnetic parts of the potential, respectively. The Fermi formula for the hyperfine structure together with the Breit relativistic correction is obtained simply by treating the magnetic potential as a small perturbation, thus

$$E_H=-ie(2\pi)^3\int\bar{\phi}_a(\mathbf{p}_2)\gamma\cdot A^{(H)}(p_2-p_1)\phi_a(\mathbf{p}_1)d\mathbf{p}_2d\mathbf{p}_1.$$

For S states, which will be our principal concern here, this formula yields [20]

$$E_H=\tfrac{2}{3}\pi\alpha g(m/M)(\phi_0^2/\kappa^3)(1+b_n\alpha^2Z^2)\langle\boldsymbol{\sigma}\cdot\boldsymbol{\Sigma}\rangle mc^2, \quad (39)$$

where ϕ_0 is the value of the Schrödinger wave function at the origin. The energy for the higher angular momentum states is of the same order of magnitude.

In considering radiative corrections to (39) we shall confine ourselves to terms which are linear in the nuclear magnetic moment. These corrections will be expressed as multiples of E_H and will be confined to terms of order α and α^2Z.

[20] E. Fermi, Z. Physik **60**, 320 (1930); and G. Breit, Phys. Rev. **35**, 1447 (1930). The subscript n in b_n refers to the principal quantum number of the state in question. Breit's results imply $b_1=3/2$, $b_2=17/8$.

EVALUATION OF THE POLARIZATION ENERGY

The polarization energy appears as the expectation value of the polarization potential for the state in question. The polarization potential can be regarded as consisting of a Coulomb part, which is independent of the nuclear moment, and a magnetic part which involves the nuclear moment linearly. The magnetic part is simply a modification of the nuclear magnetic field and can accordingly be expected to produce a modification in the hyperfine structure. There is, however, also an effect from the Coulomb part which arises from the fact that the lower energy hyperfine structure states are the more tightly bound, and therefore spend more time in the region where the Coulomb polarization potential is large. These two effects are, in fact, exactly equal, and we shall arrange our calculation in a way which makes this apparent at an early stage.

We consider first the contribution of the first term of (21),

$$\Delta E_P'=-\hbar c\alpha(2\pi)^2\left(\frac{ie}{\hbar c}\right)\int_0^1 dv\int\bar{\phi}_a(\mathbf{p}_2)$$

$$\times\frac{2v^2(1-\frac{1}{3}v^2)(p_2-p_1)^2\gamma\cdot A^e(\mathbf{p}_2-\mathbf{p}_1)}{4\kappa+(p_2-p_1)^2(1-v^2)}\phi_a(\mathbf{p}_1)d\mathbf{p}_1d\mathbf{p}_2$$

$$=-\hbar c\alpha(2\pi)^2\left(\frac{ie}{\hbar c}\right)\int_0^1 dv2v^2(1-\tfrac{1}{3}v^2)$$

$$\times\int\bar{\phi}_a(\mathbf{p}_2)\frac{\gamma\cdot A^e(\mathbf{p}_2-\mathbf{p}_1)\phi_a(\mathbf{p}_1)}{4\kappa^2+(p_2-p_1)^2(1-v^2)}[(p_2^2+\kappa^2)$$

$$+(p_1^2+\kappa^2)-2(\kappa^2-p_a^2)-2\mathbf{p}_1\cdot\mathbf{p}_2]d\mathbf{p}_1d\mathbf{p}_2,$$

where p_a is the time like component of p_1 and p_2 and is determined by the state. For hyperfine structure the third term of the above expression is, apart from a numerical factor, essentially $\Delta E_H\times(\kappa^2-p_a^2)\alpha$. $(\kappa^2-p_a^2)$ is of course proportional to the binding energy or $(\alpha Z)^2$, so that this term is a correction of order $\alpha^3Z^2E_H$ and can be ignored. The contribution of the last term to hyperfine structure is also of order $\alpha^3Z^2E_H$. Now, noting that $p^2+\kappa^2=-(i\gamma\cdot p-\kappa)(i\gamma\cdot p+\kappa)$ and recalling (23), we find that the first two terms yield

$$\Delta E_P'=\hbar c\alpha(2\pi)^2\left(\frac{ie}{\hbar c}\right)^2\int_0^1 dv2v^2(1-\tfrac{1}{3}v^2)$$

$$\times\Big[\int\bar{\phi}_a(\mathbf{p}_2)\frac{\gamma\cdot A^e(\mathbf{p}_2-\mathbf{p}_3)[i\gamma\cdot p_3-\kappa]\gamma\cdot A^e(\mathbf{p}_3-\mathbf{p}_1)}{4\kappa^2+(p_3-p_1)^2(1-v^2)}$$

$$\times\phi_a(\mathbf{p}_1)d\mathbf{p}_1d\mathbf{p}_2d\mathbf{p}_3$$

$$+\int\bar{\phi}_a(\mathbf{p}_2)\frac{\gamma\cdot A^e(\mathbf{p}_2-\mathbf{p}_3)[i\gamma\cdot p_3-\kappa]\gamma\cdot A^e(\mathbf{p}_3-\mathbf{p}_1)}{4\kappa^2+(p_3-p_2)^2(1-v^2)}$$

$$\times\phi_a(\mathbf{p}_1)d\mathbf{p}_1d\mathbf{p}_2d\mathbf{p}_3\Big]. \quad (40)$$

Equation (40) involves the external potential quadratically and makes no reference to which factor A_μ^e appeared originally in $\Delta E_P'$ and which factor arose from application of the wave equation. It is therefore clear that the two effects discussed in the first paragraph are equal. Relabeling variables and noting that the two terms of (40) are equal, we obtain

$$\Delta E_P' = 2\hbar c\alpha(2\pi)^2\left(\frac{ie}{\hbar c}\right)^2\int_0^1 dv 2v^2(1-\tfrac{1}{3}v^2)\int \bar{\phi}_a(\mathbf{p}_2) \times\frac{\gamma\cdot A^e(\mathbf{p}_2-\mathbf{p}_1-\mathbf{q})[i\gamma\cdot(p_1+q)-\kappa]\gamma\cdot A^e(\mathbf{q})}{4\kappa^2+q^2(1-v^2)} \times\phi_a(\mathbf{p}_1)d\mathbf{p}_1d\mathbf{p}_2d\mathbf{q}.$$

We now consider

$$\left(\frac{ie}{\hbar c}\right)^2\int dv 2v^2(1-\tfrac{1}{3}v^2)\int d\mathbf{q} \times\frac{\gamma\cdot A^e(\mathbf{p}_2-\mathbf{p}_1-\mathbf{q})[i\gamma\cdot(p_1+q)-\kappa]\gamma\cdot A^e(\mathbf{q})}{4\kappa^2+q^2(1-v^2)}=G(\mathbf{p}_1,\mathbf{p}_2).$$

The form of $\phi_a(\mathbf{p}_1)$, $\bar{\phi}_a(\mathbf{p}_2)$ is such as to confine $|\mathbf{p}_1|$ and $|\mathbf{p}_2|$ to values of the order of $\alpha Z\kappa$ while the q integration yields its main contribution for q's of the order of κ. Thus it is reasonable to suppose that replacing $G(\mathbf{p}_1,\mathbf{p}_2)$ by $G(0,0)$ gives rise to an error of order $\alpha Z\Delta E_P'$, which we shall soon see is of order $\alpha^3Z^2E_H$.[21] In evaluating $G(0,0)$ we may of course also replace p_a by κ. Thus,

$$G(0,0)=\left(\frac{ie}{\hbar c}\right)^2\int dv 2v^2(1-\tfrac{1}{3}v^2)\int d\mathbf{q} \times\frac{\gamma\cdot A^e(-\mathbf{q})[i\gamma\cdot\mathbf{q}-\kappa(1+\gamma_4)]\gamma\cdot A^e(\mathbf{q})}{4\kappa^2+q^2(1-v^2)}.$$

We now note that $\gamma\cdot A^e(-\mathbf{q})(1+\gamma_4)\gamma\cdot A^e(\mathbf{q})$ contains no terms linear in the nuclear moment, while

$$\left(\frac{ie}{\hbar c}\right)^2\gamma\cdot A^e(-\mathbf{q})i\gamma\cdot\mathbf{q}\gamma\cdot A^e(\mathbf{q})=\frac{\alpha^2Z}{4\pi^2\kappa}\frac{m}{M}g\gamma_4\frac{\boldsymbol{\sigma}\cdot\mathbf{q}\times(\boldsymbol{\Sigma}\times\mathbf{q})}{(q^2)^2} =\frac{\alpha^2Z}{6\pi^4\kappa}\frac{m}{M}g\gamma_4\frac{\boldsymbol{\sigma}\cdot\boldsymbol{\Sigma}}{q^2}, \tag{41}$$

on averaging over angles. Equation (41) plays an important part in the evaluation of all of the α^2Z corrections to be obtained later, as all operators which contribute to these corrections are easily reducible to the form on the left. We find therefore that

$$G(0,0)\rightarrow\frac{\alpha^2Z}{6\pi^4\kappa}\frac{m}{M}g\gamma_4\boldsymbol{\sigma}\cdot\boldsymbol{\Sigma}\int_0^1 dv 2v^2(1-\tfrac{1}{3}v^2) \times\int\frac{d\mathbf{q}}{q^2(4\kappa^2+q^2(1-v^2))} =\frac{\alpha^2Z}{6\pi^4\kappa}\frac{m}{M}g\gamma_4\boldsymbol{\sigma}\cdot\boldsymbol{\Sigma}\int_0^1 dv 2v^2(1-\tfrac{1}{3}v^2)\frac{\pi^2}{\kappa(1-v^2)^{\frac{1}{2}}} =\frac{\alpha^2Z}{16\pi\kappa^2}\frac{m}{M}g\boldsymbol{\sigma}\cdot\boldsymbol{\Sigma},$$

since

$$\int_0^1\frac{v^2(1-\frac{1}{3}v^2)}{(1-v^2)^{\frac{1}{2}}}dv=\frac{3\pi}{16}.$$

Thus[22]

$$\Delta E_P'\rightarrow\frac{1}{2}\frac{\alpha^3Z^3\pi}{\kappa^3}\frac{m}{M}g mc^2\int\bar{\phi}_a(\mathbf{p}_2)\gamma_4\boldsymbol{\sigma}\cdot\boldsymbol{\Sigma}\phi_a(\mathbf{p}_1)d\mathbf{p}_1d\mathbf{p}_2 =\frac{1}{2}\frac{\alpha^3Z^3\pi}{\kappa^3}\frac{m}{M}g\phi_0^2\langle\boldsymbol{\sigma}\cdot\boldsymbol{\Sigma}\rangle mc^2 =\tfrac{3}{4}\alpha^2ZE_H. \tag{42}$$

It is clear that there are no α^2Z corrections for states with nonzero angular momentum.

We now consider briefly the second term (21). The explicit form of $\delta A_\mu^P(q)$ is

$$\delta A_\mu^P(\mathbf{q})=\frac{2ie}{q^2}\left(\frac{ie}{\hbar c}\right)^2\int\mathrm{Tr}\Big[\gamma_\mu\frac{i\gamma\cdot p-\kappa}{p^2+\kappa^2}\gamma\cdot A^e(\mathbf{q}_2) \times S_P^e(p-q_2,\,p-q+q_1)\gamma\cdot A^e(\mathbf{q}_1) \times\frac{i\gamma\cdot(p-q)-\kappa}{(p-q)^2+\kappa^2}\Big]d\mathbf{q}_1d\mathbf{q}_2(d_4p).$$

To estimate its magnitude we again insert (18) for $S_P^e(p-q_2,\,p-q+q_1)$ and drop the last term obtaining

$$\delta A_\mu^P(q)\approx\frac{-2ie}{q^2}\left(\frac{ie}{\hbar c}\right)^3\int\mathrm{Tr}\Big[\gamma_\mu\frac{i\gamma\cdot p-\kappa}{p^2+\kappa^2}\gamma\cdot A^e(\mathbf{q}_2) \times\frac{i\gamma\cdot(p-q_2)-\kappa}{(p-q_2)^2+\kappa^2}\gamma\cdot A^e(\mathbf{q}-\mathbf{q}_1+\mathbf{q}_2) \times\frac{i\gamma\cdot(p-q+q_1)-\kappa}{(p-q+q_1)^2+\kappa^2}\gamma\cdot A^e(\mathbf{q}_1) \times\frac{i\gamma\cdot(p-q)-\kappa}{(p-q)^2+\kappa^2}\Big]d\mathbf{q}_1d\mathbf{q}_2(d_4p),$$

[21] The authors are indebted to H. A. Bethe for pointing out to them the fact that integrals like (40) might be approximated in this way.

[22] One must use Pauli-Schrödinger wave functions with spin rather than Dirac wave functions here. For Dirac wave functions the momentum space integral diverges unless $G(\mathbf{p}_1,\mathbf{p}_2)$ is used. The error is of order $\alpha^3Z^3\ln(\alpha Z)\Delta E_P'$.

the leading term having vanished as a consequence of the Furry Theorem.[23] It is clear from the occurrence of two extra factors $(ie/\hbar c)\gamma\cdot A^e$ that $\delta A_\mu{}^P$ would be at least a factor α^2Z^2 smaller than the leading term of $A_\mu{}^P$, so that the contribution of this term to the hyperfine structure is of order $\alpha^4Z^3E_H$.[24]

EVALUATION OF THE FLUCTUATION ENERGY

(a) First-Order Part

It is convenient to consider separately those parts of ΔE_F which involve $S_F{}^e(p_2, p_1)$ and those parts which do not. By the first-order part of ΔE_F we shall mean that part which comes from C and L. However, in view of the fact that L_D has been cast in a form similar to Q, we shall postpone discussing it and consider it in connection with Q.

The simplest of the first-order terms is the second term of Eq. (36), which, for convenience, we denote by $\Delta E_F{}^{(1)}$:

$$\Delta E_F{}^{(1)}=-6\pi^2\hbar c\alpha\left(\frac{ie}{\hbar c}\right)^2\int\bar{\phi}_a(\mathbf{p}_2)\Big\langle\gamma\cdot A^e(\mathbf{p}_2-\mathbf{p}_3)\times\frac{[2zi\gamma\cdot p_3+\kappa(1-2z)]}{\kappa^2-(p_3{}^2+\kappa^2)z}\gamma\cdot A^e(\mathbf{p}_3-\mathbf{p}_1)\Big\rangle\times\phi_a(\mathbf{p}_1)d\mathbf{p}_1d\mathbf{p}_2d\mathbf{p}_3dz. \quad (43)$$

This expression is very similar in form to (40). We therefore treat it in the same manner, that is, after writing $p_3=q+p_1$, we set $p_1=(0,0,0,i\kappa)=p_2$ in the portion of (43) bracketed thus $\langle\ \rangle$. Making use of (41) we find

$$\Delta E_F{}^{(1)}\rightarrow-\frac{2}{\pi^2}\frac{\hbar c\alpha^3Z}{\kappa^2}g\frac{m}{M}\langle\boldsymbol{\sigma}\cdot\boldsymbol{\Sigma}\rangle\phi_0{}^2\int zdz\frac{d\mathbf{q}}{q^2}\frac{\kappa}{\kappa^2-q^2z}=-\frac{3}{\pi^3}E_H\alpha^2Z\int zdz\frac{\kappa}{\kappa^2-q^2z}\frac{d\mathbf{q}}{q^2}.$$

We find, therefore, thus $\Delta E_F{}^{(1)}$ is a term of order α^2ZE_H multiplied by a definite integral. We now note that the real part of

$$\int\frac{\kappa dq}{\kappa^2-q^2z}d\Omega=4\pi\mathcal{P}\int_0^\infty\frac{\kappa dq}{\kappa^2-q^2z}=0,$$

where $\mathcal{P}$ denotes the principal part, so that $\Delta E_F{}^{(1)}$ does not contribute in the order of interest. The integral does have an imaginary part which we could evaluate had we paid due attention to the small imaginary quantities which should be retained in the denominators throughout the calculation.[16] As noted before, however, we are interested only in the real part of the energy. It is to be noted that the essential difference between this result and that obtained for the vacuum polarization arises from the fact that here the coefficient of q^2 in the denominator is negative for all values of the auxiliary variables. We shall see that this is a characteristic feature of the denominators of K_μ as well.

We turn now to a consideration of the first term of (36). We consider first the contribution of the first term of $K_\mu(p_1, p_2)$ which we may write

$$K_\mu{}^{(A)}(p_2, p_1)=(p_2-p_1)^2\gamma_\mu\int\left[\frac{2-6y(1-y)}{\Lambda_1{}^2}-\frac{y(1-y)}{\Lambda_2{}^2}\right]dydz,$$

yielding

$$\Delta E_F{}^{(2)}=2\pi^2\hbar c\alpha\left(\frac{ie}{\hbar c}\right)\int dydz\int\bar{\phi}_a(\mathbf{p}_2)\times(p_2-p_1)^2\gamma\cdot A^e(p_2-p_1)\phi_a(\mathbf{p}_1)\times\left[\frac{2-6y(1-y)}{\kappa^2\Lambda_1{}^2}-\frac{y(1-y)}{\kappa^2\Lambda_2{}^2}\right]d\mathbf{p}_1d\mathbf{p}_2.$$

This expression is identical in form with $\Delta E_F{}'$ and may be dealt with in a precisely similar way. One finds that

$$\Delta E_F{}^{(2)}\rightarrow-\frac{\alpha^2Z}{\pi^3}E_H\int dydz\frac{d\mathbf{q}}{q^2}\left[\frac{(2-6y(1-y))\kappa}{\kappa^2-y^2q^2}-\frac{y(1-y)\kappa}{\kappa^2-y^2zq^2}\right].$$

Again the integration over q gives rise to a vanishing real part so that like $\Delta E_P{}^{(1)}$, $\Delta E_P{}^{(2)}$ yields no α or α^2Z contributions. The third and fourth terms of K_μ are similar in structure to $K_\mu{}^A$ and can be similarly shown to give no α or α^2Z contributions.

There remains

$$K_\mu{}^{(B)}=i(p_2-p_1)_\nu\sigma_{\mu\nu}\int_0^1\frac{dy}{\kappa\Lambda_1{}^2}$$

to be considered. We note first that $K_\mu{}^{(B)}$ may be split into two terms $K_\mu{}^{(B)'}+K_\mu{}^{(B)''}$ with

$$K_\mu{}^{(B)'}=[i(p_2-p_1)_\nu/\kappa]\sigma_{\mu\nu},$$

and

$$K_\mu{}^{(B)''}=i(p_2-p_1)_\nu\sigma_{\mu\nu}\times\int dy\frac{y(p_1{}^2+\kappa^2)+(1-y)(p_2{}^2+\kappa^2)-(p_2-p_1)^2y(1-y)}{\kappa^3\Lambda_1{}^2}.$$

The contributions from $K_\mu{}^{(B)''}$ are of the same general character as those from the previously considered parts of K_μ and can similarly be shown to give no α or α^2Z contributions.

$K_\mu{}^{(B)'}$ corresponds to the anomalous moment of the electron, which appears here as a point dipole. It is clear, therefore, that it will contribute a correction to

[23] Wendell H. Furry, Phys. Rev. **51**, 125 (1937).

[24] This argument might be insufficient if $\delta A_\mu{}^P(q)$ were singular at small q. However, the gauge invariance of $j_\mu{}^P$ and the absence of charge renormalization effects in $\delta A_\mu{}^P$ imply that the momentum dependence of $\delta A_\mu{}^P(q)$ is $q^2A_\mu{}^e(q)f(q^2)$, where $f(q^2)$ is finite at $q=0$.

the hyperfine structure $\delta_H E_H$ where δ_H is the fractional change in the electron moment. Thus

$$\Delta E_F^{(3)}=2\pi^2\hbar c\alpha\left(\frac{ie}{\hbar c}\right)\int\bar{\phi}_a(\mathbf{p}_2)\frac{i(p_2-p_1)_\nu}{\kappa}\sigma_{\mu\nu}\times A_\mu^{(H)}(\mathbf{p}_2-\mathbf{p}_1)\phi_a(\mathbf{p}_1)d\mathbf{p}_1d\mathbf{p}_2. \quad (44)$$

Now,

$$i(p_2-p_1)_\nu\sigma_{\mu\nu}A_\mu^{(H)}(\mathbf{p}_2-\mathbf{p}_1)\left(\frac{ie}{\hbar c}\right)=\frac{\alpha}{2\kappa}\frac{m}{M}g\frac{\boldsymbol{\sigma}\cdot(\mathbf{p}_2-\mathbf{p}_1)\times(\boldsymbol{\Sigma}\times(\mathbf{p}_2-\mathbf{p}_1))}{2\pi^2(p_2-p_1)^2},$$

so that

$$\Delta E_F^{(3)}=\frac{\alpha^2}{2}\frac{m}{M}\frac{mc^2}{\kappa^3}\int\bar{\phi}_a(\mathbf{p}_2)\frac{\boldsymbol{\sigma}\cdot(\mathbf{p}_2-\mathbf{p}_1)\times(\boldsymbol{\Sigma}\times(\mathbf{p}_2-\mathbf{p}_1))}{(p_2-p_1)^2}\times\phi_a(\mathbf{p}_1)d\mathbf{p}_1d\mathbf{p}_2$$

$$=\frac{\alpha}{2\pi}E_H.$$

We note that the anomalous moment is $\alpha/2\pi$ Bohr magnetons, in agreement with previous calculations.

The anomalous moment also gives rise to a spin-orbit interaction obtained by using $A_\mu^{(E)}$ instead of $A_\mu^{(H)}$ in (44). Now one might inquire as to whether this interaction is different for different hyperfine structure states in a manner analogous to the interaction with the Coulomb polarization potential. One might anticipate that this will not be the case as the spin-orbit interaction is, roughly speaking, distributed throughout the atom instead of being concentrated at the center as is the case for the polarization potential. Therefore the small differences in the wave functions of different hyperfine structure states cannot have a large effect on the spin orbit energy. A detailed examination shows this effect to be of order $\alpha^3Z^2E_H$.

We summarize the results of this section with the remark that apart from L_D, the total significant contribution of the first-order part to the hyperfine structure is simply $(\alpha/2\pi)E_H$ arising from the anomalous electron moment. A more detailed investigation than has been given here indicates that the omitted terms are all of order $\alpha^3Z^2E_H$.

(b) Second-Order Part and L_D[25]

The remaining part of the fluctuation energy consists of the second-order part, which has been denoted as Q, and the infrared divergent part of L, namely L_D. These expressions both involve $S_F^e(p_2, p_1)$, for which one has either an expansion in powers of the external potential or a sum over the stationary states of the potential. On the other hand, one notes that $Q+L_D$ involves the external potential quadratically and has an over-all coefficient of order α, so that in view of the results obtained for the polarization energy and first-order part, one would expect it to yield at most an α^2Z correction. Thus one might hope to evaluate these expressions in lowest approximation by replacing $S_F^e(p_2, p_1)$ by $S_F(p_2)\delta_3(\mathbf{p}_2-\mathbf{p}_1)$. In order to see that this is in fact the case, it is worth inquiring as to the circumstances under which $S_F(p)\delta_3(\mathbf{p}-\mathbf{p}')$ is a good approximation to $S_F^e(p, p')$. Some answer to this question can be obtained by considering the first two terms in an expansion of $S_F^e(p, p')$ for the Coulomb field. Referring to (18) and (38) one finds

$$S_F^e(p, p+q)\approx S_F(p)\delta(q)-S_F(p)\gamma_4\frac{\alpha Z}{2\pi^2q^2}\frac{i\boldsymbol{\gamma}\cdot(p-q)-\kappa}{q^2-2\mathbf{p}\cdot\mathbf{q}+p^2+\kappa^2}.$$

A comparison of the two terms is simplified by integrating over q, thus

$$\int S_F^e(p, p+q)d\mathbf{q}\approx S_F(p)-S_F(p)\gamma_4\frac{\alpha Z}{2}\int_0^1 dx\frac{i\boldsymbol{\gamma}\cdot p(1+x)-\kappa}{[x(p^2+\kappa^2)-x^2\mathbf{p}^2]^{\frac{1}{2}}}.$$

It is clear that when $p^2+\kappa^2$ and $\mathbf{p}^2$ are of order $\alpha^2Z^2\kappa^2$, the two terms are of the same order of magnitude, while for "large" p (i.e., $(p^2+\kappa)$ large) the second term is a factor αZ smaller than the first. Thus the validity of replacing $S_F^e(p_2, p_1)$ by $S_F(p_2)\delta_3(\mathbf{p}_2-\mathbf{p}_1)$ depends upon the weight given low momenta in the integral in which S_F^e appears. In the case of Q the arguments of S_F^e are of the form $p+k+q$. Now $p^2+\kappa^2$ and $\mathbf{p}^2$ are kept small by the form of the wave function; low k is favored by the factors $k^2(k^2-2p\cdot k)(k^2-2p'\cdot k)$ appearing in the denominator, while low q is favored by the factors $1/q^2$ in the potentials. On the other hand, one notes that, if $\mathfrak{A}_\mu(q, p, k)$ is written

$$\mathfrak{A}_\mu(q, p, k)=\left(\frac{\boldsymbol{\gamma}\cdot A^e i\boldsymbol{\gamma}\cdot k\gamma_\mu}{k^2-2p\cdot k}-\frac{i\boldsymbol{\gamma}\cdot k\gamma_\mu\boldsymbol{\gamma}\cdot A^e}{k^2-2(p+q)\cdot k}\right)+2i\left(\frac{(p+q)_\mu}{k^2-2(p+q)\cdot k}-\frac{p_\mu}{k^2-2p\cdot k}\right)\boldsymbol{\gamma}\cdot A^e,$$

the numerator of the first term vanishes with k while the coefficient of $\boldsymbol{\gamma}\cdot A^e$ in the second term vanishes with q. In addition, the fact that one of the external potentials refers to the dipole field introduces an additional factor q. It turns out that these last two factors are just sufficient, and one can accordingly show that contributions from the next term in the expansion of S_F^e are no larger than $\alpha^3Z^2\ln(\alpha Z)E_H$.[26] It should be observed that had

[25] The treatment given Q is essentially the same as that used by M. Baranger [Phys. Rev. 84, 866 (1951)] in the evaluation of its contribution to the αZ corrections for the Lamb effect. We are indebted to him for providing us with a copy of his thesis.

[26] A more complete discussion of the validity both of this approximation and the small momentum approximation first introduced in evaluating the expression in Eq. (40) will be given by H. A. Bethe and M. Baranger in a forthcoming publication.

we based our treatment on an expansion of S_F^e as it appears in Eq. (18) rather than on the Feynman identities (22), then the terms corresponding to $\mathfrak{a}_\mu$ would not have had the afore-mentioned important property.[17] An attempt to demonstrate the validity of the expansion based on an inspection of individual portions of the higher order terms fails.[27]

The evaluation of $Q+L_D$, after replacing S_F^e by the propagation function for a free electron, is a straightforward matter and proceeds in a manner entirely similar to the previously considered terms. Considering L_D first, and recalling that

$$S_F(p)=\frac{-2i}{(2\pi)^4}\frac{i\gamma\cdot p-\kappa}{p^2+\kappa^2},$$

one obtains

$$L_D=-2i\hbar c\alpha\left(\frac{ie}{\hbar c}\right)^2\int\bar{\phi}_n(\mathbf{p}_2)\times\left[\left(\frac{2i(p_1+q)_\mu}{k^2-2(p_1+q)\cdot k}-\frac{2ip_{2\mu}}{k^2-2p_2\cdot k}\right)\gamma\cdot A^e(\mathbf{p}_2-\mathbf{p}_1-\mathbf{q})\times\frac{i\gamma\cdot(p_1+q)-\kappa}{q^2+2\mathbf{p}_1\cdot\mathbf{q}+p_1^2+\kappa^2}\gamma\cdot A^e(\mathbf{q})\times\left(\frac{2i(p_1+q)_\mu}{k^2-2(p_1+q)\cdot k}-\frac{2ip_{1\mu}}{k^2-2p_1\cdot k}\right)\frac{d_4k}{k^2}d\mathbf{q}\right]\phi_n(\mathbf{p}_1)d\mathbf{p}_1d\mathbf{p}_2.$$

Using again our previous approximation, we neglect the small momenta and binding energy of the initial and final state when these appear in the bracketed [ ] portion of the expression. That is, we set $p_1=p_2=p=(0,0,0,i\kappa)$. Making use of this fact, integrating over p_1 and p_2 and using Eq. (41) we find for hyperfine structure

$$L_D\rightarrow\frac{4i\alpha^2Z\kappa}{\pi^5}\left[\frac{2}{3}\alpha\pi\frac{\phi_0^2}{\kappa^2}g\frac{m}{M}\langle\boldsymbol{\sigma}\cdot\boldsymbol{\Sigma}\rangle mc^2\right]\int d\mathbf{q}dk\left(\frac{1}{q^2}\right)^2\frac{1}{k^2}\times\left[\frac{q^2}{(k^2-2(p+q)\cdot k)^2}-\frac{4\kappa^2(k\cdot q)^2}{(k^2-2p\cdot k)(k^2-2(p+q)\cdot k)}\right].$$

It has been remarked previously that L_D diverges in the infrared. It might therefore be preferable to combine it with Q before integrating over k. We shall see immediately, however, that in the above approximation L_D vanishes, so that the suggested combination is unnecessary. Considering the first term only and replacing $1/k^2$ by $1/(k^2+\lambda^2)$ to control the infrared divergence, we obtain

$$i\int d\mathbf{q}d_4k\frac{1}{q^2(k^2+\lambda^2)(k^2-2(p+q)\cdot k)^2}=-\pi^2\int_0^1 dx\frac{xd\mathbf{q}}{[\lambda^2(1-x)+(\kappa^2-q^2)x^2]q^2}=-4\pi^3\int xdx\frac{dq}{\kappa^2x^2+\lambda^2(1-x)-q^2x^2},$$

whose real part vanishes.

The other part of L_D vanishes similarly. The fact that the contribution from L_D vanishes in this order is not surprising in view of its similarity to the rest of the first-order part of ΔE_F.

For Q we have, on replacing $S_F^e(p,p')$ by $S_F(p)\times\delta(p-p')$,

$$Q=2i\hbar c\alpha\left(\frac{ie}{\hbar c}\right)^2\int\bar{\phi}_n(\mathbf{p}_2)\left[\mathfrak{a}_\mu'(p_2-p_1-q,p_2,k)\times\frac{i\gamma\cdot(p_1+q-k)-\kappa}{k^2-2(p_1+q)\cdot k+q^2+2\mathbf{p}_1\cdot\mathbf{q}+p_1^2+\kappa^2}\times\mathfrak{a}_\mu(q,p_1,k)\frac{d_4k}{k^2+\lambda^2}d\mathbf{q}\right]\phi_n(\mathbf{p}_1)d\mathbf{p}_2d\mathbf{p}_1.$$

Again we set $p_1=p_2=p$ in the bracketed expression so that using (28) and (29),

$$Q=2i\hbar c\alpha\phi_0^2\left(\frac{ie}{\hbar c}\right)^2\left\langle\int\frac{d_4k}{k^2+\lambda^2}d\mathbf{q}\mathfrak{a}_\mu'(-\mathbf{q},p,k)\times\frac{i\gamma\cdot(p+q-k)-\kappa}{k^2-2(p+q)\cdot k+q^2}\mathfrak{a}_\mu(\mathbf{q},p,k)\right\rangle=2i\hbar c\alpha\phi_0^2\left(\frac{ie}{\hbar c}\right)^2\langle\mathrm{I}+\mathrm{II}+\mathrm{III}\rangle,$$

with

$$\mathrm{I}=\int d\mathbf{q}d_4k\frac{(2ip_\mu-\gamma_\mu i\gamma\cdot k)\gamma\cdot A^e(-\mathbf{q})(i\gamma\cdot(p+q-k)-\kappa)\gamma\cdot A^e(\mathbf{q})(2ip_\mu-i\gamma\cdot k\gamma_\mu)}{(k^2+\lambda^2)(k^2-2p\cdot k)^2(k^2-2(p+q)\cdot k+q^2)},$$

$$\mathrm{II}=\int d\mathbf{q}d_4k\frac{\gamma\cdot A^e(-\mathbf{q})[2i(p+q)_\mu-\gamma_\mu i\gamma\cdot k][i\gamma\cdot(p+q-k)-\kappa][2i(p+q)_\mu-i\gamma\cdot k\gamma_\mu]\gamma\cdot A^e(\mathbf{q})}{(k^2+\lambda^2)(k^2-2(p+q)\cdot k)^2(k^2-2(p+q)\cdot k+q^2)},$$

$$\mathrm{III}=-\int\frac{d\mathbf{q}d_4k}{D}\{\gamma\cdot A^e(-\mathbf{q})[2i(p+q)_\mu-\gamma_\mu i\gamma\cdot k][i\gamma\cdot(p+q-k)-\kappa]\gamma\cdot A^e(\mathbf{q})[2ip_\mu-i\gamma\cdot k\gamma_\mu]+[2ip_\mu-\gamma_\mu i\gamma\cdot k]\gamma\cdot A^e(-\mathbf{q})[i\gamma\cdot p+q-k-\kappa][2i(p+q)_\mu-i\gamma\cdot k\gamma_\mu]\gamma\cdot A^e(\mathbf{q})\},$$

[27] Notwithstanding the above remark, an evaluation based on such an expansion broken off at the quadratic turn does in fact yield the same result as will be obtained here. This suggests that if one groups the higher order terms properly, a proof of their smallness might be possible.

and

$$D=(k^2+\lambda^2)(k^2-2p\cdot k)\times[k^2-2(p+q)\cdot k][k^2-2(p+q)\cdot k+q^2].$$

For brevity we confine our discussion for the moment to II. The treatments of I and III are identical. Using the well-known denominator combining formula

$$\frac{1}{ab^2c}=6\int_0^1\frac{x^2ydxdy}{[a(1-x)+bxy+cx(1-y)]^4},$$

and letting $k\to k+(p+q)x$, one finds

$$\mathrm{II}=6\int d\mathbf{q}d_4k\frac{x_2ydxdyN_2}{[k^2+\kappa^2x^2+q^2x(1-x-y)+\lambda^2(1-x)]^4}.$$

The numerator N_2 involves various products of spinor matrices and momenta from which one is to pick out contributions to the hyperfine structure. This operation is facilitated by reducing all terms to the form $\gamma\cdot A^e(-\mathbf{q})i\gamma\cdot\mathbf{q}\gamma\cdot A^e(\mathbf{q})$. For this purpose the following facts and equivalence relations are useful.

$$\gamma\cdot\mathbf{q}\gamma\cdot A^e(\mathbf{q})=-\gamma\cdot A^e(\mathbf{q})\gamma\cdot\mathbf{q},$$
$$\gamma\cdot A^e(-\mathbf{q})\gamma\cdot A^e(\mathbf{q})\to 0,$$

$(\ )\gamma\cdot A^e(-\mathbf{q})\gamma_4\gamma\cdot A^e(\mathbf{q})(\ )\to 0$ regardless of the content of the brackets. A factor γ_4 appearing on the extreme right or left of an expression may be dropped.

Using the above one finds

$$N_2\to[2(\kappa^2-q^2)(2-4x+x^2+x^3)-k^2(5+3x)]\times\gamma\cdot A^e(-\mathbf{q})i\gamma\cdot\mathbf{q}\gamma\cdot A^e(\mathbf{q}).$$

Carrying out the k space integration and inserting (41) yields

$$Q_{\mathrm{II}}=-\frac{2\hbar c\alpha}{3\pi^2\kappa}\phi_0^2\alpha^2Zg\frac{m}{M}\langle\boldsymbol{\sigma}\cdot\boldsymbol{\Sigma}\rangle\int x^2ydxdy\frac{d\mathbf{q}}{q^2}\times\left\{\frac{(2-4x+x^2+x^3)(\kappa^2-q^2)}{[\kappa^2x^2+\lambda^2(1-x)+q^2(1-x-y)]^2}-\frac{5+3x}{[x^2+\lambda^2(1-x)+q^2x(1-x-y)]}\right\}.$$

We now recall (39), carry out the angular q integration and transform $q\to q\kappa$, $\lambda\to\lambda\kappa$ so as to make the integral dimensionless, yielding

$$Q_{\mathrm{II}}=-\frac{4\alpha^2Z}{\pi^2}E_H\int dqx^2ydxdy\times\left\{\frac{(2-4x+x^2+x^3)(1-q^2)}{[x^2+\lambda^2(1-x)+q^2x(1-x-y)]^2}-\frac{5+3x}{x^2+\lambda^2(1-x)+q^2x(1-x-y)}\right\}.$$

Identical methods yield for the rest of Q,

$$Q_{\mathrm{I}}=-\frac{4\alpha^2Z}{\pi^2}E_H\int dqx^2ydxdy\left\{\frac{2-2x+3x^2-x^3-2x^2y+x^3y-q^2x^2(1-y)^2(1-x+xy)}{[x+\lambda^2(1-x)+q^2x(1-y)(1-x+xy)]^2}-\frac{1-3x(1-y)}{x^2+\lambda^2(1-x)+q^2x(1-y)(1-x+xy)}\right\},$$

$$Q_{\mathrm{III}}=\frac{8\alpha^2Z}{\pi^2}E_H\int dqx^2ydxdydz\left\{\frac{2-3x+q^2x(1-yz)[1-x(1-yz)]}{[x^2+\lambda^2(1-x)+q^2x[1-y-x(1-yz)^2]]^2}-\frac{1}{x^2+\lambda^2(1-x)+q^2x[1-y-x(1-yz)^2]}\right\}.$$

There remains only the purely numerical problem of evaluating the above integrals. The main points can be illustrated by considering the leading terms of Q_{II}, namely,

$$A=\int\frac{dqx^2ydxdy}{[x^2+\lambda^2(1-x)+q^2x(1-x-y)]^2},$$

$$B=\int\frac{q^2dqx^2ydxdy}{[x^2+\lambda^2(1-x)+q^2x(1-x-y)]^2}.$$

In the first integral it is simplest to do the q integration first, thus,

$$A=\frac{\pi}{4}\int_0^1dx\int_{1-x}^1dy\frac{x^2y}{[x^2+\lambda^2(1-x)]^{\frac{3}{2}}x^{\frac{1}{2}}(1-x-y)^{\frac{1}{2}}}.$$

It is to be observed that the coefficient of q^2 appearing in the denominator may be positive or negative, depending upon the values of the auxiliary variables. As the integral is to be evaluated as a principal part when the denominator has a pole on the real axis, it has a nonvanishing value only when this coefficient is positive. This is the origin of the lower limit $1-x$ in the y integration. The remainder of the integration is straightforward and will not be discussed further.[28]

For the integral B one must integrate over y first,[29]

[28] It might be mentioned that for Q_{III}, the fixing of the region for which the coefficient of q^2 is positive is facilitated by the substitution $z=(1-u)/y$, $1>u>1-y$.

[29] If one integrates over q first, the y integration diverges at $y=1-x$. The procedure used can be justified by remarking that the auxiliary variables have no physical significance and are in fact part of the k integration. Thus in any case in which it makes a difference one should complete the auxiliary variable integration before performing the q integration. One can also deal with the problem by rounding off the singularity of the Coulomb field. That is, one modifies the Fourier transform of the Coulomb potential by a factor $\Lambda^2/(\Lambda^2+q^2)$, where Λ is assumed to be large. With this factor present the integral is finite and independent of the order of integration. The result obtained in the limit $\Lambda\to\infty$ is identical with that given above.

obtaining

$$B=\int\left\{\frac{\ln\left(1+q^2\frac{1-x}{x}+\lambda^2\frac{1-x}{x^2}\right)}{q^2}-\frac{\ln\left|1-q^2\frac{1-x}{x}+\lambda^2\frac{1-x}{x^2}\right|}{q^2}+\frac{x}{x^2+\lambda(1-x)-x^2q^2}\right\}dqdx$$

$$=\pi\int_0^1\left(\frac{1-x}{x}\right)^{\frac{1}{2}}dx=\frac{\pi^2}{2}.$$

Only the first of the three terms contributes.

Proceeding in the manner outlined above all terms reduce to simple integrals over one, two or three auxiliary variables, a typical form being

$$\int_0^1 dx\int_0^1 dy\frac{x^m y^n}{[xy(1-xy)]^{\frac{1}{2}}}.$$

Certain of these, like A above, diverge in the limit $\lambda\to 0$, but yield a finite limit when taken together. The final result obtained is simply

$$Q=-\alpha^2 ZE_H(13/4-\ln 2). \tag{45}$$

SUMMARY AND CONCLUSIONS

The second-order radiative corrections to the hyperfine structure of S states are given by

$$\Delta E_P=\tfrac{3}{4}\alpha^2 ZE_H,$$

$$\Delta E_F=\left[\frac{\alpha}{2\pi}-\alpha^2 Z\left(\frac{13}{4}-\ln 2\right)\right]E_H,$$

yielding[30]

$$\Delta E=\left[\frac{\alpha}{2\pi}-\alpha^2 Z\left(\frac{5}{2}-\ln 2\right)\right]E_H. \tag{46}$$

For higher angular momentum states there is an order α-correction arising from the anomalous electron moment but no $\alpha^2 Z$ correction. While our derivation has been confined to hydrogenic atoms, the effect of screening on the radiative corrections is, aside from its effect on ϕ_0^2, only of order $\alpha^3 Z^2$. This result is a consequence of the fact that the $\alpha^2 Z$ correction comes chiefly from distances within a Compton wavelength of the nucleus.

A principal application of this result is to the deduction of the fine structure constant from the hyperfine structure formula. The hyperfine structure frequency of the ground state of hydrogen is related to other accurately known experimental quantities by

$$\Delta\nu=\frac{16}{3}\alpha^2 cR_\infty\left(\frac{\mu_P}{\mu_S}\right)\left(\frac{m_r}{m}\right)^3(1+\tfrac{3}{2}\alpha^2)\times\left(1+\frac{\alpha}{2\pi}-\frac{2.973\alpha^2}{\pi^2}\right)\left(1+\frac{\alpha}{2\pi}-\frac{2.973\alpha^2}{\pi^2}+\alpha^2\left(\frac{5}{2}-\ln 2\right)\right)P_r P_s. \tag{47}$$

In applying the above expression we use

$$c=2.997902\times 10^{10}\ \text{cm/sec},^4 \quad (3.0\ \text{ppm})$$
$$R_\infty=109{,}737.324\ \text{cm}^{-1},^4 \quad (0.1\ \text{ppm})$$
$$\Delta\nu=1420.4051\times 10^6\ \text{sec}^{-1},^{31} \quad (0.3\ \text{ppm})$$
$$(\mu_S/\mu_P)=658.2087,^{32} \quad (2.0\ \text{ppm})$$
$$(m_r/m)^3=0.99836790.^4$$

The small α-dependent corrections are evaluated using $1/\alpha=137.036$. The factors P_r and P_s are inserted to take into account proton recoil effects and possible departure of the proton magnetic field from that of a point dipole. From (47) one finds

$$1/\alpha=(137.03651\pm 0.00028)P_r^{\frac{1}{2}}P_s^{\frac{1}{2}}. \tag{48}$$

The contribution of the $\alpha^2 Z$ term in Eq. (46) to this result is -0.00658.

An independent determination of $1/\alpha$ by Lamb and Retherford[33] from the fine structure separation of the $2P_{\frac{1}{2}}$, $2P_{\frac{3}{2}}$ levels in deuterium yields

$$1/\alpha=137.033\pm 0.006, \tag{49}$$

a result which tends to confirm the presence of the new electrodynamic correction obtained above. It is worth noting that the comparison of (49) and (48) is independent of the values of c and R_∞, and substantially independent of the anomalous electron moment.

The factors P_r and P_s in (48) might possibly affect the value of $1/\alpha$ by a few parts per 10^5. A more accurate measurement of the fine structure of deuterium would make possible an experimental estimate of their magnitude.

It is a pleasure to acknowledge several stimulating and informative conversations with Professor H. A. Bethe.

[30] This result has been reported previously by N. M. Kroll and F. Pollock, Phys. Rev. **84**, 594 (1951). The same result has been obtained by a different method by Karplus, Klein, and Schwinger, Phys. Rev. **84**, 597 (1951).

[31] P. Kusch and A. G. Prodell, Phys. Rev. **79**, 1009 (1950).

[32] Koenig, Prodell, and Kusch, Phys. Rev. **83**, 687 (1951). The value given above is based on 658.2289 ± 0.0006 (the value quoted by P. Kusch at the 1952 Annual Meeting of the American Physical Society) for μ_S/μ_P with the proton resonance measured in oil. The diamagnetic correction used is $(1-30.5\times 10^{-6})$ and is based on the results of Ramsey [Phys. Rev. **78**, 699 (1950)] and H. S. Gutowsky and J. W. McClure [Phys. Rev. **81**, 276 (1951)]. The uncertainty given by Kusch has been doubled to allow for possible uncertainties in the diamagnetic corrections.

[33] W. E. Lamb, Jr. and R. C. Retherford (to be published).

Scattering of Plane Waves by Soft Obstacles. III. Scattering by Obstacles with Spherical and Circular Cylindrical Symmetry*

ELLIOTT W. MONTROLL AND J. MAYO GREENBERG
Institute for Fluid Dynamics and Applied Mathematics, University of Maryland, College Park, Maryland

(Received January 14, 1952)

A new variational method is devised for obtaining the "best" parameters for trial wave functions of a given type for insertion into the integral equation [see Eq. (1.4a)] for the scattering of scalar plane waves by obstacles with spherical and cylindrical symmetry.

The variational procedure is applied to the determination, in the least square sense, of the square well potential which most closely approximates the potential under consideration for a given propagation constant ($k_0=2\pi/\lambda_0$) of the incident wave. We then use as a trial function in the scattering integral equation the sphere (or cylinder) wave function (with the "best" parameters) which was derived in the first two papers of this series.

The differential and total scattering cross sections for scattering by Gaussian, exponential, and screened Coulomb potentials are obtained in simple closed forms. The Born approximation predicts the ratio of the total scattering cross section to πb^2 (where b is qualitatively the effective range of the scatterer) to be a monotone increasing function of $2\pi b/\lambda_0$, while in our theory it is a bounded function.

The main advantage of the procedure developed in this paper is that, while it is superior to the Born approximation, especially for large b/λ_0, it is equally simple to apply.

INTRODUCTION

THE tremendous volume of recent experimental data on the scattering of plane waves by obstacles (scattering of light by macromolecules, of high energy particles by nuclei, of sound waves by various types of obstacles, etc.) has led to a renewed interest in the development of approximation methods for the solution of scattering problems.

Variational principles have been derived and applied by Schwinger, Hulthén, and their collaborators and followers. In most applications to two- and three-dimensional problems the practice has been to express the scattered wave function as a series in Legendre polynomials and to find the "phases" and hence the coefficients by variational principles.

In an investigation of scattering by obstacles with sharp boundaries (spheres, circular cylinders, spheroids, etc.) Hart and one of the authors[1] have been led to approximation procedures which avoid the calculation of phases and lead to scattering cross sections directly. This paper is concerned with a generalization of these procedures to scattering by spherically and cylindrically symmetrical scatterers which have no sharp boundaries but which diminish in strength monotonically with the distance from the scattering center.

One may develop the theory of scattering by considering each infinitesimal volume element of the scatterer as a point Rayleigh scatterer and characterizing the total scattered wave at a point of observation as the sum of all the waves scattered by the point scatterers. To apply this procedure one must know the exciting field at each infinitesimal point scatterer. Mathematically the method is expressed through an integral equation (1.4a) in which the wave function at a given point is an integral over that at all other points.

The classical approximation technique is that of Rayleigh, Gans, and Born[2] (henceforth referred to as the R.G.B. or the Born approximation), in which one assumes that each infinitesimal Rayleigh scatterer is excited by the incident plane wave in the same manner that it would be in the absence of the remainder of the obstacle. In terms of the integral equation (1.4a) one substitutes the wave function of the incident wave into the integrand of the integral and carries out the required integration to compute the scattered wave function. The limitations of the R.G.B. approximation are very striking if one plots the ratio of the total scattering cross section to the geometrical cross section as a function of $2\pi a/\lambda_0$, where a is a characteristic length of the scatterer and λ_0 is the wavelength of the incident plane wave in the absence of the scatterer. This quantity is a monotone increasing function in the R.G.B. approximation, while in the exact theory[1,3] it is usually a bounded function of $2\pi a/\lambda_0$ (see Fig. 1).

In all iterative procedures for solving integral equations the quick achievement of accurate results is facilitated by a good first approximation to the solution. The problem of improving on the R.G.B. approximation then resolves itself into finding reasonably accurate and convenient forms to represent the trial wave functions.

In S-I and S-II this has been done for the scattering by spherical and elongated obstacles having sharp

* This research was supported by the ONR.

[1] R. Hart and E. Montroll, J. Appl. Phys. **22**, 376 (1951) and **22**, 1278 (1951); R. Hart, J. Acoust. Soc. Am. **23**, 373 (1951). See also A. L. Latter, Phys. Rev. **83**, 1056 (1951), where some of the same ideas have been discussed independently. The first two papers listed above will be referred to as S-I and S-II, respectively.

[2] Lord Rayleigh, Proc. Roy. Soc. (London) **A84**, 25 (1910); **A90**, 219 (1914); R. Gans, Ann. Physik **76**, 29 (1925); M. Born, Z. Physik **37**, 863 (1926); **38**, 803 (1926).

[3] H. C. van de Hulst, Recherches Astronomiques de l'observatoire d'Utrecht **11** (1946).

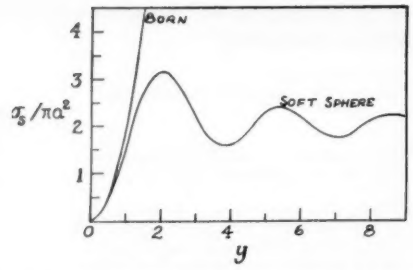

FIG. 1. Ratios of the total scattering cross section of a spherical potential well $[k^2(r)-k_0^2=k_1^2-k_0^2,\ r<a;\ =0,\ r>a]$ with geometrical cross section in the limit as $k_1/k_0\to 1$. The upper curve is the Born approximation [Eq. (3.21)]. The lower curve is the soft sphere approximation [Eq. (3.20)]. The parameter y is defined by $y=k_0a(k_1/k_0-1)$.

boundaries (square well potential). If $k_0=2\pi/\lambda_0$ and $k_1=2\pi/\lambda_1$ are the propagation constants for the exterior and interior of the scatterer, it was found that the essential features of the correct theory are retained by choosing the interior trial wave function to be of the form $\exp(ik_1z)$ rather than $\exp(ik_0z)$ as in the R.G.B. approximation.

In this paper we shall generalize the previous results by approximating the wave functions of scatterers which do not have sharp boundaries by those of spheres and cylinders with width and depth of potential well chosen so as to give the best comparison in a certain variational sense. This procedure consists essentially in determining, first, in the least square sense, the square well potential which most closely approximates the potential under consideration for a given incident propagation constant. We then use as a trial function in the original integral equation the sphere (or cylinder) wave function with the appropriate parameters.

We shall consider mainly soft scatterers ($|k_1-k_0|/k_0\ll 1$), but one should be able to extend the range of our results without too much difficulty. In particular we shall examine the scattering by Gaussian, exponential, and screened Coulomb fields. The primary merit of the new method is that while it is significantly superior to the R.G.B. theory, it is nevertheless equally simple in application, and, in fact, gives all results for the differential and total scattering cross sections in rather compact closed forms for the scatterers considered.

1. WAVE EQUATION FOR SPHERICALLY SYMMETRICAL SCATTERERS

Let us consider the scattering of a scalar plane wave of propagation constant $k_0=2\pi/\lambda_0$ (λ_0 being its wavelength in the absence of an obstacle) by an obstacle in which the wavelength of a transmitted wave and hence $k=2\pi/\lambda$ varies from point to point. The character of the scattered wave can be discussed in terms of the solution of the wave equation.

$$\nabla^2\psi+k^2(r)\psi=0. \tag{1.1}$$

We restrict ourselves in this paper to situations in which the required solutions of (1.1) are continuous and have continuous first derivatives, even though $k(r)$ might be a discontinuous function. These correspond to the usual quantum-mechanical boundary conditions, to the scattering of sound waves by obstacles whose density is the same as that of the medium in which they are embedded, and to the scalar analog of the scattering of electromagnetic waves by nonconducting dielectric particles. Equation (1.1) is equivalent to Schrödinger's equation if k_0^2 is identified with $2mE/\hbar^2$ and $k^2(r)$ with $2m(E-V)/\hbar^2$.

We locate the origin of our coordinate system at the center of a spherically symmetrical obstacle and postulate $k(r)\to k_0$ as $r\to\infty$. Actually our analysis will be limited to forms of $k(r)$ with the properties: $[k^2(r)-k_0^2]\to 0$ more rapidly than $1/r$ as $r\to\infty$ and increases as $r\to 0$ at a rate no faster than $1/r$ (if it increases at all for small r). More precisely we shall require that

$$\int_0^\infty [k^2(r)-k_0^2]^2r^2dr<\infty \quad \text{and} \quad \int_0^\infty [k^2(r)-k_0^2]rdr<\infty.$$

The wave function of an incident plane wave propagated in the direction of the unit vector $\mathbf{s}_0$ is

$$\psi_i=\exp[ik_0(\mathbf{r}\cdot\mathbf{s}_0)], \quad k_0=2\pi/\lambda_0. \tag{1.2}$$

If $\psi_s(\mathbf{r})$ is the wave function of the scattered field, the solution of (1.1) is of the form

$$\psi(\mathbf{r})=\psi_s(\mathbf{r})+\exp ik_0(\mathbf{r}\cdot\mathbf{s}_0), \tag{1.3}$$

where $\psi_s(\mathbf{r})\to 0$ as $1/r$. Hence $\psi_s(\mathbf{r})$ satisfies the integral equation[4]

$$\psi_s(\mathbf{R})=-\frac{1}{4\pi}\int\frac{e^{ik_0|\mathbf{R}-\mathbf{r}|}}{|\mathbf{R}-\mathbf{r}|}[k_0^2-k^2(r)]\psi(\mathbf{r})d\tau, \tag{1.4a}$$

where the integration extends over all space.

When $|R|$ is much larger than the range of the scatterer, the scattered wave function $\psi_s(\mathbf{R})$ can be approximated by

$$\psi_s(\mathbf{R})\sim\frac{e^{iRk_0}}{4\pi R}\int\psi(\mathbf{r})[k^2(r)-k_0^2]\times\exp[-ik_0(\mathbf{r}\cdot\mathbf{s}_1)]d\tau. \tag{1.4b}$$

The Born (Rayleigh-Gans in the case of vector waves) approximation for the scattered wave function is obtained by replacing $\psi(\mathbf{r})$ in (1.4) by the wave function of the incident wave, $\exp ik_0(\mathbf{r}\cdot\mathbf{s}_0)$, and integrating over all space.

[4] N. F. Mott and H. S. W. Massey, *The Theory of Atomic Collisions* (Oxford University Press, London, 1949), p. 114.

Equation (1.4) has, in S-II, been applied to the scattering of plane waves by uniform isotropic soft scatterers with sharp boundaries. For example, in a spherical scatterer of radius a and propagation constant k_1 (i.e., the case of scattering by a square well potential $V(r)$ of width a and height proportional to k_1^2) Eq. (1.4) becomes (since $k(r)=k_1$ for $r<a$ and $=k_0$ for $r>a$):

$$\psi_s=\frac{(k_1^2-k_0^2)}{4\pi}\int\frac{e^{ik_0|\mathbf{R}-\mathbf{r}|}\psi_t(\mathbf{r})}{|\mathbf{R}-\mathbf{r}|}d\tau \sim\frac{k_1^2-k_0^2}{4\pi R}e^{ikR_0}\int\psi_t(\mathbf{r})\exp[-ik_0(\mathbf{r}\cdot\mathbf{s}_1)]d\tau, \quad (1.5)$$

where the integration extends over the volume of the sphere and $\psi_t(\mathbf{r})$ is the wave function of the interior of the sphere.

The following approximate wave function has been derived for a sphere in S-I:

$$\psi_t=\frac{2k_1e^{ia(k_1-k_0)}[\exp\{ik_1(\mathbf{r}\cdot\mathbf{s}_0)\}-\kappa e^{2iak_1}\exp\{-ik_1(\mathbf{r}\cdot\mathbf{s}_0)\}]}{(k_1+k_0)[1-\kappa^2\exp 4iak_1]}. \quad (1.6)$$

The first term in the numerator corresponds to the transmitted wave through the sphere and the second to the internal reflected wave. The approximate scattered wave function that is derived by substituting (1.6) into (1.5) is, for $r\gg a$ ($J_{\frac{1}{2}}(z)$ is the Bessel function of order $\frac{1}{2}$),

$$\psi_s(r)=A_s r^{-1}\{J_{\frac{1}{2}}(\omega a)/(\omega a)^{\frac{1}{2}}-\kappa e^{2iak_1}J_{\frac{1}{2}}(va)/(va)^{\frac{1}{2}}\}, \quad (1.7)$$

with ω and v defined by (3.5), and

$$A_s=a^2(2\pi)^{\frac{1}{2}}k_1(k_1-k_0)e^{i(k_1-k_0)a+irk_0}/(1-\kappa^2e^{4iak_1}), \quad (1.8)$$
$$\kappa=(m-1)/(m+1), \quad m=k_1/k_0.$$

This result is quite accurate when $m=k_1/k_0<1.3$ and is useful for $m<1.5$. The ratio of the total scattering cross section to the geometrical cross section approaches the exact value for all size spheres as $k_1\to k_0$. This is not the case for the Born approximation.

Expressions similar to (1.6) and (1.7) have been obtained in S-II for the internal and scattered wave functions of infinite circular cylinders. Approximate scattered wave functions were derived for finite cylinders and oblate spheroids in S-II by approximating their internal wave functions by those of infinite cylinders, substituting these wave functions in (1.7) and integrating over the entire volume of the obstacles.

We shall now apply this technique to the determination of approximate scattered wave functions of spherically and cylindrically symmetrical scatterers which do not have sharp boundaries. We shall approximate the internal wave functions of these scatterers by those of spheres and cylinders whose radii a and propagation constants k_1 for a given propagation constant of the incident wave k_0 will be determined by the variational scheme discussed in the next section.

2. A VARIATIONAL SCHEME[6]

Let the propagation function of the scatterer of interest be $k(r)$. Then the wave equation for an incident plane wave is (1.1). Now suppose we cannot easily solve (1.1), but that we can solve the wave equation that corresponds to a similar scatterer with propagation function $k_0(r)$ (which might depend on several parameters):

$$\nabla^2\psi_0+k_0^2(r)\psi_0=0. \quad (2.1)$$

The identity,

$$\nabla^2\psi_0+k^2(r)\psi_0=[k^2(r)-k_0^2(r)]\psi_0, \quad (2.2)$$

suggests a variational scheme. If $k_0(r)$ were equal to $k(r)$, the quantities on both sides of (2.2) would vanish for all r. Hence, if we could choose the parameters in the approximating function $k_0(r)$ [and hence in $\psi_0(\mathbf{r})$] in such a way as to minimize the integral

$$I=\int|k^2(r)-k_0^2(r)|^2|\psi_0(\mathbf{r})|^2d\tau, \quad (2.3)$$

we would, in the least square sense, have the best approximating function of the initially chosen form of $k_0(r)$. Equation (2.2) implies that minimizing I is equivalent to minimizing $\nabla^2\psi_0+k^2(r)\psi_0$, or finding the parameters of ψ_0 which make ψ_0 the best solution of (1.1) of the given form.

It is to be noted that $\psi_0(\mathbf{r})$ and hence the "best" parameters of $k_0(r)$ depend on the wavelength, or energy, of the incident plane wave.

The physical meaning of the integral (2.3) is immediately apparent if the incident waves correspond to a steady stream of particles of energy E emitted in the direction of the scattering center of potential $V_0(r)$ and we interpret $|\psi_0|^2d\tau$ as a quantity proportional to the particle density in the volume element $d\tau$. Let the parameters of $k_0(r)$ be fixed, while those of $k(r)$ are varied to minimize I. Then the solution of the variational problem $\delta I=0$ yields the best least square fit of $k(r)$ to $k_0(r)$ with each volume element in space weighted by its proper quantum-mechanical particle density function. Actually it will be easier to solve the variational problem with $k_0(r)$ fixed and $k(r)$ varied, and through successive guesses of the parameters of $k_0(r)$ to find those which will give the best $k(r)$ its required parameters. In terms of the scattering potential $V(r)$, $\delta I=0$ corresponds to

$$\delta I=\delta\int|V-V_0|^2|\psi_0|^2d\tau=0. \quad (2.4)$$

Equation (2.4) is a general variational principle that can be applied either to an initially chosen form for the

[6] Variational methods for solving scattering problems have been used quite extensively by Harold Levine and Julian Schwinger, Phys. Rev. **74**, 958 (1948); **75**, 1423 (1949); W. Kohn, Phys. Rev. **74**, 1763 (1948); and others. To the best of our knowledge the simple particular variational scheme of this section has not been used explicitly before.

wave function $\psi_0(\mathbf{r})$ or of the scattering potential V_0. Let $\psi_0(\mathbf{r})$ (with several parameters) be chosen to have roughly the form which should correspond to the potential $V(r)$. Then define the approximating potential function $V_0(r)$ by

$$V_0=(1/\psi_0)\{2h^{-2}\nabla^2\psi_0+E\psi_0\}, \tag{2.5}$$

where E is the energy of the incident particles. The best values of the parameters in ψ_0 are then derived from (2.4).

The approximate wave function $\psi_0(\mathbf{r})$ with the best parameters can be improved further by inserting it into the integral equation (1.4) and integrating to obtain a better scattered wave function.

The integral (2.3) is useful for comparing two different forms of approximating wave functions. If the best parameters are found in two different forms of $\psi_0(\mathbf{r})$, that form which gives the smaller value to (2.3) is the better approximation of $\psi(\mathbf{r})$.

3. APPROXIMATE SCATTERED WAVE FUNCTIONS FOR SPHERICALLY SYMMETRICAL SCATTERERS

We shall now consider scatterers for which $|k^2(r)-k_0^2|$ is a monotone decreasing function of r. Some important examples are $k^2(r)-k_0^2=Ae^{-Br}$, $A\exp(-Br^2)$, and $Ar^{-1}e^{-Br}$. The Gaussian form occurs in scattering by randomly coiled polymer chains, and all forms have been used for the scattering of fundamental particles by nuclei.

A natural approximating form for such $k^2(r)-k_0^2$ is that of a uniform, isotropic spherical scatterer of radius a. Then

$$k_0^2(r)-k_0^2=\begin{cases}k_1^2-k_0^2 & \text{if } r<a,\\ 0 & \text{if } r>a.\end{cases} \tag{3.1}$$

Since the wave function ψ_0 is well known for this type of scatterer, one can obtain best values of k_1 and a for a given spherically symmetrical scatterer and k_0 by applying the variational principle discussed in the last section. Suppose this has been done. Then an improved scattered wave function ψ_s is derived by substituting ψ_0 for ψ in the integrand of the integral equation (1.4b).

Let ψ_i be the transmitted or internal wave function of the sphere and $\psi_s^{(0)}$ the scattered wave function. Then

$$\psi_0(\mathbf{r})=\begin{cases}\psi_i(\mathbf{r}) & r<a\\ \psi_s^{(0)}(\mathbf{r})+\exp\{ik_0(\mathbf{r}\cdot\mathbf{s}_0)\} & r>a\end{cases}$$

and

$$\psi_s(\mathbf{R})\sim\frac{e^{ikR}}{4\pi R}\Big\{2\pi\int_0^a\int_0^\pi \exp\{-ik_0(\mathbf{r}\cdot\mathbf{s}_1)\}$$
$$\times[k^2(r)-k_0^2]\psi_i r^2\sin\vartheta' dr d\vartheta'$$
$$+2\pi\int_a^\infty\int_0^\pi \exp\{-ik_0(\mathbf{r}\cdot\mathbf{s}_1)\}[k^2(r)-k_0^2]$$
$$\times[\psi_s^{(0)}(\mathbf{r})+\exp\{ik_0(\mathbf{r}\cdot\mathbf{s}_0)\}]r^2\sin\vartheta' dr d\vartheta'\}. \tag{3.2}$$

Now we could substitute the exact sphere wave functions into (3.2). This procedure gives us new scattered wave functions which are complicated infinite series of Legendre polynomials and which must be summed numerically. Since we are interested here in soft scatterers (high energies of incident waves) we can better use the closed form approximate sphere wave functions that were derived in S-I. This allows us to obtain simple closed form wave functions for many scatterers of interest (as we shall soon see, these new wave functions will be no more difficult to use than those of the Born approximation even though they are significantly more accurate). The main contribution to $\psi_s(\mathbf{R})$ in (3.2) comes from the integral from 0 to a because $k^2(r)-k_0^2$ is small for $r>a$. Hence we can use approximate wave functions in the second integral of (3.2) which need only be accurate in the neighborhood of $r=a$ but which might be rather poor (provided they are bounded) for very large values of r.

We shall use the internal sphere wave function for all values of r (including those outside the sphere) as an approximate wave function. Since $\psi_i(\mathbf{r})$ and its first derivative are equal, respectively, to $[\psi_s^{(0)}(\mathbf{r})+\exp\{ik_0(\mathbf{r}\cdot\mathbf{s}_0)\}]$ and its first derivative at $r=a$, $\psi_i(\mathbf{r})$ is a good approximation to the exterior wave function for a short distance beyond a sphere boundary (especially if $k^2(r)-k_0^2$ decreases exponentially with r). Hence we can write

$$\psi_s(R)\sim\frac{e^{ik_0R}}{4\pi R}\int\exp\{-ik_0(\mathbf{r}\cdot\mathbf{s}_1)\}$$
$$\times[k^2(r)-k_0^2]\psi_i(\mathbf{r})d\tau, \tag{3.3}$$

where the integral extends over all space.

Let us substitute the soft sphere internal wave function (1.6) into (3.3) to obtain

$$\psi_s(\mathbf{R})\sim\frac{k_1e^{ia(k_1-k_0)+iRk_0}[I_1-\kappa e^{2iak_1}I_2]}{R(k_1+k_0)[1-\kappa^2\exp(4iak_1)]}, \tag{3.4a}$$

where κ is defined by Eq. (1.8),

$$I_1=\int_0^\infty\int_0^\pi[k^2(r)-k_0^2]e^{ir\omega\cos\gamma}r^2\sin\gamma d\gamma, \tag{3.4b}$$

$$I_2=\int_0^\infty\int_0^\pi[k^2(r)-k_0^2]e^{ir\nu\cos\beta}r^2\sin\beta d\beta, \tag{3.4c}$$

γ is the polar angle between the variable vector $\mathbf{r}$ which spans space and the fixed vector $(k_1\mathbf{s}_0-k_0\mathbf{s}_1)$, and β is the polar angle between $\mathbf{r}$ and the fixed vector $(k_1\mathbf{s}_0+k_0\mathbf{s}_1)$. Also

$$\omega^2=|k_1\mathbf{s}_0-k_0\mathbf{s}_1|^2=k_1^2+k_0^2-2k_1k_0\cos\vartheta, \tag{3.5a}$$

$$\nu^2=k_1^2+k_0^2+2k_1k_0\cos\vartheta, \tag{3.5b}$$

θ being the angle of scattering (the angle between $\mathbf{s}_1$ and $\mathbf{s}_0$).

The integrations over γ and β in (3.4) are elementary and yield

$$\psi_s \sim A_s R^{-1} \int_0^\infty [k^2(r)-k_0^2] r^2 \left\{ \frac{\sin \omega r}{\omega r} - \kappa e^{2ika_1} \frac{\sin vr}{vr} \right\} dr, \quad (3.6)$$

where

$$A_s = \frac{2k_1}{(k_1+k_0)} \frac{\exp i[a(k_1-k_0)+k_0 R]}{[1-\kappa^2 \exp(4ika_1)]}. \quad (3.6a)$$

The differential scattering cross section is then

$$\sigma(\theta) = R^2 |\psi_s(R)|^2 = |A_s|^2 \left| \int_0^\infty [k^2(r)-k_0^2] r^2 \left\{ \frac{\sin \omega r}{\omega r} - \kappa e^{2ika_1} \frac{\sin vr}{vr} \right\} dr \right|^2. \quad (3.7)$$

We must now find relations between the parameters of the scattering potentials and those of the approximating sphere. This is done by applying the variational scheme of Sec. 2. At this point we derive the relations for very soft scatterers. The method of improving the accuracy of these is straightforward but leads to lengthy equations which we shall not exhibit here.

We wish to minimize the integral

$$F = \int [(k^2(r)-k_0^2)-(k_0^2(r)-k_0^2)]^2 |\psi_t|^2 d\tau, \quad (3.8)$$

for the special case

$$k^2(r)-k_0^2 = A^2 f(r/b),$$

$$k_0^2(r)-k_0^2 = \begin{cases} k_1^2-k_0^2, & r<a, \\ 0, & r>a, \end{cases}$$

with ψ_t given by (1.6). For very soft spheres we can neglect the term of order κ, which is the coefficient of the reflected wave in the sphere. Then $|\psi_t|^2 = \text{constant}$ and the variational equations,

$$\partial F/\partial(A^2) = 0 \quad \text{and} \quad \partial F/\partial b = 0, \quad (3.9)$$

imply

$$A^2 = (k_1^2-k_0^2) \int_0^{a/b} x^2 f(x) dx \Big/ \int_0^\infty x^2 f^2(x) dx, \quad (3.9a)$$

$$A^2 = (k_1^2-k_0^2) \int_0^{a/b} x^2 f'(x) dx \Big/ \int_0^\infty x^2 f(x) f'(x) dx. \quad (3.9b)$$

By equating (3.9a) to (3.9b) and integrating by parts, we find that if

$$\alpha = a/b, \quad (3.10a)$$

then we obtain the equation

$$\tfrac{2}{3}\alpha^3 f(\alpha) = \int_0^\alpha x^2 f(x) dx. \quad (3.10b)$$

Hence (3.10a) and (3.10b) give the relation between a and b. Once α has been determined, A^2 is expressed in terms of α through (3.9a) and (3.10b):

$$A^2 = \tfrac{2}{3}\alpha^3 (k_1^2-k_0^2) f(\alpha) \Big/ \int_0^\infty x^2 f^2(x) dx = \tfrac{1}{2}\beta^{-1}(k_1^2-k_0^2). \quad (3.11)$$

As $A \to 0$ this is the correct limiting relation.

Since the terms of order κ and κ^2 in all of the equations derived below (3.18–3.37) are of the same order of magnitude as the corrections required in the relations (3.10) and (3.11) between A's, b's and k_1's and a's, they should not be used without these corrections.

The total scattering cross section σ_s can be obtained in two ways: by integrating $\sigma(\theta)$ over all angles or by using the imaginary part of the scattered amplitude in the forward direction. These two results are identical only when $\sigma(\theta)$ is exact. Since it is possible to integrate our approximate expressions for $\sigma(\theta)$, we prefer to do the former to obtain a more unified presentation. It should also be noted that in the integration over θ one uses the weight function $\sin\theta$. The largest errors in our approximate formulas occur in the range of small θ. Hence the integration procedure should give the better results. We shall now summarize the formulas for $\sigma(\theta)$ and σ_s for very soft scatterers.

After neglecting the terms of order κ and κ^2 in (3.7), we have

$$\sigma(\theta) = \frac{4k_1^2 A^4 b^4}{\omega^2 (k_1+k_0)^2} \left| \int_0^\infty x f(x) \sin(bx\omega) dx \right|^2. \quad (3.12)$$

The total scattering cross section is given by

$$\sigma_s = \frac{8k_1^2 A^4 b^4 \pi}{(k_1+k_0)^2} \int_0^\pi \left| \int_0^\infty x f(x) \sin \omega bx dx \right|^2 \sin\theta \omega^{-2} d\theta. \quad (3.13)$$

It is desirable to introduce $u = b\omega$ as the new angle variable to replace θ. Then

$$\frac{\sigma}{\pi b^2} = \frac{8k_1 A^4 b^2}{k_0(k_1+k_0)^2} \times \int_{b(k_1-k_0)}^{b(k_1+k_0)} u^{-1} \left| \int_0^\infty x f(x) \sin ux dx \right|^2 du. \quad (3.14)$$

In the limit of super soft scatterers or high energies ($k_1 \to k_0$), the natural parameter in which to express the results is

$$y = (A/k_0)^2(bk_0). \tag{3.15}$$

Now

$$b(k_1+k_0) = 2\beta A^2 b/(k_1-k_0) = y\beta/[(k_1/k_0)-1],$$
$$b(k_1-k_0) = 2\beta A^2 b/(k_1+k_0) = y\beta/[(k_1/k_0)+1].$$

Hence as $k_1 \to k_0$ for fixed y, $b(k_1+k_0) \to \infty$ and $b(k_1-k_0) = y\beta$. The coefficient of the integral in (3.14) becomes $2y^2$.

With these asymptotic results, the total scattering cross section of a super soft spherically symmetrical scatterer is

$$\frac{\sigma_s}{\pi b^2} = 2y^2 \int_{y\beta}^{\infty} u^{-1} \left\{ \int_0^{\infty} x f(x) \sin ux\, dx \right\}^2 du. \tag{3.16}$$

The first special case of this formula was derived by van de Hulst[3] for a uniform spherical scatterer. There $f(x)=0$ for $r>b$, 1 for $r<b$, $\beta=1$, and $y=bk_0[(k_1/k_0)^2 - 1]$ and Eq. (3.20) results.

We shall now give the results of the application of the above equations to four types of scattering potentials.

(a) Sphere of Radius a

Let

$$k^2(r) - k_0^2 = \begin{cases} k_1^2 - k_0^2 & \text{if } r<a, \\ 0 & \text{if } r>a. \end{cases} \tag{3.17}$$

Then

$$\sigma(\theta) = \tfrac{1}{2}|A_s|^2(k_0^2-k_1^2)^2 a^6 \left\{ \frac{J_{\frac{3}{2}}^2(a\omega)}{(a\omega)^3} - 2\kappa \frac{\cos(2ak_1) J_{\frac{3}{2}}(a\omega) J_{\frac{3}{2}}(av)}{(a\omega)^{\frac{3}{2}}(av)^{\frac{3}{2}}} + \frac{\kappa^2 J_{\frac{3}{2}}^2(av)}{(av)^3} \right\}. \tag{3.18}$$

This result agrees with that derived in S-I and S-II for soft spheres.

It is shown in S-I and S-II that

$$\sigma_s \simeq 2\pi^{\frac{1}{2}} a^2 x^2 m^{-1}(m-1)^2 \left\{ \frac{\mathbf{H}_{\frac{3}{2}}(2x[m-1])}{(x[m-1])^{5/2}} - \frac{\mathbf{H}_{\frac{3}{2}}(2x[m+1])}{(x[m+1])^{5/2}} \right\}, \tag{3.19}$$

where $x = ak_0 = 2\pi a/\lambda_0$, $m = k_1/k_0$, and $\mathbf{H}_{\frac{3}{2}}(z)$ is the $\frac{3}{2}$th-order Struve function,

$$\mathbf{H}_{\frac{3}{2}}(z) = (z/2\pi)^{\frac{1}{2}}(1+2z^{-2}) - (2/\pi z)^{\frac{1}{2}}(\sin z + z^{-1}\cos z).$$

If we define $y = x(m-1)$ and let $m \to 1$, we obtain the exact total scattering cross section of super soft spheres,[2,3]

$$\sigma_s/\pi a^2 = 2(\pi/y)^{\frac{1}{2}} \mathbf{H}_{\frac{3}{2}}(2y), \tag{3.20}$$

as $y \to \infty$, $\sigma_s/\pi a^2 \to 2$.

The Born approximation expression which corresponds to (3.19) is

$$\sigma_s/\pi a^2 = 2a^2(k_1-k_0)^2\{1 - \pi^{\frac{1}{2}}\mathbf{H}_{\frac{3}{2}}(4ak_0)/(2ak_0)^{5/2}\}.$$

In the limit as $m \to 1$, the range in which the Born approximation is best (provided that $2\pi a/\lambda_0$ is small), we get

$$\sigma_s/\pi a^2 = 2y^2. \tag{3.21}$$

This equation represents $\sigma_s/\pi a^2$ as a monotonically increasing function of y, which becomes infinite as the sphere radius becomes infinite. The exact equation (3.20) represents a bounded oscillating function of y. The exact total scattering cross section is compared with the Born approximation in Fig. 1.

(b) Gaussian Scatterer

Let

$$k^2(r) - k_0^2 = \pm A^2 \exp[-(r/b)^2]. \tag{3.22}$$

Then

$$\sigma(\theta) = |A_s|^2(A^4b^6\pi/16)\{\exp(-\tfrac{1}{2}b^2\omega^2) - 2\kappa\cos(2k_1a) \times \exp[-\tfrac{1}{4}b^2(\omega^2+v^2)] + \kappa^2\exp(-\tfrac{1}{2}b^2v^2)\}. \tag{3.23}$$

Since $f(x) = \pm\exp(-x^2)$, α satisfies

$$(4/3)\alpha^3 + \alpha = \exp(\alpha^2)\int_0^{\alpha} \exp(-x^2)dx$$

so that

$$\alpha = a/b = 1.235. \tag{3.24a}$$

It follows that

$$A^2 = \pm\frac{16}{3}\left(\frac{2}{\pi}\right)^{\frac{1}{2}}(k_1^2-k_0^2)\alpha^3\exp(-\alpha^2) \simeq \pm 1.744(k_1^2-k_0^2). \tag{3.24b}$$

The total scattering cross section of a Gaussian scatterer is obtained by integrating (3.23) over all angles. Then

$$\sigma_s = \frac{\tfrac{1}{2}\pi^2A^4b^6k_1^2}{(k_1+k_0)^2(1+\kappa^4-2\kappa^2\cos 4ak_1)}\left[\frac{(1+\kappa^2)}{k_1k_0b^2} \times \{\exp[-\tfrac{1}{2}b^2(k_1-k_0)^2] - \exp[-\tfrac{1}{2}b^2(k_1+k_0)^2]\} - 4\kappa\cos(2ak_1)\exp[-\tfrac{1}{2}b^2(k_1^2+k_0^2)]\right]. \tag{3.25}$$

The limiting expression for super soft scatterers (high energies) is derived by substituting (3.24) into (3.25) and neglecting terms of order κ and κ^2. Then, for small A,

$$\sigma_s/\pi b^2 = \tfrac{1}{8}\pi y^2\exp(-\tfrac{1}{2}y^2\beta^2), \quad y = (A/k_0)^2(bk_0), \quad \beta = 0.2867. \tag{3.26}$$

This total scattering cross section is compared with

the Born approximation,

$$\sigma_s/\pi b^2=\tfrac{1}{8}\pi y^2, \tag{3.27}$$

in Fig. 2. Notice that as $y\to\infty$, $\sigma_s/\pi b^2\to\infty$ in the Born approximation and zero in our approximation.

(c) Exponential Scatterer

Let

$$k^2(r)-k_0^2=\pm A^2\exp(-r/b). \tag{3.28}$$

Then

$$\sigma(\theta)=4b^6A^4|A_s|^2\{(1+\omega^2b^2)^{-4}+\kappa^2(1+v^2b^2)^{-4} -2\kappa\cos(2ak_1)(1+v^2b^2)^{-2}(1+\omega^2b^2)^{-2}\}. \tag{3.29}$$

Here $f(x)=\pm\exp(-x)$. Hence $1+\alpha+\frac{1}{2}\alpha^2+\frac{1}{3}\alpha^3=e^\alpha$, $\alpha=2.318$, and we have

$$A^2=\pm(8/3)(k_1^2-k_0^2)\alpha^3e^{-\alpha}\simeq\pm3.270(k_1^2-k_0^2). \tag{3.30}$$

Since

$$\int_0^\pi\frac{\sin\theta d\theta}{(1+\omega^2b^2)^4}=\frac{1}{6b^2k_1k_0}\left\{\frac{1}{[1+b^2(k_1-k_0)^2]^3} -\frac{1}{[1+b^2(k_1+k_0)^2]^3}\right\}=L_1,$$

and

$$\int_0^\pi\frac{\sin\theta d\theta}{(1+\omega^2b^2)^2(1+v^2b^2)^2}=\frac{1}{4k_1k_0b^2[1+b^2(k_1^2+k_0^2)]^2} \times\left\{\frac{4k_1k_0b^2}{[1+b^2(k_1+k_0)^2][1+b^2(k_1-k_0)^2]} +\frac{1}{[1+b^2(k_1^2+k_0^2)]}\log\left(\frac{1+b^2(k_1+k_0)^2}{1+b^2(k_1-k_0)^2}\right)\right\}=L_2,$$

we have

$$\sigma_s=8b^6A^4\pi\{(1+\kappa^2)L_1-2\kappa L_2\cos(2ak_1)\}|A_s|^2. \tag{3.31}$$

The limiting expression for super soft scatterers is

$$\sigma_s/\pi b^2=(4/3)y^2(1+\beta^2y^2)^{-3},\quad \beta=0.1529. \tag{3.32}$$

The corresponding Born approximation is

$$\sigma_s/\pi b^2=(4/3)y^2. \tag{3.33}$$

Equations (3.33) and (3.32) are compared in Fig. 3.

(d) Screened Coulomb Scatterer

Let

$$k^2(r)-k_0^2=\pm[A^2/(r/b)]\exp(-r/b). \tag{3.34}$$

Then

$$\sigma(\theta)=A^4b^6|A_s|^2\{(1+\omega^2b^2)^{-2}+\kappa^2(1+v^2b^2)^{-2} -2\kappa\cos(2ak_1)(1+\omega^2b^2)^{-1}(1+v^2b^2)^{-1}\}. \tag{3.35}$$

Here $f(x)=\pm x^{-1}e^{-x}$. Then α satisfies $e^\alpha=1+\alpha+\frac{2}{3}\alpha^2$ and $\alpha=0.807$; hence,

$$A^2=\pm(4/3)\alpha^2(k_1^2-k_0^2)e^{-\alpha}\simeq\pm0.379(k_1^2-k_0^2). \tag{3.36}$$

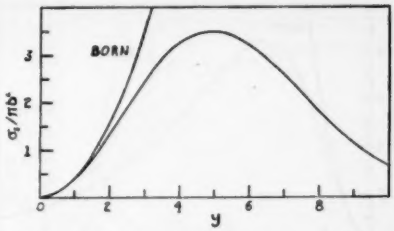

FIG. 2. Ratios of the total scattering cross section of a Gaussian sphere $[k^2(r)-k_0^2=\pm A^2\exp\{-(r/b)^2\}]$ with πb^2 in the limit as $A/k_0\to0$. The upper curve is the Born approximation [Eq. (3.27)]. The lower curve is the present approximation [Eq. (3.26)]. The parameter y is defined by $y=(A/k_0)^2(bk_0)$.

We obtain the total scattering cross section by integrating (3.35):

$$\sigma_s=\pi A^4b^4|A_s|^2(k_1k_0)^{-1} \times\left\{(1+\kappa^2)\left[\frac{1}{1+b^2(k_1-k_0)^2}-\frac{1}{1+b^2(k_1+k_0)^2}\right] -\frac{2\kappa\cos2ak_1}{1+b^2(k_1^2+k_0^2)}\log\left[\frac{1+b^2(k_1+k_0)^2}{1+b^2(k_1-k_0)^2}\right]\right\}. \tag{3.37}$$

The limiting expression for super soft scatterers is

$$\sigma_s/\pi b^2=y^2/(1+y^2\beta^2),\quad \beta=1.319, \tag{3.38}$$

while the Born approximation yields

$$\sigma_s/\pi b^2=y^2. \tag{3.39}$$

Equations (3.39) and (3.38) are compared in Fig. 4.

It is of interest at this point to see if (3.35) reduces as $b\to\infty$ to the exact differential cross section of a Coulomb scatterer. Let us consider the scattering of an electron by an ion of charge Ze. Then

$$k^2(r)-k_0^2=-(2mZe^2/rh^2)e^{-r/b},\quad k_0^2=2mE/h^2=mv^2/h^2,$$

where e = charge on the electron, m = electron mass, and v = velocity of incident electron.

From (3.34), $A^2b=2mZe^2/h^2$. Then, from (3.36),

$$2Zme^2/bh^2=0.379(k_1^2-k_0^2).$$

Hence as $b\to\infty$, $k_1\to k_0$ so that

$$\omega^2=k_1^2+k_0^2-2k_1k_0\cos\vartheta=4m^2v^2h^{-2}\sin^2\tfrac{1}{2}\vartheta,$$

and (3.35) approaches

$$\sigma(\theta)=(2mZe^2/h^2)^2\omega^{-4}\to[(Ze^2\csc^2\tfrac{1}{2}\theta)/2mv^2]^2,$$

the Rutherford scattering formula. Our approximation is equivalent to that of the Born approximation for this problem. Equations (3.18), (3.23), and (3.29) all reduce to the corresponding Born approximations when $k_1=k_0$, for then $\omega^2\to4k_0^2\sin^2\frac{1}{2}\theta$ and $\kappa=0$. The resulting expressions are independent of the parameters of the sphere whose approximate wave functions were used.

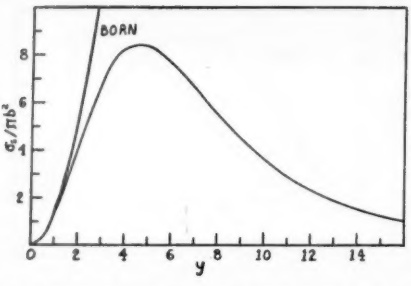

FIG. 3. Ratios of the total scattering cross section of an exponential sphere $[k^2(r)-k_0^2=\pm A^2\exp(-r/b)]$ with πb^2 in the limit as $(A/k_0)\to 0$. The upper curve is the Born approximation [Eq. (3.33)]. The lower curve is the present approximation [Eq. (3.32)]. The parameter y is defined by $y=(A/k_0)^2(bk_0)$.

As A, and therefore as $(k_1^2-k_0^2)$, increases one must use a better approximation to ψ_t in (3.8) in order to obtain more accurate relations between the sphere parameters and those of the scatterer of interest.

The above results are generalized in the next section to scatterers with the symmetry of an infinite cylinder.

4. SCATTERING BY SOFT OBSTACLES WITH SYMMETRY OF INFINITE CIRCULAR CYLINDER

Since the theory of scattering by an infinite circular cylinder is essentially the same as that of a sphere, we shall not include as much detail in this section as we did in the last. We shall merely summarize the main formulas and give a brief indication of their derivation.

We let the z axis of our coordinate system be the axis of our scatterer and let our incident plane wave be propagated in the direction of a unit vector s_0 which lies in the $x-z$ plane and makes an angle α_0 with the z axis. We shall use the approximate internal wave function of an isotropic circular cylinder of radius a and propagation constant k_1. An angle α_1 defined by

$$k_1\cos\alpha_1=k_0\cos\alpha_0, \tag{4.1}$$

and a set of "starred" parameters

$$k_j^*=k_j\sin\alpha_j,\quad m^*=k_1^*/k_0^* \tag{4.2}$$

enter naturally into the theory.

The starting point of our analysis is the integral equation (1.4a). We approximate $\psi(r)$ in the integrand by the wave function ψ_t of a soft cylinder. As was shown in S-II, the value of ψ_t at a point r, z, θ (in cylindrical coordinates) is approximately

$$\psi_t(r)=\frac{2(m^*)^{\frac{1}{2}}\exp[ia(k_1^*-k_0^*)]\exp(izk_0\cos\alpha_0)[\exp(ik_1^*r\cos\theta)-i\kappa\exp(2iak_1^*)\exp(-irk_1^*\cos\theta)]}{(1+m^*)[1+\kappa^2\exp(4iak_1^*)]}. \tag{4.3}$$

If (4.3) is substituted into (1.4a), the integration over z and θ can be carried out in the manner discussed in S–II. Then

$$\psi_s(R)=\frac{i(m^*)^{\frac{1}{2}}(2\pi/Rk_0^*)^{\frac{1}{2}}\exp[ia(k_1^*-k_0^*)+i(Rk_0^*-\frac{1}{4}\pi+k_0z\cos\alpha_0)]}{(1+m^*)[1+\kappa^2\exp(4iak_1^*)]}$$

$$\times\int_0^\infty r[k^2(r)-k_0^2][J_0(r\omega_1)-i\kappa\exp(2iak_1^*)J_0(rv_1)]dr, \tag{4.4}$$

where

$$\omega_1^2=k_1^{*2}+k_0^{*2}-2k_1^*k_0^*\cos\Theta \tag{4.5a}$$

$$v_1^2=k_1^{*2}+k_0^{*2}+2k_1^*k_0^*\cos\Theta. \tag{4.5b}$$

The differential scattering cross section is then given by

$$\sigma(\Theta)=R|\psi_s(R)|^2$$

$$=\frac{2\pi m^*}{k_0^*(1+m^*)^2(1+\kappa^4+2\kappa^2\cos 4ak_1^*)}$$

$$\times\left|\int_0^\infty r[k^2(r)-k_0^2][J_0(r\omega_1)-i\kappa\exp(2iak_1^*)J_0(rv_1)]dr\right|^2. \tag{4.6}$$

The integrations are easily carried out in three of the four special cases considered in the last section. The screened Coulomb potential leads to a divergence in the integrals needed to relate the parameters of the cylindrical scatterer with those of the screened Coulomb potential.

As in the case of scattering by spherically symmetrical scatterers, we use the variational scheme of Sec. 2 to relate a and k_1 to A and b. We again limit ourselves to soft scatterers so that we can assume $|\psi_0|^2=$constant. The integral to be minimized is

$$I=2\pi\int_0^\infty([k^2(r)-k_0^2]-[k_0^2(r)-k_0^2])^2rdr.$$

In our cases of interest

$$k^2(r)-k_0^2=A^2f(r/b),$$

while

$$k_0^2(r)-k_0^2=\begin{cases}k_1^2-k_0^2 & \text{if } r<a\\ 0 & \text{if } r>a.\end{cases}$$

The variational equations $\partial I/\partial A^2=0$ and $\partial I/\partial b=0$ imply

$$A^2=(k_1^2-k_0^2)\int_0^a xf(x)dx \Big/ \int_0^\infty xf^2(x)dx \tag{4.7}$$

$$A^2=(k_1^2-k_0^2)\int_0^a x^2f'(x)dx \Big/ \int_0^\infty x^2f(x)f'(x)dx \tag{4.8}$$

$$\alpha=a/b. \tag{4.9}$$

By equating these expressions for A^2, we find that α is the real positive root of

$$\alpha^2 f(\alpha)=\int_0^\alpha xf(x)dx, \tag{4.10}$$

and A^2 is related to k_1 by

$$A^2=(k_1^2-k_0^2)\alpha^2 f(\alpha) \Big/ \int_0^\infty xf^2(x)dx. \tag{4.11}$$

General expressions can be derived for the total scattering cross sections of very soft scatterers in the following way. Equation (4.6) implies in this case

$$\sigma_s=\frac{4\pi mA^2}{k_0(1+m)^2}\int_0^\pi\left[\int_0^\infty rf(r/b)J_0(r\omega)dr\right]^2 d\Theta.$$

Let us introduce the new integration variable $u=b\omega$. Then

$$d\Theta=udu/b^2k_1k_0\sin\Theta.$$

$\sin\Theta$ is obtained as a function of u from (4.5). Then

$$\sigma_s/2b=\frac{4\pi mA^4b^2}{k_1(1+m)^2} \times\int_{b(k_1-k_0)}^{b(k_1+k_0)}\frac{udu\left\{\int_0^\infty xf(x)J_0(xu)dx\right\}^2}{[b^2(k_0+k_1)^2-u^2]^{\frac{1}{2}}[u^2-b^2(k_1-k_0)^2]^{\frac{1}{2}}}.$$

In the limit as $A\to 0$ (i.e., $m\to 1$) it is convenient to introduce a new variable

$$y=(A/k_0)^2(bk_0)=\tfrac{1}{2}\beta^{-1}(k_1^2-k_0^2)/k_0.$$

Then for fixed y

$$(k_1+k_0)b=y\beta/[k_1/k_0-1]\to\infty$$
$$(k_1-k_0)b=y\beta/[k_1/k_0+1]\to\tfrac{1}{2}\beta y$$

and

$$\sigma_s/2b\sim\tfrac{1}{2}\pi y^2\int_{\beta y}^\infty\frac{udu\left\{\int_0^\infty xf(x)J_0(xu)dx\right\}^2}{(u^2-\beta^2y^2)^{\frac{1}{2}}}/. \tag{4.12}$$

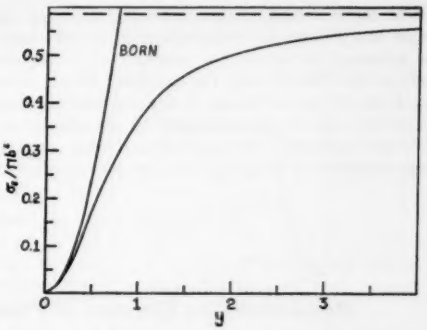

FIG. 4. Ratios of the total scattering cross section of a screened Coulomb scatterer $[k^2(r)-k_0^2=\pm\{A^2/(r/b)\}\exp(-r/b)]$ with πb^2 in the limit as $(A/k_0)\to 0$. The upper curve is the Born approximation [Eq. (3.39)]. The lower curve is the present approximation [Eq. (3.38)]. The parameter y is defined by $y=(A/k_0)^2(bk_0)$.

As an example, we shall present here only the results for the Gaussian scatterer. In that case

$$k^2(r)-k_0^2=\pm A^2\exp-(r/b)^2.$$

Hence

$$\sigma(\Theta)=\frac{\pi m^*b^4A^4}{2k_0^*(1+m^*)^2[1+\kappa^4+2\kappa^2\cos(4ak_1^*)]} \times\{\exp(-\tfrac{1}{2}b^2\omega_1^2)+\kappa^2\exp(-\tfrac{1}{2}b^2v_1^2) +2\kappa\sin(2ak_1^*)\exp[-\tfrac{1}{2}b^2(k_1^{*2}+k_0^{*2})]\}. \tag{4.13}$$

The defining equation for α for a Gaussian scatterer is $1+2\alpha^2=\exp\alpha^2$. From this we find $\alpha=1.121$ and

$$A^2=\pm 4\alpha^2\exp(-\alpha^2)(k_1^2-k_0^2)=\pm 1.431(k_1^2-k_0^2). \tag{4.14}$$

The total scattering cross section of a very soft Gaussian cylinder to plane waves where direction of propagation is normal to the cylinder axis is (we have dropped the stars on our m's and k_1's and let $m=k_1/k_0$)

$$\sigma_s=\frac{\pi mb^4A^4}{k_0(1+m)^2}\int_0^\pi\exp\{-\tfrac{1}{2}b^2(k_1^2+k_0^2-2k_1k_0\cos\Theta)\}d\Theta$$
$$=\frac{m\pi^2b^4A^4}{k_0(1+m)^2}\exp[-\tfrac{1}{2}b^2k_0^2(1+m^2)]I_0(b^2k_0^2m);$$
$$m=1+(A^2/1.431k_0^2)$$

where $I_0(x)$ is the zeroth-order Bessel function of purely imaginary argument. In the limit as $A\to 0$ we can use the asymptotic formula (4.12) to obtain

$$\sigma_s/2b\sim\tfrac{1}{8}\pi y^2\int_{\beta y}^\infty\frac{u^2\exp(-\tfrac{1}{2}u^2)du}{[u^2-\beta^2y^2]^{\frac{1}{2}}}$$
$$=\frac{\pi}{8}\left(\frac{\pi}{2}\right)^{\frac{1}{2}}y^2\exp(-\tfrac{1}{2}\beta^2y^2).$$

One might attempt to generalize the results of this paper to scatterers in which the scattering force cannot be expressed in terms of a potential which depends only on the distance from the scattering center; to the scattering of vector waves; to the scattering by shell structures; and to the scattering by periodically distributed scatterers. One might also attempt to make improvements by using step function potentials as the trial forms. Some of these problems are now under investigation. It would be desirable to investigate some slightly more complicated improved forms of the approximating wave functions then those used here.

The general program on scattering, of which this work is one phase, was initiated through a grant of the Research Corporation while one of the authors (E.W.M.) was at the University of Pittsburgh.

PHYSICAL REVIEW VOLUME 86, NUMBER 6 JUNE 15, 1952

Magnetostrictive Vibration of Prolate Spheroids. Ni-Fe and Ni-Cu Alloys*

J. S. KOUVELITES† AND L. W. MCKEEHAN
Sloane Physics Laboratory, Yale University, New Haven, Connecticut
(Received February 20, 1952)

The study of the different magnetic properties determined from the magnetostrictive vibrational behavior of small ferromagnetic prolate spheroids was extended to a large number of Ni-Fe and Ni-Cu alloys. The computed values for the saturation magnetostriction, the total change of Young's modulus with magnetization, and the initial permeability of plain-annealed (i.e., annealed in zero magnetic field) specimens of these materials, were inserted in two independent expressions, derived by Kersten, for the internal stress. The agreement between the two sets of values was quite good. The Ni-Fe alloys were also studied after having been magnetic-annealed; moreover, the 68-percent Ni Permalloy, having exceedingly strain-sensitive properties, was investigated in cold-worked, baked, and annealed conditions. In general, the changes of the calculated internal stress with heat treatment appeared consistent with the corresponding variations of properties such as the initial permeability. Even more revealing in this way were the values for the domain size determined from the computed dissipation factors and internal stresses and found to agree very well with previous measurements of Barkhausen discontinuities. When, for all the plain-annealed specimens, the relative change of Young's modulus was plotted against the relative magnetization, it was discovered that all the curves were almost identical. With the support of previous work, we were able to conclude that these curves should be similar for all plain-annealed face-centered cubic structures at room temperature.

A SMALL centrally-clamped prolate spheroid of a ferromagnetic material was forced magnetostrictively into longitudinal vibration in its fundamental mode. The perturbing agent was a small axial high frequency magnetic field superimposed on a uniform and axial static field. It was shown in a previous paper[1] how the incremental permeability, magnetostriction constant, modulus of elasticity, and dissipation factor of the ferromagnetic spheroid could be accurately computed from the resonance changes of the impedance of the high frequency magnetizing coil. Moreover, it was found that the values obtained for these parameters for a wide composition range of Ni-Fe alloys were in qualitative agreement with previous theory and experiment.

Here, the results are presented for a larger number of compositions and for a variety of heat treatments, and the extent of corroboration with previous work is indicated as quantitatively as possible. More important, on the basis of our results, it is now possible to extend present information on certain properties of ferromagnetics at low magnetizing fields.

All the measurements were made at room temperature and with a high frequency field of 0.35-oersted amplitude.

PLAIN-ANNEAL AND MAGNETIC-ANNEAL

The compositions chosen for study were nickel, the Ni-Fe alloys of atomic percent nickel: 88, 84, 79, 68, 56, 45, and the Ni-Cu alloys of atomic percent nickel: 90, 84, 81, 71. They were all commercially pure, the impurities amounting to less than 0.5 percent.

Structurally, all the above compositions are face-centered cubic. The two alloy systems represent, however, examples of addition to one ferromagnetic metal, of various amounts of either another ferromagnetic or of a nonferromagnetic. It is therefore likely that any statement found to apply to both systems will be applicable with equal validity to most other f.c.c. binary nickel alloys.

A spheroidal specimen of each composition was studied in what hereafter will be called the plain-annealed condition, which is achieved by a three-hour anneal at 700°C in a hydrogen atmosphere followed by a slow cool. The nickel and the Ni-Fe specimens were subsequently heated again to 700°C in hydrogen but

* Assisted by the ONR.
† Now in the Physics Department of the University of Leeds, England.
[1] Beck, Kouvelites, and McKeehan, Phys. Rev. **84**, 957 (1951). The following corrections for errors missed in proof should be made in this paper. On p. 958 the last part of Eq. (9) should contain the additional factor ω, the last two parts of Eq. (10) should have the first plus sign changed to a minus sign, the last part of Eq. (11) should contain the additional factor $X_a e^{2i\omega t}$.

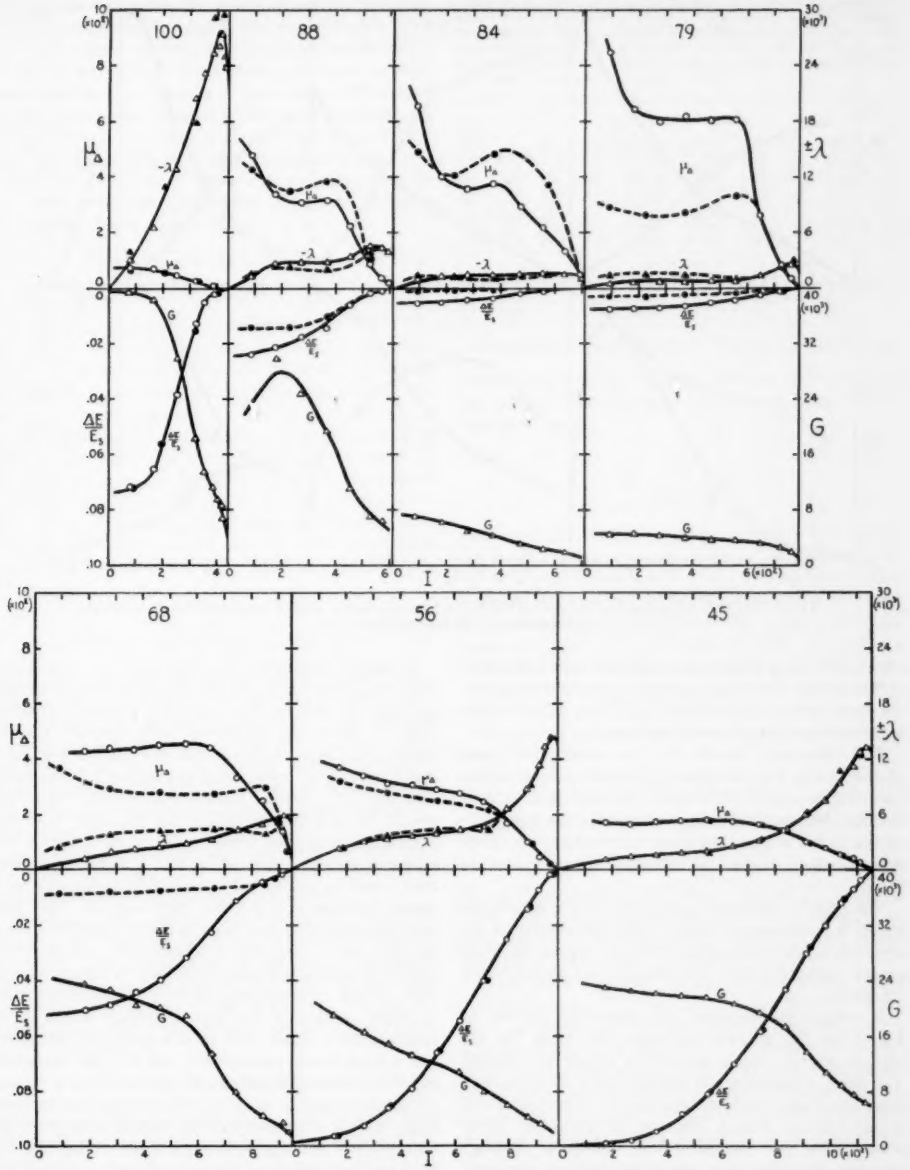

FIG. 1. The physical parameters (incremental permeability, μ_Δ; magnetostriction constant, λ; change of Young's modulus relative to its saturation value, $\Delta E/E_s$; dissipation constant, G) of nickel and the Ni-Fe alloys (atomic percent of nickel indicated), as functions of the magnetization bias. The solid curves are for the plain-annealed specimens; the dashed curves for the magnetic-annealed. All the quantities are in emu.

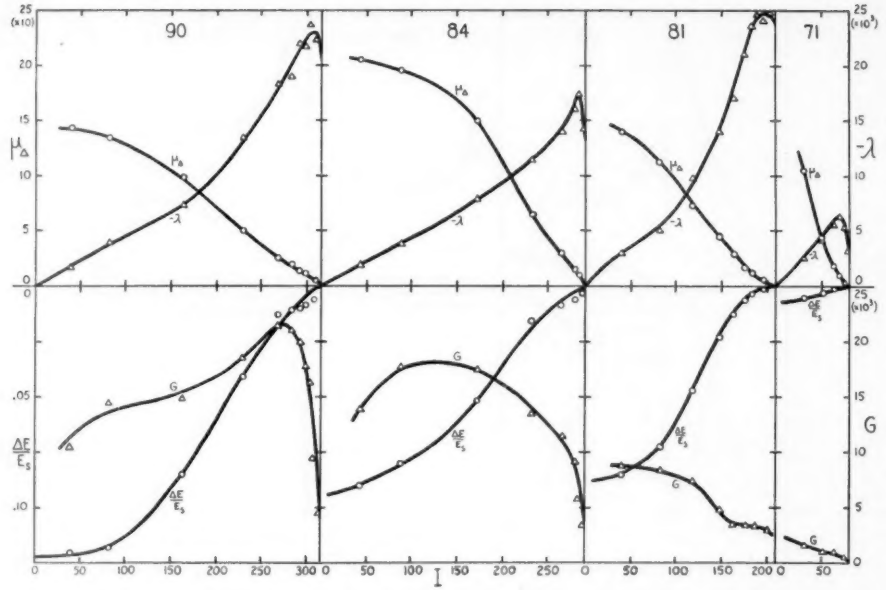

FIG. 2. The physical parameters (in emu) of the Ni-Cu alloy specimens (atomic percent of nickel indicated), as functions of the magnetization bias.

allowed to cool gradually in an applied axial static field of 90 oersteds. The Ni-Cu specimens were not magnetic-annealed since it was expected that they would not be appreciably affected by this treatment.

The calculated results for the nickel-irons were plotted in Fig. 1 as functions of the static magnetization bias. Within experimental error, no difference could be detected between the plain-anneal and the magnetic-anneal as far as the dissipation factor of any specimen was concerned; hence, only the plain-anneal values are shown.

The singular nature of a composition near 80 percent nickel is immediately evident from the computed parameters of the plain-annealed Ni-Fe specimens; their general variation with composition has already been discussed.[1]

A comparison between the quantities plotted in Fig. 1 for the magnetic-annealed and those for the plain-annealed reveals something rather unexpected. The effect of the magnetic-anneal, which is increasingly pronounced as a composition of about 70 percent nickel is approached, was a decrease of both the initial permeability and the saturation change of Young's modulus. For other than zero magnetization, the incremental permeability was either higher or lower than the corresponding value for the plain-annealed, while the magnetostriction constant was below or above, respectively, its plain-anneal value.

By static measurement,[2] it has long been established that magnetic-anneal reduces the saturation magnetostriction as well as the saturation elasticity change. This is obviously consistent with domain theory. Hence, the interpretation of the area under a λ-*versus*-I curve as a direct measure of the saturation magnetostriction is not tenable since it would appear from the results for the 68 Permalloy, for example, that the saturation magnetostriction had been increased by the magnetic-anneal. However, it may still be safely said that λ and μ_Δ signify the state of a ferromagnetic on a minor hysteresis loop. We may suppose that the magnetic-anneal locked many of the domains with their magnetic axes along the specimen axis, and that the small perturbing field was insufficient to cause as many 180° domain reversals as it did in the plain-anneal case. A larger portion of the high frequency variation of magnetization would then be due to domain rotation, and a lower initial permeability and a higher magnetostriction constant would result. It remains as a matter for further study to learn how the incremental permeability and the magnetostriction constant depend on the amplitude of the high frequency magnetizing field for both plain-annealed and magnetic-annealed permalloys.

The computed parameters for the Ni-Cu alloys are presented in Fig. 2. Although the saturation magneto-

[2] Williams, Bozorth, and Christensen, Phys. Rev. **59**, 1005 (1941).

striction and elasticity change and the maximum dissipation factor decreased rapidly and monotonously with increased copper content, the maximum permeability (which as for the Ni-Fe specimens occurred at zero magnetization) first rose and then slowly fell as the copper content was increased. This apparent anomaly was probably due to the fact that at room temperature these alloys were not far from their Curie points.

The internal stresses within the materials may be evaluated from two independent equations obtained by Kersten.[3] These expressions,

$$S_{i1}=2E_0(\Delta L/L)_s/5(\Delta E/E)_s, \tag{1}$$

$$S_{i2}=8\pi I_s^2/9\mu_0(\Delta L/L)_s, \tag{2}$$

interrelate the saturation magnetostriction: $(\Delta L/L)_s$, the saturation relative change of Young's modulus: $(\Delta E/E)_s$, the incremental permeability and the modulus of elasticity at zero magnetization: μ_0 and E_0, and the saturation magnetization: I_s. Hence, they provide a convenient index for a comparison of our results with theory. The values of internal stress, computed by means of (1) and (2) for each of the plain-annealed specimens, are shown in Table I. The agreement is fairly close when allowance is made for the fact that the $(\Delta L/L)_s$ and $(\Delta E/E)_s$ of the more permeable materials were very small and therefore less accurately determined.

The geometric mean of (1) and (2) is

$$S_{i3}=(S_{i1}S_{i2})^{\frac{1}{2}}=1.056I_s[E_0/\mu_0(\Delta E/E)_s]^{\frac{1}{2}}, \tag{3}$$

which does not contain $(\Delta L/L)_s$ and may therefore be used for the calculation of the internal stresses of the magnetic-annealed materials whose saturation magnetostriction, as was previously discussed, cannot be determined from our data. The internal stresses computed from (3) are listed in Table I for both the plain-annealed and magnetic-annealed specimens. We observe that the magnetic-anneal considerably increased the internal stresses; this is consistent with the proposed idea that the magnetic-anneal fixed the magnetic axes of the domains more rigidly than the plain-anneal.

The dissipation constant G as defined,[1] is a measure of micro-eddy current losses and magnetomechanical hysteresis,[4] but at our high frequencies of excitation (approx 160 kc/sec), it may be associated entirely with micro-eddy currents. According to Bozorth,[5] the micro-eddy current energy loss per second per cubic centimeter may be expressed as

$$P_i=42.6\sigma(fI_slS/S_i)^2, \tag{4}$$

where σ is the electric conductivity, S is the amplitude of the applied stress, and l is the length in which the internal stress, on the average, reverses sign. For S, in the case of the vibrating spheroid, we may use an average stress,

$$\bar{S}=\frac{1}{v}\int_{z=-a}^{z=a} S\,dv,$$

where the differential volume, $dv=\pi(b/a)^2(a^2-x^2)dx$, the total volume, $v=4\pi ab^2/3$, and S as a function of the major-axial coordinate x is given by $E(\pi X_a/2a)\times\cos(\pi x/2a)$ to a good approximation.[6] Thus, in terms of X_a, the absolute displacement of either end of the prolate spheroid, of a, its semimajor axis, and of E, its modulus of elasticity, the mean stress was found to be

$$\bar{S}=(12/\pi^2)EX_a/a.$$

The power loss per unit volume expressed in terms of G is[7]

$$P_G=31.6G(fX_a/a)^2. \tag{5}$$

Consequently, we find by equating (4) and (5) that

$$l=0.71(S_i/EI_s)(G/\sigma)^{\frac{1}{2}}. \tag{6}$$

By substitution in (6) of the values of S_{i3} listed in Table I, the maximum G, and the corresponding E, we were able to determine the maximum l for each of the specimens. The results are shown in Table II.

It has been suggested by Becker and Döring[8] that the significance of l lies in the identification of its value, as determined from micro-eddy current losses, with the length of a side of a cubic magnetic domain whose volume may also be calculated from Barkhausen discontinuity measurements. From the data of Bozorth and Dillinger[9] on the volume of the maximum magnetization discontinuities for a number of plain-annealed

TABLE I. The initial permeability, the saturation magnetostriction and change of Young's modulus, and the internal stress evaluated for the plain-annealed (unprimed symbols) and magnetic-annealed (primed symbols) specimens. All the quantities are in emu when the magnetostriction values are multiplied by $(10)^{-6}$ and the internal stresses by $(10)^6$.

% Ni	μ_0	μ_0'	$(\Delta L/L)_s$	$(\Delta E/E)_s$	$(\Delta E/E)_s'$	Si_1	Si_2	Si_3	Si_3'
Nickel and Ni-Fe alloys									
100	75	75	31.0	0.0725	0.0725	3.38	2.27	2.77	2.77
88	580	490	10.5	0.0240	0.0145	3.63	1.73	2.50	3.52
84	820	610	5.9	0.0058	0.0012	8.36	2.99	5.00	12.72
79	1050	330	5.1	0.0076	0.0030	5.32	3.25	4.16	11.88
68	450	420	15.6	0.0531	0.0090	2.45	3.59	2.97	7.61
56	420	370	33.4	0.0980	0.0980	2.26	1.91	2.08	2.24
45	210	210	37.9	0.1000	0.1000	2.06	4.71	3.12	3.12
Ni-Cu alloys									
90	145	...	20.4	0.1220	...	1.13	0.94	1.03	...
84	210	...	13.8	0.0920	...	1.08	0.81	0.94	...
81	160	...	13.8	0.0885	...	1.11	0.53	0.77	...
71	150	...	1.9	0.0064	...	2.08	0.63	1.14	...

[3] M. Kersten, Z. Physik **71**, 575 (1931) and **85**, 708 (1933).

[4] According to the classification of losses in ferromagnetics described in R. Becker and W. Döring, *Ferromagnetismus* (Verlag. Julius Springer, Berlin, 1939), pp. 357–382.

[5] R. M. Bozorth, *Ferromagnetism* (D. Van Nostrand and Company, Inc., New York, 1951), p. 706.

[6] As shown in J. S. Kouvelites, Quart. Appl. Math. **9**, 105 (1951), the longitudinal deflection is very closely $X_a\sin(\pi x/2a)$ for the fundamental mode.

[7] Deduced from Eq. (9) of reference 1.

[8] See reference 4, pp. 381–382.

[9] R. M. Bozorth and J. F. Dillinger, Phys. Rev. **35**, 733 (1930).

TABLE II. The maximum dissipation factor and domain dimension calculated for the plain-annealed (unprimed symbols) and magnetic-annealed (primed symbol) materials. They are in emu when the values of G are multiplied by $(10)^3$ and those of l by $(10)^{-4}$. The subscript BD refers to the quantities determined from the data of Bozorth and Dillinger.

% Ni	G_{max}	l	l_{BD}	l'
Nickel and Ni-Fe alloys				
100	39	4.4	2.8	4.4
88	28	2.7	...	3.8
84	7	2.4	...	6.2
80.5	...	...	1.4	...
79	5	1.8	...	4.8
78	...	...	2.2	...
68	25	2.5	...	6.1
56	23	2.7	...	2.9
50	...	...	3.6	...
45	24	4.9	...	4.9
Ni-Cu alloys				
90	22	2.8	...	...
84	18	3.0	...	...
81	9	2.5	...	...
71	2	5.5	...	...

Ni-Fe alloys, values were derived for the length of a side of the equivalent cubic domain. They, also, are presented in Table II. There is very definite correlation between the quantities determined by the two completely different experimental methods. There is close agreement not only in their magnitudes, but, in both sets of values for the plain-annealed Ni-Fe alloys, there is the same monotonous decrease of l as a composition of about 80 percent nickel is approached. The actual amount of variation of l with composition was rather small. Bozorth and Dillinger[9] have attributed this to a compensating effect between variations of permeability and coercivity. It follows from the data here presented that the smaller coercivity of the plain-annealed permalloys of approximately 80 percent nickel more than compensated for their higher permeability, resulting in lower values of l. Similarly, the large values of l for some of the magnetic-annealed permalloys may be the result of the dominant effect of their high permeability.

There is nothing particularly striking about the calculated values of l for the various Ni-Cu alloys (also shown in Table II) except that they have the same order of magnitude as those for the nickel-irons. The large domain size computed for the 71-percent nickel specimen is probably due to the fact that a large part of its extremely small internal dissipation was magnetomechanical hysteresis loss; thus, in this case, the assumption that the losses are almost entirely micro-eddy current dissipation may not be valid.

By the observed effects of magnetic-anneal, we have been led to believe that the modulus of elasticity was less dependent on the amplitude of the high frequency magnetic excitation than were either the incremental permeability or magnetostriction constant. Furthermore, our high frequency measurements of this physical parameter for the magnetic-annealed specimens were the most consistent with previous static measurement. Consequently, we have chosen to study its variation with magnetization bias more carefully. It should be mentioned here that due to eddy current shielding, the Young's modulus which is determined from high frequency vibration study is very closely that for constant magnetization.[10]

For each of the plain-annealed specimens (both Ni-Fe and Ni-Cu), the relative change of Young's modulus defined as

$$\epsilon=\left(\frac{1}{E_0}-\frac{1}{E}\right)\Big/\left(\frac{1}{E_0}-\frac{1}{E_s}\right),$$

subscripts 0 and s denoting zero and saturation magnetization, was plotted against the relative magnetization, $j=I/I_s$. The shaded region of Fig. 3 depicts the fairly small spread of the curves for all eleven materials. Curves a, b, and c have been constructed from the data of Siegel and Quimby[11] on plain-annealed nickel at 23.5°, 200°, and 311° C, respectively. The fact that their room temperature curve lies within the shaded region provides a very good check for our measurements. It is interesting to note that curve d, drawn from Cooke's[12] room temperature data on plain-annealed Armco iron (a body-centered rather than a face-centered cubic structure), departs markedly from the shaded region.

In a very elegant analysis of the ΔE effect in ferromagnetics, Brown[13] derived the following expression, applicable at low fields to materials of face-centered cubic symmetry,

$$\epsilon=1.54j^2. \tag{7}$$

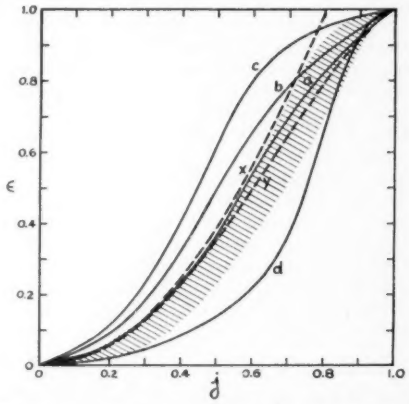

FIG. 3. The relative change ϵ of Young's modulus plotted against the relative magnetization j for the plain-annealed nickel and nickel alloy specimens (shaded region).

[10] W. F. Brown, Phys. Rev. **50**, 1165 (1936).
[11] S. Siegel and S. L. Quimby, Phys. Rev. **49**, 663 (1936).
[12] W. T. Cooke, Phys. Rev. **50**, 1158 (1936).
[13] W. F. Brown, Phys. Rev. **52**, 325 (1937).

The agreement between (7), represented by the dashed curve x, and the experimental curves, is remarkably good over a considerable range in j.

For a small applied stress, the modulus of elasticity is inversely proportional to the resultant strain which, in a magnetostrictive material, is the sum of the normal "nonmagnetic" lattice strain and the "magnetostrictive" strain associated with the change in magnetic domain orientation. Since the magnetostrictive strain ξ_m is zero at saturation, it is easily seen from the definition of ϵ that

$$\epsilon = 1 - \xi_m/\xi_{m0}, \tag{8}$$

where ξ_{m0} is the magnetostrictive strain at zero magnetization. Consequently, a convenient empirical expression for ϵ as a function of j is

$$\epsilon = 1 - (1 - j^2)^{1.54}, \tag{9}$$

which agrees with (7) at low values of j; moreover, as represented by the dashed curve y of Fig. 3, it agrees quite well with experiment over the entire range in j.

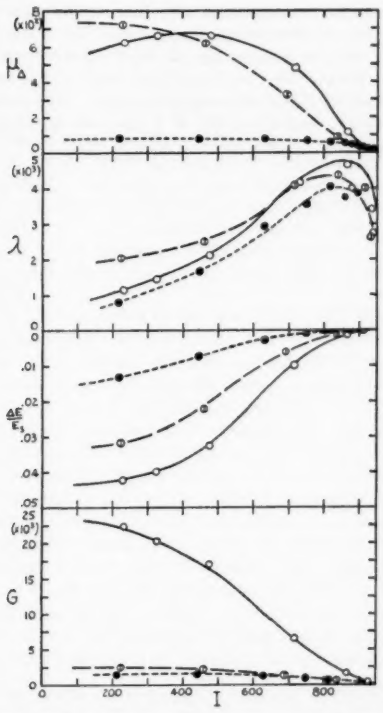

FIG. 4. The physical parameters (in emu) of 68 Permalloy when cold-worked (short-dashed curves), baked (long-dashed curves), and annealed (solid curves), as functions of the magnetization bias.

TABLE III. The physical parameters computed for the 68 Permalloy specimen after different mechanical and heat treatments. They are all in emu when multiplied by the factors indicated in Tables I and II.

Treatment	μ_0	$(\Delta E/E)_s$	S_{i1}	S_{i2}	S_{i3}	G_{max}	I
Cold-worked	80	0.0165	6.42	20.20	11.40	1.5	2.9
Baked	720	0.0335	3.11	2.24	2.64	2.5	0.9
Annealed	480	0.0430	2.58	3.36	2.94	24.0	2.7

Near saturation, when the magnetic axes of all domains are rotating more or less together, it may be said that $j = \cos\theta$, where θ is a suitable average angle between the domain axes and the direction of applied field. It follows then from (8) and (9) that

$$\xi_m \simeq \xi_{m0} \sin^{3.1}\theta.$$

In this fashion, as saturation is approached, θ goes to zero and ξ_m vanishes.

COLD-WORK, BAKE, AND ANNEAL

The large strain-sensitivity of its properties made the 68Ni-32Fe alloy the logical choice among our permalloys for a short study of the effects of different heat treatments. A spheroidal specimen was ground from a cold-drawn wire of this alloy and tested in this condition. It was then baked at 400°C for half an hour in hydrogen, furnace cooled, and tested again. Finally, it was tested after having been annealed at 700°C for three hours in hydrogen and furnace cooled.

The physical parameters calculated from the results of these tests are plotted in Fig. 4 against magnetization bias. A curious result, in reference to this figure, is that the incremental permeability for zero bias, after having been raised by the bake, was decreased by the anneal; however, at large values of magnetization bias, μ_Δ was higher after the anneal than after the bake. This situation is reminiscent of the fact that the magnetic-anneal, in all cases where it was effective, reduced the initial permeability below the value it had after the plain-anneal, but raised μ_Δ at large biases (see Fig. 1).

Again with reference to Fig. 4, the magnetostriction constant varied but little with heat treatment, while the saturation change of Young's modulus progressively increased from cold-work to bake to anneal. Hence, from (1), the internal stresses were decreased by each successive treatment. However, due to the reduction of the initial permeability by the anneal, it would seem from (2) that the internal stresses were slightly increased by the anneal after having been decreased markedly by the bake. The discrepancy between the calculated values of S_{i1} and S_{i2} appearing in Table III is hardly negligible. Nevertheless, it is indicated that the internal stresses were considerably reduced by the bake, and that, although there is disagreement in the direction of the effect, the change in the internal stresses produced by the anneal was quite small. The values of S_{i3}, determined from (3),

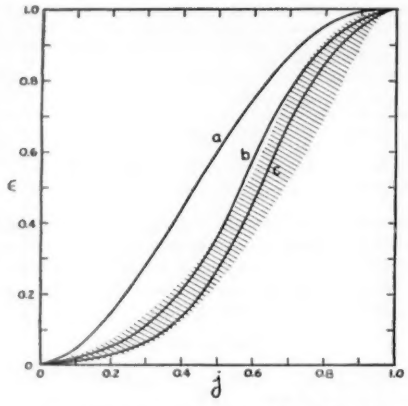

FIG. 5. The ϵ *versus* j curves for the 68 Permalloy when (a) cold-worked, (b) baked, and (c) annealed.

best portray this situation and were therefore used in conjunction with (6) in the evaluation of the domain dimension l.

It is clear from Fig. 4 that the anneal had a substantial influence on the maximum dissipation factor while the bake had practically no such influence. This fact has little intrinsic significance, but when the values for the maximum G are inserted in (6), the resultant magnitudes of l listed in Table III present a rather informative picture. Apparently, the short bake resulted in an average domain size that was smaller than that for the cold-worked material. The effect of the anneal, however, was an increase of l, and, extending the picture, we notice in Table II that a magnetic-anneal produced a further increase of l. Hence, for this material, the domain size and the initial permeability appear to be related inversely. The argument of Bozorth and Dillinger, mentioned previously in this paper, would suggest that the coercivity, varying inversely with initial permeability, is the dominant factor in the determination of the average domain size.

The ϵ *versus* j curves for the 68 Permalloy after cold-work, bake, and anneal, are presented in Fig. 5 as *a*, *b*, and *c*, respectively. The shaded region corresponding to the curves for all our plain-annealed specimens, is also shown in the figure. It is evident that each of the two successive heat treatments caused the ϵ *versus* j curve to be closer and closer to the shaded region. In this way, there is a similarity between the effects of continuing the anneal for a longer period and at a higher temperature, and that of lowering the temperature of measurement (compare Figs. 3 and 5).

We wish to express our indebtedness to Professor F. J. Beck of the Dunham Laboratory of Electrical Engineering for his encouraging interest in this research; we are also grateful to Mr. F. J. Benedict for his able assistance in experiments and computations.

Gyromagnetic Effect in a Superconductor

R. H. Pry, A. L. Lathrop, and W. V. Houston
Rice Institute, Houston, Texas
(Received February 15, 1952)

The gyromagnetic ratio of a superconducting tin sphere has been measured by the Einstein-DeHaas method. The result is approximately that to be expected on the picture of perfectly free superconducting electrons and is in agreement with the work of Kikoin and Gubar.

I. INTRODUCTION

FOR pure solid superconducting materials, Meissner and Ochsenfeld[1] have shown that the magnetic induction B inside the metal is zero. This implies either perfect diamagnetism or large surface currents in the presence of a magnetic field. In either case, the gyromagnetic effect for a superconductor should be observable.

The gyromagnetic effect has been most satisfactorily observed by the Einstein-DeHaas method. This method uses a torsion pendulum made of the magnetic material and such that a change of magnetization causes a torque and a change in angular momentum.

Kikoin and Gubar[2] carried out just such an experiment on a small superconducting lead sphere. They drove their torsion pendulum with the impulses produced by reversing a vertical magnetic field at the resonant frequency. They calculated the magnitude of these angular impulses from the resulting steady-state amplitude of the system; and in turn they determined that the ratio of the magnetic moment to the mechanical moment of the superconductor was the same as it would be in ordinary diamagnetic materials with a magnetization arising from orbital electron motions alone.

As has been shown by Meissner,[3] the model of perfect diamagnetism used by Kikoin and Gubar gives the same gyromagnetic effect as the picture of surface currents given by the London theory. According to the London picture,[4] the changing magnetic field acts on the positive charge which remains when the superconducting electrons are disregarded. The experiment then serves to measure the product of this positive charge density and the square of the penetration depth.

The report of Kikoin and Gubar did not make completely clear the direction of the effect. Since the electrons go in one direction, and the material sphere, which is observed, goes in the opposite direction rather than being dragged along by the electrons, it is important that this direction be unambiguous. We have therefore repeated their gyromagnetic experiment with a superconducting sphere to demonstrate again both the magnitude and the direction of the effect.

II. EXPERIMENTAL APPARATUS AND PROCEDURE

Figure 1, shows the details of the experimental equipment. The torsion fiber is a tungsten wire 75 cm long and 0.003 in. in diameter, and is kept at room temperature. To the bottom of the fiber is attached an octagonal Lucite cylinder. On each of the eight faces is a front surface mirror about 1 cm² in area. The connection between the Lucite cylinder and the tin sphere is made with a glass tube. The tin sphere is one inch in diameter with variations of less than 0.0004 in., and is made from spectroscopically pure tin supplied by Johnson-Mathey Company, London. The sphere is in contact with the helium vapor, but not in contact with the liquid helium. The Helmholtz coils shown are used to neutralize the horizontal component of the earth's field.

The switching of the solenoid current was controlled by a phototube and two-stage, directly coupled dc amplifier which actuated a mechanical relay. A separate contact on the relay was used to shunt out, on alternate half-cycles, a part of the plate resistance of the phototube, in order to compensate for the difference between the pull current and release current of the relay. This arrangement minimized the errors in switching time which otherwise would have occurred. The time for complete field reversal was less than 3×10^{-3} sec corresponding to less than one six-thousandth of the period of the pendulum.

The earth's field was neutralized and the solenoid field made vertical by adjustments similar to those outlined by Kikoin and Gubar. Precision was obtained by using a torsion pendulum with a one-inch magnetized iron sphere of known magnetic moment.

The amplitude and period of the oscillations were measured by observing a hairline focused on a scale 12.5 meters from the torsion pendulum.

When cooling the tin sphere through the transition temperature the earth's field was neutralized and the sphere was set into oscillation with a large amplitude. This oscillation tended to minimize further any possible frozen in moment.[5]

[1] W. Meissner and R. Ochsenfeld, Naturwiss. 21, 787 (1933).
[2] I. K. Kikoin and S. W. Gubar, J. Phys. USSR 3, 333 (1940).
[3] W. Meissner, Sitz. Bayerischen Acad. p. 321, November, 1948.
[4] F. London, Physica 3, 458 (1936); and *Superfluids* (John Wiley & Sons, Inc., New York, 1950).
[5] Alers, McWhirter, and Squire, Phys. Rev. 84, 104 (1951).

III. EXPERIMENTAL RESULTS

The results of the experiment confirm those of Kikoin and Gubar. The directions of the angular impulses are the same as one would observe if the effect were that of Faraday induction operating on a sphere composed of positive ions. Referring to Fig. 1, when the sphere is rotating in the clockwise direction as viewed from above, the field shifts from the down direction to the up direction as the oscillator passes through center. Under these switching conditions, Fig. 2 shows the approach to the steady-state condition with driving fields of 100 gauss or 10^{-2} weber/m^2 (curve A) and 51 gauss or 0.51×10^{-2} weber/m^2 (curve B). Just below these curves the zero field case (curve C) is plotted. Curve D shows the effect of reversing the cycling of the switching in the case of the larger field. Also, for the larger field, the approach to the asymptote was made from the low amplitude side, but these points are not included in the figure.

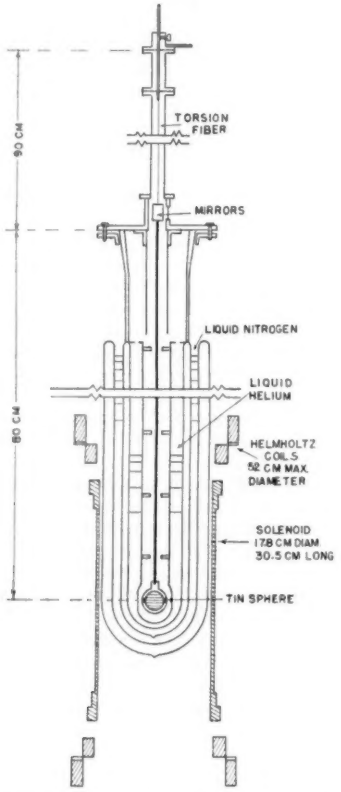

FIG. 1. Schematic outline of the cryostat and torsion pendulum.

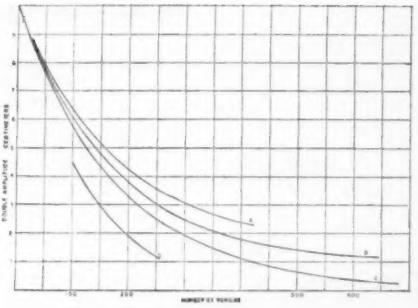

FIG. 2. Decay of the amplitude of vibration toward the limiting values.

The experimental curves show an asymptotic approach to a double amplitude of 0.95 cm at 0.51×10^{-2} weber/m^2 and 1.65 cm with 10^{-2} weber/m^2.

The observed value may be compared with the results of a simple calculation based on consideration of the impulse and momentum change of the damped oscillator.

In the steady state the system behaves like a damped oscillator for $\frac{1}{2}$ cycle. It then receives an angular impulse which just makes up for the frictional loss of the absolute value of the momentum. This frictional loss of momentum is equated to the angular impulse given the oscillator because of the magnetic field change from $+B$ to the value $-B$. The equation of motion for $\frac{1}{2}$ period is

$$\theta=\theta_0 e^{-\delta t}\cos wt,$$

with momentum: $I\dot{\theta}=-I\theta_0(we^{-\delta t}\sin wt+\delta e^{-\delta t}\cos wt)$, where the moment of inertia $I=69.4\times10^{-7}$ kg m^2 and the measured value of $\delta=2.67\times10^{-4}$ sec^{-1}. The loss in momentum in one half-period occurs in the time interval $-\pi/2w$ to $+\pi/2w$, so that the momentum change is

$$\Delta|P|=-I\theta_0\delta\pi+\text{small terms}.$$

Further detailed analysis shows that the steady state is approached exponentially and that the maximum amplitude of the nth oscillation θ_n is given by

$$\theta_n=\theta_0+Ae^{-2\pi n\delta/w}.$$

In the magnetic field B the sphere has a magnetic moment[4]

$$M=2\pi R^3B/\mu_0,$$

so that switching the field from $+B$ to $-B$ causes a change of magnetic moment $4\pi R^3B/\mu_0$. Then the change of angular momentum must be $(2m/e)(4\pi R^3B/\mu_0)$, if $2m/e$ is taken to be the ratio between the angular momentum and the magnetic moment.

Equating the frictional loss of momentum to the gain from the field change, we get a steady-state angular

amplitude:

$$\theta_0=(2m/e)(4\pi R^3B/\mu_0)(1/I\delta\pi)=3.87\times10^{-2}B \text{ radian},$$

where B is expressed in webers/m².

This angular momentum is that of the superconducting electrons, but since the total angular momentum around the vertical axis does not change, the angular momentum of the positive ions and remaining electrons composing the sphere must change in just the opposite sense and by the same amount. It is this latter change that is observed.

Another way of looking at this phenomenon was suggested by Meissner.[3] The magnetic field penetrates only a short distance below the surface of the sphere, but as it changes, an electric field is present, which acts both on the superconducting electrons and on the remaining positive ions. Since the superconducting electrons do not drag the ions with them, the two systems move independently with equal and opposite angular momenta. The motion of the positive ions is the one observed by the experimental arrangement used.

IV. DISCUSSION OF ERRORS

In spite of much care the tin sphere had a slightly ellipsoidal character, the field was not exactly uniform over the volume of the sphere, and the switching of the magnetic field did not always occur precisely at the same point. In zero field a certain rest point or zero point about which the oscillator swung was noted. With a steady upward vertical field of 10^{-2} weber/m², the zero point shifted 0.3 mm to the right on the scale corresponding to 1.2×10^{-6} radian of angle. With a steady downward vertical field of the same amount, the zero point shifted 0.9 mm to the right. These errors might be further reduced with greater effort should greater accuracy justify such action, but differences between the experimental and expected values may be attributed to these experimental errors.

V. CONCLUSION

The experiments gave rough agreement with the theory as to the magnitude of the effect. The result was 15 percent low for the 10^{-2} weber/m² driving field and 4 percent low for the 0.51×10^{-2} weber/m² driving field. The direction of driving torque was such as to produce an angular impulse on the superconducting sphere just as if the Faraday induction were operating on the positive ion lattice.

The authors are greatly indebted to the constant assistance of Professor C. F. Squire. One of us (R.H.P.) held the Shell Fellowship during this work.

PHYSICAL REVIEW VOLUME 86, NUMBER 6 JUNE 15, 1952

Angular Momentum Distributions in the Thomas-Fermi Model

J. H. D. JENSEN* AND J. M. LUTTINGER
Department of Physics, University of Wisconsin, Madison, Wisconsin

(Received January 31, 1952)

The Hartree and Thomas-Fermi models of the atom and nucleus are compared in their predictions for the angular momentum distributions. It is found that the most natural quantity to compare is not the "first appearance" of a given orbital angular momentum, but the mean squared angular momentum.

I. INTRODUCTION

RECENTLY the subject of the distribution of angular momentum in nuclei has been given considerable impetus by the discovery of certain "magic numbers"[1] which indicate a shell structure in nuclei. The interpretation of the magic numbers in terms of a "shell model"[2] enables us to make detailed statements about the angular momentum distribution in nuclei. Several authors[3] have attempted to find an interpretation of this shell structure in terms of a Thomas-Fermi model of the nucleus. Now, apart from objections to their detailed handling of the Thomas-Fermi model, it seems to us that these authors have also interpreted the appearance of closed shells in an incorrect way. They have identified the closing of a shell with the first appearance of a particle with a higher orbital angular momentum than was previously present. It is very easy to see that even in the atomic case these two phenomena are not related. In atoms the closed shells (noble gases) occur at $Z=2$, 10, 18, 36, 54, and 86, while the first appearance of electrons with orbital angular momentum 1, 2, 3 occurs at $Z=5$, 21, and 58, respectively. In the nuclear shells, say for neutrons, the shells close at $N=2$, 8, 20, 28, 50, 82, and 126 while the first appearance of $l=1$, 2, 3, 4, and 5 occur at $N=3$, 9, 21, 41, ~64, ~100. The closing of a shell is a phenomenon which is connected with the filling up of a group of energy levels which are relatively isolated

* On leave of absence from the University of Heidelberg, Heidelberg, Germany.

[1] M. Goeppert-Mayer, Phys. Rev. **74**, 235 (1948).

[2] M. Goeppert-Mayer, Phys. Rev. **75**, 1969 (1949); **78**, 16 (1950); Haxel, Jensen, and Suess, Phys. Rev. **75**, 1766 (1949); Z. Physik **121**, 259 (1950).

[3] L. M. Yang, Proc. Phys. Soc. (London) **A64**, 632 (1951); D. Ivanenko and W. Rodichew, Dokl. Akad. Nauk, SSSR **70**, 605 (1951).

from the rest, and in general has little directly to do with the emergence of new orbital angular momenta.

While we believe that the Thomas-Fermi model can give no information about the location of the closed shells, still it does give some information about the distribution of orbital angular momentum. It was thought that it might be of interest to compare its predictions with those of the shell model. The first question which arises is exactly what one should compare. Usually—in the atomic case—one has compared the "first appearance" of a certain l. This question is, however, a very poorly defined one in the Thomas-Fermi model as shown in Sec. III, since the orbital angular momentum has a continuous range of values instead of the discrete values which one obtains in a rigorous quantum mechanical theory. We prefer therefore to make the comparison between something which is well defined in the Thomas-Fermi model, and the predictions of the shell model. For this purpose we have chosen to compare the mean value of the square of the orbital angular momentum. Since the Thomas-Fermi model gives a unique expression for the number of particles with orbital momentum between L and $L+dL$ —which we will denote by $n(L)$—the mean value in question is given by

$$\langle L^2\rangle_{\text{Av}}=\int L^2 n(L)dL/Z. \tag{1}$$

Here Z is the number of particles of the type we are considering.

As soon as we have decided on a level scheme in the shell model, we then know how many particles there are with each l, and we have for comparison:[4]

$$\langle L^2\rangle_{\text{Av}}=\sum_i l_i(l_i+1)/Z,$$

where the sum goes over all the Z particles.

In Sec. II we shall make this comparison for the atomic as well as the nuclear case, and shall show that for a reasonable density distribution in the latter it is possible to obtain excellent agreement. In Sec. III we shall return to the question of the "first appearance" of a particle of given orbital angular momentum.

II. THE MEAN SQUARED ORBITAL ANGULAR MOMENTUM

Let us define $dN(\mathbf{p},\mathbf{r})$ as the number of particles with momentum $\mathbf{p}$ at the point $\mathbf{r}$ in a small element of volume of phase space. Then the basic assumption of the Thomas-Fermi model is that all states are filled equally as long as a certain maxima momentum is not exceeded, after which they are all empty. Thus, with $\hbar=1$,

$$dN(\mathbf{p},\mathbf{r})=2d^3\mathbf{r}d^3\mathbf{p}/(2\pi)^3 \quad \text{if} \quad p\leq P(r),$$
$$dN=0 \quad \text{if} \quad p>P(r).$$

The factor 2 comes from the fact that the number of states is doubled by the presence of the spin. $P(r)$ is the maximum momentum allowable at a given point. By integrating this expression over $\mathbf{p}$ one obtains

$$\rho(r)=2\cdot(4\pi/3)P^3(r)/(2\pi)^3. \tag{2}$$

This is the fundamental relationship between the density of particles $\rho(r)$ and the maximum momentum. To find the angular momentum distribution function it is convenient to consider not $n(L)$ itself but its integral,

$$N(L)\equiv\int_L^\infty n(L)dL.$$

$N(L)$ is the number of particles present with angular momentum greater than L. Now $\mathbf{L}=\mathbf{r}\times\mathbf{p}$, and therefore $L^2=r^2p^2\sin^2\vartheta$, where ϑ is the angle between $\mathbf{r}$ and $\mathbf{p}$. Hence,

$$N(L)=\int dN(\mathbf{p},\mathbf{r}),$$

where the limits of the r and p integrations are given by the conditions $pr\sin\vartheta\geqq L$ and $p\leq P(r)$. By integration over the angles and p we obtain immediately

$$N(L)=(4/3\pi)\int[P^2r^2-L^2]^{\frac{3}{2}}dr/r. \tag{3}$$

The integration over r is to be extended over that region where the radical is real. From $N(L)$ we obtain $n(L)$ by differentiation,

$$n(L)=-dN(L)/dL=(4L/\pi)\int[P^2r^2-L^2]^{-\frac{1}{2}}dr/r, \tag{4}$$

which is a well-known result.[5] Using this, we obtain from Eq. (1):

$$\langle L^2\rangle_{\text{Av}}=\frac{8}{15\pi Z}\int_0^\infty\frac{dr}{r}(rP)^5. \tag{5}$$

By means of (2) we know $\langle L^2\rangle_{\text{Av}}$ as soon as we know the density ρ.

In the case of the Thomas-Fermi atom this density is well-known and can be expressed in terms of a universal function φ for all atoms. If we put $r=\mu x$, where $\mu=3^{\frac{2}{3}}2^{-7/3}\pi^{\frac{2}{3}}Z^{-\frac{1}{3}}/me^2$, and make use of the definition $\varphi(x)=(r/Ze^2)(P^2(r)/2m)$, we obtain

$$\langle L^2\rangle_{\text{Av}}=Z^{\frac{7}{3}}\frac{2}{5}\left(\frac{3\pi}{4}\right)^{\frac{4}{3}}\left(\int_0^\infty\frac{dx}{x}(x\varphi)^{5/2}\right).$$

The integral in the brackets is a pure number and has been obtained by a numerical integration; its value is 0.370. This gives us finally

$$\langle L^2\rangle_{\text{Av}}=0.262Z^{\frac{7}{3}}. \tag{6}$$

Figure 1 gives a plot of this function along with a plot of the empirical value of $\langle L^2\rangle_{\text{Av}}$ as computed from the known ground state configurations of the elements.

[4] We have chosen units such that $\hbar=1$.

[5] E. Fermi, Z. Physik **49**, 550 (1928).

One sees that there is a general tendency to give too high angular momenta for the lighter elements, but as Z increases the Thomas-Fermi model gives a very good average variation of $\langle L^2\rangle_{Av}$ with Z. This is just in line with the usual idea that the Thomas-Fermi model improves with increasing atomic number. (Needless to say, we could not possibly hope for more than such a correctness in the average, since in the Thomas-Fermi model all properties of atoms vary smoothly with their atomic number, and therefore, all effects due to closing of shells are averaged out.)

In the nuclear case we are faced with the difficulty of not knowing ρ. The equations determining the density in the Thomas-Fermi model are not even known exactly, since the nuclear forces are unknown, and even if they were it would seem to be a prohibitively difficult task to solve them. None the less one can ask whether or not it is possible by a reasonable assumption concerning the density of protons and of neutrons in the nucleus to obtain a fit of the observed angular momenta distribution. In treating the nucleus we shall treat the Z protons and N neutrons as separate systems, each obeying its own Pauli principle, and each with its own density function. Such a treatment is certainly implicit in the usual conception of the Thomas-Fermi model. We shall therefore deal with the proton system, though of course the neutron system may be treated in an identical fashion. Let us write

$$r = Rx, \quad P(r) = P_0 f(x), \tag{7}$$

where R is a quantity of the dimension of a length and of the order of magnitude of the nuclear radius, while P_0 is a constant with the dimensions of a momentum. The function $f(x)$ is defined such that $f(0)=1$, so that P_0 is the maximum proton momentum at the center of the nucleus. Since the relationship of density to maximum momentum is given by (2), we can eliminate R and P_0 from the expression for $\langle L^2\rangle_{Av}$, by making use of $\int \rho d^3\tau = Z$, and obtain

$$\langle L^2\rangle_{Av} = \pi^{\frac{1}{2}} 2^{-\frac{1}{3}} 3^{7/3} 5^{-2} Z^{\frac{1}{3}} \frac{5\int \frac{dx}{x}\{xf(x)\}^5}{\left[3\int \frac{dx}{x}\{xf(x)\}^3\right]^{5/3}}. \tag{8}$$

The numerical factor in front of $Z^{\frac{1}{3}}$ is 0.885. Exactly the same equation holds for the neutron $\langle L^2\rangle_{Av}$ if we replace Z by N and f by another function suitable for describing the neutron density in a nucleus. Since the empirical data on neutron shells and proton shells indicates that the angular momentum distribution is roughly the same for both, we shall restrict ourselves to the same function f for both neutrons and protons.

The simplest choice of $f(x)$ would be

$$f=1 \quad \text{for} \quad x<1, \quad \text{and} \quad f=0 \quad \text{for} \quad x>1.$$

This assumes that the nucleus is a sphere of radius R and constant density. The ratio of the integrals in the expression for $\langle L^2\rangle_{Av}$ is then unity, and we obtain

$$\langle L^2\rangle_{Av} = 0.885 Z^{\frac{1}{3}}.$$

A plot of this function along with the plot of $\langle L^2\rangle_{Av}$ obtained from the shell model is given by the dashed curve in Fig. 2. One sees that this density distribution gives on the whole too large angular momenta. This result is not very surprising since the assumption of constant density right up to the edge of the nucleus over-emphasizes very much the contribution to $\langle L^2\rangle_{Av}$ from larger values of x. These however—as can be seen from the expression for $\langle L^2\rangle_{Av}$ which involves an integral over the fourth power of x—make the largest contribution to $\langle L^2\rangle_{Av}$. Therefore, our result is very sensitive to the density near the edge of the nucleus. Certainly a more realistic density distribution is given if we assume that the density is constant up to a certain point and then drops off to zero in a Gaussian fashion. Other distributions are also possible, but we choose this for ease of calculation. By a very reasonable choice of the thickness of this surface layer we shall see that it is possible to obtain as good an agreement as in the

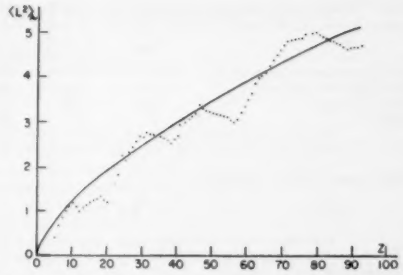

FIG. 1. Comparison of the mean squared angular momentum of an atom as calculated in the Thomas-Fermi model with the empirical values. ——— Thomas-Fermi model; ···· empirical values.

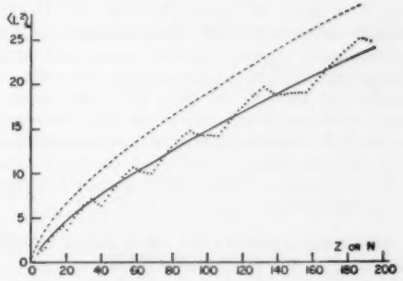

FIG. 2. Comparison of the mean squared angular momentum of the protons or neutrons in a nucleus as calculated in the Thomas-Fermi model with the values obtained from the "shell model." – – – – Constant nuclear density; ——— Gaussian drop in nuclear density at the surface; ···· values from shell model.

TABLE I. Values of Z for the first appearance of various values of l.

	$l=1$	$l=2$	$l=3$
Fermi (approximate integration)	5	21	55
Fermi (exact integration)	4.0	16.2	44.0
Definition in text	2.4	14.8	43.0
Empirical	5	21	58

atomic case. Let us choose then

$$f(x)=1 \quad \text{for} \quad x<1$$
$$=\exp(-(x-1)^2/3\beta) \quad \text{for} \quad x>1.$$

Choosing for β the value

$$\beta=\left(\frac{1.8\times10^{-13}\text{ cm}}{R}\right)^2\Big/\log 2,$$

where R is determined by the condition that inside the nucleus the proton density has the value $(Z/A)(1.4\times10^{-13}\text{ cm})^{-3}$, we obtain the solid curve given in Fig. 2. This choice means that we have chosen a surface layer of "thickness" 1.8×10^{-13} cm independent of R. We notice that the agreement with the shell model predictions is excellent, and therefore it is not necessary—as proposed by Yang[3]—to assume a surface layer with thickness proportional to $A^{\frac{1}{3}}$. Since it is not easy to decide exactly which curve is to be considered the "best fit" for the empirical facts, the β-value given is necessarily more an order of magnitude than a precise conclusion from the data.

With this choice of the constant β, we can obtain a value of the nuclear radius. Let us define the nuclear radius R_0 as the distance from the origin at which the density falls to half its value. Thus we obtain

$$R_0=R\{1+[(\log 2)\beta]^{\frac{1}{2}}\}=R+1.8\times10^{-13}\text{ cm}.$$

The resulting R_0 does not exactly satisfy the requirement that it is proportional to $A^{\frac{1}{3}}$, though it does to a very good approximation. We obtain for the ratios of the values of $R_0A^{-\frac{1}{3}}$ the values 0.95, 0.97, 0.98, 1.0 for $Z=12$, 30, 90, ∞, respectively. In the limiting case of large A we have, of course, $R_0=1.4\times10^{-13}A^{\frac{1}{3}}$. Thus although we cannot satisfy simultaneously both the requirements of constant internal density and nuclear radius proportional to $A^{\frac{1}{3}}$, we can do it well within the experimental accuracy of these facts. We could, of course, have just as well determined R by the requirement of $R_0A^{-\frac{1}{3}}=$constant, in which case we would have found that the density at the origin decreases slightly for lighter atoms; a result which in itself is perhaps not too implausible.

III. THE FIRST APPEARANCE OF A GIVEN ORBITAL ANGULAR MOMENTUM

Since in the Thomas-Fermi model the angular momentum is not quantized, but has a continuous distribution of possible values, the question, at which Z a particle with a certain $L=[l(l+1)]^{\frac{1}{2}}\cdot(l=1, 2, 3, \text{etc.})$ appears for the first time, is less unique than would appear from the literature.

We would like to discuss here a definition which we believe to be the best possible within the framework of the Thomas-Fermi model: All particles with a given angular momentum L will be said to have the quantum value l which makes $[l(l+1)]^{\frac{1}{2}}$ closest to L. In this case the "number of particles with an angular momentum l," say $\nu(l)$, will be given by

$$\nu(l)=N\left\{\frac{[l(l+1)]^{\frac{1}{2}}+[l(l-1)]^{\frac{1}{2}}}{2}\right\}$$
$$-N\left\{\frac{[l(l+1)]^{\frac{1}{2}}+[(l+1)(l+2)]^{\frac{1}{2}}}{2}\right\}.$$

This differs from the definition of Fermi in two ways: he replaces $[l(l+1)]^{\frac{1}{2}}$ by $l+\frac{1}{2}$, and replaces the integral involved in $N(L)$ by its approximate value obtained by multiplying the value of the integrand at the center of the interval by the length of the interval. The latter approximation turns out to be quite poor because the integrand is really a very rapidly varying function of L, and therefore, we have undertaken to repeat the work carrying out the integral in question numerically. As soon as one has $\nu(l)$ one may define the "first appearance" of l by the condition that for that Z, we must have $\nu(l)=1$.

The results of these calculations for the Fermi atom are given in Table I. By comparison of the first and second entries one can see the effect of replacing the exact integration by the approximate one. The exact integration leads to much poorer agreement with the empirical data. Further, the effect of replacing $[l(l+1)]^{\frac{1}{2}}$ by $l+\frac{1}{2}$ can be seen on comparing the second and third entries. With the most straightforward definition the agreement with the empirical data is poorest. If we consider the percent error we find for the Fermi case (exact integration) 20 percent, 23 percent, 24 percent, and for our case 52 percent, 32 percent, 26 percent for $l=1$, 2, 3, respectively. Thus the error for Fermi's definition increases with Z, while that for the definition above decreases. Since all properties of the Fermi model improve with increasing Z, it seems to us that definition given above would be the preferable one. However, in any case, we feel that the quantity $\nu(l)$ is so poorly defined in a model with continuous L, that it is not worth considering in the nuclear case.[3] For a comparison with experiment the natural quantities are averages such as $\langle L^2\rangle_{\text{Av}}$.

In conclusion we would like to thank the University of Wisconsin's Computing Service for having carried out the various numerical integrations involved in this paper. One of us (J.H.D.J.) participated in this work while on a Carl Schurz visiting professorship at the University of Wisconsin. He would like to indicate his thanks to the Carl Schurz committee and to the University in general for having made his stay so pleasant and profitable.

Further Considerations Regarding the Theory of Bose-Einstein Liquids*

J. G. DAUNT, T. P. TSENG, AND C. V. HEER
Department of Physics, Ohio State University, Columbus, Ohio

(Received February 11, 1952)

Model solutions of nondegenerate Fermi-Dirac systems in Bose-Einstein liquids, as proposed previously by Heer and Daunt, are discussed. A discussion is given of the physical basis for the excess partial vapor pressure of the F−D component, which is shown to be due to the degeneracy of the B−E liquid. The theory is applied to solutions of He^3 in liquid He^4, and a tentative explanation is given for the empirical hypothesis proposed by Taconis in accounting for the observed partial vapor pressures of such solutions. The results of computations of the distribution coefficient C_v/C_L and the total vapor pressure for strong solutions of He^3 in liquid He^4 are presented, these computations having been made using (a) the laws for perfect classical solutions, (b) the theory of Heer and Daunt, and (c) the theory of de Boer and Gorter. A comparison with the experimental values of C_v/C_L and of total vapor pressures for strong solutions is given, and it is deduced that the Heer and Daunt model of a quantum solution is in good agreement with the observations at temperatures below about 1.8°K and that above this temperature the model gives qualitatively the correct trend but that owing to vapor imperfections exact numerical agreement cannot be expected.

I. He^3 PARTIAL VAPOR PRESSURE FOR B-E LIQUIDS

THE measurements with solutions of He^3 in liquid He^4 up to about 2 percent He^3 of the distribution coefficient,[1–5] i.e., of the ratio of the concentration C_v of He^3 in the saturated vapor to the concentration C_L of He^3 in the solution, show that the partial vapor pressure of the He^3 is much higher than that which would be expected for perfect classical solutions at temperatures below the λ-temperature of liquid He^4.

Heer and Daunt[6] have proposed a quasi-gaseous model of a Bose-Einstein liquid which can be used to explain these properties of solutions of He^3 in liquid He^4 and which appears to be satisfactory.[6] In view of this it is considered of interest to attempt a further interpretation of the physical basis of the model, particularly with regard to the observation of the high partial vapor pressures of the He^3 component.

The basic assumptions for the model liquid proposed by Heer and Daunt were (a) that the solution of He^3 in liquid He^4 could be regarded as a statistically independent mixture of a nondegenerate Fermi-Dirac gas[7] in a smoothed potential well $-\chi_3^0$ and of a degenerate Bose-Einstein gas in a smoothed potential well $-\chi_4^0$, (b) that, following the proposal of London,[8] the onset of degeneracy in the B-E gas corresponded to the occurrence of the λ-phenomenon in liquid He^4, and (c) that the solutions were incompressible, having a volume given by

$$V=N_4v_4^0+N_3v_3^0, \tag{1}$$

where v_4^0 and v_3^0 are the volumes per atom of He^4 and He^3, respectively.

For solutions in equilibrium with their vapors the partial vapor pressure p_3 of the He^3 is given, assuming the vapor to be perfect, by

$$kT\ln(p_3/p_3^0)=\mu_3^L-\mu_3^{0L}, \tag{2}$$

where p_3^0 is the vapor pressure of pure liquid He^3 and where μ_3^L and μ_3^{0L} are the partial potentials of the He^3 in the liquid phase in the solution and in the pure liquid, respectively. (Compare with Eq. (4.6) in Heer and Daunt's paper,[6] hereafter referred to as *A*.)

If the He^3 in the liquid phase is considered as a nondegenerate F-D gas of spin ½ in a smoothed potential well $-\chi_3^0$, then the Gibbs function G for the solution is

$$\begin{aligned}G&=G_3+G_4\\&\approx F_3+F_4\\&\approx -N_3\chi_3^0+N_3kT\ln N_3-N_3kT\ln[N_3v_3^0+N_4v_4^0]\\&\quad -N_3kT-N_3kT\ln 2\left[\frac{2\pi m_3kT}{h^2}\right]^{\frac{3}{2}}+F_4,\end{aligned} \tag{3}$$

whence the partial potential, μ_3^L, is given by

$$\begin{aligned}\mu_3^L&=\left(\frac{\partial G}{\partial N_3}\right)_{T,\,p}\approx\left(\frac{\partial F}{\partial N_3}\right)_{T,\,v_3^0,\,v_4^0}\\&\approx -\chi_3^0-\frac{N_3v_3^0kT}{N_3v_3^0+N_4v_4^0}-kT\ln 2\left[\frac{2\pi m_3kT}{h^2}\right]^{\frac{3}{2}}\\&\quad +kT\ln[N_3/(N_3v_3^0+N_4v_4^0)]+\left(\frac{\partial F_4}{\partial N_3}\right)_{T,\,v_3^0,\,v_4^0}.\end{aligned} \tag{4}$$

* Assisted by a contract between the AEC and Ohio State University Research Foundation.

[1] J. G. Daunt and C. V. Heer, Proc. of Symposium on Cryogenics, Natl. Bur. Standards, March, 1951; "Proc. Intern. Conf. Low Temps." Oxford, August, 1951, p. 76; also Phys. Rev. (to be published).

[2] Lane, Fairbanks, Aldrich, and Nier, Phys. Rev. **75**, 46 (1949).

[3] Taconis, Beenakker, Aldrich, and Nier, Phys. Rev. **75**, 1966 (1949); Physica **15**, 733 (1949).

[4] H. S. Sommers, Proc. of Symposium on Cryogenics, Natl. Bur. Standards, March, 1951; Proc. Intern. Conf. Low Temps., Oxford, August, 1951, p. 78.

[5] J. G. Daunt, Phil. Mag. Suppl. on Advances in Physics **1**, 209 (1952).

[6] C. V. Heer and J. G. Daunt, Phys. Rev. **81**, 447 (1951).

[7] Heer and Daunt (reference 6) have also considered the situation when the F-D component may be degenerate.

[8] F. London, Phys. Rev. **54**, 947 (1938); J. Phys. Chem. **43**, 1 (1939).

TABLE I. Computed values of the distribution coefficient C_v/C_L, for 1.00, 5.00, and 10.00 percent solutions of He^3 in liquid He^4 according to (a) the laws for perfect classical solutions (P.C.S.), (b) the theory of Heer and Daunt, (H and D), and (c) the theory of de Boer and Gorter (their "case A"), (deB and G).

	$C_L=1$ percent			$C_L=5$ percent			$C_L=10$ percent		
T, °K	P.C.S.	H and D	deB and G	P.C.S.	H and D	deB and G	P.C.S.	H and D	deB and G
1.1	32.6	56.9	88.2	14.2	17.4	18.6	8.4	9.3	9.4
1.2	24.7	47.5	79.3	12.4	16.3	17.7	7.7	9.0	9.1
1.3	18.7	38.9	68.4	10.9	15.1	16.5	7.2	8.6	8.6
1.4	14.9	31.7	57.0	9.6	13.9	15.1	6.6	8.2	8.1
1.5	12.3	25.7	45.2	8.5	12.7	13.6	6.1	7.7	7.4
1.6	10.4	21.5	34.4	7.5	11.5	11.9	5.6	7.2	6.7
1.7	9.0	18.1	25.2	6.7	10.3	10.1	5.2	6.8	6.0
1.8	7.8	15.4	17.6	6.0	9.3	8.2	4.8	6.4	5.2
1.9	6.8	13.2	12.4	5.4	8.5	6.7	4.5	5.9	4.6
2.0	6.0	11.2	8.7	5.0	7.7	5.3	4.2	5.5	4.1
2.1	5.4	9.8	6.3	4.6	7.0	4.6	3.9	5.1	3.9
2.2	5.0	8.8	5.0	4.3	6.4	4.4	3.7	4.8	3.7
2.3	4.7	7.8	4.7	4.1	5.9	4.1	3.5	4.5	3.5
2.4	4.4	7.2	4.4	3.9	5.5	3.9	3.4	4.3	3.4
2.5	4.2	6.4	4.2	3.7	5.1	3.7	3.3	4.1	3.3

The first four terms in Eq. (4) above represent the contribution to $\mu_3{}^L$ from the nondegenerate F-D system. (They are identical with the first four terms in Eq. (4.4) in A.) The last term $(\partial F_4/\partial N_3)_{T,v_3{}^0,v_4{}^0}$, which is a cross term involving the properties of the He^4, is the term that allows $\mu_3{}^L$ and hence $p_3/p_3{}^0$ to differ from the values to be expected for classical solutions. This term, therefore, is the dominating term, producing nonclassical results when the He^4 is taken to be degenerate.

If the He^4 in solution is taken as a strongly degenerate B-E gas in a potential well $-\chi_4{}^0$, then the fourth term in Eq. (4) is given by (see Eq. (4.4) in A)

$$\left(\frac{\partial F_4}{\partial N_3}\right)_{T,v_3{}^0,v_4{}^0}=-1.341\left(\frac{2\pi m_4 kT}{h^2}\right)^{\frac{3}{2}}v_3{}^0kT. \quad (5)$$

Now if the degeneracy temperature of the He^4 in the solution is taken to be $T_\lambda{}^s$, then as shown in A,

$$(T_\lambda{}^s)^{\frac{3}{2}}=\frac{1}{2.612}\left[\frac{h^2}{2\pi m_4 k}\right]^{\frac{3}{2}}\frac{N_4}{N_3v_3{}^0+N_4v_4{}^0}, \quad (6)$$

and by substituting (6) into (5) we get

$$\left(\frac{\partial F_4}{\partial N_3}\right)_{T,v_3{}^0,v_4{}^0}=-0.514kT\left(\frac{T}{T_\lambda{}^s}\right)^{\frac{3}{2}}\frac{N_4}{N_3}\left(\frac{N_3v_3{}^0}{N_3v_3{}^0+N_4v_4{}^0}\right)$$

$$=-0.514kT\frac{N_4{}^n}{N_3}\times\left(\frac{\text{Vol of } N_3 \text{ atoms of pure liquid } He^3}{\text{Vol of solution}}\right), \quad (7)$$

since for a perfect B-E gas the number of "noncondensed," i.e., "normal," atoms $N_4{}^n$ is given by

$$N_4{}^n=N_4(T/T_\lambda{}^s)^{\frac{3}{2}}.$$

In interpreting the significance of Eq. (7) it is of value to consider another hypothetical liquid model similar to the one discussed above, except that now the He^4 is to be considered as a nondegenerate (classical) gas of N_4' active atoms in a potential well $-\chi_4{}^0$. For such a model it can be shown that the important cross term $(\partial F_4/\partial N_3)$, through which the properties of the He^4 influence the partial vapor pressures p_3 of the He^3, is given by

$$\left(\frac{\partial F_4}{\partial N_3}\right)=-kT\frac{N_4'}{N_3}\times\left(\frac{\text{Vol of } N_3 \text{ atoms of pure liquid } He^3}{\text{Vol of solution}}\right). \quad (8)$$

By comparing the evaluations of the cross term $(\partial F_4/\partial N_3)$ given in Eq. (7) for a degenerate He^4 system and in (8) for a nondegenerate (classical) He^4 system, it will be seen that, since $N_4{}^n$ is always less than the total number of He^4 atoms for temperatures below $T_\lambda{}^s$, $(\partial F_4/\partial N_3)$ will be numerically smaller for the degenerate system than for the nondegenerate system. This leads, as is evident from inspection of Eqs. (2) and (4), to increased partial pressures p_3 for the degenerate systems. This comparison of Eqs. (7) and (8) also indicates that the observed higher values of p_3

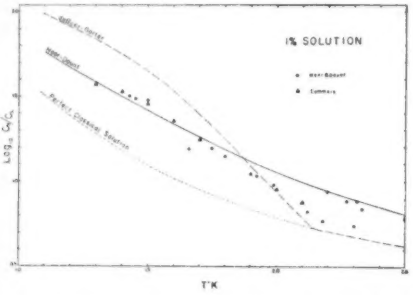

FIG. 1. Computed values of the distribution coefficient C_v/C_L for a 1.00 percent solution of He^3 in liquid He^4 according to (a) the laws for perfect classical solutions, (b) the theory of Heer and Daunt (reference 6), and (c) the theory of de Boer and Gorter (reference 14). The points indicate the experimentally determined values of C_v/C_L for a 1.00 percent solution. The points marked by circles are the results of Daunt and Heer (reference 1), and the points marked by triangles are the results of Sommers (reference 4 and private communication). (The writers are indebted to Dr. Sommers for his permission to include these results before full publication.)

below T_λ[8] could only be explained using classical theory by assuming that the effective number N_4' of active atoms is less than the total number of He^4 atoms. The complete identity of Eqs. (7) and (8) would then be obtained for $N_4' = 0.514 N_4^a$, which is a relationship very similar to that proposed by Taconis *et al.*[3] on empirical grounds. It would appear that this tentative way of explaining Taconis' hypothesis stems therefore from the fact that the kinetic energy of a degenerate B-E gas is given by $\frac{3}{2}(0.514 N_4^a)kT$ rather than by $\frac{3}{2}N_4 kT$ for a nondegenerate (classical) system.

It must be remembered that the parallelism outlined above between the results using degenerate B-E statistics and those using nondegenerate (classical) modified by a temperature dependent number of "active" atoms holds only for temperatures below T_λ. For temperatures above T_λ Eq. (5) above is not correct (see paper *A*), and the physical picture is not simple. However, since an ideal B-E gas shows deviations from classical behavior immediately above its degeneracy temperature,[7] it is to be expected that the model proposed by Heer and Daunt would show deviations from the laws for perfect classical solutions even above T_λ.

II. COMPUTATIONS OF C_v/C_L FOR STRONG SOLUTIONS IN B-E LIQUIDS

Previously Heer and Daunt (paper *A*) have presented the results of computation of the theoretical values of the distribution coefficient C_v/C_L for very dilute solutions of He^3 in liquid He^4 (i.e., for $C_L \lesssim 10^{-3}$). Since that time measurements have been made using solutions with stronger He^3 concentration,[1,4,5] and it was thought worthwhile to extend the computations to greater values of C_L.

For strong solutions the computations were made using the formulas (4.13), (4.14), (4.15), and (4.16) given in *A*, which formulas contain no adjustable parameters. The numerical evaluations were made using the 1949 He^4 temperature scale[9] for p_4^0 and using the data of Abraham, Osborne, and Weinstock[10] for p_3^0. The molar volumes of He^4 and He^3 in the pure liquid phase have been taken[11,12] to be 27.6 cc and 37.6 cc, respectively. The results are tabulated in Table I, which gives the computed value of C_v/C_L for solutions with three different solutions concentrations, namely, $C_L = 1.00$, 5.00, and 10.00 percent. In Table I also are given the evaluations of C_v/C_L calculated by assuming the laws for perfect classical solutions (P.C.S.). The results also are shown graphically in Figs. 1–3.

Figures 1–3 show that for the B-E liquid model of Heer and Daunt, as characterized by the assumptions outlined in Sec. I above, C_v/C_L has at all temperatures

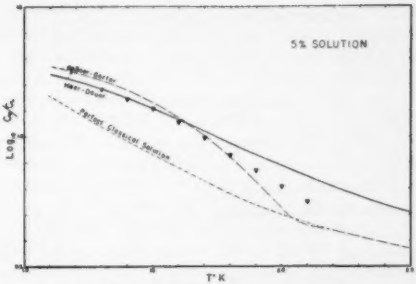

FIG. 2. The curves show the computed values of the distribution coefficient C_v/C_L for a 5.00 percent solution of He^3 in liquid He^4 according to (a) the laws for perfect classical solutions, (b) the theory of Heer and Daunt (reference 6), and (c) the theory of de Boer and Gorter (reference 14). The points indicate the experimentally determined values of C_v/C_L for a 5.00 percent solution obtained from the results of Sommers (reference 4 and private communication). (The writers are indebted to Dr. Sommers for his permission to include these results before full publication.)

values above those found for perfect classical solutions[13] (P.C.S.) and that there is no discontinuity in the slopes of the curves as they pass through T_λ. It is to be noted, moreover, that the differences between the Heer and Daunt theory and that for P.C.S. become less marked as the solution concentration increases. This is to be expected in view of the fact that theoretically these differences are introduced due to the degeneracy of the He^4 component and that as the He^4 concentration is reduced, the degeneracy becomes less marked.

The variation of C_v/C_L with the solution concentration C_L is shown in Fig. 4, which gives two computed isothermals at $T = 1.4°K$ and at $T = 2.15°K$.

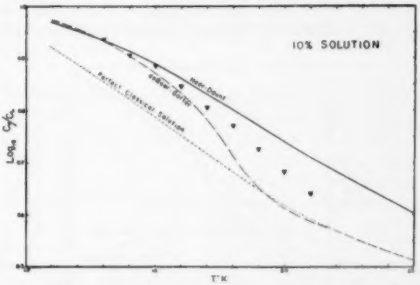

FIG. 3. The curves show the computed values of the distribution coefficient C_v/C_L for a 10.00 percent solution of He^3 in liquid He^4 according to (a) the laws for perfect classical solutions, (b) the theory of Heer and Daunt (reference 6), and (c) the theory of de Boer and Gorter (reference 14). The points indicate the experimentally determined values of C_v/C_L for a 10.00 percent solution obtained from the results of Sommers (reference 4 and private communication). (The writer are indebted to Dr. Sommers for his permission to include these results before full publication.)

[9] H. van Dijk and D. Shoenberg, Nature **169**, 151 (1949).
[10] Abraham, Osborne, and Weinstock, Phys. Rev. **80**, 366 (1950).
[11] W. H. Keesom, *Helium* (Elsevier Publishing Company, Inc., Houston, Texas, 1942).
[12] Grilly, Hammel, and Sydoriak, Phys. Rev. **75**, 1103 (1949).

[13] As pointed out in *A*, if the effects of possible degeneracy in the F-D system (He^3) are taken into account, then C_v/C_L will fall below the P.C.S. values at low temperatures. No computations of these effects have yet been made, however, in any detail.

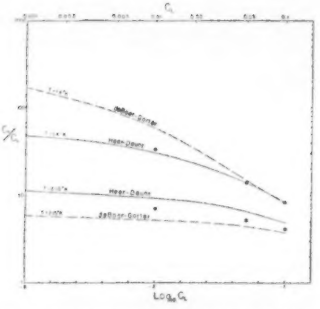

FIG. 4. The curves show the computed values of the distribution coefficient C_v/C_L for solutions of He^3 in liquid He^4 as a function of the solution concentration C_L along two isothermals (1.4°K and 2.15°K) according to (a) the theory of Heer and Daunt (reference 6) and (b) the theory of de Boer and Gorter (reference 14). The points for $C_L=1.00$ percent are taken from the experimental observations of Daunt and Heer (reference 1) and of Sommers (reference 4). The points for $C_L=5.00$ and 10.00 percent are taken from the experimental work of Sommers (reference 4 and private communication). (The writers are indebted to Dr. Sommers for his permission to include these results before full publication.)

In addition, computations have been made of C_v/C_L for solutions of He^3 in liquid He^4 based on the theory of de Boer and Gorter[14] (de Boer and Gorter's "Case *A*"). This theory treats the solutions according to classical thermodynamics and introduces the essentially quantum character of liquid He^4 by means of Taconis' hypothesis[3] (as mentioned in Sec. I above) by considering the mixing of the He^3 to take place only with the "normal" fraction of the He^4 below T_λ, i.e., by writing the Gibbs free energy of mixing as

$$\Delta G = kT[N_3 \ln N_3 + N_4^n \ln N_4^n - (N_3+N_4^n)\ln(N_3+N_4^n)].$$

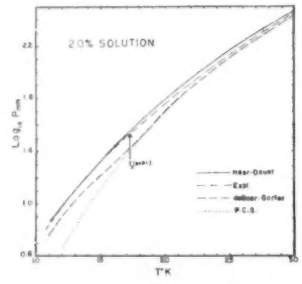

FIG. 5. Plots of the computed values of the total vapor pressure above a solution of 20 percent He^3 in liquid He^4 according to (a) the laws for perfect classical solutions, (b) the theory of Heer and Daunt (reference 6), and (c) the theory of de Boer and Gorter (reference 14). The experimental values of the observed vapor pressure are also shown by the curve marked ——·——·—— (reference 17).

[14] J. de Boer and C. J. Gorter, Physica **16**, 225, 667 (1950); Phys. Rev. **77**, 569 (1950).

TABLE II. The total vapor pressure p in mm of Hg for a 20 percent solution of He^3 in liquid He^4 as computed according to (a) the laws for perfect classical solutions (P.C.S.), (b) the theory of Heer and Daunt (H and D), and (c) the theory of de Boer and Gorter (their "Case *A*"), (deB and G). Also in the last column the experimental results of measurement on a 20.3 percent solution by Weinstock *et al.* (reference 17) are given.

T°K	(P.C.S.)	(H and D)	(deB and G)	Observed
1.1	5.70	7.24	7.64	7.00
1.2	9.31	9.77	8.91	9.48
1.4	13.5	16.6	12.9	16.6
1.6	17.4	26.9	20.0	25.7
1.8	29.9	41.7	31.3	38.0
2.0	49.0	61.7	49.6	56.2
2.4	110	126	110	115
2.6	115	170	155	159
2.8	207	224	207	214
3.0	269	292	269	276

Our computations of C_v/C_L from de Boer and Gorter's theory have been made from their Eqs. (24) to (27), using their *ad hoc* expression [Eq. (32)] for the Gibbs function of pure liquid He^4. (These equation numbers refer to de Boer and Gorter's paper.[14] Our computations have been made *ab initio* without use of de Boer and Gorter's graphs which were found not to provide sufficient accuracy at low C_L values.) The results of these computations are given in Table I and are shown in Figs. 1–4.

Recent experimental results on the evaluation of C_v/C_L for solutions of He^3 in liquid He^4 for solution concentrations of 1.00, 5.00, and 10.00 percent He^3 by Sommers[15] are included in Figs. 1–4, as well as the experimental results of Daunt and Heer[1] for 1.0 percent solutions (see Fig. 1). It will be seen that in the temperature region below about 1.8°K the theory of Heer and Daunt fits the experimental observations rather accurately. Above this temperature the observed results lie between the predictions of the two theories.

It must be remembered that in the computations reported herewith the assumption has been made, both in the theory of Heer and Daunt and in that of de Boer and Gorter, that the vapor can be treated as a perfect gas. In practice, however, at least for temperatures above about 1.8°K, the vapor is not perfect and corrections should be made for the imperfections. Such corrections have been made in a narrow temperature range (1.9°K to 2.3°K) by Kilpatrick[16] to the evaluation of p_3, p_4, and C_v/C_L according to the theory of de Boer and Gorter. These corrections have shown that the computed values of C_v/C_L must be reduced by about 10 to 15 percent in the temperature range mentioned for a 1.00 percent solution. In a similar manner it would be expected that the computed values of the theoretical C_v/C_L according to the theory of Heer and Daunt should also be reduced by a similar amount. As

[15] H. S. Sommers. The authors are indebted to Dr. Sommers for his private communications of these results and for his permission to include them here before full publication. For preliminary detail of these results see reference 4.

[16] J. E. Kilpatrick, Phys. Rev. **79**, 529 (1950).

a result it would be expected that in this higher temperature region the theory of Heer and Daunt should provide a satisfactory agreement with experiment. It would nevertheless be of value to have more experimental measurements in the region of temperature above about 2.2°K to check the basic postulates of the B-E liquid model.

III. COMPUTATIONS OF THE TOTAL VAPOR PRESSURES OF STRONG SOLUTIONS IN B-E LIQUIDS

It has already been pointed out[6] that the results of vapor pressure measurement on solutions of 20.3 percent and 25 percent He^3 concentration, as carried out by Weinstock *et al.*,[17] are in close agreement with the theoretical predictions of Heer and Daunt. Further computations have been made of the total vapor pressures above strong solutions using (a) the theory of Heer and Daunt, which involves no adjustable parameters, (b) the laws for perfect classical solution (P.C.S.), and (c) the theory of de Boer and Gorter. The results of these calculations for a 20.00 percent solution are given in Table II and in Fig. 5. Also, for comparison, the experimental observations[17] for a 20.3 percent solution are included in Table II and Fig. 5. It will be seen from Fig. 5 that the experimental results give values for the total vapor pressure everywhere above those for perfect classical solutions and that the theory of Heer and Daunt provides fair agreement with experiment, particularly at the lower temperatures. At the higher temperatures above about 1.8°K, as for the evaluations of C_v/C_L, the gas imperfections become of importance and should be taken into account. Again, as has been pointed out by Kilpatrick,[16] the vapor imperfections would result in a lowering of the theoretical evaluations of the total vapor pressure on both theories and a consequent improvement in the agreement of the theory of Heer and Daunt with observation in the higher temperature region.

[17] Weinstock, Osborne, and Abraham, Phys. Rev. **77**, 440 (1950).

PHYSICAL REVIEW VOLUME 86, NUMBER 6 JUNE 15, 1952

A Note on Wooldridge's Theory of Secondary Emission*

E. M. Baroody
Battelle Memorial Institute, Columbus, Ohio
(Received February 18, 1952)

A re-examination of Wooldridge's theory shows that the broad maximum which he obtained in the curve of secondary emission coefficient against primary energy is a result of an inconsistency in approximations, rather than an essential result of his theory. In deriving an expression for the emission coefficient from the rate of excitation of valence electrons, an estimate was needed of the probability that a typical secondary would travel in a direction favorable for emission. In making this estimate, Wooldridge neglected the momentum received from the primary, which is small compared to that received from the lattice. The present calculation shows, however, that this neglected momentum is of just the right magnitude to eliminate or drastically modify the broad maximum obtained in the emission curve.

THE recent letters[1,2] have discussed how Wooldridge's[3] final result for the variation of secondary emission with primary energy can be put into convenient form. The proposed forms avoid the graphical methods used by Wooldridge in evaluating the integral appearing in his Eq. (53). A re-examination of Wooldridge's paper has now led to the view that the term involving the integral actually lies beyond the accuracy of his theory. The importance of this lies in the fact that without this term his theory leads to an asymptotic rise to a limiting value, rather than to a curve with a broad maximum. The reasons for this view will be developed by summarizing certain of Wooldridge's results, and pointing out changes which follow if the approximations of the theory are made more consistent in one respect.

Wooldridge calculated the probability of excitation of the valence electrons of the metal through Coulomb interaction with a medium-fast primary, using the Born approximation and the Bloch model of the metal. Details were reported for a simple cubic metal with lattice constant a. The allowed transitions satisfy

$$\mathbf{k}'=\mathbf{k}+(2\pi/a)\boldsymbol{\rho}+(\mathbf{K}-\mathbf{K}'). \tag{1}$$

Here $\mathbf{k}$, $\mathbf{k}'$, and $\mathbf{K}$, $\mathbf{K}'$ are initial and final wave vectors of the metal electron and of the primary. The components of $\boldsymbol{\rho}$ are integers, and it develops that the six transitions with $|\boldsymbol{\rho}|=1$ are of most importance. For these the most probable energy transfer is of order $E_0=h^2/2ma^2$. For most of the calculations the ratio of E_0 to the primary energy is regarded as small, so that terms of order $(2\pi/aK)^2$ may be neglected.

The number of excitations per unit primary path for a given one of the six important values of $\boldsymbol{\rho}$ is approximately

$$dN_\rho/dx=(A/6)\{1-(2\pi/aK^2)\mathbf{K}\cdot\boldsymbol{\rho}\}. \tag{2}$$

* Sponsored by the Army Signal Corps and the Air Force.
[1] James J. Brophy, Phys. Rev. **82**, 757 (1951).
[2] E. M. Baroody, Phys. Rev. **83**, 857 (1951).
[3] D. E. Wooldridge, Phys. Rev. **56**, 562 (1939).

The factor A depends on various parameters, but not on the primary energy or the direction of $\boldsymbol{\rho}$. For a metal composed of small grains of random orientation, the total excitation rate is six times the average of (2), which is simply A. The corresponding rate of energy loss is $-dE/dx=AE_0$, and the range in which a primary of initial energy E_p loses the power of producing excitations, $l=(E_p-E_0)/E_0A$. These relations are Eqs. (49) and (50) of Wooldridge's paper.

The secondary emission coefficient is then written

$$\delta=A\int_0^l \exp(-\gamma x)f(x)dx, \tag{3}$$

where the integrand represents the probability that the average secondary formed at depth x is emitted. The exponential factor allows for absorption, while the probability that the secondary has sufficient energy to escape is measured by $f(x)$. This factor is estimated by considering the typical secondary to be formed with the kinetic energy, E_0+E_F, where E_F is the mean Fermi energy of the valence electrons of the metal, and taking $f(x)$ to be the probability that the initial direction of motion falls in the solid angle defined by

$$\theta\leq\theta_{\max},\quad \cos\theta_{\max}=\{W_a/(E_0+E_F)\}^{\frac{1}{2}}, \tag{4}$$

W_a being the potential energy step at the surface. It is next assumed that to sufficient approximation the typical secondary moves along $\boldsymbol{\rho}$. Equation (2) then gives,

$$f(x)=\tfrac{1}{2}\int_0^{\theta_{\max}}\{1+(2\pi/aK)\cos\theta\}\sin\theta d\theta$$
$$=\tfrac{1}{2}(1-\cos\theta_{\max})+(\pi/2aK)\sin^2\theta_{\max}. \tag{5}$$

The corresponding expression for δ is

$$\frac{\delta}{\delta_\infty}=1-\exp(-\gamma l)+\frac{\pi\gamma}{a}(1+\cos\theta_{\max})\int_0^l\frac{\exp(-\gamma x)}{K(x)}dx, \tag{6}$$

where

$$\delta_\infty=(A/2\gamma)(1-\cos\theta_{\max}). \tag{7}$$

Equation (6) is equivalent to Wooldridge's Eq. (48) and leads to his Eq. (53).

On re-examining the above procedure, which follows Wooldridge in all essentials, one notices that the term in Eq. (6) involving the integral has entered in a questionable way. The assumption that $\boldsymbol{\rho}$ specifies the direction of the secondary to sufficient accuracy, when used in Eq. (2), led to a lack of spherical symmetry in the production of secondaries, motion opposite to $\mathbf{K}$ (that is, toward the free surface) being favored. However, taking $\mathbf{k}'$ parallel to $\boldsymbol{\rho}$ involves neglecting $(\mathbf{K}-\mathbf{K}')$ in Eq. (1). Since this vector has a component directed away from the surface, taking it into account might completely alter the estimated deviation from spherical symmetry.

Now consider how the calculation would change if a distinction between $\mathbf{k}'$ and $\boldsymbol{\rho}$ were maintained. Let the orientation of $\mathbf{k}'$ with respect to the outgoing normal be again specified by θ, while a new variable β locates $\boldsymbol{\rho}$. Equation (4) is unchanged, but (5) no longer applies. Instead one has

$$f(x)=\tfrac{1}{2}\int_0^{\theta_{\max}}\{1+(2\pi/aK)\cos\beta\}\sin\beta(d\beta/d\theta)d\theta, \tag{8}$$

and requires information concerning the function $\beta(\theta)$. Since it is only intended to judge the general effect of the term $(\mathbf{K}-\mathbf{K}')=\mathbf{S}$, attention may be limited to $\mathbf{k}=0$ [as was done, in effect, in the derivation of Eq. (2)] and may later be restricted to the case when $S=|\mathbf{S}|$ has its minimum value. This is the important region, since, as shown by Wooldridge, transition probabilities are inversely proportional to S^4. For $\mathbf{k}=0$, approximate momentum and energy equations are

$$\mathbf{k}'=\mathbf{S}+(2\pi/a)\boldsymbol{\rho}, \tag{9}$$

$$k'^2=K^2-K'^2\doteq 2\mathbf{K}\cdot\mathbf{S}. \tag{10}$$

Elimination of $\mathbf{k}'$ gives

$$S^2-2\left(\mathbf{K}-\frac{2\pi}{a}\boldsymbol{\rho}\right)\cdot\mathbf{S}+\left(\frac{4\pi^2}{a^2}\right)=0. \tag{11}$$

From this one finds that to the proper approximation S is a minimum when $\mathbf{S}$ is parallel to $\mathbf{K}$ and that this minimum is

$$S_{\min}=2\pi^2/a^2K. \tag{12}$$

Equation (9) then shows that for this case

$$\cos\beta-(\pi/aK)\sin^2\beta=\cos\theta, \tag{13}$$

or

$$\{1+(2\pi/aK)\cos\beta\}\sin\beta(d\beta/d\theta)=\sin\theta. \tag{14}$$

One sees that the initial directions of motion of the secondaries are now distributed isotropically. When Eq. (14) is used in Eq. (8), one obtains

$$f(x)=\tfrac{1}{2}(1-\cos\theta_{\max}). \tag{15}$$

Thus, $f(x)$ is independent of the primary energy, and δ is simply

$$\delta=\delta_\infty\{1-\exp(-\gamma l)\}. \tag{16}$$

There is now no maximum, δ increasing exponentially toward the limit δ_∞. Although this result may depend somewhat on the fact that the influence of the term $(\mathbf{K}-\mathbf{K}')$ has not been determined in a completely general way, one may conclude that an extension or modification of the Wooldridge theory is needed if the maxima in the experimental curves are to be understood.

Analysis of the Nucleonic Component Based on Neutron Latitude Variations*

S. B. TREIMAN†
Department of Physics and Institute for Nuclear Studies, University of Chicago, Chicago, Illinois
(Received January 7, 1952)

A "specific yield" function $S_A(E, x)$ is defined which gives the production rate of disintegration neutrons at atmospheric depth x arising from a unit flux of vertically incident cosmic-ray primaries of atomic weight A and energy-per-nucleon E. The functions are obtained by comparing the latitude variations for the primary particle fluxes with the latitude variations for neutron production at various depths in the atmosphere. For atmospheric depths between at least 200 and 600 g/cm², it is found that the specific yields increase rapidly with energy up to about 4-Bev/nucleon and then become insensitive to energy up to at least 12.7-Bev/nucleon. It is also shown that this insensitivity probably extends up to considerably larger energies. The theoretical implications of these results are qualitatively discussed.

I. INTRODUCTION

IT is known from cloud chamber and photographic emulsion experiments that in energetic nuclear disruptions particles are emitted which are capable of producing further nuclear interactions. This cascade-like development of nuclear processes has been discussed phenomenologically by various authors, in connection with studies of the cosmic radiation.[1–5]

The radiations which produce nuclear disruptions in the atmosphere consist mainly of nucleons. Although recent experiments indicate that the cross section for the interaction of fast pions with nuclei is geometrical,[6–8] the process of decay can be assumed to remove all but the most energetic pions before nuclear interactions can occur with appreciable probability. Very low energy nuclear disruptions may be produced to some extent by photons and muons, but the total contribution from this source has also been shown to be small, at least below the transition maximum in the atmosphere.[5] The disruption-producing nucleons in the atmosphere constitute the nucleonic component of the cosmic radiation. In discussing the series of correlated nuclear processes generated by a single primary cosmic-ray particle, we will use the term *nucleonic chain*.

The development of a nucleonic chain can be pictured in the following way. In its first interaction with an air nucleus, an energetic primary nucleon typically produces several classes of particles: low energy evaporation fragments and disintegration nucleons; particles which decay before they can produce nuclear disruptions (except at very large energies, the bulk of the pions fall into this class); and fast particles (mainly nucleons) which are capable of producing further nuclear disruptions. As the energy of the last-mentioned particles decreases, the probability for meson production in subsequent interactions also decreases. In every nuclear process, however, evaporation and slow recoil nucleons (which we class together as disintegration nucleons) are produced, and these can be used as indicators of the development of the nucleonic chain.[3] From an energy point of view these particles represent the end products of the chain, and a knowledge of how the production rates of disintegration nucleons depend on primary particle energy should prove useful in understanding the processes involved in the nucleonic component.

In particular, we will concern ourselves here with the disintegration neutrons, for which fairly extensive experimental data are available. We introduce a "specific yield" function $S_A(E, x)$, which gives the production rate per gram of air of disintegration neutrons at atmospheric depth x arising from a unit flux of vertically incident cosmic-ray primaries of atomic weight A and energy-per-nucleon E.

For a limited range of primary particle energies, the specific yield functions can be obtained by comparing the experimentally observed neutron latitude variations in the atmosphere with the latitude variations for the fluxes of primary particles.

II. THE GEOMAGNETIC ANALYSIS

The earth's magnetic field determines a minimum value of $N \equiv p/Z$ for arrival of a primary particle from a given direction at the top of the atmosphere, where p and Z are, respectively, the total momentum and charge of the particle. It is therefore convenient to express the specific yields as a function of N. Let $N_v(\lambda)$ be the minimum value of N for arrival from the vertical direction at geomagnetic latitude λ. (Because of the eccentricity of the earth's dipole field, N_v depends slightly on longitude; this dependence is not explicitly written, but it will be taken into account in the calculations.)

Let $-dF_T/dN$ be the total (differential) flux of primary particles per unit solid angle which have

* Assisted in part by the Flight Research Laboratory, U.S.A.F.
† AEC Predoctoral Fellow.
[1] Bernardini, Cortini, and Manfredini, Phys. Rev. **76**, 1792 (1949); **79**, 952 (1950).
[2] M. Conversi, Phys. Rev. **79**, 749 (1950).
[3] Cocconi, Tongiorgi, and Widgoff, Phys. Rev. **79**, 768 (1950).
[4] G. D. Rochester and W. G. V. Rosser, *Reports on Progress in Physics* (Physical Society, London, 1951), Vol. XIV, p. 227.
[5] J. A. Simpson, Phys. Rev. **83**, 1175 (1951).
[6] Camerini, Fowler, Lock, and Muirhead, Phil. Mag. **41**, 413 (1950).
[7] A. J. Hartzler, Phys. Rev. **82**, 359 (1951).
[8] Chedester, Isaacs, Sachs, and Steinberger, Phys. Rev. **82**, 958 (1951).

TABLE I. Absorption mean free path for neutron production in the atmosphere at geomagnetic latitude λ, for atmospheric depths between 200 and 600 g/cm².

λ	L (g/cm²)
0°	212±4
19	206±4
40	181±3
53	157±2
65	157±3

momentum-to-charge ratio N (where $F_T(N)$ is then the integral flux). Let $f_A(N)$ be the fraction of these which have atomic weight A, and let $S_A(N, x)$ be the specific yield, i.e., the neutron production rate at atmospheric depth x due to a unit vertical flux of primary particles of atomic weight A and momentum-to-charge ratio N. The total production rate at depth x and latitude λ, due to the primaries arriving within a unit solid angle from the vertical direction, is given by the expression

$$R_v(\lambda, x) = -\int_{N_v(\lambda)}^{\infty} \sum S_A(N, x) f_A(N) (dF_T/dN) dN. \quad (1)$$

We define an average specific yield function $S(N, x)$ by the equation[9]

$$S(N, x) \equiv \sum S_A(N, x) f_A(N); \quad (2)$$

and from Eq. (1) we obtain the result

$$S(N, x) = dR_v(\lambda, x)/dF_T(N), \quad (3)$$

where

$$N = N_v(\lambda). \quad (3')$$

R_v is treated here as a function of F_T, λ and x being parameters. It is understood that R_v and N_v are evaluated at the same longitude.

The quantity R_v is referred to as the "vertical" neutron production rate. Experimentally, of course, one normally measures the production rate $R(\lambda, x)$ due to primary particles which arrive from all directions at the top of the atmosphere; R_v and R are related approximately by the Gross transformation

$$2\pi R_v = R - x dR/dx. \quad (4)$$

III. DETERMINATION OF THE AVERAGE SPECIFIC YIELD

A. Results at 312 g/cm²

In a recent paper Simpson[5] has presented curves showing the altitude and latitude variations of disintegration neutron intensity in the atmosphere. The neutrons detected are in the energy range ~2–30 Mev, and it has been shown that they are mainly produced in nuclear disruptions induced by higher energy nucleons. In the equilibrium region of the atmosphere, where these measurements were performed, the observed neutron intensities are proportional to the actual production rates in the vicinity of the detection apparatus. Throughout this paper, neutron production rates will be measured in counting rate units appropriate to the Simpson altitude and latitude curves. For a discussion of the absolute production rates, reference may be made to a number of recent papers.[5,10,11]

For atmospheric depths between 200 and 600 g/cm², where the measurements were performed, the production rates are observed to vary with depth in an approximately exponential manner. The absorption mean free path $L(\lambda)$, however, depends on latitude, as shown in Table I.[5] In discussing the altitude variations of various quantities, in what follows, it will always be understood that we restrict ourselves to the range of depths between 200 and 600 g/cm².

Our analysis will be based on the latitude curve for atmospheric depth 312 g/cm² and geographic longitude 80°W (see Fig. 4 in reference 5). The "vertical" production rate R_v is obtained by applying the Gross transformation of Eq. (4). Because of the exponential variation of $R(\lambda, x)$, this can be written

$$2\pi R_v(\lambda, x) = R(\lambda, x)[1 + x/L(\lambda)]. \quad (5)$$

The function $L(\lambda)$ is obtained by drawing a smoothed curve through the experimental points given in Table I.

It should be noted that if we assume $R_v(\lambda, x)$ to depend exponentially on depth, with absorption mean free path $L_1(\lambda)$, then Eq. (4) leads to the solution

$$R(x) = 2\pi R_v(0)[\exp(-x/L_1) + (x/L_1)E_i(-x/L_1)], \quad (6)$$

where we have omitted, for the moment, the explicit dependencies on λ. For $x \gtrsim L_1$, the function $R(x)$ of Eq. (6) does not differ appreciably from an exponential and, within the experimental uncertainties, can be adjusted to fit the observed neutron altitude curves by a suitable choice of $L_1(\lambda)$—at least for the limited range 200–600 g/cm². For example, at small latitudes (0°–19°) the choice

$$L_0 \equiv L_1(0°\text{–}19°) = 272 \text{ g/cm}^2 \quad (7)$$

leads to an approximately exponential function for R, where the apparent absorption mean free path L has the correct value 209 g/cm² (see Table I). We will later make use of this fact, although not in a critical way, by assuming that R_v is precisely exponential and that R is given by the corresponding (approximately exponential) function of Eq. (6).

It should also be noted here that the approximations involved in the derivation of the Gross transformation can be shown to lead only to negligible errors for the application considered in this paper.

For the primary cosmic-ray spectrum we adopt the curve given by Winckler *et al.*[12] (see Fig. 6 in reference

[9] The "yield" Y, introduced in reference 5, is related to the average specific yield S by the equation $2\pi Y = \int S dx$.

[10] L. Yuan, Phys. Rev. **81**, 175 (1951).
[11] S. Lattimore, Phil. Mag. **42**, 331 (1951).
[12] Winckler, Stix, Dwight, and Sabin, Phys. Rev. **79**, 656 (1950).

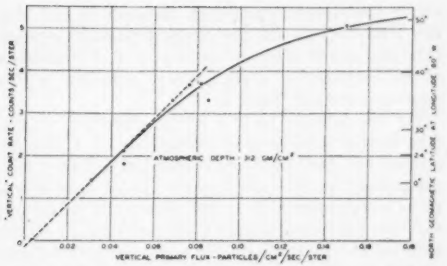
"VERTICAL" COUNT RATE - COUNTS/SEC/STER
ATMOSPHERIC DEPTH : 312 GM/CM²
VERTICAL PRIMARY FLUX - PARTICLES/CM²/SEC/STER
NORTH GEOMAGNETIC LATITUDE AT LONGITUDE 80° W

FIG. 1. "Vertical" neutron production rate at atmospheric depth 312 g/cm², plotted as a function of the total flux of primary particles which arrive from the vertical direction.

12). This curve, which includes the results of a number of investigators, gives the flux of particles with momentum-to-charge ratio greater than N, expressed as a function of the proton kinetic energy corresponding to N. The vertical cut-off value of momentum-to-charge ratio, $N_v(\lambda)$, has been given as a function of latitude for longitude 80°W by Neher.[13]

With latitude—or alternatively, the function $N_v(\lambda)$—serving as parameter, we can now obtain a plot of R_v (at 312 g/cm²) *vs* F_T. The result is shown in Fig. 1. The heavy points are the experimental flux values appearing on the Winckler curve. Two features of the R_v-F_T curve should be noticed: (1) the curve approaches very closely a straight line for latitudes between 0° and about 24° (this corresponds to a range of N_v between 13.6 and 10 Bev/c); (2) the extrapolation of this straight line passes very close to the origin. Since the slope dR_v/dF_T gives the average specific yield, it appears that the latter is virtually independent of N in the interval 10–13.6 Bev/c. The significance of (2) will be discussed later. The slope dR_v/dF_T has been obtained graphically, and the result is shown in Fig. 2, where S is plotted as a function of N. The points shown on this curve represent the results of several determinations of the slope and give an indication of the purely graphical errors involved.

B. Discussion of Errors

The experimental errors in the curves of Figs. 1 and 2 are due chiefly to uncertainties in the primary spectrum. We are mainly interested in evaluating these errors for values of N in the range 10–13.6 Bev/c, where S appears to become independent of N. Between about 3 and 15 Bev/c the Winckler spectrum is well represented by the expression

$$F_T(N)=KN^{-1.0}, \tag{8}$$

where $K=0.42$ within about 2 percent. (For smaller values of N the exponent decreases with decreasing N.)

[13] H. V. Neher, Phys. Rev. **78**, 674 (1950).

Vidale and Schein,[14] using a counter telescope, have recently determined the primary spectrum for values of N between 1.7 and 9.1 Bev/c. They find a power law with an exponent 1.0 ± 0.1 in excellent agreement with the Winckler exponent. Neher,[15] by the method of integrating ionization *vs* altitude curves, has obtained a spectrum which can be approximately represented by a power law for N between about 4 and 15 Bev/c; the exponent has the approximate value 1.1. This is considered to be in good agreement with the Winckler exponent, although the absolute flux values obtained by the ionization method are considerably smaller than the values obtained by direct measurements at the top of the atmosphere.

We are not concerned with the absolute flux of primary particles, which is subject to rather large experimental error, but rather with the shape of the primary spectrum curve. It can be shown that an error $\Delta\gamma$ in the exponent of Eq. (8) would lead to a difference ΔS between the values of S at the extremes of the interval 13.6–10 Bev/c, which is given by

$$\Delta S/S=0.31\Delta\gamma.$$

Thus, even for an error as large as $\Delta\gamma=0.2$, S would increase only by about 6 percent in going from 10 to 13.6 Bev/c.

It is probably correct, therefore, to conclude that the average specific yield function is at least very insensitive to N in the interval 10–13.6 Bev/c. For purposes of discussion we will refer to it as being constant. The choice of 10 Bev/c to mark the lower limit of the region of constant S is, of course, slightly arbitrary.

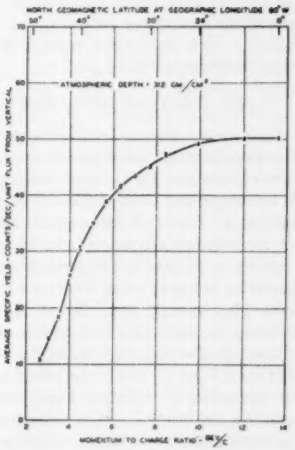
NORTH GEOMAGNETIC LATITUDE AT GEOGRAPHIC LONGITUDE 80° W
ATMOSPHERIC DEPTH : 312 GM/CM²
AVERAGE SPECIFIC YIELD - COUNTS/SEC/UNIT FLUX FROM VERTICAL
MOMENTUM TO CHARGE RATIO - BV/C

FIG. 2. Average specific yield at atmospheric depth 312 g/cm², plotted as a function of momentum-to-charge ratio N.

[14] M. L. Vidale and M. Schein, Nuovo cimento **8**, 774 (1951).
[15] H. V. Neher, Phys. Rev. **83**, 649 (1951).

C. Results at Other Atmospheric Depths

The results thus far refer only to atmospheric depth 312 g/cm². For other depths in the range 200–600 g/cm², the shape of the average specific yield curve can be inferred from Table I. The absolute value of S for any value of N will, of course, decrease with increasing depth, and the relative shape of the curve will also, in general, change with depth. Thus, for high latitudes $L(\lambda)$ decreases rapidly with increasing λ; consequently, for small values of N the average specific yield will fall off the more rapidly with decreasing N, the greater is the depth.

However, for small latitudes $L(\lambda)$ is almost independent of λ; in fact, the values at 0° and 19° agree within the experimental errors. We will not be too greatly in error, therefore, in assuming that $L(\lambda)$ is independent of λ up to 24°. The constancy of S in the interval 10–13.6 Bev/c (which corresponds to the latitude interval 0°–24°) therefore holds for all depths, at least between 200 and 600 g/cm².

We denote by $S_0(x)$ the value of S in the interval 10–13.6 Bev/c. The altitude variation of $S_0(x)$ depends, through Eq. (3), on the altitude variation of R_v. The latter, as we have seen, can be taken to be an exponential function, where for small latitudes (0°–24°) the absorption mean free path has the value L_0 given by Eq. (7). The absorption mean free path for $S_0(x)$ is also, therefore, given by L_0.

TABLE II. Composition of primary radiation at small latitudes (0°–24°).

	Percentage of primary nuclei	Percentage of primary nucleons
Protons	87	58
Helium	12	32
C, N, O	0.64	6.0
$Z \geq 9$	0.19	3.6

IV. THE INDIVIDUAL SPECIFIC YIELDS

In a recent review article, Peters[16] has summarized the experimental information on the spectra of the heavy particles ($A>1$) in the primary cosmic radiation. When expressed as a function of N, the heavy particle spectra are found to have approximately the same form as the total primary spectrum given by Winckler, at least up to 15 Bev/c. (Beyond this value the Winckler spectrum is based on an uncertain extrapolation to the very high energy spectrum of Hilberry, so that no attempt is made here to compute the relative composition of the primary radiation above 15 Bev/c.) Between 3 and 15 Bev/c the fraction of heavy particles in the primary radiation changes only by about 12 percent, the fraction of heavy particles decreasing with increasing N. It is possible that this slow variation lies within the experimental errors. Between 10 and 13.6 Bev/c (0°–24°) the fraction of heavy particles appears to be almost completely independent of N. A breakdown of the composition of the primary radiation in this interval is given in Table II.

For the interval 10–13.6 Bev/c, therefore, we can take the fractions f_A to be independent of N. But for atmospheric depths between at least 200 and 600 g/cm², the average specific yield function has also been shown to be independent of N in this interval. If we assume that the individual specific yield functions S_A do not increase with increasing N for some species of primary particles and decrease for other species, then it follows from Eq. (2) that the specific yields are individually independent of N in the interval 10–13.6 Bev/c. The corresponding ranges of kinetic energy are 9.1–12.7 Bev for protons and 4.1–5.9 Bev/nucleon for heavy primaries ($A=2Z$).

We can see now the significance of the fact that the straight-line portion of the $R_v - F_T$ curve extrapolates very close to the origin (Fig. 1). For the interval 10–13.6 Bev/c, Eq. (3) can be integrated to give

$$R_v(\lambda) = S_0 F_T(N)_{N=N_v(\lambda)} + \text{constant}, \qquad (9)$$

where the constant of integration is nearly vanishing. If we assume that the fractional composition of the primary radiation remains independent of N for $N>13.6$ Bev/c, then it follows from Eqs. (1) and (9) that the specific yields also remain independent of N above 13.6 Bev/c. Actually, the composition of the primary radiation at large N is not known with any accuracy, and it is possible that the specific yields and the fractional fluxes f_A both vary with N in such a way as to accidentally produce the almost vanishing value observed for the constant of integration in Eq. (9). However, if we rule out a sudden large change in the composition of the primary radiation just above 13.6 Bev/c, we can probably correctly conclude that the specific yields remain fairly insensitive to N up to values considerably larger than 13.6 Bev/c. However, nothing can be said about the behavior of the specific yields at very large values of N, where the flux of primary particles is in any case small and therefore unimportant in contributing to neutron production in the atmosphere.

V. COMPARISON OF PROTON AND HEAVY PARTICLE SPECIFIC YIELDS

The results of the preceding discussion were obtained directly from the experimental data on neutron and primary particle latitude variations, without reference to any particular assumptions on the properties of nucleonic chains. It was shown that for atmospheric depths between at least 200 and 600 g/cm², the production rate of disintegration neutrons arising from a unit vertical flux of primary particles becomes insensitive

[16] B. Peters, *Progress in Cosmic Ray Physics* (North Holland Publishing Company, Amsterdam, 1952).

to primary energy in the ranges 9.1–12.7 Bev for protons and 4.1–5.9 Bev/nucleon for heavy primaries. It was also shown that this energy insensitivity probably extends up to considerably larger energies.

Because of their large collision mean free paths, the residue of heavy primary nuclei below 200 g/cm² is extremely small. The heavy primaries contribute to the neutron production at large depths through their break-up into fast nucleons in the upper parts of the atmosphere, these nucleons serving as the primary particles for the development of nucleonic chains. (Fragments of atomic weight greater than unity also result from the break-up, but these, in turn, yield smaller fragments and free nucleons; and after a very few collisions the break-up into nucleons is completed.) There must exist then a close relationship between the specific yield functions for heavy particles and for free nucleons. In the absence of a reliable theory of energetic nuclear interactions, however, it is not possible to deduce the exact nature of this relationship. Thus, we have seen that the specific yield functions do not depend appreciably on primary energy in the ranges 9.1–12.7 Bev for protons and 4.1–5.9 Bev/nucleon for heavy primaries, but the relative numerical values of the specific yields cannot be determined from the empirical analysis.

However, on the basis of fairly plausible assumptions on the properties of energetic nuclear interactions, we can establish the result that the free nucleon specific yield must become insensitive to energy in the same range where the heavy particle specific yields are energy-insensitive, i.e., that the proton specific yield is actually insensitive to energy down to 4.1 Bev.

Consider the interaction of an air nucleus with an incident primary particle of atomic weight A and energy-per-nucleon E. We fix our attention on a particular nucleon in the incident particle and view the interaction, for the moment, in the rest system of the incident particle. The following possibilities occur: (1) The nucleon may have its bond broken and emerge as a low energy evaporation or recoil particle. (2) It may emerge as part of a low energy fragment of atomic weight A' greater than unity. (3) It may suffer a direct nucleon-nucleon collision and receive a considerable amount of energy, in which case it is fairly certain to emerge as a free nucleon. As viewed in the laboratory system, the nucleon emerges in processes (1) and (2) with essentially the same velocity as that of the primary particle, i.e., with energy E. In the case of (3) the nucleon has appreciably smaller energy. Let p_{A1} and $p_{AA'}$ be the respective break-up probabilities, averaged over all values of the collision parameter, for processes (1) and (2); and let $p_A(E, E')dE'$ be the probability for process (3), where the nucleon emerges with energy E' in the interval dE'. If Λ_A is the collision mean free path for the heavy primary particle in air, then the specific yield at depth x is given by

$$S_A(E, x)=\Lambda_A^{-1}\int_0^x \exp(-x'/\Lambda_A)dx' \times\left[\sum_{A'} p_{AA'}S_{A'}(E, x-x')+p_{A1}S_p(E, x-x') +\int_0^E p_A(E, E')S_p(E', x-x')dE'\right], \quad (10)$$

where $S_p(E, x-x')$ is the specific yield at depth x due to a unit flux of nucleons of energy E produced at depth x'. We do not distinguish here between the fast neutrons and protons which emerge from the break-up of the heavy particle, although the latter, of course, immediately begin to lose energy by ionization. This may be justified by observing that for the large energies which we are considering (several Bev and greater), the ionization loss per collision mean free path is small compared to the proton kinetic energy. After several collisions, when the energy is sufficiently degraded, ionization loss becomes important; but because of the possibility of charge exchange, and because of the contribution to the nucleonic chain from both charged and uncharged recoils, the charge distribution among the particles of the chain should not depend strongly, after several collisions, on the state of charge of the primary nucleon.

As we have previously seen, the heavy particle specific yields become independent of energy above 4.1 Bev/nucleon (and below an upper limit which is probably much larger than 5.9 Bev/nucleon and which we take to be larger than 9.1 Bev/nucleon). If we assume that the collision mean free path Λ_A and the break-up probabilities $p_{AA'}$ and p_{A1} are independent of energy, then it follows that the sum of the last two terms on the right-hand side of Eq. (10) must become independent of energy in this interval. This result must hold for a considerable range of depths—at least between 200 and 600 g/cm². It seems reasonable to conclude, therefore, that the last two terms in Eq. (10) are individually independent of energy above 4.1 Bev, unless we suppose that there occurs an accidental cancellation of energy and spatial dependencies. It appears then that the proton specific yield S_p, which we have previously shown to be energy-insensitive above 9.1 Bev, actually remains insensitive to energy down to 4.1 Bev.

It is apparent from Fig. 2 that for energies much below 4.1 Bev/nucleon, the proton and heavy particle specific yields both fall off rapidly with decreasing energy.

The details of the collision process are compressed into the break-up probabilities $p_{AA'}$ and p_{A1} and the distribution function $p_A(E, E')$. (For complete generality, the latter should include the fast recoil nucleons coming from the target nucleus.) An upper limit for the heavy particle specific yields, relative to the proton

specific yield, can be obtained by neglecting the last term in Eq. (10), i.e., by assuming that the collision with an air nucleus merely serves to break up the incident heavy particle into free nucleons and fragments having the same energy per nucleon as the incident particle. We have seen that in the energy-insensitive region the specific yields vary with depth in an approximately exponential manner, with absorption mean free path L_0. In this range of energies, therefore, an upper limit on S_A is obtained by setting these exponential functions into Eq. (10) and observing that for large depths ($x \gtrsim 200$ g/cm^2), $\exp(-x/L_0) \gg \exp(-x/\Lambda_A)$. We obtain the result

$$S_A < (1-\Lambda_A/L_0)^{-1}[\sum p_{AA'}S_{A'} + p_{A1}S_p]. \quad (11)$$

VI. DISCUSSION

Simpson[17] has shown that disintegration neutrons in the atmosphere are produced mainly in small stars (nuclear bursts) and that the production rates of neutrons and small stars are substantially in equilibrium, at least below 200 g/cm^2; i.e., within the experimental errors both show the same latitude and altitude variations. We can therefore redefine our specific yield functions to refer to the production of small stars without changing any of our results.

Our conclusions on the energy-insensitivity of the specific yield functions above 4.1 Bev/nucleon followed essentially from the fact that the neutron and small star latitude variations are proportional to the latitude variation of primary particle intensities in the interval 0°–24°. It would obviously be of interest to test whether or not this is also true for the production of large stars.

A question of considerable importance in the study of the nucleonic component is that of the role played by mesons. In the interaction of an energetic primary nucleon with a nucleon in an air nucleus, a pair of recoils and possibly one (or more) pions are produced, where we refer to both the target and incident nucleons as recoils after they emerge from the collision. The recoils can presumably suffer further collisions within the same nucleus, and in each elementary act, pion production presumably occurs with a probability which depends on the energies involved. If we restrict ourselves to primary energies below ~12.7 Bev, then because of the large probability for decay, the pions which are produced will not contribute appreciably to the further development of the nucleonic chain once they leave the air nucleus. On the other hand, a pion produced in an elementary act might be expected to interact within the same nucleus, producing fast recoil nucleons which can contribute to the chain.

Camerini *et al.*[18] have shown that pions of energy less than 1 Bev which are incident on the nuclei of photographic emulsions emerge with greatly reduced energy in about 50 percent of the cases. (In the remaining cases it is not possible to determine whether complete absorption or charge exchange has taken place.) This result, taken together with the evidence previously cited for a large interaction cross section between pions and nuclei, indicates a strong interaction of pions with nuclear matter. It has also been shown,[18] however, that the average number of "black" and "grey" prongs emerging from nucleon-produced stars increases only very slowly with increasing number of shower particles. If the shower particles, which consist mainly of pions, were strongly interacting within the nucleus in which they are created, one would expect to find a strong dependence of "black" and "grey" prongs on the number of shower particles. From this evidence, therefore, it appears that pions do not contribute appreciably to the production of recoil nucleons in the parent nucleus.

Our specific yield results lead to a similar conclusion. For primary proton energies between 4.1 and at least 12.7 Bev, the production rate of small stars at large atmospheric depths becomes insensitive to primary energy. On the other hand, the production of pions in the atmosphere is known to increase rapidly with increasing primary energy.[18,19] If the pions contributed appreciably to the nucleonic chains, the specific yield would also be expected to increase appreciably with primary energy. Therefore, despite the evidence of a strong interaction with nuclear matter for single, fast pions incident on nuclei, it seems to be necessary to conclude that pions do not contribute appreciably to the development of nucleonic chains, at least for primary energies below 12.7 Bev.

Theoretical treatments of the nucleonic component, in which the development of nucleonic chains is traced down to small energies, have been given by several authors.[20–22] For large energies (greater than several Bev) the calculations are based on the Heitler-Janossy theory,[23] in which it is assumed that (1) the contribution of mesons to the nucleonic component can be neglected; (2) the interaction of a nucleon with a nucleus can be decomposed into a series of independent nucleon-nucleon collisions which develop within the nucleus in a cascade-like series of events; (3) the total nucleon-nucleon collision cross section is independent of energy; (4) the distribution function for the recoil nucleon energies is a homogeneous function of the primary energy; (5) the angular deviation of the recoils with respect to the direction of the primary nucleon can be neglected.

In detailed calculations based on the above model, Messel[22] has obtained fairly good agreement between

[17] Simpson, Baldwin, and Uretz, Phys. Rev. **84**, 332 (1951).
[18] Camerini, Davies, Fowler, Franzinetti, Muirhead, Lock, Perkins, and Yekutieli, Phil. Mag. **42**, 1241 (1951).
[19] K. Sitte, Phys. Rev. **81**, 484 (1951).
[20] B. Ferretti, Nuovo cimento **6**, 379 (1949).
[21] P. Budini and N. Dallaporta, Nuovo cimento **7**, 230 (1950).
[22] H. Messel, Phys. Rev. **83**, 21 (1951); **83**, 26 (1951).
[23] W. Heitler and L. Janossy, Proc. Phys. Soc. (London) **A62**, 374 (1949).

theory and experiment for the latitude variations of small stars. This must be considered to be spurious, however, since the primary proton energy spectrum adopted by Messel (integral power law exponent = 1.7) is in serious disagreement with the spectrum deduced from the data of Winckler and Peters (exponent ≈ 1.0); and furthermore, the presence of heavy particles in the primary radiation has been neglected. Actually, the results obtained by Messel predict a specific yield function for small star production which depends strongly on primary proton energy, even for energies above 4.1 Bev.

Instead, we have found that the proton specific yield at large atmospheric depths increases rapidly with energy up to about 4 Bev but then becomes relatively insensitive to energy up to at least 12.7 Bev. If one retains all of the assumption of the Heitler-Janossy theory, with the exception of (4), then in order to explain our results it is necessary to suppose that the energy distribution of the recoil nucleons becomes insensitive to primary energy in the range from 4.1 to at least 12.7 Bev. This would imply that nucleon-nucleon collisions are on the average fairly elastic at low energies but that the elasticity begins to fall off rapidly with increasing energy in the vicinity of 4 Bev, owing, presumably, to a strong increase in meson production. The fraction of cases in which a proton-nucleus interaction leads to meson production is indeed known to increase rapidly with proton energy up to about 4 Bev, beyond which energy nearly every interaction results in meson production.[18] However, the above description of nucleon-nucleon interactions requires further that the energy carried away by the mesons increase very rapidly with primary energy above 4.1 Bev (in order that the energy remaining to the recoil nucleons be an insensitive function of primary energy). A test of this possibility must await further experiments.

The writer wishes to thank Professor J. A. Simpson for his valuable guidance and for many illuminating discussions. Thanks are also due to Professor M. Schein for several helpful discussions.

PHYSICAL REVIEW VOLUME 86, NUMBER 6 JUNE 15, 1952

Phenomenological Relationships between Photomeson Production and Meson-Nucleon Scattering*

K. A. Brueckner and K. M. Watson
Physics Department, Indiana University, Bloomington, Indiana
(Received February 25, 1952)

Photomeson production is studied on the basis of the hypothesis of charge independence combined with the suggestion from meson theory that the meson-nucleon state of angular momentum and isotopic angular momentum equal to $\frac{3}{2}$ is one of strong, resonant interaction. Reasonable agreement with experiment is obtained, both as to the energy dependence of the cross sections and as to their ratios. Similar considerations lead to a possible explanation for the angular dependence of π^+ mesons produced in p–p collisions.

I. INTRODUCTION

OUR present theoretical understanding of meson-nucleon interactions is based upon general considerations of parity and angular momentum and upon the more detailed and less reliable models of field theory. The latter have been, perhaps, surprisingly successful in many cases in predicting orders of magnitude and qualitative features of the interactions of mesons and nucleons. One of the most interesting predictions of meson theories is that meson-nucleon interactions involve relatively few states of angular momentum. This is consistent with present experimental evidence for meson-nucleon processes. However, the lack of quantitative agreement with experiment has led one to the conclusion that (among other difficulties) neither the weak nor the strong coupling limit for meson theories is correct. In view of these shortcomings of explicit models, it seems desirable to fall back on more general phenomenological analyses of the experimental data with the hope of establishing contact with meson theory where possible.

An analysis of meson nucleon scattering along these lines was made by one of us.[1] To the usual requirements of conservation of angular momentum and parity was added that of conservation of "isotopic angular momentum."[2] The suggestion of strong P-state interactions between mesons and nucleons was borrowed from meson theory and from strong-coupling theory the notion of nucleon isobars, as well as their classification in terms of spin and isotopic spin. The resulting analysis

* Supported in part by the joint program of the ONR and AEC.

[1] K. A. Brueckner, Phys. Rev. **86**, 106 (1952).
[2] K. M. Watson and K. A. Brueckner, Phys. Rev. **83**, 1 (1951); K. M. Watson, Phys. Rev. **86**, 852 (1952), discussion of the applications of the concept of "isotopic angular momentum" conservation for meson-nucleon phenomena.

led to a simple interpretation of presently known experimental cross sections.[3]

This treatment[1] began by resolving the scattering into substates of angular momentum and isotopic angular momentum. For P-state interaction (orbital angular momentum of unity), the angular momentum of the meson-nucleon system can be resolved into states of $J=\frac{1}{2}$ and $J=\frac{3}{2}$. Similarly, the meson carries one unit of isotopic angular momentum and the nucleon one-half unit, so the total isotopic angular momentum, I, can be resolved into the states $I=\frac{1}{2}$ and $I=\frac{3}{2}$. From the isobaric nucleon levels in meson theory, one would be led to expect that the state $I=\frac{3}{2}$, $J=\frac{3}{2}$ is responsible for most of the scattering, except at low energies.

This suggestion seems to be borne out by the experimental results. However, the agreement depended upon there being strong scattering in the $I=\frac{3}{2}$ state rather than in the $J=\frac{3}{2}$ state, so it cannot be taken as direct evidence for stronger scattering in the $J=\frac{3}{2}$ state than in the $J=\frac{1}{2}$ state. Measurements of the angular distribution of the scattering should help to answer this question.

Similar considerations should apply to meson production by γ-rays. An analysis by Brueckner and Case[4] of the photoproduction of mesons did indeed lend support to the idea that nucleon isobars may play an important role in photomeson production, but their analysis was made on the basis of classical meson theory and involved an average over unquantized spins and isotopic spins. In the present paper an analysis of the photomesons cross sections will be made along the lines of the previous analysis[1] of meson-nucleon scattering. One might expect the same substates of spin and isotopic spin to be of importance in both processes.[5]

A formal analysis[6] of the role played by the isotopic spin in photomeson production suggests that such a study may be promising. The admixture of the $I=\frac{3}{2}$ state is twice as great in the neutral photomeson cross section as in the charged-meson cross section. This can be expected to help increase the π^0 cross sections at the expense of the $\pi^\pm$ cross sections. Again, the angular distribution (in particular of the π^0's) can be expected to give a means of determining the angular momentum states of the meson-nucleon system which are of importance in contributing to the cross sections.

These considerations can also be applied to meson production in nucleon-nucleon collisions. Here, because of the greater complexity, the model is less specific.

[3] Lundby, Fermi, Anderson, Nagle, and Yodh, Bull. Am. Phys. Soc. **27**, No. 1, 28 (1952); and Nagle, Anderson, Fermi, Long, and Martin, Bull. Am. Phys. Soc. **27**, No. 1, 28 (1952).

[4] K. A. Brueckner and K. M. Case, Phys. Rev. **83**, 1141 (1951).

[5] H. Miyazawa, private communication, has studied the photomeson production according to charge-symmetric pseudoscalar meson theory in the limit of almost strong coupling. His results, when interpreted on the basis of the present analysis, show that there is indeed strong interaction in the $J=\frac{3}{2}$, $I=\frac{3}{2}$ state according to meson theory. His ratios of the photo cross sections represent a special case of the general isotopic spin restrictions, which are imposed in the present paper.

[6] K. M. Watson, reference 2.

II. THE ANALYSIS OF THE PHOTOMESON CROSS SECTIONS

A. Formal Considerations

It will be simplest to calculate first the radiative absorption of mesons by nucleons and then to obtain the photoproduction cross sections by detailed balancing.

We suppose the meson absorption to take place from S- and P-states of orbital angular momentum. For charged mesons the absorption is expected to take place primarily from S-states (this is the prediction of both weak- and strong-coupling meson theory and is not in disagreement with the experimental results). For neutral mesons the strong energy dependence of the cross sections suggests that P-waves rather than S-waves are important (this also is expected from meson theory).

We shall take then the mechanism of S-wave absorption as predicted by either weak- or strong-coupling meson theory. For the P-wave absorption, the angular momentum of the system can be either $J=\frac{1}{2}$ or $\frac{3}{2}$ and the emission of a γ-ray may go by either magnetic dipole or electric quadrupole interaction (in the latter case there is only the $J=\frac{3}{2}$ state). From meson theory, we would expect magnetic dipole radiation. We shall suppose this to be the case for the present, including the other possibility later.

We suppose the meson momentum to be $\mathbf{q}$ and that this is directed along the z-axis (i.e., $\mathbf{q}=q\mathbf{k}$, where $\mathbf{k}$ is the unit vector along the z-axis). $\mathbf{K}$ is the photon momentum vector and $\hat{e}$ is its polarization vector. The z-component of the angular momentum of the system is $J_z=M$, and this is just the z-component of the nucleon spin initially since the meson is moving along the z-axis.

The outgoing photon wave corresponding to an initial total isotopic spin I for the meson and nucleon and a z-component of isotopic spin m will have the form

$$\psi_0(I,m)=-\frac{h\pi^{\frac{1}{2}}}{q}\sum_{\nu}\frac{e^{i\mathbf{K}\cdot\mathbf{r}}}{r}\xi^\nu\{u_0^{\frac{1}{2}Im}(\nu|x_0^{\frac{1}{2}}|M)$$
$$-3^{\frac{1}{2}}u_1^{\frac{1}{2}Im}(\nu|x_1^{\frac{1}{2}}|M)-3^{\frac{1}{2}}u_1^{\frac{1}{2}Im}(\nu|x_1^{\frac{1}{2}}|M)\},\quad(1)$$

where the typical term $u_l^{JIm}(\nu|x_l^J|M)$ is equivalent to an element of the general U matrix given by Wigner and Eisenbud.[7] Here the x_l^J involve spherical harmonics of the outgoing photon angular variables and polarization, ν is the z-component of the nuclear spin in the final state, ξ^ν is the final nucleon spin function. The u_l^{JIm} are independent of angle but depend on energy. The superscripts J and I refer to the total angular momentum and total isotopic spin of the initial wave; the subscript l refers to the orbital angular momentum of the meson.

According to the previously mentioned analysis[6] of the role played by the isotopic spin in photomeson production, there will be one ψ_0 for the $I=\frac{3}{2}$ state, say $\psi_0(\frac{3}{2})$, and two sets of ψ_0's for the $I=\frac{1}{2}$ state which

[7] E. P. Wigner and L. Eisenbud, Phys. Rev. **72**, 29 (1947).

depend not only on the total isotopic spin but also on the total charge (related to the z-component of the isotopic spin). These we denote by $\psi_0(\frac{1}{2}+)$ and $\psi_0(\frac{1}{2}-)$, the first state corresponding to a total charge of zero and the second to a total charge of one. Thus for each angular momentum state there are three ψ_0's, corresponding to the three isotopic states, there being 9 of these quantities. From the general theory[8] we can obtain the form of the outgoing waves for initial charge eigenstates of the meson and nucleon.

$$\begin{aligned}
&\psi_0(\pi^0+n\to n+\gamma)=[\sqrt{2}\psi_0(\tfrac{3}{2})-\psi_0(\tfrac{1}{2}+)]/\sqrt{3},\\
&\psi_0(\pi^0+p\to p+\gamma)=[\sqrt{2}\psi_0(\tfrac{3}{2})-\psi_0(\tfrac{1}{2}-)]/\sqrt{3},\\
&\psi_0(\pi^-+p\to n+\gamma)=[\psi_0(\tfrac{3}{2})+\sqrt{2}\psi_0(\tfrac{1}{2}+)]/\sqrt{3},\\
&\psi_0(\pi^++n\to p+\gamma)=[\psi_0(\tfrac{3}{2})+\sqrt{2}\psi_0(\tfrac{1}{2}-)]/\sqrt{3}.
\end{aligned}\tag{2}$$

We note that the u's in Eq. (1) are the only quantities depending upon the isotopic spin, so the transformation (2) is really a transformation of the u's alone.

We observe two interesting qualitative features of Eq. (2).[9] First, if the absorption from P-states is predominantly due to the $I=\frac{3}{2}$ state, it will lead to an absorption rate for neutral mesons which is twice as great as that for charged mesons (from P-states only, of course). This can be expected to help increase the π^0 photoproduction cross section at the expense of that for the π^+ mesons, except near threshold, which is in agreement with the measured cross section.[10] Second, the $I=\frac{3}{2}$ state enters with equal weight into the cross sections for photoproduction of mesons on both neutrons and protons, so we would expect approximately equal cross sections in both cases for those energies at which the $I=\frac{3}{2}$ state gives the major contribution. This too seems to be in agreement with recent experiments.[11]

We turn next to the analysis of the angular momentum states occurring in Eq. (1). Since ψ_0 must remain invariant if the entire scattering system is rotated in space, we know that the x's must be pseudoscalar combinations (i.e., supposing the meson to be pseudoscalar) of the vectors $\mathbf{k}=\mathbf{q}/q$, $\hat{e}$, $\mathbf{K}$, and $\boldsymbol{\sigma}$, the nucleon spin. For capture of the meson from an S-state we have the unique form

$$(\nu|x_0^{\frac{1}{2}}|M)=(8\pi)^{-\frac{1}{2}}(\xi^\nu,\boldsymbol{\sigma}\cdot\hat{e}\xi^M),\tag{3}$$

which is also that given by meson theory. The ξ's are spin wave functions, and the factor $(8\pi)^{-\frac{1}{2}}$ is chosen to agree with the Wigner-Eisenbud[7] normalization.

For the capture of a meson from an orbital P-state, the incoming wave function has the form

$$\varphi=\mathbf{k}\cdot\mathbf{r}\xi^M \text{ times a function of } |\mathbf{r}|.\tag{4}$$

To resolve this into eigenstates of J, we note that ξ^M corresponds to $J=\frac{1}{2}$ and so does

$$\boldsymbol{\sigma}\cdot\mathbf{r}\xi^M,$$

since the latter form transforms under rotations like ξ^M. Then

$$\varphi_{\frac{1}{2}}{}^M=\mathbf{k}\cdot(\mathbf{r}-\tfrac{1}{3}\boldsymbol{\sigma}\cdot\mathbf{r}\boldsymbol{\sigma})\xi^M\tag{5}$$

is a state of $J=\frac{1}{2}$ since it is orthogonal to $\boldsymbol{\sigma}\cdot\mathbf{r}\xi^M$. The appropriate $J=\frac{3}{2}$ state is

$$\varphi_{\frac{3}{2}}{}^M=\tfrac{1}{3}\boldsymbol{\sigma}\cdot\mathbf{r}\boldsymbol{\sigma}\cdot\mathbf{k}\xi^M\tag{6}$$

(being just $\pm\frac{1}{3}\boldsymbol{\sigma}\cdot\mathbf{r}\xi^M$), since the sum of Eqs. (5) and (6) gives us a wave function of the type (4).

The outgoing photon wave function is also to be resolved into eigenstates of J. For magnetic dipole radiation it is simpler to use the pseudovector $\mathbf{K}\times\hat{e}$ rather than the spherical harmonics. From Eqs. (5) and (6), we see that

$$\begin{aligned}
&K(\nu|x_1^{\frac{1}{2}}|M)=(3/8\pi)^{\frac{1}{2}}(\xi^\nu,[\mathbf{K}\times\hat{e}\cdot\mathbf{k}-\tfrac{1}{3}\boldsymbol{\sigma}\cdot\mathbf{K}\times\hat{e}\boldsymbol{\sigma}\cdot\mathbf{k}]\xi^M),\\
&K(\nu|x_1^{\frac{1}{2}}|M)=(3/8\pi)^{\frac{1}{2}}(\xi^\nu,[\tfrac{1}{3}\boldsymbol{\sigma}\cdot\mathbf{K}\times\hat{e}\boldsymbol{\sigma}\cdot\mathbf{k}]\xi^M).
\end{aligned}\tag{7}$$

That these are the correct expressions can be seen if one substitutes them into Eq. (1). The resulting expression for the outgoing photon wave contains terms of the form of (5) and (6), in which $\mathbf{K}\times\hat{e}$ replaces $\mathbf{r}$.

For electric quadrupole radiation the symmetric tensor $\frac{1}{2}(K_ie_j+e_iK_j)$ enters into the x's, and we have only $J=\frac{3}{2}$. Thus

$$\begin{aligned}
&K(\nu|x,^{\frac{1}{2}}(\text{e.q.})|M)\\
&\qquad=(8\pi)^{-\frac{1}{2}}(\xi^\nu,\tfrac{1}{2}[\boldsymbol{\sigma}\cdot\mathbf{K}\hat{e}\cdot\mathbf{k}+\boldsymbol{\sigma}\cdot\hat{e}\mathbf{K}\cdot\mathbf{k}]\xi^M).
\end{aligned}\tag{8}$$

The cross section for absorption (neglecting electric quadrupole radiation) is obtained from Eq. (1),

$$\begin{aligned}
\frac{d\sigma(\text{abs})}{d\Omega}=\frac{\pi\hbar^2}{2q^2}\sum_{\nu,M,s}&|A(\nu|x_0^{\frac{1}{2}}|M)-3^{\frac{1}{2}}B(\nu|x_1^{\frac{1}{2}}|M)\\
&-3^{\frac{1}{2}}C(\nu|x_1^{\frac{1}{2}}|M)|^2,
\end{aligned}\tag{9}$$

where A, B, and C are those linear combinations of the u's in Eq. (1) which are given by the appropriate expression (2). By detailed balancing we obtain from Eq. (9) the photoproduction cross sections:

$$\begin{aligned}
d\sigma/d\Omega=(\hbar^2/8K^2)\{&|A|^2+|B|^2+\tfrac{1}{2}|C|^2(5-3\cos^2\theta)\\
&-2\,\mathrm{Im}[A^*(B-C)]\cos\theta\\
&-\tfrac{1}{2}\,\mathrm{Re}(B^*C)(3\cos^2\theta-1)\},
\end{aligned}\tag{10}$$

where θ is the angle between $\mathbf{K}$ and $\hat{e}$. For the total cross section, we have

$$\sigma=(\pi\hbar^2/4K^2)\{2|A|^2+2|B|^2+4|C|^2\}.\tag{11}$$

For pure electric quadrupole radiation [Eq. (8)], the angular distribution would be of the form

$$1+\cos^2\theta.\tag{12}$$

[8] The correspondence between the ψ_0's of Eq. (2) and the matrix elements T_1, T_2, and S_0 of reference 6 is

$$\psi_0(\tfrac{3}{2})\to\sqrt{2}T_2,\quad \psi_0(\tfrac{1}{2}+)\to\tfrac{1}{3}T_1+S_0,\quad \psi_0(\tfrac{1}{2}-)\to\tfrac{1}{3}T_1-S_0.$$

[9] Heckrotte, Henrich, and Lepore [Phys. Rev. **86**, 490 (1952)] have remarked that there should be constructive interference of the meson wave amplitudes for neutral photomeson production from deuterium if one assumes the couplings of symmetric-meson theory and the results of a perturbation calculation. Reference to Eq. (2) shows that this would be expected quite generally if production into the $I=\frac{3}{2}$ state is predominant.

[10] Panofsky, Steinberger, and Stellar, Phys. Rev. **86**, 180 (1952).

[11] A. Silverman and G. Cocconi, Bull. Am. Phys. Soc. **27**, No. 1, 27 (1952).

B. Detailed Development of the Model

We can now introduce considerable simplification into the general expression for the cross section of Eq. (10) if we make use of the results of the analysis of the scattering of mesons by nucleons. There it was shown that when the meson was in a P-state, the assumption of strong interaction in the $I=\frac{3}{2}$ state gave a good description of the ratios observed for the various processes of meson scattering. The assumption was also made that the interaction was strong in the $J=\frac{3}{2}$ state, since then the strength of the interaction could be associated with the excitation of a nucleon isobar with $I=\frac{3}{2}$, $J=\frac{3}{2}$ which is in accord with the predictions of strong coupling meson theory. We shall assume that this is also so for the photoproduction. The resulting angular dependence of the cross section can then of course be subjected to experimental verification. We shall also draw on one of the most striking features of the neutral photomeson cross section: that it increases rapidly with energy from very small values at low energies. This is due to the near absence of a contribution from meson S-states, presumably, and to the strong energy dependence to be expected from states of higher angular momentum. This feature is also given by meson theory where the large S-state contribution is present only for charged mesons. From Eqs. (1) and (2), the S-state term for neutral mesons is proportional to

$$-[u_0^{\frac{1}{2}\frac{1}{2}m}+\sqrt{2}u_0^{\frac{1}{2}\frac{1}{2}}]/\sqrt{3},$$

which is to vanish, fixing the relation

$$u_0^{\frac{1}{2}\frac{1}{2}}=u_0^{\frac{1}{2}\frac{1}{2}m}/\sqrt{2}, \tag{13}$$

which also shows that $u_0^{\frac{1}{2}\frac{1}{2}m}$ is independent of m because of the independence of m in the $I=\frac{3}{2}$ states.

Collecting these results, we find for the differential cross sections

$$\frac{d\sigma(\text{charged})}{d\Omega}=\frac{\hbar^2}{24K^2}\{(9/2)|u_0^{\frac{1}{2}\frac{1}{2}}|^2+\tfrac{1}{2}|u_1^{\frac{1}{2}\frac{1}{2}}|^2(5-3\cos^2\theta)$$
$$+3\sqrt{2}\,\mathrm{Im}[(u_0^{\frac{1}{2}\frac{1}{2}})^*u_1^{\frac{1}{2}\frac{1}{2}}]\cos\theta\}, \tag{14}$$
$$\frac{d\sigma(\text{neutral})}{d\Omega}=\frac{\hbar^2}{24K^2}|u_1^{\frac{1}{2}\frac{1}{2}}|^2(5-3\cos^2\theta).$$

The elements of the u matrix which enter into these expressions can now be expressed in terms of the generalized one-level formulas of Wigner and Eisenbud. The result is

$$u_l^{JI}=\frac{[\Gamma_l^{JI}(\pi)]^{\frac{1}{2}}[\Gamma_l^{JI}(\gamma)]^{\frac{1}{2}}}{E_l^{JI}-E-i\frac{1}{2}\Gamma_l^{JI}}, \tag{15}$$

where $\Gamma_l^{JI}(\pi)$ is the meson width, $\Gamma_l^{JI}(\gamma)$ is the gamma-width, E_l^{JI} is the resonance energy, and Γ_l^{JI} is the total width. The meson width is much greater than the gamma-width, corresponding to the much larger probability of scattering than of radiation, so the total width can be taken equal to the meson width. This equation, which is of the form given by Feshbach, Peaslee, and Weisskopf,[12] is valid only near resonance; the more general form of Wigner and Eisenbud contains explicitly a level shift but can be approximated by a formula of this type.

The resonance energy $E_1^{\frac{1}{2}\frac{1}{2}}$ and level width $\Gamma_1^{\frac{1}{2}\frac{1}{2}}$ have been given previously[1] in connection with the analysis of meson scattering. The assignment made there, which gave a good description of the scattering, was that

$$E_1^{\frac{1}{2}\frac{1}{2}}\equiv E_R=137\text{ Mev},$$
$$\frac{\Gamma_1^{\frac{1}{2}\frac{1}{2}}}{2E_1^{\frac{1}{2}\frac{1}{2}}}\equiv\rho=\rho_0\frac{q^3/\mu^3c^3}{1+(q^2a^2/\hbar^2)},\quad \rho_0=0.23, \tag{16}$$

where the parameter ρ_0 is independent of energy and is related to the reduced width of Wigner and Eisenbud; μ is the mesonic rest mass; a is the radius of the internal region of strong interaction. For the meson emitted into an S-state, both weak and strong coupling theory give an assignment to the energy $E_0^{\frac{1}{2}I}$ which is

$$|E_0^{\frac{1}{2}I}|\gg\mu c^2,$$

so that the kinetic energy E can be neglected relative to $E_0^{\frac{1}{2}I}$. For this state we shall in addition neglect the level width relative to $E_0^{\frac{1}{2}I}$. The energy variation of the u_l^{IJ} also depends on the level widths; the widths depend on K^{2l+1}, where K is the momentum. Accordingly, we can write

$$u_0^{\frac{1}{2}\frac{1}{2}}\simeq\alpha q^{\frac{1}{2}}K^{\frac{1}{2}}/\mu c,$$
$$u_1^{\frac{1}{2}\frac{1}{2}}=\beta\frac{q^{\frac{1}{2}}K^{\frac{1}{2}}}{\mu^3c^3}\frac{1}{1-E/E_R-i\rho}, \tag{17}$$

where the new dimensionless parameters α and β defined by these equations are independent of the energy.

The differential cross sections of Eq. (14) can now be expressed entirely in terms of these two constants (in general complex), with the energy and angular dependence completely specified. The constants α and β can be determined from experiment. It is interesting, however, to point out that they are given by meson theory and that their ratio is independent of the meson coupling constant. The weak coupling perturbation treatment, including the effects of the nucleon magnetic moments in nonrelativistic approximation gives

$$\alpha=-\frac{2}{\sqrt{3}\pi}g e,\quad \beta=+\frac{\sqrt{2}}{6}\frac{\mu}{M}(|\gamma_N|+|\gamma_P|)\alpha. \tag{18}$$

Here M is the nucleonic rest mass. γ_N and γ_P are the respective values of the neutron and proton magnetic moments in units of $e\hbar/2Mc$, where e is the charge on

[12] Feshbach, Peaslee, and Weisskopf, Phys. Rev. **71**, 145 (1947).

a proton. The total cross sections, with these values of α and β, are

$$\sigma(\text{charged})=\frac{g^2e^2}{\pi}\frac{q}{K}\frac{\hbar^2}{\mu^2c^2}+\tfrac{1}{2}\sigma(\text{neutral}),$$

$$\sigma(\text{neutral})=\frac{g^2e^2}{\pi}\frac{q}{K}\frac{\hbar^2}{\mu^2c^2}\left\{\frac{4}{81}\frac{q^2K^2}{M^2\mu^2c^4}(|\gamma_N|+|\gamma_P|)^2\times\frac{1}{(1-E/E_R)^2+\rho^2}\right\}. \quad (19)$$

In Fig. 1 are plotted the cross sections (19), with g chosen to fit the magnitude of the π^+ cross section to the observed value.[13] The contribution from the remaining spin and isotopic spin states was estimated by the method used[1] in connection with meson-nucleon scattering (i.e., by fitting at low energies the formal expression (1) to that obtained from perturbation theory). These further terms gave only a very small contribution to the cross sections.

We note that if we increase the nucleon magnetic moments by a factor of about 1.5 (corresponding to an energy dependence of the moments) we can make the neutral cross section larger than the charged near the resonance energy, in contrast to the predictions from classical meson theory.[4]

In Fig. (2) are plotted the predicted differential cross sections at 90° in the laboratory system. It is to be noted that the only arbitrary parameter used was g [Eq. (19)], which was chosen to fit the magnitude of the total charged meson cross section at 255 Mev. The ratio of the two cross sections is given by the theory. The fit to the experimental data of Steinberger and Bishop[13] and of Silverman and Stearns[14] seems reasonable, considering that the static values of the nucleon magnetic moments were used.

The angular distribution of the π^0 mesons from the $J=\frac{3}{2}$ state is $5-3\cos^2\theta$ in the center-of-mass system. This term is also present for the charged mesons, but is less important because of the large S-state contribution. The interference of these two terms is such as to shift the peak at 90° to somewhat larger angles. This is in qualitative agreement with the angular distribution of Steinberger and Bishop,[13] but the resulting angular asymmetry seems to be somewhat less than they find. Use of the complete meson current interaction as given by meson theory would probably help in obtaining more precise agreement.[15] Because of the inherent crudity of the present model we have not considered such refinements of the theory (the effects of which are expected from meson theory to be small).

[13] J. Steinberger and A. S. Bishop, Phys. Rev. **86**, 171 (1952).
[14] A. Silverman and M. Stearns, Phys. Rev. **83**, 206 (1951).
[15] K. A. Brueckner, Phys. Rev. **79**, 641 (1950).

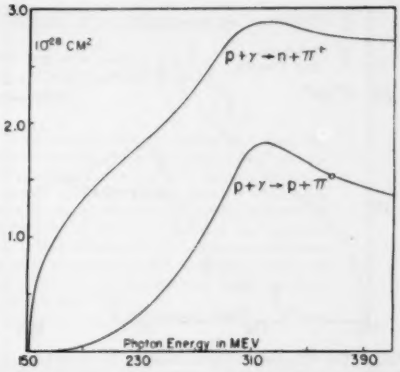

FIG. 1. The total cross sections as a function of photon energy in the laboratory system for the production of mesons from protons as predicted by the model. The only arbitrary parameter was a normalization factor used to fit the π^+ cross section at 255 Mev to that measured by Steinberger and Bishop.

III. MESON PRODUCTION IN NUCLEON-NUCLEON COLLISIONS

We shall be particularly concerned with the reaction[16] $p+p\rightarrow\pi^++d$ and its inverse.[17] An analysis[18] of the experimental results indicated that the meson is emitted predominantly into P-states. From this it was concluded that the ^1S and ^1D states of the initial p–p system contribute to the cross section. The angular distribution of the mesons (which looks approximately like $\cos^2\theta$) is then determined by the admixture of $^1S(J=0)$ and $^1D(J=2)$ states. The outgoing wave is then of the form[19]

$$(e^{i\varphi r}/r)[Q_0+\eta Q_2{}^0]\textstyle\sum_0\omega(1^+), \quad (20)$$

where Q_0 and $Q_2{}^0$ are those linear combinations of the spherical harmonics of order one and the deuteron wave function which correspond to states of angular momentum with $J=0$ and $J=2$, respectively. Σ_0 is the isotopic spin (singlet) part of the wave function of the nucleons and $\omega(1^+)$ is a symbolic factor in the wave function which implies that the meson is positive. η is a complex parameter.

The formal requirements of charge independence for the processes of meson production in nucleon-nucleon collisions have been given previously.[18] These are expected to constitute an exceedingly severe test of the hypothesis of charge independence when sufficient experimental data are available. Aside from this, however, if the suggestion introduced[1] in connection with

[16] Cartwright, Richman, Whitehead, and Wilcox, Phys. Rev. **78**, 823 (1950); C. Richman and M. H. Whitehead, Phys. Rev. **83**, 855 (1951); Peterson, Iloff, and Sherman, Phys. Rev. **84**, 372 (1951).
[17] Durbin, Loar, and Steinberger, Phys. Rev. **84**, 581 (1951); Clark, Roberts, and Wilson, Phys. Rev. **83**, 649 (1951).
[18] K. Watson and K. Brueckner, Phys. Rev. **83**, 1 (1951).
[19] K. Watson and C. Richman, Phys. Rev. **83**, 1256 (1951).

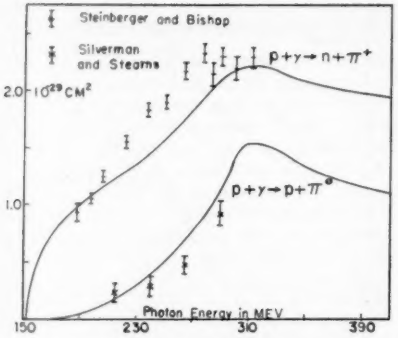

FIG. 2. The differential cross sections for the production of π^+ and π^0 mesons at 90° in the laboratory system. The only arbitrary parameter used was that of Fig. 1, which normalized the total cross section at 255 Mev to the observed value. The ratio of the two cross sections is given by the theory. The experimental data are from Steinberger and Bishop (reference 13) and Silverman and Stearns (reference 14).

meson scattering that the state ($J=\frac{3}{2}$, $I=\frac{3}{2}$) of a meson and single nucleon is a state of strong interaction, one would expect to find it also playing an important role here.

The situation is complicated by the presence of the second nucleon and consequently our model will not be so specific as before. We can expect, in general, nonlinear effects in the meson field which might tend to obscure the details of the individual meson-nucleon interaction. On the other hand, predominantly strong interactions, say in the $I=\frac{3}{2}$, $J=\frac{3}{2}$ state of the meson and either nucleon, would be expected to lead to anomalously large production cross sections from this state. To investigate such an effect in a qualitative manner, we can resolve Eq. (20) into eigenstates of angular momentum and isotopic angular momentum of the meson with respect to one of the nucleons. We use the symbols j_1, j_2 and i_1, i_2 to denote these respective quantities with respect to the nucleons "1" and "2" in the deuteron.

In considering only the reaction $p+p\rightarrow\pi^++d$ the isotopic spin properties will give us no information. However, the angular momentum considerations will give conditions on the angular distribution of the mesons.

We introduce the projection operators

$$E_{\frac{1}{2}}^{(i)}=-\tfrac{2}{3}[\mathbf{l}\cdot\mathbf{s}_i-\tfrac{1}{2}],\quad E_{\frac{3}{2}}^{(i)}=\tfrac{2}{3}[\mathbf{l}\cdot\mathbf{s}_i+1], \tag{21}$$

where the index i refers to nucleon "1" or nucleon "2". $\mathbf{l}$ is the orbital angular momentum of the meson with respect to either nucleon (assumed to a sufficient approximation to be the same as that with respect to the deuteron). $\mathbf{s}_i$ is the spin operator of the nucleon "i". $E_{\frac{1}{2}}^{(i)}$ is zero or unity, depending upon whether $j_i=\frac{3}{2}$ or $\frac{1}{2}$, respectively. $E_{\frac{3}{2}}^{(i)}$ is the corresponding projection operator for the $j_i=\frac{3}{2}$ state.

Returning to Eq. (20), we observe that

$$\begin{aligned} &E_{\frac{1}{2}}^{(i)}Q_0=Q_0, \quad E_{\frac{3}{2}}^{(i)}Q_0=0, \\ &E_{\frac{1}{2}}^{(i)}Q_2{}^0=0, \quad E_{\frac{3}{2}}^{(i)}Q_2{}^0=Q_2{}^0. \end{aligned} \tag{22}$$

Thus if the $j=\frac{3}{2}$ state is one of strong interaction, one might expect the term $Q_2{}^0$ to be predominant in Eq. (20)—i.e., η large. For strong interaction in the $j=\frac{1}{2}$ state only, one would expect η to be small and the Q_0 term to contribute. The angular distribution from either of these terms alone is

$$\begin{aligned} &Q_0\text{: spherically symmetric,} \\ &Q_2{}^0\text{: } 3\cos^2\theta+1. \end{aligned} \tag{23}$$

The first possibility is in definite disagreement with experiment, so we conclude that the $j=\frac{1}{2}$ interaction is not predominant in this case. The second possibility is perhaps a little more spherically symmetric than is indicated by present experiments, but is roughly correct. We further note that $|\eta|$ can be taken of the order of 5 to 10 (with the right phase) to give quite satisfactory agreement with experiment. This then is consistent with the previous conclusion[1] of a strong interaction in the $j=\frac{3}{2}$ state—and may indeed be a first step in the explanation of the observed angular distribution.

IV. CONCLUSIONS

A general analysis of the photomeson cross sections has been made on the assumption that only meson S- and P-waves are of importance. These have been given a simple form on basis of the joint hypotheses of charge independence and resonant interaction of the meson and nucleon in the $J=\frac{3}{2}$, $I=\frac{3}{2}$ state. Specific predictions are then obtained as to the energy and angular dependence of the cross sections. The agreement with present experimental measurements of these cross sections is reasonable (see Fig. 2).

These same considerations can be applied in a somewhat more qualitative manner to the production of mesons in nucleon-nucleon collisions. Here we obtain what may be a partial explanation of the angular distribution of π^+ mesons produced in p–p collisions.

Thermal Ionization of Trapped Electrons

RYOGO KUBO*
Institute for the Study of Metals, University of Chicago, Chicago, Illinois
(Received November 23, 1951)

The rate of thermal ionization of an electron trapped on an impurity atom is treated on a quantum mechanical basis. From the standpoint of an adiabatic approximation, the multiphonon transitions are attributed to the dependence of the atomic vibrations on the electronic states. Approximate formulas based on an Einstein model are derived for the total ionization rate by using a generating function which is intimately related to density matrices. It is shown that the rate can be expressed as $256(m/M)\omega(\rho/2)^{\epsilon_0/\hbar\omega-1}\exp(-\epsilon_0/kT)$ for low temperatures, where m is the mass of electron, M that of the atom, ω the frequency of atomic vibration, ϵ_0 the energy of ionization, and ρ is the fractional difference of the frequencies of atomic vibrations in the trapped and the ionized states, which can be of the order 0.1. For high temperatures we can expect a similar formula to that given by the activated states theory. Generally, we have reasons to expect much greater rates than those given by Goodman, Lawson, and Schiff.

INTRODUCTION

IN semiconductors and luminescent materials, electron traps play important roles in various electronic processes. The trapped electrons can be thrown up into free states by absorbing the energy of incident light, of impacting particles, or of the vibration of surrounding atoms; and conversely, a conduction electron can be trapped at a trapping center, radiating part of its energy as a photon or phonons. Quantum-mechanical theories of such elementary reaction processes are needed for thorough studies of solid-state electronics.

In this article, we confine ourselves to the study of the third process mentioned above, that is, the thermal ionization of trapped electrons. To clarify the nature of this process, one has to consider the interrelation of the electronic and vibrational states of the crystal in more detail than in the usual cases, such as in the theory of electronic conduction, because, in contrast to the latter process, thermal ionization is essentially a multiphonon process.

Twenty years ago, in his theory of the dissipation of light energy absorbed in insulating crystals, Frenkel[1] pointed out that slight differences between the modes of lattice vibrations in the electronically excited states and those in the ground state are responsible for the multiphonon emission which takes place when the electron goes back to the normal state. Möglich and Rompe,[2] on the other hand, insisted that the higher terms in the expansion of the interaction potential between the electron and the lattice give the probabilities of multiphonon jumps. Their theory was used by Riehl[3] for an explanation of luminescent phenomena. Mathematical difficulties, however, forced them to forego a quantitative treatment and to content themselves with a qualitative discussion.

More recently Goodman, Lawson, and Schiff[4] presented a simple theory of the thermal ionization process in semiconductors along similar lines to that of Möglich and Rompe. Their calculation shows that the ionization rate will decrease by the factor 10^{-6} as the ionization energy increases by $\hbar\omega$, that is the energy of a phonon. This leads one to a surprisingly small probability for the thermal ionization process of impurity levels.

The writer feels that the latter analysis is inadequate, for reasons to be clarified in the following sections. Hence, he wishes to present another theory concerned with the same problem, based on the idea of Frenkel, but differing from it in some essential points. Owing to mathematical difficulties, we also do not give any detailed treatment of actual crystals but confine ourselves to a discussion of a simplified model. Our result, however, shows that we can expect much larger probabilities for the multiphonon jumps. This conclusion will be important for the understanding, for instance, of semiconductor rectifiers. Moreover, the theory presented here will be interesting as an example of a purely quantum mechanical treatment of the reaction rate problem. The use of density matrices for such problems proves to be very helpful.

I. COUPLING BETWEEN THE LATTICE AND THE ELECTRON

Generally speaking, the Hamiltonian of a polyatomic system is of the form

$$H=H_R+H_r+V, \tag{1}$$

where H_R is the sum of the kinetic energy terms of the nuclei and their interaction potentials, H_r the similar expression for the electron system, and V the interaction energy between the nuclei and the electrons. As is well known, we can seek the eigenstates of the Hamiltonian along the lines of the adiabatic potential method. Considering the coordinates $\mathbf{R}$ of the nuclei as fixed, the eigenvalue equation,

$$[H_r+V(\mathbf{r},\mathbf{R})]\varphi_l(\mathbf{r},\mathbf{R})=E_l'(\mathbf{R})\varphi_l(\mathbf{r},\mathbf{R}), \tag{2}$$

* On leave from the Department of Physics, University of Tokyo, Tokyo, Japan.
[1] J. Frenkel, Phys. Rev. **37**, 17 and 1276 (1931); Physik. Z. Sowjetunion **9**, 158 (1936).
[2] F. Möglich and R. W. Rompe, Z. Physik **115**, 707 (1940).
[3] N. Riehl, *Physik und technische Anwendungen der Lumineszenz* (Verlag. J. Springer, Berlin, 1941).
[4] Goodman, Lawson, and Schiff, Phys. Rev. **71**, 191 (1947).

gives the adiabatic potential $E_l'(\mathbf{R})$ for the lth electronic state. Then in this electronic state the motion of the nuclear system is determined by

$$[H_R+E_l'(\mathbf{R})]\zeta_{lv}(\mathbf{R})=E_{lv}\zeta_{lv}(\mathbf{R}). \tag{3}$$

Thus a quantum state of the whole system is specified by the quantum numbers l and v, and the wave function takes the form

$$\Psi_{lv}(\mathbf{r},\mathbf{R})=\varphi_l(\mathbf{r},\mathbf{R})\zeta_{lv}(\mathbf{R}). \tag{4}$$

As shown by Born and Oppenheimer,[5] this wave function is a good approximation for stationary states. Wigner and Pelzer[6] have also shown that the adiabatic method is justified for some chemical reactions under certain conditions.

It is clear, however, that we must look for the perturbation causing the transition between different electronic states just in the approximate nature of the wave functions given by Eq. (4) if we are interested in such processes as thermal excitation. In fact, we can write

$$\begin{aligned}H\Psi_{lv}(\mathbf{r},\mathbf{R})&=[H_R+E_l'(\mathbf{R})]\zeta_{lv}(\mathbf{R})\varphi_l(\mathbf{r},\mathbf{R})\\&=E_{lv}\Psi_{lv}+H'\Psi_{lv},\end{aligned}$$

where

$$H'\Psi_{lv}\equiv H_R\zeta_{lv}\varphi_l-\varphi_l H_R\zeta_{lv}, \tag{5}$$

does not vanish because of the differentiation operators in H_R. Thus we are forced to seek a solution of the form

$$\Psi=\sum a_{lv}(t)\Psi_{lv}(\mathbf{r},\mathbf{R}). \tag{6}$$

Inserting Ψ into the time dependent wave equation, we obtain the equation,

$$i\hbar\dot{a}_{lv}=\sum_{l'v'}(lv|H|l'v')a_{l'v'}, \tag{7}$$

where the relation,

$$(lv|H|l'v')=E_{lv}\delta_{lv,l'v'}+(lv|H'|l'v'), \tag{8}$$

holds because of the orthogonality relations

$$\int\varphi_l^*(\mathbf{r},\mathbf{R})\varphi_{l'}(\mathbf{r},\mathbf{R})d\mathbf{r}=\delta_{ll'},$$

$$\int\zeta_{lv}^*(\mathbf{R})\zeta_{lv'}(\mathbf{R})d\mathbf{R}=\delta_{vv'},$$

which follow from Eqs. (2) and (3).

From a physical point of view the eigenstates described by Eq. (4) must be considered as "good." Nevertheless it is important to recognize that they are not stationary in the exact sense, and that the whole system oscillates to and fro among various good quantum states of almost the same energy. This should be interpreted as the transition from one electronic state to another, accompanied by a transition in the quantum states of the nuclear motion.[7]

The ordinary time-dependent perturbation method gives at once the transition probability from the initial (l, v) to a final $(l'v')$ state as

$$w(lv\to l'v')=(2\pi/\hbar)|(lv|H'|l'v')|^2\rho_f, \tag{9}$$

where ρ_f is the state density of the final state, and the $(l'v')$ must satisfy the law of conservation of energy,

$$E_{l'v'}=E_{lv}. \tag{10}$$

In the ionization case, the final state is that in which an electron is set free. Hence, ρ_f is approximated by

$$\rho_f=4\pi\Omega m^*hk/h^3, \tag{11}$$

where Ω is the volume of the space under consideration, m^* the effective mass of the free electron, and $\mathbf{k}$ its wave number.

The idea outlined above can be widely applied to other problems, but at present we confine ourselves to a treatment of a simplified model similar to that discussed by Goodman, Lawson, and Schiff.[4]

II. A SIMPLIFIED MODEL OF TRAPPED ELECTRONS

Suppose that a substitutional impurity atom creates a trapping center, where an electron can be trapped with a localized wave function φ_0. Strictly speaking, φ_0 is a function of the configuration of all the atoms in the crystal. However, to clarify the nature of our problem and to get a simple approximation, we assume there that only the instantaneous positions of the impurity atom affects the wave function φ_0 strongly and that the dependence of φ_0 upon the motion of other atoms can be neglected. Thus, the wave function φ_0 is regarded as a function of $\mathbf{r}$ and $\mathbf{R}$, which are the coordinates of the trapped electron and of the impurity atom, respectively. Moreover, we introduce another simplification by using an Einstein model for the vibrational motion of the atoms. In a more rigorous theory this model should be replaced by the Debye model.

With such a simplified model, it is clear that the difference of the modes of vibration, that is the difference of the vibrational frequencies of the central atom in the ground and the excited electronic states, is the cause of the multiphonon jump in the process of thermal ionization.

The Hamiltonian of the simplified model will be

[5] M. Born and F. Oppenheimer, Ann. Physik **84**, 457 (1927).
[6] H. Pelzer and E. Wigner, Z. physik Chem. **B15**, 445 (1932).

[7] This point of view has also been adopted by K. Huang and A. Rhys [Proc. Roy. Soc. (London) **A204**, 406 (1950)], who have discussed the light absorption and nonradiative transition of F-centers. Assuming a continuum model of a crystal they have treated the vibrational motion of the nuclei as lattice waves, which is, in principle, more rigorous than the Einstein model assumed in the present paper, and they gave the probabilities of nonradiative transitions in terms of the difference of the equilibrium positions of the lattice atoms between different electronic states. The author was not aware of their work when he prepared the present paper, and he wishes to leave detailed discussion to a later paper.

written as

$$H=-(\hbar^2/2M)\Delta_R+U_0(\mathbf{R})-(\hbar^2/2m)\Delta_r +V'(\mathbf{r})+V(\mathbf{R}-\mathbf{r}), \quad (12)$$

where M is the mass of the impurity atom, and $U_0(\mathbf{R})$ its interaction with the surrounding crystal atoms. $V(\mathbf{R}-\mathbf{r})$ and $V'(\mathbf{r})$ mean the Hartree fields of the electron associated with the central atom and the neighboring atoms, respectively. Although in fact $V'(\mathbf{r})$ depends on the configuration of the surrounding atoms, we have not taken this into consideration in our present simplified model.

Goodman, Lawson, and Schiff have assumed that

$$V(\mathbf{R}-\mathbf{r})=Ze^2/|\mathbf{R}-\mathbf{r}|,$$

and that $\mathbf{R}$ can be expressed as

$$\mathbf{R}=\mathbf{R}_0+\delta\mathbf{R}=\mathbf{R}_0+\sum_j \mathbf{a}_j \exp[i(\omega_j t-\mathbf{k}_j\mathbf{R}_0)].$$

Thus, expanding V in a power series of $\delta\mathbf{R}$, they obtained the probability of the multiphonon jumps from the higher terms of the expansion. It is essentially at this point that the author feels their treatment is inadequate, since the electronic state of the trapped electron should follow adiabatically the changes in $\mathbf{R}$. It is clear that any periodic displacement of the nucleus of a hydrogen atom cannot cause the ionization of its electron, unless the frequency is very high. It is true that the adiabatic approximation breaks down if the electronic energy of the excited state is very near to the ground state, in our case, for example, if the ionization energy is very small. In such cases, both theories, that of Goodman, Lawson, and Schiff and that of the writer, will give a large probability just for $w\sim\omega$, which shows that the trapped state has no real meaning. But for other cases the two theories give definitely different pictures. It should also be noticed that the situation is different for the scattering of metal electrons by lattice waves. In this case the Bloch waves of electrons remain a good approximation even for a deformed lattice, and the excitation of a few electrons has no effect on the modes of the lattice vibrations, so that the ordinary conduction theory is justifiable from a physical point of view. However, in our case, so long as we consider the wave function of the trapped electron to be localized around the impurity atom, we have to admit that the ionization definitely changes the binding of the impurity to its neighbors.

From the standpoint adopted in Sec. 1, we take

$$H'\zeta_{lv}\varphi_l\equiv-(\hbar^2/2M)(\Delta_R\zeta_{lv}\varphi_l-\varphi_l\Delta_R\zeta_{lv}), \quad (13)$$

for the reasons explained above. For our simplified model, φ_0 is a function of $(\mathbf{r}-\mathbf{R})$, so that we may write

$$\nabla_R\varphi_0=-\nabla_r\varphi_0.$$

Hence Eq. (13) is of the form

$$H'\zeta_{0v}\varphi_0=-(1/M)(\mathbf{P}\zeta_{0v}\cdot\mathbf{p}\varphi_0-\tfrac{1}{2}\zeta_{0v}\mathbf{p}^2\varphi_0), \quad (14)$$

where $\mathbf{P}$ is the momentum operator of the central atom and $\mathbf{p}$ that of the electron. Thus the matrix element in Eq. (9) is given by

$$(0v|H'|kv')=-\frac{1}{M}\int d\mathbf{R}\zeta_{kv'}{}^*\mathbf{P}\zeta_{0v}\int d\mathbf{r}\varphi_k{}^*\mathbf{p}\varphi_0 +\frac{1}{2M}\int d\mathbf{R}\zeta_{kv'}{}^*\zeta_{0v}\int d\mathbf{r}\varphi_k{}^*\mathbf{p}^2\varphi_0, \quad (15)$$

where ζ_{0v} and $\zeta_{kv'}$ are the eigenfunctions of a three-dimensional isotropic harmonic oscillator, with different frequencies for the ground state φ_0 and the ionized state φ_k of the electron.

For simplicity, we further assume the wave functions of the electron to be hydrogenlike,

$$\varphi_0=(a^3/\pi)^{\frac{1}{2}}\exp(-a|\mathbf{r}-\mathbf{R}|), \quad (16)$$

for the trapped ground state, and to be plane waves,

$$\varphi_k=e^{i\mathbf{k}\mathbf{r}}/\Omega^{\frac{1}{2}}, \quad (17)$$

for the free states. Then, we obtain

$$\int\varphi_0\mathbf{p}\varphi_k d\mathbf{r}=\hbar\mathbf{k}\left(\frac{a^3}{\Omega\pi}\right)^{\frac{1}{2}}\frac{8\pi a}{(a^2+k^2)^2}e^{i\mathbf{k}\mathbf{R}}. \quad (18)$$

$$\int\varphi_0\mathbf{p}^2\varphi_k d\mathbf{r}=-\hbar^2\mathbf{k}^2\left(\frac{a^3}{\Omega\pi}\right)^{\frac{1}{2}}\frac{8\pi a}{(a^2+k^2)^2}e^{i\mathbf{k}\mathbf{R}}. \quad (19)$$

Inserting these in Eq. (15), we may take $\exp(i\mathbf{k}\mathbf{R})\sim1$, since the higher terms of the expansion of $\exp(i\mathbf{k}\mathbf{R})$ can be neglected because of the localized nature of ζ_{0v} and $\zeta_{kv'}$.

The vibrational wave functions of the central atom are of the form

$$\zeta_{0v}=\zeta_{0v_1}(X_1)\zeta_{0v_2}(X_2)\zeta_{0v_3}(X_3),$$
$$\zeta_{kv'}=\zeta_{kv_1'}(X_1)\zeta_{kv_2'}(X_2)\zeta_{kv_3'}(X_3),$$

where X_1, X_2, and X_3 are the three orthogonal coordinates of the atom, and ζ_{0v_j} and $\zeta_{kv_j'}$ are the eigenfunctions of harmonic oscillators in quantum states v_j and v_j' with proper frequencies ω and ω', respectively. For brevity, we introduce the following notation:

$$\alpha=M\omega/\hbar, \quad \alpha'=M\omega'/\hbar, \quad (20)$$

$$(v_j|v_j')=\int\zeta_{0v_j}\zeta_{0v_j'}dX_j, \quad (21)$$

$$[v_j|v_j']=(\alpha\alpha')^{-\frac{1}{2}}\left(v_j\left|\frac{\partial}{\partial X_j}\right|v_j'\right) =(\alpha\alpha')^{-\frac{1}{2}}\int\zeta_{0v_j}\frac{\partial}{\partial x_j}\zeta_{kv_j'}dX_j, \quad (22)$$

$$\epsilon_0=\hbar^2/2ma^2, \quad \epsilon_k=\hbar^2k^2/2m. \quad (23)$$

With Eqs. (11), (15), (18), and (19) the transition probability (9) becomes, after simple calculations:

$$w(0v\to kv')=\nu_1\frac{\epsilon_0^{5/2}\epsilon_k^{3/2}}{(\epsilon_0+\epsilon_k)^4}|[v_1|v_1']|(v_2|v_2')(v_3|v_3')|^2 + \nu_2\frac{\epsilon_0^{3/2}\epsilon_k^{5/2}}{(\epsilon_0+\epsilon_k)^4}|(v_1|v_1')|(v_2|v_2')(v_3|v_3')|^2, \quad (24)$$

where,

$$\nu_1=64(m/M)(\omega\omega')^{\frac{1}{2}}, \quad \nu_2=32(m/M)^2(\epsilon_0/\hbar). \quad (25)$$

In Eq. (24), the second term may be neglected for all practical cases, because the ratio ν_2/ν_1 turns out to be $\frac{1}{2}(m/M)[\epsilon_0/\hbar(\omega\omega')^{\frac{1}{2}}]$, which is only of the order of magnitude 10^{-2} if we take $m/M\sim10^{-4}$, and $\epsilon_0\sim1$ ev.

The total rate of the thermal ionization W_t is given by the sum of $w(0v\to kv')$ over all the initial states weighted by their Boltzmann factors, and over all the final states which satisfy the condition of energy conservation (10). Thus, W_t is given by

$$W_t(x_0)=\sum_{v_1}'\cdots\sum_{v_3'}' w(0v\to kv')e^{-\beta(v_1+v_2+v_3)}(1-e^{-\beta})^3, \quad (26)$$

where the summation follows the conditions

$$(v_1+v_2+v_3+\tfrac{3}{2})-(v_1'+v_2'+v_3'+\tfrac{3}{2})(\omega'/\omega) =(\epsilon_0+\epsilon_k)/\hbar\omega\equiv x, \quad (27)$$

and

$$x\geqq x_0\equiv\epsilon_0/\hbar\omega. \quad (28)$$

The total rate $W_t(x_0)$, Eq. (26), may be written as

$$W_t(x_0)=\sum_{x\geqq x_0}W(x), \quad (29)$$

where,

$$W(x)=(1-e^{-\beta})^3\sum_{v_1}'\cdots\sum_{v_3'}' w(0v\to kv')e^{-\beta(v_1+v_2+v_3)}, \quad (30)$$

the summation being taken over all integral values of $v_1\cdots v_3'$ that satisfy the condition (27) for a fixed value of x. In these expressions β means, of course,

$$\beta=\hbar\omega/kT. \quad (31)$$

III. EVALUATION OF THE RATE OF THERMAL IONIZATION

In this section, we seek closed expressions for $W(x)$ and $W_t(x_0)$. For this purpose, as shown below, it is most convenient to use Slater sums or density matrices.

Define a function $F(x)$ by

$$F(x)=(1-e^{-\beta})^3\sum_{v_1}'\cdots \times\sum_{v_3'}'|[v_1|v_1']|(v_2|v_2')(v_3|v_3')|^2e^{-\beta(v_1+v_2+v_3)}, \quad (32)$$

in which the summation has the same meaning as in Eq. (30). $W(x)$ is then given by,

$$W(x)=\nu_1x_0^{5/2}(x-x_0)^{3/2}x^{-4}F(x), \quad (33)$$

as seen from Eq. (24).

To calculate the function $F(x)$, we introduce here its generating function $Z(\lambda)$ defined by,

$$Z(\lambda)=\sum_x F(x)e^{-\lambda x}, \quad (34)$$

which can be transformed as follows: By the condition (27)

$$\begin{aligned}Z(\lambda)&=\sum_x F(x)\exp[-\lambda(v_1+v_2+v_3+\tfrac{3}{2}) +\lambda(\omega'/\omega)(v_1'+v_2'+v_3'+\tfrac{3}{2})]\\ &=\sum_{v_1}\cdots\sum_{v_3'}|[v_1|v_1']|^2|(v_2|v_2')|^2|(v_3|v_3')|^2 \times\exp\{-(\beta+\lambda)(v_1+v_2+v_3+\tfrac{3}{2}) +\lambda(\omega'/\omega)(v_1'+v_2'+v_3'+\tfrac{3}{2})+\tfrac{3}{2}\beta\}\\ &=e^{3\beta/2}[\sum_{v_1}\sum_{v_1'}|[v_1|v_1']|^2\exp\{-(\beta+\lambda)(v_1+\tfrac{1}{2}) +\lambda(\omega'/\omega)(v_1'+\tfrac{1}{2})\}][\sum_{v_2}\sum_{v_2'}|(v_2|v_2')|^2 \times\exp\{-(\beta+\lambda)(v_2+\tfrac{1}{2})+\lambda(\omega'/\omega)(v_2'+\tfrac{1}{2})\}] \times[\sum_{v_3}\sum_{v_3'}[(v_3|v_3')|^2\exp\{-(\beta+\lambda)(v_3+\tfrac{1}{2}) +\lambda(\omega'/\omega)(v_3'+1)\}]. \quad (35)\end{aligned}$$

Using the well-known Slater sum for a harmonic oscillator,

$$\begin{aligned}\Phi(x|x',\xi)&\equiv\sum_{v=0}^{\infty}\zeta_v(x)\zeta_v(x')\exp\{-\xi(v+\tfrac{1}{2})\}\\ &=(2\pi\sinh\xi)^{-\frac{1}{2}}\exp[-\tfrac{1}{4}(\tanh\tfrac{1}{2}\xi)(x+x')^2 -\tfrac{1}{4}(\coth\tfrac{1}{2}\xi)(x-x')^2], \quad (36)\end{aligned}$$

we can easily derive the following formulas,

$$\begin{aligned}&\sum_v\sum_{v'}|(v|v')|^2\exp\{-(\beta+\lambda)(v+\tfrac{1}{2})+\lambda(\omega'/\omega)(v'+\tfrac{1}{2})\}\\ &=(\alpha\alpha')^{\frac{1}{2}}\int_{-\infty}^{\infty}\int\Phi(\alpha^{\frac{1}{2}}X|\alpha^{\frac{1}{2}}X',\beta+\lambda) \times\Phi(\alpha'^{\frac{1}{2}}X|\alpha'^{\frac{1}{2}}X',-(\omega'/\omega)\lambda)dXdX'\\ &=[2g(\beta,\lambda)]^{-\frac{1}{2}}, \quad (37)\end{aligned}$$

and,

$$\begin{aligned}&\sum_v\sum_{v'}|[v|v']|^2\exp\{-(\beta+\lambda)(v+\tfrac{1}{2})+\lambda(\omega'/\omega)(v'+\tfrac{1}{2})\}\\ &=\int_{-\infty}^{\infty}\int\Phi(\alpha^{\frac{1}{2}}X|\alpha^{\frac{1}{2}}X',\beta+\lambda)\frac{\partial}{\partial X}\frac{\partial}{\partial X'} \times\Phi(\alpha'^{\frac{1}{2}}X|\alpha'^{\frac{1}{2}}X',-(\omega'/\omega)\lambda)dXdX'\\ &=2\sqrt{2}\{(1-\rho)^{-\frac{1}{2}}\sinh(\beta+\lambda)-(1-\rho)^{\frac{1}{2}}\sinh\lambda\} \times\{g(\beta,\lambda)\}^{-3/2}, \quad (38)\end{aligned}$$

with the function $g(\beta, \lambda)$ defined by,

$$g(\beta,\lambda)=\cosh(\beta+\lambda)\cosh(1-\rho)\lambda - \tfrac{1}{2}[1-\rho+1/(1-\rho)]\sinh(\beta+\lambda)\sinh(1-\rho)\lambda, \quad (39)$$

and the parameter ρ defined by

$$\omega'/\omega=1-\rho. \quad (40)$$

Inserting Eq. (37) and Eq. (38) into Eq. (35), we then arrive at a closed expression for the generating function $Z(\lambda)$, which is conveniently written as

$$Z(\lambda)=2^{\delta/2}(\sinh\tfrac{1}{2}\beta)^{\delta}Z_1(\lambda)Z_2(\lambda), \quad (41)$$

where

$$Z_1(\lambda)=2\{(1-\rho)^{-\frac{1}{2}}\sinh(\beta+\lambda)-(1-\rho)^{\frac{1}{2}}\sinh(1-\rho)\lambda\}, \quad (42)$$

$$Z_2(\lambda)=\{g(\beta,\lambda)\}^{-\delta/2}. \quad (43)$$

The function $F(x)$ in Eq. (32), has finite values only for a discrete set of values of x defined by Eq. (27), and therefore, the series of Eq. (34) is essentially a Dirichlet series. Hence, the step-function defined by,

$$G(x)=\sum_{y\leq x}F(y),$$

is obtained by the well-known inverse formula of the bilateral Laplace-transformation,

$$G(x)=\frac{1}{2\pi i}\int_{-i\infty}^{i\infty}Z(\lambda)e^{\lambda x}\frac{d\lambda}{\lambda}.$$

From this, after a formal differentiation, we obtain

$$F(x)=\frac{1}{2\pi i}\int_{-i\infty}^{i\infty}Z(\lambda)e^{\lambda x}d\lambda, \quad (45)$$

where $F(x)$ is, however, to be interpreted as constructed from an infinite set of delta-functions. By the convolution theorem the inverse transformation, Eq. (45), is given by

$$F(x)=2^{\delta/2}(\sinh\tfrac{1}{2}\beta)^{\delta}\int f_1(x')f_2(x-x')dx', \quad (46)$$

where

$$f_1(x)=\frac{1}{2\pi i}\int_{-i\infty}^{i\infty}Z_1(\lambda)e^{\lambda x}d\lambda$$

$$=(1-\rho)^{-\frac{1}{2}}\{e^{\beta}\delta(x+1)-e^{-\beta}\delta(x-1)\} - (1-\rho)^{\frac{1}{2}}\{\delta(x+1-\rho)-\delta(x-1+\rho)\}, \quad (47)$$

and

$$f_2(x)=\frac{1}{2\pi i}\int_{-i\infty}^{i\infty}[g(\beta,\lambda)]^{-\delta/2}e^{\lambda x}d\lambda. \quad (48)$$

The function $g(\beta, \lambda)$, Eq. (39), has an infinite set of zero points because of the discrete nature of $F(x)$. On the real axis it has only two zeros, one on the positive side, and the other on the negative side. Since we are interested in the positive values of x, only the negative zero is to be considered. It must be noticed here that an exact evaluation of Eq. (45) or Eq. (48) is of little importance for us, because it leads to the series of Eq. (33), where the matrix elements may also be evaluated by direct integrations or by use of generating functions of Hermite polynomials. Such a series, in itself, is not tractable because it cannot be summed to give the desired rate $W_t(x_0)$. In fact, the merit of the method introduced here is that it is a short cut to a convenient approximation. From this standpoint, we evaluate the integral of Eq. (48) in some approximate ways.

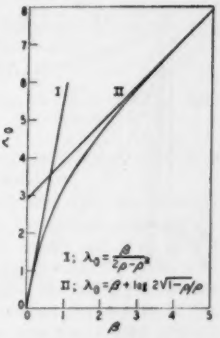

FIG. 1. The function $\lambda_0(\beta)$, which is the real solution of the equation $g(\beta, -\lambda_0)=0$ (see Eq. (49)). The parameter ρ is assumed to be 0.1. Curves I and II are the approximate solutions for high temperatures and low temperatures, respectively.

The function $g(\beta, \lambda)$ can be transformed to

$$g(\beta,\lambda)=\cosh(\beta+\rho\lambda)-1 - \frac{\rho^2}{2(1-\rho)}\sinh(\beta+\lambda)\sinh(1-\rho)\lambda$$

$$=\frac{(2-\rho)^2}{4(1-\rho)}\cosh(\beta+\rho\lambda) - \frac{\rho^2}{4(1-\rho)}\cosh\{(2-\rho)\lambda+\beta\}. \quad (49)$$

Now we assume ρ to be small, which will be true for most cases of interest. Let the negative zero point be $-\lambda_0$, which is given approximately by

$$\lambda_0\simeq\beta+\log[2(1-\rho)^{\frac{1}{2}}/|\rho|] \quad (50)$$

for large β, and by

$$\lambda_0\simeq\beta/(2\rho-\rho^2) \quad (51)$$

for small β provided that $\rho>0$. Equation (50) remains valid even for $\rho<0$, but Eq. (51) must be replaced by another formula if $\rho<0$. On physical grounds, however, ρ is usually expected to be positive, that is, $\omega'<\omega$. Figure 1 shows the numerical solution λ_0 of the equation

$$g(\beta,-\lambda_0)=0$$

for $\rho=0.1$. The function g of Eq. (49) can be written as

$$g(\beta,\lambda)=C\left[1-\frac{\cosh\{(2-\rho)\lambda+\beta\}}{\cosh\{(2-\rho)\lambda_0-\beta\}}\right], \quad (52)$$

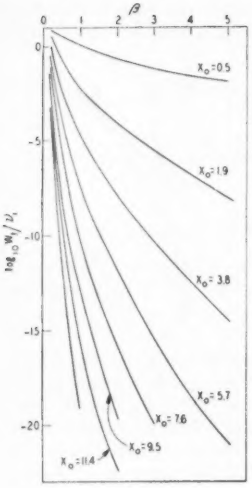

FIG. 2. Thermal ionization rates as functions of $\beta=\hbar\omega/kT$, calculated from Eq. (5.8) for some values of $x_0=\epsilon_0/\hbar\omega$, ρ being assumed to be 0.1.

where

$$C=\frac{(2-\rho)^2}{4(1-\rho)}\cosh(\beta-\rho\lambda_0)-1. \tag{53}$$

If $\lambda_0\gtrsim 1$, Eq. (52) can be approximated by

$$g(\beta,\lambda)=C[1-e^{-(2-\rho)(\lambda+\lambda_0)}], \tag{54}$$

for the domain $\Re\lambda\gtrsim-\lambda_0$. Hence, the integral of Eq. (48) will be given approximately by

$$f_2(x)=Ce^{-\lambda_0 x}\sum_{n=0}^{\infty}(-)^n\binom{-5/2}{n}\delta\{x-(2-\rho)n\}, \tag{55}$$

which is obtained by making the transformation $(2-\rho)(\lambda+\lambda_0)=z$ and expanding $[g(\beta,\lambda)]^{-5/2}$, making use of Eq. (54).

Inserting Eq. (55) into Eq. (46), we get an approximation for $F(x)$, which has positive values at $x=-1$, $1-\rho$, $3-2\rho$, $5-3\rho$, $\cdots$ and negative values at $x=-1+\rho$, 1, $3-\rho$, $5-2\rho$, $\cdots$. As defined in Eq. (33), however, $F(x)$ must have only positive values. This contradiction arises from our approximation, so it is more reasonable to introduce another approximation of $F(x)$, with the required positive character, by adding the contributions from $x=(2n-1)-n\rho$ and $(2n-1)-(n-1)\rho$ to give $F(x)$ for $x=(2n-1)(1-\frac{1}{2}\rho)$. Thus a reasonable approximation for $F(x)$ will be

$$F(x)=\sum_{n=0}^{\infty}F_n\delta(x-a_n),\quad a_n=(2n-1)(1-\tfrac{1}{2}\rho),$$
$$n=0,1,2\cdots, \tag{56}$$

where

$$F_0=2^{5/2}(\sinh\tfrac{1}{2}\beta)^2C^{-5/2}\{(1-\rho)^{-\frac{1}{2}}e^{\beta}-(1-\rho)^{\frac{1}{2}}\},$$

$$F_n=2^{5/2}(\sinh\tfrac{1}{2}\beta)^2C^{-5/2}(-)^{n-1}\binom{-5/2}{n-1}e^{-\lambda_0(2-\rho)(n-1)}$$
$$\times[\{(1-\rho)^{\frac{1}{2}}-(1-\rho)^{-\frac{1}{2}}e^{-\beta}\}+(1+3/2n)$$
$$\times e^{-\lambda_0(2-\rho)}\{(1-\rho)^{-\frac{1}{2}}e^{\beta}-(1-\rho)^{\frac{1}{2}}\}]. \tag{57}$$

Eq. (56) gives the total rate $W_i(x_0)$ as

$$W_i(x_0)=\int_{x_0}^{\infty}W(x)dx$$
$$=\nu_1\sum_{a_n>x_0}F_n x_0^{5/2}(a_n-x_0)^{3/2}a_n^{-4}, \tag{58}$$

which converges rapidly for $\lambda_0\gtrsim 1$. According to Eq. (58), $W_i(x_0)$ shows sudden decreases at the points $x_0=a_n$. This detailed behavior is not, however, particularly significant, because it originates from our approximations. The rigorous functions $W_i(x_0)$ will be much more complicated. So, rather arbitrarily, we calculate $W_i(x_0)$ for $x_0=0.5$, 1.9, 3.8, $\cdots 2n(1-\frac{1}{2}\rho)\cdots$ and replace $W_i(x_0)$ by a smoothed function. The results are shown in Fig. 2 and Fig. 3.

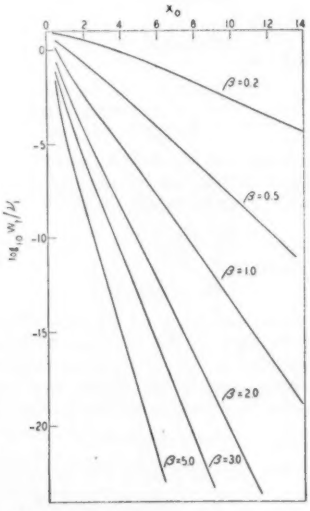

FIG. 3. Calculated rates of thermal ionization as functions of x_0 for some given values of β.

If β is very small, λ_0 will be also small. In such cases $g(\beta,\lambda)$, Eq. (39), or (49), is approximated by

$$g(\beta,\lambda)=\tfrac{1}{2}\beta^2\{1-(2\rho/\beta)(1-\tfrac{1}{2}\rho)\lambda\}. \tag{59}$$

Thus, the integral of Eq. (48) turns out to be

$$f_2(x)=2^{5/2}\beta^{-5}\lambda_0^{5/2}x^{3/2}e^{-\lambda_0 x}/\Gamma(5/2), \tag{60}$$

where λ_0 is given by Eq. (51). Then Eqs. (46) and (47) give

$$F(x)=\frac{4}{\beta^2}\frac{\lambda_0^{5/2}}{\Gamma(5/2)}e^{-\lambda_0 x}[(1-\rho)^{-\frac{1}{2}} \times\{(x+1)^{\frac{1}{2}}e^{\beta-\lambda_0}-(x-1)^{\frac{1}{2}}e^{-\beta+\lambda_0}\} +(1-\rho)^{\frac{1}{2}}\{(x-1+\rho)^{\frac{1}{2}}e^{\lambda_0(1-\rho)}-(x+1-\rho)^{\frac{1}{2}}e^{-\lambda_0(1-\rho)}],$$

which, after neglecting ρ, is approximated by

$$F(x)=\frac{4}{\beta}\frac{\lambda_0^{5/2}e^{-\lambda_0(x-1)}}{\Gamma(5/2)}\{(x-1)^{\frac{1}{2}}+(x+1)^{\frac{1}{2}}e^{-2\lambda_0}\}, \quad (61)$$

where the first term in the bracket should be put equal to zero for $x<1$ and the second term for $x<-1$.

The total rate $W_i(x_0)$ is then found to be

$$W_i(x_0)=\nu_1\int_{x_0}^{\infty}F(x)x_0^{5/2}(x-x_0)^{\frac{1}{2}}x^{-4}dx, \quad (62)$$

which cannot be evaluated in a simple form. However, if x_0 is large, $W_i(x_0)$ is roughly approximated by

$$W_i(x_0)\simeq\nu_1(4/\beta)e^{-\lambda_0 x_0}\{(1-1/x_0)^{\frac{1}{2}}e^{\lambda_0}+(1+1/x_0)^{\frac{1}{2}}e^{-\lambda_0}\}, \quad (63)$$

and if $0<x_0<1$, it is approximated by

$$W_i(x_0)\sim(4\nu_1/\beta)[x_0^{5/2}(1-x_0)^{\frac{1}{2}}+(1+1/x_0)^{\frac{1}{2}}e^{-\lambda_0}]. \quad (64)$$

Equation (63) and Eq. (64) are not good for very small λ_0; but they should be correct, at least in order of magnitude, if λ_0 is not too small, that is, except for extremely high temperatures.

IV. DISCUSSIONS

Our model is too simplified to apply quantitatively to any actual cases. However, it seems to have succeeded in clarifying some important features of the thermal ionization process, so it might be worth while to add some remarks here.

The most remarkable point is the behavior of λ_0 with changes in β [Eqs. (50) and (51)]. As shown in Eqs. (57), (58), (61), (62), etc., λ_0 has a dominant effect on the rate W_i. If β is large (and consequently λ_0 is large), Eq. (58) may be replaced by its first term, which may be simplified to read

$$W_i(x_0)\simeq 4\nu_1\left[\frac{\rho}{2(1-\rho)^{\frac{1}{2}}}\right]^{x_0-1}e^{-\beta x_0} \simeq 4\nu_1(\rho/2)^{\epsilon_0/h\omega-1}e^{-\epsilon_0/kT}, \quad (65)$$

if we remember that β is also large and use the approximation of Eq. (50). For small β, on the other hand, we can apply Eq. (51) so that the rate [see Eq. (63)] is dominated by the factor

$$W_i(x_0)\propto(4\nu_1/\beta)\exp\{-\beta x_0/(2\rho-\rho^2)\} =\frac{4\nu_1}{\beta}\exp\left\{-\frac{\epsilon_0}{2\rho-\rho^2}\Big/kT\right\}. \quad (66)$$

Intermediate to these two extremes, $W_i(x_0)$ exhibits of course a more complicated behavior.

The simple results of (65) and (66) can be easily interpreted. Figure 4 shows the energy configuration diagram of our model. The energy factor of (65) is simply the excitation probability from the level A to the level B. On the other hand, the entropy factor (or frequency factor) is governed by the square of the matrix element between two quantum states of oscillators with the difference of quantum numbers x_0 and with fractional difference ρ of the proper frequencies, and is roughly proportional to $(\frac{1}{2}\rho)^{x_0-1}$.

As shown in Fig. 4 the potential curve of our ground state crosses the continuum of ionized states at C, because we have assumed ρ to be positive, which means that the curvature of the bottom of the continuum is smaller than that of the ground state. The energy of

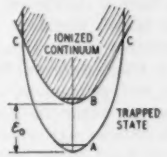

FIG. 4. The simplified model of adiabatic potentials assumed in this theory.

the intersection C is just equal to

$$\epsilon^*=\frac{\omega^2}{\omega^2-\omega'^2}\epsilon_0=\frac{\epsilon_0}{2\rho-\rho^2}. \quad (67)$$

Hence the expression (66) can be written as,

$$W_i\propto 256(m/M)(kT/h)e^{-\epsilon^*/kT}, \quad (68)$$

which is to be compared with

$$W_i=\kappa(kT/h)e^{-\Delta F^{\ddagger}/kT} =\kappa(kT/h)e^{\Delta S^{\ddagger}/k}e^{-\epsilon^*/kT}, \quad (69)$$

a formula so well known that it is often considered universal. Equation (68) means that for high temperatures the transition may take place mostly over the activation states; this seems quite reasonable.[8]

However, it must be realized that we should be led to an erroneously small rate of thermal ionization by applying Eq. (68) or Eq. (69) at low temperatures. Actually, in such cases, transitions occur not by surmounting the potential barriers but through a quantum mechanical resonance, something like a tunnel effect.

It must be admitted here that our treatment is not

[8] This fact can be established in general. A detailed discussion will be given in a later paper.

really satisfactory for the high temperature case. In fact, the simple assumptions of Eq. (16) and Eq. (17) cease to be valid for configurations where the atom moves beyond the cross points C, because there the ground level becomes higher than the lowest energy of free electron states, which means that the trapped state may cease to exist or at least it should be considered as a virtual state, something like that of a disintegrating α-particle. In this sense the adiabatic potential E_l' in (5) might be considered as a complex number, or we might add some term to the perturbation of Eq. (5) which would represent the instability of the ground state for large amplitudes of the atom. To be rigorous we must also be careful about the form of the wave functions. However, the writer prefers not to investigate these points at present, because such an investigation would inevitably introduce additional ambiguous assumptions.

In our theory, the rate of thermal ionization is governed essentially by the dependence of vibrational modes on the electronic states. As mentioned before, this idea is in sharp contrast to the theory of Goodman, Lawson, and Schiff.[4] The fractional change of frequency ρ_l (40), is to be calculated from the quantum mechanical basis. Such a calculation, too ambitious for our simplified model, would be very important for a more quantitative theory. Hence we must content ourselves with a rough estimate. In N-type semiconductors of silicon and germanium, the impurity atom has one more electron than the atom of the mother crystal does. In this state we may suppose, as a crude approximation, that the bond degree between the impurity atom and its neighbors is 5/4. If we assume that the force constant of covalent bonds is proportional to the bond degree, the ratio of the vibrational frequencies of the central atom in the ground and in the ionized state will be $(5/4)^{\frac{1}{2}}$, which gives $\rho \approx 1-(4/5)^{\frac{1}{2}}=0.108$. This suggests that it is not unreasonable to assume ρ to be the order of magnitude 0.1.

In Figs. 2 and 3 we have plotted $W_l(x_0)$ as a function of x_0 and β, where for illustration we chose arbitrarily $\rho=0.1$. It will be seen that we have the right to expect much larger rates of the thermal ionization process. ν_1 is of the order of 10^{10} sec^{-1}, so taking $x_0=3$, W_l will be 10^7 sec^{-1} for $\hbar\omega/kT=0.5$, 10^6 sec^{-1} for $\hbar\omega/kT\sim 1$, and 10^3 sec^{-1} for $\hbar\omega/kT\sim 2$. Of course these figures depend on ρ, but the effect of changing ρ can easily be estimated from Eqs. (65) and (66).

Actually the wave function of the trapped electron is not so concentrated as assumed here, but it may extend over many atoms surrounding the impurity. This circumstance requires a generalization of the model to include many atoms, which might be very complicated.[7]

We have hitherto discussed only the direct transition from the ground state to the ionized states. There may be some excited states of trapped electrons. However, it is not clear at present whether such excited levels may play the role of a staircase for the liberation of the electron, and consequently result in an increase of the rate of ionization. Analogy to the theory of recombination in discharge processes will help in developing the theory in this direction. Unfortunately, however, the latter appears to be in a rather unsatisfactory state from a quantum mechanical point of view.

Finally, it seems necessary to add remarks about the role of the temperature radiation for the establishment of the equilibrium distribution of electrons. In fact one may expect it to be dominant in some cases. Let us consider the dipole transition of a hydrogen-like 1s-state to a 2p-state in a medium with dielectric constant κ at temperature T. The transition probability is given by

$$w_{1s\to 2p}=0.94\times 10^9\kappa^{-7/3}(e^{h\nu/kT}-1)^{-1}\ \text{sec}^{-1}, \qquad (70)$$

where $h\nu$ is the energy of excitation, which has been assumed to be $(3/8)(e^2/\kappa^2 a_0)$, a_0 being the Bohr radius.

On the other hand, the total cross section of photoionization by light of frequency ν is given by

$$\phi=64\times 137^3\kappa^{3/2}\phi_0(I/h\nu)^{7/2}, \qquad (71)$$

if roughly estimated by the Born approximation, where ϕ_0 is the classical cross section of an electron, that is, 6.5×10^{-25} cm^2. It should be mentioned here that the radiation field is considered, both in Eq. (70) and Eq. (71), as that with velocity $v=c/\sqrt{\kappa}$ instead of c. The total rate of photoionization caused by the temperature radiation is given by

$$W_{\text{rad}}=\int_{\nu=I/h}^{\infty}\phi(\nu)\frac{8\pi\nu^2 d\nu}{v^2(e^{h\nu/kT}-1)}, \qquad (72)$$

which is roughly approximated by

$$W_{\text{rad}}\sim 1.5\times 10^{-16}\kappa^{5/2}(kT/\lambda_0^2 h)e^{-I/kT}, \qquad (73)$$

if $I\gg kT$, and by

$$W_{\text{rad}}\lesssim 1.5\times 10^{-16}\kappa^{5/2}c^{-2}(kT/\hbar)^3\times\text{const.}, \qquad (74)$$

if $I\ll kT$. In Eq. (73) λ_0 is the maximum wavelength of the photoionization in vacuum, and the constant in (74) is the integral $\int_0^\infty x^2(e^x-1)^{-1}dx$.

These expressions should be compared with the ionization rate W_l caused by the multiphonon jump discussed above. Generally speaking, the energy I of photoionization may be different from ϵ_0 for the thermal ionization, but in the case of nonpolar crystals these two may be considered as the same. For illustration, if we take $\kappa=16$, Eq. (73) or Eq. (74) gives $W_{\text{rad}}\sim 10^5$ sec^{-1} at room temperatures. We cannot give any definite conclusion whether this rate will prevail in the multiphonon process, but it will be seen that this gives a lower limit for the relation frequency of germanium rectifiers. It should be noted that the high dielectric constant favors photoionization, through the increase of the cross section and also through the decrease of the ionization energy.

The excitation probability (70) also gives a pretty large rate for the numerical example above mentioned. It will be $\sim e^{-h\nu/kT}\times 10^5$ sec^{-1}, which is the order of $\sim 10^4$ sec^{-1} at room temperatures. However, it seems likely that this process plays a more important role for low temperatures, $h\nu \gg kT$. If the rate of attaining equilibrium between the excited level and the ionized states is assumed to be much larger than that between the ground and the excited levels, the probability (70) is rate-determining, and it may compete with the multi-phonon process, which depends in fact on the magnitudes of the photo-exciting energy and the thermal ionization energy and also on the magnitude of ρ, or more generally on the difference of vibrational modes in different electronic states.

However, it should be noticed that the rates caused by temperature radiation are very small if the excitation energy exceeds 1 ev or so. So we are forced to believe that the thermal excitation energies may sometimes be very small. For example, Dutton, Heller, and Maurer[9] took this point of view for the explanation of their experiment on KCl, which showed that free charges are liberated from V_1 and F centers at $-132°$ in KCl crystals irradiated by x-rays at liquid nitrogen temperature. These authors concluded that the thermal ionization energy of V_1 is only one-tenth of its optical excitation energy, which seems somewhat surprising.

The writer wishes to suggest another possible explanation. In this kind of experiment it seems important to notice that the crystal is not in a state of thermal equilibrium, so that the relaxation process taking place in heating may possibly supply energy to liberate free charges from deep traps. To clarify these points, further experiments would be required.

This work was undertaken three years ago but has been completed during the author's visit in the United States. On this occasion, he wishes to express his gratitude for the opportunity to work for a year at the Institute for the Study of Metals of the University of Chicago. Also, he wishes to thank Professor M. Kotani of Tokyo University for his interest in this work.

[9] Dutton, Heller, and Maurer, Phys. Rev. **84**, 363 (1951).

PHYSICAL REVIEW VOLUME 86, NUMBER 6 JUNE 15, 1952

Measurement of Neutron Densities with Crystals of NaI(Tl)

BERTEL GRIMELAND
Joint Establishment for Nuclear Energy Research, Kjeller, Lillestrøm, Norway
(Received January 18, 1952)

Crystals of NaI(Tl) were irradiated in a nuclear reactor and the induced activity in sodium and iodine registered with a photomultiplier tube. It was found that an absolute measurement of the activities can be made in this way. Since sodium is an almost pure "one over v" absorber the neutron density can be determined from its activity.

Comparisons have also been made between the sodium and iodine cross sections for capture of thermal neutrons. With the sodium cross section equal to 0.47 barn, the cross section of iodine was found to be 5.00 barns.

We consider an element with only one stable isotope which, after neutron capture, gives a radioactive isotope decaying with a single period. The number of radioactive nuclei formed when such an element is irradiated in a neutron flux will be

$$B = K\nu \cdot \int_0^\infty n(v)\cdot v\sigma(v)dv, \tag{1}$$

where

$$K = (1/\lambda)(1-e^{-\lambda t}). \tag{2}$$

λ is the radioactivity constant of the isotope formed, t the time of irradiation, ν the number of nuclei exposed to irradiation, $n(v)$ the neutron density as a function of neutron velocity, and $\sigma(v)$ the cross section of the stable isotope for neutron capture. In the region of thermal energies we shall usually have

$$\sigma(v) = (\sigma_0 \cdot v_0/v), \tag{3}$$

with $v_0 = 2.2\cdot 10^5$ cm/sec and σ_0 the value of the cross section at this velocity. In the region above thermal energies there will often be one or more resonances, and we can put

$$\sigma(v) = (\sigma_0 v_0/v) + \sigma_r(v), \tag{4}$$

where $\sigma_r(v)$ stands for the pure resonance part of the cross section. It is assumed that all resonances are outside the thermal region, so that $\sigma_r(v)=0$ for all thermal velocities. We may then write

$$B = K\nu\sigma_0 v_0 N + K\nu \int_0^\infty n(v)v\sigma_r(v)dv, \tag{5}$$

where

$$N = \int_0^\infty n(v)dv. \tag{6}$$

If we work with a pure "one over v" absorber we can determine N, the total neutron density, from Eq. (5)

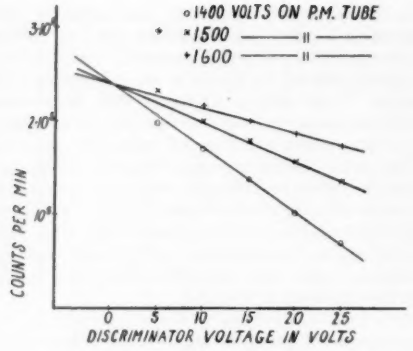

FIG. 1. Discriminator-bias curves, drawn to determine absolute β-activity.

since the last integral vanishes and we get

$$N = B/K\nu\sigma_0 v_0, \tag{7}$$

which can be determined if B is known. To find B an absolute measurement of β-particles must be made. For that purpose one can use the coincidence method described by Putman,[1] or the 4π-counter described by Cohen.[2]

A variation of the 4π-counter method would be to introduce the element whose activity is to be measured into a scintillating material and count the activity by means of a photomultiplier tube. The best thing would be to use a scintillating material which could itself be activated. Such a material is NaI(Tl). Both sodium and iodine fullfill our conditions of having one stable isotope and one activity only. Iodine has some resonances at about 30 ev,[3] whereas sodium is an almost pure "one over v" absorber.[4] Sodium would therefore be very well suited for the measurement of neutron densities. The half-life of Na_{11}^{24} is 15.06 hours[5] and that of I_{53}^{128} is 24.99 min.[6] The two activities can therefore be separated completely.

Experiments have been carried out to try the method. Small crystals of weights 0.1 g–1.5 g and thickness 0.1 cm–0.25 cm were used. During irradiation the crystals were kept in oily paper to prevent damage by moisture. To register the activity the crystals were placed in a glass tube which was glued on to the top of an E.I.M. 5311 photomultiplier tube and filled with paraffin.

Discriminator-bias curves were taken with different voltages on the P.M. tube, usually 1400 volts, 1500 volts, and 1600 volts, and all countings referred to the time of the end of irradiation. The bias curves were found to be almost straight lines cutting each other in the same point. Trying different crystals, it was found that the intersection point was usually situated at a fixed discriminator-voltage, which would then be the true zero-point of the discriminator. A typical set of curves is shown in Fig. 1. With low discriminator-bias and high voltages on the P.M. tube, points were often found which were situated well above the straight lines drawn. It is supposed that this must be due to a weak delayed light emission from the crystal, and these points were not taken into account. The counting rate corresponding to the intersection point was therefore considered to be the true rate of decay of radioactive nuclei. As pointed out by Cohen,[2] γ-radiation following the emission of a β-particle, will have no effect unless it is delayed with respect to the β-emission. This is not the case with either sodium or iodine. Many experiments were made in which 2, 3, or 4 crystals were irradiated at the same place and during the same time interval. Usually the values obtained for N agreed within 5 percent.

These experiments were started while the author had the opportunity to work at the laboratories of the Commissariat à l'Energie Atomique in Châtillon, France. There a comparison was made with the method used at that laboratory. This method was based on measurements made with the 4π-counter already mentioned,[2] and the element activated was manganese. The measured activity of sodium indicated a neutron density about 12 percent higher than the one found with manganese. This result was considered satisfactory because the difference might well be due to errors in the cross sections used.

At this institute (Kjeller, Norway) comparisons have been made with measurements by the coincidence method.[1] Sodium carbonate was irradiated in this case, and therefore the value used for the cross section of sodium would not influence the result. The agreement between the values obtained for N as a result of measurements on sodium iodide and sodium carbonate was found to be satisfactory. The use of a NaI(Tl) crystal for absolute measurement of neutron densities therefore appears to be an easy and reliable method. The accuracy seems to be better than 5 percent, if possible errors in the cross section are not taken into account.

TABLE I. Ratio between σ_0^* for iodine and σ_0 for sodium.

Pile	Place of irradiation in pile	$\sigma_0^*(I)^a / \sigma_0(Na)$	$\sigma_0^*(I)$ (barns)
Chatillon	Center of reactor	14.15	6.65
Chatillon	Outer part of graphite reflector	11.29	5.31
Kjeller	Center of reactor[b]	14.30	6.71
Kjeller	50 cm from axis[b]	13.91	6.55
Kjeller	150 cm from axis[b]	11.50	5.40
Kjeller	Thermal column	10.71	5.03

[a] $\sigma_0(Na)$ is the thermal absorption cross section of sodium. $\sigma_0^*(I)$ is the thermal absorption cross section that one would get for iodine at the place indicated if it were supposed to be a pure "one over v" absorber.
[b] Measurements made in a channel leading through the reactor tank. The tank has a radius of 100 cm and the point at 150 cm is thus situated in the graphite reflector.

[1] J. L. Putman, Brit. J. of Radiology **23**, No. 265, 46 (1950).
[2] R. A. Cohen, Compt rend. **229**, 356 (1949).
[3] R. K. Adair, Revs. Modern Phys. **22**, 249 (1950).
[4] Harris, Muehlhause, and Thomas, Phys. Rev. **79**, 11 (1950).
[5] J. Sreb, Phys. Rev. **81**, 469 (1951).
[6] *Nuclear Data*, Natl. Bur. Standards Circular No. 499 (1950).

TABLE II. Capture cross section of sodium and iodine.

Authors	Pile	Method	Position in pile	σ_{Na} barn	σ_I barns	σ_I/σ_{Na}
Seren *et al.*[a]	Argonne[e]	Activation	Center	0.63		9.92
Seren *et al.*[a]	Argonne[e]	Activation	Thermal col.		6.25	
Harris *et al.*[b]	Argonne[f]	Pile oscillator	Center	0.52	9.23	17.75
Colmer and Littler[c]	Gleep, Harwell	Pile oscillator	Center	0.50	7.4	14.80
Pomerance[d]	Oak Ridge	Pile oscillator	Graphite refl.	0.47	6.1	12.96

[a] See reference 8.
[b] See reference 10.
[c] See reference 9.
[d] See reference 7.
[e] Not stated whether heavy-water or graphite pile.
[f] Heavy-water pile.

Evidently the same experimental procedure that has been described here for sodium can be carried out with iodine, and its absolute activity can be measured. If we solve Eq. (5) with respect to σ_0 we get

$$\sigma_0=\left[B-K\nu\int_0^\infty n(v)v\sigma_r(v)dv\right]\Big/K\nu Nv_0. \quad (8)$$

At the same time we introduce a quantity σ_0^* defined by the equation

$$\sigma_0^*=B/K\nu Nv_0. \quad (9)$$

Obviously σ_0^* can be determined if B and N are known from measurements. For a true "one over v" absorber σ_0^* will be equal to the true thermal absorption cross section σ_0. For an element with resonances, such as iodine, σ_0^* will vary with the form of the function $n(v)$, and only in the case of a pure thermal neutron flux will we have $\sigma_0=\sigma_0^*$. Otherwise $\sigma_0<\sigma_0^*$. It is evident that the ratio between σ_0^* of iodine and σ_0 of sodium can be determined with the crystal method if the two activities are measured separately.

This ratio has been measured both at Châtillon and at Kjeller at different positions in the piles. The results are shown in Table I. We also give the calculated values of σ_0^* for iodine, assuming $\sigma_0=0.47$ barn for sodium.[7] It is seen that the figures from the two reactors agree well. This is what might be expected, since we have to do with two heavy-water reactors of about the same geometrical size.

According to the figure of Table I the true thermal absorption cross section of iodine can not be greater than 5.03 barns. This value is lower than values obtained by earlier measurements. In Table II we have listed values of σ_{Na} and σ_I as given by four different groups of experimenters. We also give σ_I/σ_{Na} for comparison with the results obtained here.

The value obtained by Seren *et al.*[8] seems to fit best with the value in the thermal column of the Kjeller pile. Since, however, Seren *et al.* give a probable error of ±20 percent, the value of the agreement is doubtful. The Harwell figure[9] fits quite well with the figures from the center of the Châtillon and Kjeller piles. On the other hand, it is remarkable that Harris *et al.*[10] have obtained a much higher value at the center of the Argonne heavy-water reactor. It should be stated in this connection that no corrections for self-absorption have been applied to the NaI(Tl) crystals used. For thermal neutrons such a correction would not amount to more than 1 or 2 percent, and even if it were more it would not affect the value of σ_I/σ_{Na}. But self-absorption of the iodine resonance neutrons will of course not be without influence on the ratio. Since this self-absorption has probably been rather high, the correct values of σ_I/σ_{Na} at the center of the Chatillon and Kjeller piles are perhaps somewhat higher than those given here. Still it is believed that these values will not be as high as that of Harris *et al.*

Pomerance[7] states that according to measurements of the cadmium ratio of indium there should be very few epithermal neutrons at the place in the pile where he made his experiments. His value for σ_I/σ_{Na} is however much higher than the value from the thermal column of the Kjeller pile, and also higher than the values obtained in the graphite reflector of both the Chatillon and Kjeller piles. To find an explanation of this discrepancy it would be of interest to make measurements with both oscillator and crystal at the same pile.

[7] H. Pomerance, Phys. Rev. **83**, 641 (1951).

[8] Seren, Friedlander, and Turkel, Phys. Rev. **72**, 888 (1947).
[9] F. C. W. Colmer and D. J. Littler, Proc. Phys. Soc. (London) **A63**, 1175 (1950).
[10] Harris, Muehlhause, Rasmussen, Schroeder, and Thomas, Phys. Rev. **80**, 342 (1950).

Momentum Spectra of Cosmic-Ray Mesons and Protons at Sea Level and 3.4-km Altitude*

W. L. WHITTEMORE AND R. P. SHUTT
Brookhaven National Laboratory, Upton, Long Island, New York

(Received January 31, 1952)

A cloud-chamber experiment has been performed at sea level and 3.4-km altitude to collect data on the momentum and scattering distributions of 15,000 mesons and protons. The momentum spectra and derived conclusions are discussed here. The meson momentum distribution at sea level is in accord with the results of others. A comparison of the sea-level and altitude spectra indicates that, for momenta between 0.7 and 3 Bev/c, 0 to 15 percent of the mesons observed at sea level are produced below 3.4 km. Assuming that production of the fast mesons observed takes place within the top 125 g/cm² of the atmosphere, the differential momentum distribution of mesons at production can be represented adequately as an inverse power law with an exponent equal to 2.75 ± 0.07, in good agreement with previous published results. The relative numbers of positive and negative particles at sea level agree well with those of other workers. At altitude the $+/-$ ratio becomes quite large for the lower momenta (up to 2.5 as against 1.2 at sea level), while it approaches the sea-level ratio (1.3) for high momenta. Assuming that the difference between the sea-level and altitude ratios is due to protons, one can compute that above 0.3 Bev/c protons form 19 ± 2 percent of all ionizing particles (excluding electrons) at 3.4 km. From the observed $+/-$ ratios the proton momentum spectrum has been calculated.

I. INTRODUCTION

BY means of a cloud-chamber experiment carried out both at sea level and at 3.4-km altitude, data have been obtained on the momentum and scattering distributions of mesons and protons. 15,000 meson and proton tracks have been measured. The purpose of this article is to make available the data concerning the momentum spectra, particularly those obtained at 3.4 km, to present the information which can be deduced concerning the production of mesons and the spectrum of protons, and to compare the results with some already existing in the literature.[1–6]

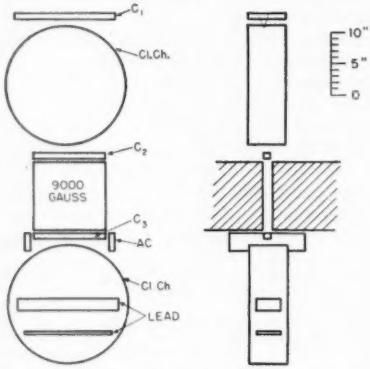

FIG. 1. Geometric arrangement of cloud chambers, magnetic field, and Geiger counters.

II. APPARATUS

The equipment consisted of two nineteen-inch cloud chambers mounted one above and one below the air gap of a permanent magnet which provided a field of 9000 gauss. Figure 1 shows the geometrical arrangement with the location of Geiger counters. The two chambers were triggered by a simple threefold counter telescope $C_1C_2C_3$ if no particles set off the anticoincidence counters AC. The AC were used only during the altitude run in an effort to reduce the number of expansions which showed no counter-controlled track in the bottom chamber. Some of these expansions were caused by side showers while most were caused by particles of low momentum which triggered all the coincidence trays but were deflected away from the bottom chamber by the magnetic field. The AC were not as necessary at sea level because of the presence of relatively fewer particles of low momentum. Stereoscopic pictures were taken of both chambers. A system of mirrors was used to allow a single camera to photograph both cloud chambers simultaneously. One camera viewed the cloud chambers along the axis of each, while another camera viewed each chamber with a stereoscopic angle of 20°. At the top and bottom of the top chamber were sets of fiducial wires which could be used together with a third set of wires in the bottom chamber to ascertain the path of the particles through the cloud chambers and the air gap of the magnet. The equipment had a small vertical aperture of only 20° in the east–west direction and 6° in the north–south direction. The roof of the trailer housing the equipment was the only absorber over the apparatus and amounted to only one or two g/cm² of wood and steel.

The angle between the tracks produced in the upper

* Work done at Brookhaven National Laboratory under the auspices of the AEC.

[1] M. Sands, Phys. Rev. **77**, 180 (1950).
[2] J. C. Street, J. Franklin Inst. **227**, 765 (1939).
[3] B. G. Owen and J. G. Wilson, Proc. Phys. Soc. (London) **A64**, 417 (1951).
[4] Caro, Parry, and Rathgeber, Australian J. Sci. Research **A4**, 16 (1951).
[5] B. Rossi, Revs. Modern Phys. **20**, 537 (1948).
[6] Miller, Henderson, Potter, Todd, and Wotring, Phys. Rev. **79**, 459 (1950); Miller, Henderson, Potter, and Todd, Phys. Rev. **84**, 981 (1951).

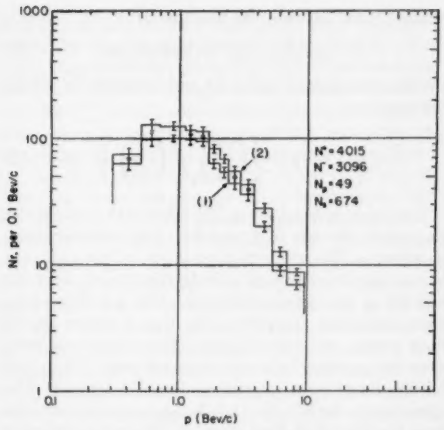

FIG. 2. The differential momentum distributions of positive and negative particles observed at sea level. No electrons are included. (1) refers to negative particles, (2) to positive particles after subtraction of identified protons. For absolute intensity multiply ordinate by 1.07×10^{-6} cm^{-2} sec^{-1} sterad^{-1} (Mev/c)$^{-1}$.

chamber and that in the top half of the bottom chamber was used to determine the momentum in a manner already described.[7–9] The lower section of the bottom chamber contained a 5-cm and a 1-cm lead plate and thereby gave information on the projected angle of scattering in lead for a particle whose momentum was also measured. The plates also aided in the identification of electrons and slow protons. The momentum p was measured in the range 0.300 ± 0.006 to 11 ± 4 Bev/c. The errors are caused mainly by distortion in the chambers. Scattering in the two cloud-chamber walls and four Geiger counter walls (total thickness $\frac{3}{16}$-in. Lucite, 0.006-in. aluminum[10]) caused an error of less than one percent for mesons. For some tracks of exceptional quality the momentum could be measured up to 30 Bev/c, both at sea level and at altitude. The "cut-off" effect of the magnetic field on the momentum distribution at low momenta has been investigated and found to be negligible for momenta larger than 0.5 Bev/c. For smaller momenta the spectrum must be increased by a factor which increases with decreasing momentum to 1.15 for $p=0.3$ Bev/c. This correction is not included in the histograms discussed in the next section but is included later on.

[7] R. B. Brode, Revs. Modern Phys. **21**, 37 (1949).
[8] Glaser, Hamermesh, and Safanov, Phys. Rev. **80**, 625 (1950).
[9] R. P. Shutt and W. L. Whittemore, Rev. Sci. Instr. **22**, 73 (1950).
[10] The counters C_2 and C_3 were especially constructed in order to minimize scattering in their walls. The top and bottom walls consisted of 0.0015-in. aluminum foils while the effective counting volume was limited at the sides by a series of fine wires spaced $\frac{1}{2}$-in. from the solid side walls. The counters were operated at atmospheric pressure by means of "Q"-gas passed through the counters at the slow rate of 1 cm^3/sec. The "Q"-gas was obtained from the Matheson Company, East Rutherford, New Jersey.

III. MOMENTUM DISTRIBUTIONS

The differential momentum spectra are given in Figs. 2 and 3 for runs made at sea level and altitude, respectively. N^+ and N^- refer, respectively, to the total number of positive and negative particles after all recognized electrons are deducted; the appropriate values are stated in each histogram. At sea level 42 electrons were recognized by the showers produced in the 5-cm and 1-cm lead plates. At altitude 43 electrons were similarly observed. The ratio of these numbers of electrons has no significance because the anticoincidence counters were used at altitude and not at sea level. On each histogram the number of particles N_s whose momenta were too large to be measured is also included. N_p refers to the number of protons which were identified by their absorption in the 6 cm of lead in the lower cloud chamber and also by their heavy ionization in the gas. Protons which are stopped by ionization losses in 6 cm of lead must produce in the gas an ionization density I greater than 2.2 times the minimum rate. Hence, N_p should include all protons for which $I/I_{\min}>2.2$. It was not possible to separate, on the basis of ionization alone, other protons whose ionization was less than 2.2 $I_{\min}$. Therefore, the distribution (2), Fig. 3, represents data for particles ionizing in the range 1 to 2.2 times the minimum rate. In what follows these particles will be referred to as ionizing at the minimum rate.

No accurate record of running time was kept; hence the absolute intensity is not plotted in these histograms. However, if Greisen's value[11] of 0.82×10^{-2} cm^{-2} sec^{-1}

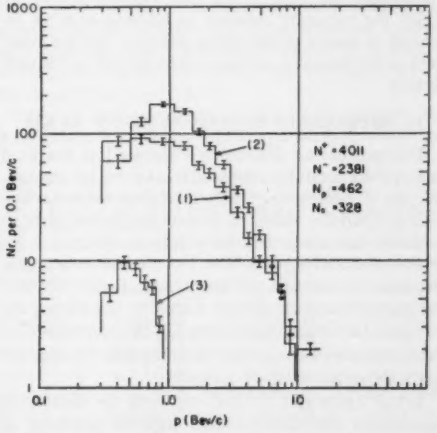

FIG. 3. The differential momentum distributions of positive and negative particles observed at 3.4-km altitude. No electrons are included. (1), (2), as in Fig. 2; (3) refers to identified protons. For absolute intensity multiply ordinate by 2.41×10^{-6} cm^{-2} sec^{-1} sterad^{-1} (Mev/c)$^{-1}$. For simplification of the graph the ordinate of (3) has been divided by 10.

[11] K. Greisen, Phys. Rev. **61**, 212 (1949).

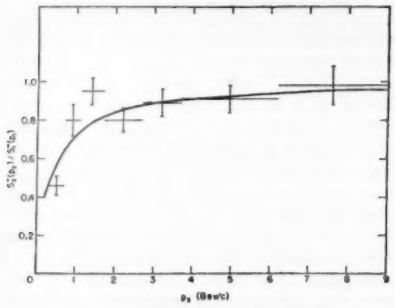

FIG. 4. Experimental and theoretical variation of $S_2^-(p_2)/S_1^-(p_1)$ with momentum.

sterad^{-1} for the total intensity of the penetrating component at sea level is used to normalize the combined data for positive and negative particles ionizing at the minimum rate, the ordinate in Fig. 2 should be multiplied by 1.07×10^{-8} cm^{-2} sec^{-1} sterad^{-1} (Mev/c)$^{-1}$ to give the absolute differential intensity at sea level. If this change of scale is made, the resulting differential momentum spectrum agrees very well with that of Wilson as exhibited by Rossi.[6] In particular, for low momenta the present spectrum follows closely that of Wilson rather than the one Rossi has deduced from counter absorption measurements. The ordinate of Fig. 3 should be multiplied by $2.25\times1.07\times10^{-8}$ cm^{-2} sec^{-1} sterad^{-1} (Mev/c)$^{-1}$ to give the absolute differential momentum spectrum at 3.4 km. The factor 2.25 by which the spectrum obtained at altitude must be increased to take account of the different running times used at sea level and altitude will be derived in the next section.

IV. PRODUCTION OF MESONS BELOW 3.4 KM

The momentum distributions obtained at sea level and at 3.4 km can be compared so as to reveal any production of mesons which may take place below 3.4 km. This comparison, which will be described below, gives no evidence that a large fraction of mesons observed at sea level is produced below 3.4 km. For this comparison only the data for negative particles are used since the data for positive particles include a number of protons, unrecognizable because they ionized at the minimum rate. Since electrons were not included, the data for negative particles pertain solely to mesons.

Let $S_1^-(p)dp$ and $S_2^-(p)dp$ represent the differential momentum distributions for negative particles at 3.4-km altitude and at sea level, respectively. Let $P_1(p_2)$ be the probability that a meson with momentum p_1 at 3.4 km will arrive at sea level with momentum p_2, suffering a momentum loss p_1-p_2 due to ionization. The quantity $P_1(p_2)$ is evaluated from data given by Sands.[1] Except for mesons produced below 3.4 km, the following relation holds between the two spectra

$$S_2^-(p_2)(dp)_2=S_1^-(p_1)(dp)_1P_1(p_2). \quad (1)$$

Divide both sides of (1) by dx and rearrange to obtain the equation

$$S_2^-(p_2)/S_1^-(p_1)=\left[\left(\frac{dp}{dx}\right)_1\Big/\left(\frac{dp}{dx}\right)_2\right]P_1(p_2). \quad (2)$$

The term in brackets in (2) takes into account the changes in the rate of momentum loss with increasing momentum. The theoretical quantity on the right can be evaluated on the basis of ionization theory, since the half-life of mu-mesons is known. This quantity represents essentially the probability that a meson known to be present at 3.4-km altitude will survive to sea level, since the quantity in brackets ranges from 1.08 to 1.03 for the momentum interval under consideration. The quantity on the left, $S_2^-(p_2)/S_1^-(p_1)$, can be evaluated from the spectra in Figs. 2 and 3. This ratio cannot be compared directly with the theoretical expression but must be decreased by a factor K to take into account the fact that the running times at altitude and sea level were different. Since it can be shown from different considerations that only a few percent of the radiation at 3.4 km consist of protons with momenta greater than 5 Bev/c, one can reasonably conclude that only few mesons with momenta larger than 5 Bev/c are produced below 3.4 km. Under these circumstances the experimental and theoretical curves should agree at high momenta even if production should occur for smaller momenta. Figure 4 shows the theoretical curve and experimental points together with the standard errors. The value $K=2.25$ was chosen to make the best over-all fit with particular attention paid to high momenta. This choice of K implies that the intensity at 3.4 km as measured by a Geiger counter telescope containing 167 g/cm^2 of lead would increase by a factor of 1.9 over that at sea level. Rossi[5] has shown that the increase as measured by such a counter telescope is 2.0. The discrepancy may be due to statistical fluctuations, due to a residual effect of side showers on the counter telescope, or due to the fact that the counter experiment covered a larger solid angle than covered in the present experiment.

A comparison of the experimental points and theoretical values of $S_2^-(p_2)/S_1^-(p_1)$ in Fig. 4 shows that two experimental points fall considerably above the theoretical curve in the range from about 0.7 to 3 Bev/c. Except for mesons produced below 3.4 km, the two functions should agree everywhere. Hence, the difference between the theoretical curve and the curve determined by the experimental points, unless wholly due to statistical fluctuations, indicates the magnitude of meson production. A computation based on this difference shows that of the 1600 negative sea-level mesons between 0.7 and 3 Bev/c about 120 ± 90 or between 0 and 15 percent were produced below 3.4 km. Therefore

260 ± 200 mesons of both signs could have been produced. The experimental point at 0.5 Bev/c falls below rather than above the theoretical curve. The detection of sea-level particles in this momentum range ($0.3<p_2<0.7$ Bev/c) is made somewhat uncertain by magnetic cutoff and also by increased scattering, while the corresponding high altitude particles are not so affected due to their higher momenta ($1.0<p_1<1.4$ Bev/c). Thus the latter discrepancy is understandable. We conclude that the experimental data are mainly in agreement with the assumption advanced by other workers that mesons observed at sea level are largely produced in the upper atmosphere; however, there is some evidence that a few of the sea-level mesons with momenta less than 3 Bev/c are produced in the lower one-third of the atmosphere. As shown later there are about 200 protons and probably about as many neutrons present in the altitude spectrum, possessing sufficient energy to produce one or more mesons in the indicated momentum range. Thus, a small amount of meson production, as indicated here, is entirely feasible.

V. DERIVATION OF THE DIFFERENTIAL PRODUCTION SPECTRUM FOR MESONS

Using a method similar in principle to that used first by Euler and Heisenberg[12] and later by Janossy and Wilson,[13] one can derive a spectrum for mesons at production, assuming that production of mesons takes place near the top of the atmosphere. The method for deriving the production spectrum follows closely the material presented in Sec. IV. Equation (2) can be rewritten to represent the spectrum observed at sea level, $S_2^-(p)dp$, in terms of the production spectrum $S_0^-(p)dp$. For particles starting with momentum p_0 one has

$$S_0^-(p_0)=S_2^-(p_2)\Big/\left[\left(\frac{dp}{dx}\right)_0\Big/\left(\frac{dp}{dx}\right)_2\right]P_0(p_2). \quad (3)$$

In this case the momentum at sea level and at the place of production differ by an amount p_0-p_2, which is the momentum loss in traversing the atmosphere between these two depths. Furthermore, $P_0(p_2)$ has the same significance as before but different values since it now represents the probability that a meson with momentum p_0 at the place of production will survive to sea level. When $S_0^-(p)dp$ is evaluated by means of (3) and plotted as a function of p, it is found that it follows a power law $p^{-\gamma}dp$ (except for a scale factor) where $\gamma=2.92\pm0.08$ for $2<p<10$ Bev/c. A similar calculation using the spectrum of negative particles observed at 3.4 km together with the appropriate changes in the momentum loss and survival probabily leads to $\gamma=2.61\pm0.15$. These values of γ differ by more than the standard errors. If no production occurs except near the top of the atmosphere, the two values of γ should agree. On the other hand, if some production does occur down through the atmosphere, the two values of γ obtained would not necessarily agree, the production process having been over-simplified. The results of Sec. IV indicate that some production may indeed take place in the lower atmosphere and, in particular, that up to 15 percent of the mesons with momenta lower than 3 Bev/c could be produced below 3.4 km. If these mesons are subtracted from the spectrum observed at sea level a value of $\gamma=2.82\pm0.08$ is found, in better agreement with the altitude value. By averaging the two values for γ in the appropriate manner one finds $\gamma_M=2.75\pm0.07$. However, it must be kept in mind that the power law is only an approximation because some production takes place through the whole atmosphere, particularly, of course, at the lower momenta as shown by Sands.[1] It is interesting to note that this value agrees with the value $\gamma=2.87$ deduced by Euler and Heisenberg,[12] but is less than the value $\gamma=3.3$ cited by Janossy and Wilson.[13]

If the observed momentum spectra are first transformed to range distributions expressed in g/cm^2 of air and the above computations are repeated, it is found that $S_{0R}^-(R)dR\sim R^{-\gamma_R}dR$ where $\gamma_{RM}=2.90\pm0.07$ for $900<R_0<4100$ g/cm^2 of air. This value is in good agreement with $\gamma_R=2.92$, cited by Sands.[1]

VI. DIFFERENTIAL PROTON SPECTRUM AT 3.4 KM

The ratio of the number of positive particles to the number of negative particles observed at any given altitude and momentum, defined as r, has been investigated previously by several workers.[3,4,6,8,14–17] Each of the given references includes many additional ones. Several detailed studies of the variation of r with momentum have been performed at sea level. The results of the present study obtained at sea level and also at 3.4 km are shown in Table I.

Protons with momenta >0.7 Bev/c cannot be stopped by ionization losses in 6 cm of lead. However, in

TABLE I. Ratio (r) of number of positive particles to number of negative particles and proton fraction (f) of total number of mesons and protons at 3.4 km. Values for $r=r_m$ in parenthesis pertain solely to mesons.

Range of momentum Bev/c	r Sea level	r 3.4 km	f 3.4 km
0.30–0.70	1.38 ± 0.09 (1.24 ± 0.08)	2.50 ± 0.14 (1.35 ± 0.10)	$0.34^a\pm0.06$
0.70–1.10	1.22 ± 0.07	2.10 ± 0.12	0.28 ± 0.06
1.10–1.9	1.21 ± 0.07	1.87 ± 0.10	0.22 ± 0.05
1.9 –3.5	1.28 ± 0.07	1.52 ± 0.07	0.11 ± 0.04
3.5 –9.6	1.32 ± 0.06	1.41 ± 0.08	0.06 ± 0.04
0.3 –9.6			0.19 ± 0.02

[a] Observed directly.

[12] H. Euler and W. Heisenberg, Ergeb. Exact. Naturwiss. **17**, 1 (1938).
[13] L. Janossy and J. G. Wilson, Nature **158**, 450 (1946).
[14] W. R. Brode, Phys. Rev. **78**, 92 (1950).
[15] M. G. Mylroi and J. G. Wilson, Proc. Phys. Soc. (London) **A64**, 404 (1951).
[16] M. Correll, Phys. Rev. **72**, 1054 (1947).
[17] Quercia, Rispoli, and Sciuti, Phys. Rev. **74**, 1728 (1948).

histogram (3), Fig. 3, "stopped" protons with apparent momenta up to 0.9 Bev/c are shown. Near 0.7 Bev/c the criterion for proton identification based on ionization density becomes quite uncertain while the criterion based on the stopping power of lead also becomes uncertain since some of the protons that normally would emerge from the lead with low energies may well be scattered out of the field of view, may be stopped by the greater effective path length caused by scattering, or may be absorbed by nuclear interaction.[18] On the other hand, a slow ($p<0.7$ Bev/c) heavily ionizing proton is more subject to scattering than a meson with the same momentum, and its track is relatively wide. These facts combined with still other sources of small errors may lead to slightly falsified proton momentum measurements. A rough estimate shows that about one half of the particles in question may actually belong in the range 0.3 to 0.7 Bev/c. With this correction the values for r have been calculated as given in Table I. (Without this correction the directly observed value for f in the range $0.3<p<0.7$ Bev/c would be 0.31 instead of 0.34.)

The values of $r(=r_m)$ for mesons alone are shown in parenthesis for the momentum interval 0.3 to 0.7 Bev/c, since here protons could be identified directly. The other values of r include the effects of protons. However, at sea level, Mylroi and Wilson[16] have shown that for $p>0.7$ Bev/c less than four percent of all ionizing particles at sea level are protons and that for higher momenta the fraction is much less. Hence the values of r at sea level for $p>0.7$ Bev/c pertain mostly to mesons. In addition, the following argument indicates that essentially no energetic protons are left at sea level. The intensity of primary protons at the top of the atmosphere is about twenty times the mu-meson intensity at sea level.[19] For a mean free path of 125 g/cm^2 (see reference 5) one would have $[20\exp(-1030/125)]$ or about 0.5 percent of the sea-level intensity left as protons of high energy. Of course, secondary protons would increase somewhat this number, which is a lower limit; however, one would expect that most secondary protons have relatively low energy.

The present experimental data at sea level (Table I) also represent adequately the results of other workers. The results of Owen and Wilson[3] and Caro *et al.*[4] indicate that there is a flat maximum for r at about 5 Bev/c. Our results are consistent with this view, although there are not sufficient data above 10 Bev/c to check this point quantitatively. The good agreement between the present data and those of others obtained at sea level leads one to have confidence in the values of r obtained with the same equipment at 3.4-km altitude.

Concerning the variation of r with momentum at 3.4 km (Table I), the first important point to notice is the large excess of positive particles observed at low momenta. Except for the small positive excess known to be characteristic of mesons at sea level, this large excess of positive particles must be caused by protons. This idea has been previously used by Miller *et al.*[6] and by Adams *et al.*[20] for results obtained at airplane altitudes. Practically all the pi-mesons which are produced will quickly decay into non-interacting mu-mesons. These mu-mesons will be removed by decay or by ionization losses regardless of the sign of their charge; therefore, any r_m inherent in the production of the mesons must be maintained through all altitudes thereafter, provided, of course, that no meaons are produced below 3.4 km with a different positive to negative ratio. In particular, if a certain r_m exists at 3.4 km this same value should exist at sea level for mesons having a momentum reduced by the ionization loss. If this reasoning is correct, the large values of r observed at 3.4 km must be caused by a component of cosmic rays which is positively charged and almost completely absorbed in the atmosphere below 3.4 km. Thus one is justified in identifying this component with protons since they have the required properties and are known to be much more abundant at high altitudes than at sea level. Furthermore, the values of r_m at sea level and altitude for $0.3<p<0.7$ Bev/c agree within the limits of error (see Table I, values in parenthesis). Finally, the values of r at sea level and altitude approach each other for large momenta. This would imply that there are relatively few energetic protons at 3.4-km altitude, a result in agreement with what one expects on the basis of the following computation. Since the intensity of primary protons at the top of the atmosphere is about ten times the intensity of the hard component observed at 3.4 km, $[10\exp(-670/125)]$ or only 5 percent of the observed high energy intensity at altitude consist of high energy protons. Of course this number will be increased somewhat by secondary protons, as mentioned previously.

Before calculating the proton spectrum from the variation of r with altitude and momentum, some results of other workers will be examined. Miller *et al.*[6] (1950) observed 950 particles at 3.4 km under 5 cm of lead for which $r=1.50\pm0.05$ in the range $0.05<p<2.5$ Bev/c. A value can be deduced in the following manner for the present data and compared with that of Miller. Miller observed all particles below 5 cm of lead. This is roughly equivalent to the present results when we deduct all particles which stop in 5 cm of lead from the total observed for $0.3<p<2.5$ Bev/c. For this case, $r=1.68\pm0.06$, in fair agreement with Miller. For mesons having ranges >60 cm of iron and momenta of $1.0<p<2.5$ Bev/c Brode[14] reports values of $r_m=1.32\pm0.02$ near sea level and $r_m=1.30\pm0.03$ at 3.65 km. The present results agree sufficiently with these values. In Brode's experiment protons are practically eliminated

[18] The effects of nuclear interaction of the protons in the lead will be considered in detail in a later paper.

[19] Winckler, Stix, Dwight, and Sabin, Phys. Rev. **79**, 656 (1950).

[20] Adams, Anderson, Lloyd, Rau, and Saxena, Revs. Modern Phys. **20**, 334 (1948).

by ionization losses, scattering, and nuclear interactions in the interposed iron. Correll[16] has observed r_m for slow mesons at 3.4 km and found for about 350 particles that $r_m=1.0$. Considering the poor statistics, this value is in agreement with the value $r_m=1.35\pm0.10$ deduced from the present work. It is interesting to compare our value with a value of $r_m=1.26$ which Quercia *et al.*[17] have deduced from counter experiments at altitude for the region of low momenta. Identification of the charge was made in this case by deflecting the charged particles through magnetized iron plates. This experiment was operated at sea level, at 5.1 and 7.3 km.

In order to determine the proton spectrum at 3.4 km we proceed as follows. As just described, for mesons we must have

$$S_2^+(p_2)/S_2^-(p_2)=r_{m2}(p_2)=r_{m1}(p_1)=S_1^+(p_1)/S_1^-(p_1), \quad (4)$$

where the subscripts were defined for Eq. (1) and S_1^+, S_1^-, S_2^+, S_2^- refer to mesons only. Because of the presence of only few protons with momenta >0.7 Bev/c at sea level we may put the sea-level values of r equal to r_{m2}. If $S_{T1}^+(p)dp$ is the differential spectrum of the total positive component at 3.4-km altitude, then the proton component $S_{P1}(p)dp$ is given by

$$S_{P1}(p_1)=S_{T1}^+(p_1)-S_1^+(p_1)$$
$$=S_{T1}^+(p_1)-S_1^-(p_1)r_{m2}(p_2). \quad (5)$$

The results obtained by performing this computation are shown in Fig. 5, where both the total spectrum $[S_{T1}^+(p)+S_1^-(p)]dp$ and the proton spectrum are exhibited. The spectrum of protons for $p>2$ Bev/c can be represented fairly well as $S_{P1}(p)dp\sim p^{-\alpha}dp$, where $\alpha=2.5\pm0.5$. From these spectra one can find the fraction f of the protons in the total spectrum as shown in the last column of Table I. One also finds that protons form 19 ± 2 percent of all ionizing particles with $p>0.3$ Bev/c. The value of about 6 percent for high momenta agrees with the approximate value of 5 percent calculated from the proton primary intensity.

Figure 5 includes from the data of Miller *et al.*[6] (1951) three points which fall somewhat below the proton spectrum derived here. Protons of momenta <0.7 Bev/c are quite subject to multiple Coulomb scattering in the 2.5 cm of lead located above Miller's cloud chamber, and some of them may have been scattered out of the field of view. Furthermore, a number of protons (~10 percent) may have been removed by nuclear interaction in the same lead. From the results of Miller *et al.* one infers the value for the total intensity near 0.5 Bev/c shown in Fig. 5. This value agrees well with the present result. The data of Winckler *et al.*[19] obtained at high altitudes have been used to compute the expected number of protons at 3.4 km for high momenta. The point entered at 5 Bev/c is in agreement with the present results, taking into account the large experimental errors in this momentum range.

The proton spectrum at 3.4 km consists of a small number of high energy primaries and a larger number of lower energy secondaries produced in the atmosphere by nuclear interaction of the primaries. Particularly the number of secondaries is modified by ionization losses in the atmosphere. Messel[21] has calculated several values for the integral spectrum of the proton component at different altitudes, making use of an interaction model first proposed by Heitler and Janossy,[22] including a mean free path of 65 g/cm² for interaction and of 130 g/cm² for absorption. An energy power law for the primaries with an exponent of -2.7 was chosen. From these calculations one expects that at 3.4 km the ratio of the number of protons with $p>0.78$ Bev/c to the number of protons with $p>2.9$ Bev/c should be 5, in rough agreement with a value of 7 ± 2 found from our data.

Most of the protons observed at 3.4 km disappear before reaching sea level in the following manner. In the first place, a proton must have a momentum of at least 1.67 Bev/c to arrive at sea level. 19 ± 2 percent of all ionizing particles (excluding electrons) at altitude are protons, but the spectrum of Fig. 5 shows that only one quarter of these have $p>1.67$ Bev/c and hence can reach sea level. Furthermore, since the 353 g/cm² of air between 3.4 km and sea level correspond to about 2.8 mean free paths for interaction, these remaining protons become reduced to about $[\exp(-2.8)]$ or 0.06 of those initially present. Finally, the proton component capable of reaching sea level becomes $(19)\times(0.25)\times(0.06)$ or 0.3 percent of all ionizing particles observed at altitude. Since the total intensity of the hard component at sea level is only half that at altitude, the above predicts

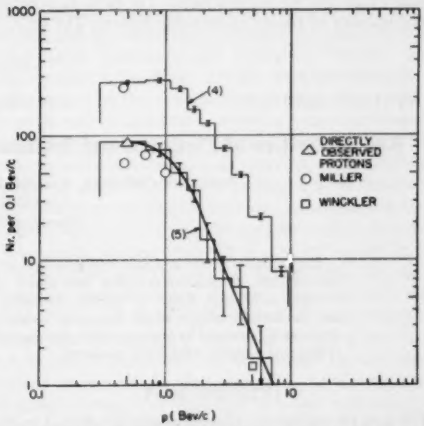

FIG. 5. The spectrum for combined negative and positive particles, including protons, observed at altitude (4) and the deduced spectrum for protons (5). Multiply ordinate by 2.41×10^{-4} cm^{-2} sec^{-1} sterad^{-1} (Mev/c)$^{-1}$ for absolute intensity.

[21] H. Messel, Phys. Rev. **83**, 26 (1951).
[22] W. Heitler and L. Janossy, Proc. Phys. Soc. (London) **A63**, 374 (1949).

that 0.6 percent of the penetrating component at sea level should consist of protons, a value comparable to what has already been deduced. Of course, many of the protons absorbed between 3.4 km and sea level produce nuclear stars, the products of which are secondary protons, neutrons, and mesons, all with energies still lower than those of the incident protons. These secondary protons will be absorbed in the atmosphere for the most part. Some of the mesons produced below 3.4 km should penetrate to sea level, although many should be absorbed or arrive with too little momentum to be measured by the present apparatus. The results of Sec. IV indicate that up to 15 percent of the mesons observed at sea level with momenta less than 3 Bev/c could be produced below 3.4 km.

Finally, one can deduce from the positive to negative meson ratio r_m something concerning the multiplicity with which mesons are produced. The ratio r_m depends on a number of poorly understood factors. The specific mechanism by which mesons are produced is not known. Whether mesons are produced multiply or plurally in several acts all occurring in one nucleus is not yet clear. However, one can make some very simple assumptions about the production of mesons by saying that in half of all cases the extra charge due to the protons is not projected forward but goes off as some low or medium energy proton instead of a high energy meson. Then $r_m=1.32\pm0.06$ implies an average multiplicity of 4 for meson production by high energy protons which agrees with other arguments. For instance, see the discussion of Owen and Wilson.[3]

The writers wish to thank members of this laboratory for their cooperation and assistance which contributed materially to the success of the experiment. In particular, Mr. Arnold Roesch was very helpful in constructing most of the electronic equipment and in assisting in the operation of the cloud chamber at Upton, New York and at Berthoud Pass, Colorado.

PHYSICAL REVIEW VOLUME 86, NUMBER 6 JUNE 15, 1952

Radioactivities of Platinum and Iridium from Photonuclear Reactions in Platinum*

DARLEANE CHRISTIAN, RUSSELL F. MITCHELL, AND DON S. MARTIN, JR.
Iowa State College, Ames, Iowa

(Received February 21, 1952)

The products of photonuclear reactions induced in platinum by a 70-Mev synchrotron x-ray beam have been studied. No osmium activities were found. The iridium fraction included Ir^{193} and Ir^{194} and two new isotopes: a 140-min, 1-Mev β^- emitter, probably Ir^{196}, and a 7-min activity, probably Ir^{197}. Pt^{193}, Pt^{197}, and the 88-min isotope which decays by isomeric transition were found in the platinum fraction. Some evidence is presented to question the assignment of the 88-min activity to Pt^{195}. Relative yields of all these radioactive isotopes have been measured.

INTRODUCTION

IN this investigation, platinum was irradiated in the x-ray beam of the Iowa State College 70-Mev synchrotron in order to identify and characterize the osmium, iridium, and platinum activities produced and to determine their relative yields.

Prior to this work an 87-min platinum activity and the 18-hr Pt^{197} had been reported from photonuclear reactions in platinum.[1,2] Also, Butement[3] reported a new 66-min activity and the well-known 19-hr Ir^{194} in the iridium fraction from $PtCl_4\cdot xH_2O$ which had been irradiated with x-rays.

EXPERIMENTAL DETAILS

Irradiations

Samples of 1 to 5 grams to be irradiated were contained in test tubes of 1-cm diameter. The tubes were mounted close to the synchrotron doughnut by a plastic holder which was carefully aligned in the x-ray beam of the synchrotron. The intensity of the beam was monitored by an ionization chamber whose current was continuously recorded. All of the samples for yield determinations were irradiated at nearly constant beam intensities at the maximum energy of the synchrotron unless otherwise indicated. In early experiments, platinum metal was irradiated. However, dissolving the platinum metal was time consuming and in subsequent irradiations, $PtCl_4\cdot xH_2O$ was used. In spectroscopic analyses of the platinum and $PtCl_4\cdot xH_2O$ no osmium or iridium was found. The principal impurity was copper estimated at about 0.01–0.1 percent.

Chemical Separations

The various components of the irradiated samples were separated by the chemical methods outlined below.

1. Chlorine. A small fraction of the $PtCl_4\cdot xH_2O$ was fused with Na_2CO_3. The melt was extracted with water, and silver nitrate was added to precipitate AgCl.

2. Osmium. The $PtCl_4\cdot xH_2O$ was dissolved in concentrated HNO_3. Osmium and iridium carriers were

* Contribution No. 190 from the Institute for Atomic Research and Department of Chemistry, Iowa State College, Ames, Iowa. Work performed in the Ames Laboratory of the AEC.

[1] H. Wäffler and O. Hirzel, Helv. Phys. Acta **21**, 200 (1948).
[2] Mock, Waddel, Fagg, and Tobin, Phys. Rev. **74**, 1536 (1948).
[3] F. D. S. Butement, Nature **165**, 149 (1950).

added. The osmium was distilled as OsO_4, collected in 6 *N* NaOH solution, and precipitated by passing H_2S into the solution as it was gradually acidified.

3. Iridium. $NaBrO_3$ was added to the HNO_3 solution from which osmium had been distilled. If no osmium separation was performed, the $NaBrO_3$ was added to a water solution of the irradiated $PtCl_4 \cdot xH_2O$ containing iridium carrier. IrO_2 was precipitated by neutralization of the heated solution by $NaHCO_3$. Unless the IrO_2 was dissolved in acid and reprecipitated, a small fraction of the platinum activity carried with the iridium. A second precipitation removed the platinum activity beyond the limits of detection.

4. Platinum. After precipitation of IrO_2, platinum metal was prepared from the filtrate by the addition of powdered magnesium.

The conditions for these chemical separations are given adequately in standard works.[4,5]

All counting samples were prepared by filtering the precipitates through previously washed and weighed Whatman No. 50 filter papers. The filter paper was supported on a sintered glass disk so that an even deposit was obtained over an area of 5.3 cm². The filter paper and deposit were weighed after washing with alcohol and ether and drying. Then without disturbing the deposits, the filter papers were mounted on a cardboard backing and covered with known thicknesses of Cellophane or Scotch tape. In this manner the chemical recovery was determined.

Various platinum complex compounds were irradiated in the synchrotron x-ray beam in an attempt to attain by a Szilard-Chalmers process the high specific platinum activities needed for counting experiments. Several different schemes for separating the active platinum atoms from the bulk of the complex were investigated which were only partially successful in attaining the desired ends. Of these schemes the most effective one was the precipitation of $[Pt(NH_3)_4][PtCl_4]$ by the addition of either $PtCl_4^{=}$ or $PtCl_6^{=}$ to solutions of irradiated $[Pt(NH_3)_4]Cl_2$ or $[Pt(NH_3)_4]C_2O_4$ crystals. In this manner 30–40 percent of the platinum activity could be separated from 400-mg samples of irradiated complex by precipitating samples of $[Pt(NH_3)_4][PtCl_4]$ weighing 20–40 mg.

Measurements

All samples were counted in standard mica end-window G-M tubes mounted in lead or heavy iron housings in conjunction with conventional scale of 64 scalers. A Co^{60} sample of 0.1 mg/cm² thickness electroplated on platinum was used as an absolute radioactive standard. Its absolute beta-disintegration rate was determined in this Laboratory by the coincidence counting method. This standard was always counted in the same geometry as each experimental sample. From aluminum absorption data of the standard, the magnitude of the gamma-ray component was determined and the beta-ray counting rate, found by difference, was corrected for absorption and backscattering. By a comparison of the beta-counting rates of the yield samples and the standard after multiplication by the proper total scattering and absorption factors, the disintegration rates of the samples were determined.

TABLE I. Relative yields of photonuclear reactions of platinum with 70-Mev maximum energy beam per atom of natural isotopic abundance ($Cl^{34}/Cl = 1$).

Isotope produced	Half-life	Yield Av. values
Pt^{199}	3.6–4 days	30.4
Pt^{197}	18 hr	11.4
Pt?	88 min	1.9
Ir^{192}	70 days	0.56
Ir^{194}	19 hr	0.61
Ir^{196}?	140 min	0.33
Ir^{197}?	7 min	0.09

The corrections for absorption in the sample covering, air path and mica-counter window were determined from aluminum absorption curves of the activities. The combined self-absorption, backscattering, and scattering corrections applied to the yield samples were obtained from data given by Engelkemeir and co-workers[6] when possible. Most of the platinum samples were, for intensity purposes, thicker than the 15-mg/cm² upper limit of Engelkemeir and co-workers. Accordingly, the self-absorption and scattering correction factors for the 0.7-Mev beta of 18-hr Pt^{197} were determined experimentally in the following way. The counting rate per unit weight of platinum was determined by counting samples of irradiated platinum of 4 to 85 mg/cm² thickness. A curve of counting rate per unit weight *versus* sample thickness was plotted and matched to the curve for a 0.6-Mev beta presented by Engelkemeir and co-workers. From this curve the correction factor for samples mounted on cardboard, covered with 3.5-mg/cm² Cellophane and 20 mm from the counter window, was read.

The yields of the various radioactivities (i.e., the rate of formation of the radioisotopes or alternatively their saturation disintegration rates in the synchrotron beam) were computed from the observed disintegration rates of the counting samples by the standard equations of radioactive growth and decay. They were reported in Table I compared to the yield of Cl^{34}. The yields have been tabulated on the basis of the naturally occurring isotopic mixture for both chlorine and platinum because at the energies available, some of the activities can be formed by different photonuclear reactions of more than

[4] F. P. Treadwell and W. T. Hall, *Analytical Chemistry* (John Wiley & Sons, Inc., New York, 1949), ninth edition.

[5] W. F. Hillebrand and G. E. F. Lundell, *Applied Inorganic Analysis* (John Wiley & Sons, Inc., New York, 1929).

[6] Engelkemeir, Seiler, Steinberg, and Winsberg, *Radiochemical Studies: The Fission Products* (McGraw-Hill Book Company, Inc., New York, 1951), Paper No. 4, National Nuclear Energy Series, Plutonium Project Record, Vol. 9, Div. IV.

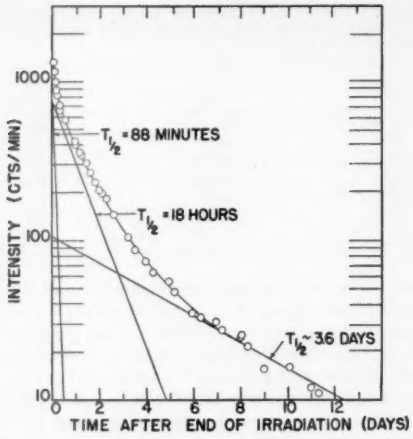

FIG. 1. Decay curve for platinum fraction of 1.5-hr irradiation of $PtCl_4 \cdot xH_2O$ with 70-Mev maximum beam energy.

one target isotope. Since Perlman and Friedlander[7,8] have measured relative yields including that of Cl^{34} at 50- and 100-Mev maximum beam energies, the values reported here can be compared with the general trends of their results if the appropriate effects of isotopic abundances are included.

PLATINUM ACTIVITIES

18-Hr Pt^{197}

A decay curve for the platinum fraction is shown in Fig. 1. The strong component with the 18-hr half-life, together with an absorption curve that indicated a 0.7-Mev beta, showed that the well-established Pt^{197} was formed in high yield. For convenience the yields of the other activities were compared to that of the Pt^{197}. However, in several experiments the Pt^{197}/Cl^{34} yield ratio was determined for comparison with the trends shown by Perlman and Friedlander. Pt^{197} could be produced only by the process $Pt^{198}(\gamma,n)$. Assuming Cl^{34} to be formed predominantly by (γ,n) rather than by $(\gamma,3n)$ reaction, then the Pt^{197}/Cl^{34} yield ration on an isotopic basis would be 119. This value is significantly larger than the yield ratio of 35 which was reported by Perlman and Friedlander for the neighboring heavy isotope Re^{186}/Cl^{34}. All other activities which they reported were of much lower atomic mass.

3.6-Day Pt^{193}

In the platinum yield samples, the longest decay period with measurable intensity was 3.6–4.0 days which was present in low intensity. The aluminum absorption curve indicated soft electrons with this period. It was undoubtedly the same activity which Wilkinson[9] showed must be associated with Pt^{193}, an isotope which should decay by orbital capture. It is to be noted, however, that the half-life in conjunction with the high conversion ratio and the high L to K ratio suggests a delayed isomeric transition which has sometimes been assigned as Pt^{195} or Pt^{197}.[10] Because of the low intensity and uncertainty caused by the corrections which must be applied in converting counting rates into disintegration rates, its yield ratio is approximate. The ratio on an isotopic basis, assuming that it was formed only by a (γ,n) process, was calculated assuming a conversion electron for each disintegration. This value, 70, for Pt^{193}/Cl^{34} was again well in excess of the Re^{186} value.

88-Min Pt Activity

An 88-min activity was the shortest component found in the platinum fraction. It is the same activity which has been tentatively assigned as Pt^{195}.[11] L. J. Laslett and S. H. Cox of this Laboratory observed conversion-electron lines with a scintillation crystal spectrometer in good agreement with the previously reported values of 0.26 and 0.32 Mev. If the activity is isomeric with a stable nucleus, it could be formed by a (γ,γ') process or perhaps by (γ,n) if the next isotope of platinum is stable. The yield was high for a (γ,γ') process, hence a (γ,n) is indicated. However, its low value, about 16 percent of $Pt^{198}(\gamma,n)$, would be expected

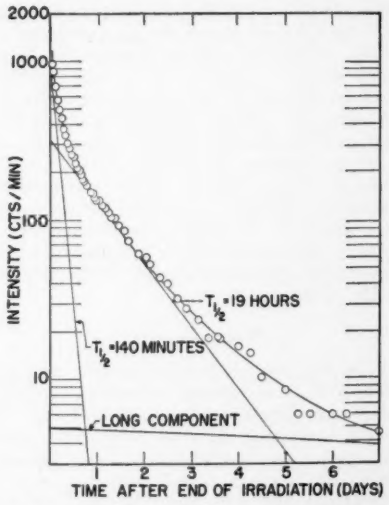

FIG. 2. Decay curve for iridium fraction of 1.5-hr irradiation of $PtCl_4 \cdot xH_2O$ with 70-Mev maximum beam energy.

[7] M. L. Perlman and G. Friedlander, Phys. Rev. **74**, 442 (1948).
[8] M. L. Perlman, Phys. Rev. **75**, 988 (1949).
[9] G. Wilkinson, Phys. Rev. **75**, 1019 (1949).
[10] M. Goldhaber and A. W. Sunyar, Phys. Rev. **83**, 906 (1951).
[11] *Nuclear Data*, Natl. Bur. Standards Circular 499 (1950).

for an isomeric state since a large fraction of the photonuclear reactions might lead to the ground state.

Since the mass assignment of this activity is uncertain, an experiment was performed to determine whether the 88-min platinum activity could be produced by a photonuclear reaction on Au^{197}, a stable isotope of 100 percent abundance. Pt^{196} would therefore be formed by a (γ,pn) process. If the activity is a metastable isomer of Pt^{196}, which is unlikely since Pt^{196} is even-even, it would be formed by a (γ,p) reaction of Au^{197}. Sherr, Bainbridge, and Anderson[12] have shown that the 88-min activity must have a mass assignment greater Pt^{194}. The yields of these (γ,p) and (γ,pn) reactions in several instances have been reported by Perlman[8] and Moses and Martin[13] to be of nearly the same magnitude at the beam energies in question. As can be seen from Table I, (γ,p) reactions in platinum are in all cases about 0.01 of the yield of the (γ,n) reactions on an isotopic basis. Therefore, if the 88-min activity is a metastable state of either of the above platinum isotopes, it is to be expected that it would be produced in a yield of at least 0.0005 that of the 5.6-day Au^{196}. This value assumes a factor of 0.05 to give the fraction of processes ending in the metastable state. Such a factor is consistent with the yields obtained for platinum irradiations.

A 1.2-gram sample of gold was irradiated by the synchrotron x-rays for 80 minutes. It was dissolved, platinum carrier was added, and two samples of ammonium chloroplatinate (IV) were precipitated and counted. A 132-mg sample of gold was also precipitated for counting. By counting the two samples it was estimated that the yield of 88-min platinum relative to that of 5.6-day Au^{196} must have been less than 0.00003, i.e., less than 6 percent of the expected amount. From these results it appears highly improbable that the 88-min platinum activity is a metastable state of either Pt^{195} or Pt^{196}. Assignment to a metastable state of Pt^{197} appears reasonable in view of the above results and those of Sherr and co-workers.[12]

OSMIUM ACTIVITIES

No more than 5–10 counts/min were found in the osmium samples. However, very short activities would not have been detected as the samples could not be counted until 1–2 hours after the end of the irradiations.

IRIDIUM ACTIVITIES

19-Hr Ir^{194}

A decay curve of the iridium fraction is presented in Fig. 2. The 19-hr period with the 2.1-Mev beta-energy found by a Feather analysis of the aluminum absorption curve of this component were in agreement with those expected for the well-established Ir^{194}. It would be expected to form in about equal yield by $Pt^{195}(\gamma,p)$ and $Pt^{196}(\gamma,pn)$ reactions on an isotopic basis.

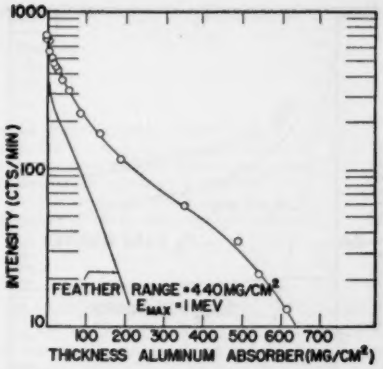

FIG. 3. Aluminum absorption curve of combined 140-min and 19-hr iridium activities 3 hours after end of irradiation. Lower curve for 140-min activity obtained by subtraction of 19-hr component from upper curve.

Then the value of each of these referred to Cl^{34} would be about 0.8, a value comparable to those obtained for similar reactions in tungsten.[13]

70-Day Ir^{192}

A low intensity of a long-lived component (Fig. 2) was found to be present in the iridium samples. It was not due to platinum contamination in the iridium sample since its half-life was much longer than 4 days, which was the longest platinum activity observed. When phosphorus holdback carrier was added before the precipitation of IrO_2, the intensity of this long component was reduced to about one-sixth its value. Apparently, the majority of the long-lived activity was due to P^{32} or P^{33} formed by $(\gamma,2p)$ or $(\gamma,2pn)$ reactions in Cl^{35}.[14] The remaining very low intensity of long-lived activity had a much longer half-life and may be due to 70-day Ir^{192} formed by a (γ,pn) reaction in Pt^{194}. From a five-hour irradiation the half-life of this component was estimated to be about 65 days. Its yield as given in Table I could be estimated only approximately. It appears to be comparable to the value for Ir^{194}.

140-Min Iridium Activity

A new iridium activity having a half-life of 140 min (Fig. 2) was found in the iridium fraction. The activity emitted beta-rays; an aluminum absorption curve of an iridium sample was taken about three hours after the end of irradiation (Fig. 3). Another was taken 20 hours later after most of the 140-min activity had decayed. The latter curve was corrected for the decay of Ir^{194} during the 20-hour period and subtracted from the

[12] Sherr, Bainbridge, and Anderson, Phys. Rev. **60**, 473 (1941).
[13] A. J. Moses and D. S. Martin, Jr., Phys. Rev. **84**, 336 (1951).
[14] Jensen, Nichols, Clement, and Pohm, AEC Report ISC-157 (1951).

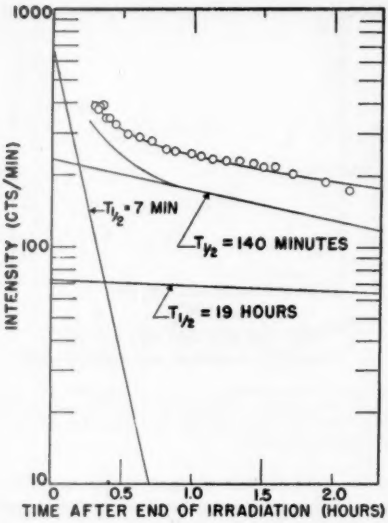

FIG. 4. Iridium fraction from 15-min irradiation of $PtCl_4 \cdot xH_2O$ with 70-Mev maximum beam energy.

upper curve shown in Fig. 3. The lower curve in Fig. 3 shows the absorption curve for the 140-min component obtained by the subtraction. From a rough Feather analysis the maximum beta-energy was estimated to be 1 Mev.

In order to determine if the 140-min iridium was the parent of the 18-hr Pt^{197}, an IrO_2 sample was separated after a five-hour irradiation. It was immediately dissolved and reprecipitated after the addition of platinum carrier to insure complete separation from the platinum activities formed during irradiation. The IrO_2 sample was redissolved, platinum carrier was added, and after varying periods of time iridium was separated from the platinum carrier. The platinum samples carried only 5–10 counts/min of activity. On the basis of the iridium counting rate they should have contained 500 counts/min if the 140-min iridium activity activity were the parent of the 18-hr Pt^{197}. These results indicate that the 140-min activity cannot be assigned to Ir^{197}. The 140-min activity would logically be assigned to either Ir^{195} or Ir^{196}.

The relative yield of the 140-min activity (Table I) was 0.54 the yield of Ir^{194}. However, in an irradiation with a 30-Mev maximum beam energy the relative yield ratio, 140-min Ir/Ir^{194} increased to 0.70. Such a result indicates that the 140-min activity is formed by a $(\gamma,\dot{p})$ but not by a $(\gamma,\dot{p}n)$ process. Therefore, an assignment to Ir^{195} appears likely. The observed beta-ray energy of 1 Mev is in agreement with the difference in the atomic masses of Ir^{195} and Pt^{195} as calculated by Metropolis and Reitwiesner.[15] This assignment would also be supported by the higher yield of Ir^{194} at the 70-Mev beam energy because Ir^{194} can form by the two processes, $(\gamma,\dot{p})$ and $(\gamma,\dot{p}n)$.

7-Min Iridium Activity

The decay curve of an iridium fraction which was separated rapidly following a 15-minute irradiation of $PtCl_4 \cdot xH_2O$ is given in Fig. 4. The curve shows a 7-minute component. In an irradiation at 30-Mev maximum beam energy the yield ratio of the 7-min to the 140-min activity was unchanged. Hence, it also was formed primarily by a $(\gamma,\dot{p})$ process. These features seem to eliminate Ir^{196} as a possibility and indicate Ir^{197} as the most likely assignment. Its yield which is lower than the yield of the 140-min activity may reflect the lower abundance of the target isotope. However, an assignment to an isomeric state of Ir^{195} has not been excluded.

The authors wish to thank Dr. L. J. Laslett and Dr. D. J. Zaffarano and the synchrotron crew for their assistance in providing the necessary irradiations, also Dr. V. A. Fassel and his assistants for performing the spectroscopic analyses.

[15] N. Metropolis and G. Reitweisner, "Table of Atomic Masses," AEC Report NP 1980 (1950).

Q Values of the $C^{12}(d,p)C^{13}$, $Be^{9}(d,p)Be^{10}$, and $O^{16}(d,p)O^{17}$ Reactions

E. D. KLEMA* AND G. C. PHILLIPS
Rice Institute, Houston, Texas

(Received March 10, 1952)

The Q values of the reactions listed above have been obtained by measuring the energies of the disintegration protons by means of an annular magnet whose magnetic field was measured and kept constant by a proton magnetic moment regulator. The energy of the incident deuterons was measured in terms of the 0.8735-Mev $F^{19}(p,\alpha'\gamma)O^{16}$ resonance. The values obtained for the above reactions are 2.732 ± 0.006 Mev, 4.591 ± 0.008 Mev, and 1.918 ± 0.008 Mev, respectively. The neutron-proton mass difference as calculated from the present data for carbon and the data given by other workers for the Q's of a closed cycle of reactions involving C^{12} and C^{13} is 0.789 ± 0.008 Mev.

INTRODUCTION

THE precise measurement of the ground-state masses and of the energy levels of light nuclei is of importance in the development of a satisfactory theory of nuclear forces. One method of approach to this problem is the measurement, by magnetic analysis, of the momenta of charged particles produced in nuclear reactions. A large annular magnet for this purpose was first designed by Cockcroft[1] and used by Rutherford[2] and his co-workers to measure accurately the energies of the natural alpha-particle groups. A magnet similar to the one of Rutherford is being used at M.I.T. by Buechner[3] and his associated in studying nuclear energy levels. A magnet based on a modification of this design has been constructed at Rice Institute. The performance of this instrument has been checked by using it to measure the Q values of several nuclear reactions previously investigated by the M.I.T. group.[4]

In the present measurements a beam of deuterons was incident on a thin target of beryllium. The target was centered in the uniform field of the magnet, and the direction of the deuterons was at about 45° to the target plane. Those protons which came off the target at an angle of about 90° with respect to the incident deuteron beam were deflected by the magnetic field and brought to a focus 180° around from the target. At this point they passed through an energy resolution slit and then were counted in a mica window proportional counter. Because the incident deuteron beam was at right angles to the field of the annular magnet and was brought to the target through the field of the magnet, the angle between the incident beam and the emitted protons was not exactly 90°. Knowledge of the magnetic field necessary to deflect the emitted protons through the slit, together with the incident deuteron energy, enables one to calculate the Q value of the reaction.

In the experiments to be described, both the method used for determining the energy of the incident deuterons and that for measuring the field of the magnet were different from those used by Buechner. In the M.I.T. work the energy of the deuterons was measured by the magnetic analysis of those elastically scattered from thin foils placed in the target position. The magnetic field was measured by means of a fluxmeter calibrated in terms of polonium alpha-particles. In the present work the energy of the incident beam was determined by means of the 0.8735-Mev $F^{19}(p,\alpha'\gamma)O^{16}$ resonance as measured by Herb[5] and his associates. The magnetic field was measured in terms of the magnetic moment of the proton.

APPARATUS AND EXPERIMENTAL METHOD

The annular magnet was constructed of S.A.E. 4815 forging steel, which has satisfactory magnetic properties and excellent machining characteristics.[6] The outside and inside diameters of the annular region of the magnet were 29.500 inches and 25.560 inches, respectively. The gap between the pole pieces was 0.562 of an inch. The magnet began to saturate at about 16,000 gauss. It was supported on a stainless steel table by 1-inch bronze ball bearings so that it could be rotated through small angles when connected to the vacuum system of the Van de Graaff generator by a sylphon. This adjustment allowed the beam to be centered accurately on the target.

The magnetic field of the annular magnet was both measured and held constant by means of a proton magnetic moment regulator designed and constructed at this laboratory by Richard D. Jones. The proton magnetic moment absorption signal was presented on an oscilloscope screen and was used to monitor visually the constancy of the magnetic field. The width of the oscilloscope sweep was found to be equal to approximately 6 gauss, and the magnetic field was held constant to within ±1.5 gauss during the runs.

The frequency of the oscillator used to provide the energy at the Larmor frequency of the protons was

* Now at Oak Ridge National Laboratory, Oak Ridge, Tennessee.

[1] J. D. Cockcroft, J. Sci. Instr. **10**, 71 (1933).

[2] Rutherford, Wynn-Williams, Lewis, and Boden, Proc. Roy. Soc. (London) **A139**, 617 (1933).

[3] Buechner, Van de Graaff, Strait, Stergiopoulos, and Sperduto, Phys. Rev. **74**, 1226 (1948).

[4] Buechner, Strait, Sperduto, and Malm, Phys. Rev. **76**, 1543 (1949), and W. W. Buechner and E. N. Strait, Phys. Rev. **76**, 1547 (1949).

[5] Herb, Snowdon, and Sala, Phys. Rev. **75**, 246 (1949).

[6] Herbert C. Roters, *Electromagnetic Devices* (John Wiley and Sons, Inc., New York, 1941), p. 48.

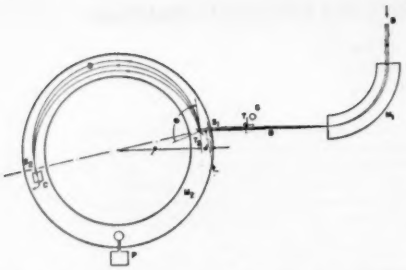

FIG. 1. Schematic diagram of the experimental arrangement: B is the trajectory of the bombarding deuterons; D, the trajectory of the disintegration particles; M_1, the 90° beam analyzing magnetic field; M_2, the annular analyzing magnet for 180° disintegration particle focusing (with radius of curvature ρ); T_1, the rotatable CaF_2 calibrating target; G, the Geiger counter for energy calibration with the $F^{19}(p,\alpha'\gamma)$ reaction; d, the distance between beam entrance slit S_1 and the target T_2; r, the radius of curvature of the entering deuteron mean in the magnetic field M_2; S_3, the energy resolution slit placed at the focal point; C, the proportion counter; and P, the proton moment magnetometer.

measured by means of a U.S. Army Signal Corps Frequency Meter Model No. BC-221-D. The oscillator frequency was checked often at the ends of bombardments, which lasted about 10 minutes; it was found that the drift of the oscillator during a measurement was of the order of a few thousand cycles/sec. The frequency meter was checked by beating its signal with that of radio station *WWV*.

The vacuum system placed in the annular gap of the the magnet was made by bending copper tubing of 2-inch outside diameter and $\frac{1}{16}$-inch wall thickness into the arc of a semicircle and then flattening it. The housing for the target assembly was formed of brass sides with phosphor bronze lids. This housing was silver-soldered to the copper vacuum tube and had entry ports for the beam and for the target assembly. Defining slits of chosen width could be inserted into the beam entry port. For one-half percent energy resolution, the slit width was 0.060 cm. A glass viewing port allowed the region about the target to be seen. Inside this chamber insulated silver electrodes electrically shielded the target and, when held at about 90 volts below ground, suppressed secondary electron emission from the target. The target assembly was constructed to slip very snugly into the target chamber and could be accurately repositioned. The vacuum seal was made with an "O" ring. A rod that could be rotated through a simple teflon seal carried (at 90° to each other) both the target and a quartz disk with a fine quartz fiber cemented to the disk at right angles to the rod. This arrangement allowed the beam spot on the target to be positioned precisely. A silver cylinder behind the target was carried by this assembly to stop the beam. This silver cylinder and the silver electron suppressor formed a Faraday cage for measuring the beam passing through the target.

The detector for the disintegration protons was a mica window proportional counter. This counter could be removed from a brass and phosphor bronze housing silver-soldered to the other end of the copper vacuum tube. The counter, which could be repositioned accurately, carried chosen focal plane slits in front of its window. The mica window thickness of 2.1-cm air equivalence was suffivient to stop scattered deuterons that otherwise would contribute a background of counts. The slit width for one-half percent resolution was 0.0875 cm.

The radius of curvature of the circular path from target to slit along the middle of the annular region was measured accurately by means of the calibrated screw on a milling machine. This radius was 34.895 cm. The angle which the direction of the incident deuterons made with the direction of the outgoing protons moving along the central path of the annular region, θ_0, was measured in the following manner: The deuteron beam was made to pass through a slit placed in the uniform field on the line joining the target and its focal point, and the beam was then centered on the target. The centering of the beam spot on the target was accomplished by rotating the quartz disk into the position otherwise occupied by the target. Stops on the target rotation system accurately aligned the target or quartz disk into the same position. If the distance between the slit and the target is d and the radius of curvature of the deuterons in the uniform field of the annular magnet is r, then to the first order,

$$\cos\theta_0 = -d/2r.$$

The quantity r was calculated from the known energy of the deuterons and the known magnetic field of the annular magnet. The distance d was 2.600 cm. Figure 1 schematically shows the geometry of the experimental arrangement.

The monoenergetic deuterons used in these experiments were furnished by the Rice Institute pressurized Van de Graaff accelerator[7] and 90° magnetic analyzer. The energy of the deuterons was determined in terms of the accurately measured 0.8735-Mev $(p\alpha',\gamma)$ resonance in fluorine.[5] For the energy calibration of the Van de Graaff, a target of zinc fluoride about 2 kev thick for the incident protons (as determined by weighing on a microbalance) was rotated into the beam after the 90° analysis and was bombarded with a molecular hydrogen beam. The current in the coils of the analyzing magnet of the accelerator was varied until the peak of the resonance was reached. The 90° beam analyzing magnet current was then held constant at this value while the electrostatic generator was being changed over from the acceleration of the molecular hydrogen beam to the acceleration of an atomic deuterium beam and then the (d,p) reactions were investigated. At the conclusion

[7] Bennett, Bonner, Mandeville, and Watt, Phys. Rev. **70**, 882 (1946).

of a measurement, molecular hydrogen ions were again accelerated and the γ-ray counting rate was again determined. A 1-kev correction to the incident deuteron energy was made because of the target thickness. The difference in the masses of a deuteron and a molecular hydrogen ion were taken into account in calculating the deuteron energy. The determination of the electrostatic generator energy with the $F^{19}(p,\alpha'\gamma)O^{16}$ resonance was made with the anngular magnet off. However, when it was energized its fringing field influenced the 90° analyzer. The interaction of the field of the annular magnet with that of the analyzing magnet was measured experimentally, and this effect was corrected for in calculating the energy of the incident deuterons. The corrections to the deuteron energy were of the order of 20 kev.

The target used in the present experiments was a thin beryllium foil, about 80 μg/cm^2, kindly supplied to us by Dr. Hugh Bradner.[8] Oxygen was present on the surface of the beryllium in the form of a protective oxide, and the carbon was deposited by the action of the deuteron beam. The beryllium data were taken before any visible carbon deposit had been formed. The oxygen data were taken after a layer of carbon not over a few kev thick had been built up. The effect of the carbon deposit was taken into account in estimating the probable error to be assigned the oxygen Q value.

The (d,p) runs were made by measuring the proton counts per unit of charge passing through the target for various fields of the annular magnet. Since the field of the annular magnet was influenced by that of the analyzing magnet, an experiment was carried out by probing the field with the proton resonance magnetometer to give corrections to the observed frequencies due to the effect of the other magnet and to the natural inhomogeneities in the field of the annular magnet along the path of the protons from the target to the counter. The correction factors were of the order of 1.001. Some ferromagnetic materials were in the vicinity of the magnetic field: two Kovar glass seals and some iron in the proportional counter preamplifier. Probing the field in the regions of these materials, however, showed their effect was at the most one part in two thousand, and thus this small error has been neglected.

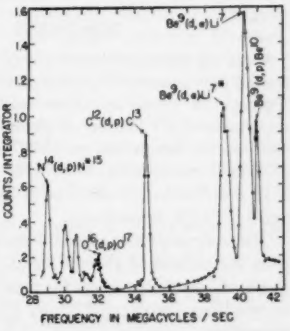

FIG. 2. The yield of disintegration particles, in arbitrary units, *versus* the magnetic field strength in units of Mc/sec for the bombardment of an 80 μg/cm^2 Be foil by 1747-kev deuterons.

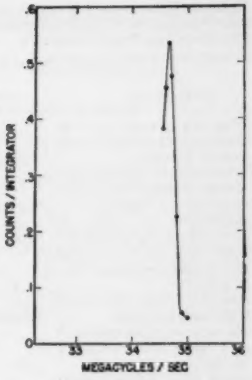

FIG. 3. Proton group from the $C^{13}(d,p)C^{13}$ reaction. The proton count per unit charge of deuterons striking the target is plotted as a function of the magnetic field as measured by the proton moment resonant frequency.

In taking data a beryllium target was first bombarded with the defining slits set to make $\Delta E/E$ one percent for the analyzed protons and the momentum position of the proton groups ascertained. These data are shown in Fig. 2. For the final experiments the energy resolution was set at one-half percent, and a fresh target was installed. Only the oxygen, beryllium, and carbon proton groups were investigated with the greater resolution. The criterion used for determining the proton energies to be associated with the observed peaks was that given by Rutherford.[2] From the observed points one-third the heights of the peaks on the high velocity side, the nonrelativistic energies of the protons were calculated by means of the following expression:

$$E_2 = 2(\pi^2/10^{14})(\nu_c/\nu_n)(1/\gamma)\rho^2 f^2,$$

where E_2 is the proton energy in Mev; ν_c/ν_n is the ratio of the cyclotron frequency to the nuclear resonance frequency of the proton. The value used, 0.358079 $\pm$0.000008, is that given by Sommer *et al.*;[9] γ is the gyromagnetic ratio of the proton. The value used is that given by Thomas *et al.*:[10] 2.67528$\pm$0.00006$\times 10^4$ sec^{-1} gauss^{-1}; ρ is the average radius of curvature of the paths of the protons in the field of the annular magnet; and f is the observed "momentum" (chosen at one-third the height of the peak on the high velocity side) in cycles/sec.

The relativistic correction to the proton energy is given by $E_2^2/2m_0c^2$, where m_0c^2 is the rest energy of the proton in Mev. The mass of the proton used, 1.0081374, is that given by Tollestrup *et al.*[11] The energy equivalence of 1 atomic mass unit, 931.04$\pm$0.07 Mev, is that given by Dumond and Cohen.[12]

[8] Hugh Bradner, Rev. Sci. Instr. **19**, 662 (1948).

[9] Sommer, Thomas, and Hipple, Phys. Rev. **80**, 487 (1950).
[10] Thomas, Driscoll, and Hipple, Phys. Rev. **78**, 787 (1950).
[11] Tollestrup, Fowler, and Lauritsen, Phys. Rev. **78**, 372 (1950).
[12] J. W. M. Dumond and E. Richard Cohen, Revs. Modern Phys. **21**, 651 (1949).

TABLE I. The sources of error and estimates of their magnitude in the determination of the Q values of the (d,p) nuclear reactions for the three target nuclei indicated.

Source of error	Probable error Carbon	Beryllium	Oxygen
Uncertainty in angle between directions of incident and emitted particles	2.4 kev	3.2 kev	4.0 kev
Measurement of magnetic field of annular magnet (including interaction of magnets)	2.0	2.4	1.8
Measurement of radius of curvature of particle paths	1.2	1.7	1.0
Measurement of bombarding energy (including interaction of magnets)	1.4	1.7	1.4
Determination of peak location	2.9	3.8	4.6
Target contamination	negligible	negligible	4.0
Probable error of measurement of $F^{19}(p,\alpha',\gamma)O^{16}$ resonance energy	1.5	1.4	1.5
Probable error of measurement of γ_e/γ_m and γ	0.1	0.2	0.1
Energy resolution of annular magnet	4.2	6.0	3.4

Figure 3 shows the proton yield per incident deuteron for the $C^{12}(d,p)C^{13}$ reaction plotted as a function of the magnetic field strength as measured by the proton moment resonance frequency, and is typical of the data obtained for the other groups.

The Q values of the reactions investigated were calculated from the following formula given by Livingston and Bethe:[12]

$$Q=(M_1-M_3)E_1/M_3 + (M_2+M_3)E_2/M_3-2(M_1M_2E_1E_2)^{\frac{1}{2}}\cos\theta/M_3,$$

where the subscripts 1, 2, and 3 refer to the incident particle, produced particle, and residual nucleus, respectively. The M's refer to the masses and the E's to the energies of the particles in question. The values of the masses used are those given by Tollestrup *et al.*[11] θ is the angle between the directions of motion of the incident and produced particles.

The values of θ_0 for the various proton groups, calculated from the formula given previously, are as follows: carbon—92.268°; beryllium—92.862°; oxygen —92.074°. Protons whose direction of motion made a greater angle than θ_0 with the direction of the motion of the incident beam at the target could not pass through the slit in front of the counter; their energy was lower than that of those moving along the central path of the annular region, and their radius of curvature was too small to enable them to pass through the slit. Protons making a smaller angle than θ_0 with the incident beam had a higher energy than those moving along the central path and could pass through the slit. The maximum angle such protons could make with the central path and still be detected was determined by the width of the vacuum chamber at a point 90° around from the target toward the counter. This angle χ, between the tangents to the paths of the protons traveling along the central path and those just striking the wall of the vacuum chamber, was 4.25°. The average angle between the incident deuterons and emitted protons was then $\theta_0-\chi/2$. These average angles for the various proton groups measured are as follows: carbon—90.14°; beryllium—90.56°; oxygen 89.95°.

Thus to a very good approximation the average angle between incident and emitted particles in the present experiments was 90°; and since the sign of $\cos\theta$ changes about $\theta=90°$, the Q values for the reactions were calculated for an angle θ of 90°. The uncertainty in the Q obtained due to the deviation of the average angle from 90° was calculated in each case from the following expression:

$$\Delta Q=2(M_1M_2E_1E_2)^{\frac{1}{2}}\Delta\theta/M_3,$$

where $\Delta\theta$ is the deviation of the average angle between incident and emitted particles from 90°. In combining this uncertainty with the others involved in the measurement of a given Q, the whole ΔQ (instead of $\frac{1}{4}$ of it) as calculated above was included in the probable error because of the uncertainty in the measurement of the angle χ. Similarly, the value of ρ used in the calculations of E_3 was that of the average path, not the ρ as measured for the path along the middle of the annular region. This correction factor to the measured ρ was 1.0007.

RESULTS

The values obtained for the Q's of the three (d,p) reactions studied in the present work are as follows:

$C^{12}(d,p)C^{13}$	$Q=2.732\pm0.006$ Mev
$Be^{9}(d,p)Be^{10}$	$Q=4.591\pm0.008$ Mev
$O^{16}(d,p)O^{17}$	$Q=1.918\pm0.008$ Mev.

The probable errors given above were determined from the estimated probable errors of the various measurements. These estimates are given in Table I.

DISCUSSION

From the measured Q's of the (d,p) reactions investigated the masses of C^{13}, Be^{10}, and O^{17} can be calculated. Taking the conversion from mass to energy and the masses of C^{12} and Be^{9} as given by Tollestrup *et al.*, one obtains the masses as 13.007555, 10.016756, and 17.004529, respectively, while if the more recent masses of Li *et al.*[14] are used, one obtains 13.007463, 10.016705, and 17,004529, respectively.

The neutron-proton mass difference can be calculated from the present (d,p) data for carbon and the values obtained by other workers for the Q's of a closed cycle of reactions involving C^{12} and C^{13}. Considering the

[12] M. Stanley Livingston and H. A. Bethe, Revs. Modern Phys. **9**, 277 (1937).

[14] Li, Whaling, Fowler, and Lauritsen, Phys. Rev. **83**, 512 (1951).

reactions

$$C^{13}+H^2\rightarrow C^{13}+H^1+Q_1,$$
$$C^{12}+H^2\rightarrow N^{13}+n^1+Q_2,$$
$$N^{13}\rightarrow C^{13}+2m_e+Q_3,$$

one obtains the following expression for the neutron-proton mass difference:

$$n^1-H^1=Q_1-Q_2-Q_3-2m_e.$$

The present measurements yield a value for Q_1. A value for Q_2 or -0.281 ± 0.003 Mev has been found by Bonner *et al.*,[15] and for Q_3 of 1.202 ± 0.005 Mev by Hornyak *et al.*[16] Using the value of the electron mass of 0.51079 ± 0.00006 Mev as given by Dumond and Cohen,[17] one obtains

$$n^1-H^1=0.789\pm0.008 \text{ Mev}.$$

[15] Bonner, Evans, and Hill, Phys. Rev. **75**, 1398 (1949).
[16] Hornyak, Dougherty, and Lauritsen, Phys. Rev. **74**, 1727 (1948).

ACKNOWLEDGMENTS

The authors wish to express their appreciation to Professor T. W. Bonner, who suggested this work. They wish to thank Mr. James W. Butler and Mr. Kendall Famularo for their aid in carrying out the measurements, and Mr. J. F. Van der Henst and Mr. E. J. Harmening for invaluable aid in constructing the apparatus. The Cameron Iron Works constructed the magnet and generously presented it to the Rice Institute. A grant from the Research Corporation, which aided this work, is gratefully acknowledged.

PHYSICAL REVIEW VOLUME 86, NUMBER 6 JUNE 15, 1952

Impedance Measurements on PbS Photoconductive Cells*

E. S. Rittner and F. Grace†
Philips Laboratories, Inc., Irvington-on-Hudson, New York
(Received January 7, 1952)

It is concluded from an analysis of existing and of new impedance measurements on PbS photoconductive cells that the observed decrease in parallel resistance with frequency is attributable to a known effect of distributed capacitance and should no longer be cited as convincing evidence for the existence of internal barriers in these photocells. These results, however, should not be construed as evidence against a barrier picture.

I. INTRODUCTION

It has been postulated by Sosnowski, Starkiewicz, and Simpson[1,2] that in PbS photoconductive cells the intercrystalline contacts between *n*- and *p*-type material constitute a controlling influence on the dark resistance and photosensitivity. The most direct experimental evidence yet advanced in support of this hypothesis is Chasmar's[3] observation that the resistance component of an equivalent parallel *RC* circuit decreases with increasing frequency, ostensibly due to capacitative shunting of the intercrystalline barriers. However, according to a theory of Howe,[4] which is briefly outlined in Sec. II, even a homogeneous resistor should exhibit a decrease in parallel resistance with frequency because of distributed capacitance effects. An analysis of Chasmar's data in this light, which is presented in Sec. III, indicates that distributed capacitance represents an alternative explanation of the data. In Sec. IV new impedance measurements of our own are presented which confirm this conclusion and which in addition indicate that the barrier picture is inadequate to account quantitatively for the observed decrease with frequency of the parallel resistance. The conclusions of the present study are explicitly set forth in Sec. V along with a statement of opinion regarding the *p–n* barrier hypothesis.

II. THE HOWE THEORY

It has been argued by Howe[4] that if a steady potential difference is applied across a resistor R, there will be a linear fall in potential along it and an electrostatic field will be set up as indicated in Fig. 1 (a). Each pair of elements like a, a' will act like a condenser with a capacitance given by the quotient of the surface charge on the element to the potential difference between the elements. If the capacitance per unit length is assumed to be a constant C over the entire length $2l$ of the resistor and if the latter is "folded" in half, then it may be seen that the resistor is equivalent to a shorted transmission line of length l, dc resistance per unit length R/l, and capacitance per unit length C [see Fig. 1 (b)]. The impedance of such a line is

$$Z=Z_0\tanh al, \qquad (1)$$

* Presented at the 311th meeting of the American Physical Society.
† Present address: International Business Machines Corporation, Poughkeepsie, New York.
[1] Starkiewicz, Sosnowski, and Simpson, Nature **158**, 28 (1946).
[2] Sosnowski, Starkiewicz, and Simpson, Nature **159**, 818 (1947).
[3] R. P. Chasmar, Nature **161**, 281 (1948).
[4] G. W. O. Howe, Wireless Engineer **12**, 291 (1935); **12**, 413 (1935); **17**, 471 (1940).

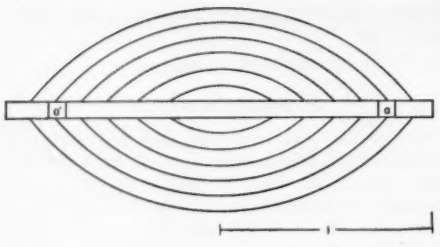

FIG. 1(a). Edge view of resistor showing the electrostatic field.

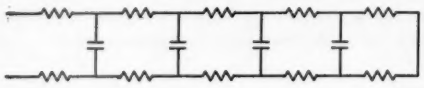

b

FIG. 1(b). Howe's equivalent circuit.

where $Z_0=(R/j\omega Cl)^{\frac{1}{2}}$ and $\alpha=(j\omega CR/l)^{\frac{1}{2}}$. If this impedance is expressed as an equivalent parallel combination, then the resistance component $R_{||}$ and the capacitance component $C_{||}$ will both be functions of frequency. This is illustrated in Fig. 2, using as abscissa the dimensionless quantity $flCR$, where $f=\omega/2\pi$.

In order to justify the use of the transmission line analogy, it is necessary to show that the capacitance per unit length is reasonably constant. To this end Howe has made the simplifying assumption that the surface charge density is a linear function of distance and has shown by numerical computation that the resulting potential is reasonably linear with distance. The value of the corresponding capacitance per unit length C is found to depend only upon geometric factors. For a flat plate resistor supported by an insulator of dielectric constant ϵ, with an electrode width $2w$ much greater than the electrode separation $2l$, which is a reasonable representation of the photoconductive cells discussed in this paper, the capacitance per unit length is

$$C=0.35(\epsilon+1)w/l\ \mu\mu f/\text{cm}. \qquad (2)$$

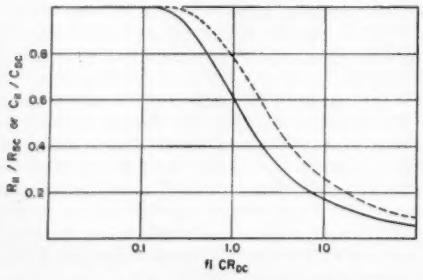

FIG. 2. Howe's theoretical curves. ——— resistance, - - - - - - capacitance.

The dielectric constant of the glass envelope is in the neighborhood of 5. However, since the thickness of the glass is by no means large compared to the electrode separation, the effective dielectric constant may assume a value between 1 and 5.

The Howe theory applies only to resistors so well isolated that all the lines of force may be considered to start and to terminate somewhere on the resistor. In practice it is extremely difficult to avoid a small amount of distributed capacitance to ground without employing long leads, thereby introducing inductance difficulties. It is important to appreciate that the combination of the end-grounded resistor and its grounded surroundings represents a shorted transmission line of length $2l$. Figure 2 of Howe's is applicable to this configuration, but in this case it is the distributed capacitance between the resistor and the grounded shield which determines the frequency dispersion of the impedance. Thus, in any case, if the impedance of the resistor is determined by distributed capacitance effects, the parallel resistance should behave in accordance with Fig. 2. If the distributed capacitance to ground is negligible, the results should be in accord with Eq. (2); otherwise, the observed distributed capacitance should be higher than the limiting value characteristic of the isolated resistor.

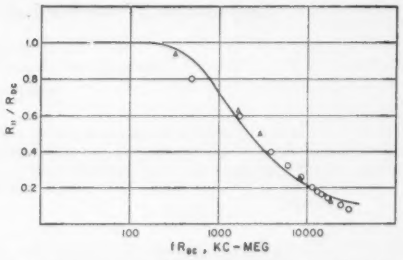

FIG. 3. Comparison of Chasmar's data with the Howe theory. ○ Points scaled from Chasmar's curve (3), 297°K, cell in darkness. △ Points scaled from Chasmar's curve (4), 297°K, cell illuminated. ——— Howe curve, $lC=0.7\mu\mu f$.

III. ANALYSIS OF CHASMAR'S IMPEDANCE MEASUREMENTS

Chasmar's room temperature data are replotted in Fig. 3 in a form suitable for analysis in terms of the Howe theory. The solid line represents a theoretical Howe curve with a value of lC best fitting the points, which are scaled directly from the experimental plots. The theoretical curve with $lC=0.7\mu\mu f$ fits the experimental points reasonably well both for the cell in the dark and under illumination. The range of values of lC following from the cell dimensions (0.1×1 cm) and Eq. (2), taking ϵ to be between 1 and 5, is $0.3-1.1\mu\mu f$, which represents excellent agreement between theory

and experiment in view of the drastic simplifications made in Howe's treatment.

Although the low temperature (194.5°C) data (not plotted) do not follow the Howe theory as well as do the room temperature data, it appears that distributed capacitance effects represent at least an alternative explanation of Chasmar's data.

IV. NEW IMPEDANCE MEASUREMENTS

We have carried out further impedance measurements on a number of commercial PbS photocells with the use of a Boonton Type 160-A Q-meter. The experimental arrangement employed in most of the work is illustrated in Fig. 4. The photocell was surrounded by an electrostatically shielded glass tube through which cp benzene, taken from a large supply thermostatted to within ±0.1°C, could be circulated. The temperature of the benzene, monitored by means of a thermocouple, was variable over the range +5°C to +40°C, the lower limit being set by the freezing point of benzene and the upper limit by possible irreversible changes in the cell characteristics at high temperatures. Care was exercised to ensure that all substances in the vicinity of the layer (i.e., benzene, glass, polyethylene) possessed sufficiently low dielectric losses so as not to influence the measurements. At the highest frequency employed (*ca* 10 mc) it is estimated that the contribution to the impedance from lead and layer inductances is negligible. The separation between electrodes was in all cases small compared to the distance (1.8 cm) between the layer and the electrostatic shield. In order to test whether or not the observed distributed capacitance was characteristic of the isolated photocell, additional measurements were carried out in air at room temperature with the photocell at the center of a 6-in. metal box and with the photocell unshielded at a distance of 12-in. from the ground plane of the Q-meter.

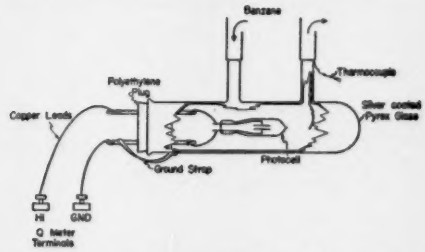

FIG. 4. Experimental arrangement for impedance measurements.

Typical experimental results obtained with the apparatus of Fig. 4 are displayed in Fig. 5, showing the fall-off with frequency of the parallel resistance at three different temperatures for a PbS cell manufactured by the Electron-Radar Products, Inc. In this particular cell the electrode separation separation was 0.5 cm and the electrode length 1.1 cm. The data are replotted in Fig. 6 as a Howe curve. The points for all three temperatures fall reasonably well about the solid line, which represents the theoretical curve for a value of $lC=0.9\mu\mu f$. On repeating the measurements with the photocell much further removed from ground and plotting the data as a Howe curve, the dashed curve of Fig. 6 is obtained characterized by a value of $lC=0.4\mu\mu f$. Thus, it appears that the frequency dispersion observed for the cell in the apparatus of Fig. 4 was determined by distributed capacitance between the photocell and ground, whereas the lower lC value found in the measurements with the cell far removed from ground arose from the self-capacitance of the photocell. The range of values of lC following from Eq. (2) and from the cell geometry is 0.4–1.1$\mu\mu f$. In view of the fact that lower values of lC are to be preferred in this particular case because of the unusually large interelectrode separation, agreement between experiment and theory may be regarded as satisfactory.

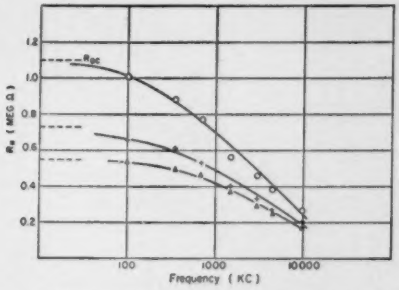

FIG. 5. Resistance *vs* frequency for PbS photoconductive cell in darkness. ○ $T=8°C$, + $T=27°C$, △ $T=40°C$.

Thus far, it is possible to conclude only that the impedance data can be adequately explained on the basis of distributed capacitance; however, the picture of p–n barriers as an alternative explanation of the data has not yet been ruled out. Differentiation between these two alternatives is possible on the basis that the

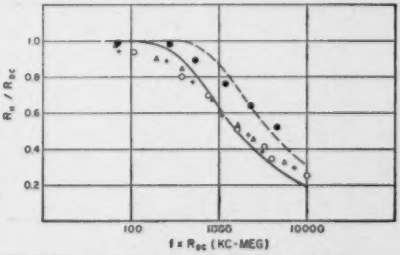

FIG. 6. Comparison of data of Fig. 5 with the Howe theory. Measurements in apparatus of Fig. 4: ○ $T=8°C$, + $T=27°C$, △ $T=40°C$. Cell far removed from ground: ● $T=20°C$. ——— Howe curve, $lC=0.9\mu\mu f$; ------- Howe curve, $lC=0.4\mu\mu f$.

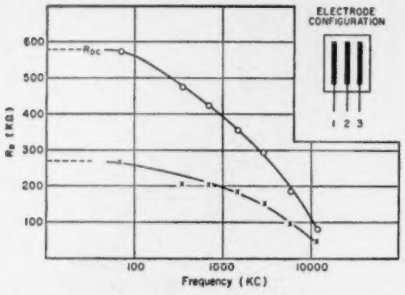

FIG. 7. Electrode configuration (inset) and resistance *vs* frequency data for three-electrode PbS photoconductive cell. ○ $R_{1,3}$, × $R_{1,2}$.

frequency dependence of the parallel resistance is a known function of the cell geometry in the case of distributed capacitance, whereas it is an intrinsic property of the layer in the case of the *p–n* barrier picture. Thus, if the impedance measurements are made on a photocell containing more than two electrodes at varying spacings, it should be possible to choose between these two explanations.

The inset in Fig. 7 shows schematically the electrode configuration in a number of special PbS cells obtained from the Continental Electric Company for the present purpose. The plots in Fig. 7 show typical data of parallel resistance *vs* frequency for that portion of the layer between electrodes 1 and 3 and between electrodes 1 and 2 under conditions where distributed capacitance to ground is negligible. In this particular cell the electrode length was 0.8 cm, the 1–3 electrode separation 0.12 cm, and the 1–2 electrode separation 0.05 cm. If the *p–n* barrier picture were the correct explanation of the data, then the ratio $R_{1,2}/R_{1,3}$ should be independent of frequency. That this is not the case may be seen by reference to Fig. 8. On the other hand, all the experimental points fall about a theoretical Howe curve with $lC=1.4\mu\mu$f (see Fig. 9); moreover, the range of values of lC predicted by Eq. (2) from the above dimensions

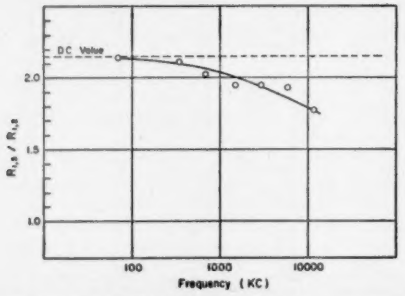

FIG. 8. Replot of data of Fig. 7 to test the barrier explanation.

is 0.3–0.9$\mu\mu$f, which, in view of the small interelectrode separation, represents not unreasonable agreement with the experimental value.

V. DISCUSSION

Since the results of the impedance measurements can be adequately understood on the basis of distributed capacitance effects, whereas some of them cannot be explained by the barrier picture, it is clear that the observed fall-off in parallel resistance with frequency can no longer be cited as evidence for the existence of *p–n* barriers in photoconductive cells. However, the impedance work should not be construed as evidence against the barrier picture, as the dispersion due to capacitative shunting of the barriers may occur at high frequencies and hence be masked by the lower frequency dispersion due to distributed capacitance.

Indeed, we would like again to venture the opinion that *p–n* barriers represent an essential feature of the

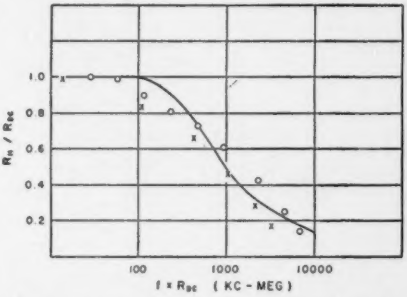

FIG. 9. Replot of data of Fig. 7 to test the distributed capacitance explanation. ○ $R_{1,2}$; × $R_{1,3}$; ——— Howe curve, $lC=1.4\mu\mu$f.

photoconductivity mechanism in PbS and in similar semiconducting films. In accordance with the argument previously advanced by one of us[5] the configuration of *n*-type crystallites separated by thin *p*-type regions seems to be an inevitable consequence of the evaporation and oxidation processes commonly employed in making photocell layers. In this connection we view as highly significant the recently acquired facts[6,7] that *n–p–n* junctions of Ge constitute very sensitive photoconductive units.

ACKNOWLEDGMENT

We wish to express our appreciation to some of our colleagues for a number of valuable discussions, particularly to F. K. du Pré, T. R. Kohler, N. C. Jamison, and R. A. Hutner. An exchange of letters with Dr. R. P. Chasmar has likewise proved helpful.

[5] E. S. Rittner, Science **111**, 685 (1950).
[6] Shockley, Sparks, and Teal, Phys. Rev. **83**, 151 (1951).
[7] K. G. McKay, Phys. Rev. **84**, 833 (1951).

Comparison of Magnetoelastic Energy Losses and Magnetic Hysteresis in Ferromagnetic Materials

G. Bonfiglioli, A. Ferro, and G. Montalenti
Center for Electrophysics Studies, Galileo Ferraris National Electrical Institute, Torino, Italy
(Received January 8, 1952)

In the present work it is shown that in several samples of ferromagnetic materials, with medium coercive forces, magnetic hysteresis energy losses in a saturation loop are higher than, but of the same order as, magnetoelastic energy losses in a stress cycle described between values of stress not far from the yield point.

Moreover, it is observed that the law that expresses the magnetoelastic energy loss of a stress loop as a function of the difference between maximum remanence $J_r(\tau)$ (measured at the maximum value of stress) and the initial value $J_r(0)$ (measured on material at rest) is of the type,

$$E=K[\Delta J_r(\tau)]^n,$$

where E is the energy loss and n is an exponent comprised between 1.2 and 2.2.

This law is very similar to the Steinmetz law, with the value of ΔJ_r substituted for the value of J (intrinsic induction at the tip of a magnetic loop).

I

FERROMAGNETIC materials, as is well known, show a high value of internal friction which, as was observed by Becker and Kornetzky[1] and Zacharias,[2] markedly decreases when the material is brought to magnetic saturation or is heated above the Curie temperature. (For a complete bibliography on the problem see the books of Becker and Döring[3] and Bozorth.[4]) Two of the authors[5] have shown in a previous article that the high value of internal friction is due to Weiss domain motion induced by mechanical stress; this movement is foreseen by domain theory and confirmed by several experimental results.[6] To draw these conclusions, the ratio J_r/J_s (where J_r=retentivity and J_s=saturation intrinsic induction) was assumed to be an index of domain motion,[7,8] and for several materials curves of the ratio J_r/J_s and curves of the magnetoelastic internal friction, both as functions of the applied stress, were compared. Magnetoelastic internal friction was defined as the magnetic part of the energy loss per unit volume and per mechanical cycle. In order to separate this part of the loss from the purely mechanical or viscous loss, which is always present, the magnetoelastic loss was measured as the difference between a measure of the total internal friction and a measure of the same on a saturated specimen. In that work it was observed that both curves show the same shape and show abrupt changes of slope at practically identical values of the stress. It was then concluded that the high value of internal friction of ferromagnetic materials was induced by domain motion under the applied stress.

The purpose of this paper is to compare the values of the losses in mechanical and magnetic hysteresis loops when the alteration (disregarding the sign) of domain structure, produced by magnetic field or by mechanical stress, is the same.

We have not been able to date to find the relation which establishes the equivalence between magnetic field and stress as an extension of the theory of Brown,[9] keeping in mind the well-known fact that in one case we are concerned with domains at 90° and in the other with domains at 180°. We therefore limited ourselves to finding the empirical relation between the values of the magnetoelastic energy loss and the variation $\Delta J_r(\tau)=J_r(\tau)-J_r(0)$ of the remanence, where $J_r(\tau)$ is

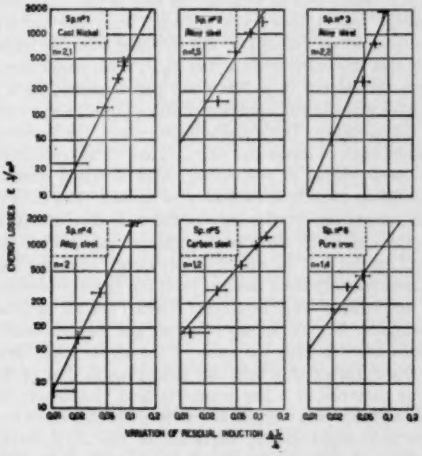

FIG. 1. Magnetoelastic energy loss values for different materials as functions of $\Delta J_r/J_s$. The reported energy loss is an average value in the specimen cross section.

[1] R. Becker and M. Kornetzky, Z. Physik 88, 634 (1934).
[2] J. Zacharias, Phys. Rev. 44, 116 (1933).
[3] R. Becker and W. Döring, *Ferromagnetismus* (J. Springer, Berlin, 1939), pp. 357–382.
[4] R. M. Bozorth, *Ferromagnetism* (D. Van Nostrand Company, Inc., New York, 1951), pp. 699–712.
[5] A. Ferro and G. Montalenti, J. Appl. Phys. 22, 565 (1951).
[6] R. M. Bozorth, J. phys. et radium 12, 308 (1951).
[7] R. M. Bozorth, Z. Physik 124, 519 (1948).
[8] G. Montalenti, Nuovo cimento 7 (1950).
[9] William Fuller Brown, Jr., Phys. Rev. 75, 147 (1949).

TABLE I. The magnetoelastic losses observed on the maximum stress cycle which the material can stand without yielding, and the corresponding energy loss area of a magnetic loop up to saturation.

No.	Material	Coercive force Asp/m	Saturation intrinsic induction Wb/m^2	J_τ/J_s initial value ($\tau=0$)	J_τ/J_s maximum stress in the loop	Maximum magneto-elastic energy losses, joule/m³	Saturation magnetic hysteresis, joule/m³	Ratio between max. magneto-elastic losses and magnetic hysteresis to saturation
1	Cast nickel	600	0.61	0.52	0.60	480	1720	0.28
2 and 3	Alloy steel quenched and tempered	1200	1.91	0.74	0.66	3100	7800	0.40
4	Idem	1300	1.91	0.77	0.65	3300	8500	0.38
5	Carbon steel $C=0.4$ percent quenched and tempered	1000	1.97	0.67	0.56	2250	4500	0.49
6	Pure annealed iron	320	2.13	0.51	0.46	525	2630	0.20
7	Armco iron[a]	80	2.15	...	...	340	720	0.45

[a] Source, for magnetoelastic losses, Boulanger (reference 10); for magnetic hysteresis R. A. Chegwidden, Metal Progress **54**, 705 (1948).

measured when the mechanical stress reaches the maximum value for the mechanical loop under consideration, and $J_\tau(0)$ is measured when the mechanical stress is zero. The meaning of $\Delta J_\tau(\tau)$ will be more clearly explained later.

II

The measurement methods have been amply described in a preceding paper.[6] Internal friction measurements have been carried out using a torsion pendulum with a frequency of about 4 *Hz*. It is to be observed that magnetoelastic losses in a stress cycle are largely independent of frequency, as was already shown by other authors[4,10] and was confirmed by the authors in preliminary tests. In our case the frequency was varied between about 1 and 80 *Hz*. The test piece was rigidly clamped at one end to a heavy bench and at the other to a flywheel free to turn on the axis of the test piece. Energy loss values were deduced from the natural decrease in oscillations of the flywheel after an initial impulse. Measurements of the J_τ/J_s ratio under stress were carried out in a Neumann permeameter, with a special attachment applying static torque to the ends of the specimen. The stress being torsional, the observed values both of losses and of J_τ/J_s are to be considered as mean values in a specimen with shearing stresses increasing linearly from center to surface. The data of the present paper refer only to the tests carried out on samples in which there was significant variation of the J_τ/J_s ratio; i.e., in which, under stress, domains had moved sensibly from the rest position. It was observed, in accordance with Boulanger,[10] that, for all samples examined, for low values of stress the magnetoelastic losses increase with the cube of the stress itself, thus giving evidence of a behavior analogous to that of the same material in a low magnetic field (Rayleigh). In this region it was not possible to test whether there was also any slight elastic variation of the J_τ/J_s ratio, because these low changes of domain orientation are below the sensitivity of the measurement method (± 2 percent). For higher values of the magnetoelastic losses, if these are plotted on logarithmic paper (Fig. 1) as functions of the variation of J_τ (i.e., of the difference between the value measured at the maximum stress of the mechanical cycle and the initial value at rest), it was observed that, within experimental error, the points lie on straight lines. Then the following relation holds:

$$E=K[\Delta J_\tau(\tau)]^n,$$

where E is the energy loss and n is found to be an exponent lying between 1.2 and 2.2. For magnetic hysteresis losses in all the materials tested, the law of Steinmetz with exponent about 1.6 holds; this was experimentally confirmed by the authors. It may be concluded that a similar law is also valid for magnetoelastic losses when ΔJ_τ is substituted for J.

At this point it should be noted that ΔJ_τ and J have very similar physical meanings. In fact J, as is evident, is the sum of the projections on the field direction of the vectors which may be assumed to represent domain magnetizations, and whose orientation is a function of the applied field. As this sum is zero when the material is unmagnetized, J is the variation with field of the projection, starting from the initial distribution. Similarly, it is easy to see that ΔJ_τ is the variation of the projection on the field direction of the domain magnetizations induced in this case by the stress. Thus, the observed validity of a law relating magnetoelastic energy losses and ΔJ_τ, very similar quantitatively to the law of Steinmetz, lends evidence to the thought that the process from which magnetoelastic losses arise in a stress cycle is of the same type as magnetic hysteresis; i.e., there is a Barkausen effect due to the stress applied.

In Table I are shown and compared the magnetoelastic losses observed on the maximum stress cycle which the material can stand without yielding, and the corresponding energy loss area of a magnetic loop up to saturation. The magnetoelastic loss values in the table correspond to the case of uniform stress in the specimen, equal to that at the surface, and have been deduced analytically from the observed values by taking into account the fact that the stress increases

[10] C. Boulanger, Rev. mét. **255** (1949).

linearly from the central axis, where its value is zero, to the external surface where its value reaches a maximum. It may thus be seen that the two values of maximum energy losses, magnetoelastic and magnetic, are of the same order of magnitude.

From these results it is not clear whether the differences observed between the two values are to be attributed to the fact that, on materials with not too low coercive forces, stresses below the yield point are unable to orient the domains completely in one direction, or to the fact that in one case 90° domains and in the other 180° domains participate in the process. For these reasons the question of the interpretation of the observed results still remains open.

We would like to thank Dr. W. F. Brown, Jr., for his kind advice regarding the present paper.

PHYSICAL REVIEW VOLUME 86, NUMBER 6 JUNE 15, 1952

An Hysteresis Effect in the Transmission of Electrons through Thin Dielectric Foils*

PAUL H. OWEN† AND C. SHARP COOK
Physics Department, Washington University, St. Louis, Missouri
(Received December 26, 1951)

The relative transmission of monoenergetic electrons through a dielectric foil suspended in vacuum has been observed to depend upon the previous history of the foil. A plot of this transmission against energy of incident electrons shows something resembling a type of hysteresis loop. Experiments are discussed which give evidence that this hysteresis loop is produced through the collection of negative charge within the foil.

I. INTRODUCTION

THE many nuclear and electronic phenomena which depend upon the passage of electrons through matter have made experimental studies of such a process of considerable interest. In this laboratory one of the chief reasons for desiring information on this subject is for the purpose of determining the relative transmission of beta-particles through Geiger-Müller (G-M) counter windows. Since the ratio of the number of beta-particles actually entering the sensitive region of the G-M counter to the number striking the outer surface of its window depends both upon the absorption and upon the scattering of the particles within the window, the ratio is not easily obtained from theoretical considerations.

A method utilizing the electrostatic acceleration of beta-particles from the source of a thin lens spectrometer[1] is being use to study this effect as it actually appears in the window of a G-M counter. It was thought advisable to have, if possible, in addition, some independent check on the results. The apparatus constructed for this purpose has led to some interesting results with regard to the transmission of electrons through nonconducting matter, but has not necessarily served as an independent check of the results of the other study.

II. APPARATUS

For these studies electrons were accelerated from a type of electron gun, focused by a semicircular, uniform field magnetic spectrometer, and collected in a Faraday cage. The magnitude of the charge thus collected was measured by means of a Lindemann electrometer. A movable window assembly was placed immediately in front of the Faraday cage. By proper rotation of the window assembly a zapon foil could be alternately inserted into or removed from the path of the beam of electrons. This arrangement was constructed as an insert for the 5.7-cm radius of curvature magnetic spectrometer.[2] This insert is shown in Fig. 1.

There are certain distinct differences between the two methods of attacking the problem. In the first place, the electron currents are orders of magnitude apart. In the G-M counter experiment individual electrons are recorded (in range of 10^{-16} to 10^{-19} ampere). In the experiment described by this paper electron currents of the order of magnitude of 10^{-10} ampere were collected by the Faraday cage. Secondly, whereas gas is always in contact with one surface of the G-M counter window, the foil on the rotatable foil holder always existed within a relatively well-evacuated region.

Because of the larger electron currents involved, the conditions appear, so far as applications are concerned, to approach more closely to many electronic problems than to the nuclear problem for which we attempted to use it.

The mechanical fragility of the thin zapon foils makes it difficult to weigh the foils without damaging them. For this reason, it has become the practice in this laboratory to specify the thickness of thin G-M counter windows in terms of the lowest energy electron

* Assisted by the joint program of the ONR and AEC.
† Now Ensign, U. S. Navy.
[1] C. H. Chang and C. S. Cook, Nucleonics **10**, No. 4, 24 (1952).
[2] G. E. Owen and C. S. Cook, Rev. Sci. Instr. **20**, 768 (1949).

which can be transmitted through them. Zapon windows as thin as 3 kev have been used.[3] As discussed later, the very nature of the current investigation has made this method of measurement of foil thicknesses experimentally impossible. Estimates of foil thicknesses were made by comparing production techniques against those for making foils to be used as G-M counter windows.

III. RESULTS AND DISCUSSION

A typical result of the experiment is shown in Fig. 2. Production methods would indicate that the foil should transmit electrons having a kinetic energy somewhat

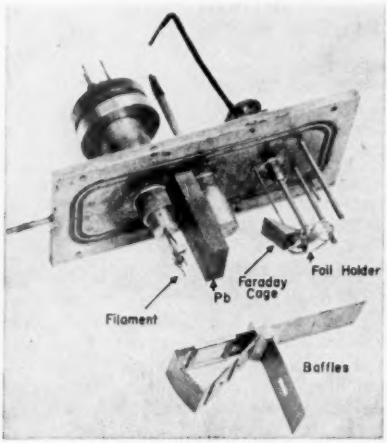

FIG. 1. Photograph of spectrometer insert used for this set of experiments. Filament structure for electron-gun is that portion immediately to the left of the lead block. Cup immediately to the right of the lead block holds flip coil assembly to be used with ballistic galvanometer for measurement of magnetic field. Movable window assembly, with six equally spaced openings for holding foils, and Faraday cage, immediately behind it, are further to the right. The baffle system, which under normal operating conditions is attached to the lead block, is shown at the bottom, detached from the rest of the system. The screen on this assembly, which sits immediately in front of the filament, is normally at ground potential and acts to accelerate electrons emanating from the filament, which is at a negative potential.

less than 2 kev. However, a transmission coefficient of zero is reached at an energy twice this. This in itself would not be significant were it not for the fact that the whole curve is somewhat anomalous.

Beginning at about 8 kev the transmission curve appears relatively smooth, steadily decreasing in magnitude to an energy slightly less than 4 kev. At this energy it exhibits a rather abrupt drop to zero transmission. Following this sharp drop it is impossible to pass through the foil any electrons having a kinetic energy within a few kilovolts (either up or down) of

[3] Owen, Cook, and Owen, Phys. Rev. 78, 686 (1950).

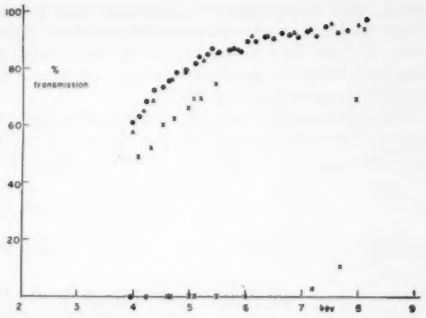

FIG. 2. Transmission curve for a thin zapon foil using the apparatus shown in Fig. 1. The circles represent the original data with the new foil, starting at about 8 kev. The crosses represent a continuation of these same data around the hysteresis loop. The triangles represent the data obtained after the spectrometer vacuum chamber was opened to air and the foil allowed to discharge.

4 kev. However, if the energy of the incident electrons is raised sufficiently (in this case to 7 kev) a finite positive transmission appears. A further slight increase in electron energy greatly increases the transmission such that at slightly less than 8 kev it has reached a value approximately the same as it initially had at this energy. This closes a pattern which might be considered as a sort of hysteresis loop.

A lowering of the energy again does not repeat the original curve (see Fig. 2). However, the initial curve can be repeated if air is let into the spectrometer vacuum system and the whole system again pumped down to a good vacuum.

The abrupt drop does not present so striking an appearance in Fig. 2 as it does if slightly thicker foils are used. Partial hysteresis loops are shown for two such foils in Fig. 3. The abrupt drops in transmission

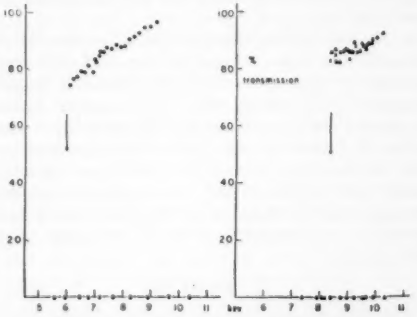

FIG. 3. Transmission curves obtained in the same way as the curve of Fig. 2 but using somewhat thicker zapon foils. The curve on the right shows three different sets of data obtained using a single foil. Air was let into the spectrometer chamber between each measurement in order to discharge the foil.

take place in these two cases at about 6 kev and 8 kev, respectively. Since the apparatus did not operate in a stable manner for applied filament voltages greater than 11 kev, it was impossible in both cases illustrated by Fig. 3 to complete the hysteresis loops.

Once the transmission had dropped to zero, the only way found again to transmit electrons was by the process of letting the vacuum system down to air and repumping a vacuum. It might also be indicated that if initial measurements were made at an energy greater than the energy of the abrupt drop, the value of the relative transmission initially obtained could be repeated. If, however, after repumping a vacuum the first measurements were made below the critical drop-off energy, the transmission coefficient remained zero throughout subsequent measurements until air was once again let into the spectrometer's vacuum chamber. The condition of zero transmission was observed to remain for as long as 24 hours. No attempt was made to see how long a period of time would be required before finite transmission could once again be observed.

The nature of the results led to the suspicion that a negative charge was developing inside the dielectric zapon foil, thus building up a potential which prevented further electrons from penetrating the foil. Further evidence for this arose from the fact that occasionally when the apparatus was operating in the immediate vicinity of the critical drop-off energy, the transmission over a period of time fell to zero even though no change was made in operating conditions.

This drop in transmission was never observed to occur instantaneously; instead it required at least several minutes to take place. The nature of the experiment made it impossible to measure this time with precision. However, a time in the order of minutes seems reasonable since a current of 10^{-10} ampere for a few minutes (say five for convenience in calculation) would build up a charge of 10^{-7} to 10^{-8} coulomb. With a voltage of a few kilovolts on the foil this would mean that the capacitance of the foil should be several micro-micro farads, which seems entirely reasonable.

If it were possible to make the foil conducting, further proof of this charging effect should be evident. All attempts to apply a conducting coating, such as a dag dispersion of colloidal graphite or an evaporated aluminum coating, led to foils too thick to allow successful operation in the energy region below 11 kev

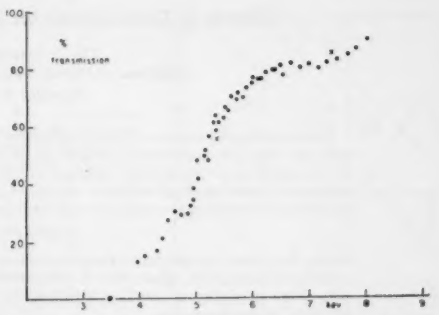

FIG. 4. Transmission curve for a zapon foil mounted on a mesh of fine, electrically grounded wire (1-mm spacing). Circles represent data taken as energy of beam progressed toward lower values. Crosses represent relative transmission obtained following the measurement of zero transmission at 3.46 kev.

(the upper limit of our stabilized high voltage supply). An alternate method involved a reduction of the distances between positions of ground potential on the surface of the foil. This was done by mounting the foil on a mesh of fine wire, the spacing between wires being approximately one millimeter. The resulting transmission curve was entirely different as indicated in Fig. 4. After traversing the region from higher energies to a point of zero transmission, a rise in energy again repeated the initial results.

In conclusion it must be said that the relative transmission of an electron beam through a dielectric foil appears to depend very strongly upon the previous history of the foil. In the present case it seems that the manner in which the foil has been electrically charged is the item which determines the anomalous behavior of the transmission curve and which leads to a transmission-energy type of hysteresis loop. The fact that the foil can be so charged is a result of the fact that many of the electrons entering the foil are elastically scattered so many times before leaving, that their effective path becomes of the order of magnitude of their range as determined by their inelastic collisions.

The authors wish to thank Professor H. Primakoff for many helpful suggestions about the methods for presenting the data and Mr. Lisle Morseman for doing the photography work necessary to produce Fig. 1.

Effects of Dislocations on Mobilities in Semiconductors*

D. L. DEXTER AND F. SEITZ
Department of Physics, University of Illinois, Urbana, Illinois
(Received February 29, 1952)

The scattering of electrons or holes in semiconductors by the dilation of the lattice around rigid, randomly-arranged edge-type dislocations is treated by the method of the deformation potential. The contribution of this scattering to the electrical resistance is determined from the Boltzmann transport equation by the method of Mackenzie and Sondheimer, except for the use of Maxwell-Boltzmann, rather than Fermi-Dirac statistics. The temperature dependence of the reciprocal of the mobility μ is given by

$$1/\mu=\alpha_l T^{\frac{1}{2}}+\alpha_i T^{-\frac{1}{2}}+\alpha_d T^{-1},$$

where the α's are temperature-independent quantities referring to scattering from the lattice, impurity atoms, and dislocations, respectively. A discussion is given of the relative magnitudes of these three terms, and of the possibility of obtaining experimental information concerning dislocations in semiconductors by electrical measurements.

THE electrical properties of nonpolar semiconductors have been intensively investigated[1] in recent years, particularly in regards to the effects of scattering of electrons and holes by lattice vibrations and impurity atoms. As is well-known, the electrical conductivity of metals is changed appreciably (of the order of 2 percent in Cu at room temperature) upon cold-working, which fact suggests that the scattering of electrons by dislocations[2] is an important effect in metals, when the density of dislocations becomes as high as 10^{12} per cm^2. Although there seems as yet no evidence for the presence of appreciable numbers of dislocations in semiconductors, it is nevertheless clear that if they do exist they will have an effect on the mobilities of electrons and holes, and in fact the well-developed electrical measurements provide a possible source of information concerning their presence; it is consequently the purpose of this note to investigate the expected magnitude of the scattering by stationary dislocations in these materials.

Bardeen and Shockley[3] have shown that, in an appropriate approximation, the scattering potential for a charge carrier in a distorted nonpolar, nonmetallic crystal can be written in the form

$$V(\mathbf{r})=(E_1/\epsilon)\Delta(\mathbf{r}), \tag{1}$$

where $\Delta(\mathbf{r})$ is the dilation of the lattice at the point $\mathbf{r}$, and E_1 is an experimentally determined parameter of the order of several electron volts. The dilation around an edge-type dislocation has been evaluated[4] by the use of the theory of elasticity for a continuous isotropic medium; thus the scattering potential may be written

$$V(\mathbf{r})=(E_1/\epsilon)(\lambda/2\pi)[(1-2\nu)/(1-\nu)]\sin\theta/r, \tag{2}$$

where λ is the unit crystallographic slip distance, ν the Poisson ratio, r the distance from the dislocation axis (assumed straight) and θ the angle measured from the slip direction. The necessary matrix elements $\langle\mathbf{k}'|eV|\mathbf{k}\rangle$ for the scattering of electrons in momentum states $\mathbf{k}$ to states $\mathbf{k}'$ have already been evaluated[5] (in reference 5, the parameter $2E/3$ is to be replaced by E_1). The calculation of the change in electrical resistance proceeds exactly as in reference 5 except that one uses Maxwell-Boltzmann, rather than Fermi-Dirac, statistics. Assuming the dislocations to be arranged isotropically, we obtain for the average change in resistivity

$$\Delta\rho=\frac{3\pi}{32}\frac{E_1^2\lambda^2}{k_0Th}\left(\frac{1-2\nu}{1-\nu}\right)^2 N\frac{m^*}{ne^2}, \tag{3}$$

where k_0 is Boltzmann's constant, T the absolute temperature, N the density of dislocation lines per unit area, and n is the density of carriers. Making the usual assumption of the additivity of the reciprocal collision times for the several scattering processes, we may write the reciprocal mobility as

$$1/\mu=\alpha_l T^{\frac{1}{2}}+\alpha_i T^{-\frac{1}{2}}+\alpha_d T^{-1}, \tag{4}$$

where the α's are temperature independent parameters and the subscripts l, i, d denote the contributions to the scattering from the lattice, the impurities, and the dislocations. α_d is then given by $300enT\Delta\rho$ (in practical units). Evaluating this for electrons in Si, so that $E_1=6.5$ ev, $\lambda^2=5\times10^{-16}$ cm^2, and $\nu=0.37$, we find $\alpha_d=1.1\times10^{-11}Nm^*/m$ (practical units). Pearson and Bardeen[6] have measured α_l and α_i for certain samples of Si with P impurities and find $\alpha_l=0.67\times10^{-6}$ (practical units) and, for samples containing $\sim10^{18}$ impurity atoms per cm^3, $\alpha_i\sim5$. The relative values of dislocation scattering and lattice scattering are about the same as the foregoing in diamond, tellurium, and germanium, and are about the same for electrons as for holes.[7]

* Research supported by the ONR.

[1] See, for example, W. Shockley, *Electrons and Holes in Semiconductors* (D. Van Nostrand Company, Inc., New York, 1950).

[2] J. S. Koehler, Phys. Rev. **75**, 106 (1949); see also D. L. Dexter, Phys. Rev. **86**, 770 (1952).

[3] J. Bardeen and W. Shockley, Phys. Rev. **80**, 72 (1950).

[4] J. S. Koehler, Phys. Rev. **60**, 398 (1941).

[5] D. L. Dexter, Phys. Rev. **85**, 936 (1952).

[6] G. L. Pearson and J. Bardeen, Phys. Rev. **75**, 865 (1949).

[7] We are assuming in these numerical estimates that the effective mass of the carrier is equal to the electronic mass m. Since

Using these values of the coefficients α, we see that the scattering from the fixed dislocation becomes as large as the lattice scattering at room temperature only for dislocation densities of the order of 10^{11} per cm^2. Since densities of this magnitude are found in metals only after severe cold-working, it seems unreasonable to expect dislocation scattering to be important in well-annealed semiconductors near room temperature, unless thermal motion possibly alters the scattering from dislocations in an appreciable way. In general, the density of dislocations N for which, at temperature T, the dislocation scattering is equal to the lattice scattering is given by

$$N=0.6\times10^{5}T^{6/2},$$

so that at hydrogen temperature a density of $\sim10^{8}$ lines per cm^2 would result in scattering comparable to or somewhat larger than that from the lattice. But, of course, the scattering by neither mechanism would be observable in silicon crystals having impurity contents as high as those described in the literature, namely, of the order of 10^{18} per cm^3. In such cases the impurity scattering at 20°K would be 3 orders of magnitude larger than that from the lattice. Thus it appears that evidence for the effects of scattering from fixed dislocations on the electrical properties of semiconductors should be sought in specimens having impurity content of the order 10^{15} per cm^3 or less and at temperatures in the hydrogen range.

Figure 1 shows the dependence of each of the terms in (4) upon temperature for the interesting range of temperature and several values of dislocation and impurity density for the case of electrons in silicon. The cross points of a given line of negative slope with the line having positive slope, which corresponds to $1/\mu$ for lattice scattering, gives the temperature below which the density of dislocations or impurity atoms associated with the given line of negative slope is sufficiently high to dominate the scattering.

It should be mentioned that the increase of dislocation scattering with decreasing temperature, as described by the third term in Eq. (4), is associated with the fact that the wavelength of the conduction electrons in a nondegenerate semiconductor increases as temperature decreases, and with the circumstance that the distortion associated with a dislocation is distributed over a large distance.

Although the dislocations have been treated as if rigid in the foregoing calculation, it is difficult to believe that the change in scattering which results from their thermal agitation can be important unless the scattering evaluated above is important. In any event the additional contribution should be small at low temperatures.

It should be emphasized that each dislocation is treated independently of others in the foregoing as if they are randomly distributed. Actually, dislocations may have additional effects upon resistivity if they are correlated into definite patterns. For example, regions where the residual strain is tensile over regions large compared to the wavelength of the electron may represent potential "pockets" in which carriers may be trapped.

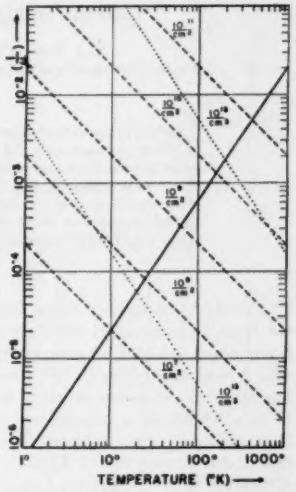

FIG. 1. Logarithm of the reciprocal mobility of electrons in Si *versus* the logarithm of the absolute temperature. The contribution to the scattering by the lattice is shown in the solid line of positive slope, that by impurity atoms (of density 10^{13}/cm^3 and 10^{18}/cm^3) in the dotted lines, and that by dislocations (of density 10^{7} to 10^{11} lines/cm^2) in the broken lines.

Essentially nothing is known at present about the type of lattice defect which is most prominent in silicon and germanium at high temperatures. Since only half the sites in a body-centered cubic lattice are occupied in the diamond structure, one might suppose that interstitial atoms introduced from the surface, grain boundaries, or from dislocations represent the type most strongly favored. This is supported by the fact that the liquid has a higher density than the solid at the melting point, as if disordering resulted in a more economical use of volume. In any case, it does not seem unreasonable to suppose that the disorder contributes to the formation of dislocations when crystals are prepared from the melt, perhaps by condensation of interstitial atoms or vacancies at suitable nuclei. Although the plastic properties frequently associated with the presence of dislocations are suppressed in these materials, this fact does not preclude the presence of dislocations inasmuch as there exists a number of mechanisms whereby dislocations are made stationary and do not contribute to plastic flow, e.g., pinning-down by nodes, impurities, and by topology. The density of dislocation lines formed in this way could be varied by quenching specimens from temperatures near the melting point at different rates. Thus a search for a contribution to the scattering of conduction electrons by dislocations might benefit by a study of specimens quenched from temperatures near the melting point.

the product $E_1^2m^*$ in Eq. (3) is proportional to m^{*-1}, dislocation scattering is about an order of magnitude more important than is indicated by the foregoing estimate for carriers whose effective mass is $\frac{1}{3}m$.

Search for Alpha-Particles from the $O^{16}(d,\alpha)N^{14*}$ Reaction*

R. J. VAN DE GRAAFF, A. SPERDUTO, W. W. BUECHNER, AND H. A. ENGE
Physics Department and Laboratory for Nuclear Science and Engineering, M.I.T., Cambridge, Massachusetts
(Received February 18, 1952)

Studies of the gamma-rays from several nuclear reactions have indicated the existence of an energy level in N^{14} at approximately 2.3 Mev. An investigation of the $O^{16}(d,\alpha)N^{14}$ reaction has been carried out in order to investigate this region of excitation in N^{14}. Two-million-volt deuterons from an electrostatic generator were employed, and the alpha-particles were analyzed with a magnetic spectrograph. The region of excitation studied was from 0 to 2.8 Mev. With the exception of the ground-state group, no alpha-particle groups were found, although any group with an intensity greater than 2 percent of the ground-state group would have been observed.

SEVERAL researches,[1] using different nuclear reactions, have reported the observation of a gamma-ray of about 2.3 Mev which appeared to be associated with a level at 2.3 Mev in N^{14}. Fowler, Lauritsen, and Lauritsen[2] in the re-evaluation of data for the reaction $C^{13}(p,\gamma)N^{14}$ found a gamma-ray of about 2.3 Mev. Bombarding C^{13} with deuterons, Thomas and Lauritsen[3] reported a gamma-ray of 2.318 ± 0.008 Mev which is attributed to N^{14*}. Beghian, Grace, and Halban[4] have bombarded B^{11} with polonium alpha-particles and report a gamma-ray of 2.2 ± 0.2 Mev as probably due to an excited state in N^{14}. Alburger,[5] bombarding PbO_2 with 3.7-Mev deuterons, observed indications of a gamma-ray of about 2.1 Mev. Sherr, Muether, and White[6] have investigated the decay of O^{14} and have observed the emission of 1.8-Mev positrons and a gamma-ray of about 2.3 Mev.

Mandeville and Swann[7] have investigated neutron groups from the reaction $C^{13}(d,n)N^{14}$, and they reported groups corresponding with levels in N^{14} at 4.90, 3.87, 3.47, and 2.19 Mev.

However, Fulbright and Bush,[8] using the reaction $N^{14}(p,p')N^{14*}$, found no proton group that might be associated with a 2.3-Mev level in N^{14}. It occurred to the present authors that suitable observations of alpha-particles from the reaction $O^{16}(d,\alpha)N^{14*}$ might make more definite the assignment of the 2.3-Mev gamma-ray and, moreover, might give further evidence regarding the possibility that an additional unresolved state may be involved. A search for such alpha-particles has therefore been made.

Deuteron bombardments of targets containing oxygen have been carried out at 2.0 and 2.1 Mev. The charged particles emitted at 90 degrees to the incident beam were analyzed with a 180-degree magnetic spectrograph. The results of the bombardments at 2.1 Mev are shown in Fig. 1, where the number of particle tracks per unit area of emulsion is shown as a function of $H\rho$. The deuterons elastically scattered from the target nuclei are shown, together with the alpha-particles observed. The survey shown extends over a range of values of $H\rho$ corresponding to alpha-particle energies that would be associated with N^{14} levels between 2.8 Mev and the ground state. This range corresponds to alpha-particle energies from about 1.6 to 3.8 Mev.

In the figure, the peaks due to oxygen and to carbon are double. This is because of the composite nature of the target, which was a film of Formvar, upon one side of which a thin layer of aluminum had been evaporated. The aluminum serves to increase the exposure that the Formvar can withstand without failure. The target was placed at an angle of 45 degrees to the deuteron beam, the aluminum being on the front side facing the oncoming beam and also facing the main part of the spectrograph.

In Fig. 1, the peak resulting from the ground-state alpha-particles is double, as is also the peak resulting from the deuterons elastically scattered from oxygen. This shows the presence of oxygen at the front of the aluminum in addition to the oxygen at the back of the aluminum. The fact that the peak due to the deuterons elastically scattered from carbon is double shows that there is also a layer of carbon contamination in the region of the front surface of the aluminum. Analysis of the data plotted in the figure shows a layer of contamination about 2.5 kev thick lying on top of the front-surface oxygen layer.

Using the ground-state alpha-particle peak shown in Fig. 1, the Q value for the reaction $O^{16}(d,\alpha)N^{14}$ has been computed. With proper correction for the layer of contamination just mentioned, the result for the Q value is 3.111 Mev, which is in good agreement with that obtained in previous measurements.[9]

Except for the ground state, only one small group of alpha-particles was observed. This group has a maximum count of 15 and in Fig. 1 occurs at a value of

* This work has been supported by the joint program of the ONR and AEC.

[1] Hornyak, Lauritsen, Morrison, and Fowler, Revs. Modern Phys. **22**, 291 (1950).

[2] Fowler, Lauritsen, and Lauritsen, Revs. Modern Phys. **20**, 236 (1948).

[3] R. G. Thomas and T. Lauritsen, Phys. Rev. **78**, 88 (1950).

[4] Beghian, Grace, and Halban, Proc. Phys. Soc. (London) **63**, 913 (1951).

[5] D. E. Alburger, Phys. Rev. **75**, 51 (1949).

[6] Sherr, Muether, and White, Phys. Rev. **75**, 282 (1949).

[7] C. E. Mandeville and C. P. Swann, Phys. Rev. **79**, 787 (1950).

[8] H. W. Fulbright and R. R. Bush, Phys. Rev. **74**, 1323 (1948).

[9] Strait, Van Patter, Buechner, and Sperduto, Phys. Rev. **81**, 747 (1951).

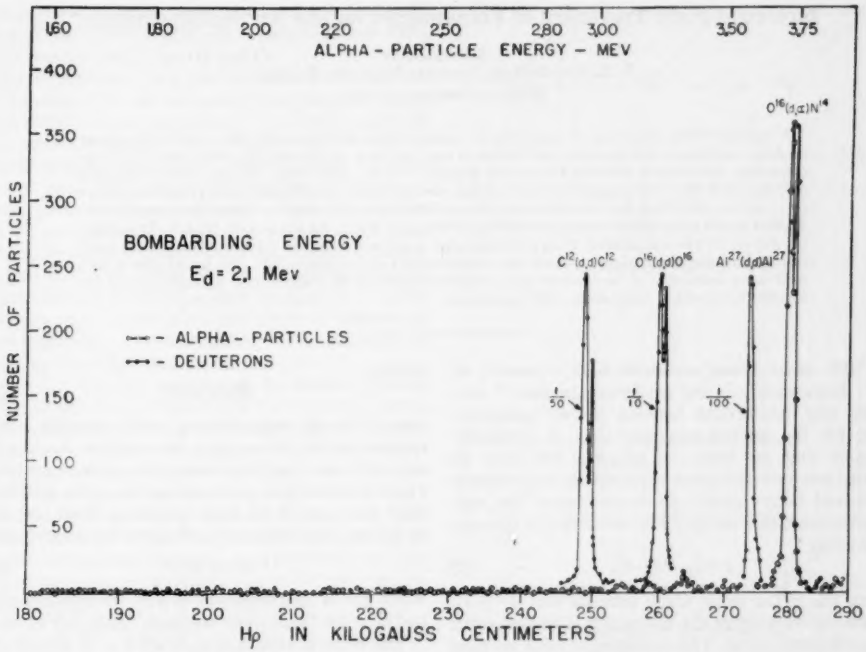

FIG. 1. Particle groups from aluminum-Formvar target bombarded with 2.1-Mev deuterons.

$H\rho = 264$ gauss-centimeters. Measurement of the shift in energy of the alpha-particles when the bombarding voltage was shifted from 2.1 to 2.0 Mev indicated that the target nucleus involved was not oxygen, but one of considerably higher atomic number, possibly aluminum. A test bombardment was then made, using a target of Formvar backed with copper. As the alpha-particle group was no longer observable, it was concluded that the group previously observed was not from oxygen.

Thus, there were observed within the range of the survey no alpha-particle groups that could be associated with an excited level in the N^{14} nucleus. It is estimated that a group equal in intensity to about 2 percent of the ground-state group could have been observed. However, it is evident that the alpha-particle yield, if it exists, might be much greater under other conditions of angle and voltage.

This result is in agreement with the recently reported work of Ashmore and Raffle[10] who studied the region of excitation in N^{14} from 2.0 to 6.1 Mev using 6.8-Mev cyclotron deuterons and magnetic analysis of the alpha-particles from this reaction. They found no levels in N^{14} between 2.0 and 3.95 Mev.

[10] A. Ashmore and J. R. Raffle, Proc. Phys. Soc. (London) **64A**, 754 (1951).

Molecular Field Treatment of Ferromagnetism and Antiferromagnetism*

J. SAMUEL SMART
U. S. Naval Ordnance Laboratory, White Oak, Maryland
(Received February 20, 1952)

A modified Weiss treatment of magnetism in crystals which considers both first and second nearest neighbor interactions with all four combinations of signs has been carried out. The usual results for ferromagnetism are obtained for both interactions positive. For the other cases, various types of magnetic ordering below the Curie temperature are predicted, the exact kind depending on the signs and magnitudes of γ_1 and γ_2, the Weiss field coefficients for first and second nearest neighbor interactions, respectively. Explicit results are given for the kind of ordering as functions of θ/T_c for bcc and fcc lattices. Expressions are derived for the susceptibility of an antiferromagnet above and below the Curie temperature, the latter calculation being given for only a single axis of spontaneous magnetization only. The theory gives a good qualitative description of the behavior of an antiferromagnet for all temperatures, although some of the detailed results are in disagreement with experiment.

THE usual Weiss molecular field treatment of ferromagnetism and antiferromagnetism[1-3] considers only interactions between nearest neighbors. Also, for the antiferromagnetic case, it is usually assumed that the lattice of magnetic ions may be divided into two equivalent sublattices as in the simple cubic and body-centered cubic structures. The high temperature molar susceptibility calculated in this way is given by

$$\chi = C_M/(T-\theta), \tag{1}$$

where C_M is the molar Curie constant and $\theta = \pm T_c$, depending on whether the interaction is ferromagnetic or antiferromagnetic. The experimental data on most antiferromagnetic compounds can be fitted reasonably well to an equation of this form. However, the value of θ/T_c, instead of being -1 as predicted, varies between rather wide limits, the observed values ranging all the way from $+0.7$ for MnAs to -5.0 for MnO.

Recent work by Néel[4] and Anderson[5] has shown that theoretical values of θ/T_c more in line with the experimental results may be obtained by including second nearest neighbor interactions and by considering magnetic lattices appropriate to actual antiferromagnetic compounds. The calculations of Anderson were carried out only for the case of both first and second nearest neighbor interactions antiferromagnetic while Néel's results are in a form not easily applied to antiferromagnetism. It seems worthwhile to generalize the method of Anderson to include all four possible combinations of sign.

THE HIGH TEMPERATURE SUSCEPTIBILITY AND THE MAGNETIC ORDERING

The starting point for calculating the high temperature susceptibility is the high temperature approximation of Langevin's equation of state for a paramagnetic material.

$$M = CH/T, \tag{2a}$$

where M is the magnetization in the direction of the applied field H. We assume the material contains N magnetic atoms, each with a magnetic moment $\mu = g\beta S_0$, where S_0 is the spin quantum number, g the gyromagnetic ratio, and β the Bohr magneton. Then (2a) can be written in a form more convenient for our purposes:

$$S = C'H/T, \tag{2b}$$

where $g\beta S$ is the component of μ in the direction of H and C' is the "spin Curie constant," $g\beta S_0(S_0+1)/3k$.

The Weiss procedure is to redefine H to include the effects of internal fields due to neighboring atoms. We shall denote the Weiss field coefficients for first and second nearest neighbor interactions by γ_1 and γ_2 respectively. It is convenient to define the γ_i as positive quantities and to write in the signs of the interactions explicitly. In terms of the Heisenberg theory, the γ_i are given by

$$\gamma_i = 2z_i|J_i|/g\beta, \tag{3}$$

where z_i is the number of ith nearest neighbors and J_i is the exchange interaction between electrons on ith neighbors. However, for the purpose of this paper, the γ_i may be considered merely as phenomenological constants with the J's being a measure of the difference in interaction energy of parallel and antiparallel spins.

In substituting into Eq. (2), γ_i will be multiplied by $\epsilon_i = \pm 1$, which specifies whether the ith neighbor interaction is ferromagnetic or antiferromagnetic. For convenience in discussion, the various combinations of signs of the ϵ_i are classified as indicated below.

Case	I	II	III	IV
ϵ_1	$+1$	-1	-1	$+1$
ϵ_2	$+1$	-1	$+1$	-1

Case I should of course lead to the usual results for ferromagnetism in the Weiss theory, except that the Curie temperature is defined in terms of two Weiss coefficients instead of one. Anderson has worked out Case II for a face-centered cubic lattice, and analogous

* Supported in part by the ONR.
[1] L. Néel, Ann. Phys. **18**, 64 (1932); **5**, 256 (1936).
[2] F. Bitter, Phys. Rev. **54**, 79 (1938).
[3] J. H. Van Vleck, J. Chem. Phys. **9**, 85 (1941).
[4] L. Néel, Ann. Phys. **3**, 137 (1948).
[5] P. W. Anderson, Phys. Rev. **79**, 705 (1950).

results for a body-centered cubic lattice are given by Van Vleck.[6] Their results will be rederived here along with new ones for Cases III and IV.

In problems involving antiferromagnetic interactions, it is necessary to divide the lattice of magnetic atoms into sublattices to take account of various possibilities of magnetic ordering. The method of subdivision depends on the symmetry of the specific lattice, but there should be at least division into enough sublattices so that a given atom has neither first nor second neighbors on its own sublattice. Also, we consider only cases where the sublattices have the same number of atoms. In general, for both first and second nearest neighbor interactions, there will be at least two kinds of magnetic ordering, one favorable to each type of interaction. The possibility of intermediate kinds of magnetic ordering is certainly not excluded.

We first give the calculations for a body-centered cubic lattice. In accordance with the discussion above, it is subdivided into four fcc lattices. We denote the four lattices by the subscripts 1, 2, 3, 4 at the risk of causing confusion with the subscripts 1 and 2 for the γ's. The division is made so that sublattices 1 and 2 contain the center atoms and sublattices 3 and 4 the corner atoms. Then an atom on sublattice 1 has all its second nearest neighbors each on sublattice 2 and half of its first nearest neighbors each on sublattices 3 and 4. The equations corresponding to (2b) are

$$S_k=(C'/T)[H_0+\sum_{\substack{l\neq k\\ k,l=1,2,3,4.}}\epsilon_{kl}\gamma_{kl}S_l], \quad \text{(4a, b, c, d)}$$

where H_0 is the applied magnetic field and $\gamma_{kl}S_l$ is the internal field acting on an atom on the kth sublattice due to its neighbors on the lth sublattice. The γ_{kl} are simply related to γ_1 and γ_2, the Weiss field coefficients for first and second nearest neighbor interactions. For example, $\gamma_{12}=\gamma_2$; $\gamma_{13}=\gamma_{14}=\frac{1}{2}\gamma_1$. The ϵ_{kl} are ±1, depending on whether the given interaction is ferromagnetic or antiferromagnetic.

From Eqs. (4) we can easily calculate the molar susceptibility

$$\chi=(Ng\beta/4H_0)\sum_k S_k=C_M/(T-\theta), \quad (5)$$

where N is Avogadro's number, $C_M=Ng\beta C'$, and

$$\theta=C'\sum_{l\neq k}\epsilon_{kl}\gamma_{kl}=C'\sum_i \epsilon_i\gamma_i. \quad (6)$$

The factor $\frac{1}{4}$ appears in Eq. (5) because the sum is over four atoms, one on each sublattice. The second summation in Eq. (6) is over the different shells of neighbors ($i=1, 2$, in this case).

The possible Curie temperatures can be found by setting $H_0=0$ in Eqs. (4) and finding what temperature allows nonzero solutions for the S_k. This procedure leads to a determinantal equation of the form

$$\begin{vmatrix} 1 & a_2 & \frac{1}{2}a_1 & \frac{1}{2}a_1 \\ a_2 & 1 & \frac{1}{2}a_1 & \frac{1}{2}a_1 \\ \frac{1}{2}a_1 & \frac{1}{2}a_1 & 1 & a_2 \\ \frac{1}{2}a_1 & \frac{1}{2}a_1 & a_2 & 1 \end{vmatrix}=0 \quad (7)$$

[6] J. H. Van Vleck, J. phys. et radium **12**, 262 (1951).

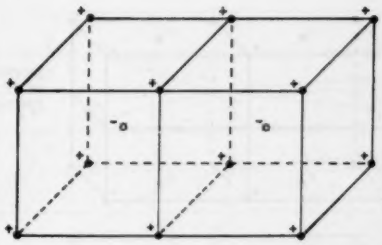

ORDERING OF THE FIRST KIND

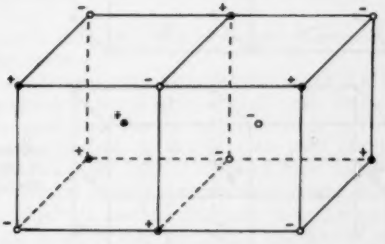

ORDERING OF THE SECOND KIND

FIG. 1. Possible kinds of magnetic ordering for a body-centered cubic lattice.

where $a_i=-C'\epsilon_i\gamma_i/T$. By the usual methods, this determinant may be factored into

$$[(1+a_2)^2-a_1^2][(1-a_2)^2]=0$$

giving

$$T_{c1}=-C'(\epsilon_1\gamma_1-\epsilon_2\gamma_2), \quad T_{c2}=-C'\epsilon_2\gamma_2,$$
$$T_{cF}=C'(\epsilon_1\gamma_1+\epsilon_2\gamma_2). \quad \text{(8a, b, c)}$$

Resubstituting the values of T_c, we find that T_{c1} corresponds to $S_1=S_2=-S_3=-S_4$, which is just the condition for ordering with respect to nearest neighbors, or ordering of the first kind, as Van Vleck has designated it. T_{c2} corresponds to $S_1+S_2=0$, $S_3+S_4=0$, which is the second nearest neighbor ordering, or ordering of the second kind. Figure 1 shows the two kinds of magnetic ordering for a bcc lattice. T_{cF} corresponds to $S_1=S_2=S_3=S_4$ or the ferromagnetic case. For each combination of signs of ϵ_1 and ϵ_2, one or more of the Curie temperatures may be negative, indicating that for this case, the particular kind of ordering has a higher energy than the random state.

The kind of magnetic ordering which actually exists below the Curie temperature will be that which corresponds to the highest value of T_c. For example, in Case II with $\epsilon_1=\epsilon_2=-1$, we have $T_{c1}=C'(\gamma_1-\gamma_2)$ and $T_{c2}=C'\gamma_2$. Then the ordering will be of the first or

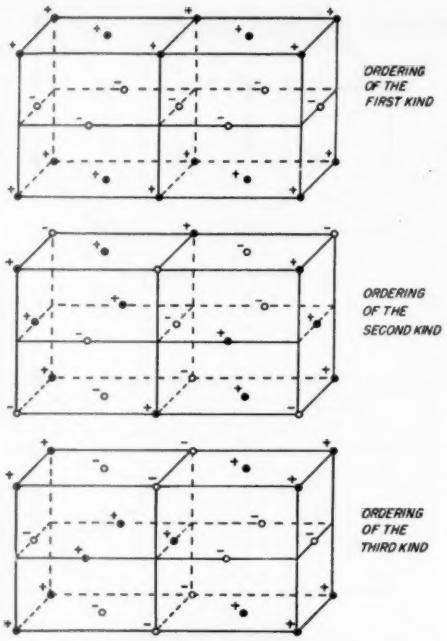

FIG. 2. Possible kinds of magnetic ordering for a face-centered cubic lattice.

second kind depending on whether γ_2 is less than or greater than $\frac{1}{3}\gamma_1$.

We should be able to obtain the Curie temperature for a specified type of magnetic ordering without solving Eq. (7). Suppose the ordering is specified by $S_k=\eta_{kl}S_l$ where $\eta_{kl}=\pm 1$. Then we note that T_c is given by

$$T_c=C'\sum_{l\neq k}\eta_{kl}\epsilon_{kl}\gamma_{kl}, \tag{9}$$

an expression equivalent to Eqs. (8).

One significant result of the calculations with different signs of first and second nearest neighbor interactions is that they help clarify the difference in the physical interpretations of the quantities θ and T_c. The quantity θ appearing in the susceptibility formula indicates the effect of the internal field on the susceptibility. If the internal field favors ferromagnetism, then it aids the applied field in aligning the moments. For this case, $\theta>0$, and for a given temperature (above T_c) χ is greater than its "pure paramagnetic" value C/T. On the other hand, if the internal field favors antiferromagnetism, then it hinders the applied field by tending to keep the total moment zero. In this case $\theta<0$, and for a given temperature χ is less than C/T. θ for a particular material is obtained by adding algebraically the contributions from first and second nearest neighbor interactions (and others, if more are considered) as indicated by Eq. (6).

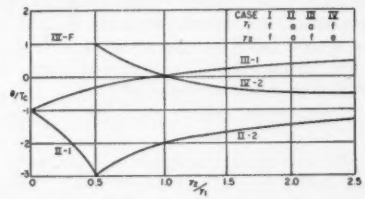

FIG. 3. θ/T_c values for a body-centered cubic lattice. The Roman numerals on each curve refer to the signs of the interactions; the Arabic numerals refer to the kind of magnetic ordering.

TABLE I. Values of θ and T_c for a body-centered cubic lattice.

Case	θ/C'	T_c/C' Ferro	1st	2nd	Magnetic structure
I	$\gamma_1+\gamma_2$	$\gamma_1+\gamma_2$			ferro
II	$-\gamma_1-\gamma_2$		$\gamma_1-\gamma_2$	γ_2	1st for $\gamma_2<\frac{1}{3}\gamma_1$; 2nd for $\gamma_2>\frac{1}{3}\gamma_1$
III	$-\gamma_1+\gamma_2$		$\gamma_1+\gamma_2$		1st
IV	$\gamma_1-\gamma_2$	$\gamma_1-\gamma_2$		γ_2	1st for $\gamma_2<\frac{1}{3}\gamma_1$; 2nd for $\gamma_2>\frac{1}{3}\gamma_1$

TABLE II. Values of θ and T_c for a face-centered cubic lattice.

Case	θ/C'	T_c/C' Ferro	1st	2nd	3rd	Magnetic structure
I	$3\gamma_1+\gamma_2$	$3\gamma_1+\gamma_2$				ferro
II	$-3\gamma_1-\gamma_2$			γ_2	$\gamma_1-\frac{1}{3}\gamma_2$	3rd for $\gamma_2<\frac{3}{4}\gamma_1$; 2nd for $\gamma_2>\frac{3}{4}\gamma_1$
III	$-3\gamma_1+\gamma_2$		$\gamma_1+\gamma_2$			1st
IV	$3\gamma_1-\gamma_2$	$3\gamma_1-\gamma_2$		γ_2		ferro for $\gamma_2<\frac{3}{4}\gamma_1$; 2nd for $\gamma_2>\frac{3}{4}\gamma_1$

The quantity T_c depends on the actual magnetic configuration existing below the Curie temperature—θ, on the other hand, is independent of what happens below the Curie temperature. Essentially, kT_c is a measure of the energy which has to be supplied to bring the material from a state of perfect order to one where the long-range order is destroyed. To find T_c, we combine the same terms as were used in finding θ but with plus or minus signs according to whether or not the magnetic structure is favorable or unfavorable to a given interaction, as indicated by Eq. (9).

The previous considerations enable us to write down θ and T_c for any magnetic lattice by inspection, once the molecular field coefficients and the magnetic structure are assigned. Thus, in considering the fcc lattice, we find that it is convenient to divide it into eight fcc sublattices. Then Eqs. (6) and (9) with appropriate generalizations to the eight sublattice case may be used to obtain θ and T_c directly. Figure 2 shows three possible kinds of antiferromagnetic ordering for the fcc lattice, the third kind being a compromise version

suggested by Anderson[5] which under certain conditions has a lower energy than either of the other two.

Tables I and II give values of θ and T_c for the bcc and fcc lattices, respectively. Only values of T_c which are largest for some range of γ_2/γ_1 and thus may correspond to actual structures, are listed.

θ and T_c are easily determined from susceptibility measurements, so that γ_1 and γ_2 can be calculated from the relations in Tables I and II, except for Case I where θ and T_c are identical. However, a convenient way of demonstrating the relation between the experimental results and the Weiss field coefficients is to plot θ/T_c as a function of γ_2/γ_1. These curves are shown in Figs. 3 and 4. The Roman numerals labeling the curves refer to the type of interactions and the Arabic numerals to the kind of ordering. Thus, for Case III, the ordering is of the first kind for all values of γ_2/γ_1. For Case IV, the material is ferromagnetic for low values of γ_2/γ_1 and antiferromagnetic with ordering of the second kind for high values of γ_2/γ_1. These two cases extend the theoretical upper limit for θ/T_c for an antiferromagnet from -1 to $+1$, and cover some experimental results which were not allowed by Case II alone. In general, there are two possible values of γ_2/γ_1 for a given θ/T_c ratio; thus there is an ambiguity in the theory. In order to determine the correct value of γ_2/γ_1 the magnetic structure must be established by neutron diffraction.

Table III gives experimental values of θ and T_c for some antiferromagnetic compounds. The columns designated "Low" and "High" give the two values of γ_2/γ_1, corresponding to the observed θ/T_c ratio and list the curves of Figs. 3 and 4 from which they were taken. In some cases, the kind of ordering has been determined by neutron diffraction; this information is recorded in the last column.

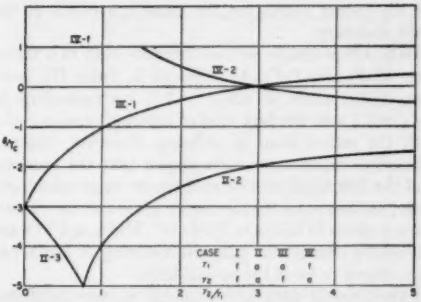

FIG. 4. θ/T_c values for a face-centered cubic lattice. The Roman numerals on each curve refer to the signs of the interactions; the Arabic numerals refer to the kind of magnetic ordering.

No antiferromagnetic compounds are known in which the magnetic lattice is body-centered cubic. However, in the rutile structure the magnetic lattice is body-centered tetragonal. In this case, an atom has two neighbors along the c axis at distance c, eight neighbors on the corners of the rectangular parallepiped at distance $(a^2+c^2)^{\frac{1}{2}}/2$, and four neighbors along the a axes at distance a. We may divide this structure so that the central atom is on the A sublattice, the corner atoms on the B sublattice, and the other two sets of neighbors on the A sublattice. For convenience, we will assign the coefficient γ_1 to the corner atoms and γ_2 to the combined effect of the other two sets. Actually, the atoms along the c axis are nearer the central atom than

TABLE III. Experimental data on antiferromagnetic compounds.

Compound	Crystal structure	Magnetic lattice structure	$-\theta$	T_c	$-\theta/T_c$	γ_1/γ_2 Low	γ_1/γ_2 High	Ordering from neutron diffraction
MnF_2	Rutile	bc				II-1	II-2	
		tetragonal	113	72	1.57	*0.22*	1.75	1st[a]
FeF_2	Rutile	bc				II-1	II-2	
		tetragonal	117	79	1.48	*0.19*	2.10	1st[a]
MnO_2	Rutile	bc						
		tetragonal		92				2nd[b]
VO_2	Rutile	bc						
		tetragonal		338				
MnO	NaCl	fcc	610	122	5.0	II-3	II-2	2nd[c]
						0.75	*0.75*	
FeO	NaCl	fcc	570	198	2.9	III-1	II-2	2nd[c]
						0.02	*1.57*	
CoO	NaCl	fcc	280[d]	292[d]	0.96	III-1	IV-2	2nd[c]
						1.05	*75*	
NiO	NaCl	fcc	2470[e]	647[d,f]	3.8	II-3	II-2	2nd[e]
						0.35	*1.07*	
MnS	NaCl	fcc	435	140	3.1	II-3	II-2	
						0.05	1.43	
$FeCO_3$	Calcite		14	57	0.25			

[a] R. A. Erickson and C. G. Shull, Bull. Am. Phys. Soc. **26**, No. 3, 17 (1951).
[b] R. A. Erickson, Phys. Rev. **85**, 745 (1952).
[c] Shull, Strauser, and Wollan, Phys. Rev. **83**, 333 (1951).
[d] C. Henry La Blanchetais, J. phys. et radium **12**, 765 (1951).
[e] T. R. McGuire, unpublished work.
[f] Approximate temperature of the susceptibility maximum. A crystal structure transition occurs about 520°K. The remainder of the data in this table were taken from the review article of H. Blaette, Ann. phys. **1**, 306 (1946).

are the corner atoms for the usual c/a ratios in the rutile structure.

Data are available on two fluorides with this structure, MnF_2 and FeF_2. As indicated in Table III, both have θ/T_c values of about -1.5, corresponding to $\gamma_2/\gamma_1 \sim 0.2$ with the first kind of ordering or $\gamma_2/\gamma_1 \sim 2.0$ with the second kind of ordering. However, neutron diffraction experiments have shown that the ordering is of the first kind; this determines the ratio unambiguously, as far as this simple theory goes, and the correct value is given in italics in Table III. MnO_2 and VO_2 are interesting because the magnetic ordering of MnO_2 has been shown to be of the second kind.

Experimental data are available on five antiferromagnetic compounds with the NaCl structure. For four of these, the magnetic structure has been determined to be of the second kind. For MnO, FeO, and NiO the second kind of ordering is allowed for the observed θ/T_c values with $\gamma_2/\gamma_1 = 0.75$, 1.57, and 1.07, respectively. In the case of CoO, however, where the ordering is also of the second kind, the value of γ_2/γ_1 is about 75, which seems unreasonably large. It is not clear whether the theory fails here or whether some special feature of the Co^{++} ion such as the relatively large spin-orbit coupling acts to give a very large effective γ_2/γ_1 ratio. The magnetic structure of MnS has not been determined but from the data it appears to be of the second kind with $\gamma_2/\gamma_1 = 1.43$.

$FeCO_3$ is an interesting case because it has a value of θ/T_c of -0.25. Such values are not allowed by the previous calculations of Néel and Anderson which consider only Case II. $FeCO_3$ has the calcite structure, a distortion of NaCl which suggests the subdivision into eight sublattices. If the results for the fcc lattice are used as a guide, the θ/T_c value could be explained either by Case IV with ordering of the second kind or Case III with ordering of the first kind. In view of the lack of experimental data on materials with the calcite structure, it does not seem worthwhile to make special calculations for this case.

THE SUSCEPTIBILITY BELOW THE CURIE TEMPERATURE

In an antiferromagnetic material below the Curie temperature, each of the sublattices acquires a spontaneous magnetization and the internal field becomes very large. This means we can no longer use the approximation $\mu H/kT \ll 1$ which leads to Eq. (2). Also the susceptibility depends upon the direction of the applied magnetic field with respect to the antiferromagnetic axis. Van Vleck[3] has calculated the susceptibility of a simple AB type antiferromagnet considering only first nearest neighbor interactions. For this case $\chi_\perp$ is constant for $T < T_c$ and $\chi_\parallel$ is zero at absolute zero, rising to $\chi_\perp$ at $T = T_c$ where $\chi_\parallel$ and $\chi_\perp$ refer to the susceptibility with the magnetic field applied respectively parallel and perpendicular to the antiferromagnetic axis. To obtain the powder susceptibility, $\chi_\parallel$ and $\chi_\perp$ are weighted in the ratio 1:2 giving the results that $\chi(0) = \frac{2}{3}\chi(T_c)$ and that the susceptibility should have a cusp at the Curie temperature. In this way, the qualitative features of the $\chi - T$ curve for an antiferromagnet are explained although the experimental value of $\chi(0)/\chi(T_c)$ is not always close to $\frac{2}{3}$. Anderson[6] has pointed out that if there is more than one antiferromagnetic axis within a single domain, then the $\chi(0)/\chi(T_c)$ ratio should be expected to be different from $\frac{2}{3}$. This seems to be actually the case in MnO_2 where both the susceptibility data[7] and the neutron diffraction data referred to in Table III suggest that the antiferromagnetic axis for sublattices 1 and 2 is perpendicular to that for sublattices 3 and 4. However, for most antiferromagnetic materials, the ratio is reasonably close to $\frac{2}{3}$, suggesting that there is only one antiferromagnetic axis; also, most of the observed crystal structure changes[8] at the Curie temperature support this idea. In the calculations to be given here, we consider only the case of a single antiferromagnetic axis.

As in the preceding section, the calculations are given explicitly for the bcc lattice. Let $\mathbf{S}_k$ be the average spin per atom on the kth sublattice with an external magnetic field applied and $\mathbf{S}_k{}^0$ be the spontaneous value in zero applied field. Then

$$\begin{aligned} H_k &= \mathbf{H}_0 + \textstyle\sum_{l \neq k} \epsilon_{kl}\gamma_{kl}\mathbf{S}_l \\ &= \mathbf{H}_0 + \textstyle\sum_{l \neq k} \epsilon_{kl}\gamma_{kl}[\mathbf{S}_l{}^0 + \boldsymbol{\delta}\mathbf{S}_l], \end{aligned} \tag{10}$$

where $\boldsymbol{\delta}\mathbf{S}_l$ is the change produced in $\mathbf{S}_l$ by application of the external magnetic field. (In the previous section, the quantities $\mathbf{S}_k$ were written as scalars because it was implicitly assumed they were either parallel or antiparallel to $\mathbf{H}_0$. For $T < T_c$ it is necessary to take into account differences in direction between $\mathbf{H}_0$ and $\mathbf{S}_k{}^0$.) Let the type of magnetic ordering existing be given by $\mathbf{S}_k{}^0 = \eta_{kl}\mathbf{S}_l{}^0$ where $\eta_{kl} = \pm 1$. Also, we assume that all of the $\boldsymbol{\delta}\mathbf{S}_l$ are equal. Then Eq. (10) may be rewritten

$$\begin{aligned} \mathbf{H}_k &= \mathbf{H}_0 + \mathbf{S}_k{}^0 \textstyle\sum_{l \neq k} \eta_{kl}\epsilon_{kl}\gamma_{kl} + \boldsymbol{\delta}\mathbf{S} \textstyle\sum_{l \neq k} \epsilon_{kl}\gamma_{kl} \\ &= \mathbf{H}_0 + (T_c/C')\mathbf{S}_k{}^0 + (\theta/C')\boldsymbol{\delta}\mathbf{S}. \end{aligned} \tag{11}$$

Then straightforward application of the Langevin-Weiss theory gives

$$S = |\textstyle\sum_k \mathbf{S}_k| = 4\delta S = S_0[\sum_k \cos(\mathbf{H}_k, \mathbf{H}_0) B(y_k)], \tag{12}$$

where B is the Brillouin function for spin S_0 and

$$y_k = g\beta S_0 |\mathbf{H}_k| / kT. \tag{13}$$

When $\mathbf{H}_0 = 0$, $\boldsymbol{\delta}\mathbf{S} = 0$ and

$$y_k = y^0 = 3S_0(S_0+1)^{-1} T_c T^{-1} |\mathbf{S}_k{}^0 / S_0|. \tag{14}$$

Now consider separately the cases where $\mathbf{H}_0$ is parallel and perpendicular to $\mathbf{S}_k{}^0$.

$$T < T_c,\ \mathbf{H}_0 \| \mathbf{S}_k{}^0$$

[7] H. Bizette and B. Tsai, *Colloque sur la polarisation de la matiere* (Paris, 1949).

[8] J. S. Smart and S. Greenwald, Phys. Rev. **82**, 113 (1951).

The applied field is assumed to be small in comparison with the internal field so that the Brillouin function may be expanded about $H_0=0$, giving

$$B(y_l)=B(y^0)+\eta_{kl}g\beta S_0[H_0+(\theta/C')\delta S]B'(y^0)/kT. \quad (15)$$

Also $\cos(\mathbf{H}_l,\mathbf{H}_0)=\eta_{kl}$. Substituting into Eq. (12) we find

$$S=\frac{4g\beta S_0^2}{kT}H_0B'(y^0)\left[1-\frac{g\beta S_0^2}{kT}\frac{\theta}{C'}B'(y^0)\right]^{-1}. \quad (16)$$

Expressing the result in terms of the molar susceptibility,

$$\chi_{II}=C_M\frac{3S_0(S_0+1)^{-1}B'(y^0)}{T-3S_0(S_0+1)^{-1}B'(y^0)\theta}. \quad (17)$$

Equation (17) reduces to Van Vleck's result[3] for his approximations ($S_0=\frac{1}{2}$, $\gamma_2=0$).

$$T<T_c,\ \mathbf{H}_0\perp\mathbf{S}_k^0$$

Let the z axis be the axis of spontaneous antiferromagnetism and the x axis be the direction of the applied magnetic field. Then since $|\mathbf{H}_0|\ll|\mathbf{H}_k|$, we may write

$$S=4\delta S=4|\mathbf{S}_k^0|\frac{|\mathbf{H}_z|}{|\mathbf{H}_e|}=4|\mathbf{S}_k^0|\frac{|\mathbf{H}_0+(\theta/C')\delta\mathbf{S}|}{|(T_c/C')\mathbf{S}_k^0|}, \quad (18)$$

and

$$S=4C'H_0/(T_c-\theta). \quad (19)$$

The molar susceptibility is then

$$\chi_\perp=C_M/(T_c-\theta)=\chi_{II}(T_c)=\chi(T_c). \quad (20)$$

T_c is determined experimentally as the point at which the maximum in the $\chi-T$ curve occurs, while θ may be found by fitting the high temperature ($T>T_c$) susceptibility data to Eq. (5). If the theory is consistent, then we should be able to use the values of θ and T_c determined in this way to calculate the susceptibility for $T<T_c$ from Eqs. (17) and (20). Figure 5 shows the results of such a calculation for MnO which has $\theta/T_c=-5$. The agreement between the theoretical and experimental curves is not very good, their shapes being considerably different. Actually, the curve for $\theta=-T_c$ has more nearly the shape of the experimental curve. However, Fig. 5 is plotted on a reduced scale; on an absolute scale the curve for $\theta=-T_c$ gives a susceptibility which is much too large.

One reason for the discrepancy between theory and experiment may be the neglect of anisotropy effects. Recently, Nagamiya[9] has calculated the susceptibility for a simple AB type antiferromagnet, including an anisotropy field. If this type of calculation were extended to second nearest neighbors and to more complicated lattices, the agreement might be improved. It is also possible that the reason for the discrepancy lies in a basic defect of the Weiss theory itself. Holstein and Primakoff[10] have shown that the Weiss theory and the spin-wave theory give quite different results for the intrinsic susceptibility of a ferromagnet below its Curie temperature.

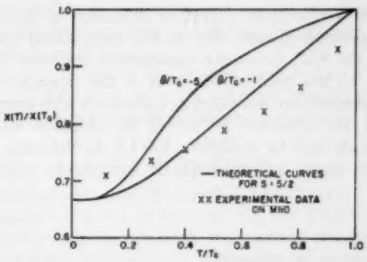

FIG. 5. $\chi(T)/\chi(T_c)$ vs T/T_c for a material with a single antiferromagnetic axis. The experimental data are taken from Bizette, Squire, and Tsai, Compt. rend. **207**, 449 (1938).

GENERAL DISCUSSION

This simple extension of the Weiss theory given above is a good qualitative description of the behavior of an antiferromagnet for all temperatures although some of the detailed results are in disagreement with the experiments. In this respect, it is quite similar to the usual Weiss theory of ferromagnetism. In particular the theory gives an adequate account of the θ/T_c values although it is uncertain as to just how much significance can be attached to the corresponding γ_2/γ_1. Since these quantities cannot be computed theoretically at the present time, we are forced to consider them merely as adjustable constants. The theory also gives explicit conditions for the different kinds of magnetic ordering, although here it is necessary to have the magnetic lattice subdivided properly.

It is an interesting question as to whether a simple Weiss theory which takes account of both first and second nearest neighbor interactions or a more sophisticated theory which considers only nearest neighbor interactions gives the better results in antiferromagnetism. Certainly the fact that both types of ordering have been observed in compounds with the same magnetic lattice (rutile) points up the importance of considering both interactions. It is interesting to compare the results of the Weiss field treatment to those of Li,[11] who applied the more elegant Bethe-P. R. Weiss method to the problem of a simple AB type antiferromagnet with first neighbor interactions only. His results indicate that there should be some curvature in the $1/\chi-T$ curve just above the Curie temperature (due to short range ordering) but that at high temperatures, the susceptibility should be given by Eq. (1) with $\theta\cong-T_c$.

[9] T. Nagamiya, Prog. Theoret. Phys. **6**, 342 (1951).

[10] T. Holstein and H. Primakoff, Phys. Rev. **58**, 1098 (1940).

[11] Y.-Y. Li, Phys. Rev. **84**, 721 (1951).

The low temperature curvature is evident in much of the experimental data, but as has been stated previously, the θ/T_c ratios are considerably different from unity. Li has pointed out that if the susceptibility measurements are not taken at sufficiently high temperatures, an apparent θ/T_c will be obtained whose magnitude may be as high as 1.5–1.7. In this way, the data on some antiferromagnetic compounds, such as MnF_2 and FeF_2, might be fitted, but for most the θ/T_c values fall considerably outside the range allowed by Li's theory. Presumably a Bethe-Weiss treatment including both types of interactions and appropriate magnetic lattices should correct some of the deficiencies of both Li's theory and the present theory (at high temperatures) but the amount of calculation involved seems formidable.

PHYSICAL REVIEW VOLUME 86, NUMBER 6 JUNE 15, 1952

A Note on the Absorber Theory of Radiation

PETER HAVAS
Department of Physics, Lehigh University, Bethlehem, Pennsylvania
(Received August 14, 1951)

The Wheeler-Feynman theory, starting with fields symmetric in time, obtained the Lorentz-Dirac equations of motion, which use retarded fields only, together with a condition on the total field of all particles in the universe. It is shown that if the field acting on a particle produced by all other particles is static but not zero, no motion of the system satisfying this condition exists. Some implications of this result for the physical interpretation of the Wheeler-Feynman theory are discussed.

RECENT attempts to obtain the force of radiative reaction on a moving charge in classical electrodynamics have proceeded from two different viewpoints. One is that of field theory, which considers the *total* field at all points in space to be the fundamental physical quantity. The other is that of action at a distance, which considers only the forces exerted on a charge by *other* charges to be physically meaningful.

The field theoretical point of view was first applied successfully to the problem of the motion of a point charge by Dirac,[1] who succeeded in obtaining the equations of motion first found by Lorentz on the basis of a model of an extended charge. These equations can be written

$$m_a v_a'^{\mu} = e_a \sum_{k \neq a} {}_{\rm ret}F_{\nu}^{\mu(k)} v_a^{\nu} + \tfrac{2}{3} e_a (v_a''^{\mu} + v_a'^2 v_a^{\mu}), \qquad (1)$$

where ${}_{\rm ret}F^{(k)}$ is the retarded field of the kth particle evaluated at the position of the ath one, and where we have assumed that there are no fields present except those due to charges.

The first derivation of the Lorentz-Dirac equations on the basis of action at a distance is due to the absorber theory of radiation of Wheeler and Feynman.[2] This was achieved taking the forces on the charges as determined by half the sum of the retarded and the advanced field, while the previous field theoretical derivations all had been based on the use of retarded fields alone.

In a previous paper[3] it was pointed out that the need for the exclusive use of retarded fields for the explanation of the radiative reaction arose only in the field theoretical derivations for the one-particle problem, but that the considerations of Wheeler and Feynman on the total field due to all particles are applicable to field theory as well as to action at a distance. It was concluded that one can obtain the Lorentz-Dirac equations in both theories starting with fields symmetric in time, in spite of the fundamentally different underlying physical ideas.

It was noted, however, that there was not complete equivalence of the retarded and symmetric cases. The considerations of Wheeler and Feynman led to the symmetry condition

$$\sum_{\text{all } k} {}_{\rm ret}F^{(k)} = \sum_{\text{all } k} {}_{\rm adv}F^{(k)} \text{ everywhere.} \qquad (2)$$

Therefore the solutions of (1) are subject to this condition in the symmetric case both in field theory and in action at a distance, while there is no such restriction imposed upon them in the retarded case.

It appears that present mathematical methods are not powerful enough to enable us to discuss the effect of this restriction in the general case.[4] We shall only discuss the case that the effect on a single charge of all other charges in the universe is that of a static field, i.e., that

$$\sum_{k \neq a} {}_{\rm ret}F^{(k)} = \text{const} = \sum_{k \neq a} {}_{\rm adv}F^{(k)} \text{ everywhere.} \qquad (3)$$

From this and condition (2) we must have

$${}_{\rm ret}F^{(a)} = {}_{\rm adv}F^{(a)} \text{ everywhere.} \qquad (4)$$

[1] P. A. M. Dirac, Proc. Roy. Soc. (London) **A167**, 148 (1938).
[2] J. A. Wheeler and R. P. Feynman, Revs. Modern Phys. **17**, 157 (1945).
[3] P. Havas, Phys. Rev. **74**, 456 (1948).
[4] For a discussion of some of the difficulties of the two-body problem, see P. Havas, Acta Phys. Austriaca **3**, 342 (1949).

A necessary, but not sufficient, condition for the validity of (4) is that

$$_{\text{ret}}F^{(a)}-{}_{\text{adv}}F^{(a)}=0 \text{ on the world line of particle } a. \quad (5)$$

But according to Dirac[1] we have on the world line

$$\tfrac{1}{2}e_a({}_{\text{ret}}F_\mu{}^{(a)}-{}_{\text{adv}}F_\mu{}^{(a)})v_a{}^\mu=\tfrac{2}{3}e_a{}^2(v_a{}''{}^\mu+v_a{}'{}^2v_a{}^\mu). \quad (6)$$

Therefore the condition (5) implies the vanishing of (6) or the vanishing of the radiation terms in (1).

Now the problem of determining the conditions under which Eq. (1) possesses solutions with vanishing radiation terms has already been solved by Schott.[5] He obtained the result that the only such solutions are motions in a plane; taking it as the x–y plane and having the particle at $t=0$ at $x=\frac{2}{3}ae_a{}^2/m_a$ and $y=0$, moving in the y direction with velocity $b(a^2+b^2)^{-\frac{1}{2}}$, such a motion will be produced by the combination of a uniform electric field E in the x direction of magnitude $\frac{2}{3}m_a{}^2(a^2+b^2)^{\frac{1}{2}}/(a^2e_a{}^3)$ and a uniform magnetic field H in the negative z direction of magnitude $\frac{2}{3}m_a{}^2b/(a^2e_a{}^3)$. The resultant motion is a hyperbola, with a constant y component of the velocity.

This result can be considerably simplified by changing to a frame of reference moving with a velocity $b(a^2+b^2)^{-\frac{1}{2}}$ in the y direction. In this frame the particle is moving in a straight line parallel to the electric field in the x direction; the magnetic field is zero. Therefore Schott's result can be expressed as follows: The only radiationless motions of a particle obeying the Lorentz-Dirac equations are those which in some frame of reference are parallel to a uniform electrostatic field causing the motion.

The motion of a charge in such a field has first been studied by Born,[6] who called it a "hyperbolic motion." It is given by

$$x=\pm(t^2+\text{const})^{\frac{1}{2}}, \quad y=z=0, \quad (7)$$

the upper and lower sign corresponding to the motion of a positive and a negative charge, respectively. This is a hyperbola with asymptotes $x=\pm t$ in the $x-t$ plane. In this plane the retarded field progresses parallel to these asymptotes in the direction of increasing t, and the advanced field similarly in the direction of decreasing t. Consequently for a positive charge the region to the left of the asymptote $x=t$ is not reached by the advanced field (similarly the region to the right of $x=-t$ for a negative charge), while the part of this region above the asymptotes is reached by the retarded field. Therefore the difference between the retarded and the advanced field does not vanish everywhere, i.e., Eq. (4) does not hold.

The only exception is provided by the case of zero field. In this case Schott's solution breaks down; however, this radiationless solutions is obviously given by

$$x=v_0t, \quad y=z=0 \quad (8)$$

if the reference frame is chosen appropriately. It can easily be shown that in this case Eq. (4) does hold.

Therefore the only motions of a particle obeying the Lorentz-Dirac equations in which the retarded field produced by the particle equals its advanced field everywhere are those with constant velocity.

Consequently, *if the field acting on a particle produced by all other particles is static but not zero, no motion of the system satisfying the symmetry condition (2) of the Wheeler-Feynman theory exists.* If we do not want to reject this theory, we have therefore to reject the original assumption of a static field; we have to assume that the field is only approximately static and therefore the retarded and advanced fields are not quite equal; their difference depends on the motion of all the particles in the universe.

This, however, amounts in effect to abandoning the application of the specific features of this theory to any practical problem, as we cannot hope ever to possess enough information about the initial conditions for such a problem even within classical theory. In practice we shall be forced to operate with the assumption of a knowledge of some average field acting on a particle. But then the symmetry condition (2) does not provide us with any information useful for the solution of our problem. If we accept the statistical interpretation suggested by Wheeler and Feynman we are in effect assuming that initially we possess knowledge of the retarded field only, but not of the advanced one.[7] Therefore, e.g., in the example treated above, we would mean by "static field" that the retarded field is static within the time and space interval of our experiment and nothing is known about the advanced one, and consequently we have to solve Eq. (1) without the restriction of the symmetry condition.

Therefore, at least for the one-particle problem, the absorber theory of radiation is not equivalent mathematically to a field theory using retarded fields only. An interpretation allowing operational equivalence appears to be possible, however.

[5] G. A. Schott, Phil. Mag. **45**, 769 (1923).
[6] M. Born, Ann. Physik **30**, 1 (1909).
[7] For a criticism of this interpretation see A. Landé, Phys. Rev. **80**, 283 (1950).

Nuclear Recoil Following Neutrino Emission from Beryllium 7*

RAYMOND DAVIS, JR.
Chemistry Department, Brookhaven National Laboratory, Upton, New York
(Received March 6, 1952)

The nuclear recoil spectrum of the electron capture isotope Be^7 was measured from nearly monolayer deposits of the isotope on lithium fluoride and wolfram surfaces. The recoil spectrum was measured with an electrostatic analyzer having a two percent resolution. The spectra exhibited a peak at the high energy end of the spectrum consistent with the hypothesis of single neutrino emission in Be^7. The maximum recoil ion energy observed was 55.9±1.0 electron volts.

I. INTRODUCTION

IN the theory of beta-radioactivity it has been assumed that part of the energy of the decaying nucleus is carried away by a single neutrino. Crane,[1] in a review of the subject of energy and momentum relations in beta-decay, pointed out that this assumption could be examined experimentally by studying the nuclear recoil spectrum of an electron capture isotope. If the energy is emitted as a single neutrino, the momentum of the recoiling nucleus must be equal to the momentum of the emitted neutrino, with the result that all nuclei should recoil with the same momentum. However, if the energy is emitted in the form of several neutrinos in random directions, the momentum of the recoiling nucleus will be equal and opposite to the resultant momenta of the neutrinos, and the recoil spectrum will be continuous extending from zero to a maximum corresponding to the emission of all neutrinos in the same direction. Another method of testing the single neutrino hypothesis is to examine the nuclear recoil spectrum from a beta-emitting nucleus by defining the direction and energy of the electron and the direction of the recoil. Single neutrino emission should then lead to monoenergetic recoils. This point has been tested by the experiments of Sherwin with P^{32}. He concludes that the missing energy is carried away by a single neutrino.[2]

Two experiments have been conducted with the electron capture isotope Be^7, by Allen[3] and by Smith and Allen.[4] This isotope has the largest recoil energy of the known pure electron capture isotopes and is therefore a good choice for the experiment. The recoil spectra observed by these experimenters, from a source of Be^7 on the surface of a solid, showed a distribution in recoil ion energies which was attributable to the recoiling ion losing energy by collisions with neighboring atoms on the surface. Because of this difficulty, definite conclusions could not be reached concerning the question of single or multiple neutrino emission. In the later work, the end point of the recoil spectrum was measured at 56.6±1.0 ev, a value that agrees with the expected result.

More recently, Rodeback and Allen[5] have reported an experiment with the electron capture isotope A^{37} in which the recoil spectrum was measured in the gas phase. A peak was observed at the correct energy, 9.7 electron volts, which had a width corresponding to the resolution of the apparatus and was therefore in agreement with the hypothesis of single neutrino emission. A further experiment with A^{37} is in progress,[6] but to date only the experimental method has been reported.

So far, no recoil experiments have been reported with positron-emitting isotopes, although many of them have high recoil energies and would be well suited for an experiment. These isotopes should exhibit a continuous recoil spectrum displaying a sharp peak beyond the continuous spectrum resulting from single neutrino emission in the K-capture branch. Isotopes with high transition energies will in general have a weak K-capture branch, and the peak will be small compared to the continuous spectrum. However, if future recoil experiments reveal this peak cleanly, it will serve as an added verification of the single neutrino hypothesis.

It might be pointed out that recoil experiments of the type discussed can only show that the missing energy disappears in one parcel in a defined direction, but they are not capable of conclusively demonstrating that the parcel is composed of one or more particles. The only means of examining this possibility is to measure the cross section for the absorption of neutrinos and compare the results with the theoretically expected cross section for single neutrino emission. But neutrino absorption experiments are barely within the limit of available experimental techniques.

The present study is a reinvestigation of the recoil spectrum of Be^7. In this work the spectrum was observed from a solid surface with an electrostatic analyzer of relatively high resolution, $\Delta E/E=0.018$. A study was made of the methods of preparing the recoil sources in an effort to obtain a monolayer distribution of Be^7 on a surface, and thereby obtain a recoil spectrum free from surface effects. This was accomplished to a

* Research carried out under the auspices of the AEC.
[1] H. R. Crane, Revs. Modern Phys. **20**, 278 (1948).
[2] C. W. Sherwin, Phys. Rev. **75**, 1799 (1949).
[3] J. S. Allen, Phys. Rev. **61**, 692 (1942).
[4] P. B. Smith and J. S. Allen, Phys. Rev. **81**, 381 (1951).
[5] G. W. Rodeback and J. S. Allen, Phys. Rev. **83**, 215 (1951).
[6] T. Ohkawa, J. Phys. Soc. Japan **6**, 197 (1951).

degree that permitted conclusions to be reached in favor of single neutrino emission in Be^7.

The nuclear recoil energy E_R resulting from the emission of a single neutrino of momentum E_ν/c is given by

$$E_R = E_\nu^2/2Mc^2, \tag{1}$$

where M is the mass of the recoiling atom and c is the velocity of light. The isotope Be^7 decays according to the scheme given in Fig. 1.[7-9] In 89 percent of the decays 0.864±0.003 Mev of energy is emitted, and if this amount of energy is carried away by a single neutrino all nuclei should recoil with 57.3±0.5 electron volts energy according to (1).

The 11-percent branch which goes to the excited state of Li^7 would exhibit a continuous recoil spectrum extending from zero to 57.3±0.5 ev from the nearly simultaneous emission of a neutrino and a gamma-ray.[10]

To study the neutrino recoil spectrum of Be^7 one observes the recoils from a solid surface, since it is very difficult to prepare carrier-free gaseous compounds of beryllium that would be suitable for the experiment. In using a surface as a site of recoils one must prepare the radioactive isotope as an extremely thin layer on the surface, approaching a bare monolayer if the observed recoil spectrum from the surface is to be a true representation of the initial recoil spectrum. In the present case, the recoil energy is low, only about twenty times the magnitude of chemical bond energies, and the surface effects must be made small if one is to distinguish between single and multiple neutrino emission. Thin layers of radioactive atoms on surfaces can be prepared by selectively evaporating the contaminents from a thick deposit on a surface leaving the desired radioactive atoms on the surface, or by evaporating the radioactive atoms and condensing them on a fresh surface. The first method was used by Allen[3] in the first experiment with Be^7. A combination of these two means has been employed successfully by Sherwin[11] in preparing monolayer sources of both P^{32} and Y^{91} for recoil studies of electron-neutrino angular correlations and by Smith and Allen[4] in their work on Be^7. In the present work, both of these means of preparing surfaces were used.

Since the energy spectrum was measured by electrostatic means, a further requisite is that excited lithium atoms leaving the surface and traveling at 4×10^6 cm/sec be ionized. If the time required for the atom to move away from the surface is long compared to the time of adjustment of the electrons on the surface, then the recoiling atom will be in equilibrium with the

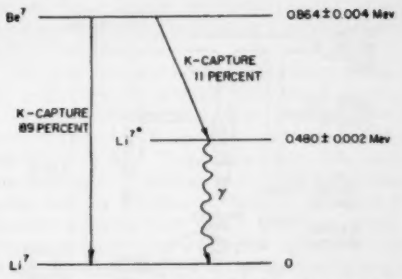

FIG. 1. The decay scheme of Be^7. The Be^7-Li^7 mass difference of 0.864±0.003 Mev was computed from the Q value (see references 7 and 8) of 1.646±0.002 Mev for the reaction $Li^7(p,n)Be^7$ and the neutron-proton mass difference of 0.782±0.002 Mev (see reference 9).

surface, and the ratio of the number of ionized atoms to neutral atoms will be given by

$$n_+/n_a = (\omega_+/\omega_a)\exp[-(I-\phi)/kT], \tag{2}$$

where ω_+ and ω_a are statistical weights, I is the ionization potential of the atom, and ϕ the work function of the surface. This equation has been verified for potassium atoms in thermal equilibrium with tungsten surfaces.[12] In recoil experiments one insures that the conditions are favorable for ionization by employing surfaces with high work functions. For experiments with Be^7 the work function of the surface should be greater than 5.36 volts, the ionization potential of lithium. Surfaces of high work function, oxygenated wolfram and lithium fluoride, were used in the present experiments.

II. EXPERIMENTAL

Chemical Separation

The Be^7 was prepared by bombarding cp metallic lithium for 500 microampere hours with the 8.5-Mev proton beam from the University of Pittsburgh cyclotron. The portion of the target struck by the beam was removed and dissolved in water. The solution was made acid and 50 mg of $CuCl_2$ and $FeCl_3$ were added as carrier. After adjusting the solution to 0.3N in HCl, copper was precipitated and removed as sulfide. Following this the solution was boiled to remove hydrogen sulfide, and a few drops of hydrogen peroxide were added to oxidize the ferrous ion. The solution was made alkaline with ammonium hydroxide precipitating ferric hydroxide which serves to carry the Be^7. The precipitate was dissolved in acid, and reprecipitated with ammonium hydroxide. This precipitation was repeated once more, and the final ferric hydroxide precipitate dissolved in about 5 milliliters of 7.8N HCl. The aqueous solution was extracted three times with 10 milliliter portions of isopropyl ether which serves to

[7] Herb, Snowden, and Sala, Phys. Rev. **75**, 246 (1949).
[8] Shoupp, Jennings, and Jones, Phys. Rev. **76**, 502 (1949).
[9] Taschek, Argo, Hemmendinger, and Jarvis, Phys. Rev. **76**, 325 (1949).
[10] R. E. Bell and L. G. Elliott, Phys. Rev. **76**, 168 (1949), have shown that the lifetime of the excited state of Li^7 is $(0.75\pm0.25)\times10^{-13}$ second.
[11] C. W. Sherwin, Phys. Rev. **82**, 52 (1951); Rev. Sci. Instr. **22**, 339 (1951).
[12] M. J. Copley and T. E. Phipps, Phys. Rev. **48**, 960 (1935).

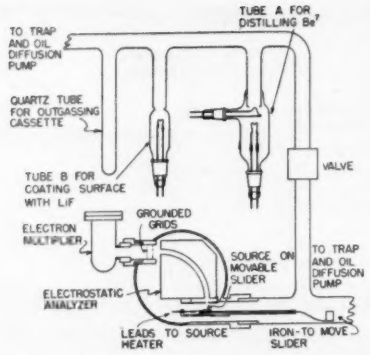

FIG. 2. Schematic diagram of the apparatus used to study the recoil spectrum of Be^7.

extract the iron leaving the Be^7 in the solution. The solution was adjusted to pH 5.8 with ammonium hydroxide and extracted with a 5-milliliter portion of 10 percent solution of acetylacetone in benzene. The organic phase containing the activity was washed with 20-milliliter portions of distilled water until the wash water on evaporation showed no signs of a residue. The Be^7 was back-extracted from the organic phase with a 1-milliliter portion of constant boiling hydrochloric acid or a 5 percent oxalic acid solution. The Be^7 contained in 1 milliliter of solution was evaporated in a drying oven, a drop at a time, on a wolfram ribbon which could be installed in the vacuum system for the evaporations.

Source Preparations

Sources were prepared by selective evaporation in vacuum from wolfram ribbons that were heated by passing a current through them. Wolfram was chosen because the evaporations were carried out at temperatures in the range 1400° to 1600°C, and it was necessary to use a metal with a very low vapor pressure at high temperatures. Either wolfram or tantalum would serve this purpose equally well, but these metals do have the disadvantage of reacting to some extent with acids. In some experiments, iridium was used and it was found that the metal evaporates slightly at temperatures above 1650°C, but it does have the advantage of resistance to acids. A wolfram ribbon 0.005×0.125 inch was bent in the form of a flattened M as shown in Fig. 2 (lower ribbon of the tube A) and spot welded to two heavy wolfram leads held parallel by a glass bridge. This assembly was connected by means of steel couplings to wolfram leads sealed through a taper joint. The ribbon holder was arranged in this way so that it could be removed from the vacuum line and weighed. It was found that these ribbon assemblies could be weighed reproducibly with an Ainsworth microbalance to about 2×10^{-6} gram.

Preliminary studies were made of the distillation behavior of Be^7. Evaporations were made from the metal ribbons onto weighed platinum foils about two centimeters in diameter that could be removed from the vacuum line and weighed after the evaporation. By measuring the weight loss of the ribbon, the gain in weight of the platinum disks, and determining the amount of Be^7 by counting, the vaporization properties of Be^7 and its contaminants could be studied as a function of temperature. The temperature of the wolfram ribbon was measured with an optical pyrometer. In these preliminary experiments the optimum conditions for distilling a Be^7 source were determined. It was found that upon evaporating a hydrochloric or oxalic acid solution containing the Be^7, the residues amounted to 100 to 200 micrograms. Upon heating the ribbon to around 1400°C in vacuum most of these residues distilled off leaving 70 to 90 percent of the Be^7 on the ribbon. The weight of the wolfram ribbon upon heating from 1400° to 1500° loses about 5 to 10 micrograms, and the platinum disk receiving the distillate did not increase in weight within the limit of sensitivity of the weighing, less than 2 micrograms. By following the procedure of heating the ribbon to 1400° to remove contaminants, then distilling onto a surface by increasing the temperature to about 1500°, the activity could be transferred forming a deposit weighing less than 2×10^{-6} g/cm².

The weighing technique used in these preliminary experiments was sufficiently accurate to establish the optimum conditions for separating the contaminants from the Be^7 by evaporation. However, much more accurate weighings would be required to insure that the amount of material distilled onto a surface was less than an amount corresponding to a monolayer. A monolayer 3×10^{-8} cm thick with an average density of 3 g/cm³ would weigh 10^{-7} gram, and to detect weight changes of this order would require about a twenty-fold increase in sensitivity. It should be pointed out that the weight of Be^7 itself distilled in the sources as only around 4×10^{-10} gram, an amount corresponding to 1/200th of a monolayer. In addition to the requirement of reducing the contaminants distilling along with the Be^7 to less than 10^{-7} g/cm², it is essential that all beryllium atoms be on the surface, and not imbedded in crystalline aggregates. In the present experiments the only way of knowing whether the latter condition was attained was to examine the quality of the recoil spectrum.

The preparation of the recoil sources used in the measurements to be described were based upon the distillation behavior experienced in the preliminary trials. The recoil spectra will be reported for two sources prepared by quite different techniques. Source I was prepared by evaporation onto a freshly deposited lithium fluoride surface in which a double evaporation was employed to reduce the quantity of contaminants accompanying the Be^7 evaporation. After preparation,

this source was transported through the vacuum system and placed under the electrostatic analyzer. Source II was prepared by evaporation of contaminants from a wolfram ribbon leaving some of the Be^7 remaining on the ribbon. The recoil spectrum of the Be^7 remaining on the wolfram ribbon was measured. The details of preparing these sources are as follows.

Source I, prepared by double vacuum evaporation. One milliliter of a 5 percent oxalic acid solution containing the separated activity was evaporated, a drop at a time, on the lower wolfram ribbon in tube *A* shown in Fig. 2. It was heated to 1380°C in vacuum to distill off the easily vaporizable impurities. The upper ribbon of tube *A* was heated to 2000°C to clean it thoroughly, and then rotated down over the lower ribbon. The lower ribbon was heated to 1830°C to distill the activity to the upper ribbon. The upper ribbon was then heated to 1300°C to remove contaminants vaporizing at this temperature that may have accompanied the activity on the first distillation. The upper ribbon was then rotated in position to distill a second time onto the lithium fluoride surface. The lithium fluoride surface was prepared by distilling the fused salt from a wolfram ribbon in tube *B* (Fig. 2). The lithium fluoride was distilled onto a one-inch disk of 0.005 inch platinum foil spot welded to a nickel ring so that it could be moved inside the vacuum line with an external bar magnet. Prior to coating with lithium fluoride this assembly was outgassed by heating it for 17 hours at 890°C. The lithium fluoride coated disk was then placed over the upper ribbon, and the second distillation of Be^7 was accomplished by heating the ribbon to 1525°C. The recoil source thus prepared was moved through the valve into the side of the vacuum system containing the electrostatic analyzer. Later the source was compared to a Co^{60} standard and found to contain about 5×10^6 disintegrations per second of Be^7.

Source II, prepared by evaporation. A milliliter of hydrochloric acid solution containing Be^7 was evaporated on a wolfram ribbon. A ribbon was heated to 1560°C in a vacuum system to evaporate contaminants, and the cleaned-up ribbon used as a recoil source. The ribbon lost about 90 percent of the Be^7 activity from this treatment. The resulting source contained about 5×10^6 disintegrations per second. The source was removed from the vacuum system and installed under the entrance slit of the electrostatic analyser.

The Vacuum System and the Electrostatic Analyzer

The apparatus, shown in Fig. 2, consists of two separately pumped vacuum systems interconnected by a valve. On one side of the valve was located apparatus for preparing the sources and on the opposite side the electrostatic analyzer and the electron multiplier for measuring the recoil ion spectra. The valve served to protect the measuring apparatus from becoming contaminated during the evaporation operations. The side of the vacuum system used to distill the sources was pumped by a 2-stage oil diffusion pump through a liquid nitrogen cooled trap giving a vacuum of around 5×10^{-7} mm of Hg.

The recoil ion spectra were measured by means of a 90° cylindrical electrostatic analyzer of plate radii 3.750 and 4.125 inches. The plates of the analyzer were made of brass 1.63 inches thick, and were bolted to a one-half inch thick Pyrex glass plate. The analyzer was held in a cylindrical brass vacuum chamber 3 inches deep by 8 inches in diameter, having a 6-cm diameter pumping tube and a port into which the electron multiplier case is fitted. A vacuum of 5×10^{-7} mm of Hg was maintained in the chamber by means of a glass 3-stage oil diffusion pump and a large liquid nitrogen cooled trap. A track was located in the pumping tube on which rode a small platform slider that could be moved back and forth by means of an armature and an external bar magnet. The source fitted on a stainless steel hot plate attached to the sliding platform. A wolfram wire heating element attached to the brass chamber fitted under the hot plate when the source was located under the entrance of the analyzer. A calibration of the hot plate temperature at various settings of the heater current was made with a source disk identical to the one used in the experiment and having a fine wire thermocouple spot welded to its surface. By means of this hot plate the source could be heated to over 300°C.

An electron multiplier designed by Dr. Robert P. Stone[13] of the RCA laboratory was used to detect the recoiling ions. The multiplier was held in a case (Fig. 2) which was operated at a high negative potential and was insulated from the grounded vacuum case by a Lucite adapter. The multiplier was operated with its center dynode grounded, and a total applied potential across the tube of 4000 volts. The first dynode was made negative so that the low energy ions leaving the analyzer were accelerated by 2000 volts onto the first dynode. To screen the analyzer from the high potential two grids were placed between the multiplier and the exit of the analyzer. The analyzer was initially designed so that the source and the screen grid were located at the foci of the analyzer. With this arrangement the resolution of the analyzer, $\Delta E/E$, was 0.11. To improve the resolution a slit 0.199 inch wide was placed 0.375 inch from the entrance, and a second slit 0.063 inch wide by 0.75 inch long was placed 1.5 inches from the exit of the analyzer. With these slits in place the resolution $\Delta E/E$ was increased to 0.018. A resistor, center tapped to ground, was connected between the plates of the analyzer so that the outer and inner plates ran at equal potentials above and below ground, respectively.

The energy E of an ion of charge z passing through

[13] The electron multiplier was loaned to me through the courtesy of Dr. Irving Wolff, and Dr. Stone of the RCA Laboratories Division, Radio Corporation of America, Princeton, New Jersey. The multiplier is described in Dr. Stone's article, Rev. Sci. Instr. **20**, 935 (1949).

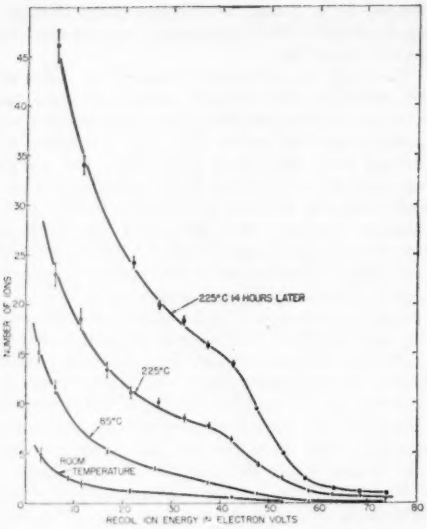

FIG. 3. Recoil spectra from a double distilled Be^7 source on a lithium fluoride surface measured at a series of surface temperatures.

the center of the analyzer is related to the applied potential difference, $V_1 - V_2$, and the radii of the inner and outer plates r_1 and r_2 respectively by,

$$E = z(V_1 - V_2)/2 \ln(r_1/r_2). \quad (3)$$

For the analyzer used in these experiments the expression becomes for singly charged ions,

$$E = 5.246(V_1 - V_2). \quad (4)$$

The performance of the analyzer was checked with thermal ions from a heated wolfram ribbon placed under the entrance slit (Fig. 4). The ribbon was set at a measured negative potential with respect to the entrance slit to accelerate the ions into the analyzer. The peak position and shape were measured at several ion energies. The resolution expressed above was taken as the half-width of the peak divided by the ion energy. The position of the monoenergetic ion peaks for various ion energies agreed with Eq. (4) except that each peak was displaced an equal amount from the energy expressed by the equation as a result of the contact difference in potential between the thermal ion source and the brass analyzer.

Recoil spectra were measured by observing the counting rate on the electron multiplier at various voltage settings on the electrostatic analyzer. To obtain the energy spectrum as a plot of the number of ions in equal energy intervals along the energy axis, each observed counting rate was divided by the corresponding energy setting of the analyzer, and this quotient plotted as the ordinate in the accompanying figures showing the recoil energy spectrum.

III. RESULTS AND DISCUSSION

Results with a Double Evaporated Source on a Lithium Fluoride Surface

After preparing Source I it was transferred to the electrostatic analyzer and placed on the hot plate. Measurements were attempted with the source at room temperature with entrance and exit slits on the analyzer, but no measurable ion current was observed. The source was transferred back through the valve to the preparation side of the line where it was stored while the analyzer vacuum system was opened and both the entrance and exit slits removed. Upon obtaining a satisfactory vacuum the source was placed back in position under the analyzer. The set of measurements shown in the lower curve of Fig. 3 were obtained. Upon increasing the surface temperature of the source to 85°C, a much higher counting rate resulted. The measurements at this temperature shown in the figure were taken after the source had been at 85°C for about one hour, but it was noticed that the counting rate increased with time at a rate corresponding to an increase of 30 percent in an hour. The source was heated further until the surface temperature reached 225°C and again a large increase in counting rate was observed. The measurements shown in Fig. 3 were started at the time the source reached temperature, and at this time an increase of around 15 percent in counting rate per hour was observed. After this the source remained at 225°C for 14 hours and then the series of measurements shown in the upper curve of Fig. 3 were obtained. The counting rate exhibited an average increase of about 7 percent per hour during this heating period. The increase in counting rate in standing at 225°C for 14 hours was uniform over the whole spectrum, so that the treatment served to increase the yield of ions without effecting a change in the shape of the recoil spectrum. The end point of the recoil spectrum is about 51 ev as determined by the knee of the curve and substracting 6 volts to allow for the resolution of the analyzer. The maximum recoil energy as observed must

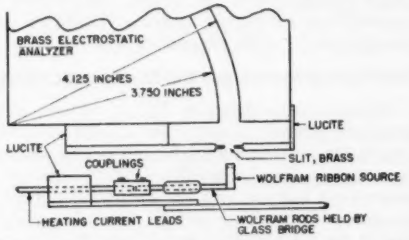

FIG. 4. Drawing showing the location of the wolfram ribbon recoil Source II under the entrance slits of the electrostatic analyzer.

be corrected for the difference in contact potential between the LiF surface and the brass analyzer and also for the binding energy of the recoiling lithium ion to the surface. Neither of these corrections could be made in the measurements on Source I. Also the shape of the recoil spectrum observed exhibited an increase in the number of ions with decreasing energy, a result that would be expected if a large fraction of the ions leaving to the surface were degraded in energy by collisions. The quality of the spectrum therefore does not allow conclusions to be drawn concerning single or multiple neutrino emission in Be^7.

After making the measurements at 225°C just described, the analyzer was set for 35 electron volt ions and the heater current of the hot plate turned off. The counting rate was found to drop slowly and after forty minutes the counting rate had dropped to 87 percent of the value at 225°C. The surface temperature dropped to about 70°C in this period of time. The reduction in counting rate was probably due to the surface being covered with an adsorbed layer of gas, and this observation gives an approximate measure of the effect. This is reasonable when one notes that at a pressure of 5×10^{-7} mm of Hg the surface is bombarded by the residual gas molecules in the vacuum system at a rate sufficient to build up a monolayer in 15 seconds if none evaporated.

It was clear from the results that this source, although evaporated twice onto a fresh LiF surface, was of low quality, and that ions leaving the surface had to penetrate several layers of atoms. The increase in ion yield from the surface upon increasing the surface temperature indicated that the surface was covered with an adsorbed layer and to improve the results heating to even higher temperatures would be necessary. An attempt was made to heat the source to 320°C but at this temperature the LiF substrate vaporized partially, and measurements were discontinued.

It is well known that evaporated films on surfaces tend to agglomerate under certain conditions. For agglomeration of a condensed monolayer on a surface to take place, the condensed layer must be energetically more stable in the form of agglomerates, and the atoms or molecules composing the layer must have sufficient mobility to migrate over the surface and form crystalline agglomerates.[14] For the agglomerates to be more stable energetically the heat of evaporation of the substance from the agglomerates, which can be taken equal to the heat of evaporation of the bulk material, must be greater than the heat of evaporation of the adsorbed layer from the surface. The Be^7 activity evaporating from the wolfram ribbon exhibits a vapor pressure of beryllium oxide,[15] and lower than the vapor pressure of beryllium metal. Furthermore, upon considering the conditions under which the Be^7 was placed on the ribbon initially, and the subsequent heat treatment, one would expect that the beryllium would be in the form of the oxide. It is entirely possible that the poor recoil spectrum obtained from the LiF surface is a result of agglomeration of the Be^7 in the form of BeO crystals. If this conclusion is correct, a distilled source using BeO as a substrate may yield better results.

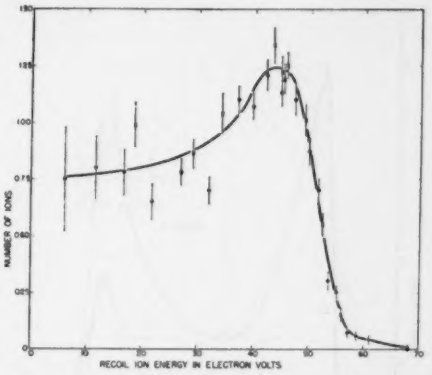

FIG. 5. Recoil spectrum from wolfram ribbon Source II at a surface temperature of 300°.

Results with an Evaporated Source on a Wolfram Surface

In view of the large increase in ion yield with temperature, an experiment was performed using the wolfram ribbon itself as a recoil source. The Be^7 activity remaining on the wolfram ribbon after vaporizing off the contaminants may be spread on the surface and be clean enough to serve as a recoil source. Further, a more vigorous thermal treatment could be given to clean the surface of absorbed gases by passing a current through the ribbon sufficient to heat it to 1000°C. With these possibilities in mind recoil Source II was prepared as described above.

Recoil Source II was installed under the entrance slits of the analyzer as shown in Fig. 4. After obtaining a satisfactory vacuum, a current was passed through the ribbon sufficient to heat it to 1000°C for 15 seconds to outgas its surface. Previously the ribbon had been heated to 1560°C, and by only heating to 1000°C there was no danger of distilling Be^7 from the surface and contaminating the analyzer and electron multiplier. The recoil spectrum was then measured while the ribbon was at room temperature with the result that only a very low counting rate was observed over the entire spectrum. The temperature of the ribbon was increased to about 300° and after a period of three and one-half hours the measurements shown in Fig. 5 were

[14] For a discussion see papers of G. I. Finch, E. T. S. Applegard, and J. E. Lennard-Jones from Report of a Conference on the Conduction of Electricity in Solids, Proc. Phys. Soc. (London) 49 (Extra Part) 113–154 (1937).

[15] N. D. Erway and R. L. Seifert, Manhattan District Declassified Contribution No. 1030 (1946).

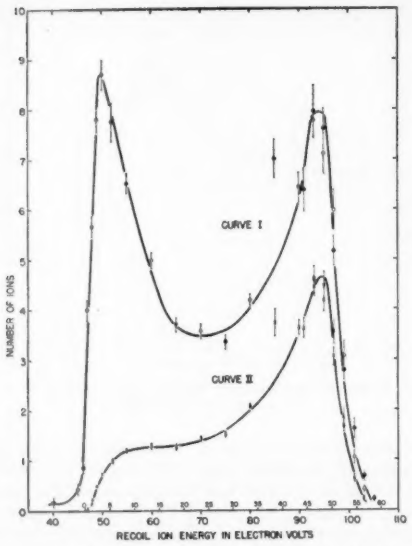

FIG. 6. Recoil spectrum observed from Source II with 46.4 volts between the source and the electrostatic analyzer. Curve I shows the experimentally observed spectrum, and Curve II represents the spectrum corrected for discrimination effects.

obtained. The spectrum shows a peak around 45 ev recoil energy. Comparison with the spectrum from the double evaporated source on lithium fluoride at 225°C surface temperature shows clearly that a relatively larger number of high energy ions was obtained from the wolfram surface. The counting errors are much greater at low energies and are indicated by the bars. The series of points indicated by the plane bars were taken in sequence from low to high energy, then following these the points marked with crosses were taken randomly over the spectra. A slight increase in counting rate with time was noticeable.

The temperature of the ribbon cannot be increased very much above 300° because thermal ions are given off in abundance at around 550°. However, a more vigorous thermal treatment of the surface could be achieved by flashing the ribbon for about 15 seconds at 1000°, then reducing the temperature of the ribbon to around 300° for counting. Experiments of this sort were conducted and it was found that the yield of ions increased by a factor of about three. The recoil spectra exhibited a sharper peak and the relative number of low energy ions was greatly reduced. The recoil spectrum shown in the upper curve of Fig. 7 illustrates these improvements. This spectrum was taken by flashing the ribbon at around 1000° for fifteen seconds and the recoil ions counted for a three minute period at 300° starting five seconds after the current was reduced. The counting rate was observed as a function of the time, and it was found to remain constant during the three minute period within the counting statistics.

Measurements were made in which the recoil source was placed at a positive potential with respect to the grounded entrance slit of the analyzer. This accelerating potential gives each ion entering the analyzer an energy of V electron volts in addition to its initial recoil energy. In this way the entire recoil spectrum is shifted along the energy axis by V electron volts. The spectrum shown in the upper curve of Fig. 6 was obtained with 46.4 volts accelerating potential. This procedure had two advantages. First, by shifting the entire spectrum to higher energies the counting efficiencies for all ions entering the analyzer were made more nearly comparable. This follows from the fact that the aperture of the analyzer increases linearly with the energy. When potential between the source and the analyzer was zero, 50-volt ions were counted with fifty times greater efficiency than one-volt ions, and therefore, large errors were introduced in the measurements at the low energy side of the spectrum (Figs. 3, 5, and 7). But, by applying a potential comparable in magnitude to the maximum recoil energy, the aperture of the analyzer only changed by a factor of about 2 over the spectrum. There was, however, a discrimination effect in favor of low energy ions, which will be discussed later. The second advantage of the applied potential was that the maximum energy of the recoiling ions could be obtained free of a contact potential error.

The recoil spectrum shown in Fig. 6 was obtained following the above-mentioned flashing technique, and the counting rate observed as a function of the time for a three minute period. For each point a plot of counting rate *versus* time was made and the value taken by extrapolating to zero time. However, it was found that the counting rate did not change appreciably during the three minute period. The results presented represent two separate sweeps over the spectrum as indicated by the solid and open circles. The spectrum exhibits two distinct peaks, one at the low energy end that is very steep sided, and one at the high energy end which is similar in shape to the spectrum obtained without an accelerating potential. To obtain the maximum recoil energy of the ions from this spectrum, the following procedure was used. The low and high energy sides of the spectrum were extrapolated to the energy axis. The energies obtained were then corrected for the resolution of the analyzer by adding to the extrapolated energy at the low energy side the resolution half-width and subtracting the corresponding resolution half-width from the extrapolated value at the high energy side. The difference in these two corrected energies gave a maximum recoil energy of 55.9 ± 1.0 ev. The largest error was in determining the end point at the high energy side. This value agrees with the results of Smith and Allen.[4] They observed a maximum recoil energy of

56.6±1.0 ev from an evaporated source of Be^7 on a tantalum substrate.

The strong peak at the low energy side of the spectrum in Fig. 6 results from a discrimination effect in favor of low energy ions. An ion leaving the surface with an energy E and direction θ with respect to the normal was accelerated by the applied field in the direction normal to the surface. Upon passing through the entrance slit the ion had an energy equal to the sum of the initial energy and the applied potential, $E+V$, but also had its direction of motion changed to a smaller angle with respect to the normal. The change in direction of the ions was small for high energy ions and large for low energy ions, and thus gives rise to a greater relative collection of efficiency for low energy ions. An estimate of this effect was calculated in the following manner. The ion was considered to move in a uniform electric field between the wolfram ribbon and the entrance slit. After passing through the slit the ion travels a short distance and enters the radial field of the analyzer. For the purpose of making the geometrical efficiency correction the exact orbit of the ions through the analyzer was not used, but was regarded as a pure geometrical baffle having an acceptance angle as defined by half the distance between the plates at a distance halfway through the analyzer. The arrangement used for these calculations is shown in Fig. 8. The motion of the ion of initial energy E and initial direction θ between the source and the slit is given by the expression

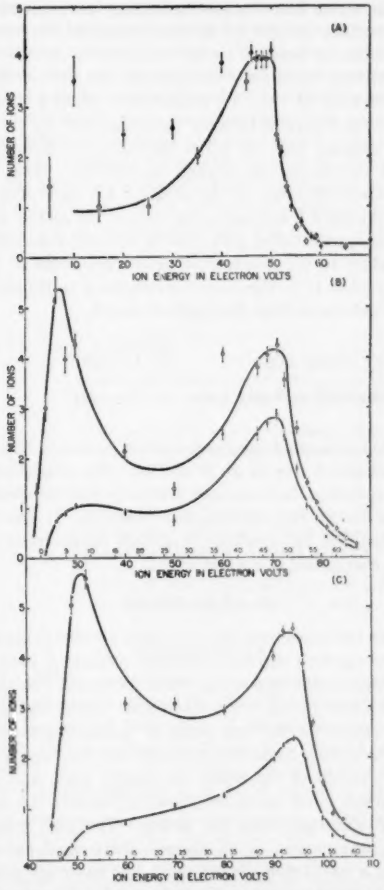

FIG. 7. A series of three recoil spectra observed successively at several accelerating potentials between the source and the entrance slit. These were at zero (Curve A), 23 (Curve B), and 46 (Curve C) volts. The recoil curves B and C were corrected for discrimination correction using the factor g plotted in Curves B and C of Fig. 9. The corrected spectra are shown below the observed spectra in each case.

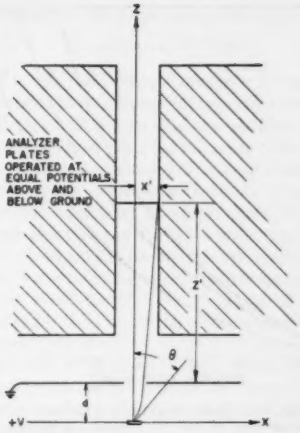

FIG. 8. The schematic representation of the relation between the source, slit, and analyzer used in calculating the discrimination effect.

$$z=\frac{x}{\tan\theta}+\frac{Vx^2}{4dE\sin^2\theta}. \tag{5}$$

After leaving the slit the ion was assumed to travel in a straight line, and after moving a distance z' from the slit, it will be displaced a distance x' in the X-direction.

$$x'=\frac{2dE}{V}\sin\theta\left[-\cos\theta+\left(\cos^2\theta+\frac{V}{E}\right)^{\frac{1}{2}}\right]+\frac{z'\sin\theta}{\left(\cos^2\theta+\frac{V}{E}\right)^{\frac{1}{2}}}. \tag{6}$$

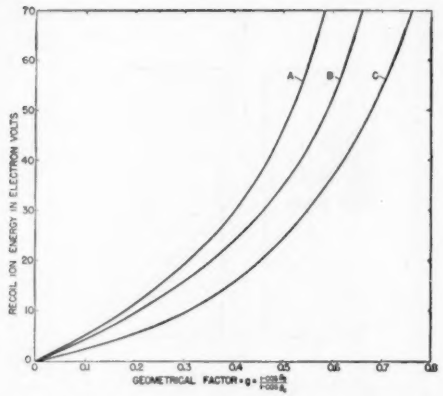

FIG. 9. Plot of the geometrical factor g for various ion energies calculated from Eqs. (6) and (7). Curve A is calculated for 46.4 volts between the source and the analyzer using the geometrical acceptance angle of the analyzer, three degrees. Curves B and C are for 46.4 and 23.3 volts, and using one-sixth the geometrical acceptance angle of the analyzer, around 30 minutes.

Setting the distance as one-half the spacing between the plates of the analyzer, z' the distance from the slit to the center of the analyzer, and the values for d, and V, a calculation was made of the angles θ_c and the corresponding energies E. One has then as a result of the calculation the maximum angle from the normal that an ion of energy E leaving the surface, can have in order to enter the analyzer and be counted. The acceptance angle for the analyzer in the plane parallel to the plates is determined by the width of the exit slit and the total distance through the analyzer. For the analyzer used in these experiments the acceptance angle is almost identical in the radial and axial directions, and the critical angles θ_c calculated by the above formula may be used as defining a cone at the surface within which ions of a specified energy are counted. It is clear that the cone will be much larger for low energy ions than for the high energy ions, and the calculation shows that cones for 2 and 42-volt ions have critical angles θ_c of 18° and 4°, respectively, when a 46-volt potential is applied between the source and the slit. If it is assumed that the initial distribution of recoil ions from the surface is random in direction, then the collection efficiency of the analyzer for recoil ions of initial energy E is equal to the ratio of the surface area of the corresponding unit cone to the unit cone corresponding to the geometrical acceptance angle of the analyzer θ_g (3°). The collection efficiency so defined is then calculated from the angles θ_c and θ_g.

$$\text{Efficiency factor} = \frac{\text{volume of cone defined by critical angle}}{\text{volume of cone defined by geometrical acceptance angle}} = \frac{1}{g} = \frac{1-\cos\theta_c}{1-\cos\theta_g}. \tag{7}$$

Each measured value was multiplied by the factor g which corrected the spectrum for the variation of collection efficiency of the analyzer with initial ion energy. The results of applying the discrimination correction to the recoil spectrum are shown in the lower curve of Fig. 6. A plot of g *versus* E is shown in Fig. 9. Since the estimation of the defining geometry of the analyzer was only approximate, a calculation of the factor g was repeated using one-sixth the value of x' used in the first calculation and the results of this calculation are shown in Fig. 9.

To check the above described discrimination correction it was applied to recoil spectra measured successively at two different values of the accelerating potential, 23 and 46 volts, and also with the source grounded. The measurements were taken in sequence having the source at zero potential, then at 23 volts and finally at 46 volts. After this the spectrum at zero potential was repeated, the measurements being shown by the solid circles in Fig. 7(a). These points were higher at the low energy and this was attributed to a change in the source during the measurements which extended over a period of four and one-half hours. The observed spectra and the spectra corrected for discrimination are shown in Fig. 7. Comparison of the three spectra shows that the discrimination correction reduces the observed spectra at 23 and 46 volts, respectively, to a spectrum that compares favorably with the spectra observed at zero accelerating potential. It can be noticed that the correction is perhaps too severe at the high energy end of the spectrum.

IV. CONCLUSIONS

The recoil spectrum obtained from a wolfram surface under vigorous thermal treatment exhibits a peak at the high energy end of the recoil spectrum. The spectrum shown in Fig. 6 was taken under these conditions and represents the best series of measurements. The discrimination correction discussed above accounts for the presence of the sharp low energy peak, and the corrected recoil spectrum shown represents the true recoil spectrum from the surface. The high energy peak was located at 48 electron volts recoil energy, about 8 volts below the end point, and has a half-width in the neighborhood of 10 electron volts. The number of recoil ions leaving the surface with the full recoil energy was vanishingly small. The appearance of the peak at a lower energy indicates that the majority of the recoiling ions leaving the surface lose energy through

collisions with neighboring atoms. However, the quality of the recoil spectrum was good enough to allow one to draw conclusions concerning single or multiple neutrino emission in Be^7. Multiple neutrino emission should lead to a bell-shaped recoil distribution spectrum, and if surface collision effects were present in the experimental curve it would be distorted toward larger numbers of low energy ions. Since the observed spectrum exhibits a peak near the high energy end of the spectrum one can conclude that Be^7 electron capture decays are accompanied by the emission of a single neutrino.

The observed end point of the spectrum 55.9 ± 1.0 ev, should be compared to the initial recoil energy of the nucleus of 57.3 ± 0.5 ev minus the binding energy of the lithium ion to the surface. The binding energy of lithium ions to the surface could not be measured experimentally, nor be evaluated theoretically because of the uncertainties in the knowledge of the nature of the surface from which the ion recoiled. The main reason for desiring an accurate value for the end point of the recoil spectrum and the surface binding energy is to obtain the mass of the neutrino directly from a measure of its recoil momentum. The recoil energy E_R for an ion of mass M resulting from the emission of a single neutrino of rest mass m_ν is given by

$$E_R=(E^2-m_\nu^2c^4)/2Mc^2, \tag{8}$$

where E is the total energy available for the process (0.864 ± 0.003 Mev). Upon taking the observed end point of 55.9 ± 1.0 ev as E_R one obtains from this experiment an upper limit for the mass of the neutrino of 0.27 ± 0.14 electron masses. The limit obtained from this experiment is much higher than the upper limit of 0.001 electron masses set by observations of the shape of the end point of the He^3 beta-spectrum,[16] and the limit of (-0.04 ± 0.05) set by nuclear reaction data.[17]

The author would like to express his appreciation to Dr. Irving Wolff and Dr. R. P. Stone of the RCA laboratories for the loan of the electron multiplier tube used in these experiments, and to Dr. Oliver A. Schaeffer and Dr. James A. Amick for their helpful discussions during the course of the experiments. The author would like further to thank Professor O. Kofoed-Hansen for reading the manuscript.

[16] Hamilton, Alford, and Gross, Phys. Rev. **83**, 215 (1951); H. A. Tolhoek, Ned. T. Natuurkde **15**, 96 (1949); Curran, Angus, and Cockcroft, Phil. Mag. **40**, 53 (1949); and O. Kofoed-Hansen, Phil. Mag. **42**, 1448 (1951).

[17] Shoupp, Jennings, and Sun, Phys. Rev. **75**, 1 (1949).

PHYSICAL REVIEW VOLUME 86, NUMBER 6 JUNE 15, 1952

On the Stress Tensor of the Electron*

SIDNEY BOROWITZ† AND WALTER KOHN‡
Department of Physics, Harvard University, Cambridge, Massachusetts

(Received July 25, 1951)

A suggestion by Schwinger for dealing with problems of gauge invariance has been adapted for treating the radiative corrections to the stress tensor of an electron. The divergencelessness of the stress tensor implies that a certain divergent integral be invariant with respect to translation. Application of this rule gives a zero self-stress and shows that the matrix elements of the symmetric tensor between states of unequal momenta are finite. The canonical tensor however remains infinite. The connection with the results of Rohrlich, and Villars, and Pais and Epstein, is discussed.

INTRODUCTION

RECENT developments in quantum electrodynamics[1] have shown that the difficulties connected with the infinite self-energy of the electron and the infinite charge induced in the electron vacuum by an external field can be circumvented by appropriate covariant renormalizations. It was of interest to investigate whether these techniques were sufficient to give unambiguous and self-consistent answers to other questions in quantum electrodynamics.

The calculation of the self-stress of an electron by Pais and Epstein[2] seemed to show that this was not the case. These authors found that after carrying out the renormalization procedure, the self-stress emerged as a finite quantity, whereas Lorentz covariance demands that it must vanish. It was clear that this difficulty had its origin in the infinite integrals which occur in the expression for the stress-tensor and whose evaluation may lead to inconsistent results.

In the present paper the basic idea underlying the calculation was to investigate carefully the divergent integrals that occur and to use physical principles in

* A preliminary report was given at the January, 1950 meeting of the Am. Phys. Soc., Phys. Rev. **78**, 345 (1950).

† Present address—Department of Physics, New York University, University Heights, New York 53, New York.

‡ Present address—Institute for Theoretical Physics, Copenhagen, Denmark; on leave of absence from Department of Physics, Carnegie Institute of Technology, Schenley Park, Pittsburgh, Pennsylvania.

[1] S. Tomonaga, Prog. Theor. Phys. **1**, 27 (1946); J. Schwinger, Phys. Rev. **74**, 1439 (1948); **75**, 651 (1949); **76**, 790 (1949). The last three papers will be referred to as SI, SII, and SIII, respectively.

[2] A. Pais and S. T. Epstein, Revs. Modern Phys. **21**, 445 (1949).

their evaluation. The point of view is quite analogous to a proposal by Schwinger[3] to deal with the question of gauge invariance. It was found that to insure the conservation of the charge induced in the electron vacuum by a prescribed electromagnetic field, a certain divergent integral over the entire momentum space had to be considered as zero. It was significant that the integrand had the form of a difference of two terms which differed only by a translation of the variable of integration. Clearly, such an integral would be unambiguously zero if each part were separately convergent. In the present, incomplete theory of electrodynamics its vanishing is dictated by the requirement of gauge invariance. Thus one may say that a conservation theorem—in this case conservation of charge—extends the translational invariance of convergent integrals to a certain divergent integral. Once the zero value of this integral is recognized, it can be eliminated wherever it appears, leaving remainders which are either finite or can be interpreted as charge renormalizations.

The situation is quite parallel in the case of the stress-tensor of an electron interacting with the radiation field of the vacuum. Again there is a conservation theorem—this time energy conservation—which enables one to recognize as zero a certain integral whose integrand has the characteristic difference form. When one then calculates the corrections to the matrix elements of the stress tensor, taken between electron states of equal momenta, one is led to integrals of the same class and hence concludes that these correction vanish. In particular one thus finds a zero self-stress. The matrix elements between states of unequal momenta also contain divergent integrals of the above-mentioned class, but these matrix elements become finite and unambiguous once the zero value of these integrals is recognized. It is interesting to note that the canonical stress tensor remains infinite which bespeaks its unphysical nature.[4]

The problem may also be regarded from the following point of view. The formal proof of the vanishing of the self-stress rests on the four-vector character of the energy momentum, which in turn is a consequence of the divergencelessness of the stress tensor.[5] When one calculates the radiative corrections of the divergence of the stress tensor and of the self-stress, one finds divergent and consequently ambiguous integrals for both. The satisfactory feature of the present calculation is that these integrals are of the same type; when one therefore insists that the former be set equal to zero—a reasonable assignment in view of its gradient form—the latter necessarily vanishes. The formal connection between self-stress and the divergence of the stress tensor is thus preserved in the radiative corrections.

A different approach to the problem of the stress-tensor has been followed by Rohrlich[6] and Villars.[7] These authors found that formal regularization[8] led to the inconsistent result of Pais and Epstein. However, they obtained a vanishing self-stress and divergenceless stress tensor by going outside the framework of pure electrodynamics and introducing an auxiliary neutral vector meson field coupled to the electron by an imaginary coupling constant. The contributions of this additional field to the self stress and to the divergence of the stress tensor cancel those of the electron-photon fields. The present analysis shows the reason for the failure of formal regularization and for the success of the auxiliary field procedure adopted by Rohrlich and Villars.

In Sec. 1 of the present paper an expression for the radiative correction to the canonical stress tensor of an electron is derived. Sections 2 and 3 deal with the vanishing divergence of the canonical tensor and its implications for the diagonal elements[9] of the canonical and symmetrical tensors and in particular for the self-stress. In Sec. 4 the off-diagonal elements[9] of the symmetrical tensor are calculated, which apply to an electron in a superposition of momentum states (wave packet). Appendix I contains a discussion of the result of Pais and Epstein and Appendix II deals with regularization procedures applied to the stress-tensor, in the light of the present analysis.

1. THE RADIATIVE CORRECTION OF THE CANONICAL STRESS TENSOR

The stress tensor of any physical system must be symmetrical, as can be shown by considering the gravitational field it produces.[10] While the canonical tensor does not satisfy this requirement it is nevertheless a suitable starting point for our discussion, for the following reasons: (a) It is simpler in form than the symmetrical tensor. (b) The main difficulties occur in the calculation of the canonical tensor, the transition to the symmetrical tensor being relatively straightforward. (c) The corrections to the important diagonal elements[9] can be calculated equally well from either tensor.

The canonical stress tensor of the electron and radiation field consists of two parts, composed, respectively, of the matter and electromagnetic field operators[11]:

$$\mathbf{T}_{\mu\nu}=\mathbf{T}_{\mu\nu}^{(\mathrm{m})}+\mathbf{T}_{\mu\nu}^{(\mathrm{e.m.})} \tag{1.1}$$

[3] J. Schwinger, unpublished lectures on quantum electrodynamics (Harvard University, Cambridge, Massachusetts, 1950).

[4] When this calculation was completed, Schwinger [Phys. Rev. 82, 664, 1951)] proposed an improved treatment of vacuum polarization which suggests an analogous approach to the stress tensor problem. The present paper corresponds to Schwinger's older work on vacuum polarization (see reference 3).

[5] W. Heitler, *Quantum Theory of Radiation* (Oxford University Press, London, England, 1944), second edition, pp. 17–18.

[6] F. Rohrlich, Phys. Rev. **77**, 357 (1950).

[7] F. Villars, Phys. Rev. **79**, 122 (1950).

[8] W. Pauli and F. Villars, Revs. Modern Phys. **21**, 434 (1949).

[9] The words "diagonal" and "off-diagonal" here refer to the matrix of the stress tensor in the space of state vectors which describe electrons in various momentum states.

[10] L. Rosenfeld, Mém. Acad. Roy. Belgique (1940). F. J. Belinfante, Physica **7**, 449 (1940).

[11] Boldface type indicates operators in the Heisenberg representation.

with

$$\mathbf{T}_{\mu\nu}{}^{(\mathrm{m})}=\frac{1}{2}\left[\bar{\psi},\gamma_\mu\frac{\partial}{\partial x_\nu}\psi\right],$$
$$\mathbf{T}_{\mu\nu}{}^{(\mathrm{e.m.})}=\frac{1}{2}\left[\left\{\frac{\partial\mathbf{A}_\lambda}{\partial x_\mu},\frac{\partial\mathbf{A}_\lambda}{\partial x_\nu}\right\}-\delta_{\mu\nu}\left(\frac{\partial\mathbf{A}_\lambda}{\partial x_\sigma}\right)^2\right]; \tag{1.2}$$

where $\hbar$ and c have been set equal to 1. The operators ψ, $\bar{\psi}$ and $\mathbf{A}_\mu$ satisfy the equations[12]

$$[\gamma_\mu(\partial/\partial x_\mu-ie\mathbf{A}_\mu)+m_0]\psi=0,$$
$$[\gamma_\mu{}^T(\partial/\partial x_\mu+ie\mathbf{A}_\mu)-m_0]\bar{\psi}=0, \tag{1.3}$$
$$\Box^2\mathbf{A}_\mu=-\mathbf{j}_\mu.$$

Here m_0 is the mechanical mass of the electron.

The object of the present section is to write $\mathbf{T}_{\mu\nu}$ in the form

$$\mathbf{T}_{\mu\nu}=T_{\mu\nu}+\delta T_{\mu\nu},^{13} \tag{1.4}$$

where $T_{\mu\nu}$ has the same form as $\mathbf{T}_{\mu\nu}$ but is expressed in terms of interaction variables ψ, $\bar{\psi}$, A_μ which include the effects of mass renormalization. These variables satisfy the equations

$$(\gamma_\mu\partial/\partial x_\mu+m)\psi=0,\quad(\gamma_\mu{}^T\partial/\partial x_\mu-m)\bar{\psi}=0,$$
$$\Box^2A_\mu=0, \tag{1.5}$$

where m is the experimental mass of the electron. The additional term, $\delta T_{\mu\nu}$, then describes the observable correction to the stress tensor. It will be calculated to order e^2 for a single electron.

Matter Part

The transition to the representation which incorporates the mass renormalization will be carried out in two stages. We first express $\tilde{T}_{\mu\nu}$ in interaction variables $\tilde{\psi}$, $\tilde{\bar{\psi}}$, $\bar{A}_\mu$ which do not include the mass renormalization; subsequently we shall transform to the interaction representation, with mass renormalization.

The tilde variables are related to the Heisenberg variables by integral equations of the following kind:

$$\psi(x)=\tilde{\psi}(x)-ie\int G^{(\mathrm{m})}(x-x')\gamma_\lambda\mathbf{A}_\lambda(x')\psi(x')d\omega',$$
$$\mathbf{A}_\mu(x)=\bar{A}_\mu(x)+\int G^{(\mathrm{e.m.})}(x-x')\mathbf{j}_\mu(x')d\omega', \tag{1.6}$$

where $G^{(\mathrm{m})}$ and $G^{(\mathrm{e.m.})}$ are Green's functions satisfying the equations

$$(\gamma_\mu\partial/\partial x_\mu+m_0)G^{(\mathrm{m})}(x-x')=-\delta(x-x'),$$
$$\Box^2G^{(\mathrm{e.m.})}(x-x')=-\delta(x-x'). \tag{1.7}$$

Since in the present work we are concerned only with virtual processes, we may choose

$$G^{(\mathrm{m})}(x-x')=S_+(x-x'),$$
$$G^{(\mathrm{e.m.})}(x-x')=D_+(x-x'), \tag{1.8}$$

where S_+ and D_+ are defined in SIII, Eq. (1.63). Equations (1.6) may be solved, by successive substitution for ψ, $\bar{\psi}$, and $\mathbf{A}_\mu$ in terms of $\tilde{\psi}$, $\tilde{\bar{\psi}}$, and $\bar{A}_\mu$, which allows one to express $\mathbf{T}_{\mu\nu}{}^{(\mathrm{m})}$ in terms of the interaction variables without mass renormalization

$$\begin{aligned}\mathbf{T}_{\mu\nu}{}^{(\mathrm{m})}=\tilde{T}_{\mu\nu}{}^{(\mathrm{m})}&-\frac{e^2}{2i}\int\bar{\tilde{\psi}}(x')\gamma_\lambda\Big[S_+(x'-x)\gamma_\mu\frac{\partial}{\partial x_\nu}S_+(x-x')\\&-\frac{\partial}{\partial x_\nu}S_+(x'-x)\gamma_\mu S_+(x-x'')\Big]\gamma_\lambda\\&\times D_+(x'-x'')\tilde{\bar{\psi}}(x'')d\omega'd\omega''\\&-\frac{e^2}{2i}\int\Big[\bar{\tilde{\psi}}(x)\gamma_\mu\frac{\partial}{\partial x_\nu}S_+(x-x')\\&\times\gamma_\lambda S_+(x'-x'')D_+(x'-x'')\gamma_\lambda\tilde{\bar{\psi}}(x'')\\&+\tilde{\bar{\psi}}(x'')\gamma_\lambda S_+(x''-x')D_+(x''-x')\gamma_\lambda\\&\times S_+(x'-x)\gamma_\mu\frac{\partial}{\partial x_\nu}\tilde{\bar{\psi}}(x)\Big]d\omega'd\omega''.\end{aligned} \tag{1.9}$$

Next we need the connection between the tilde variables and the renormalized interaction variables ψ, $\bar{\psi}$, and A_μ. Clearly,

$$\bar{A}_\mu=A_\mu.$$

ψ and $\tilde{\psi}$ are related by the equation

$$\psi(x)=(1+\zeta)^{\frac{1}{2}}\Big[\tilde{\psi}(x)+\int S_+(x-x')\times\delta M(x'-x'')\psi(x'')d\omega'd\omega''\Big], \tag{1.10}$$

where the mass operators δM is

$$\delta M(x-x')=ie^2\gamma_\lambda S_+(x-x')D_+(x-x')\gamma_\lambda, \tag{1.11}$$

and ζ is a number, of order e^2, which renormalizes the over-all scale of the operator and will be discussed further.

It is easy to see that the ψ so defined satisfies the Dirac equation with altered mass, m. For operating on (1.10) with $(\gamma_\mu\partial/\partial x_\mu+m_0)$ gives

$$\begin{aligned}(\gamma_\mu\partial/\partial x_\mu+m_0)\psi&=-\int\delta M(x-x'')\psi(x'')d\omega''\\&=-\delta m\psi,\end{aligned} \tag{1.12}$$

where $\delta m=m-m_0$ (see SII, Eqs. (3.78), (3.79)).

[12] For details, see SI, p. 1443.

[13] In what follows, we shall be concerned only with the one electron part of $T_{\mu\nu}$ and $\delta T_{\mu\nu}$.

Solving (1.10) for $\tilde{\psi}$ in terms of ψ, gives, to order e^2,

$$\tilde{\psi}=\psi-\int S_+(x-x')\delta M(x'-x'')\psi(x'')dx'dx''-\tfrac{1}{2}\zeta\psi. \quad (1.13)$$

Substitution into (1.9) gives $\mathbf{T}_{\mu\nu}^{(m)}$ in terms of the renormalized interaction variables. The integral in (1.9) containing the mass operator is canceled and one obtains

$$\mathbf{T}_{\mu\nu}^{(m)}=T_{\mu\nu}^{(m)}+\delta T_{\mu\nu}^{(m)}, \quad (1.14)$$

where $\delta T_{\mu\nu}^{(m)}$ is the physically observable correction, given by

$$\delta T_{\mu\nu}^{(m)}(x)=-\zeta T_{\mu\nu}(x)$$
$$-\frac{e^2}{2i}\int\bar{\psi}(x')\gamma_\lambda\Big[S_+(x'-x)\gamma_\mu\frac{\partial}{\partial x_\nu}S_+(x-x'')$$
$$-\frac{\partial}{\partial x_\nu}S_+(x'-x)\gamma_\mu S_+(x-x'')\Big]\gamma_\lambda D_+(x'-x'')$$
$$\times\psi(x'')dx'dx''. \quad (1.15)$$

To evaluate this correction we pass into momentum space. We write

$$\bar{\psi}(x')=\int\bar{\varphi}(p')e^{-ip'x'}d\mathbf{p}',$$
$$\psi(x'')=\int\varphi(p'')e^{ip''x''}d\mathbf{p}'', \quad (1.16)$$

where $d\mathbf{p}'$ and $d\mathbf{p}''$ indicate integrations over the space components of the momentum four-vectors, p' and p'';

$$S_+(x)=-(2\pi)^{-4}\int(dk)e^{ikx}/(i\gamma k+m), \quad (1.17)$$

$$D_+(x)=(2\pi)^{-4}\int(dk)e^{ikx}/k^2,$$

where (dk) indicates an integration over the entire four-dimensional momentum space (see SIII, Eqs. (1.69)). With these substitutions and the usual simplifications, $\delta T_{\mu\nu}^{(m)}$ becomes

$$\delta T_{\mu\nu}^{(m)}(x)=\int\bar{\varphi}(p')\delta T_{\mu\nu}^{(m)}(p',p'')\varphi(p'')$$
$$\times e^{i(p''-p')x}dp'dp'', \quad (1.18)$$

where the momentum representatives $\delta T_{\mu\nu}^{(m)}(p',p'')$ are given by

$$\delta T_{\mu\nu}^{(m)}(p',p'')$$
$$=\frac{ie^2}{2(2\pi)^4}\int(dk)\Big[\frac{(p'+p''-2k)_\nu}{k^2}\gamma_\lambda\frac{1}{i\gamma(p'-k)+m}$$
$$\times i\gamma_\mu\frac{1}{i\gamma(p''-k)+m}\gamma_\lambda\Big]-\tfrac{1}{2}\zeta i(p'+p'')_\nu\gamma_\mu. \quad (1.19)$$

The renormalization constant ζ is related to the kernel $K_\mu^{(2)}$ of SIII, Eqs. (1.62), (1.97) by the equation

$$\zeta\gamma_\mu\delta(x'-x)\delta(x-x'')=\frac{e^2}{2}K_\mu^{(2)}(x'-x,x-x'); \quad (1.20)$$

it is conveniently expressed as $\zeta=$ coefficients of $i\gamma_\sigma$ in

$$\frac{\partial}{\partial p_\sigma}\delta M(p)\Big|_{i\gamma p+m=0}=\frac{ie^2}{(2\pi)^4}\int\frac{(dk)}{k^2}\Big[\gamma_\lambda\frac{1}{i\gamma(p-k)+m}$$
$$\times i\gamma_\sigma\frac{1}{i\gamma(p-k)+m}\gamma_\lambda\Big]_{i\gamma p+m=0}. \quad (1.21)$$

Using this expression in (1.19) gives, finally,

$$\delta T_{\mu\nu}^{(m)}(p',p'')=\frac{ie^2}{(2\pi)^4}\int\frac{(dk)}{k^2}$$
$$\times\Big\{\Big[\gamma_\lambda\frac{1}{i\gamma(p'-k)+m}i\gamma_\mu\frac{1}{i\gamma(p''-k)+m}\gamma_\lambda\Big](-k_\nu)$$
$$+\frac{(p'+p'')_\nu}{2}\gamma_\lambda\Big[\frac{1}{i\gamma(p'-k)+m}i\gamma_\mu\frac{1}{i\gamma(p''-k)+m}$$
$$-\Big(\frac{1}{i\gamma(p-k)+m}i\gamma_\mu\frac{1}{i\gamma(p-k)+m}\Big)_{i\gamma p+m=0}\Big]\gamma_\lambda\Big\}. \quad (1.22)$$

The Electromagnetic Part

Here the mass renormalization does not affect the second-order correction and hence one can make directly the transition from the Heisenberg to the final interaction variables. The basic equation is

$$\delta(\mathbf{A}_\rho(x_1)\mathbf{A}_\sigma(x_2)+\mathbf{A}_\sigma(x_2)\mathbf{A}_\rho(x_1))$$
$$=-2ie^2\int\bar{\psi}(x')[\gamma_\rho D_+(x_1-x')S_+(x'-x'')D_+(x''-x_2)\gamma_\sigma$$
$$+\gamma_\sigma D_+(x_2-x')S_+(x'-x'')D_+(x''-x_1)\gamma_\rho]$$
$$\times\psi(x'')dx'dx'', \quad (1.23)$$

which is easily derived from (1.6) and (1.8), when one uses the fact that $\bar{A}_\mu(x)=A_\mu(x)$.

The correction to $\mathbf{T}_{\mu\nu}^{(e.m.)}$, Eq. (1.2), is then obtained by setting ρ and σ equal to λ in the above expression and operating on it with

$$\frac{1}{2}\Big[\frac{\partial}{\partial x_{1\mu}}\frac{\partial}{\partial x_{2\nu}}-\frac{1}{2}\delta_{\mu\nu}\frac{\partial}{\partial x_{1\sigma}}\frac{\partial}{\partial x_{2\sigma}}\Big]_{\substack{x_1\to x\\ x_2\to x}}. \quad (1.24)$$

This results in

$$\mathbf{T}_{\mu\nu}^{(e.m.)}=T_{\mu\nu}^{(e.m.)}+\delta T_{\mu\nu}^{(e.m.)} \quad (1.25)$$

where

$$\delta T_{\mu\nu}^{(\mathrm{e.m.})}(x) = -ie^2 \int \bar{\psi}(x')\gamma_\lambda S_+(x'-x'')\gamma_\lambda \psi(x'') \times \Big[\frac{\partial}{\partial x_\mu} D_+(x-x') \frac{\partial}{\partial x_\nu} D_+(x''-x) + \frac{\partial}{\partial x_\nu} D_+(x-x') \frac{\partial}{\partial x_\mu} D_+(x''-x) - \delta_{\mu\nu} \frac{\partial}{\partial x_\sigma} D_+(x-x') \frac{\partial}{\partial x_\sigma} D_+(x''-x) \Big] d\omega' d\omega''. \quad (1.26)$$

In momentum space this corresponds to

$$\delta T_{\mu\nu}^{(\mathrm{e.m.})}(p', p'') = -\frac{ie^2}{(2\pi)^4} \int (dk)\gamma_\lambda \frac{1}{i\gamma(p''-k)+m} \gamma_\lambda \times \Big[\frac{k_\mu(p''-p'-k)_\nu + k_\nu(p''-p'-k)_\mu - \delta_{\mu\nu}k_\sigma(p''-p'-k)_\sigma}{k^2(p''-p'-k)^2} \Big]. \quad (1.27)$$

The total correction to $T_{\mu\nu}(p', p'')$ is

$$\delta T_{\mu\nu}(p', p'') = \delta T_{\mu\nu}^{(\mathrm{m})}(p', p'') + \delta T_{\mu\nu}^{(\mathrm{e.m.})}(p', p'') \quad (1.28)$$

where $\delta T_{\mu\nu}^{(\mathrm{m})}$ and $\delta T_{\mu\nu}^{(\mathrm{e.m.})}$ are given by (1.22) and (1.27).

2. THE DIVERGENCE OF THE CANONICAL STRESS TENSOR

The conservation of energy of the electron-photon system is expressed by the equation

$$\partial \mathbf{T}_{\mu\nu}/\partial x_\mu = 0 \quad (2.1)$$

which is a consequence of the definition of $\mathbf{T}_{\mu\nu}$, (1.1), (1.2), and the equations of motion, (1.3). Expressing $\mathbf{T}_{\mu\nu}$ in the form $T_{\mu\nu}+\delta T_{\mu\nu}$, it follows from the divergence-free nature of $\mathbf{T}_{\mu\nu}$ that

$$(\partial/\partial x_\mu)\delta T_{\mu\nu} = 0. \quad (2.2)$$

Transforming to the momentum space, this equation becomes

$$0 = (\partial/\partial x_\mu) \int \bar{\varphi}(p')\delta T_{\mu\nu}(p', p'')\varphi(p'') \times e^{i(p''-p')x} d\mathbf{p}' d\mathbf{p}'' = i \int \bar{\varphi}(p')[(p''-p')_\mu \delta T_{\mu\nu}(p', p'')]\varphi(p'') \times e^{i(p''-p')x} d\mathbf{p}' d\mathbf{p}'', \quad (2.3)$$

so that

$$(p''-p')_\mu \delta T_{\mu\nu}(p', p'') = 0. \quad (2.4)$$

In a convergent theory, the verification of (2.4) from (1.28), (1.22), and (1.27) would constitute merely a check on the algebra. In the present divergent electrodynamics, however, an explicit calculation of $(p''-p')_\mu \delta T_{\mu\nu}$ gives an infinite, ambiguous integral and (2.4) is to be used as a directive to attach the value zero to this integral, here and wherever else it may occur.

When (1.28) is substituted into (2.4), one obtains after some rearrangement

$$(p''-p')_\mu \delta T_{\mu\nu}(p', p'') = -\frac{ie^2}{2(2\pi)^4} \int (dk)\gamma_\lambda \Big[\frac{1}{(i\gamma(p'-k)+m)} \frac{k_\nu}{k^2} - \frac{1}{(i\gamma(p''-k)+m)} \frac{(k-p''+p')_\nu}{(k-p''+p')^2} \Big] \gamma_\lambda. \quad (2.5)$$

For large values of k, the integrand in (2.5) behaves like k^{-3} so that the integral is linearly divergent. It is, however, noteworthy that the second term of the integrand arises from the first by the translation of the variable of integration, $k \to k+p'-p''$. Thus if the theory were convergent and the contributions from the two terms were finite, they would automatically cancel, in accordance with the requirement of conservation of energy. To maintain energy conservation in the present, divergent theory, it is evidently necessary to *regard integrals of the form*

$$\int (dk)\gamma_\lambda \frac{k_\nu}{k^2} \frac{1}{i\gamma(p'-k)+m} \gamma_\lambda \quad (2.6)$$

as independent of translations of the variable of integration. This rule will enable us to calculate the symmetrical stress tensor in a self-consistent, unambiguous manner.

3. THE DIAGONAL ELEMENTS OF THE CANONICAL AND SYMMETRICAL STRESS TENSORS

The diagonal elements of the canonical and symmetrical tensors, $\mathbf{T}_{\mu\nu}(p', p')$ and $\mathbf{\Theta}_{\mu\nu}(p', p')$ are of special interest since they alone are needed to calculate space integrals of the components of these tensors. Thus, for example, if dv indicates integration over the three space-coordinates,

$$\int \mathbf{T}_{\mu\nu}(x)dv = \int \bar{\varphi}(p')\mathbf{T}_{\mu\nu}(p', p')\varphi(p'')e^{i(p''-p')x} d\mathbf{p}' d\mathbf{p}'' dv = (2\pi)^3 \int \bar{\varphi}(p')\mathbf{T}_{\mu\nu}(p', p')\varphi(p')d\mathbf{p}'. \quad (3.1)$$

Further, it is well known that the difference, $\mathbf{\Theta}_{\mu\nu}(x) - \mathbf{T}_{\mu\nu}(x)$ has the form of a divergence, $\partial \mathbf{F}_{\lambda\mu\nu}/\partial x_\lambda$. Hence $\mathbf{\Theta}_{\mu\nu}(p', p'') - \mathbf{T}_{\mu\nu}(p', p'')$ contains $(p''-p')_\lambda$ as a factor and therefore vanishes when $p''=p'$. This

means that

$$\mathbf{T}_{\mu\nu}(p', p') = \mathbf{\Theta}_{\mu\nu}(p', p') \tag{3.2}$$

so that $\delta T_{\mu\nu}(p', p')$ is also the correction of the physically important symmetrical tensor.

From Eqs. (1.28), (1.22), and (1.26) one finds that when $p'' = p'$, the total correction of $\mathbf{T}_{\mu\nu}(p', p')$ can be written in the form

$$\delta T_{\mu\nu}(p', p'') = -\frac{ie^2}{(2\pi)^4}\int (dk)\frac{\partial}{\partial k_\mu}\left(\frac{k_\nu}{k^2}\gamma_\lambda\frac{1}{i\gamma(p'-k)+m}\gamma_\lambda\right). \tag{3.3}$$

This integral is linearly divergent. However, the integrand is the momentum derivative of the integrand in (2.6). Such a derivative corresponds, of course, to an infinitesimal translation of the variable of integration, and hence, by the discussion of the last section, conservation of energy requires that the integral be set equal to zero:

$$\delta T_{\mu\nu}(p', p') = \delta\Theta_{\mu\nu}(p', p'') = 0. \tag{3.4}$$

In particular, the correction to the so-called self-stress of the electron,

$$\delta S = \frac{1}{3}\left[\int \delta\Theta_{ii}(x)dv\right]_{\text{electron at rest}}, \quad i = 1, 2, 3 \tag{3.5}$$

vanishes.

4. THE OFF DIAGONAL[9] ELEMENTS OF THE SYMMETRICAL STRESS TENSOR

In the preceding section we have seen that the space integrals of $\delta T_{\mu\nu}(x)$ and $\delta\Theta_{\mu\nu}(x)$ are equal and involve only the diagonal[9] matrix elements $\delta T_{\mu\nu}(p', p')$ which were shown to be zero. Clearly, these diagonal matrix elements are also sufficient to describe the non-integrated stress tensors at any given point, if the electron is in a state of definite momentum, p'.

It is, however, also of some interest to investigate the non-integrated stress-tensor of an electron in a superposition of momentum states (wave packet), and in particular to ascertain that it is free from singularities. For this purpose one must calculate the correction $\delta\Theta_{\mu\nu}(x)$ of the symmetrical, rather than the canonical stress-tensor. Equivalently, we may compute $\delta\Theta_{\mu\nu}(p', p'')$, defined by the equation

$$\delta\Theta_{\mu\nu}(x) = \int \bar{\varphi}(p')\delta\Theta_{\mu\nu}(p', p'')\varphi(p'') \times e^{i(p''-p')x}dp'dp''. \tag{4.1}$$

In Heisenberg variables, $\mathbf{\Theta}_{\mu\nu}(x)$ is given by the expression

$$\mathbf{\Theta}_{\mu\nu}(x) = \tfrac{1}{2}(\mathbf{F}_{(\mu\lambda}\mathbf{F}_{\nu)\lambda} - \tfrac{1}{2}\delta_{\mu\nu}\mathbf{F}_{\lambda\sigma}^2) + \tfrac{1}{4}[\bar{\psi}, \gamma_{(\mu}\partial\psi/\partial x_{\nu)}] - \tfrac{1}{2}\mathbf{j}_{(\mu}\mathbf{A}_{\nu)}, \tag{4.2}$$

where the symbol $(\mu\ \ \nu)$ indicates symmetrization in the following sense: $A_{(\mu}B_{\nu)} \sim A_\mu B_\nu + A_\nu B_\mu$; and

$$\mathbf{F}_{\mu\nu} = \partial\mathbf{A}_\nu/\partial x_\mu - \partial\mathbf{A}_\mu/\partial x_\nu. \tag{4.3}$$

Using the equation of motion $\mathbf{j}_\mu = -\Box^2\mathbf{A}_\mu$ in the last term of (4.2), we may re-write $\mathbf{\Theta}_{\mu\nu}$ in the form

$$\begin{aligned}\mathbf{\Theta}_{\mu\nu} &= \tfrac{1}{2}\mathbf{T}_{(\mu\nu)} \\ &+\frac{1}{2}\frac{\partial}{\partial x_\lambda}\Big[\frac{1}{2}\Big(\frac{\partial\mathbf{A}_{(\mu}}{\partial x_\lambda}\mathbf{A}_{\nu)} + \mathbf{A}_{(\mu}\frac{\partial\mathbf{A}_{\nu)}}{\partial x_\lambda}\Big) \\ &\quad -\Big(\frac{\partial\mathbf{A}_\lambda}{\partial x_{(\mu}}\mathbf{A}_{\nu)} + \mathbf{A}_{(\nu}\frac{\partial\mathbf{A}_\lambda}{\partial x_{\mu)}}\Big) \\ &\quad +\tfrac{1}{2}\delta_{\mu\nu}\Big(\frac{\partial\mathbf{A}_\lambda}{\partial x_\sigma}\mathbf{A}_\sigma + \mathbf{A}_\sigma\frac{\partial\mathbf{A}_\lambda}{\partial x_\sigma}\Big)\Big] \\ &+\frac{1}{2}\Big[\frac{\partial^2\mathbf{A}_\lambda}{\partial x_{(\mu}\partial x_\lambda}\mathbf{A}_{\nu)} + \mathbf{A}_{(\nu}\frac{\partial^2\mathbf{A}_\lambda}{\partial x_{\mu)}\partial x_\lambda} \\ &\quad -\tfrac{1}{2}\delta_{\mu\nu}\Big(\frac{\partial^2\mathbf{A}_\lambda}{\partial x_\sigma\partial x_\lambda}\mathbf{A}_\sigma + \mathbf{A}_\sigma\frac{\partial^2\mathbf{A}_\lambda}{\partial x_\sigma\partial x_\lambda}\Big)\Big]\end{aligned} \tag{4.4}$$

(see Eqs. (1.1), (1.2) for $\mathbf{T}_{\mu\nu}$). The last square bracket in (4.4) may be set equal to zero by invoking the subsidiary condition $\partial\mathbf{A}_\lambda/\partial x_\lambda = 0$.[14] Thus $\mathbf{\Theta}_{\mu\nu}$ may finally be written in the simple form

$$\mathbf{\Theta}_{\mu\nu} = \mathbf{\Theta}_{\mu\nu}{}^{(1)} + \mathbf{\Theta}_{\mu\nu}{}^{(2)}, \tag{4.5}$$

where

$$\begin{aligned}\mathbf{\Theta}_{\mu\nu}{}^{(1)} &= \tfrac{1}{2}\mathbf{T}_{(\mu\nu)}, \\ \mathbf{\Theta}_{\mu\nu}{}^{(2)} &= -\frac{1}{4}\frac{\partial^2}{\partial x_\lambda{}^2}(\mathbf{A}_{(\mu}\mathbf{A}_{\nu)}) + \frac{1}{2}\delta_{\mu\nu}\frac{\partial^2}{\partial x_\lambda\partial x_\sigma}(\mathbf{A}_\lambda\mathbf{A}_\sigma) \\ &\quad -\frac{1}{2}\frac{\partial}{\partial x_\lambda}\Big(\frac{\partial\mathbf{A}_\lambda}{\partial x_{(\mu}}\mathbf{A}_{\nu)} + \mathbf{A}_{(\nu}\frac{\partial\mathbf{A}_\lambda}{\partial x_{\mu)}}\Big).\end{aligned} \tag{4.6}$$

The Radiative Correction of $\mathbf{\Theta}_{\mu\nu}{}^{(1)} = \tfrac{1}{2}\mathbf{T}_{(\mu\nu)}$

In Sec. 1, Eqs. (1.28), (1.22), and (1.27), we derived integral expressions for $\delta T_{\mu\nu}(p', p'')$. We saw later, in Sec. 3, that in the special case, $p'' = p'$, these integrals are divergent yet must be regarded as zero. In the present case, where $p'' \neq p'$, the integrals are still divergent, but on subtracting out, from $\frac{1}{2}\delta T_{(\mu\nu)}(p', p'')$, the Hermitian expression,

$$\delta R_{(\mu\nu)}(p', p'') = \tfrac{1}{4}(\delta T_{(\mu\nu)}(p', p') + \delta T_{(\mu\nu)}(p'', p'')) \tag{4.7}$$

[14] Actually these terms can be shown to have a vanishing radiative correction independently of the subsidiary condition. For we may note that since $\Box^2(\partial\mathbf{A}_\lambda/\partial x_\lambda) = \partial(\Box^2\mathbf{A}_\lambda)/\partial x_\lambda = -\partial\mathbf{j}_\lambda/\partial x_\lambda = 0$, the scalar field $\partial\mathbf{A}_\lambda/\partial x_\lambda$ is not coupled to the electron field. An explicit calculation of the correction of the above terms leads to infinite integrals; however, their integrands have the characteristic difference form, so that in accordance with a rule dictated by the conservation of charge (see reference 3), these integrals must be regarded as zero.

which we know to be zero, we shall obtain a finite result for $\delta\Theta_{\mu\nu}$. Following are the details of the calculation.

We consider first the unsymmetrized (in μ and ν) expression, $\delta T_{\mu\nu}(p', p'') - \delta R_{\mu\nu}(p', p'')$ and break it up into three parts,

$$\delta T_{\mu\nu} - \delta R_{\mu\nu} = \delta L_{\mu\nu} + \delta M_{\mu\nu} + \delta N_{\mu\nu}, \tag{4.7'}$$

where

(a) the matter part, $\delta L_{\mu\nu}$, is

$$\delta L_{\mu\nu} = \frac{ie^2}{(2\pi)^4}\int (dk)\frac{(-k_\nu)}{k^2}$$
$$\times\gamma_\lambda\Big[\frac{1}{i\gamma(p'-k)+m}i\gamma_\mu\frac{1}{i\gamma(p''-k)+m}$$
$$-\frac{1}{2}\frac{1}{i\gamma(p'-k)+m}i\gamma_\mu\frac{1}{i\gamma(p'-k)+m}$$
$$-\frac{1}{2}\frac{1}{i\gamma(p''-k)+m}i\gamma_\mu\frac{1}{i\gamma(p''-k)+m}\Big]\gamma_\lambda \tag{4.8}$$

(see Eq. (1.22)).

(b) The mass renormalization term, $\delta M_{\mu\nu}$, is

$$\delta M_{\mu\nu} = \frac{ie^2}{(2\pi)^4}\int (dk)\frac{1}{k^2}$$
$$\times\gamma_\lambda\Big[\frac{(p'+p'')_\nu}{2}\frac{1}{i\gamma(p'-k)+m}i\gamma_\mu\frac{1}{i\gamma(p''-k)+m}$$
$$-\frac{p_\nu'}{2}\Big(\frac{1}{i\gamma(p'-k)+m}i\gamma_\mu\frac{1}{i\gamma(p'-k)+m}\Big)_{i\gamma p'+m=0}$$
$$-\frac{p_\nu''}{2}\Big(\frac{1}{i\gamma(p''-k)+m}i\gamma_\mu\frac{1}{i\gamma(p''-k)+m}\Big)_{i\gamma p''+m=0}\Big]\gamma_\lambda \tag{4.9}$$

(see Eq. (1.22)).

(c) To obtain a convenient expression for the electromagnetic term, $\delta N_{\mu\nu}$, we first rewrite $\delta T_{\mu\nu}^{(e.m.)}$, Eq. (1.27), in a form symmetrical in p' and p'':

$$\delta T_{\mu\nu}^{(e.m.)} = -\frac{1}{2}\frac{ie^2}{(2\pi)^4}\int (dk)\Big[\gamma_\lambda\frac{1}{i\gamma(p''-k)+m}\gamma_\lambda$$
$$\times\frac{k_\mu(p''-p'-k)_\nu - \delta_{\mu\nu}k_\sigma(p''-p'-k)_\sigma}{k^2(p''-p'-k)^2}$$
$$+(p''\rightleftharpoons p')\Big], \tag{4.10}$$

so that

$$\delta N_{\mu\nu} = -\frac{1}{2}\frac{ie^2}{(2\pi)^4}\int (dk)\Big[\gamma_\lambda\frac{1}{i\gamma(p''-k)+m}\gamma_\lambda$$
$$\times\Big(\frac{k_\mu(p''-p'-k)_\nu - \delta_{\mu\nu}k_\sigma(p''-p'-k)_\sigma}{k^2(p''-p'-k)^2}$$
$$-\frac{-k_\mu k_\nu + \delta_{\mu\nu}k^2}{(k^2)^2}\Big)+(p''\rightleftharpoons p')\Big]. \tag{4.11}$$

We now turn to a calculation of these three parts.

(a) *The Matter Part, $\delta L_{\mu\nu}$*

The expression (4.8), when rationalized and upon introduction of the usual auxiliary variables u and v, becomes

$$\delta L_{\mu\nu} = \frac{-e^2}{(2\pi)^3}\int_0^1 u\,du\int_{-1}^1 dv\int (dk)k_\nu$$
$$\times\{[(i\gamma k\gamma_\mu\gamma k + m(\gamma_\mu\gamma k+\gamma k\gamma_\mu)+2i\gamma_\mu k^2$$
$$-4i\gamma k k_\mu)(\delta''-\tfrac{1}{2}\delta_+''-\tfrac{1}{2}\delta_-'')]$$
$$+[(-2i\gamma_\mu kP+2i\gamma kP_\mu)\delta''$$
$$-(-2i\gamma_\mu kp''+2i\gamma kp'')\delta_+''$$
$$-(-2i\gamma_\mu kp'+2i\gamma kp')\delta_-'']$$
$$+[2i\gamma_\mu p'p''\delta''+mp_\mu''\delta_+''+mp_\mu'\delta_-'']$$
$$+[(1/2i)(\gamma_\mu k\Delta p-\gamma k\Delta p_\mu)(\delta_+''-\delta_-'')]$$
$$+[(i/4m)(P_\mu\sigma_{\mu\lambda}-P_\mu\sigma_{\mu\lambda})k_\mu\Delta p_\lambda(\delta_+''+\delta_-'')]\}, \tag{4.12}$$

where $P_\mu = p_\mu'' + p_\mu'$, $\Delta p_\mu = p_\mu'' - p_\mu'$, and δ'', δ_+'', δ_-'' are abbreviations for

$$\begin{aligned}\delta'' &= \delta''(k^2 - ku(P+\Delta pv)),\\ \delta_+'' &= \delta''|_{v=+1} = \delta''(k^2-2kup''),\\ \delta_-'' &= \delta''|_{v=-1} = \delta''(k^2-2kup').\end{aligned} \tag{4.13}$$

The terms have been grouped to facilitate recognition of any infinities. We shall now show that all terms, except those in the last square bracket, are in fact finite.

To show that the first term is finite, we note the identity

$$\int_{-1}^1 f(v)dv = \int_{-1}^1\Big\{\tfrac{1}{2}[f(1)+f(-1)]-v\frac{\partial f}{\partial v}\Big\}dv$$
$$= \int_{-1}^1\Big\{\tfrac{1}{2}[f(1)+f(-1)]+\frac{v^2-1}{2}\frac{\partial^2 f}{\partial v^2}\Big\}dv. \tag{4.14}$$

Hence we have

$$\int_{-1}^{1} dv(\delta''-\tfrac{1}{2}\delta_+''-\tfrac{1}{2}\delta_-'')=\int_{-1}^{1} dv\frac{v^2-1}{2}u^2(k\Delta p)^2\delta^{IV}. \tag{4.15}$$

Recalling that for large k, $\delta(k^2-ku(P+\Delta pv))\sim k^{-2}$ and hence $\delta^{IV}\sim k^{-10}$, we see that the first term behaves like k^{-5}; since the volume element, $(dk)\sim k^3dk$, the integral of the first term is finite.

The second term may be transformed as follows: By (4.14),

$$\int_{-1}^{1}\delta''dv=\int_{-1}^{1} dv[\tfrac{1}{2}(\delta_+''+\delta_-'')+uvk\Delta p\delta'''], \tag{4.16}$$

so that

$$\int_{-1}^{1}[(p'+p'')_\sigma\delta''-p_\sigma''\delta_+''-p_\sigma'\delta_-'']dv$$

$$=-\Delta p_\sigma(\delta_+''-\delta_-'')+\int_{-1}^{1} dvP_\sigma uvk\Delta p\delta'''$$

$$=uk\Delta p\int_{-1}^{1} dv(\Delta p_\sigma+vP_\sigma^2)\delta'''. \tag{4.17}$$

Since $\delta'''\sim k^{-6}$, the second term is $\sim k^{-5}$ and hence has a finite integral.

The third term may at once be seen to be of order k^{-5}.

The fourth term may be shown to be finite by noting that

$$\delta_+''-\delta_-''=-\int_{-1}^{1} uk\Delta p\delta'''dv\sim k^{-7}. \tag{4.18}$$

However, the integrand of the last term is k^{-4}, and hence this term is logarithmically infinite. Since all other contributions to $\delta T_{\mu\nu}-\delta R_{\mu\nu}$ will be seen to be finite, it follows that, even after mass renormalization the radiative corrections to the canonical stress tensor remain infinite.

Fortunately these infinities disappear when one constructs the symmetrical combination $\delta T_{(\mu\nu)}$, which enters the expression for the physically important symmetrical tensor. To show this we return to the last term of (4.12) and note that

$$\delta_+''=\delta''(k^2-2kup'')$$

$$=\delta''(k^2)+\int_0^1\frac{\partial}{\partial w}\delta''(k^2-2kuwp'')dw$$

$$=\delta''(k^2)-2kup''\int_0^1\delta'''(k^2-2kuwp'')dw. \tag{4.19}$$

and similarly for δ_-''. Only the $\delta''(k^2)$ gives an infinite contribution to $\delta L_{\mu\nu}$. Hence on symmetrization one is left with the following, possibly divergent terms:

$$(i/4m)(P_{(\mu}\sigma_{\rho\lambda}-P_\rho\sigma_{(\mu\lambda)})k_\nu)k_\mu\Delta p_\lambda\delta''(k^2). \tag{4.20}$$

For purposes of integrating over k we may replace

$$k_\alpha k_\beta\to\tfrac{1}{4}k^2\delta_{\alpha\beta}. \tag{4.21}$$

Hence (4.20) becomes

$$\tfrac{1}{16}k^2(P_{(\mu}\sigma_{\nu)\lambda}-P_{(\nu}\sigma_{\mu)\lambda})\Delta p_\lambda\delta''(k^2), \tag{4.22}$$

which vanishes since the bracket is both symmetrical and antisymmetrical in μ and ν.

The actual evaluation of $\delta L_{(\mu\nu)}$ was carried out by the usual methods and gave the following result:

$$\tfrac{1}{2}\delta L_{\mu\nu}(p',p'')=-\frac{e^2}{4(2\pi)^3}\int_0^1 du\,\tfrac{1}{2}\int_{-1}^{1} dv\int(dk)$$

$$\times\{[-2u^3(1+u)v^2]m\delta_{\mu\nu}\Delta p^2$$

$$+[-m^2u^2(2-4u+u^2)-u^2(1-u+\tfrac{1}{4}u^2(1-v^2))\Delta p^2$$

$$-\tfrac{1}{2}u^4v^2\Delta p^2]i\gamma_{(\mu}P_{\nu)}$$

$$+[-2u^3(1-u)]mP_\mu P_\nu$$

$$+[2u^3(1+u)v^2]m\Delta p_\mu\Delta p_\nu\}$$

$$\times\delta''(k^2+m^2u^2+\tfrac{1}{4}\Delta p^2u^2(1-v^2))$$

$$+\{[u^3(u-2)]m^2i\gamma_{(\mu}P_{\nu)}$$

$$+[2u^2(1-u^2)]m(P_\mu P_\nu+\Delta p_\mu\Delta p_\nu)\}$$

$$\times\delta''(k^2+m^2u^2)]. \tag{4.24}$$

(b) The Mass Renormalization Term, $\delta M_{\mu\nu}$

After rationalization and introduction of the variables u and v, this term, Eq. (4.9) becomes

$$\delta M_{\mu\nu}=\frac{-e^2}{2(2\pi)^3}\int_0^1 udu\tfrac{1}{2}\int_{-1}^{1} dv\int(dk)$$

$$\times\gamma_\lambda\{\tfrac{1}{2}P_\nu(i\gamma(p'-k)-m)i\gamma_\mu(i\gamma(p''-k)-m)\delta''$$

$$-\tfrac{1}{2}p_\nu''[(i\gamma(p''-k)-m)i\gamma_\mu$$

$$\times(i\gamma(p''-k)-m)]_{i\gamma p''+m=0}\delta_+''$$

$$-\tfrac{1}{2}p_\nu'[(i\gamma(p'-k)-m)i\gamma_\mu$$

$$\times(i\gamma(p'-k)-m)]_{i\gamma p'+m=0}\delta_-''\}\gamma_\lambda. \tag{4.25}$$

These terms contain logarithmic infinities which, however, cancel. For collecting the terms of highest power in k we have

$$\gamma_\lambda i\gamma ki\gamma_\mu i\gamma k\gamma_\lambda\int_{-1}^{1} dv(\tfrac{1}{2}P_\nu\delta''-\tfrac{1}{2}p_\nu''\delta_+''-\tfrac{1}{2}p_\nu'\delta_-''). \tag{4.26}$$

The integral over v is precisely that encountered in (4.17). Hence we see that the logarithmic infinities in (4.25) combine to give a term $\sim k^{-5}$ which has a finite

integral. Direct evaluation gives

$$\tfrac{1}{2}\delta M_{(\mu\nu)}(p',p'')=-\frac{e^2}{4(2\pi)^3}\int_0^1 du\,\tfrac{1}{2}\int_{-1}^1 dv\int(dk)$$
$$\times\{[\tfrac{1}{4}u^3v^2\Delta p^2+u(1-u+\tfrac{1}{4}u^2(1-v^2))\Delta p^2$$
$$+m^2u(2-2u-u^2)]i\gamma_{(\mu}P_{\nu)}$$
$$+[-u^2(1-u)]\mathrm{im}\sigma_{(\mu\lambda}P_{\nu)}\Delta p_\lambda\}$$
$$\times\delta''(k^2+m^2u^2+\tfrac{1}{4}\Delta p^2u^2(1-v^2))$$
$$+\{[-m^2u(2-2u-u^2)]i\gamma_{(\mu}P_{\nu)}\}\delta''(k^2+m^2u^2)]. \tag{4.27}$$

(c) The Electromagnetic Part, $\delta N_{\mu\nu}$

A discussion similar to that given for the matter part shows without difficulty that $\delta N_{(\mu\nu)}$ is finite. It is given by the following final expression:

$$\tfrac{1}{2}\delta N_{(\mu\nu)}(p',p'')=-\frac{e^2}{4(2\pi)^3}\int_0^1 du\,\tfrac{1}{2}\int_{-1}^1 dv\int(dk)$$
$$\times[\{[2u(1-u^2)+2(1-u)^3(2u+1)v^2]m\Delta p^2\delta_{\mu\nu}$$
$$+[u(1-u)^3v^2]i\gamma_{(\mu}P_{\nu)}\Delta p^2$$
$$+[2u^2(1-u^2)]mP_\mu P_\nu$$
$$+[-2(1-u^2)(1-(1-u)^2v^2)]m\Delta p_\mu\Delta p_\nu\}$$
$$\times\delta''(k^2+m^2u^2+\tfrac{1}{4}\Delta p^2(1-u)^2v^2)$$
$$+\{[-2u^2(1-u^2)]m(P_\mu P_\nu+\Delta p_\mu\Delta p_\nu)\}$$
$$\times\delta''(k^2+m^2u^2)]. \tag{4.28}$$

This completes the calculation of

$$\delta\Theta_{\mu\nu}{}^{(1)}=\tfrac{1}{2}\delta T_{(\mu\nu)}=\tfrac{1}{2}[\delta L_{(\mu\nu)}+\delta M_{(\mu\nu)}+\delta N_{(\mu\nu)}], \tag{4.29}$$

Eqs. (4.24), (4.27), and (4.28).

The Radiative Correction of $\Theta_{\mu\nu}{}^{(2)}$

The second portion of the symmetrical tensor is given by Eq. (4.6). The calculation is based on Eq. (1.23) and leads, in a straightforward manner, to the following finite result:

$$\delta\Theta_{\mu\nu}{}^{(2)}(p',p'')=-\frac{e^2}{4(2\pi)^3}\int_0^1 du\,\tfrac{1}{2}\int_{-1}^1 dv\int(dk)$$
$$\times\{-4u(1-u)m\Delta p^2\delta_{\mu\nu}+(1-u)^3\Delta p^2 i\gamma_{(\mu}P_{\nu)}$$
$$+4u(1-u)m\Delta p_\mu\Delta p_\nu+2imu^2(1-u)\Delta p_\lambda\sigma_{(\mu\lambda}P_{\nu)}\}$$
$$\times\delta''(k^2+m^2u^2+\tfrac{1}{4}\Delta p^2(1-u)^2(1-v^2)). \tag{4.30}$$

The Total Radiative Correction of the Symmetrical Stress Tensor

We now collect the corrections of $\Theta_{\mu\nu}{}^{(1)}$ and $\Theta_{\mu\nu}{}^{(2)}$, Eqs. (4.29) and (4.30), to obtain the total correction of $\Theta_{\mu\nu}$:

$$\delta\Theta_{\mu\nu}(p',p'')=-\frac{e^2}{4(2\pi)^3}\int_0^1 du\,\tfrac{1}{2}\int_{-1}^1 dv\int(dk)$$
$$\times\{i\gamma_{(\mu}P_{\nu)}m^2[u(u-1)(u^2+2u-2)\delta_1''$$
$$+2u^2(1-u^2)\delta_2''+(u^3(u-2)+u(u^2+2u-2))\delta_3'']$$
$$+imP_{(\mu}\sigma_{\nu)\lambda}\Delta p_\lambda[-u^2(1-u)^2\delta_1''+u^2(1-u)^2\delta_2'']$$
$$+i\gamma_{(\mu}P_{\nu)}\Delta p^2[u(1-u)(1-u+\tfrac{1}{4}u^2(1-v^2))\delta_1''$$
$$+(1-u)^3\delta_2''-\tfrac{1}{2}u^3(u-1)v^2\delta_1''+(1-u)^3uv^2\delta_2'']$$
$$+m(\Delta p_\mu\Delta p_\nu-\delta_{\mu\nu}\Delta p^2)[2u^3(1+u)v^2\delta_1''$$
$$+2(1-u)^2((1-u^2)v^2-1)\delta_2'']$$
$$+\delta_{\mu\nu}m\Delta p^2[(1-u)^3(3u+2)v^2+(u-1)(1-u^2)]\delta_2''\}, \tag{4.31}$$

where

$$\delta_1=\delta(k^2+m^2u^2+\tfrac{1}{4}\Delta p^2u^2(1-v^2)),$$
$$\delta_2=\delta(k^2+m^2u^2+\tfrac{1}{4}\Delta p^2(1-u)^2(1-v^2)), \tag{4.32}$$
$$\delta_3=\delta(k^2+m^2u^2).$$

The integration over k leads to infrared infinites (see reference 1, SIII, p. 800), which may be formally circumvented by introducing a finite photon mass, or must be eliminated by a Bloch-Nordsieck calculation. The last term in (4.31) can be shown to vanish as a result of integrating over u and v. Since all other terms are individually divergenceless, we see that the entire tensor has, correctly, a vanishing divergence. Equation (4.31) is in agreement with the result of Villars,[15] as is further discussed in Appendix II.

ACKNOWLEDGMENT

We should like to thank Professor J. Schwinger for proposing this research and for many discussions about the general nature of the problem and its details. He has contributed many suggestions which have been incorporated into the body of the paper.

APPENDIX 1. THE RESULT OF PAIS AND EPSTEIN[16]

Pais and Epstein[2] have shown by a simple and elegant argument that the self-stress can be calculated from the equation

$$S=\frac{m_0{}^2}{3}\frac{\partial}{\partial m_0}\left(\frac{\delta m}{m_0}\right), \tag{A1.1}$$

[15] Equation (4.31) does not appear to be identical with Villars' equations (22), (28), reference 6, for two reasons: One is an oversight in Villars' paper, in which the second term of the first line of (26a) was partly omitted in (28). The other is that we calculated the correction to $-\Box^2A_\mu A_\nu$ in different variables from those used by Villars; as a result our expression looks different from that obtained by Villars but can, in fact, be shown to be identical with it.

[16] A discussion of the Pais and Epstein result also appears in J. Yukawa and H. Umezawa, Prog. Theoret. Phys. **6** (1), 112 (1951); **6** (2), 197 (1951).

where m_0 is the mechanical and δm the electromagnetic mass of the electron. On using the expression

$$\delta m=\frac{3e^2}{2\pi}m_0\log\left(\frac{1}{m_0 a}+\text{const}\right), \tag{A1.2}$$

where the cut-off length a is supposed to be *independent of* m_0, they obtained the nonvanishing result

$$S=-(e^2/2\pi)m_0, \tag{A1.3}$$

which is in contradiction to Lorentz covariance.

We should like to make the following comments on this result. First, we believe it to be unsafe to draw conclusions from explicit expressions for infinite integrals, into which a cut-off length has been introduced. However, if this is done, as in (A1.2), the statement that the cut-off length a is independent of m_0 introduces a foreign element into the theory, at the very last stage. For the only lengths which can be constructed from the constants e, $\hbar$, c, and m_0, which occur in quantum electrodynamics, are numerical multiples of the Compton wavelength of the electron, $\hbar/m_0c$; hence in our units ($\hbar=1$, $c=1$) any cut-off length must be given by an expression of the type

$$a=d/m_0, \tag{A1.4}$$

where d is independent of m_0. If, instead, a is assumed as independent of m_0—which could be the case if other particles and their Compton wavelengths were introduced—it is not surprising that a result, inconsistent with the original equations of quantum electrodynamics, is obtained.

When one uses the dimensionally correct expression (A1.4), Eq. (A1.2) takes the form

$$\delta m=\epsilon m_0, \tag{A1.5}$$

where ϵ is a pure number. This equation can of course be written down directly from dimensional considerations, without explicit use of (A1.2); for since m_0 is the only mass occurring in the original equations of quantum electrodynamics, any derived quantity, of the dimension of a mass, must be just a numerical multiple of m_0. It is clear that substitution of (A1.5) into (A1.1) gives the correct result, $S=0$.[17] We may remark that Eq. (A1.1) must be considered as reliable since it is derived by a formal argument, which is based entirely on the equations of quantum electrodynamics.

Next we should like to show that even if the cut-off is chosen independent of m_0, as was done by Pais and Epstein, S is given by an integral of the type (3.3) which according to our basic prescription (2.6) must be regarded as zero.

The electromagnetic mass of the electron is given by the integral (see reference 1, SIII, Eq. (3.78))

$$\delta m=\frac{e^2}{i(2\pi)^4}\int_V\frac{(dk)}{k^2}\left[\gamma_\lambda\frac{1}{i\gamma(p-k)+m_0}\gamma_\lambda\right]_{i\gamma p+m_0=0}, \tag{A1.6}$$

where V is a large volume bounded by the surface σ, which may be described by the parametric representation

$$\sigma:\quad k_\mu=k_\mu(u,v,w;m_0). \tag{A1.7}$$

It is convenient to change to dimensionless variables,

$$k=m_0k';\quad p=m_0p' \tag{A1.7'}$$

which gives

$$\delta m=\frac{e^2}{i(2\pi)^4}m_0\int_{V'}(dk')\left[\gamma_\lambda\frac{1}{k'^2(i\gamma(p'-k')+1)}\gamma_\lambda\right]_{i\gamma p'+1=0}, \tag{A1.8}$$

where V' is bounded by the surface,

$$\sigma':\quad k_\mu'=(1/m_0)k_\mu(u,v,w;m_0). \tag{A1.9}$$

We note from (A1.8) that $\delta m/m_0$ is a function of m_0 only through σ', the bounding surface of V'. Thus,

$$\begin{aligned}\frac{\partial}{\partial m_0}\left(\frac{\delta m}{m_0}\right)&=\frac{e^2}{(2\pi)^4 i}\int_{\sigma'}d\sigma_\mu'\left[\gamma_\lambda\frac{1}{k'^2(i\gamma(p'-k')+1)}\gamma_\lambda\right]\frac{\partial k_\mu'}{\partial m_0}\\&=\frac{e^2}{(2\pi)^4 i}\int_{V'}(dk')\frac{\partial}{\partial k_\mu'}\left[\gamma_\lambda\frac{\partial k_\mu'/\partial m_0}{k'^2(i\gamma(p'-k')+1)}\gamma_\lambda\right]\\&=\frac{e^2}{(2\pi)^4 i}\int_V(dk)\frac{\partial}{\partial k_\mu}\left[\gamma_\lambda\frac{\partial/\partial m_0(k_\mu/m_0)}{k^2(i\gamma(p-k)+m_0)}\gamma_\lambda\right],\end{aligned} \tag{A1.10}$$

where we have first converted the surface integral to a volume integral and then changed back to the original variables. Here we see again that if $k_\mu\propto m_0$, which means that the cut-off length is inversely proportional to m_0, then $(\partial/\partial m)(k_\mu/m_0)=0$ and hence $S=0$. If, however, k_μ were independent of m_0, as assumed by Pais and Epstein, one obtains in agreement with (3.3)[18]

$$S=-\frac{1}{3}\frac{e^2}{(2\pi)^4 i}\int_V(dk)\frac{\partial}{\partial k_\mu}\left[\frac{k_\mu}{k^2}\gamma_\lambda\frac{1}{i\gamma(p-k)+m_0}\gamma_\lambda\right]. \tag{A1.11}$$

Explicit calculation of S from (A1.11) or (3.3) gives the finite result (A1.3). However, our previous discussion applies, according to which integrals of the type (A1.11) must be regarded as zero. Thus we see that the incorrect, finite result for S is obtained only when one works out explicitly the infinite integral for the electromagnetic mass δm of the electron (see A1.2)

[17] Rohrlich, reference 5, has used a similar dimensional argument to show that the self-stress of an electron interacting with the electromagnetic field as well as a number of neutral vector meson fields vanishes. However, we have shown that the argument does not require the introduction of the vector meson fields.

[18] The minus sign in Eq. (A1.11) has its origin in the fact that Pais and Epstein have defined their stress tensor as the negative of ours; δT_{44} vanishes.

and uses a mass-independent cut-off length. As long as one leaves δm in the form of an integral, the conservation of energy leads correctly to a null result for the self-stress.

APPENDIX II. THE SEMI-REALISTIC REGULARIZATION PROCEDURE OF ROHRLICH AND VILLARS

Villars[7,8] has tried to calculate the correction to the stress tensor by means of the regulator method of Pauli and Villars.[9] However, this procedure still led to a nonvanishing self-stress, in fact to the same result as was obtained by Pais and Epstein.[2] This showed that quantum electrodynamics, supplemented by formal regularization rules is not a self-consistent scheme.

It was noticed, however, by Rohrlich[6] that a vanishing self-stress can be obtained by replacing the stress tensor $\Theta_{\mu\nu}$ of the electron photon fields by the sum $\lim_{M\to\infty}(\Theta_{\mu\nu}+\Theta_{\mu\nu}{}^{M})$, where the second term represents the stress tensor of a neutral vector meson field, of mass M, coupled to the electron field by the imaginary coupling constant ie. Physically, this situation was interpreted[7] as indicating that pure quantum electrodynamics was not self-consistent, but must be supplemented by additional fields with imaginary coupling.

It has been shown in the body of the present paper that no unphysical additional fields are necessary to obtain consistent results for the stress tensor.

Furthermore, one can see clearly why the inclusion of a neutral vector meson field gives consistent results, while formal regularization reproduces the result of Pais and Epstein.

We consider first the integrated stress tensor. If the electron is coupled to both a photon and vector meson field, in the manner of Rohrlich and Villars, the radiative corrections are finite. Under these circumstances, a direct calculation of the radiative corrections of the self-stress must give the zero result which follows formally from the divergencelessness of the total tensor. This is confirmed by an explicit calculation which gives

$$\delta T_{\mu\nu}{}'(p',p'')=\frac{-ie^2}{(2\pi)^4}\int(dk)\frac{\partial}{\partial k_\mu}\left[k_\nu\left(\frac{1}{k^2}-\frac{1}{k^2+M^2}\right)\gamma_\lambda\frac{1}{i\gamma(p'-k)+m}\gamma_\lambda\right] \quad \text{(A2.1)}$$

for the correction of the total tensor. In contrast to (3.3), this is a convergent integral, and hence, because of the derivative form of the integrand, it is unambiguously zero.

On the other hand, if the electron-photon tensor is formally regularized, the property of having a vanishing divergence, on which the vanishing of the self-stress rests, is destroyed. Hence the radiative correction to the self-stress, even though finite, need no longer be zero.

We shall now show that the result of such a calculation must in fact be identical with the nonvanishing result, (A1.3), of Pais and Epstein.

The formal argument of Pais and Epstein can be applied to the total stress tensor of the system: electron+photon field+vector meson field (with imaginary coupling). We write this tensor as

$$\Theta_{\mu\nu}=\Theta_{\mu\nu}{}^{reg}+M^2(\mathbf{A}_\mu{}^{(M)}\mathbf{A}_\nu{}^{(M)}-\tfrac{1}{2}\delta_{\mu\nu}\mathbf{A}_\lambda{}^{(M)}A_\lambda{}^{(M)}), \quad \text{(A2.2)}$$

where $\Theta_{\mu\nu}{}^{reg}$ is that part of the tensor whose correction is calculated in a formal regularization procedure. Explicit calculation shows that the correction to the 4–4 component of the term in parentheses vanishes in the rest system. One can now follow the procedure of Pais and Epstein which leads to the relation

$$S^{reg}=\frac{m^2}{3}\frac{\partial}{\partial m_0}\left(\frac{\delta m_{reg}}{m_0}\right) \quad \text{(A2.3)}$$

between the self-stress and mass-correction calculated by formal regularization. Since δm_{reg} is just of the form (A1.2) with a $\sim 1/M$, we see that formal regularization is exactly equivalent to introducing a cutoff in (A1.1) which is independent of m_0. Under these conditions the result of Pais and Epstein must be regained. This is confirmed by the calculations of Villars.[8]

Next we consider the off-diagonal elements, $\delta\Theta_{\mu\nu}(p',p'')$ which were calculated by Villars. In our own work they were calculated from

$$\delta\Theta_{\mu\nu}(p',p'')-\tfrac{1}{4}(\delta T_{(\mu\nu)}(p',p')+\delta T_{(\mu\nu)}(p'',p'')), \quad \text{(A2.4)}$$

(see Eq. (4.7)). On the other hand, Villars computed

$$\lim_{M\to\infty}(\delta\Theta_{\mu\nu}(p',p'')+\delta\Theta_{\mu\nu}{}^{M}(p',p'')). \quad \text{(A2.5)}$$

To see that the two methods lead to the same results, we note that the difference between (A2.5) and (A2.4) can be written as

$$\lim_{M\to\infty}\{[\delta\Theta_{\mu\nu}{}^{M}(p',p'')-\tfrac{1}{4}(\delta T_{(\mu\nu)}{}^{M}(p',p')+\delta T_{(\mu\nu)}{}^{M}(p'',p''))]+\tfrac{1}{4}[(\delta T_{(\mu\nu)}{}^{M}(p',p')+\delta T_{(\mu\nu)}(p',p'))+(\delta T_{(\mu\nu)}{}^{M}(p'',p'')+\delta T_{(\mu\nu)}(p'',p''))]\}. \quad \text{(A2.6)}$$

For a given M, the first square bracket is a finite quantity as in electrodynamics (essentially, because $\propto\Delta p^2$); while, as we saw above the second bracket vanishes identically in M. As now $M\to\infty$, the first bracket approaches zero because of the $(k^2+M^2)^{-1}$ terms which replace our previous $(k^2)^{-1}$ in all integrals. Thus the equivalence of Villars' calculation and ours is established.

Nuclear Matrix Elements in the Theory of Beta-Decay*

HENRY BRYSK†
Department of Physics, Duke University, Durham, North Carolina
(Received January 14, 1952)

An approach has been developed whereby the nuclear matrix elements can be calculated for the odd-A and half of the even-A beta-radioactive nuclei. The designation of nuclear states is made in accordance with the Mayer shell model and its extension by Nordheim to the even-A nuclei. The transforming nucleon is assigned the wave functions of a Dirac particle in a "square-well" potential representing the nuclear "core." Expressions for the matrix elements have been determined and compared with the data. Consistent agreement is found for the tensor interaction.

I. INTRODUCTION

ACCORDING to the Fermi theory of beta-radioactivity,[1,2] the probability P per unit time that a radioactive nucleus will emit an electron of energy (in units of the rest-energy of the electron) between W and $W+dW$ is

$$PdW=(G^2/2\pi^3)|M|^2F(Z,W)W \times(W^2-1)^{\frac{1}{2}}(W_0-W)^2dW, \quad (1)$$

where G is the interaction constant, F the Fermi function expressing the distortion, due to the electric field of the nucleus, of the statistical distribution, W_0 the maximum (end-point) energy of the emitted electron, and $|M|^2$ the square of the nuclear matrix element. More precisely, $|M|^2$ is a sum $\sum_{\Omega\Omega'}M_\Omega{}^*M_{\Omega'}C_{\Omega\Omega'}$ of terms quadratic in the matrix elements and each multiplied by a spectral correction factor $C_{\Omega\Omega'}(Z,W,W_0,R)$.

The Fermi function has been explicitly calculated and investigated in considerable detail.[3] The various spectral correction factors have also been explicitly determined.[4–7] The nuclear matrix elements, however, have heretofore only been crudely estimated on the basis of rather loose qualitative arguments (except for the allowed transitions for which angular factors alone determine M_Ω[8]). It is the purpose of this paper to remedy that lacuna for the majority of ground-to-ground transitions.

The matrix elements are formed by irreducible tensor operators compounded out of the Dirac operators and the position vector.[4,5] On the basis of their transformation properties, these operators fall into five categories or interactions: scalar, vector, axial vector, tensor, and pseudoscalar (S, V, A, T, and P). For each interaction, an $|M|^2$ is constructed from the M_Ω's having the desired transformation property and the appropriate correction factors. A knowledge of the matrix elements permits us to predict spectral distributions for the five interactions (or combinations of them) and thus, by comparison with the experimental data, to determine the correct interaction form. Angular correlation measurements give further clues in the same direction.

Integration of Eq. (1) over the whole range of electron energies (from 1 to W_0) yields $1/\tau$, the reciprocal of the theoretical lifetime. The M_Ω's are functions of nuclear quantities only and are strictly independent of W. In order to reduce greatly the calculations necessary, we can replace the C's by average values, thus taking all of $|M|^2$ outside the integral; the error introduced is not significant to the accuracy at present required. Thus,

$$(1/\tau)=(G^2/2\pi^3)|M|^2f(Z,W_0), \quad (2)$$

where $f(Z,W_0)$ is the energy integral. Substituting into this equation the experimental values of the mean life t and the end-point energy W_0, the theory predicts that

$$(G^2/2\pi^3)|M|^2ft=1. \quad (3)$$

Since the experimental ft values (now easily and quickly obtainable from the data[9]) vary over a very wide range, it is customary to list the common logarithm of the ft value instead. Then

$$\log ft+\log|M|^2=\text{constant}, \quad (4)$$

for all transitions for the proper choice of interaction.

The determination of the matrix elements presents two difficulties: the identification of the nuclear states, and the formation of appropriate nuclear wave functions. To resolve these two problems we have to postulate a model or formalism, and for each problem the approach involves elements not essential for the other. Such a model was evolved for the odd-A nuclei and for half the even-A. For those categories, our survey covers all allowed, first-forbidden, and second-forbidden transitions which occur ground-to-ground (and a few involving isomeric states where the spin assignment is clear) and for which the data (decay scheme, half-life, end-

* Based, in part, on a thesis submitted to the Graduate School of Arts and Sciences of Duke University, April 16, 1951, in partial fulfillment of the requirements for the Ph.D. degree.
† Now at the Westinghouse Atomic Power Division, Pittsburgh, Pennsylvania.
[1] E. Fermi, Z. Physik **88**, 161 (1934).
[2] E. J. Konopinski, Revs. Modern Phys. **15**, 209 (1943).
[3] E. Feenberg and G. Trigg, Revs. Modern Phys. **22**, 399 (1950).
[4] E. J. Konopinski and G. E. Uhlenbeck, Phys. Rev. **60**, 308 (1941).
[5] E. Greuling, Phys. Rev. **61**, 568 (1942).
[6] R. Nataf, thesis, University of Paris (1951).
[7] R. Nataf and R. Bouchez, J. phys. et radium **13**, 81 (1952).
[8] B. O. Grönblom, Phys. Rev. **56**, 508 (1939).
[9] S. A. Moszkowski, Phys. Rev. **82**, 35 (1951).

point energy, branching ratio if the decay is complex, optionally spectral shape) is complete and reliable,[10,11] up to neutron number 100. Heavier isotopes are omitted because they lie in the region of alpha-radioactivity where the competition of the latter process masks beta-decay in all but a very few cases, and where consequently spin assignments are very uncertain, especially in view of the extended choice of possible states for high particle number. The superallowed group does not fall within the model. Higher forbidden transitions were not dealt with because only three scattered cases were found with sufficient information; where the spin difference between the initial and final nuclei is high, the decay usually does not proceed ground-to-ground but instead via excited states and gamma-rays.

II. THE MODEL

Treating the nucleus strictly as a many-body problem, Wigner found that as a result of space, spin, and isotopic spin orthogonalities only the superallowed group of beta-transitions should occur to first order.[12] No quantitative information about the unfavored transitions has been obtained by this method. Since most decays are not superallowed, the Wigner theory is not wholly satisfactory. We are led to consider the Wigner approach as a first approximation, and to postulate some mechanism on a different basis whose contribution will yield the unfavored allowed and the forbidden transitions.

Such a mechanism is provided by the nuclear shell model.[7,13–19] We shall use the Mayer version of this model.[18,19] We consider each nucleon to behave as a particle in an attractive potential due to the other nucleons, all confined to a sphere of radius R. In the ground state, like nucleons are assumed to pair off to form an inert core as far as beta-decay is concerned; the whole interaction is ascribed to the remaining odd nucleon (for odd-A) or nucleons (for even-A). The spin and parity of an odd-A nucleus are those of the odd nucleon; the nucleon—and thus the nucleus—is assigned a spectroscopic term in analogy to atomic structure. For even-A, even-Z nuclei, there is only the core, and we take the nuclear spin as zero and all resultant nucleonic angular momenta also as zero. For even-A, odd-Z, the spins of the two odd nucleons add vectorially: If $J_1=l_1-\frac{1}{2}$ and $J_2=l_2+\frac{1}{2}$ (J and l are the total and orbital angular momenta of the nucleon), the resultant spin is the minimum $|J_1-J_2|$; if both are $l-\frac{1}{2}$ or $l+\frac{1}{2}$, the resultant spin is high (probably the maximum).[20] Experimental agreement with the spin predictions has been found in a number of cases.[21] In the ground state, a nucleon occupies the lowest available state of a single particle in the potential well due to all the other nucleons, subject to the Pauli principle. In order to make the energy levels break at the empirical "magic numbers," Mayer introduces spin-orbit coupling in such a manner that the $l+\frac{1}{2}$ term falls below the $l-\frac{1}{2}$ term. The order of levels in the Mayer scheme is shown in Appendix A; within a shell, this order is not rigid, rather there is quite a bit of crossing-over. While the spin-orbit coupling is essential for shell assignments, its effect on the energy levels is neglected in our calculations.

The shell model, which singles out the odd nucleon(s) and disregards the structure of the core, cannot of course account for the superallowed transitions since the latter are clearly related to correspondence of the proton and neutron number in the core. From the point of view of the shell model, superallowed behavior is a kind of resonance phenomenon. We shall not concern ourselves further with the superallowed transitions, but direct our attention to a comparison of the ordinary allowed and the forbidden decays.

For the odd-A nuclei, we take for the nuclear wave functions simply the wave functions (initial and final) of the transforming nucleon viewed as a Dirac particle in a three-dimensional "square-well" potential. The square well is selected for simplicity, though any other sufficiently steep well would do. For the even-A-minimum-spin-coupling nuclei, we adhere strictly to the same formalism, disregarding any limitation on the operators due to consideration of the resultant spin of the nucleus. No consistently satisfactory extension of the model has been found which will cover the even-A-high spin-coupling group.

III. DIRAC PARTICLE IN A SQUARE-WELL POTENTIAL

For a potential which is a function of r alone, the Dirac wave equation for the motion of a single particle[22] is separable, and yields the wave functions[23]

$$\psi_a=\begin{bmatrix} D_\kappa & Y_\kappa^{m-\frac{1}{2}} & if_{-\kappa} \\ -I_\kappa & Y_\kappa^{m+\frac{1}{2}} & if_{-\kappa} \\ I_{\kappa-1} & Y_{\kappa-1}^{m-\frac{1}{2}} & g_{-\kappa} \\ D_{\kappa-1} & Y_{\kappa-1}^{m+\frac{1}{2}} & g_{-\kappa} \end{bmatrix}$$

and

$$\psi_b=\begin{bmatrix} I_{\kappa-1} & Y_{\kappa-1}^{m-\frac{1}{2}} & if_\kappa \\ D_{\kappa-1} & Y_{\kappa-1}^{m+\frac{1}{2}} & if_\kappa \\ D_\kappa & Y_\kappa^{m-\frac{1}{2}} & g_\kappa \\ -I_\kappa & Y_\kappa^{m+\frac{1}{2}} & g_\kappa \end{bmatrix}, \qquad (5)$$

[10] A. M. Feingold, Revs. Modern Phys. **23**, 10 (1951).
[11] K. Way *et al.*, *Nuclear Data*, National Bureau of Standards Circular 499, (1949).
[12] E. P. Wigner, Phys. Rev. **56**, 519 (1939).
[13] W. M. Elsasser, J. phys. et radium (Sér. 7) **4**, 549 (1933); **5**, 389, 635 (1934).
[14] H. Margenau, Phys. Rev. **46**, 613 (1934).
[15] Haxel, Jensen, and Suess, Phys. Rev. **75**, 1766 (1949).
[16] E. Feenberg and K. C. Hammack, Phys. Rev. **75**, 1877 (1949).
[17] L. W. Nordheim, Phys. Rev. **75**, 1894 (1949).
[18] M. G. Mayer, Phys. Rev. **75**, 1969 (1949).
[19] Haxel, Jensen, and Suess, Z. Physik **128**, 295 (1950).
[20] L. W. Nordheim, Phys. Rev. **78**, 294 (1950).
[21] J. E. Mack, Revs. Modern Phys. **22**, 64 (1950).
[22] E. L. Hill and R. Landshoff, Revs. Modern Phys. **10**, 87 (1938).
[23] M. E. Rose, Phys. Rev. **51**, 484 (1937).

where

$$I_\kappa=[(\kappa+m+\tfrac{1}{2})/(2\kappa+1)]^{\frac{1}{2}},\ D_\kappa=[(\kappa-m+\tfrac{1}{2})/(2\kappa+1)]^{\frac{1}{2}},$$

and $\kappa=|K|$, where K is the Dirac quantum number such that

$$\begin{aligned}&\text{for } \psi_a\text{:}\quad K=-(J+\tfrac{1}{2})=-l-1;\\&\text{for } \psi_b\text{:}\quad K=(J+\tfrac{1}{2})=l.\end{aligned}\tag{6}$$

In the Dirac representation, the orbital angular momentum l is no longer a good quantum number (i.e., it is not an eigenvalue of the problem); instead there is the new good quantum number K.

The spherical harmonics Y appearing above have been defined in agreement with Condon and Shortley[24] (leading to some sign differences from Rose). The radial functions $f(r)$ and $g(r)$ are real.

The Dirac radial equations for a single particle moving in a central field are[25]

$$\begin{aligned}(E+Mc^2-V)rf_K-\hbar c(d/dr)rg_K-\hbar cKg_K=0,\\(E-Mc^2-V)rg_K-\hbar c(d/dr)rf_K-\hbar cKf_K=0,\end{aligned}\tag{7}$$

where M is the rest mass, E and V the total and potential energy. For a square well of depth V_0, we substitute for the interior solution $e=(E+V_0)/Mc^2$ and $x=(Mc/\hbar)r(e^2-1)^{\frac{1}{2}}$ to recast the equations into

$$\begin{aligned}[(d/dx)+(K/x)](e-1)^{\frac{1}{2}}xg_K-(e+1)^{\frac{1}{2}}xf_K=0,\\[(d/dx)-(K/x)](e+1)^{\frac{1}{2}}xf_K+(e-1)^{\frac{1}{2}}xg_K=0.\end{aligned}\tag{8}$$

The solutions of these equations which are regular at the origin are spherical Bessel functions.[26] For K positive or negative, they are

$$\begin{aligned}f_\kappa=A_\kappa(e+1)^{-\frac{1}{2}}j_{\kappa-1}(x),\quad f_{-\kappa}=A_{-\kappa}(e+1)^{-\frac{1}{2}}j_\kappa(x),\\g_\kappa=A_\kappa(e-1)^{-\frac{1}{2}}j_\kappa(x),\qquad g_{-\kappa}=-A_{-\kappa}(e-1)^{-\frac{1}{2}}j_{\kappa-1}(x),\end{aligned}\tag{9}$$

where A_κ and $A_{-\kappa}$ are normalization factors.

For the external solution, we can let $w=E/Mc^2$ and obtain equations of exactly the same form. However, while $e>1$, $w<1$, so that the argument of the Bessel functions is now imaginary. The solutions that vanish at ∞ and are real are spherical Macdonald functions.[26] Letting $y=(Mc/\hbar)r(1-w^2)^{\frac{1}{2}}$, we obtain

$$\begin{aligned}f_\kappa=B_\kappa(1+w)^{-\frac{1}{2}}k_{\kappa-1}(y),\\g_\kappa=-B_\kappa(1-w)^{-\frac{1}{2}}k_\kappa(y),\\f_{-\kappa}=B_{-\kappa}(1+w)^{-\frac{1}{2}}k_\kappa(y),\\g_{-\kappa}=-B_{-\kappa}(1-w)^{-\frac{1}{2}}k_{\kappa-1}(y).\end{aligned}\tag{10}$$

If we match the inner and outer solutions for f and g at the walls of the well, the ratio of the two equalities yields the boundary value equation. Using the rather good approximation $e+1\approx 2\approx 1+w$ and applying the recursion relations, the boundary value equation takes on the same form as in the nonrelativistic treatment.[14] If by each function we understand its value for $r=R$, we have

$$\begin{aligned}&\text{for } \psi_a\text{:}\quad j_{\kappa-2}/j_\kappa=-k_{\kappa-2}/k_\kappa;\\&\text{for } \psi_b\text{:}\quad j_{\kappa-1}/j_{\kappa+1}=-k_{\kappa-1}/k_{\kappa+1}.\end{aligned}\tag{11}$$

The consecutive solutions of the equation as x and y increase correspond to the successive nodal quantum numbers n.

For the normalization factors, the same approximation yields

$$B_\kappa/A_\kappa=j_{\kappa-1}/k_{\kappa-1},\quad B_{-\kappa}/A_{-\kappa}=j_\kappa/k_\kappa.\tag{12}$$

Using for the well range the usual nuclear radius $3.5\times10^{-13}A^{\frac{1}{3}}$ in units of the Compton wavelength of the electron, we find consistently a binding energy of the order of 8 Mev (as it should be) and a well depth of the order of 40 Mev. The results of numerical solution for the boundary values are listed in Appendix A. The spherical Bessel functions have been tabulated[27] and a polynomial expansion exists for the Macdonald functions.[26]

TABLE I. Transitions $K'-K=\pm1$ ($\Delta J=\pm1$, $\Delta l=\pm1$).—By the coupling rule, this can occur only for odd A.

Isotope	Decay	Spin assignment	log ft	S	log($\lvert M\rvert^2 ft$) V	A	T
35 Br 87	–	$2p_{3/2}-2d_{5/2}$	6.8	4.4	5.4	4.4	5.4
36 Kr 87	–	$2d_{5/2}-2p_{3/2}$*	7.0	4.4	5.4	4.4	5.4
37 Rb 89	–	$2p_{3/2}-2d_{5/2}$	6.6	4.2	5.2	4.2	5.2
57 La 141	–	$2d_{5/2}-2f_{7/2}$	7.5	5.2	6.0	5.2	6.0
58 Co 141	–	$2f_{7/2}-2d_{5/2}$*	7.7	5.3	6.0	5.3	6.0
59 Pr 143	–	$2d_{5/2}-2f_{7/2}$	7.6	5.3	6.1	5.3	6.1
59 Pr 145	–	$2d_{5/2}-2f_{7/2}$	7.8	5.5	6.3	5.5	6.3
61 Pm 147	–	$2d_{5/2}-2f_{7/2}$	7.6	5.3	6.1	5.3	6.1

IV. THE MATRIX ELEMENTS

Instead of irreducible tensors, the nuclear operators can be expressed in terms of solid spherical harmonics $\mathcal{Y}_{LM}(\Omega)$, where L is the order of the tensor and M is an integer such that $|M|\leq L$;[28] this leads to considerable simplification for $L>1$.

Making use of group-theoretical theorems,[28] we can prove that the square of the nuclear matrix element reduces to

$$|M_\Omega|^2=\frac{2L+1}{2J+1}\sum_{m'=-J'}^{J'}|(nKm'|\,\mathcal{Y}_{LO}(\Omega)\,|n'K'm')|^2.\tag{13}$$

Cross terms vanish unless both Ω's have the same L,

[24] E. U. Condon and G. H. Shortley, *Theory of Atomic Spectra* (Cambridge University Press, London, 1935).
[25] L. I. Schiff, *Quantum Mechanics* (McGraw-Hill Book Company, Inc., New York, 1949).
[26] G. N. Watson, *A Treatise on the Theory of Bessel Functions* (Cambridge University Press, London, 1944), second edition.
[27] *Tables of Spherical Bessel Functions*, Mathematical Tables Project, National Bureau of Standards (Columbia University Press, New York, 1947).
[28] D. L. Falkoff and G. E. Uhlenbeck, Phys. Rev. **79**, 323 (1950).

TABLE II. Transitions $K'+K=0$ ($\Delta J=0$, $\Delta l=\pm 1$).

Isotope	Decay	Spin assignment	log fi	log(|M|²/fi) S	V	A	T	P
46 Pd 111	−	$3s_{1/2}-2p_{1/2}$	6.8	3.1	4.9	5.2	5.4	3.6
47 Ag 111	−	$2p_{1/2}-3s_{1/2}$*	7.3	3.6	5.4	5.7	5.9	4.1
47 Ag 113	−	$2p_{1/2}-3s_{1/2}$*	7.0	3.3	5.1	5.4	5.6	3.8
47 Ag 115	−	$2p_{1/2}-3s_{1/2}$	6.4	2.7	4.5	4.8	5.0	3.2
48 Cd 117	−	$3s_{1/2}-2p_{1/2}$	6.1	2.4	4.2	4.5	4.7	2.9
49 In 115m	−	$2p_{1/2}-3s_{1/2}$*	6.4	2.7	4.5	4.8	5.0	3.2
49 In 117	−	$2p_{1/2}-3s_{1/2}$*	6.2	2.5	4.3	4.6	4.8	3.0
49 In 119	−	$2p_{1/2}-3s_{1/2}$*	6.2	2.5	4.3	4.6	4.8	3.0
54 Xe 137	−	$2f_{7/2}-1g_{7/2}$*	6.3	1.7	3.7	4.7	4.7	3.0
56 Ba 139	−	$2f_{7/2}-1g_{7/2}$*	6.7	2.1	4.1	5.1	5.1	3.4
66 Dy 165	−	$2f_{7/2}-1g_{7/2}$*	6.2	1.6	3.6	4.6	4.6	2.9
7 N 16	−	$2s_{1/2}-1p_{1/2}$	6.8	1.5	4.8	4.8	5.0	3.8
36 Kr 88	−	$2d_{5/2}-1f_{5/2}$	6.8	0.0	3.8	5.1	5.2	2.3
37 Rb 88	−	$2d_{5/2}-1f_{5/2}$	7.1	0.3	4.1	5.4	5.5	2.6
54 Xe 138	−	$2f_{7/2}-1g_{7/2}$	6.5	1.9	3.9	4.9	4.9	3.2
58 Ce 144	−	$2f_{7/2}-1g_{7/2}$	7.2	2.6	4.6	5.6	5.6	3.9

in which case

$$M_\Omega M_{\Omega'}{}^* = \frac{2L+1}{2J+1} \sum_{m'=-J'}^{J'} (nKm'|\,\mathcal{Y}_{LO}(\Omega)\,|n'K'm') \times (nKm'|\,\mathcal{Y}_{LO}(\Omega')\,|n'K'm')^*. \quad (14)$$

A great simplification is introduced by neglecting the difference between the initial and final energy levels in computing the matrix elements, i.e., by assigning the Bessel functions the same argument. The error introduced is not too large because of the smallness of the binding energy and well depth relative to the rest-energy of a nucleon. With this approximation, numerical integration for each individual case is replaced by the use of analytic expressions for the integrals. These expressions, based on the properties given by Watson,[26] were computed and are listed in Appendix B.

The procedure for calculating the matrix elements is as follows: Form $\psi'^*\mathcal{Y}_{LO}(\Omega)\psi$ by matrix multiplication for each of the four possibilities ($a\to a$, $a\to b$, $b\to a$, $b\to b$). Next integrate over the region (i.e., inside or outside the well); the angular integration will yield zero except possible for some special values of $\kappa'-\kappa$. The sum of the inner and outer integrals for one such value is the $(nKm'|\,\mathcal{Y}_{LO}(\Omega)\,|n'K'm')$ corresponding to the particular set of quantum numbers. Substitute this into Eq. (13) or (14) and carry out the indicated multiplications and summation.

It should be noted that the first two components of ψ are pure imaginary, the last two real. The operators acting on ψ either leave this order unchanged or reverse the groups of two; beyond the matrix operation, the factors introduced by the operators are either real or pure imaginary. Thus the product is pure imaginary or real, and consequently so is $(nKm'|\,\mathcal{Y}_{LO}(\Omega)\,|n'K'm')$. As a result, we find automatic agreement with the independent theoretical prediction that all cross terms of matrix elements are real[29]—the i factors being always present in the correction factors when the product inside the summation in Eq. (14) is pure imaginary, and not otherwise. Cross terms play no significant role till the second-forbidden transitions.

The values of the matrix elements appear in Appendix C.

V. EXAMINATION OF THE DATA

We proceed to tabulate the forbidden transitions, assigning nuclear states[30] and computing $\log(|M|^2 fl)$ for each of the five interactions, $|M|^2$ being normalized to $|M_1|^2=1$ (ordinary allowed, not superallowed, matrix elements of magnitude 1). For comparison, it should be noted that for odd-A nuclei the ordinary allowed transitions have logft values in the range 4.9–6.1, while the superallowed are 3.1–3.8; for even-A, there appears to exist only one allowed category with intermediate values 3.9–5.3, though there is some meager evidence for superallowed logft values. Allowed matrix elements can occur with the $K'-K=0$ ($\Delta J=0$, $\Delta l=0$) group for S, V, A, or T; with the $K'-K=-1$ ($\Delta J=\pm 1$, $\Delta l=0$) group only for A or T.

In the tabulation (Tables I–V), the nonoccurrence of an interaction means that its matrix elements are not comparable in magnitude with those entered. Spins marked with asterisks indicate measured values. In the "decay" column, − or + identifies negatron or

TABLE III. Transitions $K'+K=-2$ ($\Delta J=\pm 2$, $\Delta l=\pm 1$).—This group has its significant matrix elements for A or T only, these two being in fact equal. Here we first expect to find a definitely forbidden spectral shape, of which there is indeed considerable experimental corroboration.[31]

Isotope	Decay	Spin assignment	log fi	log (Cfi)	log $(\|M\|^2/fi)$
16 S 37	−	$1f_{7/2}-1d_{3/2}$*	7.0	7.6	4.0
17 Cl 38	−	$1f_{7/2}-1d_{3/2}$	7.4	8.1	4.5
18 A 41	−	$1f_{7/2}-1d_{3/2}$*	8.6	8.8	5.2
19 K 42	−	$1f_{7/2}-1d_{3/2}$	8.0	8.4	4.8
33 As 72	+	$1f_{5/2}-1g_{9/2}$	8.2	8.6	5.0
33 As 76	−	$1g_{9/2}-1f_{5/2}$	8.4	8.7	4.9
36 Kr 85	−	$1g_{9/2}-1f_{5/2}$*	9.2	8.4	4.6
37 Rb 86	−	$1g_{9/2}-1f_{5/2}$	8.6	8.5	4.7
38 Sr 89	−	$2d_{5/2}-2p_{1/2}$*	8.6	8.4	4.3
38 Sr 90	−	$2d_{5/2}-2p_{1/2}$	9.2	8.3	4.2
38 Sr 91	−	$2d_{5/2}-2p_{1/2}$	8.1	8.4	4.3
39 Y 90	−	$2d_{5/2}-2p_{1/2}$	8.0	8.1	4.0
39 Y 91	−	$2p_{1/2}-2d_{5/2}$*	8.7	8.5	4.9
45 Rh 102	+	$2p_{1/2}-2d_{5/2}$	8.4	7.9	4.3
45 Rh 102	−	$2d_{5/2}-2p_{1/2}$	9.4	9.0	4.9
50 Sn 123m	−	$1h_{11/2}-1g_{7/2}$*	9.1	8.8	5.1
50 Sn 125	−	$1h_{11/2}-1g_{7/2}$	8.9	9.0	5.3
51 Sb 122	−	$1h_{11/2}-1g_{7/2}$	8.0	8.0	4.3
51 Sb 125	−	$1g_{7/2}-1h_{11/2}$	9.4	8.6	5.1
53 I 126	−	$1h_{11/2}-1g_{7/2}$	8.5	8.2	4.5
55 Cs 137	−	$1g_{7/2}$*$-1h_{11/2}$	9.6	8.7	5.2

[29] C. L. Longmire and A. M. L. Messiah, Phys. Rev. **83**, 464 (1951).

[30] Mayer, Moszkowski, and Nordheim, Revs. Modern Phys. **23**, 315 (1951); L. W. Nordheim, Revs. Modern Phys. **23**, 322 (1951)—with minor deviations.

[31] C. S. Wu, Revs. Modern Phys. **22**, 386 (1950).

TABLE IV. Transitions $K'+K=1$ ($\Delta J=\pm1$, $\Delta l=\pm2$).—This is the l-forbidden group. Nuclear shell assignments are a bit shaky for this group, in that the state for which the transition is l-forbidden and the state for which it is allowed both lie in the same shell, so that they are in competition.

Isotope	Decay	Spin assignment	log ft	log $(\lvert M\rvert^2 ft)$
8 O 19	−	$1d_{3/2}-2s_{1/2}^m$	5.6	1.9
14 Si 31	−	$1d_{3/2}-2s_{1/2}^m$	5.9	2.2
15 P 32	−	$1d_{3/2}-2s_{1/2}$	7.9	4.2
28 Ni 63	−	$1f_{5/2}-2p_{3/2}^m$	7.1	3.4
28 Ni 65	−	$1f_{5/2}-2p_{3/2}^m$	6.6	2.9
29 Cu 64	−	$1f_{5/2}-2p_{3/2}$	5.3	1.6
29 Cu 64	+	$2p_{3/2}-1f_{5/2}$	4.9	1.3
31 Ga 66	+	$2p_{3/2}-1f_{5/2}$	7.9	4.3
32 Ge 69	+	$1f_{5/2}-2p_{3/2}^m$	6.0	2.3

positron decay. A superscript m indicates that the initial state is isomeric, an m in the "decay" column that the final state is isomeric.

The last five interactions in the $K'+K=0$ ($\Delta J=0$, $\Delta l=\pm1$) tabulation are even-A nuclei treated on a strict one-particle model. From the point of view of the nucleus as a whole, these are $J=0\rightarrow0$ (parity change) cases. However, this does not restrict the spin of the transforming nucleon, but merely requires that the two odd nucleons at the odd-Z end of the transition have equal spins coupling to zero resultant. Hence, it is consistent to ignore the limitations usually imposed on the matrix elements as a result of the $0\rightarrow0$ identification. These matrix elements correspond to the spin-orbit coupling implicit in the Dirac equation; for the larger empirical spin-orbit coupling (from shell breaks), they would presumably be considerably larger.

Nonrelativistically, the l-forbidden transitions can only occur with a forbidden shape. In the Dirac representation, however, we find that the largest possible matrix elements are $\boldsymbol{\sigma}$ and $\beta\boldsymbol{\sigma}$ (for A and T), with allowed shape. These do not occur nonrelativistically, when l is a good quantum number, but here K is the good quantum number and l is not; the contributions are from the small components of the Dirac wave functions. Satisfactory $\log(\lvert M\rvert^2 ft)$ values can be obtained by considering the states involved in these transitions to be an admixture, in varying proportions, of allowed and l-forbidden; for A and T, the spectral shape is allowed (as found experimentally for P^{32}, Cu^{64}, and Ga^{66}).

Finally, for the second-forbidden transitions (Table V), our theoretical expressions yield an $\lvert A_{ij}/T_{ij}\rvert$ ratio of about 9 (or $\lvert A_{ij}/R_{ij}\rvert$ about 18) with the S_{ijk} term negligible—to very little precision because the calculational approximations used became serious for the small overlap of initial and final wave functions here encountered. The cross term is predicted positive for Tc^{99} ($a\rightarrow a$) and negative for the other two ($b\rightarrow b$). Experimentally, the Tc^{99} spectrum is fitted with $\lvert A_{ij}/T_{ij}\rvert=6.65$ for T (or $\lvert A_{ij}/R_{ij}\rvert=13.30$ for V) with the sign uncertain.[32] For Cs^{137}, $\lvert A_{ij}/T_{ij}\rvert=7.43$ with cross term negative has been reported,[33] though the fit with Konopinski's correction factors appears to be imperfect for any ratio.[32]

The P^{32} electron-neutrino angular correlation,[34] reinterpreted in the light of our spin assignment and of an improved theory,[35] is consistent only with T.

The beta-gamma angular correlation of Rb^{86} agrees with T only,[36] and this is probably also true for I^{126}.[37]

VI. CONCLUSIONS

The theoretical classification of the degree of forbiddenness of a transition was based upon a qualitative estimation of the magnitude of the various matrix elements; the values of $\lvert M\rvert^2$ fell into groups differing by a factor of the order of 100. Later, some refinements were made, mainly on an empirical basis. According to the calculations just presented, this classification loses much of its validity. Within the same order of forbiddenness, there are values differing by several orders of magnitude. On the other hand, there is no sharp demarcation in size as we go from allowed to first-forbidden to l-forbidden matrix elements. This roughly continuous distribution of $\lvert M\rvert^2$ values, and thus also of ft values, agrees with the data. A break does occur before the second-forbidden group. The finer subdivision we obtain eliminates much of the "straggling" observed in the experimental ft values; the range of $\log ft$ values found for a particular assignment of initial and final configurations is at most 1 and usually less.

In earlier discussions of the nuclear matrix elements, it has always been assumed that there is no appreciable error in replacing β by 1 in the matrix expressions. This assumption turns out to be correct in most cases, but not for $\Delta J=0$. In that category, the matrix element of $\beta\gamma_5$ is very much smaller than that of γ_5; the matrix element of $\boldsymbol{\alpha}$ is less than that of $\beta\boldsymbol{\alpha}$, and decreases with increasing κ.

Another simplification can lead to totally wrong results. As hitherto unsuspected, for l-forbidden transitions the dominant role is played by the small components of the Dirac wave functions—an effect ignored in nonrelativistic approximations.

TABLE V. Transition $K'-K=\pm2$ ($\Delta J=\pm2$, $\Delta l=\pm2$).—For the first time, in this group, A and T differ considerably in spectral shape, thus allowing discrimination (differences in $\log(\lvert M\rvert^2 ft)$ have to be quite large to be decisive).

Isotopes	Decay	Spin assignment	log ft	S	$\log(\lvert M\rvert^2 ft)$ V	A	T
43 Tc 99	−	$1g_{9/2}-2d_{5/2}$	12.6	4.9	5.9	4.9	5.9
55 Cs 135	−	$1g_{7/2}^m-2d_{3/2}^m$	13.1	5.1	5.1	5.1	5.1
55 Cs 137	−	$1g_{7/2}^m-2d_{3/2}^m$	12.2	5.3	5.1	5.3	5.1

[32] F. Wagner, Jr., and M. S. Freedman, private communication.

[33] L. M. Langer and R. J. D. Moffat, Phys. Rev. **82**, 635 (1951).
[34] C. W. Sherwin, Phys. Rev. **82**, 52 (1951).
[35] E. Greuling and M. L. Meeks, Phys. Rev. **82**, 531 (1951).
[36] D. T. Stevenson and M. Deutsch, Phys. Rev. **83**, 1202 (1951).
[37] D. T. Stevenson and M. Deutsch, Phys. Rev. **84**, 1071 (1951).

The experimental evidence (logft values, spectral shapes, angular correlations) is always consistent with the theoretical predictions for the tensor interaction, but not so for the other interactions. Agreement is not achieved by any linear combination of interactions unless T predominates in it.

There is still need for considerable experimental information. Careful determination of the spectral shapes of the more highly forbidden decays should be carried out; all but the most recent such work is unreliable because of thick sources and other uncertainties. For first-forbidden, $\Delta J=0, \pm 1$ decays, the small deviation from the allowed spectrum is very difficult to detect, but angular correlation experiments could serve the same end. Many decay schemes bear reinvestigation because of lacking or inadequate gamma-ray search, or failure to ascertain whether a gamma-ray is in series with a beta-ray; this applies to essentially all the older data. Of particular theoretical interest are the even-A-high-spin-coupling nuclei, which do not lend themselves to our formalism; too few are now known, especially as to shape. Further verification of our interpretation of the l-forbidden ($\Delta J=\pm 1$, $\Delta l=\pm 2$) group is desirable. Most of the data for high-Z nuclei is too old and sketchy. Despite the difficulties, more electron-neutrino angular correlations should be undertaken. The shell assignments would be more secure and many equivocal interpretations could be eliminated if more spins of nuclei were known.

I wish to express my grateful appreciation to Professor E. Greuling for his essential and untiring guidance and for his friendly encouragement in the course of this work.

APPENDIX A

Boundary Values

Term	K	x	$j_\kappa(x)$	$j_{\kappa-1}(x)$	y	$k_\kappa(y)$	$k_{\kappa-1}(y)$
$1s_{1/2}$	-1	2.1	0.44	0.41	0.89	2.1	1.0
→							
$1p_{3/2}$	-2	3.4	0.31	0.26	1.5	4.3	1.7
$1p_{1/2}$	1	3.4	0.26	-0.073	1.5	1.7	1.0
→							
$1d_{5/2}$	-3	4.7	0.24	0.19	2.1	9.2	3.1
$1d_{3/2}$	2	4.7	0.19	-0.039	2.1	3.1	1.5
$2s_{1/2}$	-1	5.1	-0.11	-0.18	2.3	1.4	1.0
→							
$1f_{7/2}$	-4	5.9	0.20	0.15	2.7	19.0	6.0
→							
$1f_{5/2}$	3	5.9	0.15	-0.027	2.7	6.0	2.5
$2p_{3/2}$	-2	6.6	-0.11	-0.14	2.9	2.4	1.3
$2p_{1/2}$	1	6.6	-0.14	0.046	2.9	1.3	1.0
$1g_{9/2}$	-5	7.1	0.17	0.12	3.2	42.0	13.0
→							
$1g_{7/2}$	4	7.1	0.12	-0.020	3.2	13.0	5.0
$2d_{5/2}$	-3	8.0	-0.10	-0.11	3.6	4.2	2.1
$2d_{3/2}$	2	8.0	-0.11	0.031	3.6	2.1	1.3
$3s_{1/2}$	-1	8.3	0.060	0.11	3.7	1.3	1.0
$1h_{11/2}$	-6	8.3	0.15	0.10	3.7	90.0	27.0
→							
$2f_{7/2}$	-4	9.3	-0.095	-0.096	4.1	7.8	3.5

The function

$$\bar{k}_\kappa=(2/\pi)ye^y k_\kappa$$

here tabulated can be used instead of k_κ, since the k_κ's always occur in ratios in which the common factor $(2/\pi)ye^y$ cancels out. It is more convenient to compute $\bar{k}_\kappa$ because it can be expressed as a polynomial in $1/y$ of order κ.[23]

The arrows set off nuclear shells.

APPENDIX B

The Radial Integrals

It should be understood that by the expressions on the right side of the equations below we mean their value at $r=R$ (listed in Appendix A).

$$(2/R^3)\int_0^R j_\kappa^2 r^2 dr = j_\kappa^2 + j_{\kappa-1}^2 - (2\kappa+1) j_\kappa j_{\kappa-1}/x$$

$$(2/R^3)\int_R^\infty k_\kappa^2 r^2 dr = -k_\kappa^2 + k_{\kappa-1}^2 + (2\kappa+1) k_\kappa k_{\kappa-1}/y$$

$$(2/R^3)\int_0^R j_{\kappa-1}^2 r^2 dr = j_\kappa^2 + j_{\kappa-1}^2 - (2\kappa-1) j_\kappa j_{\kappa-1}/x$$

$$(2/R^3)\int_R^\infty k_{\kappa-1}^2 r^2 dr = k_\kappa^2 - k_{\kappa-1}^2 - (2\kappa-1) k_\kappa k_{\kappa-1}/y$$

$$(2/R^3)\int_0^R j_{\kappa+1} j_\kappa r^3 dr = (R/2x)[(2\kappa+1) j_\kappa^2 + (2\kappa+3) j_{\kappa-1}^2 - (2\kappa+1)(2\kappa+3) j_\kappa j_{\kappa-1}/x]$$

$$(2/R^3)\int_R^\infty k_{\kappa+1} k_\kappa r^3 dr = (R/2y)[-(2\kappa+1) k_\kappa^2 + (2\kappa+3) k_{\kappa-1}^2 + (2\kappa+1)(2\kappa+3) k_\kappa k_{\kappa-1}/y]$$

$$(2/R^3)\int_0^R j_\kappa j_{\kappa-1}r^3dr=(R/2x)[(2\kappa+1)j_\kappa^2+(2\kappa-1)j_{\kappa-1}^2-(2\kappa+1)(2\kappa-1)j_\kappa j_{\kappa-1}/x]$$

$$(2/R^3)\int_R^\infty k_\kappa k_{\kappa-1}r^3dr=(R/2y)[(2\kappa+1)k_\kappa^2-(2\kappa-1)k_{\kappa-1}^2-(2\kappa+1)(2\kappa-1)k_\kappa k_{\kappa-1}/y]$$

$$(2/R^3)\int_0^R j_{\kappa-1}j_{\kappa-2}r^3dr=(R/2x)[(2\kappa-3)j_\kappa^2+(2\kappa-1)j_{\kappa-1}^2-(2\kappa-1)(2\kappa-3)j_\kappa j_{\kappa-1}/x]$$

$$(2/R^3)\int_R^\infty k_{\kappa-1}k_{\kappa-2}r^3dr=(R/2y)[-(2\kappa-3)k_\kappa^2+(2\kappa-1)k_{\kappa-1}^2+(2\kappa-1)(2\kappa-3)k_\kappa k_{\kappa-1}/y]$$

$$(2/R^3)\int_0^R j_{\kappa+2}j_\kappa r^4dr=(R^2/3x^2)\{[-x^2+(2\kappa+1)(2\kappa+3)]j_\kappa^2+[-x^2+(2\kappa+3)(2\kappa+5)]j_{\kappa-1}^2$$
$$-[-(2\kappa+3)x^2+(2\kappa+1)(2\kappa+3)(2\kappa+5)]j_\kappa j_{\kappa-1}/x\}$$

$$(2/R^3)\int_R^\infty k_{\kappa+2}k_\kappa r^4dr=(R^2/3y^2)\{[-y^2-(2\kappa+1)(2\kappa+3)]k_\kappa^2+[y^2+(2\kappa+3)(2\kappa+5)]k_{\kappa-1}^2$$
$$-[-(2\kappa+3)y^2-(2\kappa+1)(2\kappa+3)(2\kappa+5)]k_\kappa k_{\kappa-1}/y\}$$

$$(2/R^3)\int_0^R j_{\kappa+1}j_{\kappa-1}r^4dr=(R^2/3x^2)\{[-x^2+(2\kappa+1)(2\kappa+3)]j_\kappa^2+[-x^2+(2\kappa-1)(2\kappa+3)]j_{\kappa-1}^2$$
$$-[-(2\kappa-3)x^2+(2\kappa-1)(2\kappa+1)(2\kappa+3)]j_\kappa j_{\kappa-1}/x\}$$

$$(2/R^3)\int_R^\infty k_{\kappa+1}k_{\kappa-1}r^4dr=(R^2/3y^2)\{[y^2+(2\kappa+1)(2\kappa+3)]k_\kappa^2+[-y^2-(2\kappa-1)(2\kappa+3)]k_{\kappa-1}^2$$
$$-[(2\kappa-3)y^2+(2\kappa-1)(2\kappa+1)(2\kappa+3)]k_\kappa k_{\kappa-1}/y\}$$

$$(2/R^3)\int_0^R j_\kappa j_{\kappa-2}r^4dr=(R^2/3x^2)\{[-x^2+(2\kappa+1)(2\kappa-3)]j_\kappa^2+[-x^2+(2\kappa-1)(2\kappa-3)]j_{\kappa-1}^2$$
$$-[-(2\kappa+3)x^2+(2\kappa+1)(2\kappa-1)(2\kappa-3)]j_\kappa j_{\kappa-1}/x\}$$

$$(2/R^3)\int_R^\infty k_\kappa k_{\kappa-2}r^4dr=(R^2/3y^2)\{[-y^2-(2\kappa+1)(2\kappa-3)]k_\kappa^2+[y^2+(2\kappa-1)(2\kappa-3)]k_{\kappa-1}^2$$
$$-[-(2\kappa+3)y^2-(2\kappa+1)(2\kappa-1)(2\kappa-3)]k_\kappa k_{\kappa-1}/y\}$$

$$(2/R^3)\int_0^R j_{\kappa-1}j_{\kappa-3}r^4dr=(R^2/3x^2)\{[-x^2+(2\kappa-3)(2\kappa-5)]j_\kappa^2+[-x^2+(2\kappa-1)(2\kappa-3)]j_{\kappa-1}^2$$
$$-[-(2\kappa-3)x^2+(2\kappa-1)(2\kappa-3)(2\kappa-5)]j_\kappa j_{\kappa-1}/x\}$$

$$(2/R^3)\int_R^\infty k_{\kappa-1}k_{\kappa-3}r^4dr=(R^2/3y^2)\{[y^2+(2\kappa-3)(2\kappa-5)]k_\kappa^2+[-y^2-(2\kappa-1)(2\kappa-3)]k_{\kappa-1}^2$$
$$-[(2\kappa-3)y^2+(2\kappa-1)(2\kappa-3)(2\kappa-5)]k_\kappa k_{\kappa-1}/y\}.$$

APPENDIX C

The Matrix Elements

This table contains all matrix elements from allowed through second-forbidden, except those for $\gamma_5\mathbf{r}$, $\beta\gamma_5\mathbf{r}$, $\boldsymbol{\alpha}\cdot\mathbf{r}$, $\beta\boldsymbol{\alpha}\cdot\mathbf{r}$, $\boldsymbol{\alpha}\times\mathbf{r}$, and $\beta\boldsymbol{\alpha}\times\mathbf{r}$, which have been omitted because they have no practical significance inasmuch as they only occur in competition with much larger less forbidden matrix elements.

The following abbreviations are used:

$$M=\int_0^R j_{\kappa'}{}^2r^2dr, \qquad m=\lambda\int_R^\infty k_{\kappa'}{}^2r^2dr,$$

$$N=\int_0^R j_{\kappa'-1}{}^2r^2dr, \qquad n=\lambda\int_R^\infty k_{\kappa'-1}{}^2r^2dr,$$

$$O=\int_0^R j_{\kappa'+1}j_{\kappa'}r^3dr, \qquad o=\lambda\int_R^\infty k_{\kappa'+1}k_{\kappa'}r^3dr,$$

$$P=\int_0^R j_{\kappa'}j_{\kappa'-1}r^3dr, \qquad p=\lambda\int_R^\infty k_{\kappa'}k_{\kappa'-1}r^3dr,$$

$$Q=\int_0^R j_{\kappa'-1}j_{\kappa'-2}r^3dr, \qquad q=\lambda\int_R^\infty k_{\kappa'-1}k_{\kappa'-2}r^3dr,$$

$$S=\int_0^R j_{\kappa'+2}j_{\kappa'}r^4dr, \qquad s=\lambda\int_R^\infty k_{\kappa'+2}k_{\kappa'}r^4dr,$$

$$T=\int_0^R j_{\kappa'+1}j_{\kappa'-1}r^4dr, \qquad t=\lambda\int_R^\infty k_{\kappa'+1}k_{\kappa'-1}r^4dr,$$

$$U=\int_0^R j_{\kappa'}j_{\kappa'-2}r^4dr, \qquad u=\lambda\int_R^\infty k_{\kappa'}k_{\kappa'-2}r^4dr,$$

$$V=\int_0^R j_{\kappa'-1}j_{\kappa'-2}r^4dr, \qquad v=\lambda\int_R^\infty k_{\kappa'-1}k_{\kappa'-2}r^4dr.$$

$$\lambda=(B_KB_{K'})/(A_KA_{K'}).$$

We have neglected the discrepancy between the values of e and w for the initial and final states, and set $e\approx 1\approx w$ so that

$$1/(e+1)=\tfrac{1}{2}, \qquad 1/(1+w)=\tfrac{1}{2},$$
$$1/(e-1)=\tfrac{1}{2}H^2, \qquad 1/(1-w)=\tfrac{1}{2}h^2,$$
$$1/(e^2-1)^{\frac{1}{2}}=\tfrac{1}{2}H, \qquad 1/(1-w^2)^{\frac{1}{2}}=\tfrac{1}{2}h.$$

Since $1/(e-1)\approx 33$ and $1/(1-w)\approx 164$, we neglect terms in $1/(e+1)$ and $1/(1+w)$ in comparison with the former.

We follow the Konopinski nomenclature:[2]

$$|B_{ij}|\leftrightarrow|\mathcal{Y}_{2M}(\boldsymbol{\sigma},\mathbf{r})|=|\mathcal{Y}_{2M}(\beta\boldsymbol{\sigma},\mathbf{r})|$$
$$|A_{ij}|\leftrightarrow|\mathcal{Y}_{2M}(\boldsymbol{\alpha},\mathbf{r})|=|\mathcal{Y}_{2M}(\beta\boldsymbol{\alpha},\mathbf{r})|$$
$$|R_{ij}|\leftrightarrow\tfrac{1}{2}|\mathcal{Y}_{2M}(\mathbf{r},\mathbf{r})|=\tfrac{1}{2}|\mathcal{Y}_{2M}(\beta\mathbf{r},\mathbf{r})|$$
$$|T_{ij}|\leftrightarrow|\mathcal{Y}_{2M}(\boldsymbol{\sigma}\times\mathbf{r},\mathbf{r})|=|\mathcal{Y}_{2M}(\beta\boldsymbol{\sigma}\times\mathbf{r},\mathbf{r})|$$
$$|S_{ijk}|\leftrightarrow|\mathcal{Y}_{3M}(\boldsymbol{\sigma},\mathbf{r},\mathbf{r})|=|\mathcal{Y}_{3M}(\beta\boldsymbol{\sigma},\mathbf{r},\mathbf{r})|.$$

For convenience, we define

$$|M_\Omega'|_{KK'}{}^2=4|M_\Omega|^2/(A_K{}^2A_{K'}{}^2).$$

Normalization consists in setting $|M_1|^2=1$. Then

$$|M_1'|_K{}^2=4/A_K{}^4,$$

and we have the working relation

$$|M_\Omega|_{KK'}{}^2=|M_\Omega'|_{KK'}{}^2/(|M_1'|_K|M_1'|_{K'}).$$

The quantum number n is not explicit here, but is present via the boundary values.

Ω	ψ	ψ'	ΔJ	$\lvert M_\Omega'\rvert^2$
			(a) $K'-K=0$ ($\Delta J=0$, $\Delta l=0$)	
$1,\beta$	a	a		$(H^2N+h^2n)^2$
	b	b		$(H^2M+h^2m)^2$
$\boldsymbol{\sigma},\beta\boldsymbol{\sigma}$	a	a		$[(2\kappa'+1)/(2\kappa'-1)](H^2N+h^2n)^2$
	b	b		$[(2\kappa'-1)/(2\kappa'+1)](H^2M+h^2m)^2$
			(b) $K'+K=-1$ ($\Delta J=\pm 1$, $\Delta l=0$)	
$\boldsymbol{\sigma},\beta\boldsymbol{\sigma}$	a	b		$[4\kappa'/(2\kappa'+1)](H^2M-h^2m)^2$
	b	a		$[4\kappa'/(2\kappa'-1)](H^2N-h^2n)^2$

(c) $K'-K=\pm1$ ($\Delta J=\pm1$, $\Delta l=\pm1$)

α, $\beta\alpha$	a	a	1	$[4\kappa'/(2\kappa'+1)](HN+hn)^2$
	a	a	-1	$[4\kappa'/(2\kappa'-1)](HM+hm)^2$
	b	b	1	$[4\kappa'/(2\kappa'-1)](HN-hn)^2$
	b	b	-1	$[4\kappa'/(2\kappa'+1)](HM-hm)^2$
$\mathfrak{r}$, $\beta\mathfrak{r}$, $\sigma\times\mathfrak{r}$, $\beta\sigma\times\mathfrak{r}$	a	a	1	$[\kappa'/(2\kappa'-1)](H^2Q+h^2q)^2$
	a	a	-1	$[\kappa'/(2\kappa'+1)](H^2P+h^2p)^2$
	b	b	1	$[\kappa'/(2\kappa'-1)](H^2P+h^2p)^2$
	b	b	-1	$[\kappa'/(2\kappa'+1)](H^2O+h^2o)^2$
B_{ij}	a	a	1	$\{2\kappa'(2\kappa'+1)/[(2\kappa'-1)(2\kappa'-3)]\}(H^2Q+h^2q)^2$
	a	a	-1	$\{2\kappa'(2\kappa'+3)/[(2\kappa'-1)(2\kappa'+1)]\}(H^2P+h^2p)^2$
	b	b	1	$\{2\kappa'(2\kappa'-3)/[(2\kappa'-1)(2\kappa'+1)]\}(H^2P+h^2p)^2$
	b	b	-1	$\{2\kappa'(2\kappa'-1)/[(2\kappa'+1)(2\kappa'+3)]\}(H^2O+h^2o)^2$

(d) $K'+K=0$ ($\Delta J=0$, $\Delta l=\pm1$)

γ_5	$[H(M+N)-h(m-n)]^2$
$\beta\gamma_5$	$[H(M-N)-h(m+n)]^2$
α	$\{[(2\kappa'-1)/(2\kappa'+1)]^{\frac{1}{2}}(HM-hm)-[(2\kappa'+1)/(2\kappa'-1)]^{\frac{1}{2}}(HN+hn)\}^2$
$\beta\alpha$	$\{[(2\kappa'-1)/(2\kappa'+1)]^{\frac{1}{2}}(HM-hm)+[(2\kappa'+1)/(2\kappa'-1)]^{\frac{1}{2}}(HN+hn)\}^2$
$\mathfrak{r}$, $\beta\mathfrak{r}$	$\{1/[(2\kappa'-1)(2\kappa'+1)]\}(H^2P-h^2p)^2$
$\sigma\cdot\mathfrak{r}$, $\beta\sigma\cdot\mathfrak{r}$	$(H^2P-h^2p)^2$
$\sigma\times\mathfrak{r}$, $\beta\sigma\times\mathfrak{r}$	$\{4\kappa'^2/[(2\kappa'-1)(2\kappa'+1)]\}(H^2P-h^2p)^2$
B_{ij}	$\{8(\kappa'-1)(\kappa'+1)/[3(2\kappa'-1)(2\kappa'+1)]\}(H^2P-h^2p)^2$

(e) $K'+K=-2$ ($\Delta J=\pm2$, $\Delta l=\pm1$)

B_{ij}	a	b	$\{16\kappa'(\kappa'+1)/[(2\kappa'+1)(2\kappa'+3)]\}(H^2O-h^2o)^2$
	b	a	$\{16\kappa'(\kappa'-1)/[(2\kappa'-1)(2\kappa'-3)]\}(H^2Q-h^2q)^2$

(f) $K'+K=1$ ($\Delta J=\pm1$, $\Delta l=\pm2$)

σ, $\beta\sigma$	a	b	$[4\kappa'/(2\kappa'-1)](N+n)^2$
	b	a	$[4\kappa'/(2\kappa'+1)](M+m)^2$

(g) $K'-K=\pm2$ ($\Delta J=\pm2$, $\Delta l=\pm2$)

A_{ij}	a	a	2	$\{16\kappa'(\kappa'-1)/[(2\kappa'-1)(2\kappa'-3)]\}(HQ+hq)^2$
	a	a	-2	$\{16\kappa'(\kappa'+1)/[(2\kappa'+1)(2\kappa'+3)]\}(HO+ho)^2$
	b	b	2	$\{16\kappa'(\kappa'-1)/[(2\kappa'-1)(2\kappa'-3)]\}(HQ-hq)^2$
	b	b	-2	$\{16\kappa'(\kappa'+1)/[(2\kappa'+1)(2\kappa'+3)]\}(HO-ho)^2$
R_{ij}	a	a	2	$\{\kappa'(\kappa'-1)/[(2\kappa'-1)(2\kappa'-3)]\}(H^2V+h^2v)^2$
	a	a	-2	$\{\kappa'(\kappa'+1)/[(2\kappa'+1)(2\kappa'+3)]\}(H^2T+h^2t)^2$
	b	b	2	$\{\kappa'(\kappa'-1)/[(2\kappa'-1)(2\kappa'-3)]\}(H^2U+h^2u)^2$
	b	b	-2	$\{\kappa'(\kappa'+1)/[(2\kappa'+1)(2\kappa'+3)]\}(H^2S+h^2s)^2$
T_{ij}	a	a	2	$\{4\kappa'(\kappa'-1)/[(2\kappa'-1)(2\kappa'-3)]\}(H^2V+h^2v)^2$
	a	a	-2	$\{4\kappa'(\kappa'+1)/[(2\kappa'+1)(2\kappa'+3)]\}(H^2T+h^2t)^2$
	b	b	2	$\{4\kappa'(\kappa'-1)/[(2\kappa'-1)(2\kappa'-3)]\}(H^2U+h^2u)^2$
	b	b	-2	$\{4\kappa'(\kappa'+1)/[(2\kappa'+1)(2\kappa'+3)]\}(H^2S+h^2s)^2$
S_{ijk}	a	a	2	$\{12\kappa'(\kappa'-1)(2\kappa'+1)/[(2\kappa'-1)(2\kappa'-3)(2\kappa'-5)]\}(H^2V+h^2v)^2$
	a	a	-2	$\{12\kappa'(\kappa'+1)(2\kappa'+5)/[(2\kappa'-1)(2\kappa'+1)(2\kappa'+3)]\}(H^2T+h^2t)^2$
	b	b	2	$\{12\kappa'(\kappa'-1)(2\kappa'-5)/[(2\kappa'+1)(2\kappa'-1)(2\kappa'-3)]\}(H^2U+h^2u)^2$
	b	b	-2	$\{12\kappa'(\kappa'+1)(2\kappa'-1)/[(2\kappa'+1)(2\kappa'+3)(2\kappa'+5)]\}(H^2S+h^2s)^2$

(h) $K'+K=2$ ($\Delta J=\pm2$, $\Delta l=\pm3$)

B_{ij}	a	b	$\{16\kappa'(\kappa'-1)/[(2\kappa'-1)(2\kappa'-3)]\}(Q+q)^2$
	b	a	$\{16\kappa'(\kappa'+1)/[(2\kappa'+1)(2\kappa'+3)]\}(O+o)^2$

(i) $K'+K=-3$ ($\Delta J=\pm 3$, $\Delta l=\pm 2$)

S_{ijk}	a	b	$\{144\kappa'(\kappa'+1)(\kappa'+2)/[(2\kappa'+1)(2\kappa'+3)(2\kappa'+5)]\}(H^2S-h^2s)^2$
	b	a	$\{144\kappa'(\kappa'-1)(\kappa'-2)/[(2\kappa'-1)(2\kappa'-3)(2\kappa'-5)]\}(H^2V-h^2v)^2$.

Where the cross terms occur, their magnitude is given simply by

$$|M_\Omega M_{\Omega'}{}^*|^2=|M_\Omega|^2|M_{\Omega'}|^2$$

and the sign of the cross term, i.e., the sign of each of the real expressions $(-iM_rM_a{}^*)$, etc. . . ., is as follows:

Group	ψ	ψ'	ΔJ	Sign
$K'-K=\pm 1$			1	+
			−1	−
$K'+K=0$	a	b		+
	b	a		−
$K'-K=\pm 2$	a	a		+
	b	b		−

PHYSICAL REVIEW VOLUME 86, NUMBER 6 JUNE 15, 1952

Hyperfine Structure Anomalies in the $^2P_{\frac{1}{2}}$ State of Tl^{205} and Tl^{203}†

ALAN BERMAN*
Columbia University, New York, New York

(Received March 3, 1952)

The atomic beam magnetic resonance method has been used to make a precision measurement of the hyperfine structure separation of the ground state of Tl^{205} and Tl^{203}. The experimentally determined ratio $\Delta\nu^{205}/\Delta\nu^{203}=1.00974\pm 0.00003$ is to be compared with the ratio of the magnetic moments, determined by nuclear induction techniques, of $g_I{}^{205}/g_I{}^{203}=1.00986\pm 0.00005$. It is shown that the difference between the two ratios can be accounted for by consideration of effects predicted by Bohr and Weisskopf and by Crawford and Schawlow. In particular, the agreement between theory and experiment can be construed as evidence of the reality of the effects postulated by Crawford and Schawlow, which have not been heretofore directly observed.

INTRODUCTION

A PREVIOUS determination[1] of the ratio of the hyperfine structure separations ($\Delta\nu$) of the $^2P_{\frac{1}{2}}$ ground states of Tl^{205} and Tl^{203} differed by about 40 parts in 10^5 from the ratio of the magnetic moments of the two isotopes. This discrepancy was approximately four times as large as could be accounted for on the basis of any extant theories of hfs anomalies. Unfortunately, the combined experimental uncertainties of the two ratios was 25 parts in 10^5, with the principal contribution to the uncertainties arising from the ratio of the $\Delta\nu$'s. Since an ability to account for a hfs anomaly in Tl would be a stringent test, of a type not heretofore made, of the validity of certain aspects of current theories on the subject, a new and more precise determination of the ratio of the hfs separations has been made by use of atomic beam techniques.

THEORY

A direct determination of the $\Delta\nu$'s of Tl^{203} and Tl^{205}, from observation of the transitions $\Delta F=\pm 1$, would require frequencies that are inconveniently high (~21,300 Mc). The value of the $\Delta\nu$'s may, however, be determined from measurements of the $\Delta F=0$, $\Delta m_F=\pm 1$ transitions (1, 1↔1, 0) and (1, 0↔1, −1). The expressions for the frequencies of these lines at an arbitrary magnetic field are[2]

$$f_1=\tfrac{1}{2}\Delta\nu[(1+x)-(1+x^2)^{\frac{1}{2}}+2x(g_J/g_I'-1)^{-1}] \quad \text{for } (1, 1\leftrightarrow 1, 0), \quad (1)$$

$$f_2=\tfrac{1}{2}\Delta\nu[(1+x^2)^{\frac{1}{2}}-(1-x)+2x(g_J/g_I'-1)^{-1}] \quad \text{for } (1, 0\leftrightarrow 1, -1), \quad (2)$$

where $x=(g_J-g_I')\mu_0H/h\Delta\nu$, and g_I' differs slightly from the nuclear g value as determined by nuclear resonance methods because of a partial decoupling of the **L** and **S** vectors in the $^2P_{\frac{1}{2}}$ state.

If the transitions are observed at a fixed magnetic field, then a measurement of the frequencies of the two lines will be sufficient to determine both x and $\Delta\nu$, provided that the value of the ratio g_J/g_I' is known.

The value of $\Delta\nu$ deduced from the Breit-Rabi formula will not be the true hfs separation. Nonvanishing matrix elements of the electron-nucleus interaction operator, which are not diagonal in J, lead to a per-

† This work has been supported in part by the ONR.
* Submitted in partial fulfillment of the requirements for the degree of Doctor of Philosophy in the Faculty of Pure Science at Columbia University.
[1] Berman, Kusch, and Mann, Phys. Rev. 77, 140 (1950).
[2] Millman, Rabi, and Zacharias, Phys. Rev. 55, 384 (1938).

turbation of levels of the same F (in this case $F=1$) in the $P_{\frac{1}{2}}$ and $P_{\frac{3}{2}}$ fine structure levels. Thus, if $\Delta\nu'$ is the true hfs separation and $\Delta\nu$ the hfs deduced from the Breit-Rabi formula, then

$$\Delta\nu'=\Delta\nu-\frac{|\langle J=\frac{1}{2}|H'|J=\frac{3}{2}\rangle|^2}{E_{\frac{1}{2}}-E_{\frac{3}{2}}},$$

where H' is the operator connecting the fine structure levels. This relation can be shown[3] to reduce to the form

$$\Delta\nu'=\Delta\nu(1-k\Delta\nu/\delta),$$

where k is a constant and δ is the separation between the $^2P_{\frac{1}{2}}$ and $^2P_{\frac{3}{2}}$ levels. This correction has been calculated by Robert Frosch for a number of elements. In the case of thallium it amounts to 15.2 kc for Tl^{205} and 14.9 kc for Tl^{203}. Within the precision of this experiment the effect may be neglected.

For an atom in a state for which $J=\frac{1}{2}$ and $I\geqslant 1$, doublets occur in the hfs spectrum, from which the value of g_J/g_I' can be determined. When $I=\frac{1}{2}$, as in the case of both Tl isotopes, this ratio cannot be determined simply by measurements of lines in the hfs spectrum.

No precision measurement of the g_J value of the $^2P_{\frac{1}{2}}$ state of Tl has been reported. However, it may be expected that to an accuracy of 1 part in 10^4 the g_J values of atoms are characteristic of the atomic state rather than of the particular atom. Indeed, the measured values of $g_J(^2P_{\frac{1}{2}}$ In) and $g_J(^2P_{\frac{1}{2}}$ Ga) reported by Kusch and Foley[4] do agree to within 1 part in 10^5, although the stated precision is not quite as great. For the similar electronic configuration of Tl, it is plausible to assume that $g_J(^2P_{\frac{1}{2}}\text{ In})=g_J(^2P_{\frac{1}{2}}\text{ Tl})$. Using the value

$$g_H/g_J(^2P_{\frac{1}{2}})=-45.6877\times10^{-4} \tag{3}$$

given by Taub and Kusch[5] and the values

$$\begin{aligned} g_I(Tl^{203})/g_H&=0.571499\pm0.00005,\\ g_I(Tl^{205})/g_H&=0.577135\pm0.00005 \end{aligned} \tag{4}$$

obtained by Poss[6] by means of nuclear resonance techniques, it is then possible to determine a value of g_J/g_I for each isotope.

Foley[7] has considered the effect of the partial decoupling of the **L** and **S** vectors in the $^2P_{\frac{1}{2}}$ state. This effect was shown to reduce the apparent value of the magnetic moment of the nucleus, as deduced from observation of the Zeeman effect of hfs to a value below that determined by nuclear resonance experiments. If g_I' is the apparent value of the nuclear gyromagnetic ratio, then

$$g_I'/g_I=1-\Delta\nu/[g_I(2I+1)6\delta], \tag{5}$$

where δ is the fine structure separation between the $^2P_{\frac{1}{2}}$ and $^2P_{\frac{3}{2}}$ states. For the case of Tl the magnitude of the values of g_I used in computing the ratio g_J/g_I' must accordingly be reduced by 0.429 percent from the values determined by the nuclear resonance method.

METHOD

A field of 3000 gauss, in the vicinity of which most of the measurements of this experiment were made, corresponds to $x\approx0.14$. An expansion of (1) and (2) for small values of x leads to the approximate relationships

$$f_{1,2}=g_F\mu_0H/h\pm\tfrac{1}{4}x^2\Delta\nu+\cdots, \tag{6}$$

$$f_2-f_1=\tfrac{1}{2}x^2\Delta\nu+\cdots, \tag{7}$$

where $g_F\cong g_J/2$, $g_J=\frac{2}{3}$, and $\mu_0/h=1.3998\times10^6$ sec^{-1}.

Equation (6) indicates that the primary field dependence of the observed lines is through the term $g_F\mu_0H/h$ and is 0.467 Mc/gauss. Dependence of the frequencies on $\Delta\nu$ enters only through a small term quadratic in the field.

The product $x\Delta\nu$, which is proportional to (g_J-g_I'), can in general be determined to a high degree of precision since it is determined from the sum of the two frequencies. However, the same fractional error will occur in $\Delta\nu$ as occurs in the difference of the two frequencies. At $x=0.14$, for example, the absolute error in $\Delta\nu$ will then be about 100 times as great as the absolute error in f_2-f_1. The conditions under which the experiment was performed, and the attainable accuracy of the results were largely determined by the considerations of these implications of Eqs. (6) and (7).

Stringent requirements of stability and homogeneity were necessarily imposed on the magnetic field in which the transitions occurred. The current of 160 amperes, required for the "C" field coils, was supplied by two two-volt submarine batteries. This current had to be maintained constant to within at least 0.0005 ampere for extended periods of time in order that measurements of f_2 and f_1 could be made at values of the fields which did not differ by more than 1 part in 300,000. A greater shift in the field between successive observations of f_1 and f_2 would result in an error $>\frac{1}{2}$ Mc in the value of $\Delta\nu$. The necessary stability was obtained most readily by maintaining a continuously monitored voltage drop across a 0.001-ohm resistor constant, by the introduction of a small manually controlled bucking current.

A small fraction of the absolute magnitude of the "C" field arose from stray fields from the "A" and "B" magnets. As no attempt was made to stabilize these fields against drift, an approximately monotonic drift of 1 part in 60,000 per hour occurred in the magnitude of the "C" field. However, by a proper sequential observation of the transitions the effect of this drift, as well as effects arising from drifts in the "C" field not dependent on fluctuations in the field coil currents, could be averaged out.

The rf region used in this experiment was 1.25 cm long. Since an oven temperature of 750°C is necessary

[3] Robert Frosch, private communication.
[4] P. Kusch and H. M. Foley, Phys. Rev. **74**, 250 (1948).
[5] H. Taub and P. Kusch, Phys. Rev. **75**, 1481 (1949).
[6] H. L. Poss, Phys. Rev. **75**, 600 (1949).
[7] H. M. Foley, Phys. Rev. **80**, 288 (1950).

to generate the beam, the theoretical half-widths of the resonances is 20 kc. Although extreme care was taken to obtain as small half-widths as possible, inhomogeneities in the magnetic field increased the half-widths of the lines to about three times the theoretical value.

In view of the sensitivity of the values of $\Delta\nu$ to the accuracy of measurement of the position of the center of the lines, it was essential that no significant overlap between the lines occurred. If any overlap did occur, it would cause an asymmetry in the shapes of the lines which would result in a mismeasurement of the position of the center of the lines. At values of the magnetic field corresponding to $x=0.14$, the separations between the same line for each isotope are ~950 kc for the f_1 lines and ~1050 kc for the f_2 lines. Thus, the resonances observed in this experiment appeared as two completely resolved doublets.

In the experiment reported by Berman, Kusch, and Mann,[1] the $\Delta\nu$ was determined at fields corresponding to an $x\approx 0.1$. At such fields the separations between the lines corresponding to the same transition for each isotope was ~450 kc. The possibility of systematic errors arising from an overlapping of the "tails" of the resonance peaks was, therefore, considerably greater than in this experiment. As can be seen from Eq. (7), at such a value of x, the same absolute error of measurement of f_2-f_1, would result in twice as great an error in $\Delta\nu$ as would result at a value of $x=0.14$.

RESULTS

Six runs, productive of significant data, were obtained in the present set of experiments. Each run was taken at a somewhat different value of the magnetic field. A check on the internal consistency of the data may be obtained from consideration of the fact that the ratio,

$$\frac{f_2^{203}+f_1^{203}}{f_2^{205}+f_1^{205}}=\frac{g_J+g_I'^{203}}{g_J+g_I'^{205}}\equiv\omega,$$

should be a constant for all values of the magnetic field. The values of $\Delta\nu^{205}$, $\Delta\nu^{203}$, and ω calculated in each of these runs are given in Table I.

The value of $\omega=1.0000278\pm0.0000014$ is in good agreement with the value $\omega=1.000026$ which may be calculated from the values of g_I^{205}/g_H, g_I^{203}/g_H, and $g_H/g_J(^2P_{\frac{1}{2}})$ given in Eqs. (3) and (4).

The values of ω given in Table I indicate that both g_I are negative. Since it is known that $|g_I^{205}|>|g_I^{203}|$, a value of $\omega<1$ indicates that both g_I are positive, while a value of $\omega>1$ indicates that both g_I are negative. The possibility that only one of the g_I's is negative may be precluded by the good agreement of the observed and calculated values.

The mean values of $\Delta\nu$ obtained from the experimental data are

$$\Delta\nu(\mathrm{Tl}^{205})=21311.48\pm0.19\times10^6\ \mathrm{sec}^{-1},$$
$$\Delta\nu(\mathrm{Tl}^{203})=21106.06\pm0.49\times10^6\ \mathrm{sec}^{-1},$$

TABLE I. Values of $\Delta\nu^{205}$ and $\Delta\nu^{203}$ obtained from measurements of the transitions $F=0$, $m_F=\pm1$, together with corresponding values of $\omega=(g_J+g_I'^{203})/(g_J+g_I'^{205})$. Frequencies are given in Mc.

$\Delta\nu^{203}$	$\Delta\nu^{205}$	ω
21106.21	21311.05	1.000025
21107.52	21311.32	1.000024
21106.31	21311.32	1.000028
21105.61	21311.64	1.000022
21106.15	21311.26	1.000029
21104.81	21311.53	1.000031
Weighted average of all data		
21106.06±0.49	21311.48±0.19	1.0000278±0.0000014

which lead to a value of the ratio,

$$\Delta\nu^{205}/\Delta\nu^{203}=1.00974\pm0.00003.$$

The ratio of the uncertainties of $\Delta\nu^{203}$ and $\Delta\nu^{205}$ is approximately the same as the ratio of the isotope abundances, indicating that the differential uncertainties may be attributed to the differential intensities of the resonance lines for each isotope.

The quoted errors are purely statistical in nature. A systematic error is possible, as the values given for $\Delta\nu^{205}$ and $\Delta\nu^{203}$ are directly dependant upon the assumed values of g_J/g_I'. However, it may be seen from (1) and (2) that at magnetic fields corresponding to an $x=0.14$, an error as great as 0.1 percent in the assumed value of g_J/g_I' will cause a maximum error in the resultant $\Delta\nu$ of 0.001 percent. An error of this magnitude, if assumed to be in the same directions for both isotopes, will cause an error in the ratio $\Delta\nu^{205}/\Delta\nu^{203}$ of only 1 part in 10^6. Hence any reasonable departure of g_J(Tl) from g_J(In) or an effect arising from an incomplete calculation of g_I'/g_I will have no significant effect on the important datum of this experiment, the ratio $\Delta\nu^{205}/\Delta\nu^{203}$. Similarly, a systematic error of this nature should not appreciably affect the value of the isotope shift $(\Delta\nu^{205}-\Delta\nu^{203})$, which the results of this experiment indicate to be 205.4±0.4 Mc.

Poss[6] has reported that the ratio of the magnetic moments is

$$g_I^{205}/g_I^{203}=1.00986\pm0.00005.$$

Defining

$$\Delta\equiv g_I^{205}/g_I^{203}-\Delta\nu^{205}/\Delta\nu^{203},$$

gives

$$\Delta=0.00012\pm0.00008.$$

DISCUSSION OF RESULTS

First-order theory of hyperfine structure predicts a null value for Δ. The theory is, however, based on two assumptions. The first assumes that the Coulomb attraction between the electron and the nucleus becomes infinite as $r\to0$, while the second assumes that the hfs splittings arise from the interaction between the magnetic field produced by the orbital electrons and a point dipole located at the center. For electrons whose wave functions do not have appreciable values in the nuclear

region, the error introduced by these assumptions should be negligible. However, for electrons in the $P_{\frac{1}{2}}$ and $S_{\frac{1}{2}}$ states a nonzero value of Δ may be expected, because the radial wave functions of these states remain finite in the nuclear region. The expected value of Δ would be composed of two parts, Δ_1 and Δ_2. Δ_1 arises from the cutoff of the Coulomb potential, while Δ_2 arises from the finite distribution of the magnetic moment in the nucleus.

If it is assumed that for a nucleus of finite radius the Coulomb field is cut off in some appropriate manner, then the wave functions for electrons in the $P_{\frac{1}{2}}$ and $S_{\frac{1}{2}}$ states will differ markedly within the nuclear region from values corresponding to a pure Coulomb field. Rosenthal and Breit[8] have pointed out, that since the coupling of the electron and the nuclear magnetic moment is proportional to the integral

$$\int \phi_1\phi_2 y^{-2}dy = I, \tag{8}$$

where ϕ_1 and ϕ_2 are the Darwin-Gordon radial functions, and $y=2Zr/a_H$, special consideration of the behavior of the wave functions at values of $r \leqslant r_0$, the nuclear radius, is necessary. It is evident from the form of (8), that the values of the product $\phi_1\phi_2$ are weighted most heavily for small values of y where, for a nucleus of finite size, ϕ_1 and ϕ_2 depart most from their values in a pure Coulomb field. Taking into account the actual perturbed nature of the wave functions at values of $r<r_0$, Rosenthal and Breit were led to a correction factor for nuclear magnetic moments deduced from hfs splittings of the form

$$\Delta\nu \sim g_I(1-KA^{(2\rho-1)/2}), \tag{9}$$

where $\rho=(1-Z^2\alpha^2)^{\frac{1}{2}}$.

The factor K in Eq. (9) is a function of the electronic state, the atomic number, an assumed variation of the nuclear radius of $r_0=1.5\times10^{-13}A^{\frac{1}{3}}$ cm, and the exact form of the electrostatic potential within the nuclear region. It is clear from the form of Eq. (9) that for two isotopes of the same atom a differential correction will exist. Thus

$$\Delta\nu_1/\Delta\nu_2=(g_{I^1}/g_{I^2})\{1-K(A_1^{(2\rho-1)/2}-A_2^{(2\rho-1)/2})+\cdots\},$$

or

$$\Delta_1=g_{I^1}/g_{I^2}K(A_1^{(2\rho-1)/2}-A_2^{(2\rho-1)/2}). \tag{10}$$

Crawford and Schawlow[9] have calculated the factor K for two specific models of nuclear charge distribution. For the case of a uniform distribution of charge and negligible nonelectrical forces in the nucleus, they are led to a value of

$$\Delta_1(^2P_{\frac{1}{2}}\ \mathrm{Tl}^{203,205})=9.3\times10^{-5},$$

while for the case of charge concentrated on the surface of the nucleus and similarly negligible nonelectrical forces within, they are led to a value of

$$\Delta_1(^2P_{\frac{1}{2}}\ \mathrm{Tl}^{203,205})=10.4\times10^{-5}.$$

Bohr and Weisskopf[10] have considered the interaction of $S_{\frac{1}{2}}$ and $P_{\frac{1}{2}}$ electrons with a magnetic moment that has a finite distribution over the nuclear region. They are led to expect a nonzero value of Δ_2 which depends not only on the size of the nucleus, but also on the intrinsic structure of the nuclear magnetic moments. Assuming that the spin g-factor is that of the proton, and that the orbital momentum is that of the odd particle in the nucleus, they were able to account for observed anomalies[11,12] in K and Rb. Using the same assumptions, the maximum expected value on the basis of this effect alone will be

$$\Delta_2(^2P_{\frac{1}{2}}\ \mathrm{Tl})=1.4\times10^{-5}.$$

The smallness of the expected effect results from the great similarity in the magnitudes of the magnetic moments of the two isotopes, and also from the fact that the effect will in general be considerably less for $P_{\frac{1}{2}}$ states than for $S_{\frac{1}{2}}$ states.

A combination of the predictions of the theories of Crawford and Schawlow, and of Bohr and Weisskopf leads to

$$\Delta_{\mathrm{calc}}=11\pm1\times10^{-5}.$$

This is to be compared with the experimental value of

$$\Delta_{\mathrm{obs}}=12\pm8\times10^{-5}.$$

The agreement seems to be quite good but, unfortunately, the combined precision to which the two experimental ratios is known precludes any significant discrimination between the proposed nuclear models. However, the general accordance of theory and experiment may be construed as further evidence of the essential validity of current theories of hfs anomalies.

In particular, as the principal effect observed was that of Rosenthal and Breit, this experiment may be considered as an additional indication of the accuracy of the correction factors calculated by Crawford and Schawlow, which are to be applied when magnetic moments are deduced from spectroscopic measurements of hyperfine structure splittings in heavy elements.

The author takes great pleasure in thanking Professor P. Kusch for aid and encouragement, and Mr. R. G. Gould for his many active contributions to this research.

[8] J. E. Rosenthal and G. Breit, Phys. Rev. **41**, 459 (1932).
[9] M. F. Crawford and A. L. Schawlow, Phys. Rev. **76**, 1310 (1949).
[10] A. Bohr and V. F. Weisskopf, Phys. Rev. **77**, 94 (1950).
[11] Ochs, Logan, and Kusch, Phys. Rev. **78**, 184 (1950).
[12] F. Bitter, Phys. Rev. **76**, 150 (1949).

Ferromagnetic Resonance in Nickel Ferrite as a Function of Temperature*

D. W. Healy, Jr.†
Cruft Laboratory, Harvard University, Cambridge, Massachusetts
(Received January 16, 1952)

Ferromagnetic resonance in $NiOFe_2O_3$ has been studied over a temperature range of −195°C to 588°C. From this study the variation in line width with temperature, g value, and magnetic anisotropy constants K_1 and K_2 have been determined. Results show that the line width decreases with increasing temperature, the g value remains essentially constant, and the two anisotropy constants show different sign behavior over the temperature range.

I. INTRODUCTION

THE phenomenon of ferromagnetic resonance originally observed by Griffiths[1] has since received extensive study both theoretically[2,3] and experimentally.[4–7] In particular, Yager *et al.*[8] have studied the resonance phenomenon in single crystals of $NiOFe_2O_3$ at room temperature.

This paper discusses the experimental results of a study made on $NiOFe_2O_3$ over a temperature range of −195°C to 588°C. The Curie temperature of $NiOFe_2O_3$ is approximately 600°C. The investigation was carried out at a frequency of about 9000 Mc/sec on small spherical samples. These spheres were about 0.019 inch in diameter, and hence, were small enough so that the rf electromagnetic field could be considered uniform throughout their volume. In addition, their small size relative to the exciting wavelength insured the avoidance of dimensional resonance effects.

A study has been made of the line width of the resonance curve, the variation of the spectroscopic splitting factor, g, and the magnetic anisotropy constants, K_1 and K_2, as a function of temperature.

II. EXPERIMENTAL

The experimental technique of measurement was similar to that used by Bloembergen[7] in studying the resonance phenomenon in nickel and Supermalloy. A block diagram of the measuring equipment is shown in Fig. 1. A sample was placed in a rectangular microwave cavity excited by a fixed frequency rf field, and the power absorbed by the sample then was measured as a function of the magnitude of a constant magnetic field H_0. This field was so oriented that its lines of flux were perpendicular to those of the rf field.

In order to measure the power absorbed in the sample, the unloaded Q, Q_u, of the cavity and the coupling Q, Q_e, were determined by conventional techniques. Q_u at zero value of H_0 was measured both with the sample in the cavity and also without a sample. The two Q_u's were nearly identical; therefore, the sample did not materially contribute to loss either of a dielectric or eddy current nature in the cavity. Since nickel ferrite has a high resistivity[9] and since the sample was located at a region of rf magnetic field maximum (electric field minimum), it is expected that such losses would be small.

Once Q_u for the cavity and sample had been determined at zero H_0, the technique was to measure the power reflected from the cavity as a function of H_0. Since the power incident on the cavity was held constant, the variation in power absorbed in the sample could be found in terms of the power reflected from the cavity. The power absorbed in the cavity in turn could be expressed in terms of a change of the Q_u of the cavity.

The imaginary component, μ'', of the permeability of the ferrite sample can be evaluated from a knowledge of the change in Q of the cavity by using a perturbation technique such as described by Bethe and Schwinger.[10] In order to employ this technique we must know the field configuration in the cavity and we must assume that the distortion of these fields produced by the

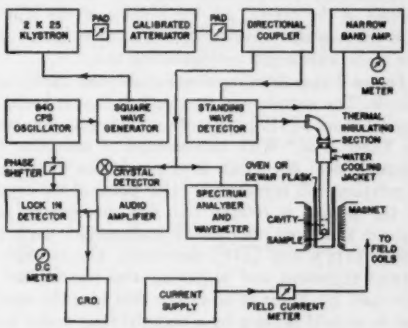

FIG. 1. Block diagram of measuring equipment.

* This work was supported by the ONR.
† Now at College of Applied Science, Syracuse University, Syracuse, New York.
[1] J. H. E. Griffiths, Nature **158**, 670 (1946).
[2] C. Kittel, Phys. Rev. **73**, 155 (1948).
[3] J. H. Van Vleck, Phys. Rev. **78**, 266 (1950).
[4] H. G. Beljers, Physica **14**, 629 (1949).
[5] A. F. Kip and R. D. Arnold, Phys. Rev. **75**, 1556 (1949).
[6] L. R. Bickford, Tech. Rept. XXIII Lab. Insulation Research MIT (October 1949).
[7] N. Bloembergen, Phys. Rev. **78**, 572 (1950).
[8] Yager, Galt, Merritt, and Wood, Phys. Rev. **80**, 744 (1950).
[9] J. L. Snoek, *New Developments in Magnetic Materials* (Elsevier Publishing Company, Houston, Texas, 1946).
[10] H. A. Bethe and J. Schwinger, Natl. Defense Research Committee Report D1-117, March 1943.

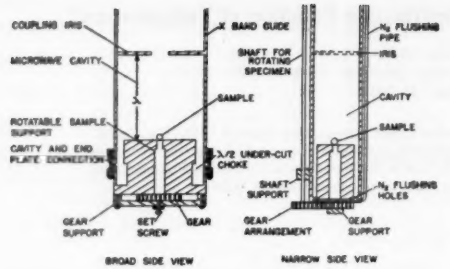

FIG. 2. Detail of microwave cavity.

introduction of the sample into the cavity is negligibly small. For this case we have

$$(\delta f/f)+j\delta(1/2Q_u)=\delta W/W, \tag{1}$$

where f is the resonant frequency of the cavity, δf the change in the resonant frequency produced by the introduction of the sample, Q_u the unloaded Q of the cavity, δW the change in stored energy in the cavity produced by the introduction of the sample, and W is the total stored energy of the cavity. If we know the field configuration, we can compute W and also δW in terms of $\mu=\mu'+j\mu''$. In computing W and δW we take advantage of the fact that the sample was placed in a region of the cavity where the electric rf field is negligibly small.

By this means μ'' can be calculated from the relationship

$$\mu''=\frac{\Delta Q_u}{2Q_u^2}\frac{V}{\Delta V}\frac{\lambda_g^2}{2\lambda_1^2}, \tag{2}$$

where ΔQ is the change in the value of Q_u measured as a function of the constant magnetic field, V is the volume of the cavity, ΔV the volume of the sample, λ_g is the resonant wavelength in the cavity, and λ_1 the free space wavelength corresponding to λ_g.

Figure 2 is a drawing showing the test cavity and sample. The sample was mounted so that it could be rotated about a [110] axis in the same fashion employed by Yager *et al.*[8] With this method of mounting the magnetic field H_0, which is perpendicular to the axis of rotation, will remain in a (110) plane of the crystal as the sample is rotated but will successively pass through the three principal crystallographic axes, the [100], [110], and [111] directions. The method of crystal alignment and mounting also was similar to that used by Yager *et al.* except that here the sample had to be held in place by a material that would withstand a large temperature variation. Insalute cement was used for this purpose.

Since the cavity was to be used over a wide temperature range it was necessary to prevent oxidation of the copper cavity walls at the high temperature and also prohibit the condensation of water vapor and oxygen at the low temperatures. For this purpose a slight positive pressure of dry nitrogen was maintained in the cavity at all times.

The spherical samples were prepared by a technique similar to that described by Bond.[11]

The steady magnetic field was measured in terms of the current through the field coils. The calibration of the magnetic field in terms of the field current was made by means of a proton resonance device of the type reported by Pound and Knight.[12]

III. THEORETICAL

Kittel has shown that the general resonance condition is

$$\omega=\gamma H_{eff}, \tag{3}$$

where γ is the gyromagnetic ratio, $g(e/2mc)$, and g is the spectroscopic splitting factor.[13] H_{eff}, the effective value of the constant magnetic field, is given by

$$H_{eff}=\{[H_0+(N_y+N_y^{a1}+N_y^{a2}-N_z)M_z] \times[H_0+(N_z+N_z^{a1}+N_z^{a2}-N_z)M_z]\}^{\frac{1}{2}}. \tag{4}$$

H_0 is the externally applied field, assumed here to be in the z direction, N_x, N_y, and N_z are the shape dependent demagnetizing factors, and N_x^{a1}, N_y^{a1} and N_x^{a2}, N_y^{a2} are effective demagnetizing factors introduced to account for the presence of magnetic anisotropy energy. Kittel[2] and Bickford[6] have shown that, when H_0 is in a (110) plane and is strong enough to saturate the sample magnetically, these effective demagnetizing factors are given by

$$\left.\begin{aligned} N_x^{a1}&=(1-\sin^2\theta-3\sin^2 2\theta)(K_1/M_s^2),\\ N_y^{a1}&=2(1-2\sin^2\theta-\tfrac{3}{8}\sin^2 2\theta)(K_1/M_s^2),\\ N_x^{a2}&=\tfrac{1}{2}\sin^2\theta(6\cos^4\theta-11\sin^2\theta\cos^2\theta +\sin^4\theta)(K_2/M_s^2),\\ N_y^{a2}&=-\tfrac{1}{2}\sin^2\theta\cos^2\theta(3\sin^2\theta+2)(K_2/M_s^2). \end{aligned}\right\} \tag{5}$$

Here θ measures the angle between H_0 and a [100] axis of the crystal, and K_1 and K_2 are the first and second order anisotropy constants, respectively. From

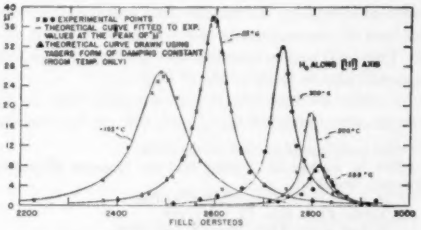

FIG. 3. μ'' vs H_0 for $NiOFe_2O_3$ single crystal sphere.

[11] W. L. Bond, Rev. Sci. Instr. **5**, 344 (1951).
[12] R. V. Pound and W. D. Knight, Rev. Sci. Instr. **21**, 219 (1950).
[13] C. Kittel, Phys. Rev. **76**, 743 (1949).

these expressions, knowing the value of M_s, H_0, and θ, the anisotropy constants K_1 and K_2 and g value have been calculated.

The classical equations of motion as first set up by Kittel have the form,

$$\left.\begin{aligned} dM_{x,y}/dt&=\gamma(\mathbf{M}\times\mathbf{H}_{\text{eff}})_{x,y}-(M_{x,y}/T_2),\\ dM_z/dt&=\gamma(\mathbf{M}\times\mathbf{H}_{\text{eff}})_z-[(M_z-M_0)/T_1].\end{aligned}\right\} \quad (6)$$

The relaxation terms are those used by Bloembergen and were based upon the form used by Bloch in describing nuclear magnetic resonance. An alternative form for these relaxation terms is that used by Yager *et al.* and first put forward by Landau and Lifshitz.[14] In the equation of motion this form appears as

$$d\mathbf{M}/dt=\gamma(\mathbf{M}\times\mathbf{H}_{\text{eff}})-(\gamma\alpha/M)[\mathbf{M}\times(\mathbf{M}\times\mathbf{H})]. \quad (7)$$

Since the physical mechanisms which lead to a broadening of the resonance line are not well understood, both of these damping terms have been introduced on purely empirical grounds.

The steady state solution of Eq. (6) yields

$$\mu''=\frac{4\pi\gamma^2M_0[H_0+(N_y^{e1}+N_y^{e2})M_0](2\omega/T_2)}{(-\omega^2+\omega_0^2)^2+(4\omega^2/T_2^2)}, \quad (8)$$

where we assume that $M_z=M_0$ and the sample is spherical so that $N_x=N_y=N_z$. Here $\omega_0^2=\gamma^2H^2_{\text{eff res.}}$

The solution of Eq. (7) is

$$\mu''=\frac{4\pi\dfrac{\alpha}{1+\alpha^2}\dfrac{\omega}{\gamma}\dfrac{1}{l_yH_z}\left[\dfrac{\omega^2}{\gamma^2}\dfrac{1}{l_xl_yH_z^2(1+\alpha^2)}+\dfrac{l_z}{l_y}\right]}{\left[1-\dfrac{\omega^2}{\gamma^2}\dfrac{1}{l_xl_yH_z^2(1+\alpha^2)}\right]^2+\dfrac{\alpha^2}{1+\alpha^2}\dfrac{(l_z+l_y)^2}{l_xl_y}\dfrac{\omega^2}{\gamma^2}\dfrac{1}{l_xl_yH_z^2(1+\alpha^2)}}\dfrac{M_0}{l_zH_z}, \quad (9)$$

where we have used Yager's notation that $l_zH_z=H_0+(N_x^{e1}+N_x^{e2})M_0$ and $l_yH_z=H_0+(N_y^{e1}+N_y^{e2})M_0$.

From either Eq. (8) or (9) we can calculate T_2 or its equivalent in terms of α by equating the peak value of μ'' as determined experimentally to the theoretical expression at resonance.

IV. RESULTS

The absorption resonance curves at several temperatures are shown in Fig. 3. The solid curves represent the theoretical curves where the damping term has been adjusted so that the value of μ'' at resonance agrees with the experimental value. For the room temperature data two sets of theoretical curves are drawn, one indicated by the solid curve and the other by solid triangles. The solid curve was drawn for the theoretical expression using a damping term of the form used by Bloembergen,[7] while the solid triangles are derived from the theoretical expression using the form of damping term used by Yager *et al.*[8] It is readily seen that there is is little difference between these two curves.

The room temperature data agree very well with those of Yager *et al.*[8] and give an absorption curve width of about 70 oersteds independent of the crystallographic orientation of the sample. At −195°C the width of the absorption curve is about 110 oersteds, and this decreases to about 50 oersteds at 588°C.

Figure 4 shows a plot of $1/T_2$ *vs* temperature. T_2 is the over-all relaxation time as determined from the width of the absorption curve. The decrease of $1/T_2$ with temperature was unexpected and is a different behavior from that observed in ferromagnetic metals. The fact that $1/T_2$ decreases with increase in temperature would suggest that spin lattice relaxation effects play only a small role in contributing to the over-all line width.

Figure 5 shows the variation of H_0 required for resonance measured as a function of the angle between the direction of H_0 and a [100] direction in the sample. In order to explain this angular variation it was necessary to include two anisotropy terms in the expression for the magnetic anisotropy energy. From the angular variation shown in Fig. 5, therefore, the anisotropy constants K_1 and K_2 were measured. Their variation with temperature is given in Fig. 6.

Referring again to Fig. 5, we have plotted a curve for 25°C showing the best fit to the observed angular variation of the resonant value of H_0 that can be made using only the first term in the expansion for the anistropy energy. We see that this curve does not fit the experimental data very well and that it is necessary to include the second-order term to get a good agreement. This result is different from that observed by

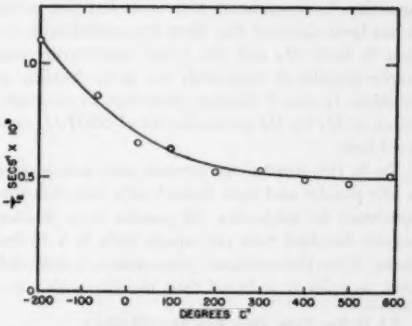

FIG. 4. $1/T_2$ *vs* temperature from $NiOFe_2O_3$ resonance curves.

[14] L. Landau and E. Lifshitz, Physik. Z. U.S.S.R. **8**, 153 (1935).

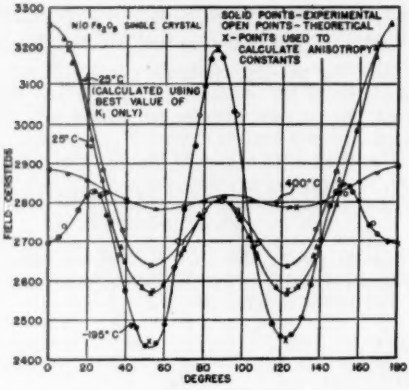

FIG. 5. H_{res} *vs* θ. θ equals angle in (110) plane between static field and cube edge.

Yager *et al.* and indicates that there may be considerable variation in the anisotropy energy from crystal to crystal depending on the impurity content and method of preparation.

Table I shows the variation in the g value as a function of temperature. This g value is calculated from the value of H_0 required for resonance and remains essentially constant over the whole temperature range. It had been expected that there would be some correlation between the value of g and that of the magnetic anisotropy energy. This correlation was expected since it is believed[15] that the spin system "feels" the crystal lattice through the agency of the spin-orbit and orbit-lattice coupling parameters. Thus any variation in the strength of the orbit-lattice coupling would be manifested by a change in both the g value and the anisotropy energy. Such a correlation is not evident here.

In calculating both the g values and the anisotropy constants it is necessary to know the saturation magnetization, M_0, of the nickel ferrite as a function of temperature. Pauthenet[16] has published data on this quantity. In experiments with other ferrities, however, it has been observed that there was considerable variation in both M_0 and the Curie temperature among ferrite samples of supposedly the same chemical composition. It was of interest, therefore, to ascertain the value of M_0 for the particular lot of $NiOF_2O_3$ crystals used here.

To do this some of the crystals used were ground to a fine powder and then formed into thin disk-shaped specimens by subjecting the powder to a pressure of several hundred tons per square inch in a hydraulic press. When the resonance phenomenon is observed for such samples it is found that the line width is considerably increased by the so-called "powder broadening." It is not expected that the resonant value of H_0 will be displaced due to this "powder broadening;" however, the resonant value of H_0 will be considerably affected by the demagnetizing field.

The demagnetizing field can be calculated using the formulas compiled by Osborne[17] considering the disks as limiting cases of flattened oblate spheroids. A value for M_0 can be determined by comparing the value of the field required for resonance in a spherical sample, where M_0 enters only through the anisotropy field, with the field required for resonance in a disk-shaped sample, which is strongly affected by M_0 through the agency of the demagnetizing fields. Figure 7 shows the temperature variation of M_0 calculated in this fashion compared with the data prepared by Pauthenet.

Table I also lists the g value computed for the disk-shaped samples using the calculated value of M_0. These values of g are quite sensitive to any error in determining M_0 and thus agree with the values of g computed for the spherical samples within the accuracy of the experiment. In addition, we have listed in Table I the value of H_0 required for resonance and the computed value of H_{eff}.

V. CONCLUSIONS

Comparison of the experimental data with the curves predicted by Kittel's theory shows that a resonance type curve fits the observations very well. The physical reasons for this are not clear. Measurements made by Damon[18] on spin-lattice relaxation times indicate that the spin lattice interaction contributes little to the line width. Since the other mechanisms which are responsible for the line width are not evident, it seems fruitless to discuss the more difficult problem of line shape.

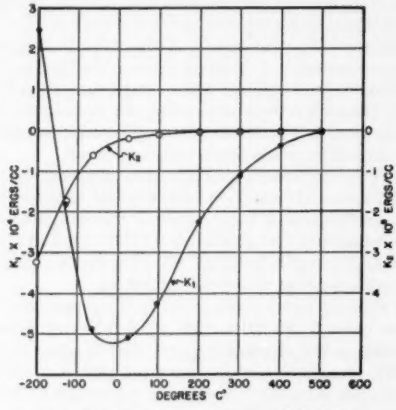

FIG. 6. K_1 and K_2 *vs* temperature ($NiOFe_2O_3$).

[15] J. H. Van Vleck, Phys. Rev. **52**, 1178 (1937).
[16] R. Pauthenet, Compt. rend. **230**, 1842 (1950).
[17] J. A. Osborne, Phys. Rev. **67**, 351 (1945).
[18] R. W. Damon, Ph.D. thesis, Harvard University (1951).

The increase of T_2 with temperature shown in Fig. 4 is unexpected. This increase rules out the possibility that spin lattice relaxation and dipolar forces contribute materially to the line width since their temperature variation would be the inverse of that observed. The fact that the line width increases along with the increase in ordering of the electron spins, as 0°K is approached, indicates that the cause for the line broadening might be sought in action of the pseudo-dipolar forces mentioned by Van Vleck.[5] He points out that, if crystalline imperfections exist, these forces may couple together microcrystals of slightly different resonance frequencies, thus broadening the line. Such forces could increase with the increase in anisotropy energy and thus become more pronounced at low temperatures.

In this connection it would be of interest to make measurements at lower temperatures to determine whether or not ordering of the magnetic lattice eventually overcomes the tendency for the line to broaden. It may be, as Van Vleck suggested, that the effect of impurities in the crystal lattice would obscure such tendency and no narrowing would be observed.

Experiments at lower temperature would likewise be of interest in connection with the anisotropy energy. The measurements made here show that the anisotropy constants increase in magnitude very rapidly with temperature in the vicinity of −195°C, and it is not expected that such a temperature variation would continue. At higher temperatures, as has been observed in the ferromagnetic metals, the anisotropy energy falls to zero before the Curie temperature is reached.

TABLE I. g values of $NiOFe_2O_3$.

Single crystal sphere				Polycrystalline material	
Temp	H_{res}	H_{eff}	g	Temp	g
−195°C	2486	2856	2.26	−195°C	2.28
−65°C	2567	2878	2.24		
25°C	2597	2866	2.25	25°C	2.24
100°C	2677	2878	2.23	115°C	2.19
200°C	2693	2834	2.26	233°C	2.20
300°C	2735	2844	2.25	360°C	2.16
400°C	2792	2828	2.26	488°C	2.20
500°C	2795	2813	2.27	542°C	2.30
588°C	2813	2812	2.27		

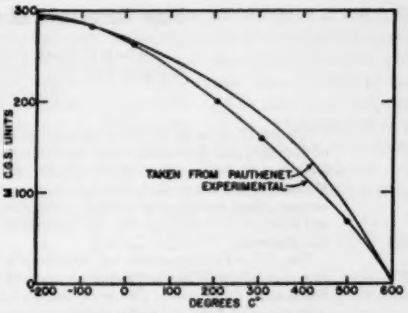

FIG. 7. M vs temperature for $NiOFe_2O_3$ polycrystalline material.

The g value as seen from Table I remains essentially constant over the whole temperature range studied. This is a different behavior from that reported by Bickford[6] for magnetite. In the case of magnetite the change in g value could be correlated with the change in anistropy energy, the lowest g value occurring near the temperature where magnetite undergoes a transition and becomes magnetically isotropic. No such correlation is possible here, and reasons for this different behavior are not known.

In conclusion the writer would like to acknowledge his debt to Professor N. Bloembergen who has given generously of his time and advice during this investigation. He would also like to acknowledge his gratitude to the Bell Telephone Laboratories who supplied the single crystals of $NiOFe_2O_3$ studied.

Fine Structure of the Hydrogen Atom. IV*

WILLIS E. LAMB, JR.,† AND ROBERT C. RETHERFORD‡
Radiation Laboratory, Columbia University, New York, New York

(Received February 29, 1952)

The fourth paper of this series contains an analysis of measurements made in 1950 on the fine structure of hydrogen and deuterium. After application of numerous experimental and theoretical corrections the following results are obtained. The displacement $2^2S_{\frac{1}{2}}-2^2P_{\frac{1}{2}}$ is 1058.27 Mc/sec for hydrogen and 1059.71 Mc/sec for deuterium, each with a limit of error ± 1.0 Mc/sec. There seems to be satisfactory agreement between these and the most recently calculated values. The difference of 1.44 Mc/sec between deuterium and hydrogen is compatible with an explanation based on reduced mass effects and the finite extension of the deuteron.

The $2^2P_{\frac{3}{2}}-2^2P_{\frac{1}{2}}$ separation for deuterium is 10,972.11 Mc/sec (limit of error ± 1.0 Mc/sec). With assumption of a well-justified theoretical formula for the doublet splitting, one may calculate a value for the fine structure constant α. The result for $1/\alpha = 137.033$ (limit of error ± 0.006) is in distinct disagreement with the value $1/\alpha = 137.0429 \pm 0.0009$ derived from the hyperfine splitting of the ground state of hydrogen. The formula used for this was in error due to neglect of corrections of relative order $Z\alpha^2$, and is still in doubt because of reduced mass effects and spatial extent of nuclear magnetism.

THE preceding papers[97] of this series have laid a foundation in experiment and theory for analysis of more accurate measurements of the fine structure splittings of hydrogen and deuterium. Results of such an analysis are given in the present paper.

The provisional goal was to measure the fine structure pattern with an accuracy of 1 Mc/sec. Considering that the resonances are more than 100 Mc/sec broad, this required working within 1 percent of the half-width which is not usually possible in radiofrequency spectroscopy. In the course of the measurements, however, it became apparent that the internal consistency of data accumulated in a single run was an order of magnitude better than this, while the external consistency of different runs was about at the 0.5 percent level. A number of possible improvements in procedure were suggested as the data accumulated, and it is now hoped that even more accurate results will subsequently be obtained in this laboratory. It is felt, however, that the values here obtained are of sufficient interest to justify their publication now.

Prior to an analysis of data in Sec. 75, a few additional matters not incorporated in Parts II and III require discussion.

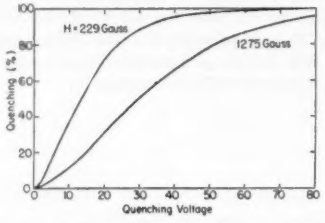

FIG. 54. Percentage of quenching of metastable hydrogen atoms as a function of dc voltage applied to transmission line. The plate separation was roughly $\frac{1}{4}$ cm. Curves are shown for magnetic fields of 229 and 1275 gauss.

O. ADDITIONAL EFFECTS

73. Quenching of beam by Electrostatic Fields

The calculated effect of motional electric fields on metastable hydrogen atoms in states α and β was indicated in Fig. 34. Additional quenching may be produced by application of a static electric field in the rf interaction region, or elsewhere along the beam. Examples of this quenching are given in Fig. 54 for magnetic fields of 229 and 1275 gauss. The electrode geometry was not sufficiently good to warrant an attempt to fit these data accurately to a theoretical formula based on an equation like (42). The ease of quenching, however, seems to vary with magnetic field in the manner expected if the beam were composed mostly of atoms in the α-state. According to Fig. 34 this should be the case for a range of magnetic fields extending from perhaps 400 to 1200 gauss. Outside of this range the beam should have an appreciable fraction of atoms in the β-state. In practice, however, this fraction is reduced by the presence of electric fields in the electron bombarder, detector, and possibly elsewhere along the beam, for the β-state is more easily quenched than α up to $H=3400$ gauss. This is especially true in the vicinity of the crossing point of β and f, which occurs at about 1188 gauss where very weak stray electric fields in the z direction may cause a decay of β. The behavior at higher fields is shown in Fig. 55, which was taken at 1450 gauss. This indicates that the beam

* Work supported jointly by the Signal Corps and ONR.

† Present address. Department of Physics, Stanford University, Stanford, California. This author is responsible for the calculation of theoretical and experimental corrections.

‡ Present address: Department of Electrical Engineering, University of Wisconsin, Madison, Wisconsin.

[97] I, W. E. Lamb, Jr., and R. C. Retherford, Phys. Rev. **79**, 549 (1950); II, **81**, 222 (1951); III, W. E. Lamb, Jr., Phys. Rev. **85**, 259 (1952). Frequent references to these papers are made. Sections, figures, equations, footnotes, tables, and appendices are numbered consecutively after those of Parts I–III. The designation of states by letters α, β, a, b, c, d, e, and f is explained in Fig. 14.

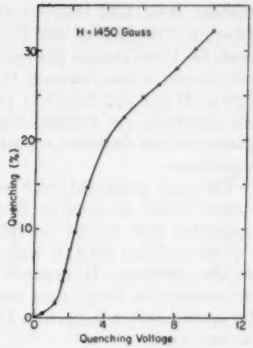

FIG. 55. Percentage of quenching of metastable hydrogen atoms as a function of dc voltage applied to transmission line. The curve was taken at 1450 gauss where the beam contains an appreciable fraction of easily quenched atoms in the lower metastable state β.

is composed of an easily quenched "soft" component formed by atoms in the β-state, and a "hard" component of atoms in state α. In such a case, the fractional quenching may be written as

$$\phi=\phi_\alpha[1-\exp-(V/V_\alpha)^2]+\phi_\beta[1-\exp-(V/V_\beta)^2], \quad (245)$$

where V is the voltage applied to quenching electrodes, V_α and V_β are constants characterizing the ease of quenching, and ϕ_α and ϕ_β are the fractions of the two kinds of atoms α and β in the beam. In Eq. (245) it is assumed that the beam consists only of two components α and β and no attempt is made to consider hyperfine splitting or velocity distribution. For $|V|\ll V_\alpha$ one may write

$$\phi=\phi_\alpha(V/V_\alpha)^2+\phi_\beta[1-\exp-(V/V_\beta)^2], \quad (246)$$

so that when ϕ is plotted against V^2 in the range

$$V_\beta\ll|V|\ll V_\alpha,$$

a straight line results whose slope is ϕ_α/V_α^2 and whose intercept on the vertical axis is just ϕ_β. In the case of Fig. 55 this analysis yields Fig. 56 with $\phi_\beta=20.6$ percent; $\phi_\alpha=79.4$ percent, and $V_\alpha=26.2$ volts. From the behavior for $|V|<V_\beta$, one may estimate that $V_\beta\sim 2.88$ volts.

When such measurements are made at various magnetic fields between 850 and 1450 gauss, it is found that the fraction ϕ_β decreases rapidly as the field is decreased from 1450 gauss, passes through a minimum near the βf crossing point 1188 gauss and increases slightly and then falls off sharply as the field is lowered further. Typical results have been $\phi_\beta=22$ percent at $H=1450$ gauss, and $\phi_\beta=3$ percent at $H=1188$ gauss when the apparatus is in a "clean" condition, but lower figures such as 14 percent and 0.5 percent, respectively, have been observed even though the beam was not excessively poisoned. The variation is probably to be attributed to varying conditions in the electron bombarder of the sort discussed in Sec. 43.

It was discovered that on some occasions there was a rather considerable effect on the beam when the quenching voltage was merely reversed in sign. This was attributed to the existence of a contact-like potential difference between the quenching electrodes which could amount to as much as one volt. The actual figure varied considerably from day to day, and sometimes during a run. Presumably this potential difference was in part due to contact potentials and partly to charges produced on insulating films by illumination with ultraviolet light. To allow for this effect, the portion of Eq. (246) linear in V^2 was rewritten as

$$\phi=(\phi_\alpha/V_\alpha^2)(V-V_0)^2+\phi_\beta, \quad (247)$$

with V_0 the potential difference with no applied electric field. A procedure was developed whereby the constants ϕ_β, V_0, and V_α could be calculated rapidly for magnetic fields of interest from measurements of ϕ at three voltages in the range $V_\beta\ll|V|\ll V_\alpha$.

The presence of soft component β requires a correction to the observed rf quenching by a factor $1+(\phi_\beta/\phi_\alpha)=1+s$. For observations between 400 and 850 gauss the motional quenching keeps the beam sufficiently pure α, and no soft component correction is needed. It was, however, necessary for data taken at magnetic fields near the βf crossing point. One of the unsatisfactory features of the present work is the possible error introduced in application of the rather variable soft component correction. Of course, the frequency was chosen so that ϕ_β was small not only at the resonance peaks but also at the two working points. Only a difference in soft component at these two points would lead to a significant differential correction that might be in error. It is planned, however, in future work to treat the problem in a somewhat better fashion.

The above complications impose a very severe limitation on the possible ranges of frequency *versus* magnetic field plot (Fig. 15) which can be explored accurately. The soft component becomes unmanageably large above 1450 gauss, difficult either to correct for or to quench

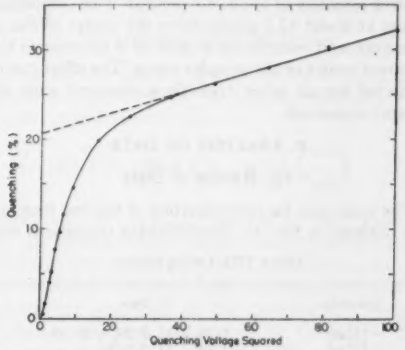

FIG. 56. Analysis of data shown in Fig. 55 whereby quenching is plotted against square of voltage. The beam is found to contain 20.6 percent of atoms in the more easily quenched lower metastable state.

differentially. The best choice in perhaps $H\sim1158$ gauss, i.e., the second β-crossing. The first β-crossing $H\sim575$ gauss would also be satisfactory except that for $\alpha\epsilon$ the sharp resonances $\alpha\beta$ (Sec. 47) are superimposed, while for all transitions there is a considerable overlap from other transitions. It is somewhat better to have the resonances occur at a higher field, such as 700 gauss, in order to obtain more separation from nearby peaks, but not yet to have appreciable soft component contamination in the beam. These criteria have guided the choice of transitions for accurate study.

74. Forbidden Component

The possibility of transitions with $\Delta m_I\neq0$ has been previously ignored. In one case, namely H(αf), such a transition can occur with appreciable intensity in the present apparatus. Referring to Fig. 17, this is the one from state α, $m_I=-\frac{1}{2}$ to state f, $m_I=+\frac{1}{2}$, which can be regarded as produced by matrix elements of the hyperfine interaction energy $\Delta w\mathbf{I}\cdot\mathbf{J}$ which are off diagonal in m_I and m_J. These mix in with the state α, $m_I=-\frac{1}{2}$ some contamination of state β, $m_I=+\frac{1}{2}$ which is coupled by electric dipole radiation to f, $m_I=+\frac{1}{2}$. Likewise, some of e, $m_I=-\frac{1}{2}$ is mixed in with f, $m_I=+\frac{1}{2}$ and makes transitions possible from α, $m_I=-\frac{1}{2}$.

The relative intensity of transition α, $m_I=-\frac{1}{2}\rightarrow f$, $m_I=+\frac{1}{2}$ to the allowed transitions α, $m_I\rightarrow f$, m_I is

$$\text{Ratio}=\left(\frac{\Delta w}{g_s\mu_0 H}\right)^2\cdot\frac{|(e|\mathbf{E}\cdot\mathbf{r}|\alpha)|^2}{|(f|\mathbf{E}\cdot\mathbf{r}|\alpha)|^2}. \qquad (248)$$

For H(αf), $H\sim704$ gauss, one has $\Delta w/g_s\mu_0 H\sim\frac{1}{10}$. With the particular rf field geometry used, the electric field was primarily in the z direction and therefore favored the αe transition over αf. From calculations on the amount of overlap of αe on αf, it was estimated that the ratio of squared matrix elements in (248) was 4.74, so that the forbidden component would have a relative intensity of about 4.7 percent. This component occurs at about 12.5 gauss above the center of the αf resonance and contributes a shift of 0.10 gauss to the apparent center of the complex curve. The effect can be neglected for all other transitions observed with the present apparatus.

P. ANALYSIS OF DATA

75. Nature of Data

The basic plan for determination of the fine structure was outlined in Sec. 45. The following transitions were studied: H(αe) and D(αe) at 2195 Mc/sec, H(αf) and D(αf) at 2395 Mc/sec, and D(αc) at 7195 Mc/sec. The basis for these choices is explained in Sec. 73. It had been hoped to also measure H(αc) at 7195 Mc/sec as well as H(αe) and D(αa) at 11,800 Mc/sec, but after the possibility of further improvements became apparent, it was decided to postpone the study of these transitions.

TABLE VIII. Listing of runs.

Transition	Date
H(αe)	1/28, 3/17, 3/23, 4/28/50
D(αe)	2/14, 2/23, 5/2/50
H(αf)	7/10, 7/12, 7/13, 10/27/50
D(αf)	7/14, 8/1/50
D(αc)	8/14, 10/19/50

The data presented here were obtained in fifteen "runs" which are listed in Table VIII. In general, the apparatus was turned on fully in the morning for "seasoning" and the data were taken during four hours in the afternoon. It required about nine months to accumulate the fifteen runs, since the apparatus had to be opened rather frequently for cleaning as described in Sec. 43.

Data taken for each run consisted basically of about fifteen comparisons of the rf quenching at two points of approximately equal heights on opposite sides of the resonance curve. Each comparison was obtained from the average of six measurements of the fractional quenching on each side. A typical sample of data for one such comparison is given in Table IX from the run of 7/13/50 on transition H(αf).

The values in column R_{nom} are the nominal resistance box settings on the variable side of the bridge circuit used for determining magnetic field. To these must be added previously determined corrections due to departures from nominal values as well as a measured value of the search coil resistance. After calibration of the permanent magnet by observations of transition D($\alpha\beta$), the magnetic fields corresponding to R_a and R_b could be obtained and were 649.86 and 753.86 gauss, respectively, for this case. Readings of the galvanometer were taken at 20-second intervals, some with rf on or off, and some with dc quenching voltage applied to the beam. Columns 1, 3, 5, 7, and 9 correspond to rf and dc fields off; columns 2, 4, and 6 to rf on and dc off; while column 8 was taken with dc on and rf off. The column marked Δf gives the frequency interval below 2400 Mc/sec for the rf on readings in the row in question. Since the frequency drift was small it sufficed to record Δf once for each line of data. In order to keep track of rf power variations, the crystal current I_x was recorded in some convenient unit on the intermediate rows in columns 1, 3, and 5. The remaining figures shown under columns, 2, 4, and 6 are the calculated galvanometer deflections due to rf. Thus, in column 2

$$(\text{rf quenching})_2=\tfrac{1}{2}(G_1+G_3)-G_2, \qquad (249)$$

where G_n is the galvanometer reading recorded in column n. The dc quenchings in column 8 were similarly calculated. Also shown are calculations of average dc and rf quenching, average crystal current for each row, and in the final column, the average percentage of rf quenching for each line.

Much auxiliary data were required in order to make the calculations necessary to obtain from each com-

TABLE IX. Transition H(αf), 7/13/50, 2400$-\Delta f$ Mc/sec. Sample data showing intercomparisons on two sides of resonance at magnetic fields corresponding to nominal bridge resistances R_{nom}. The frequency is 2400$-\Delta f$ Mc/sec, subject to corrections applied later because of departure of the standard crystal from 5 Mc/sec. The measurement cycle consists of a reading of dc quenching followed by three determinations of rf quenching, then of dc quenching, then three more rf quenchings, and a final determination of dc quenching. Listed vertically in columns 1, 3, and 5 are galvanometer readings with quenching fields off, and also crystal current readings obtained when the rf is next turned on. In columns 2, 4, and 6 are galvanometer readings with rf on and calculated galvanometer deflections due to rf. In columns 7 and 9 are galvanometer readings and calculated galvanometer deflections due to dc quenching. Also given are the average dc and rf quenchings, average crystal currents, and finally the average percentage of quenching for each line of data.

R_{nom}	Δf	1	2	3	4	5	6	7	8	9	dc	rf	ϕ%
4162								144.5	6.0	144.3			
									138.4				
	4.68	144.3	116.3	144.5	116.3	144.7	116.5	145.2	6.0	144.8	138.7	28.28	20.39
		179.5	28.1	180.0	28.3	180.5	28.45		139.0			180.0	
	4.68	144.8	116.1	144.7	116.1	144.6	116.2	144.4	6.0	144.3	138.68	28.5	20.55
		181.5	28.65	181.0	28.55	181.5	28.3		138.35			181.33	
4846								141.2	5.0	141.2			
									136.2				
	4.68	141.2	110.0	140.9	110.4	141.7	110.3	141.5	5.1	141.5	136.3	31.08	22.81
		181.5	31.05	181.5	30.9	181.5	31.3		136.4			181.5	
	4.68	141.5	110.4	142.0	110.5	142.2	110.8	142.1	5.2	141.6	136.53	31.43	23.02
		182.5	31.35	183.0	31.6	182.5	31.25		136.65			182.67	

parison the magnetic field of the center of the resonance. Thus the quenching was measured several times at the nominal center of the resonance to insure that the rf power setting was approximately right. Values of $d\phi/dI_x$ were obtained so that all data might be adjusted to the desired rf power level. The slope $d\phi/dR$ was measured at the working level so that the center of the resonance could be calculated if ϕ_a was not exactly equal to ϕ_b. In cases of transitions $\alpha\epsilon$ and αc a measure of the small amount of β-component in the beam was obtained at several magnetic fields (see Sec. 73). One or more calibrations of permanent magnet were made by observing the sharp resonance D($\alpha\beta$). Temperatures in the vicinity of electro- and permanent-magnets were recorded at frequent intervals during the run. Various pressures, oven and bombarding currents and voltages, etc., were recorded, although they were not needed in analysis of the data. The small difference of the crystal frequency standard from *WWV* was determined several times during the year and interpolation was used for the day in question.

76. Corrections Applied in Calculation of a Run

(a) *Soft component correction.*—If appreciable contamination of the beam by β-state was expected, a measurement of

$$s=\phi_\beta/\phi_\alpha \tag{250}$$

was made at the two magnetic fields H_a and H_b of the working points, at the nominal central field H_x and, for reference, also at 1450 gauss where a large value of s is obtained. The method of making these measurements was indicated in Sec. 73. Values of ϕ obtained during the run must be corrected by a factor $1+s$.

(b) *Power variation correction.*—The crystal current was measured each time the rf was applied. Since the variations were small, it sufficed to associate the average crystal current with the average percentage of quenching for each row of data. The value of $d\phi/dI_x$ was measured for the working point level and was calculated with sufficient accuracy for other levels by Eq. (102). The height of the nominal center was then brought to the desired level of quenching, e.g., 31 percent for H($\alpha\epsilon$), thereby determining a standard value of crystal current for the run. The remaining data were then reduced to this crystal current.

(c) *Frequency variation corrections.*—All quenchings were then adjusted to the same frequency, e.g., 2195 Mc/sec for H($\alpha\epsilon$), by applying a correction

$$\delta\phi=\pm\left(\left|\frac{d\phi}{dR}\right|\frac{R}{H}\Big/\frac{df}{dH}\right)\delta f \tag{251}$$

to the quenching, where R/H is given by the magnetic field calibration, df/dH is the calculated slope of the Zeeman frequency *versus* magnetic field curves, and $\delta f=5.00-\Delta f$. The $+$ and $-$ signs are taken for points on the low and high field sides of the resonance, respectively.

77. Determination of Center

Denoting the average of both ϕ's for R_a by $\bar{\phi}_a$ and likewise for R_b, one finds that the nominal center corresponds to a resistance $\bar{R}$,

$$\bar{R}=\tfrac{1}{2}(R_a+R_b)+\tfrac{1}{2}[\bar{\phi}_b-\bar{\phi}_a]\Big/\left(\frac{d\phi}{dR}\right), \tag{252}$$

where corrected values of R_a and R_b are used. From $\bar{R}$ one may calculate the apparent central field $\bar{H}$ by use of the field calibration figure R/H for the day in question.

To illustrate the calculations outlined above, and to indicate the magnitude of the corrections, a sample calculation of central field is given in Table X for the data presented in Table IX. The necessary auxiliary information shown in the table has been obtained from measurements not indicated in Table IX. It should be recalled that a "run" consisted primarily of about

TABLE X. Calculation of sample data from run of 7/13/50 on transition H(αf). The table gives crystal current calculated to give desired central quenching, dependence of quenching on crystal current, magnetic field calibration R/H, correction for departure of frequency from 2395 Mc/sec. Crystal current and frequency corrections are then calculated. In the last part of the table, the magnetic field of the resonance center is computed. For this, the slope in percent per ohm, the difference in quenching $\Delta\phi$ on the two sides of the resonance and the field calibration are combined to give a resonance field of $H_c = 704.27$ gauss.

$I_0 = 178.68$		$d\phi/dI_s = (0.004076)\phi$			$R/H = 6.577649$			$\delta\phi_2 = \pm 0.231\ \delta f$	
R_{nom}	R_{total}	$\bar{\phi}_0$	$\bar{I}_s$	ΔI_s	$\delta\phi_1$	ϕ_1	δf	$\delta\phi_2$	ϕ
4162	4274.57	20.47	180.67	1.99	0.17	20.30	0.32	0.08	20.38
4846	4958.63	22.92	182.09	3.41	0.32	22.60	0.32	−0.08	22.52
	Av = 4616.60								

$d\phi/dR = 0.06762$ at $R_{nom} = 4162$ ohm

$\Delta\phi = 22.52 - 20.38 = 2.14$ percent

$\frac{1}{2}\Delta R = \frac{1}{2}(2.14)/(0.06762) = 15.82$ ohm

$R_c = 4632.42$ ohm $H_c = 4632.42/(6.577649) = 704.27$ gauss

fifteen such comparisons. Table XI shows the distribution of central fields obtained from the entire run devoted to transition H(αf), 2195 Mc/sec of 7/13/50. The average field center is $H = 704.06$ gauss with an average deviation (av dev) = 0.06 gauss. This deviation gives a measure of the internal consistency of the data, but does not show external errors due to various causes discussed below.

78. Summary of Central Field Measurements

The results of all fifteen runs are given in Tables XII and XIII, together with a number of other quantities which are of significance in judging the accuracy of the data. The runs on transitions αe and αc differ from those on αf because for the former a correction for β-component is necessary, while instead for αf overlap from αe must be considered. Columns headed s_a and s_b show the percentages of β-state in the beam for the working points, while under ϕ_c and ϕ_{930}, respectively, are indicated the amounts of rf quenching at the nominal center and 930 gauss. The latter field lies between the αf and αe peaks, and the value of ϕ_{930} serves to determine the effect of overlap from αe.

Q. ASYMMETRY AND SHIFT CORRECTIONS

79. Asymmetry and Stark Effect Corrections

Although the resonance curves are highly symmetrical there are a number of small effects leading to slight asymmetries which must be allowed for if the level shifts are to be determined to the desired accuracy. These have been listed in Sec. 45 and equations for their calculation given in Part III and Sec. 74. Since the completion of Part III, it was realized that the velocity distribution in the quenching function $G(\psi)$ should have had a v^2 instead of v^3 dependence. This defect will be corrected in connection with later more accurate work. Fortunately, for our purposes, the effect of this error will be negligible except in the case of Stark effect. The correction to S should be reduced by a factor closely approximating one-half, and the calculations of this paper are modified accordingly. There are also somewhat smaller changes in effects of quenching asymmetry, but since these corrections are small, the changes can be neglected here.

The resulting corrections for the case of transition H(αe) at 2195 Mc/sec with $\phi_0 = 31$ percent are given in Table XIV. (There is no overlap correction here, and the β-component correction was made at the earlier stage indicated by Table X.) Each $\Delta\phi$ is the calculated difference in quenching on opposite sides produced by the indicated asymmetry. The corresponding contribution to the expected frequency of the transition is

TABLE XI. Results of run on H(αf) of 7/13/50 based on calculations like those given in Table X for the first two lines of data.

$R_a = 4274.57$ ohm		$R_b = 4958.63$ ohm		$\bar{R}_{ab} = 4616.60$ ohm		
R	ϕ_a	ϕ_b	$\Delta\phi$	$\frac{1}{2}\Delta R$	R_c	δR_c
R_a	20.380					
			2.142	15.84	4632.44	1.35
R_b		22.522				
			1.987	14.69	4631.29	0.20
R_a	20.535					
			1.864	13.78	4630.38	0.71
R_b		22.399				
			1.864	13.78	4630.38	0.71
R_a	20.535					
			1.867	13.81	4630.41	0.68
R_b		22.402				
			1.933	14.29	4630.89	0.20
R_a	20.469					
			1.929	14.26	4630.86	0.23
R_b		22.398				
			2.022	14.95	4631.55	0.46
R_a	20.376					
			1.957	14.47	4631.07	0.02
R_b		22.333				
			1.917	14.17	4630.77	0.32
R_a	20.416					
			1.988	14.70	4631.30	0.21
R_b		22.404				
			2.032	15.03	4631.63	0.54
R_a	20.372					
			1.954	14.45	4631.05	0.04
R_b		22.326				
			1.938	14.33	4630.93	0.16
R_a	20.388					
			2.008	14.85	4631.45	0.36
R_b		22.396				
Average	20.434%	22.398%	1.960%		4631.09 ohm	
Av dev	0.059	0.034	0.056		0.41	
$R/H = 6.577649$ ohm/gauss					$\bar{H}_c = 704.06$ gauss	
					(Av dev) = 0.06 gauss	

TABLE XII. Summary of runs on $\alpha\epsilon$ and $\alpha\zeta$. The table gives separation in gauss of working points, average quenching for these, magnetic field calibration R/H. The measured slopes $d\phi/dH$ are based on relatively little data, since they are needed only for adjusting ϕ_a and ϕ_b to the same level. The calculated quenching and slope values are given for comparison. The columns s_a and s_b give percentages of soft component at the working points, while the last two columns contain average magnetic fields for the various runs together with the average deviations of individual values from these averages.

Date	H_b-H_a gauss	$\bar{\phi}$%	R/H	$d\phi/dH$	s_a%	s_b%	$\bar{H}_\epsilon$ gauss	Av dev
Transition H(α/ϵ) (2195 Mc/sec)								
1/27	114.47	20.87	6.57076	0.3218	...	...	1159.11	0.14
3/17	114.81	21.15	6.55112	0.3463	2.0	1.6	1159.41	0.19
3/23	114.78	20.99	6.55277	0.2932	0.2	0.1	1158.70	0.25
4/28	115.70	20.76	6.55310	0.3162	0.0	0.0	1158.94	0.20
Calculated	115.25	20.92		0.310				
Transition D($\alpha\epsilon$) (2195 Mc/sec)								
2/14	84.20	20.01	6.56792	0.3411	2.7	0.6	1158.73	0.07
2/23	84.15	20.10	6.57110	0.3642	1.3	0.8	1158.71	0.09
5/2	84.25	19.89	6.55256	0.3398	0.6	0.4	1159.07	0.15
Calculated	84.29	19.92		0.343				
Transition D($\alpha\zeta$) (7195 Mc/sec)								
8/14	35.80	22.85	6.58090	0.9154	6.1	5.9	1188.94	0.10
10/19	35.78	22.12	6.58438	0.7552	0.6	0.6	1188.98	0.09
Calculated	35.82	21.66		0.742				

given by

$$\delta F=\Delta\phi\Big/\left(\left|\frac{d\phi}{df}\right|\right). \tag{253}$$

The total correction is $\Delta F=1.34$ Mc/sec and the effect $\Delta\delta$ on the desired level shift δ is just the negative of this.

A summary of such corrections to the frequencies of all five transitions is given in Table XV.

80. Miscellaneous Corrections

For various reasons no temperature corrections were made. The most serious error involved is caused by reversible changes of magnetization of the permanent magnet due to temperature changes during a run. The method contemplated for these corrections was somewhat defective and must be improved in future work. However, the possible order of magnitude of error due to this cause is well below the 0.5 Mc/sec level and is allowed for in the limits of error given for the final results.

Corrections for departure of the frequency standard from 5 Mc/sec are necessary. If the true frequency is $(1+\epsilon)$ times the nominal frequency, then all microwave oscillator frequencies are increased by a factor $(1+\epsilon)$. Such a factor must also be applied to all magnetic fields as they are determined by Eq. (164) in terms of a measured frequency. Because of the near linearity of the Zeeman splitting with magnetic field, all results for δ and $\Delta E-\delta$ must be multiplied by the same factor $(1+\epsilon)$. The correction amounts to about 0.08 Mc/sec for δ and about 0.6 Mc/sec for $\Delta E-\delta$.

The error in field calibration due to the Stark effect produced by distant levels was shown in Sec. 57 to be negligible. Since the calibrations were made at 1613.5 to 1615 Mc/sec, while the crossing point for β and ϵ is now known to be nearer 1610 Mc/sec, there is a slight error in field determination which can be estimated from Eq. (219) (see Fig. 53). This might amount to a correction to δ at most of order 0.1 Mc/sec, and will be neglected. Care will be taken in future work to calibrate much nearer the crossing point. Of course it was not possible to calculate this point exactly until a fairly accurate value for δ was available.

TABLE XIII. Summary of runs on transitions αf. Similar to Table XII except that no soft component is present in beam. Instead, a measure of overlap from the $\alpha\epsilon$ peak is given in columns ϕ_ϵ and $\phi_{\alpha\epsilon}$.

Date	H_b-H_a	$\bar{\phi}$%	R/H	$(d\phi/dH)_a$	ϕ_ϵ%	$\phi_{\alpha\epsilon}$%	$\bar{H}$, gauss	Av dev
Transition H(αf)								
7/10	103.85	21.30	6.56780	0.5238	28.3	5.53	704.26	0.12
7/12	104.04	21.40	6.57522	0.4672	28.3	5.78	704.02	0.11
7/13	104.00	21.42	6.57765	0.4448	28.3	5.82	704.07	0.06
10/27	101.78	21.90	6.58308	0.5160	28.3	5.89	704.53	0.17
Calculated	103.98	22.11		0.558				
Transition D(αf)								
7/14	46.89	23.51	6.57702	0.5909	33.26	3.84	704.32	0.08
8/1	46.83	23.86	6.58754	0.5721	33.19	3.96	704.37	0.07
Calculated	46.84	22.57		0.638				

TABLE XIV. Some details of calculation of theoretical asymmetry and shift corrections for transition H(αe). The theory required has been given in Part III.

Nominal frequency 2195 Mc/sec. Nominal magnetic field of resonance center 1159 gauss.

Constants for undistorted resonance
$a_{\frac{1}{2}}=28.388$, $a_{-\frac{1}{2}}=-28.388$ Mc/sec
$b=49.846$ Mc/sec, $A=0.57918$
Working point frequency $\xi=58.8$ Mc/sec
Calculated quenching $\phi=20.917\%$
Calculated slope $d\phi/d\xi=0.3077\%$/Mc/sec
Distortion due to variation of matrix element
$\phi(+\xi)=21.096\%$, $\phi(-\xi)=20.741\%$
$\Delta\phi=\phi(+\xi)-\phi(-\xi)=0.355\%$
Required correction to shift is $\Delta\delta=-0.577$ Mc/sec
Quenching asymmetry
$\phi(+\xi)=21.528\%$, $\phi(-\xi)=21.478\%$
$\Delta\phi=0.050\%$
$\Delta\delta=-0.081$ Mc/sec
Incomplete Back-Gousdmit effect and Zeeman curvature
$a_{\frac{1}{2}}=29.197$, $a_{-\frac{1}{2}}=-27.579$ Mc/sec
$c_{\frac{1}{2}}=1.020793$, $c_{-\frac{1}{2}}=1.020027$ Mc sec^{-1} gauss^{-1}
$d_{\frac{1}{2}}=3.328\times10^{-4}$, $d_{-\frac{1}{2}}=3.388\times10^{-4}$ Mc sec^{-1} gauss^{-2}
$\phi(h=-57.5)=21.238\%$, $\phi(h=+57.5)=20.675\%$
$\Delta\phi=\phi(-57.5)-\phi(+57.5)=0.563\%$
$\Delta\delta=-0.915$ Mc/sec
Stark effect
$\Delta\delta=0.230$ Mc/sec
Total asymmetry and shift correction to level separation
$\Delta\delta=-1.34$ Mc/sec

A calculation of the effect of contamination of the deuterium by hydrogen and a mass spectroscopic analysis[98] for hydrogen showed that only a negligible error could be due to this cause.

R. RESULTS

81. Quantities Which Can Be Determined

From each run on αe and αf we have now determined a magnetic field H_c. If there were no level shift δ, one could calculate a theoretical frequency $F(H_c)$ from Eqs. (164)–(172) with $y_0=0$. If the actual frequency is f, the level shift is given by $\delta=f-F(H_c)$ to which should be added the correction $\Delta\delta$ from Table XV as well as the miscellaneous corrections of Sec. 80. For the low frequency transitions, the result obtained for δ is highly independent of the assumed value of ΔE. For transition $D(\alpha c)$, however, only the combination $\Delta E-\delta$ is really determined. By using the adopted value of δ it is possible to calculate ΔE and, if Eq. (135) is assumed, to determine a value for the fine structure constant α.

82. Weights Assigned to Data

As will be seen from Table XVI, the average deviation (av dev) for a single run is usually somewhat smaller than the differences in δ obtained from different runs on a given transition. The question arises whether one should give each run an equal weight or should assign weights proportional to the number of lines of data of the run and inversely proportional to (av dev)^2. The correct procedure depends on the kinds of errors which lead to the discrepancies, and these are not known. Fortunately, the results obtained by the two methods differ at most by 0.1 Mc/sec except in case of transition $H(\alpha f)$ where the run of 10/27/50, having a very low weight, accounts for the larger difference. Rather arbitrarily, the first method of assigning weights was adopted.

83. Results

The results are as follows: For hydrogen, the same value for the $2^2S_{\frac{1}{2}}-2^2P_{\frac{1}{2}}$ shift $\delta_H=1058.27$ Mc/sec is obtained from transitions αe and αf. For deuterium, the values of δ_D are 1059.81 and 1059.61, respectively, with average $\delta_D=1059.71$ Mc/sec. The limit of error is conservatively estimated as 1.0 Mc/sec for each isotope. The deuterium-hydrogen difference is $\delta_D-\delta_H=1.44$ Mc/sec with limit of error set also at 1.0 Mc/sec, since it is felt that there should be some cancellation of errors.

Assuming the above value of δ_D, the high frequency transition $D(\alpha c)$ can be used to calculate $\Delta E=10{,}972.11$ Mc/sec with limit of error of 1.0 Mc/sec.

84. Discussion of Results

The agreement between values of δ obtained from transitions αe and αf must be regarded as somewhat fortuitous. Of course, the results would be vitiated if some shift or resonance asymmetry had been omitted from the theory. The likelihood of this may perhaps be judged by comparing the observed and calculated quenching ϕ and slope $d\phi/sH$ values shown in Tables XII and XIII. The agreement is fairly good, but much better for H(αe) and D(αe) than for the other transitions. It is not known whether the discrepancies are of experimental[99] or theoretical origin. More accurate

TABLE XV. Summary of asymmetry and shift corrections to δ for transitions αe and αf, and to $\Delta E-\delta$ for transition D(αc).

Transition	H(αe)	D(αe)	H(αf)	D(αf)	D(αc)
Frequency	2195	2195	2395	2395	7195
Overlap correction	0	0	+0.984	+0.243	0
Matrix element variation	−0.577	−0.381	−0.279	−0.124	−0.156
Quenching asymmetry	−0.081	+0.031	−0.141	+0.015	−0.033
Incomplete Back-Goudsmit effect and Zeeman curvature	−0.915	−0.113	−2.474	−0.150	+0.064
Stark effect	+0.230	+0.115	−0.065	−0.032	+0.012
Forbidden component	0	0	+0.192	0	0
Total correction (Mc/sec)	−1.34	−0.35	−1.78	−0.05	−0.11

[98] This analysis was kindly made for us by Mr. R. Crom of Professor T. I. Taylor's laboratory.

[99] Since transitions αf and αc occur in the fringing region of the rf field, it is possible that magnetic field inhomogeneity (Sec. 38) might contribute to the discrepancies. The indicated limits of error allow for this effect.

measurements now in progress at Columbia may answer the question. Tests of this kind provide an indirect qualitative confirmation of the theory of hyperfine splitting for the $2p$ states.

Taking the above uncertainty and the sizes of the known corrections (as shown in Table XV) into account, it would appear that the values of δ obtained from transitions $(a\varepsilon)$ would be more accurate than δ values obtained from transitions af. Since the corrections are smaller for deuterium than for hydrogen, the shift for the former isotope should be the more accurate of the two.

The difference between the present values for δ and the previously quoted 1062 ± 5 Mc/sec[100] can mostly be attributed to use of an improved theory of the hydrogen atom including effects due to reduced mass and the anomalous magnetic moment of the electron.

When the value of $\Delta E=10{,}972.11$ Mc/sec obtained above for deuterium is compared to the input value 10,970.45 Mc/sec, the following is seen: (a) There is very good evidence for the bulk of the 25.07 Mc/sec contribution to ΔE arising from the anomalous magnetic moment of the electron, and (b) there appears to be a 1.66 Mc/sec discrepancy between observed and input values of ΔE. If the very well-founded theoretical formula (135) for ΔE is assumed, a fractional increase in the value of the fine structure constant α of 76 parts per million (ppm) would be required. The input value for $1/\alpha$ of 137.043 would accordingly emerge as 137.033 with a limit of error of ±0.006. Future work should give considerably better precision, but it is believed that the above represents a significant indication of the need for a thoroughgoing revision of physical constants related to α. Recent discussions by Bearden and Watts[101] and by DuMond and Cohen[102] determine α primarily from the extremely accurate measurements of hyperfine splitting of the ground state of hydrogen by Prodell and Kusch.[103] For this purpose they must use a theoretical formula connecting the hyperfine splitting with α. Radiative corrections to this formula have recently been given by Kroll and Pollock[104] and others[105] which in themselves would lead to $1/\alpha=137.036$, a change by more than seven times the probable error assigned by DuMond and Cohen, and ten times that given by Bearden and Watts. However, additional corrections due to spatial distribution of nuclear magnetism[105,106] and reduced mass effects are still necessary. Until these can be made with confidence, the value of the fine structure constant will be more reliably determined from fine structure than from hyperfine structure. Ultimately, one may hope that α-values determined by the two very different and independent methods will be in agreement.

TABLE XVI. Summary of corrections applied to data to obtain level shifts. All frequencies are in Mc/sec.

Run	H_c (gauss)	δ (apparent)	Frequency correction	Asymmetry and shift correction	δ (final)	Av dev for run
H($a\varepsilon$)						
1/27	1159.11	1059.46	+0.09	−1.34	1058.21	0.14
3/17	1159.41	1059.15	0.08	−1.34	1057.89	0.19
3/23	1158.70	1059.88	0.08	−1.34	1058.62	0.25
4/28	1158.94	1059.62	0.08	−1.34	1058.36	0.20
					Av=1058.27	
H(af)						
7/10	704.26	1059.91	+0.07	−1.78	1058.20	0.23
7/12	704.02	1060.38	0.07	−1.78	1058.67	0.21
7/13	704.07	1060.28	0.07	−1.78	1058.57	0.11
10/27	704.53	1059.38	0.06	−1.78	1057.66	0.32
					Av=1058.27	
D($a\varepsilon$)						
2/14	1158.73	1060.18	+0.09	−0.35	1059.92	0.07
2/23	1158.71	1060.20	0.09	−0.35	1059.94	0.09
5/2	1159.07	1059.83	0.08	−0.35	1059.56	0.15
					Av=1059.81	
D(af)						
7/14	704.32	1059.64	+0.07	−0.05	1059.66	0.15
8/1	704.37	1059.54	0.07	−0.05	1059.56	0.13
					Av=1059.51	
			($\Delta E-\delta$) (apparent)		($\Delta E-\delta$) (final)	
D($a\varepsilon$)						
8/14	1188.94	9911.87	+0.62	−0.11	9912.38	0.23
10/19	1188.98	9911.96	0.56	−0.11	9912.41	0.21
					Av=9912.40	

The value of $\delta_H=1058.27$ Mc/sec for hydrogen differs considerably from the value 1051.41 Mc/sec computed[107] on the basis of second-order quantum electrodynamics. A number of corrections to this have now been calculated. Among these are -0.94 Mc/sec[108] on account of the fourth-order anomalous magnetic moment of the electron, and a calculation by Baranger[109] of contributions to δ of order $Z^5\alpha^6$ amounting to 6.89 Mc/sec. Kroll[108] has found corresponding vacuum polarization terms to be 0.25 Mc/sec. Bersohn, Weneser, and Kroll[110] have estimated the higher order corrections of order $Z^4\alpha^6$ to be in the range 0.25 ± 0.10 Mc/sec.

In order to calculate the resulting level shift for infinite nuclear mass, we must remove the reduced mass

[100] Part II, Sec. 46.
[101] J. A. Bearden and H. M. Watts, Phys. Rev. **81**, 73 (1951).
[102] J. W. M. DuMond and E. R. Cohen, Phys. Rev. **82**, 555 (1951).
[103] A. G. Prodell and P. Kusch, Phys. Rev. **79**, 1009 (1950).
[104] N. M. Kroll and F. Pollock, Phys. Rev. **84**, 594 (1951).
[105] Karplus, Klein, and Schwinger, Phys. Rev. **84**, 597 (1951).
[106] F. E. Low and E. E. Salpeter, Phys. Rev. **83**, 478 (1951).
[107] Bethe, Brown, and Stehn, Phys. Rev. **77**, 370 (1950). This paper is essentially concerned with the calculation of the average atomic excitation energy which enters the logarithm of Eq. (137). The rest of the equation is derived from relativistic calculations by N. M. Kroll and W. E. Lamb, Phys. Rev. **75**, 388 (1949) and by J. B. French and V. F. Weisskopf, Phys. Rev. **75**, 1240 (1949). No detailed calculation of the level shift by the new covariant methods has yet appeared.
[108] N. M. Kroll, private communication.
[109] M. Baranger, Phys. Rev. **84**, 866 (1951). Our earlier result $\delta=1062\pm5$ Mc/sec is misquoted here.
[110] Bersohn, Weneser, and Kroll, Bull. Am. Phys. Soc. **27**, No. 1, 21 (1952).

correction $-\delta/M=-0.575$ Mc/sec assumed by Bethe, Brown, and Stehn[107] for hydrogen. A further correction of 3×76 ppm or $+0.24$ Mc/sec is needed because of the indicated change in value of $1/\alpha$ from 137.043 to 137.033. The result is

$$\delta=1051.41-0.94+6.89+0.25+0.25+0.575+0.24$$
$$=1058.67 \text{ Mc/sec.}$$

This figure cannot be compared with the experimental results for hydrogen and deuterium until it has been corrected for reduced mass effects.

According to indications of present theory, the shifts δ_H and δ_D are related to δ for infinite nuclear mass by equations of the form

$$\begin{aligned}\delta_H&=\delta(1-aM^{-1})+0.08,\\ \delta_D&=\delta(1-\tfrac{1}{2}aM^{-1})+0.74+0.04.\end{aligned}\tag{254}$$

The factors $(1-aM^{-1})$ and $(1-\frac{1}{2}aM^{-1})$ express the form of reduced mass dependence. Bethe, Brown, and Stehn[107] took the coefficient $a=1$. It is known that this proportionality of δ to reduced mass is incorrect. According to an argument of Welton in which δ depends on the probability of finding the electron at the nucleus, one might expect $a=3$. However, there are also radiative contributions from the proton. These are being considered by Gourary[111] and by Salpeter.[112] Since their values for a are not yet final, we shall determine a semi-empirical value from the observed $\delta_D-\delta_H$ difference. The additive constant 0.74 Mc/sec in Eq. (254) represents the effect of finite deuteron size[105,112] (the value 0.45 Mc/sec of Part III, Appendix VI was calculated with a zero-range deuteron wave function.) The remaining terms 0.08 and 0.04 Mc/sec express the reduced mass dependence of the denominator of the argument of Bethe's logarithm. It is assumed that no reduced mass enters the numerator mc^2. No attempt is made to include estimates of possible mesonic effects (Appendix VI b). When the observed difference $\delta_D-\delta_H=1.44$ Mc/sec is inserted into Eqs. (254), one obtains $a=2.58$. With this semi-empirical determination of the reduced mass effect, one finds calculated values $\delta_H=1057.27$ and $\delta_D=1058.71$ Mc/sec. The observed values for δ_H and δ_D are 1.00 Mc/sec larger than these.

It would be premature to claim that this difference represents a real discrepancy between observation and theory. It is quite possible that further calculations on the basis of present quantum electrodynamics will improve the agreement. In view of the surprisingly large magnitude of the Baranger[109] correction, it may be that contributions of order $Z^6\alpha^7$ and higher must yet be calculated in order to make possible a significant comparison between theory and experiment. An experimental test of this conjecture will be possible when more accurate measurements are available for both $Z=1$ and $Z=2$. Any residual deviation might be ascribed to a departure from the Coulomb law for electron and proton. An effect of this sort would arise from the presence of a meson cloud about the nucleus, but according to such estimates as have been made from the theory of the electron neutron interaction (Appendix VI b) would not suffice. On the other hand, the f field considered by Pais[113] would give a contribution for a proton and not for a neutron.

The authors have benefited greatly from many valuable discussions of the theoretical aspects of this work with Professor N. M. Kroll, and of experimental questions with E. S. Dayhoff and S. Triebwasser, who are continuing the measurements.

[111] B. S. Gourary, private communication.
[112] E. E. Salpeter, Bull. Am. Phys. Soc. **27**, No. 1, 20 (1952), and private communication.
[113] A. Pais, Phys. Rev. **68**, 227 (1945); Verh. Kon. Nederland Akad. Wet. Afdel. Natuurk., Sec. 1, **19**, 5 (1947).

Decay of Sr^{85} and Sr^{85m}

A. W. SUNYAR, J. W. MIHELICH, G. SCHARFF-GOLDHABER, AND M. GOLDHABER,
Brookhaven National Laboratory, Upton, New York,*

AND

N. S. WALL AND M. DEUTSCH, *Laboratory for Nuclear Science and Engineering and Department of Physics, Massachusetts Institute of Technology,† Cambridge, Massachusetts*

(Received February 29, 1952)

Sr^{85} (65 day) decays by K-capture to an excited state of Rb^{85} of 513-kev energy. This state is found to have a half-life of (0.9 ± 0.2) μsec. It decays to the ground state of Rb^{85} by an $M2$ transition, identified by its internal conversion coefficient. Sr^{85m} (70 min) decays in three ways: 14 percent by K-capture to an excited state of Rb^{85} of 150 kev, 84.7 percent by an $E3$ transition of 7.5 ± 1 kev followed by an $M1$ transition of 225 kev, and 1.3 percent by an $M4$ crossover transition of 232.5 kev. A decay scheme for Sr^{85}, Rb^{85m}, and Sr^{85m} consistent with shell theory and isomer systematics is given. The existence of large ft values for allowed β-transitions near closed shells is interpreted as due to a rearrangement of nucleons in the even–even core of an odd A nucleus.

I. INTRODUCTION

In its ground state Sr^{85} (65 days) decays[1] by orbital electron capture followed by emission of a 513-kev gamma-ray. No positrons have been observed. An isomeric state of 70-minute half-life has been reported to decay with the emission of two gamma-rays[1] of 152 kev and 233 kev. This even–odd isomer which contains 47 neutrons is one of the systematically occurring isomers[2,3] of odd mass number found just before the number of odd nucleons reaches "magic number" 50. In terms of the strong spin-orbit coupling shell model[4,5] $g_{9/2}$ and $p_{1/2}$ levels are here expected to be adjacent in energy. Isomeric transitions in this region should thus be of the $M4$ type ($\Delta I=4$, yes). This prediction is fulfilled in somewhat less than half the cases. The remainder of the isomeric transitions occurring in the $g_{9/2}$ shell have considerably shorter radiation lifetimes (by factors of 10^5 in some cases) and have been identified[6] as $E3$ transitions ($\Delta I=3$, yes), in apparent contradiction to shell-theoretical expectations. This contradiction has been removed[6,7] by a simple extension of the strong spin-orbit coupling shell model, in which it is assumed that an odd number of nucleons (3, 5, or 7) in $g_{9/2}$ states may couple to form a $7/2+$ state which lies lower in energy than the $g_{9/2}$ state. The isomeric transition then takes place between the $7/2+$ state and the $p_{1/2}$ state and is of the $E3$ type. Whenever the ground state of a nucleus is of the $g_{9/2}$ type, it may occasionally happen that the $7/2+$ state lies intermediate in energy between the $p_{1/2}$ and $g_{9/2}$ states. A two-step isomeric transition then becomes possible, $p_{1/2}\rightarrow 7/2+\rightarrow g_{9/2}$, or the transition may proceed competitively via the crossover $M4$ transition, $p_{1/2}\rightarrow g_{9/2}$. One such example, the isomeric transition in Tc^{99m}, has previously been established.[8]

A number of alternatives had to be considered in the attempts to understand the features of the 70-minute isomeric transition in Sr^{85m}. The isomeric transition may proceed in two steps, or one of the two observed gamma-rays may appear as a result of a competing mode of decay from the isomeric state. One must then decide which gamma-ray is responsible for the lifetime. A comparison of the observed lifetime with the semi-empirical lifetime-energy relation of Goldhaber and Sunyar[6] for $M4$ transitions shows that the 70-minute lifetime is approximately 100 times shorter than expected for an $M4$ transition of 233 kev. If, therefore, we are actually dealing with an $M4$ transition, a competitive process like K-capture must be acting to shorten the lifetime by a large factor. The 152-kev gamma-ray could then be identical with the 149-kev gamma-ray which follows the β-decay from Kr^{85m} and which was identified as a mixed $M1+E2$ transition on the basis of its internal conversion coefficient of 0.051.[9] We also considered the possibility that the isomeric transition is of the $E3$ type, involving a transition between the previously discussed $7/2+$ configuration and a $p_{1/2}$ state, with the 152-kev gamma-ray again appearing in a competitive K-branch. However, when compared to the mean lifetime[6] for all other $E3$ transitions, the Sr^{85m} isomeric transition is slower by a factor of several hundred. When account is taken of the presumed K-branch, the radiative lifetime of the isomeric state is lengthened still further.

A further possibility was that the decay of Sr^{85m} does not involve K-capture, but a two-step isomeric transition between the configurations $p_{1/2}\rightarrow 7/2+\rightarrow g_{9/2}$, with

* Research carried out under contract with the AEC.
† Research supported in part by the joint program of ONR and AEC.

[1] M. Ter-Pogossian and F. T. Porter, Phys. Rev. **81**, 1057 (1951).
[2] E. Feenberg and K. C. Hammack, Phys. Rev. **75**, 1877 (1949).
[3] L. W. Nordheim, Phys. Rev. **75**, 1894 (1949).
[4] M. G. Mayer, Phys. Rev. **78**, 16 (1950).
[5] Haxel, Jensen, and Suess, Z. Physik **128**, 301 (1950).
[6] M. Goldhaber and A. W. Sunyar, Phys. Rev. **83**, 906 (1951).
[7] S. A. Moszkowski, Phys. Rev. **83**, 906 (1951).
[8] Mihelich, Goldhaber, and Wilson, Phys. Rev. **81**, 638 (1951).
[9] I. Bergström and S. Thulin, Phys. Rev. **79**, 537 (1950); I. Bergström, Manne Siegbahn Anniversary volume, Upsala (1951), p. 360.

the 152-kev and the 233-kev gamma-rays emitted in cascade. This situation seemed unlikely for the following reasons: The crossover $M4$ transition would in this case have an energy of 385 kev, which is about the same as that of the isomeric transition in Sr^{87m} (2.7 hr). The remarkable uniformity[6] of the matrix elements of $M4$ transitions makes it appear very likely that the lifetime of such a crossover $M4$ transition in Sr^{85} would be approximately the same as that of Sr^{87m}, since the initial spins would in this case be the same. The 385-kev transition should have been easily observed, unless it was obscured by the presence of Sr^{87m} in the sources used previously. Finally it appeared possible that the 70-minute lifetime is determined by a low energy and as yet unobserved $E3$ transition while the 233-kev gamma-ray is the second step in the cascade. In this case one should also expect the crossover $M4$ transition to occur with an observable intensity. It might have previously escaped detection owing to the fact that the conversion electrons of the 233-kev gamma-ray had not been examined in a spectrometer with sufficient resolution to resolve two close electron groups.

To decide between these possibilities the radiations of Sr^{85m} and Sr^{85} have been studied in detail by various techniques. A unique decay scheme has been established which does involve a complex decay of Sr^{85m} (K-capture, a two-step isomeric transition, as well as a crossover transition). A new short-lived isomer, Rb^{85m}, following K-capture in Sr^{85} has been detected.

II. GROUND-STATE DECAY OF Sr^{85} (65 DAYS)

In order to study the disintegration scheme of the 65-day activity we investigated the coincidences between K x-rays and gamma-rays. The x-rays were detected with an argon-filled proportional counter and single channel pulse-height analyzer. The gamma-rays were detected with a NaI(Tl) scintillation counter and discriminator. By counting coincidences between K x-rays and 513-kev gamma-rays as a function of delay introduced into the x-ray channel, we could establish that the 513-kev state of Rb^{85} is metastable with a half-life of $(9\pm2)\times10^{-7}$ second. By a comparison of the number of 513-kev gamma-rays with the number of x-rays from Sr^{85} we found that substantially all K-capture events lead to the 513-kev state of Rb^{85}.

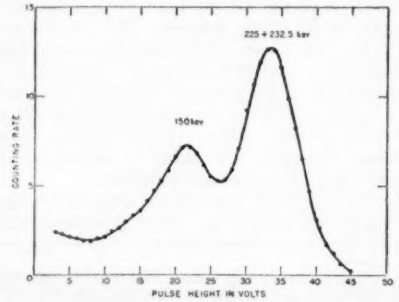

FIG. 1. γ-ray spectrum of Sr^{85m} taken with a scintillation spectrometer [1.4-cm cube NaI(Tl)].

We then measured the internal conversion coefficient of the 513-kev gamma-ray.[10] The result obtained, $\epsilon=(8.1\pm1)\times10^{-3}$, is compatible with either an $M2$ or $E3$ transition,[11] but the measured lifetime excludes an $E3$ transition. The theoretical K conversion coefficient[11] for an $M2$ transition is 6.8×10^{-3}. The empirical K/L ratio curves of Goldhaber and Sunyar[6] indicate that the K/L ratio should be ~9, which leads to a total conversion coefficient of 7.5×10^{-3}. The observed lifetime of 0.9 μsec is slightly higher than the one given by Weisskopf's[12] formula, which yields a value

$$\tau_{M2}(513\text{ kev})=1.6\times10^{-7}\text{ sec.}$$

The conversion coefficient was determined by comparing the number of electrons in the 513-kev line observed in a magnetic lens spectrometer with the number of Rb K x-rays observed in a proportional counter spectrometer. The efficiencies of the two spectrometers for the relevant radiations were calibrated by comparing the corresponding counting rates for Sr^{87m}.

Let N_0 be the number of Sr^{85} atoms decaying per second and $N(e)$ the number of electrons counted in the 500-kev line. $\epsilon=\epsilon_K+\epsilon_L+\cdots$ is the total conversion coefficient and $\eta(e)$ the transmission of the lens spectrometer. Then $N(e)=N_0\epsilon\eta(e)$. Similarly for the x-ray spectrometer, $N(x)=N_0(f_K+\epsilon_K)F\eta(x)$. F is the fluorescence yield for Rb K-shell excitation and f_K is that fraction of electron capture events in which a K electron is captured. Thus $\epsilon=F(f_K+\epsilon_K)N(e)\eta(x)/N(x)\eta(e)$. For Sr^{87m} we denote corresponding quantities with a prime: $N'(e)=N_0'\epsilon'\eta'(e)$ and $N'(x)=N_0'\epsilon_K'F'\eta'(x)$. In this case, of course, observed counting rates must be corrected for decay of the source. Then $N'(x)/N'(e)=(\epsilon_K'/\epsilon')\times F'[\eta'(x)/\eta'(e)]$. Combining this expression with that for ϵ we obtain

$$\epsilon=\frac{N(e)}{N'(e)}\frac{N'(x)}{N(x)}\frac{\epsilon'}{\epsilon_K'}(f_K+\epsilon_K)\frac{F}{F'}\frac{\eta(x)}{\eta'(x)}\frac{\eta'(e)}{\eta(e)}.$$

From the empirical K/L curves[6] we find $\epsilon'/\epsilon_K'=1.15$. We shall not make any serious error if we assume $f_K=0.9$ and $\epsilon_K=0.008$. Thus $(f_K+\epsilon_K)\epsilon'/\epsilon_K'=1.05$. From the standard reference work[13] we find $F/F'=0.97$. The ratio of the x-ray efficiencies involves the prob-

[10] W. S. Emmerich and J. D. Kurbatov [Phys. Rev. **85**, 149 (1952)] have recently come to the same conclusion. In addition, they have found a value of 13 for the K/L ratio of the 513-kev transition. They have measured the internal conversion coefficient of this gamma-ray as 7×10^{-3}. They have been unable to observe K x-ray and gamma-ray coincidences.

[11] Rose, Goertzel, Spinrad, Harr, and Strong, Phys. Rev. **83**, 79 (1951).

[12] V. F. Weisskopf, Phys. Rev. **83**, 1073 (1951).

[13] A. H. Compton and S. K. Allison, *X-Rays in Theory and Experiment* (D. Van Nostrand and Company, Inc., New York, 1935).

ability of absorption in the counter gas and the loss in the counter window. From data in the same work[13] we calculate $\eta(x)/\eta'(x)=1.10$. The transmission of the lens spectrometer is substantially independent of energy so that $\eta'(e)/\eta(e)=1$. Thus finally $\epsilon=1.12N(e)N'(x)/N'(e)N(x)$.

Sr^{85} was prepared by deuteron bombardment of rubidium carbonate in the MIT cyclotron. The target was dissolved in dilute acid and the strontium coprecipitated with lead carrier as carbonate. The lead was removed as sulfide from acid solution and the strontium purified further by repeated precipitation as nitrate from fuming nitric acid, using about 0.5 mg of inactive strontium carrier. Y^{87} (80 hr) was prepared by deuteron bombardment of strontium carbonate, and Sr^{87m} was extracted from it periodically by precipitating the nitrate as in the case of Sr^{85}. Sources of both Sr species were prepared by drying a drop containing the radioactive nitrate in an atmosphere of ammonia. This results in a rather uniform deposit of the hydroxide. The ammonium nitrate formed was destroyed by gentle heating. The sources weighed less than 0.3 mg/cm² and were deposited on mica weighing about 2 mg/cm².

From such sources we obtained $N(e)N'(x)/N'(e)N(x)=7.4\times10^{-3}$, yielding a value for the total conversion coefficient $\epsilon=(8.1\pm1)\times10^{-3}$.

III. DECAY OF Sr^{85m} (70 MIN)

To investigate the radiations from Sr^{85m} this isomer was produced by bombarding Sr^{84} (enriched to 63.7 percent)[14] in the Brookhaven reactor.

We have observed coincidences between K x-rays detected in a proportional counter and gamma-rays detected by a NaI(Tl) scintillation counter. Coincident x-rays characteristic of either Sr or Rb were selected by means of a pulse-height analyzer and critical absorbers. Coincident gamma-ray energies were roughly selected by varying the discrimination level in the scintillation counter. In this manner we could show that the 150-kev gamma-ray but not the 233-kev gamma-ray coincides with K x-rays. The K x-rays coincident with the 150-kev radiation are characteristic of Rb. It is, therefore, clear that the 150-kev radiation appears in a K-electron capture branch from Sr^{85m}, and is very probably the same gamma-ray which is observed to follow β-decay from Kr^{85m}. In the following it will be assumed that these γ-rays are identical.

The intensity ratio of unconverted 233-kev gamma-rays to unconverted 150-kev gamma-rays will yield information about the magnitude of the electron capture branch. This ratio was determined from the pulse-height distribution from a scintillation counter employing a 1.4-cm cube crystal of NaI(Tl). The pulse-height distribution measured with a single channel differential discriminator is shown in Fig. 1. The degree of absorption of the radiations in the crystal was computed from standard reference data.[13] The fraction of the absorbed radiation which appears finally in the photoelectron peak (including multiple Compton effect) was determined by interpolation from experimental data.[15] With these corrections the gamma-ray intensity ratio may be obtained from areas under the photo peaks. This ratio may also be obtained from peak heights of the photoelectron peaks, after additional corrections for variation of the half-width of a photoelectron peak with gamma-ray energy and for change in the relative channel width $\Delta E/E$ with discriminator setting have been made. We obtain the ratio $\gamma_{233}/\gamma_{150}=6\pm2$. This result clearly indicates that the K-branch is relatively small, since the conversion coefficient[9] for the 150-kev gamma-ray is only 0.051. Before the absolute magnitude of the K-branch can be stated, the conversion coefficient for the 233-kev gamma-ray must be determined.

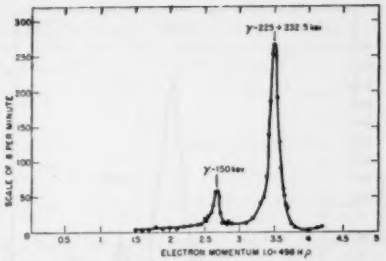

FIG. 2. Internal conversion electrons from Sr^{85m} taken with a lens spectrometer.

This was done by a comparison of the number of conversion electrons from the 150-kev transition with the number of conversion electrons from the 233-kev transition. From the known values of the unconverted gamma-ray intensity ratio and the total conversion coefficient of the 150-kev transition one may then deduce the conversion coefficient for the 233-kev transition. The conversion electron spectrum of the 70-minute activity as measured with a magnetic lens spectrometer is shown in Fig. 2.[16] We obtain a value of 5.0 ± 0.8 for the ratio of the number of conversion electrons of the 233-kev gamma-ray to the number from the 150-kev gamma-ray. If we assume for the moment that the 233-kev transition is simple, this results in a conversion coefficient for the transition of 0.042 which is compatible only with the interpretation that the transition is of an $M1$, $E2$, or mixed $M1+E2$ character. The conversion coefficient is far too small to be compatible with the interpretation that the transition is either an $M4$ or an $E3$ transition. Theoretical K-conversion coefficients[11] for these alternatives are 1.93 and 0.22, respectively, while $\beta_1\sim0.018$ and $\alpha_2\sim0.047$. It is, therefore,

[14] The enriched Sr^{84} was obtained from the Isotopes Division, AEC, Oak Ridge National Laboratory, Oak Ridge, Tennessee.

[15] A. W. Sunyar, unpublished.

[16] We wish to thank Dr. D. E. Alburger for kindly putting his lens spectrometer at our disposal.

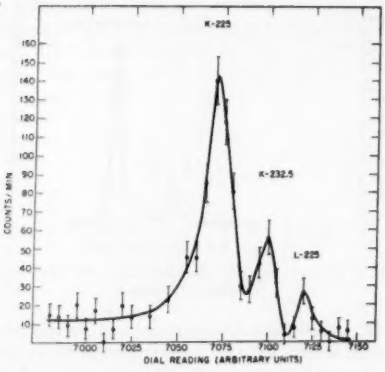

FIG. 3. Internal conversion electrons from Sr^{85m} taken with a 180°-permanent magnet beta-spectrograph and Geiger counter detection. The 225-kev and 232.5-kev transitions are now resolved.

clear that the 233-kev transition cannot be responsible for the 70-minute lifetime.

The approximate value of the conversion coefficient for the 233-kev transition strongly suggests that it is the second step in a $p_{1/2}\rightarrow 7/2+\rightarrow g_{9/2}$ cascade. The energy of the lifetime-determining $p_{1/2}\rightarrow 7/2+$ transition ($E3$) may then be indirectly measured by observation of the crossover $M4$ transition. A search for this transition has been made by examination of the internal conversion electron spectrum of Sr^{85m} in a high resolution, 180° type, fixed magnet spectrograph employing photographic detection. The transition previously called the 233-kev transition was found to be a doublet. K-electron lines of two gamma-rays of 225 and 232.5 kev were observed. The 7.5±1 kev separation of the lines shows that we are not dealing with K and L lines of a single gamma-ray converted in Sr. The 7.5-kev step is accordingly interpreted as the $p_{1/2}\rightarrow 7/2+E3$ transition which is mainly responsible for the 70-minute half-life.

In order to obtain a more reliable intensity ratio of the two K lines than is possible from the weak lines on the film, we have employed detection of electrons with a Geiger counter inside the fixed magnet spectrograph. The Geiger counter with a 1.6-mm entrance slit over the window (2.5 mg/cm² mica) was movable along the film plane by a screw-driven mechanism. The counting rate as a function of position of the Geiger tube along the film plane is shown in Fig. 3. We find that the ratio of the number of K-electrons from the 225-kev gamma-ray to those from the 232.5-kev gamma-ray is 3±1. The K/L ratio for the 225-kev transition is found to be 5.5±2. The K/L ratio expected for the 232.5-kev $M4$ transition from the empirical curve[6] is 5.2. Thus the ratio of the total number of conversion electrons from the 225-kev transition to those from the 232.5-kev transition is also ~3. The number of electrons from the 225-kev transition relative to those from the 150-kev transition then is $5.0\times 3/4=3.75$. The experimentally found ratio $(\gamma_{225}+\gamma_{232.5})/\gamma_{150}=6$ is essentially the ratio $\gamma_{225}/\gamma_{150}$. The total conversion coefficient for the 225-kev transition is $\epsilon_{225}=\epsilon_{150}\times 3.75/6=0.031$. Employing the above K/L ratio we find $\epsilon_K=0.026$ with an estimated uncertainty of a factor of 2. We can, therefore, conclude that the 225-kev transition is either an $M1$, $E2$ or a mixed $M1+E2$ transition. This is in agreement with the interpretation that the transition occurs between a 7/2+ state and a $g_{9/2}$ ground state.

Direct observation of conversion electrons from the lifetime-determining 7.5-kev transition has been attempted by means of absorption measurements in a flow proportional counter. We have observed about 3 times as many soft electrons as can be attributed to the Auger effect. This is below the total number expected by a factor of about 3, a result which can probably be attributed to source absorption effects.

The radiative lifetime for the crossover $M4$ transition may be computed from the available data. Since $\epsilon_K=0.026$ for the 225-kev transition, we have 2.5 K-electrons of this transition appearing for each 100 transitions via the 7.5-kev step, and $2.5/3=0.84$ K-electrons of the 232.5-kev transition. Then the number of crossover transitions $N_c=N_\gamma+N_K+N_L+N_M$. Since $N_\gamma=N_K/\beta_4{}^K=0.84/1.93=0.44$ and $N_L/N_M\sim 3$ for $M4$ transitions, we find $N_c=1.5$ for each 100 transitions of 7.5-kev energy. Similarly, there are 16.5 K-branching events per 100 7.5-kev transitions. This leads to a radiative mean life $\tau_\gamma(232.5\text{ kev})=1.5\times 10^6$ seconds. From the semi-empirical formula[6] for $M4$ transitions for an initial spin of 1/2, the calculated radiative mean life is 1.39×10^6 sec, in good agreement with the observed value.

IV. DISCUSSION

From available experimental data one can now construct a complete disintegration scheme (Fig. 4) involving both ground states and isomeric states of the three isobars Sr^{85}, Rb^{85}, and Kr^{85}. The measured spin and magnetic moment[17] of the ground state of Rb^{85} allow it to be designated as an $f_{5/2}$ state. The spins of Kr^{85m}, Kr^{85} and of the 150-kev state of Rb^{85} have previously been assigned[9] as $p_{1/2}$, $g_{9/2}$ and $p_{3/2}$, respec-

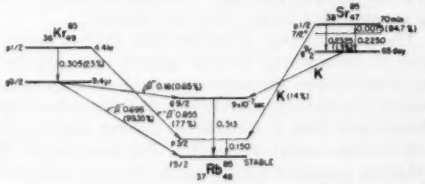

FIG. 4. Proposed disintegration scheme of Kr^{85}, Rb^{85}, and Sr^{85} and their isomers.

[17] National Bureau of Standards Circular 499 (1950).

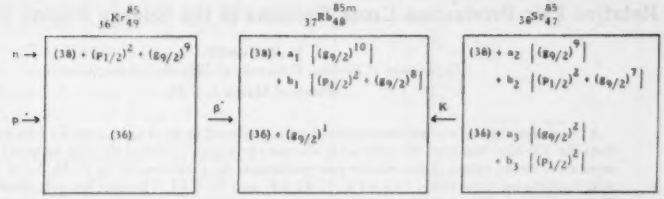

FIG. 5. Suggested neutron and proton configurations for the three isobars Kr^{85}, Rb^{85m}, and Sr^{85}.

tively. We have established that the decay of Sr^{85m} proceeds via a two-step isomeric transition and competitively via the crossover transition between the states $p_{1/2}$, 7/2+ and $g_{9/2}$. The K-capture branch from the isomeric $p_{1/2}$ state of Sr^{85} to the 150-kev state of Rb^{85} is in agreement with the $p_{3/2}$ assignment for the latter state. A search for annihilation radiation was unsuccessful. Positrons, if present, are <15 percent of the K-branch. Using the Feenberg and Trigg curves[18] for the ratio of f_K/f_+ we find a disintegration energy <1.75 Mev for the K-branch. This leads to $ft<10^5$, indicating an allowed transition. For the 65-day Sr^{85} it follows that $ft<5.7\times10^6$, which is also compatible with an allowed transition. The established fact that K-electron capture from the ground state of Sr^{85} does not lead directly to the $f_{5/2}$ ground state of Rb^{85} in any appreciable fraction of the disintegrations, is in agreement with the $g_{9/2}$ designation for the Sr^{85} ground state. Since substantially all such K-capture events lead to the 513-kev excited state of Rb^{85}, and since we have established that the transition to the ground state of Rb^{85} is an $M2$ transition, we must interpret the 513-kev state as a $g_{9/2}$ state. The level assignments from gamma-transitions are thus in excellent agreement with shell-theoretical expectations.

However, an apparent contradiction with beta-theory arises if we consider the beta-emission from Kr^{85}. Zeldes, Ketelle, and Brosi[19] have found that the decay of the ground state of Kr^{85} leads, in 0.65 percent of the disintegrations, to an excited state of Rb^{85}. This state decays by the emission of a 540±20 kev gamma-ray, determined by scintillation spectrometer and absorption techniques. The gamma-ray is in coincidence with the low energy β-group of about 150 kev. We tentatively interpret this gamma-ray as being identical with the 513-kev gamma-ray following K-capture from Sr^{85}, which would, however, imply a slightly higher energy (~180 kev) for the β-rays which precede it.

Our level assignments have an important bearing upon the relation of comparative half-lives in β-decay to the forbiddenness of the β-transition. The ft value for the 150-kev β-transition from Kr^{85} is of the order of 10^9. The transition takes place between the $g_{9/2}$ ground state of Kr^{85} and the $g_{9/2}$ state of Rb^{85m}. Such a β-transition should be allowed. Accordingly, the ft value would be expected to be of the order of 10^5. Nevertheless, in spite of its allowed character, the transition appears to be slowed down by a factor of the order of 10^4. In the following an explanation for the excessively long half-life of this β-transition is attempted.

The possible neutron and proton configurations for Kr^{85}, Rb^{85m}, and Sr^{85} are shown in Fig. 5. The β-transition from $Kr^{85}\rightarrow Rb^{85m}$ changes a $g_{9/2}$ neutron into a $g_{9/2}$ proton. To the two possibilities for the final neutron configuration of Rb^{85m} are attached probability coefficients "a" and "b". A value of unity for the coefficient b_3 should make the transition proceed as a normal allowed transition. The fact that the transition probability is reduced by a factor of the order of 10^4 is interpreted as evidence that 10 neutrons in $g_{9/2}$ states form a particularly stable configuration preferred to the other possible configuration $(p_{1/2})^2+(g_{9/2})^8$. If the coefficient a_3 were exactly one, the β-transition could not take place, except as a multiple particle transition. The fact that the transition proceeds with $ft\simeq10^9$ indicates that $b\simeq10^{-4}$. The neutron configuration of Rb^{85m} is thus a remarkably pure configuration containing $10g_{9/2}$ neutrons, with an extremely small admixture ($\sim10^{-4}$) of a configuration involving $2p_{1/2}$ neutrons and $8g_{9/2}$ neutrons. Similar shell rearrangements appear to be responsible for large ft values observed in other cases (Zr^{89} and Zr^{89m},[20,21] Y^{87} and Y^{87m}[22]).

[18] E. Feenberg and G. Trigg, Revs. Modern Phys. **22**, 399 (1950).
[19] Zeldes, Ketelle, and Brosi, Phys. Rev. **79**, 901 (1950).
[20] Goldhaber, der Mateosian, Scharff-Goldhaber, Sunyar, Deutsch, and Wall, Phys. Rev. **83**, 661 (1951).
[21] Shore, Bendel, and Becker, Phys. Rev. **83**, 688 (1951).
[22] L. G. Mann and P. Axel, Phys. Rev. **84**, 221 (1951).

Relative Pair Production Cross Sections in the Energy Region 50 to 300 Mev*

C. R. EMIGH†
Department of Physics, University of Illinois, Urbana, Illinois
(Received March 3, 1952)

A cloud-chamber survey has been made of pairs produced in Al, Ag, Au, and Th foils by an x-ray beam from the 300-Mev betatron. By comparing the pairs produced in two of the foils mounted to intercept the same x-ray beam, values of the relative pair production cross sections for Ag to Al, Au to Al, and Th to Al were found to be, respectively, (3.4±1.4), (7.9±1.5), and (11.7±1.7) percent low compared with the Bethe-Heitler theory predictions. The results are consistent with a correction factor to the theoretical pair cross section given by $[1-(1.4\pm0.1)10^{-4}Z^2]$. The calculated number of Compton electrons between 50 and 200 Mev expected from the Al foil is 1201, from the Ag foil is 355, and from the Au foil is 113. The observed numbers with statistical errors indicated are, respectively. 1170±40, 354±30, and 70±18.

INTRODUCTION

THE Bethe-Heitler theory[1] for pair production in the field of the nucleus, the Wheeler-Lamb theory[2] for pair production in the field of the atomic orbital electrons, and the Klein-Nishina equation[3] for the Compton scattering are generally used in accounting for the absorption of gamma-rays for energies much larger than mc^2. It is sometimes necessary to take into account the absorption caused by photonuclear disintegration and the photoelectric effect. The usual methods for studying the absorption of gamma-rays are measurement of the beam intensity before and after its passage through an absorber and measurement of the beam intensity alternately with and without an absorber placed in the beam between the source of gamma-rays and the detector. It has been well established by such experiments that the absorption coefficients for the heavy elements are low compared with the values predicted by the above theories. This discrepancy has been blamed on the failure of the Born approximation in the development of the pair production theory when applied to the heavy elements. It is the purpose of this experiment to measure unambiguously the Z dependence of the pair production cross section. In addition, by measuring the energies of the pair members, the cross sections for the distribution of energy between the pair members are studied for Al, Ag, and Au.

Using the information obtained from the pair spectrum observed, the quantum spectrum from the 300-Mev betatron is calculated and compared with the quantum spectrum which one might expect from the thick W target of the betatron. Also, by using the calculated quantum spectrum, the energy distribution of the Compton electrons as calculated by the Klein-Nishina formula is compared with the observed Compton electron spectrum.

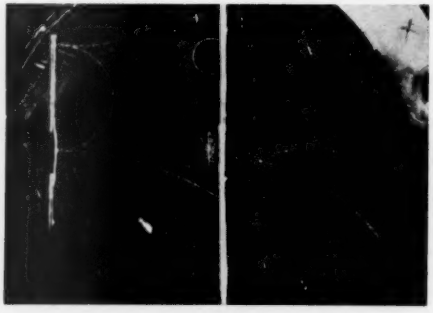

FIG. 1. Photograph of the cloud chamber showing pairs created in Au and Al foils by a beam of photons traversing the chamber from left to right. Note Pb absorbers on which the foils were mounted.

THE EXPERIMENT

The foil arrangement was such that two foils of different atomic numbers were placed parallel to one another and spaced 14 cm apart in a 35-cm cloud chamber. A horizontal x-ray beam from the betatron entered the chamber through a 5-mil Al window and passed through both foils, thus making sure that the quantum spectrum for each foil was practically the same. The foils were approximately 1 inch high and 1½ inches long. Their thicknesses were 0.6295±0.0005, 0.2844±0.004, 0.1008±0.0001, and 0.1274±0.0002 grams per cm², respectively, for Al, Ag, Au, and Th. They were mounted by small pieces of black Scotch electrical tape on Pb foil frames which were 1 inch high, ⅛ inch thick and extended completely across the chamber, except for a 1½ inch gap where the foils were mounted in the beam. These Pb absorbers degraded the energy of any pair member whose energy was low enough to curve around and hit one of the absorbers. This prevented the particles from forming tracks which would have been complete circles, obliterating the origin of the pair. A clear origin was necessary to determine with certainty the two tracks which constitute a

* This work was assisted in part by the joint program of the ONR and AEC.
† Now at Los Alamos Scientific Laboratory, Los Alamos, New Mexico.
[1] H. Bethe and W. Heitler, Proc. Roy. Soc. (London) **A146**, 83 (1934).
[2] J. Wheeler and W. Lamb, Phys. Rev. **55**, 858 (1939).
[3] O. Klein and Y. Nishina, Z. Physik **52**, 852 (1929).

pair. Figure 1 is a photograph showing a pair created in the Au foil (left) and a pair created in the Al foil. The tracks which are deflected up are made by electrons.

The experiment was divided into two parts. In the first part two foils of different Z's were placed in the chamber. The ratio of the number of pairs of total energy greater than 50 Mev produced in one foil to those produced in the other was determined. The direct ratios for Au to Al, Ag to Al, and Au to Ag were obtained by successive cloud chamber runs. An indirect ratio for Au to Al was determined from the Ag to Al and Au to Ag ratios. The final ratio of Au to Al was calculated by a statistically weighted average of the direct and indirect ratios. In a similar manner, the ratio for Ag to Al was determined.

The second part of the experiment was to determine the ratio for Th to Al. This was done by the direct method only. The Th was wrapped in a thin sheet of Al to absorb the emitted alpha-particles and very low energy beta-particles which would otherwise obliterate the origin of the pairs. The Al shield required a correction of about 10 percent to be made on the number of pairs observed from the shielded Th.

In order to eliminate any systematic error in measuring the radii of curvature due to the relative positions of the foils and also to compensate for the almost negligible degradation of the x-ray beam through the first foil, the foils were interchanged in position. Approximately an equal number of pairs was measured in each position. The foil thicknesses were chosen to produce about the same number of pairs when bombarded by the same x-ray beam.

The apparatus alignment is shown in Fig. 2. The chamber was placed directly in the x-ray beam at about 7 meters from the betatron target. Because the lighted region of the cloud chamber was only an inch deep, an x-ray beam $\frac{1}{4}$ inch high at the foil was used. The width of the x-ray beam at the foil was approximately $\frac{3}{4}$ inch long. The collimation of the beam was obtained primarily by a 12-inch long, 4-inch square lead brick containing a vertically and horizontally tapered slot. The collimator was placed at about 3 meters from the betatron target and the taper of the slot was matched to the divergence of the beam. A crotch collimator was used to restrict the size of the beam coming out of the betatron crotch and with a secondary collimator reduced the background in the chamber caused by scattered secondary electrons and photons. As the betatron target did not appear to act as a point source, the crotch collimator also helped to define the beam at the foils by reducing the apparent size of the target. Behind the collimation system at about 4 meters a large magnet with a 5000-gauss field was used to sweep out all electrons and positrons which were produced by the beam in coming through the collimation system.

The pulse lights and cameras were arranged so that the illumination used to expose the film was the light

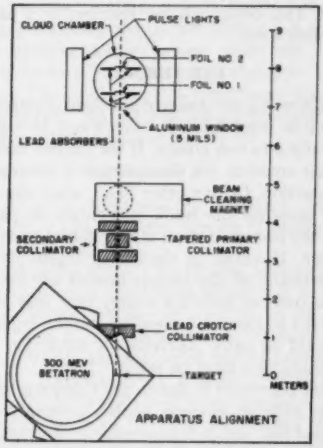

FIG. 2. The collimation scheme for obtaining a small beam in the chamber.

which was scattered by the track droplets through an angle of approximately 90 degrees from the incident light. The pulse lights were mounted and collimated so as to give a horizontal light beam 1 inch high, of the same width as the chamber, and which illuminated the region between the foils and absorbers without forming any shadows. The camera shutters were always open and the amount of illumination used for proper exposure was determined by the intensity of the light from the flash tubes.

Operational time sequencing of the cloud-chamber functions, the operation of a diesel-driven generator which supplied a pulsed field for the cloud chamber, and the operation of the betatron were controlled by a magnetic pulse time delay circuit.[4] The cloud chamber was expanded when the magnetic field reached its maximum value of $10{,}000 \pm 100$ gauss. The betatron was triggered 0.04 second later. The track droplets were allowed to grow for approximately 0.15 second. After this time had elapsed the pulse lights were triggered and the film exposed. The chamber was compressed 0.01 second after the pictures were taken, thus readying the chamber for the next expansion. At this same time the camera motors were operated to advance the 35-mm film one frame. This sequence had a cycle time of 10 seconds.

The analyzing consisted of measuring the radii of curvature of all the electron and positron tracks which were photographed. Using the radius of curvature and the relativistic equation for the motion of an electron in a magnetic field, the total energy of each pair member was determined. A special curvature measuring device enabling a very rapid accumulation of good statistics

[4] C. R. Emigh, Rev. Sci. Instr. **21**, 142 (1950).

was used. This device will be described in a paper to be published later.

THE THEORY

The pairs which are observed in a cloud chamber when a thin foil is bombarded by x-rays can be separated theoretically into two groups. If the nucleus takes part in the pair creation, the phenomenon is referred to as pair production. On the other hand, when the orbital electron takes up the recoil momentum of pair production, the process is more often referred to as triplet production. However, in the energy region 50 to 300 Mev practically all the triplets formed will have their recoil electrons of such low energy that they will not be observed in the cloud chamber and the triplets will be analyzed as pairs. Therefore, a correction due to triplet production must be made.

Another correction is due to the Compton effect. In this case only an electron is seen coming from the bombarded foil, and it is impossible to distinguish this Compton electron from a pair whose positron has such a low energy that it is not observed in the cloud chamber. However, the number of pairs of this type can be estimated from the number of pairs in which the electron has such a low energy that only the positron is observed. Therefore, it is possible to make a comparison between the experimental and theoretical Compton cross sections. The following sections outline the three theories—pair production, triplet production, and the Compton effect—in a manner which is most useful in the analysis of the pair production data.

The theory of pair production which takes into account the screening of the nucleus by the orbital electrons was published by Bethe and Heitler in 1934. Their theory is based on a first-order Born approximation. The condition for the applicability of the Born approximation is that $(Z/137)\ll(v_1/c)$ and $(Z/137)\ll(v_2/c)$, where v_1 and v_2 are the velocities of the electron and the positron, respectively. For energies greater than mc^2 this condition is probably satisfied for Al. For the heavier elements, such as Ag, Au, and Th, the condition is not fulfilled. However, the condition for validity, although sufficient, may be a much too stringent one, because even for the heaviest elements the correction to the theory is only of the order of 10 percent.

Bethe and Heitler consider the screening effect of the orbital electrons by assuming a Fermi-Thomas distribution of the atomic electrons. Their calculations show that screening is very important for energies greater than 15 Mev. Because the Fermi-Thomas electron density distribution function leads to a numerical integration, the cross section for pair creation is given only numerically. A convenient form for the cross section, $\phi_p(E_1)$, for the creation of a pair whose electron has an energy in the range E_1 to E_1+dE_1, and for an incident quantum whose energy is k_0, is given by the relation

$$\phi_p(E_1)dE_1=\frac{Z^2e^4dE_1}{137(mc^2)^2k_0^3}\left\{(E_1^2+E_2^2)\left[\phi_1(\gamma)-\frac{4}{3}\ln Z\right]+\frac{2}{3}E_1E_2\left[\phi_2(\gamma)-\frac{4}{3}\ln Z\right]\right\}, \quad (1)$$

where $\phi_1(\gamma)$ and $\phi_2(\gamma)$ are given graphically by Bethe and Heitler as functions of $\gamma=100\ mc^2k_0/E_1E_2Z^{\frac{1}{3}}$. The total integral cross sections are obtained by graphical integrations of the above expression.

The triplet production cross section which includes the effects of screening is given by Wheeler and Lamb. The results of their calculations for the cross section per atom, $\phi_t(E_1)$, for the creation of a pair whose electron has an energy in the range E_1 to E_1+dE_1, when the primary quantum energy is k_0 is given by the relation

$$\phi_t(E_1)dE_1=\frac{Ze^4dE_1}{137(mc^2)^2k_0^3}\left\{(E_1^2+E_2^2)\left[\psi_1(\epsilon)-\frac{8}{3}\ln Z\right]+\frac{2}{3}E_1E_2\left[\psi_2(\epsilon)-\frac{8}{3}\ln Z\right]\right\}, \quad (2)$$

where $\psi_1(\epsilon)$ and $\psi_2(\epsilon)$ are given graphically as functions of $\epsilon=100\ mc^2k_0/E_1E_2Z^{\frac{1}{3}}$.

The cross section for both pair production and triplet production can be expressed in the following form:

$$\phi_p(E_1)+\phi_t(E_1)=\phi_p(E_1)[1+\phi_t(E_1)/\phi_p(E_1)]. \quad (3)$$

The fraction $\phi_t(E_1)/\phi_p(E_1)$ is small compared with 1 for $Z>13$ and to the degree of accuracy for which this experiment is designed, we are justified in equating the numerical functions $\phi_1(\gamma)$ to $\phi_2(\gamma)$ in Eq. (1) and $\psi_1(\epsilon)$ to $\psi_2(\epsilon)$ in (2). The term $\phi_t(E_1)/\phi_p(E_1)$ reduces to $[\psi_1(\epsilon)-(8/3)\ln Z]/[Z\phi_1(\gamma)-(4/3)\ln Z]$. This term is practically independent of the sharing ratio E_1/k_0, and the incident quantum energy k_0, and it varies as $1/Z$. The average value for this term is $1.1/Z$ in the energy range 50 to 300 Mev. The cross section for both pair production and triplet production becomes

$$\phi_p(E_1)+\phi_t(E_1)=\phi_p(E_1)[1+1.1/Z]. \quad (4)$$

The Compton effect contributes an appreciable number of tracks observed in the cloud chamber when a foil is bombarded by x-rays. The number of Compton electrons which one expects to observe in a certain energy region E_1 to E_2 is dependent upon the intensity of the incident spectrum for all energies of the primary quanta greater than E_1. In order to calculate this number, the Klein-Nishina formula is used. The differential cross section per atom can be expressed in terms of the scattered quantum, k, for values of primary

radiation $k_0 > 50$ Mev as follows:

$$\frac{Zd\sigma_c}{\tilde{\phi}} = \frac{137\pi}{a}\left[\frac{k_0}{k} + \frac{k}{k_0}\right]\frac{dk}{k_0}; \quad \tilde{\phi} = Z^2 r_0/137, \quad a = k_0/mc^2. \tag{5}$$

Because the pair electrons and the Compton electrons have been analyzed into energy bins which are 10 Mev wide the next step is to calculate the cross section per atom for Compton scattering of the electron into the energy bin, E_1 to E_2, due to an incident quantum whose energy is greater than E_1. Integrating the expression (5) we obtain

$$\frac{Z\sigma_c}{\tilde{\phi}} = \frac{137\pi}{a}\left[\ln k + \frac{1}{2}\left(\frac{k}{k_0}\right)^2\right]_{k_1}^{k_2}. \tag{6}$$

We consider first the cross section per atom, σ_c', for producing a Compton electron whose total energy lies in the range, E_1 to E_2, due to an incident quantum whose energy, k_0, is such that $E_1 \leqslant k_0 \leqslant E_2$. From the Compton formula for the frequency shift of the scattered radiation the minimum value for the scattered quantum, k_1, is given to a very good approximation by $k_0/2a$. The maximum value from energy conservation is $k_2 = k_0 - E_1 + mc^2$. Making these substitutions for the limits of the relation (6) and noting that the term $\frac{1}{2}(k/k_0)^2$ contributes practically nothing, we obtain

$$\frac{Z\sigma_c'}{\tilde{\phi}} = \frac{137\pi}{a}\ln\left\{2a\left[\frac{k_0 - E_1 + mc^2}{k_0}\right]\right\}. \tag{7}$$

Next consider the cross section, σ_c'', for producing a Compton electron whose total energy lies in the range, E_1 to E_2, resulting from an incident quantum $k_0 > E_2$. From energy conservation $k_1 = k_0 - E_1 + mc^2$ and $k_2 = k_0 - E_2 + mc^2$. Making these substitutions into (6) we obtain

$$\frac{Z\sigma_c''}{\tilde{\phi}} = \frac{-137\pi}{a}\left\{\ln\left(\frac{k_0 - E_2 + mc^2}{k_0 - E_1 + mc^2}\right) + \frac{1}{2}\left[\frac{k_0 - E_2 + mc^2}{k_0} - \frac{k_0 - E_1 + mc^2}{k_0}\right]\right\}. \tag{8}$$

In order to calculate the number of Compton electrons expected in a bin E_1 to E_2, we must know, in addition to the cross sections σ_c' and σ_c'', the quantum spectrum in the energy range 50 to 300 Mev. The only information on this spectrum is the number of pairs recorded in each bin. By using the pair data obtained and dividing the number of pairs in each bin by the pair production cross section for that energy, an accurate estimate of the quantum spectrum is obtained. The pair cross sections are corrected for the discrepancies observed in this experiment. However, as the spectrum of the incident quanta is not constant across the 10-Mev wide bin, E_3 to E_4, we make the assumption that its variation across the bin is proportional to $1/k_0$. This is a reasonable assumption, as the spectrum is generated by the bremsstrahlung process when the betatron target is bombarded by a mono-energetic beam of electrons. The results of this experiment also justify the assumption. Stating this assumption mathematically the number of quanta is given by

$$dN = (A/k_0)dk_0, \tag{9}$$

where A is a normalization constant equal to $N_3/\ln(E_4/E_3)$, and N_3 is the number of quanta calculated for the bin E_3 to E_4.

By multiplying Eq. (7) by (9) and integrating over k_0 a new function, ϕ_c', is defined as the cross section per atom for finding a Compton electron in the energy interval, E_1 to E_2, due to quanta in the same energy interval, provided the number of quanta varies as $1/k_0$ across that energy interval. Also by multiplying Eq. (8) by (9) and integrating over k_0, we can define another new function, ϕ_c'', as the cross section per atom for finding a Compton electron in the energy interval, E_1 to E_2, due to quanta in the energy interval, E_3 to E_4, provided the number of quanta varies as $1/k_0$ across the energy interval, E_3 to E_4, and where $E_3 \geqslant E_2$. The integral expressions for ϕ_c' and ϕ_c'' are

$$\phi_c' = \int_{E_1}^{E_2} \frac{\sigma_c' dk_0}{\ln(E_2/E_1)k_0}; \quad \phi_c'' = \int_{E_3}^{E_4} \frac{\sigma_c'' dk_0}{\ln(E_4/E_3)k_0}. \tag{10}$$

These expressions have been normalized to a single incident quantum. The integrations are rather long but straightforward.

Assuming the corrected pair and triplet cross sections are valid, the number of Compton electrons expected in any single energy bin, i, due to quanta in the same bin plus those due to quanta in all the higher energy bins, is given by the relation

$$N_c(i) = \frac{N_p(i)\phi_c'}{\phi_p(i)} + \sum_{j=i+1}^{26} \frac{N_p(j)\phi_c''(j)}{\phi_p(j)}, \tag{11}$$

where $N_c(i)$ is the number of Compton electrons in bin i, $N_p(i)$ is the number of pairs (including triplets) in bin i, ϕ_c' and ϕ_c'' are the Compton cross sections previously derived, and $\phi_p(i)$ is the average pair-plus-triplet cross section for the bin i. The running index, i, indicates the number of the bin on an increasing energy scale, 50 to 60 Mev is bin 1, 60 to 70 Mev is bin 2, and so forth up to bin 26. As $N_p(i)$ is not known exactly, only the total number of pairs-plus-triplets, plus Compton electrons are observed, Eq. (11) can be written

$$N_c(i) = \frac{N_T(i)F'(i)}{1+F'(i)} + \frac{1}{1+F'(i)}\sum_{j=i+1}^{26} N_p(j)F''(j), \tag{12}$$

where $N_T(i) = N_p(i) + N_c(i)$, $F'(i)$ is the ratio of the Compton cross section to the pair-plus-triplet cross section for the bin i, and $F''(j)$ is the same for the bin j.

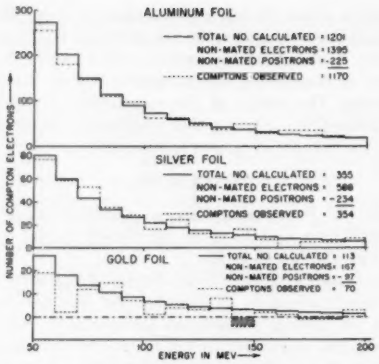

FIG. 3. Histogram showing both the calculated and observed number of Compton electrons from the Al, Ag, and Au foils.

This is the form of the relation used in computing the expected Compton spectra from the Al, Ag, and Au foils. Although the quantities $N_p(j)$'s are not known to start with, they can be found by calculating the $N_c(i)$'s in the order of i_{max} to $i=1$. The $N_p(i)$ can be calculated from the relation $N_T=N_p(i)+N_c(i)$, and the resulting $N_p(i)$ becomes one of the $N_p(j)$'s for the next calculation.

THE RESULTS

The data compiled by analyzing 46,592 pairs can be summarized in several ways. Each way is designed to compare most easily the experimental results with certain features of the theory of gamma-ray absorption. The interesting features of the theory investigated in this experiment are the Compton effect, the energy sharing in pair creation, and the Z dependence on the pair production cross section.

Using all the data from the Al foil, the calculated number of Compton electrons which one might expect in each 10-Mev wide bin is obtained by applying formula (12). This assumes that the pair and triplet cross sections for Al are given accurately by the Bethe-Heitler and the Wheeler-Lamb theories, respectively. A direct comparison between the calculated number of Compton electrons expected in each bin can be made if it is assumed that in a given energy bin the number of pairs in which only the positron is observed is equal to the number of pairs in which only the electron is observed. Then the observed number of Compton electrons can be obtained by subtracting the number of nonmated positrons observed from the number of nonmated electrons observed. The results of these calculations are shown by the histograms in Fig. 3. In the case of Ag and Au, the pair cross sections used in formula (12) for the calculations of the number of Compton electrons expected in each bin are corrected for the observed low values. For Al and Ag the calculated and observed values are in agreement within the statistical errors. For the case of Au the observed values seem low. The shaded portions in the histogram for Au indicate that more nonmated positrons than nonmated electrons were observed in those bins. A possible explanation for the low values observed for Au is that the Born approximation is not quite valid and therefore an asymmetry in the electron-positron energy distribution curve might be expected in the end regions. If we consider that the low energy electron is attracted to the nucleus while a low energy positron is repelled, then more nonmated positrons than nonmated electrons should be observed. A correction for this asymmetry would have the effect of bringing up the values of observed Compton electrons.

The data from all the experimental runs for each element are plotted in the histograms of Fig. 4 according to the distribution of energy between the pair members (these data include triplets). The data are divided into bins of approximately the same number of pairs: 50 to 100 Mev, 100 to 150 Mev, and 150 to 300 Mev. The calculated numbers of Compton electrons are indicated. For comparison, the Bethe-Heitler and Wheeler-Lamb theoretical curve is plotted for the distribution calculated by using the average energy of the incident quanta intensity for each bin. The theoretical curve is normalized by making the area under it equal to the area under the experimental pair distribution histogram. The relative agreement with the theory is within the statistical errors.

The observed number of pairs-plus-triplets-plus-Compton electrons, $N_e(Z)$, for each foil is corrected for the Compton electrons and triplets. The resulting number of pairs, $N_p(z)$, is normalized to one atom to give the cross section multiplied by the incident number

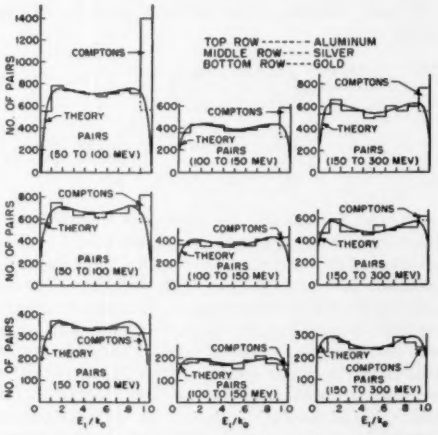

FIG. 4. Theoretical curves and experimentally observed histograms for the energy distribution among the pair members created in the Al, Ag, and Au foils.

of quanta per cm², $\phi_p(Z)N(k_0)$. As $N(k_0)$ is the same for each foil used in a particular experimental run, the ratio of the normalized $N_p(Z)$'s is a measure of the relative pair production cross section. The results of these calculations are shown in Fig. 5 for Au to Al, Ag to Al, and Th to Al. The data are divided into energy bins of approximately the same number of pairs. The cross sections are expressed in units of $Z^2r_0/137$. The Bethe-Heitler theoretical ratios are also plotted. For Th a correction was made for the pairs formed in the thin Al shield. The apparent energy dependence of the relative pair production cross sections for Th to Al, as shown by the dotted lines in Fig. 5 is probably not real. It is possible that the errors due to the bin edge resolution in making a measurement of the pair energy and the human error in making a wrong choice of pair members (only in the case of Th where the origin was sometimes obscured by the emitted beta-particles) could account for the effect. However, most errors of these types are canceled out when the pairs are counted in an over-all bin, 50 to 300 Mev. (See the solid line in Fig. 5 for Th to Al.)

By comparing the relative pair production cross sections obtained from the experiment for each 10-Mev bin with those predicted by the Bethe-Heitler theory, and calculating the weighted average (weighted according to the number of pairs in each bin) of all the bins from 50 to 300 Mev, the relative pair production cross sections for Ag to Al, for Au to Al, and for Th to Al are found to be, respectively, (3.4 ± 1.4), (7.9 ± 1.5), and (11.7 ± 1.7) percent low compared with the values predicted by the Bethe-Heitler theory.

From all the data on pairs produced in the Al foil we can find the quantum spectrum from the 300-Mev betatron's 0.02-inch W target. The theoretical cross sections for Al were used in the calculations. The results are shown in Fig. 6. The theoretical curve for comparison was calculated by Professor Walter Aron

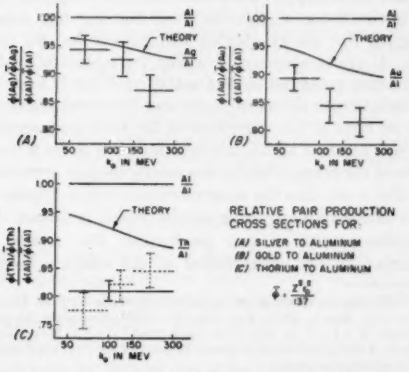

FIG. 5. Comparison of the calculated relative pair production cross sections with the experimentally observed values.

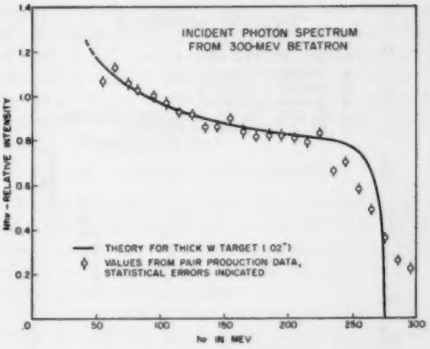
INCIDENT PHOTON SPECTRUM FROM 300-MEV BETATRON
$h\nu$ - RELATIVE INTENSITY
THEORY FOR THICK W TARGET (.02")
VALUES FROM PAIR PRODUCTION DATA, STATISTICAL ERRORS INDICATED
$h\nu$ IN MEV

FIG. 6. Comparison of the thick target theoretical bremsstrahlung to the experimental points.

of the University of California. The calculated curve shown by Aron was for a 0.02-inch Pt target; however, the shape of the curve should be practically the same for a W target. The spectrum is in excellent agreement with the thick target calculations of Aron. The discrepancy at the high energy end of the curve is due primarily to the fact that no attempt was made during the experiment to hold the maximum energy of the betatron at a given value. Its average value was around 275 Mev. The fluctuation has practically no effect on the low energy portion of the curve.

COMPARISON WITH OTHER EXPERIMENTS

Several experiments have been reported in the literature on the absorption coefficient in the energy range 10 to 300 Mev. Dewire, Ashkin, and Beach[5] have measured the transmission through several different elements of a 280-Mev photon beam from the Cornell Synchrotron using an electron pair spectrometer. Lawson,[6] also using a pair spectrometer, measured the absorption coefficient of several elements for an 88-Mev photon beam from the G-E 100-Mev betatron. Their experimental results are compared with the theories of Bethe-Heitler for pair production in the field of the nucleus, of Wheeler-Lamb for the pairs produced in the field of the atomic electrons, and with the Klein-Nishina formula for the Compton scattering. The gamma-ray absorption cross section measurements at 17.6 Mev obtained by Walker,[7] also using a magnetic pair spectrometer, are plotted in Fig. 7 along with the results of Dewire *et al.*, and Lawson. In this case the theoretical cross section includes a small contribution from the atomic photoelectric effect in the lead absorber. This correction only amounts to a factor of 0.7 percent in the total cross section. Walker uses the results of Borsellino,[8] who gives the ratio of the pair cross section

[5] Dewire, Ashkin, and Beach, Phys. Rev. **82**, 447 (1951).
[6] J. L. Lawson, Phys. Rev. **75**, 433 (1949).
[7] R. L. Walker, Phys. Rev. **76**, 527 (1949).
[8] A Borsellino, Helv. Phys. Acta **20**, 136 (1947).

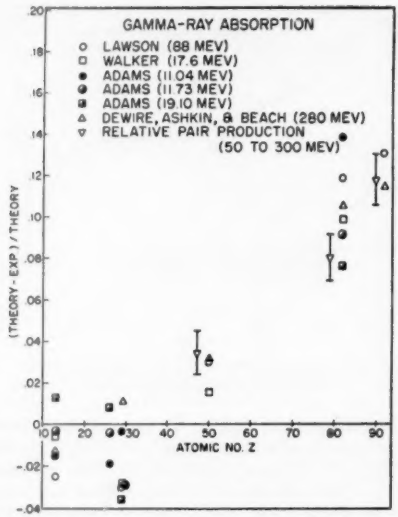

FIG. 7. A presentation of the gamma-ray absorption discrepancy between theory and experiment as found by several experimenters. Relative pair production discrepancies are also shown for comparison.

for an electron to that of a proton. However, the difference between Borsellino's results and those of Wheeler and Lamb should not make much difference in the total theoretical cross section used by Walker.

Adams[9] has measured the absorption of quanta between 11 and 20 Mev using the x-rays from the 22-Mev University of Illinois betatron. Copper, iron, and carbon threshold detectors were used to measure the absorption coefficient at energies of 11.04, 13.73, and 19.10 Mev, respectively. In comparing his results with the theory, Adams uses the modified Bethe-Heitler theory to account for pair production in the field of the atomic nucleus and its surrounding electrons by replacing Z^2 by $Z(Z+1)$, which is essentially the same as that given by the Bethe-Heitler theory and the more exact calculations by Wheeler and Lamb. He also used the form of the Bethe-Heitler theory which assumes no screening. No account is taken of the atomic photoelectric effect in the heavier elements, or the photoneutron effect in the lighter elements. The results of his experiment are also plotted in Fig. 7.

Figure 7 gives a comparative view of all the reliable data on gamma-ray absorption published to date. There is a consistent agreement among all the data presented that the total absorption cross section for the heavy elements are less than that predicted by theory. In the region of Pb the discrepancy from absorption measurements is of the order of 10 percent. The experimental discrepancy found in this experiment is (3.4 $\pm$1.4) percent for the relative pair production between Ag and Al, (7.9$\pm$1.5) percent between Au and Al, and (11.7$\pm$1.5) percent between Th and Al. If we assume that the pair and triplet production cross sections are given correctly for Al by the Bethe-Heitler and Wheeler-Lamb theories, respectively, then the experimental discrepancies found in this experiment can be compared with the discrepancies found from absorption experiments.

[9] G. D. Adams, Phys. Rev. **74**, 1707 (1948).

TABLE I.

	Al	Cu	Ag	Sn	Au	Pb	Th	U
Experimental error	−0.01	1.1	3.4[a]	3.1	7.9[a]	10.3	11.7[a]	11.4
Correction term	0.02	1.18	3.09	3.5	8.7	9.4	11.3	11.9

[a] These data from the relative pair production experiment. Other data are taken from experiment by Dewire *et al.*

To summarize, the discrepancy found in the absorption measurement can be ascribed to the failure of the pair production cross section theory to give the correct results. If the blame is placed on the 1st-order Born approximation then one might expect a second-order Born approximation would bring in a correction term proportional to Z^3. The results of this experiment can be fitted to a correction term of this type. A good approximation is obtained by replacing the Z^2 factor in the theoretical pair production cross section by $Z^2[1-(1.4\pm0.1)10^{-3}Z^2]$. Table I compares this approximation with the results of this experiment and the data of Dewire *et al.* Dewire's data are used because at the enegy of 280 Mev the Compton and photoelectric effects can be ignored.

In a very recent experiment by A. I. Berman at Los Alamos, very accurate absorption measurements at 20 Mev for 19 elements from H to U were made using a carbon threshold detector. His experimentally determined correction for pair production is $(1.5\pm0.1)10^{-3}Z^2$.

In conclusion it might be noted that the data representing the energy sharing distribution for Au (see Fig. 4) are in agreement[10] within the statistical errors with that predicted by Bethe-Heitler. Thus it leads us to believe that the discrepancy may be caused primarily by an error in the magnitude of the total cross section as was assumed above, and that the error is not a function of the energy distribution among the pair members. If this is so, then the same discrepancy may appear in the bremsstrahlung cross section which is almost the reverse process of pair production. The results of Curtis[11] on the measurement of the absolute brems-

[10] The sharing distribution has been verified also by J. W. Dewire and L. A. Beach, Phys. Rev. **83**, 476 (1950), measuring the pairs formed in a $\frac{1}{2}$-mil Au foil when bombarded by a 270-Mev photon beam. A statistical error of about 10 percent for the experimental points were obtained.

[11] C. D. Curtis, Phys. Rev. **81**, 308 (1951), and by private communications.

strahlung cross sections for 60-Mev electrons incident on a thin Pb foil give results which are (8±3) percent low compared with the Bethe-Heitler theory for bremsstrahlung.

The results obtained by Walker[12] on the relative pair production cross sections for incident quanta of 17.6 Mev as presented give discrepancies which are somewhat larger than those given by recent absorption measurements and the results of this experiment. However, the results of Walker can be made compatible by using the Wheeler and Lamb theory for triplet production in making the correction to the number of pairs observed to obtain the number of pairs created in the field of the nucleus. The triplet correction term obtained experimentally by Walker is $0.8/Z$, although his data are not inconsistent with a correction term $1.1/Z$ which is given by the Wheeler and Lamb theory. By applying this latter correction to his data, the relative pair production cross section discrepancy for Pb to Al, Sn to Al, and Cu to Al becomes respectively (13±3), (8±4), and (3±3) percent. Further correction to Walker's results should be made to account for the fact that he measured only the pairs produced in the central half of the differential cross section ($0.25<E_1/k_0<0.75$), where the effects of screening are greater in proportion to the effects of screening where $E_1k_0<0.25$ and $E_1/k_0>0.75$, especially in the case of the lower Z elements. The effect of a correction of this type would be to reduce his values of relative pair production cross sections by another percent or two. If one makes these corrections, the results of Walker should be compatible with the results of absorption measurements and those of this experiment.

[12] R. L. Walker, Phys. Rev. **76**, 1440 (1949).

ACKNOWLEDGMENTS

The author wishes to express his appreciation to the large number of people who contributed to the experiment. Interest in cloud-chamber apparatus and techniques was stimulated by Dr. H. W. Koch, to whom the author is indebted especially.

The author wishes to express his gratitude to Professor Donald W. Kerst, under whose direction the experiment was performed, for the many helpful suggestions and criticisms rendered; and also to Professor A. T. Nordsieck, whose views on the problem initiated interest in this experiment.

The task of performing the experiment was carried out with the able assistance of the 300-Mev betatron crew, the diesel operators, and the continual assistance of graduate research assistants Philip Fisher and Irwin Janney. It was a pleasure to have Donald Vermillion as an aid throughout the experiment's entire program.

Analyzing and calculating were assisted by Wilna Johnson, Robert Turner, Jim Bauerle, and others.

PHYSICAL REVIEW VOLUME 86, NUMBER 6 JUNE 15, 1952

An Investigation into the Nuclear Scattering of High Energy Protons

KANTILAL M. GATHA AND R. J. RIDDELL, JR.
Department of Physics, University of California, Berkeley, California
(Received March 5, 1952)

The angular distributions of high energy protons, elastically scattered from various nuclei, have been considered theoretically. For this purpose, the optical model of the nucleus, hitherto developed on the basis of the nuclear scattering of high energy neutrons, has been suitably modified to account for the proton scattering. Appropriate proton wave equations have been established and solved exactly. However, these solutions have been found unsuitable for numerical computations. Next, the WKB and the Born approximations have been used, within their respective regions of validity, to yield appropriate expressions for the differential scattering cross section. Finally, the theoretical and the experimental diffraction patterns for the nuclear scattering of 340-Mev protons have been compared. It has been found that the above nuclear model gives only an approximate account of such a scattering. It is further indicated that the effective nuclear radii, appropriate for this energy, are about 10 percent smaller than those calculated on the basis of the nuclear scattering of 90-Mev neutrons.

I. INTRODUCTION

THE experimental observations and the corresponding theoretical considerations on the scattering of high energy nucleons by nuclei have provided valuable information about nuclear structure. In this connection, the theoretical investigations have been carried out by making use of the optical model of the nucleus, employing the concept of a partially transparent nucleus as introduced by Serber.[1] Fernbach, Serber, and Taylor[2] have accounted for the nuclear scattering of 90-Mev neutrons on this basis and Fernbach[3] has extended the same considerations to

[1] R. Serber, Phys. Rev. **72**, 1114 (1947).
[2] Fernbach, Serber, and Taylor, Phys. Rev. **75**, 1352 (1949).
[3] S. Fernbach, *The Scattering of High Energy Neutrons by Nuclei* (unpublished Ph.D. dissertation, Physics Department, University of California, 1951), pp. 16–18.

give an approximate account of the nuclear scattering of 280-Mev neutrons.

Richardson, Ball, Leith, and Moyer[4] have recently observed the angular distributions for 340-Mev protons elastically scattered from various nuclei. It is the purpose of the present investigation to examine whether the above nuclear model, with reasonable modifications, can be employed to account for the nuclear scattering of such high energy protons.

II. THE OPTICAL MODEL OF THE NUCLEUS

A. The Optical Model for Neutron Scattering

In the optical model for the transparent nucleus, one regards the nucleus as a uniform sphere of nuclear matter, characterized by a complex refractive index, in which the real part is due to the effect of the nuclear potential well and the imaginary part is considered to be due to inelastic collisions. Using optical considerations as well as the equivalent WKB approximation, Fernbach, Serber, and Taylor[2] have obtained expressions for the total cross section σ_t and its two components, namely, the absorption cross section σ_a and the cross section for elastic scattering σ_e. These expressions involve the nuclear parameters $r_0=R/(A^{\frac{1}{3}}\times 10^{-13})$, (k_1/k), and $(K/2k)$, where R is the nuclear radius

$$k=(E^2-\mu^2c^4)^{\frac{1}{2}}/\hbar c, \tag{1}$$

$$\frac{k_1}{k}=\left\{\left[\frac{(E-V_n)^2-\mu^2c^4}{E^2-\mu^2c^4}\right]^{\frac{1}{2}}-1\right\}, \tag{2}$$

and

$$\frac{K}{2k}=\frac{\epsilon}{2k}\left[\frac{D}{2}(\sigma_{nn}+\sigma_{np})\right]. \tag{3}$$

In these equations, E is the energy of the incoming neutron and μ is its rest mass; V_n is the nuclear potential and D is the nucleon density, inside the nucleus; σ_{nn} and σ_{np} are the (n,n) and (n,p) scattering cross sections, respectively, and ϵ is a factor, smaller than unity, introduced to account for the effects due to the exclusion principle. In terms of these parameters, the complex refractive index is

$$n=1+(k_1/k)+i(K/2k). \tag{4}$$

The above expressions have been collected here, since they are useful in the present investigation. It may also be noted that the nuclear scattering of 90-Mev neutrons is reasonably accounted for by using the nuclear parameters $r_0=1.39$ cm, $k_1=3.3\times 10^{12}$ cm^{-1}, and $K=3.0\times 10^{12}$ cm^{-1}. At 280 Mev an approximate account of the scattering is given by using $r_0=1.39$ cm, $k_1=0$, and $K=2.5\times 10^{12}$ cm^{-1}, although the theory is less successful at this energy than at 90 Mev.

[4] Richardson, Ball, Leith, and Moyer, Phys. Rev. **83**, 859 (1951).

B. The Optical Model for the Proton Scattering

It will be assumed that the only modification in the nuclear model required to account for the scattering of protons will be the inclusion of the electrostatic potential due to the nucleus. Since the optical model of the nucleus is based upon the tacit assumption that the nucleon density within the nucleus is uniform, one can replace V_n by

$$V_p=Ze^2/r \text{ for } r>R,$$

and

$$V_p=V_n+(3R^2-r^2)Ze^2/2R^3 \text{ for } r<R, \tag{5}$$

where Z is the atomic number of the nucleus.

One can now define a quantity k_2, analogous to k_1 on the basis of Eq. (2), by replacing the potential V_n therein by the new potential V_p. One can also obtain an expression for the complex refractive index for the scattering of protons by substituting k_2 in place of k_1 in Eq. (4). Then the magnitude of the momentum, which is now complex, is

$$k_c=k+k_2+\tfrac{1}{2}iK. \tag{6}$$

This expression will be used to obtain the appropriate proton wave equations.

III. THE THEORETICAL NUCLEAR SCATTERING OF HIGH ENERGY PROTONS

A. The Proton Wave Equations

As a reasonable wave equation for high energy protons one may take the Dirac equation with an additional term, due to Pauli,[5] to account for the anomalous magnetic moment. However, if one neglects this term for the present, one obtains the usual Dirac equation. Next, following Williams,[6] one can square the Dirac operator and obtain a second-order equation in which the term containing all the spin effects naturally separates out. This term, being of the same order of magnitude as the Pauli term, may be similarly neglected for the present. Thus one obtains the Klein-Gordon equation

$$(E-V)^2\psi=(c^2p^2+\mu^2c^4)\psi. \tag{7}$$

One can now substitute for $[(E-V)^2-\mu^2c^4]$ in the above equation the quantity $(\hbar ck_c)^2$ from Eq. (6). Neglecting small second-order terms and separating into spherical coordinates, one obtains the proton wave equations for the regions outside and inside the nucleus, respectively:

$$\left[\frac{1}{\rho^2}\frac{d}{d\rho}\left(\rho^2\frac{d}{d\rho}\right)+1-\frac{2\chi}{\rho}-\frac{l(l+1)}{\rho^2}\right]W_l^0=0, \tag{8}$$

$$\left[\frac{1}{\rho'^2}\frac{d}{d\rho'}\left(\rho'^2\frac{d}{d\rho'}\right)+1+\frac{\bar{\chi}}{\eta'^3}\rho'^2-\frac{l(l+1)}{\rho'^2}\right]W_l^i=0. \tag{9}$$

In these equations, $\rho=kr$, $\rho'=k'r$, $\eta=kR$, and $\eta'=k'R$.

[5] W. Pauli, Revs. Modern Phys. **13**, 223 (1941).
[6] E. J. Williams, Proc. Roy. Soc. (London) **A169**, 531 (1938).

We also have $\chi=\alpha\gamma k_0/k$ and $\bar{\chi}=\alpha\bar{\gamma}k_0/k$, where $\alpha=Z/137$, $\gamma=E/\mu c^2$, $\bar{\gamma}=(E-\bar{V})/\mu c^2$, $k_0=\mu c/\hbar$, and $k'=\bar{k}+\frac{1}{2}iK$, in which $\bar{k}=[(E-\bar{V})^2-\mu^2c^4]^{\frac{1}{2}}/\hbar c$ and $\bar{V}=V_n+(3Ze^2/2R)$.

The errors introduced in the phase shifts by neglecting the various terms so far mentioned have been estimated and found to be negligible. The above equations can also be written as a single equation

$$\left[\frac{1}{\rho^2}\frac{d}{d\rho}\left(\rho^2\frac{d}{d\rho}\right)+1-U-\frac{l(l+1)}{\rho^2}\right]W_l=0, \quad (10)$$

where $U=2\chi/\rho$ for $\rho>\eta$, and $U=-[(k'^2-k^2)/k^2]-[(\alpha\bar{\gamma}k_0k')/(k\bar{k}\eta^3)]$ for $\rho<\eta$.

Equations (8) and (9) will be used to obtain the exact solutions, while Eq. (10) will be useful in the WKB and the Born approximations for the scattering.

B. The Exact Phase Shifts

Only a sketch of the results of the exact treatment will be presented here. It can be shown that Eqs. (8) and (9), with suitable substitutions, can be brought into the form of the equation for the confluent hypergeometric functions, in Kummer's notation, as defined by Whittaker and Watson.[7] Imposing the requirements of continuity at the boundary on the resulting solutions, one obtains an exact expression for the phase shifts

$$\delta_l{}^e=\eta_l+\lambda_l, \quad (11)$$

where $\eta_l=\arg\Gamma(l+1+i\chi)$ and $\lambda_l=-\tan^{-1}(A_l/B_l)$. A_l and B_l, are given by

$$A_l=F_t{}^0F^i-aF^0F_\xi{}^i+bF^0F^i, \quad B_l=G_t{}^0F^i-aG^0F_\xi{}^i+bG^0F^i,$$

where the subscripts denote differentiation with respect to the corresponding variables. One also has

$$F^0=F(p,q,\zeta), \quad G^0=G(p,q,\zeta),$$
$$F^i=F(p',q',\xi), \quad G^i=G(p',q',\zeta),$$

where F and G, respectively, are the regular and irregular confluent hypergeometric functions. The parameters of these functions are given by $p=l+1+i\chi$, $q=2l+2$, $p'=[(2l+3)-i(\eta'^3/\bar{\chi})^{\frac{1}{2}}]/4$, $q'=(2l+3)/2$, $\zeta=-2i\eta$, and $\xi=-i(\eta'\bar{\chi})^{\frac{1}{2}}$; while $a=(\eta'\bar{\chi})^{\frac{1}{2}}/\eta$ and $b=\frac{1}{2}(a-1)$.

We have not found it possible in this investigation to compute the exact phase shifts, because of a lack of tabulated values for the functions involved. Also, neither the ascending nor the descending series of these confluent hypergeometric functions converge rapidly enough for numerical computations. Moreover, the exact solutions considered above are not necessarily exact representations of the true solutions for a physical nucleus, where the boundary is surely not as abrupt as in the nuclear model employed here. Thus it is both necessary and reasonable to use approximation methods for the treatment of this problem.

C. The WKB Approximation

Since one has $\eta\gg1$ for high energy protons, one may expect that the WKB approximation may be valid. The Phase shifts, using Langer's modification,[8] are given by

$$\delta_l{}^L=\lim_{\rho\to\infty}\left[\int_{\rho_1}^{\rho}(\rho^2-\rho^2U-\nu^2)^{\frac{1}{2}}\frac{d\rho}{\rho}-\int_{\nu}^{\rho}(\rho^2-\nu^2)^{\frac{1}{2}}\frac{d\rho}{\rho}\right], \quad (12)$$

where $\rho_1{}^2-\rho_1{}^2U(\rho_1)-\nu^2=0$ and $\nu=l+\frac{1}{2}$.

There is no reliable criterion for the validity of the above expression for phase shifts. However, the potential for the proton scattering consists of the Coulomb potential and an approximate square well. Exact expressions for the phase shifts are known both for the pure Coulomb potential and for the square-well potential separately. Thus, one may use these potentials as test cases to obtain some insight into the errors introduced by using the above approximation. In the former case, an analytical comparison showed that the errors diminish for large values of l, while a numerical comparison showed that, for $l=0$, the errors at 340 Mev are quite small for all nuclei. On the other hand, for the square well, analytical as well as numerical comparisons showed that the errors are small for small values of l, while for larger values of l, significant errors are encountered. The contributions to these errors due to the steepness of the boundary would be smaller for the physical nucleus where one may expect the potential to change gradually. However, even when the boundary is not steep, experience has shown[9] that this approximation overestimates positive phase shifts, particularly when they are smaller than about 0.5 radian. These errors may have some effect on the shapes of the theoretical diffraction patterns. In the present approximate investigation, all these errors will be neglected.

Now, as is done by Fernbach,[8] one may simplify the expression for the phase shifts given by Eq. (12), to obtain

$$\delta_l=-\tfrac{1}{2}\lim_{\rho\to\infty}\left[\int_{\nu}^{\rho}(\rho^2-\nu^2)^{-\frac{1}{2}}U\rho d\rho\right]. \quad (13)$$

Appropriate numerical comparisons for suitable test cases have shown that this simplification introduces additional errors which become significant only when l is close to η. These errors may have some effect on the value of σ_l, but they can only affect the diffraction patterns at very small angles. Such errors also will be neglected in the present investigation.

Substituting the expression under Eq. (10) for U in Eq. (13), one obtains the phase shifts for the proton

[7] E. T. Whittaker and G. M. Watson, *A Course of Modern Analysis* (The McMillan Company, New York, 1946), pp. 337–354.

[8] N. F. Mott and H. S. W. Massey, *The Theory of Atomic Collisions* (Oxford University Press, London, 1949), p. 127.

[9] See reference 8, p. 213.

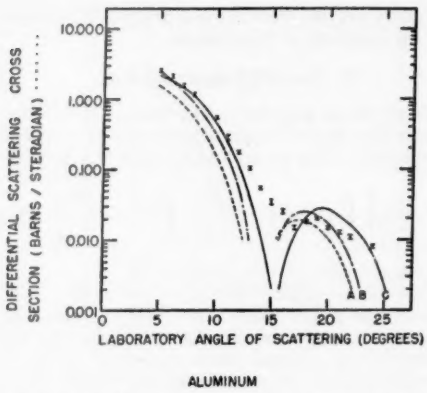

FIG. 1. The proton diffraction patterns for aluminum. Curves *A* and *B*, respectively, represent the WKB and the Born patterns with $r_0=1.39$ cm. Curve *C* represents the WKB pattern with $r_0=1.25$ cm.

scattering as

$$\delta_l=\delta_l'+i\delta_l'', \tag{14}$$

where, for $\nu>\eta$, $\delta_l'=\chi\ln\nu$, $\delta_l''=0$, and for $\nu<\eta$,

$$\delta_l'=\chi\ln[\eta+(\eta^2-\nu^2)^{\frac{1}{2}}]-(\eta^2-\nu^2)^{\frac{1}{2}}[u-v(\eta^2+2\nu^2)],$$
$$\delta_l''=w(\eta^2-\nu^2)^{\frac{1}{2}}.$$

In this, one has approximately

$$u=(\gamma k_0\bar{k}_0)/k^2,\quad v=(\alpha\gamma k_0)/(6k\eta^3),$$

and $w=K/(2k)$ with $\bar{k}_0=\bar{V}/\hbar c$.

Following the usual procedure[10] for such a modified Coulomb potential, one obtains the differential scattering cross section

$$\sigma(\theta)=[f(\theta)]^2+[g(\theta)]^2, \tag{15}$$

where

$$f(\theta)=-\frac{1}{2k}\Big\{\chi\csc^2\tfrac{1}{2}\theta\cos[\chi\ln(\csc^2\tfrac{1}{2}\theta)+2\eta_0]$$
$$-\sum_{l=0}^{\bar{l}}(2l+1)[\exp(-2\delta_l'')\sin2\delta_l'$$
$$-\sin2\eta_l]P_l(\cos\theta)\Big\},$$

$$g(\theta)=-\frac{1}{2k}\Big\{\chi\csc^2\tfrac{1}{2}\theta\sin[\chi\ln(\csc^2\tfrac{1}{2}\theta)+2\eta_0]$$
$$+\sum_{l=0}^{\bar{l}}(2l+1)[\exp(-2\delta_l'')\cos2\delta_l'$$
$$-\cos2\eta_l]P_l(\cos\theta)\Big\},$$

and $\eta_{\bar{l}}=\chi\ln\nu$ in this approximation, while $\bar{l}$ is the largest l less than η.

D. The Born Approximation

The usual criterion of validity for the Born approximation shows that this approximation can be used for the Coulomb scattering at 340 Mev in the case of light elements only. Moreover, experience has shown[9] that this approximation gives a good account of the scattering by a potential well when the phase shifts are smaller than about 0.5 radian. Positive phase shifts larger than this value are expected to be significantly underestimated. With reasonable values of the nuclear parameters, as obtained from the neutron scattering, one finds that a considerable number of phase shifts for light elements would be closely approximated by this approximation. Thus one may use the Born approximation for the proton scattering for such elements. In this case, one obtains an expression for the differential scattering cross section

$$\sigma(\theta)=[f(\theta)]^2+[g(\theta)]^2, \tag{16}$$

where

$$f(\theta)=\{[(a+3c\eta^2)\omega^2-6c]\sin(\omega\eta)$$
$$-[(2\chi+a\eta+c\eta^3)\omega^3-6c\eta\omega]\cos(\omega\eta)\}/k\omega^5,$$
$$g(\theta)=\{b\omega^2\sin(\omega\eta)-b\eta\omega^3\cos(\omega\eta)\}/k\omega^5.$$

In these equations, $\omega=2\sin\frac{1}{2}\theta$, and, approximately, $a=-(2\gamma k_0\bar{k}_0)/k^2$, $b=K/k$ and $c=(\alpha\gamma k_0)/(k\eta^3)$.

One may also note here, that in this approximation σ_s for the neutron scattering can be expressed as

$$\sigma_s=\pi R^4(4k_1^2+K^2)/2, \tag{17}$$

where it is assumed that $\eta\gg1$.

IV. COMPARISON WITH THE EXPERIMENTAL OBSERVATIONS

Aluminum and lead have been chosen as representative elements on which to compare the theoretical and the experimental diffraction patterns for 340-Mev protons. As an illustrative example, Fig. 1 shows such patterns for aluminum. The experimental values, together with probable errors, for $\frac{1}{2}°$ angular resolution, obtained by Richardson, Ball, Leith, and Moyer,[4] are indicated thereon. The WKB patterns for aluminum were computed with $r_0=1.39$ cm and various values of k_1 and K. It may be noted here that the potential V_n determines k_1. Curve *A* in Fig. 1 represents the WKB pattern for $k_1=0$ and $K=1.7\times10^{13}$ cm^{-1} as a typical example. Curve *B* similarly represents the Born pattern with the same parameters.

One can immediately make the significant observation that the theoretical patterns exhibit rather deep minima, unlike the experimental patterns for both elements. If the absence of such deep minima in the observed patterns is not due to some undetermined experimental errors, one must ascribe this disagreement

[10] Leonard I. Schiff, *Quantum Mechanics* (McGraw-Hill Book Company, Inc., New York, 1949), pp. 119–120.

to some defect in the theoretical patterns. It seems unlikely that the use of approximation methods is responsible for this defect, Thus, one is led to the conclusion that the rather idealized nuclear model of a uniform sphere with a sharp boundary as used here, should be regarded only as an approximate representation of the physical nucleus.

In spite of this difficulty, it would be of some interest to obtain appropriate values of the nuclear parameters for this model. It has been found that both for aluminum and lead the theoretical patterns with the above parameters have their maxima at smaller angles than the corresponding maxima of the experimental patterns. In view of the errors discussed before, one would expect the WKB patterns to show some such deviation. However, it is difficult to understand why the Born pattern for aluminum deviates in the same direction. Moreover, this deviation for the WKB pattern of lead is not smaller than that for aluminum, and the deviation for lead at the third maximum is not smaller than that at the second maximum. This behavior is contrary to what one would expect if these deviations were due to errors in the WKB approximation. These arguments indicate that the above values of the nuclear parameters should be corrected. Modifications in the values of k_1 and K, within reasonable limits, have been found to have practically no influence on these deviations. However, such deviations can be removed by changing r_0. It has been estimated that within the limits of both theoretical and experimental uncertainties involved, it would be sufficient to take $r_0=1.25$ cm. This value somewhat overcompensates for this deviation in the case of aluminum, but it similarly undercompensates for it in case of lead.

With the above value of r_0, one can calculate K from Eq. (3), assuming $\sigma_{nn}=\sigma_{np}$ and using the experimental value of about 26 mb both for σ_{pp} and σ_{np}. Allowing less than 10 percent for the exclusion principle according to Fernbach's[8] prescription, one obtains $K=3.0\times10^{12}$ cm^{-1}, approximately. Since the Born approximation reasonably accounts for a number of the phase shifts for large values of l, which contribute to σ_e, one may use Eq. (17) with the above parameters together with $k_1=0$ to obtain $\sigma_e=95$ mb for the neutron scattering due to carbon, even though this nucleus is perhaps slightly small for the optical model to be strictly valid. The electrostatic potential inside the nucleus is small for this element, and thus would not affect this value significantly. Richardson[11] has estimated the corresponding σ_e by a graphical integration of the experimental pattern for carbon, after eliminating the small angle effects due to the electrostatic potential outside the nucleus. He obtains $\sigma_e=98$ mb in this case. This agreement shows that one may still take $k_1=0$, approximately.

Extrapolating the curves of σ_t *versus* E prepared by Hildebrand,[12] approximate values of σ_t for the neutron scattering at 340 Mev were obtained for various elements. The corresponding WKB values of σ_t were computed with the above parameters from the formula given by Fernbach, Serber, and Taylor.[3] The calculated values are smaller by 18 percent for aluminum and by 10 percent for lead than the extrapolated experimental values. This underestimation may be largely due to the use of the rather simplified WKB approximation. Similar underestimation is shown by the comparison of the WKB and the exact calculations for 90-Mev neutrons scattered from aluminum as calculated by Pasternack and Snyder.[13] Thus, one may regard the above values of the nuclear parameters as appropriate for 340 Mev. Curve C in Fig. 1 shows the WKB pattern with the above parameters. In view of the various approximations involved, this curve gives a reasonable correlation with the experimental observations.

V. CONCLUSIONS

On the basis of the present investigation, one can conclude that the approximations inherent in the optical model of the nucleus, developed to account for the scattering of 90-Mev neutrons, become significant at higher energies of the order of 340 Mev. However, this model can be reasonably modified and appropriate nuclear parameters can be determined to give an approximate account of the scattering of 340-Mev protons. In this connection, it is indicated that the effective nuclear radii, appropriate for this energy, are about 10 percent smaller than those obtained from the neutron scattering at 90 Mev.

The authors wish to express their thanks to Professor R. Serber and Dr. T. D. Lee for valuable help during this work. They also wish to thank Dr. R. H. Good and Dr. Robert Jastrow for useful discussions on theoretical questions, and Dr. Burton J. Moyer and Dr. R. E. Richardson for similar discussions on the experimental aspects of the problem. Thanks are due Mrs. Ardith Kenney of the Radiation Laboratory at the University of California for all numerical computations. Lastly, K. M. Gatha wishes to express his gratitude to the Watumull Foundation for supporting his graduate studies in the United States.

[11] R. E. Richardson (to be published).

[12] R. H. Hildebrand (private communication).

[13] S. Pasternack and H. S. Snyder, Phys. Rev. **80**, 921 (1950).

Letters to the Editor

PUBLICATION of brief reports of important discoveries in physics may be secured by addressing them to this department. The closing date for this department is five weeks prior to the date of issue. No proof will be sent to the authors. The Board of Editors does not hold itself responsible for the opinions expressed by the correspondents. Communications should not exceed 600 words in length and should be submitted in duplicate.

Thermal and Electrical Conductivities of Carbon Materials

S. MIZUSHIMA
Department of Applied Physics, Keiogijuku University, Tokyo, Japan
(Received April 7, 1952)

IN a previous note,[1] the large difference in thermal conductivity (1:100) between so-called amorphous carbon and graphite was attributed to the difference in crystallite sizes. Experiments have been carried out to test this relationship by measuring the physical changes and crystallite sizes for coke specimens. These were prepared from pitch coke (0.5 percent ash) manufactured at the Yahata Steel Company and widely used for the production of electrodes in Japan. After prebaking at 1300°, each sample was heated in an electric furnace at different temperatures over a range from 1500° to 2700° for 20 min. The results are shown in Fig. 1. It can be seen that the curves for the thermal conductivity

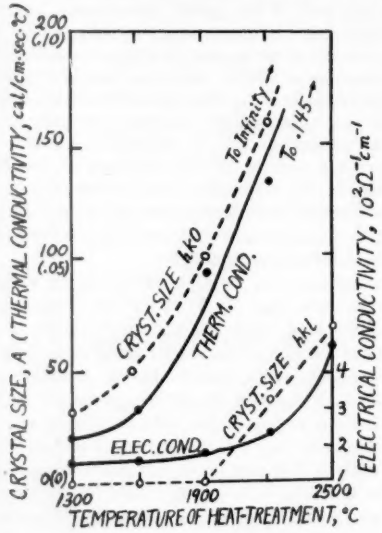

FIG. 1. Changes of crystal size and of electric and thermal conductivities by heat treatment at different temperatures.

and for the crystallite size in the *hk*0 direction are nearly parallel to each other and both show a rapid rise with temperature even in the region where the electrical conductivity remains constant. Inasmuch as the *hk*0 size represents the (mean) diameter of the layers in a crystallite, this resemblance means that the lattice waves which carry the heat current are scattered by the crystallite boundaries with the mean free path being proportional to the layer diameter. On the other hand, the curve for the electrical conductivity appears to correspond to that representing the temperature dependence of the crystallite size in the *hkl* direction. Since the *hkl* size is related to the degree of the change from the randomly oriented layer structure to the regular three-dimensional one, the electronic waves which carry the electric current are scattered by the irregular potential caused by the random neighboring layers.

So-called amorphous carbons having a completely random layer structure may therefore be supposed to have electrical resistivity independent of crystallite size, as long as the layer diameter in a crystallite is sufficiently large. After heating at temperatures in the range from 1500° to 1900°, solid carbon samples, prepared from pitch coke, formaldehyde resin, or charcoal, show nearly the same and constant resistivity, 3.6, 3.6, and 2.3Ω cm (in the fiber direction).

Though a number of experiments on the crystallite growth of carbon have been carried out by others, these new relations found for solid samples seemed worth mentioning.

[1] S. Mizushima and J. Okada, Phys. Rev. **82**, 94 (1951).

Ferromagnetic Resonance in Copper Ferrite

TOSHIKO OKAMURA AND YUZO KOJIMA
Research Institute for Scientific Measurements, Sendai, Japan
(Received March 10, 1952)

THE ferromagnetic resonance absorption in a single crystal of copper ferrite was studied from −195°C to *ca* +470°C at 24,000 Mc/sec, and the resonance phenomena in some sintered polycrystalline specimens were also studied.

The *g*-factor, the first-order magnetocrystalline anisotropy K_1, and the saturation magnetization M_s were determined from the resonance data as functions of the temperature.

The crystals were grown by a method similar to that by which crystals of manganese zinc ferrite and cobalt zinc ferrite had been grown previously.[1] A mixture of 8.0 g of Fe_2O_3, 4.0 g of CuO and 12 g of borax was kept at 1200°C for 3 hours in a platinum crucible and slowly cooled at a rate of 1°C/min till 900°C; then the current to heat the furnace was turned off, and the sample was cooled to room temperature in the furnace.

We were afraid that the specimen obtained in this manner might have tetragonal symmetry; but since its deviation from

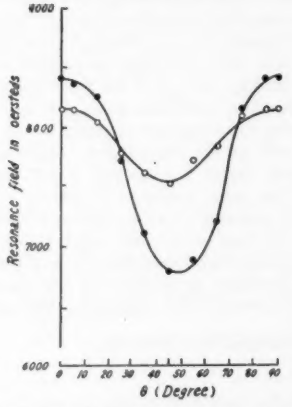

FIG. 1. The resonance field as a function of crystal orientation; θ equals the angle in the (100) plane between the static field and the cube edge; the open circles denote the results at room temperature and the solid circles denote the results at liquid nitrogen temperature.

cubic symmetry might be negligibly small, we assumed the crystal symmetry to be cubic for the calculation of K_1 and g.

The measuring procedure was the same as in the earlier experiments,[2] so it is omitted here.

The single crystal was so mounted as to make the (100) plane consistent with both the directions of the rf field and the dc magnetic field. The resonance field was observed as a function of crystal orientation at room and liquid nitrogen temperatures, as shown in Fig. 1.

TABLE I. Measurements on copper ferrite.

Temp. (°C)	M_s (gauss/cc)	K_1 (ergs/cc)	g	g^a
−195	315	-2.06×10^6	2.20	2.17
−150	310	−1.80	2.13	2.13
−100	305	−1.43	2.09	2.08
− 50	295	−1.01	2.06	2.05
15	280	−0.63	2.04	2.04
50	250	−0.43	2.04	2.05
100	220	−0.24	2.07	2.05
150	180	−0.16	2.01	2.05
200	165	−0.10	2.01	2.05
250	135	−0.07	2.03	2.05
300	110	−0.04	2.04	2.05
350	80	−0.02	2.04	2.06
400	60	−0.01	2.05	2.06
450	30	—	2.05	2.06

[a] Determined by the resonance experiment on a polycrystalline spherical specimen.

The saturation magnetization M_s at various temperatures was calculated from the resonance data for polycrystalline spherical and disk-formed specimens. Substituting these values of M_s in Kittel's formula, g and K_1 were calculated from the resonance field for both the [100] and [110] directions parallel to the static field. The results are given in Table I. In the table, the g-factors determined for a spherical polycrystalline specimen of diameter 0.8 mm are also listed.

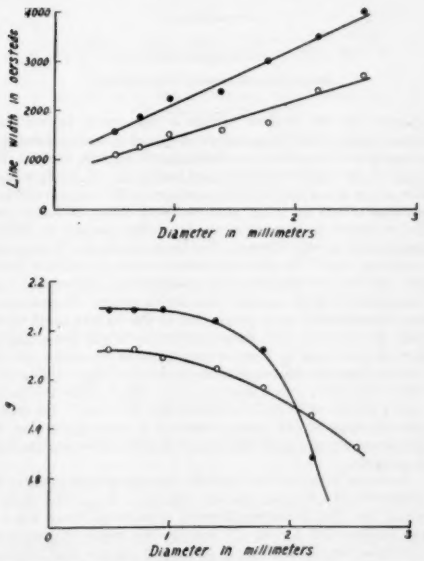

FIG. 2. The half-linewidth and apparent g-factor of various spheres at room and liquid nitrogen temperatures; the open circles denote the results at room temperature and the solid circles denote the results at liquid nitrogen temperature.

K_1 did not change its sign in the whole temperature region, contrary to the cases of nickel ferrite,[3] manganese zinc ferrite and cobalt zinc ferrite,[3] for which K_1 changes sign at *ca* −160°C, −100°C and +70°C, respectively.

The g-factor increases in value below room temperature with falling temperature, similar to the inclination of g-factors in other ferrites[4] when plotted against temperature; but it shows an almost constant value above room temperature up to the Curie point *ca* +470°C, at which temperature the resonance disappeared.

To determine the g-factor in polycrystalline specimens, the size effect was studied for various spheres whose diameter varied from 2.6 mm to 0.5 mm, and a similar effect was observed to that found in other ferrites by Yager and his co-workers[5] and recently by the writer.[6] Figure 2 shows the half-linewidth and apparent g of various spheres at room and liquid nitrogen temperatures. An interesting effect was found, that is, g at a low temperature was smaller than g at room temperature for a very large sphere, and the discrepancies of the half-linewidth between room temperature and a lower temperature became smaller as the size of the sphere approached zero.

Details of the present experiment will be published in Science Reports of the Research Institute of Tôhoku University.

[1] T. Okamura, Phys. Rev. **85**, No. 4 (1952).
[2] Okamura, Kojima, and Torizuka, Sci. Repts. Research Inst., Tôhoku University, 4, No. 1 (1952).
[3] D. W. Healy, Technical Report of Harvard University, No. 135 (1951).
[4] T. Okamura and Y. Torizuka, Nature **168**, 162 (1951).
[5] W. A. Yager and F. R. Merritt, Phys. Rev. **81**, 477 (1951).
[6] T. Okamura and Y. Kojima (to be published in Sci. Repts. Research Inst., Tôhoku University).

The β-Spectrum of RaD

A. A. JAFFE AND S. G. COHEN
Hebrew University, Department of Physics, Jerusalem, Israel
(Received May 5, 1952)

THE radioactive decay of RaD has been investigated by introducing it in the form of lead tetramethyl vapor into a proportional counter. Excellent proportionality was obtained (as checked by the line width obtained from superimposed external sources) using dry lead tetramethyl at a pressure of a few mm together with methane and argon, to a total pressure of one atmosphere. The counter was 75 cm long and 9 cm in diameter and was provided with a window for calibration with an external source. The amount of lead tetramethyl that sticks to the counter wall during the course of an experiment (not more than 4 hours) was found to be very small.

The pulse distribution, obtained with a single channel pulse analyzer, is shown in Fig. 1, for an experiment in which 2 mm of lead tetramethyl vapor gave a total counting rate of about 3000/sec.

Other work[1,2] has shown that a 46.7-kev γ-ray occurs in about 70 percent of disintegrations, and is highly converted (97 percent). If this γ-ray is emitted in a time short compared with the resolving time of the counter (2 microseconds) we would expect that 70 percent of the pulses should correspond to the sum of the energies of the γ-ray and the β-particle, if all the secondary radiations after internal conversion are re-absorbed in the counter gas. This is seen in the region of peak A, which is much broader than that obtained with an external source of RaD providing 46.7 kev γ-rays. In some cases, however, the L x-rays of bismuth (mainly 10.8 kev and 13.0 kev) escape from the counter, giving rise to the peak at B (36.7 kev).

Careful examination using the 46.7 γ-rays from an external source of RaD (0.5 millicurie) indicated that the maximum at A occurs at an energy 2.7±0.5 kev greater than 46.7 kev; this together with the sharpness of the peak probably indicates the existence of a maximum in the β-spectrum. The point at 46.7 kev corresponds to the zero of energy for the β-spectrum. After comparison with the pulse distribution obtained for the 46.7-kev γ-ray (semi-half width 1.7 kev), it is possible to estimate the

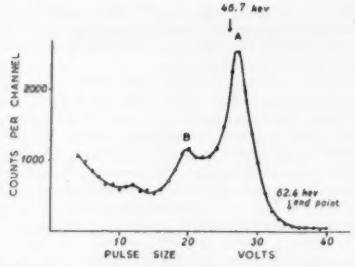

FIG. 1. Pulse-size distribution from proportional counter with RaD in the form of lead tetramethyl vapor.

amount of distortion of the shape of the β-spectrum associated with A. The necessary correction is small, and the curve closely approximates the shape of the β-spectrum except in the neighborhood of the maximum. A Fermi plot for an allowed transition (neglecting the effect of screening on the Coulomb factor for which no adequate calculations are as yet available to us), somewhat surprisingly, gives a good straight line from 3 kev to 13.0 kev. Extrapolation gives an end point corresponding to a maximum energy of 15.7 kev. From several determinations, the mean value for the end point was found to be 16.7 ± 1 kev, which is in good agreement with the value of 18 ± 2 kev reported recently by Bannerman and Curran[2] using scintillation counters. The residual tail of low intensity can be accounted for by the random superposition of pulses due to the finite pulse duration and high counting rate, and probably also to the presence of a very small amount of RaE, perhaps in the form of bismuth trimethyl.

The low energy part of the pulse distribution should include the pure β-spectrum (i.e., when all γ-rays coincident with the decay are unconverted and escape from the counter or if all the accompanying γ-rays are metastable). This was examined at higher amplifications down to 0.9 kev, and the results also indicate the existence of a maximum at 2.4 kev. Even after subtracting the maximum possible unaccompanied β-spectrum, using the shape obtained from the results at higher energy, as described above, the remaining pulse distribution extends appreciably down to 7 kev. A consideration of our detailed results, together with other published data, provide evidence, we believe, for a branching in the β-decay, so that in at least 10 percent of the disintegrations a β-spectrum of maximum energy 55.6 kev is followed by a 7.8-kev γ-ray.

A detailed account of these experiments and their interpretation is in preparation.

[1] D. K. Butt and W. D. Brodie, Proc. Phys. Soc. (London) **A64**, 791 (1951).
[2] R. C. Bannerman and S. C. Curran, Phys. Rev. **85**, 134 (1952).
[3] N. Feather, Nucleonics **5**, 22 (July, 1949).

Excitation in High Energy Nuclear Reactions*

NORTON M. HINTZ†
Nuclear Laboratory, Harvard University, Cambridge, Massachusetts
(Received April 9, 1952)

A QUANTITY of special interest in a high energy nuclear reaction is the energy transferred to the struck nucleus by the incoming nucleon. Because of the possibility of noncapture excitation at high energies,[1] the excitation of the nucleus immediately after the collision may be less than the maximum possible value which is obtained when the incident particle is captured to form a compound nucleus.

It is the purpose of this note to point out that direct evidence for this may be obtained, in the case of certain nuclear reactions, by measuring the range of the struck nucleus in the target foil. This has been done for the nuclear reactions $Al^{27}(p, 3pn)Na^{24}$ and $C^{12}(p, pn)C^{11}$ by determining the fractional loss of the residual nuclei, Na^{24} and C^{11}, from thin foils of the target element. The experimental arrangement makes use of 180° focused protons from the internal beam of the Harvard cyclotron.[2] The target assembly consists of a stack of absorbers, interspersed with target foils, each foil backed with a receptor foil of 0.001 in. polyethylene to catch the recoil nuclei.

Figure 1 shows preliminary results for the ratio of the activity in the receptor foil N_r, to the total activity N_t, plotted as a function of the incident proton energy for two nuclear reactions. The receptor foil itself has a strong activity after irradiation due to the $C^{12}(p, pn)C^{11}$ reaction, so the method is limited to reactions leading to residual nuclei having half lives long as compared to C^{11}. Beryllium foils might be used as receptors for shorter lived nuclei, since only a relatively weak activity due to Be^7 would be present. In the case of the $C^{12}(p, pn)C^{11}$ reaction, the difference between the counting rates per unit mass in the target and receptor foils was taken as the quantity N_r, resulting in considerably poorer statistics than for the Na^{24} reaction.

The dashed lines in Fig. 1 show the expected ratio N_r/N_t if it is

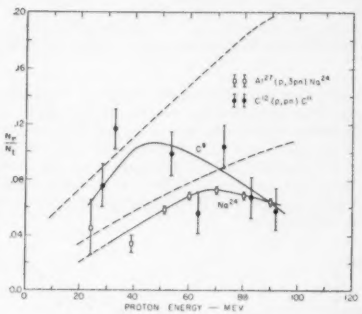

FIG. 1. Ratio of recoil to total activation.

assumed that the incident particle is captured to form a compound nucleus which subsequently de-excites by isotropic emission of particles. If particles are emitted preferentially forward, the range of the recoil fragments, and hence N_r, will be decreased. The ranges of the Na^{24} and C^{11} recoil ions in Al^{27} and polyethylene were calculated using the semi-empirical theory of Knipp and Teller[3] based on measurements of nuclear recoils in various gaseous mixtures by Blackett, Feather, and others. The ranges so calculated should be quite approximate since, in addition to the low accuracy of cloud-chamber measurements, the original data was presented in the form of "reduced air ranges." The reduction was accomplished by a comparison of the nuclear recoil tracks with the tracks of fast alpha-particles for which the electronic part of the stopping cross section alone is important. In the velocity range of this experiment roughly $\frac{1}{4}$ of the stopping cross section for heavy ions is due to nuclear effects. Thus the dashed curves should probably be renormalized so as to fit the experimental points at low energy where it is quite likely that the maximum energy transfer occurs and that the subsequent emission is isotropic.

It should be pointed out that the experiment does not give the nuclear recoil for typical nuclear collisions, but only for those in which the residual nucleus detected is produced. From Fig. 1 it can be seen that for the C^{11} reaction the region of noncapture excitation begins from 40–50 Mev, and for the Na^{24} reaction, about 65 to 70 Mev. For the reaction $Al^{27}(p, 3pn)Na^{24}$, a calculation based on the evaporation theory[4] gives 4 as the average number of particles emitted if the excitation lies within the range

corresponding to capture of protons of energy 53 to 75 Mev. Thus one expects, if the yield of Na^{24} is to vary slowly above 70 Mev as is observed,[2] that noncapture processes should become important above 75 Mev. A similar argument can relate the slow variation with energy in the C^{11} reaction above 40 Mev[4] to the observed departure of the C^{11} recoil range (Fig. 1) from its maximum value at approximately the same energy.

In order to calculate the actual nuclear excitation, W, from the recoil data of Fig. 1 a knowledge of the angular distribution of the recoil fragments is necessary. In the case of noncapture excitation, followed by isotropic emission of particles, the nuclear excitation is given by

$$W = W_m(2\gamma \cos\theta - \gamma^2), \tag{1}$$

where W_m is the relative kinetic energy in the center-of-mass system before collision, $\gamma = v_r/v_c$ is the ratio of the nuclear recoil velocity to the velocity of the center of mass, and θ is the nuclear recoil angle. Over the velocity range of this experiment the range varies approximately linearly with velocity, so that

$$N_r/N_t = \langle R\cos\theta\rangle_{\Delta v}/t \simeq R(\langle v_r\cos\theta\rangle_{\Delta v})/t, \tag{2}$$

where $R = R(v)$ is the range of the recoil fragment in the target foil whose total thickness is t. Placing $\theta = 0$ in Eq. (1) gives the upper limit to W for a given γ. From the data of Fig. 1 this upper limit is approximately 80 Mev in the Na^{24} reaction and 55 Mev in the C^{11} reaction when $W_m = 90$ Mev in both cases. If $\langle\cos^2\theta\rangle_{\Delta v}$ is taken as 0.75, W becomes 50 Mev for C^{11} and 65 Mev for Na^{24}. Measurements of the angular distribution of nuclear recoils in photographic plates or cloud chambers would enable a more precise value of W to be calculated.

* Assisted by the joint program of the ONR and AEC.
† Present address: Cavendish Laboratory, Cambridge, England.
[1] R. Serber, Phys. Rev. **72**, 1114 (1947).
[2] Norton M. Hintz, Phys. Rev. **83**, 185 (1951).
[3] J. Knipp and E. Teller, Phys. Rev. **59**, 659 (1941).
[4] V. Weisskopf, Phys. Rev. **52**, 295 (1937).
[5] Aamodt, Peterson, and Phillips, unpublished University of California Radiation Laboratory Report No. 1400 (1951).

(γ, α) Reactions on Li^7, O^{16}, and $Br^{79,81}$

H. Nabholz, P. Stoll, and H. Wäffler*
Swiss Federal Institute of Technology, Zürich, Switzerland
(Received April 14, 1952)

IN light as well as in middle-weight nuclei, (γ, α) reactions have exceedingly small cross sections ($\approx 10^{-29}$ cm^2). Therefore, an investigation of these processes needs a highly sensitive detecting device. The nuclear emulsion turned out to be very suitable to a study of (γ, α) reactions in the above mentioned elements, since emulsions can easily be loaded with lithium, and oxygen as well as bromine, form a great part of the emulsion itself.

1. Li^7.—200μ Kodak NT 1a plates loaded with lithium have been exposed to the $\sim$6.13 Mev gamma-rays from the $F^{19}(p, \alpha)O^{16} + \gamma$ reaction at a bombarding energy of $\sim$430 kev. About 600 events consisting of an α-particle ($E \cong 1.5$ Mev) and a triton ($E_T \cong 2$ Mev) emitted in opposite directions have been observed in 30 cm^2 of the emulsion. They belong to the reaction

$$Li^7(\gamma, \alpha)T^3 (Q = -2.51 \text{ Mev}).$$

From the geometry of the arrangement, the number of tracks counted, and the absolute intensity of the gamma-rays measured according to the method of Fowler *et al.*,[1] the cross section has been determined to be

$$\sigma[Li^7(\gamma_{6.13}, \alpha)] = (2.65 \pm 1.0) \times 10^{-29} \text{ cm}^2.$$

The angular distribution (350 tracks) of the tritons with respect to the incident gamma-rays is given by

$$J(\theta) = 1 - (0.1 \pm 0.09)\cos\theta.$$

This result is in qualitative agreement with the following assumptions: $Li^7(^2P_{\frac{1}{2}}^-)$ absorbs in its ground state EQ and MD radiation. Both kinds of transitions lead to a $^2P_{\frac{1}{2}}^-$ state and accordingly to an isotropic distribution. From an admixture of ED absorption there results a $^2P_{\frac{1}{2}}^+$ state, which together with the $^2P_{\frac{1}{2}}^-$ state causes a $\cos\theta$ interference term in the angular distribution.

2. O^{16}.—200μ Kodak NT 1a plates have been irradiated by the 17.6-Mev gamma-rays from the $Li^7(p, \gamma)$ reaction. Figure 1 shows the energy-distribution of 600 α-particle tracks measured in 15 cm^3 of emulsion. As follows from the well-known masses of O^{16}, C^{12}, and He^4, the peak at 7.8 Mev corresponds to the $O^{16}(\gamma, \alpha)$ reaction leading to the ground state of the rest nucleus C^{12}. Since the first excited state of C^{12} lies at $\sim$4.5 Mev, a second maximum at $\sim$4.4-Mev α-particle energy could be expected from the 17.6-Mev gamma-line. This maximum would partially interfere with the 5.7-Mev α-particles from the 14.8-Mev gamma-line present in the lithium gamma-ray spectrum, as well as with polonium contamination tracks (5.3 Mev) always present in the emulsion. But since the number of α-tracks between 4 and 6 Mev is only 25 percent of the number of those between 7 and 9 Mev, one can say that the predominant part of the $O^{16}(\gamma_{17.6}, \alpha)$ transitions leads to the ground state of the C^{12} nucleus. From a comparison of the number of tracks which belong to this peak with the number of "carbon stars" arising from the reaction $C^{12}(\gamma, \alpha)2\alpha$, the following cross section ratio results:

$$\sigma[O^{16}(\gamma_{17.6}, \alpha)]/\sigma[C^{12}(\gamma_{17.6}, \alpha)] = 0.82 \pm 0.1.$$

A new determination of the carbon cross section has been made recently.[2] The result is $\sigma[C^{12}(\gamma, \alpha)2\alpha] = 1.7 \pm 0.3 \times 10^{-28}$ cm^2 for γ-rays from lithium. Assuming this new value tentatively as correct, we get after a correction for the three Li γ-ray lines (17.6; 14.8; $\approx$12.5 Mev) an absolute value of the oxygen cross section:

$$\sigma[O^{16}(\gamma_{17.6}, \alpha)] = (1.8 \pm 0.5) \times 10^{-28} \text{ cm}^2,$$

which is in agreement with a former determination.[3]

3. $Br^{79,81}$.—An interpretation of the peak at 10.2 Mev in the α-particle distribution is not possible by a (γ, α) process on one of the light elements of the emulsion, as calculations with the well-known masses show. Only bromine and silver remain. But the emission probability for an α-particle of 10 Mev from a silver

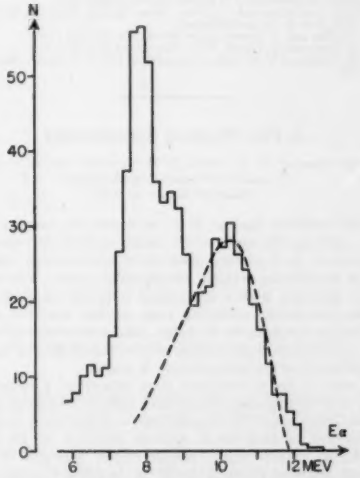

FIG. 1. α-particle distribution in a nuclear plate exposed to lithium gamma-rays. Block-diagram: experimental distribution; dashed curve: theoretical α-particle distribution for bromine.

nucleus excited at 17.6 Mev is about 1000 times smaller than for a bromine nucleus under the same conditions. (This is calculated by means of the statistical theory of nuclear reactions.) Therefore, one can safely ascribe the overwhelming number of α-particles at 10 Mev to the $Br^{79,81}(\gamma, \alpha)$ reaction. Under this assumption, the cross section for both bromine isotopes relative to that of the $C^{12}(\gamma, \alpha)2\alpha$ reaction has been computed to be

$$\sigma[Br^{79,81}(\gamma_{17.6}, \alpha)]/\sigma[C^{12}(\gamma_{17.6}, \alpha)] = 0.51 \pm 0.05. \quad (1)$$

This value may be compared with the result calculated according to statistical theory. From the mass formula one gets $E_b(Br^{81}) - E_b(Br^{79}) = 0.5$ Mev for the difference of the α-particle binding energies in Br^{79} and Br^{81}. The α-particle distribution (see Fig. 1) gives immediately $E_b(Br^{79}) = 5.7$ Mev. Since the neutron binding energies are also known for both bromine isotopes, namely, 10.6 and 9.95 Mev for Br^{79} and Br^{81}, respectively, the theoretical cross section ratios $(\gamma, \alpha)/(\gamma, n)$ can be calculated. The result is $\approx 8\times10^{-4}$ for Br^{79} and 3×10^{-4} for Br^{81}. With these values and the experimental cross section ratios $\sigma[Cu^{63}(\gamma, n)]/\sigma[Br^{79}(\gamma, n)]$ and $\sigma[Cu^{63}(\gamma, n)]/\sigma[Br^{81}(\gamma, n)]$ given by Wäffler,[4] we obtain

$$\sigma[Br^{79,81}(\gamma_{17.6}, \alpha)]/\sigma[Cu^{63}(\gamma_{17.6}, \alpha)] = 4.2\times10^{-4}. \quad (2)$$

To get the absolute value of $\sigma[Br^{79,81}(\gamma_{17.6}, \alpha)]$ we put $\sigma[Cu^{63}(\gamma, n)] = 10^{-26}$ cm^2.

Experimental value $\sigma[Br^{79,81}(\gamma_{17.6}, \alpha)] = (1.2\pm0.5)\times10^{-29}$ cm^2.

Theoretical value $\sigma[Br^{79,81}(\gamma_{17.6}, \alpha)] = 4\times10^{-29}$ cm^2.

This theoretical value is obtained for $r_0 = 1.3\times10^{-13}$ cm in the nuclear radius formulas; with $r_0 = 1.5\times10^{-13}$ cm the theoretical cross section increases by a factor of about 6. Our results demonstrate, therefore, that in the present case statistical nuclear theory gives the correct magnitude for the ratio $(\gamma, \alpha)/(\gamma, n)$.

From the level distribution of the residual nucleus, the energy distribution of the emitted α-particles can be calculated. The dotted curve in Fig. 1 shows the theoretical distribution, based on the level density formula $\omega(E) \propto \exp\{2[a(A)\cdot E]^{\frac{1}{2}}\}$ with $a(A) = 2.7$ Mev^{-1} as given by Blatt and Weisskopf.[5]

As one may learn from the figure, the calculation based on the above-mentioned assumptions is in satisfactory agreement with the experiment.

* Now at the University of Zürich, Zürich, Switzerland.
[3] Fowler, Lauritsen, and Lauritsen, Revs. Modern Phys. **20**, 236 (1948).
[3] H. Glattli *et al.* (to be published).
[4] H. Wäffler and S. Younis, Helv. Phys. Acta **22**, 614 (1949).
[4] H. Wäffler and O. Hirzel, Helv. Phys. Acta **21**, 200 (1948).
[5] J. M. Blatt and V. Weisskopf, unpublished ONR Technical Report No. 42 (1950).

A Fast Neutron Spectrometer

L. E. Beghian, R. A. Allen, J. M. Calvert, and H. Halban
Clarendon Laboratory, Oxford, England
(Received March 11, 1952)

THE methods used so far to determine the energies of fast neutrons rely mostly on the measurement of the pulse-height spectrum of recoil protons (hydrogen-filled ionization chambers, organic scintillating crystals, photographic plates). The neutron energy spectrum is then determined from the recoil spectrum, the neutron-proton scattering cross section, and the angular distribution as a function of energy. All these techniques however have the common disadvantage of poor resolution and considerable difficulty in the interpretation of results.

In order to try to overcome these difficulties, a technique to select only recoil protons which have suffered a head-on collision has been developed. The simplest way of doing this is to measure coincidences between recoil protons produced in an organic scintillating crystal and a second crystal arranged to detect neutrons scattered at practically 90° to the primary neutron beam. In principle, the scattering angle could be defined by geometrical alignment of the two crystals relative to the neutron beam, but this would lead to an intolerably low over all sensitivity of the apparatus.

We have, therefore, adopted a time-of-flight method which selects only coincidences which are due to neutrons traveling from the first to the second crystal with energies less than 30 kev. It is thus clear that for a primary energy of several million volts, the recoil proton in C_1 carries away more than 99 percent of the primary energy which in turn is dissipated in scintillation energy. Hence by measuring the pulse-height distribution of such recoils by a multi-channel kicksorter, the neutron energy spectrum can be directly determined.

As shown in Fig. 1, the two crystals C_1 and C_2 are viewed by 14-stage photomultipliers (E.M.I. type 6262) whose outputs feed into a fast coincidence circuit of total resolving time 3×10^{-8} second. The pulse from C_1 is delayed by 3.5×10^{-8} second. Thus a coincidence will be favored if the time of flight of the scattered neutron from C_1 to C_2 (distance 6 cm) is between 2×10^{-8} and 5×10^{-8} second: i.e., if its energy is between 3×10^6 ev and 5×10^6 ev approximately.

For C_1, a stilbene crystal (1.5 cm diameter, 0.5 cm thick) is

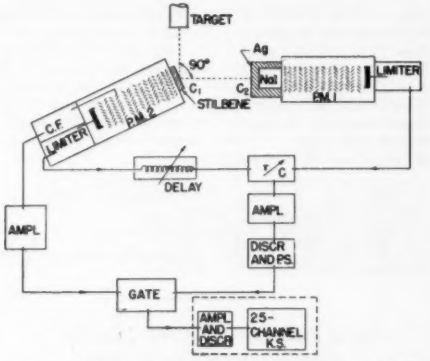

FIG. 1. Block diagram of spectrometer. C—coincidence unit; AMPL—amplifier; DISCR—discriminator; C. F.—cathode follower; P. S.—pulse shaper; K. S.—kicksorter; P. M. photomultiplier. Arrow indicates variable settings.

used. We find the scintillation energy for this is closely proportional to proton recoil energy [results to be published in Proc. Phys. Soc. (London)]. For C_2, a one-inch cube of NaI (Tl), surrounded by $\frac{1}{4}$ cm silver is used. The capture of neutrons by silver or iodine nuclei results in a γ-ray cascade which can then be detected by the crystal. The over-all efficiency of this combination for detecting neutrons of 3×10^6 ev is calculated to be about 6 percent from the known radiative capture cross sections. The pulse-rise time from sodium iodide is slow (0.25×10^{-6} second) for the present purpose; however, since proportionality of pulse height is not required from this crystal (it is anyhow limited to feed into the coincidence circuit), it is possible to operate on the initial portion of the leading edge of the pulse with a rise time of less than 10^{-8} second.

The output of the coincident circuit is amplified by a 5-megacycle bandwidth amplifier, and is then used to gate proportional pulses from C_1 (resolving time of gate 2×10^{-6} second). This insures that only those pulses from C_1 are selected for analysis which correspond to a head-on neutron-proton collision in the crystal, apart from a background due to random coincidences. The gated pulses are then analyzed by a multi-channel kicksorter. The normal output electrode of photomultiplier "C_1" cannot be used to supply the proportional pulses, since the output from this electrode has to be limited before being fed into the coincidence circuit. Instead, pulses from the 11th dynode are used since these have been found to be closely proportional to scintillation energy.

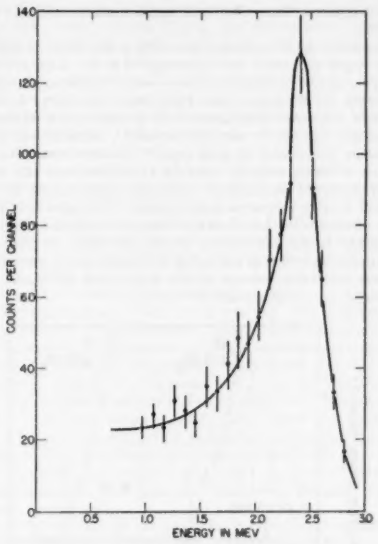

FIG. 2. Neutron peak.

The first measurements have been made with D-D neutrons of energy 2.8 Mev. Figure 2 shows the corresponding peak registered on the kicksorter.

The sensitivity of the instrument to gamma-radiation is very much lower than to neutrons: because of the delay introduced into the coincidence circuit, only fortuitous coincidences can be produced by γ-rays.

We wish to thank the Paul Foundation of the Royal Society for a grant which made this work possible and Lord Cherwell for his interest and encouragement.

Collision of Heavy Primary Cosmic-Ray Nucleus

N. L. ALLEN,* J. Y. MEI,* E. PICKUP, AND L. VOYVODIC
Physics Division, National Research Council, Ottawa, Canada
(Received April 30, 1952)

IN an investigation of the types of disintegrations caused by heavy primary nuclei in collisions with nuclei in emulsions, an unusually interesting example has been found in a 600-micron Ilford G5 emulsion exposed at about 85,000 feet.[1] The incoming nucleus with $Z=17\pm3$, as estimated by delta-ray counting, makes a collision in which 45 singly charged particles with minimum or near minimum ionization are produced with half-angle $\theta_1\simeq12.5°$. There is also a relativistic α-particle at about 3.5° to the forward direction. A microprojection tracing of the event is shown in Fig. 1, and the angular distribution in Fig. 2. Some particles were identified (see the following note), including 5 pions, one proton and a possible kappa-meson, with energies ($p\beta$) approximately 170, 300, 390, 570, 740, 770, and 710 Mev at angles about 36, 35, 11, 6, 10, 15, and 22 degrees relative to the incident direction respectively. An associated electron pair, C, starting about 80 microns from the star center also indicates that neutral pions were emitted.

Conservation of charge before and after the collision rules out silver as target nucleus, and also bromine since we know that there are pions created. There is no detectable heavy recoil. A collision with hydrogen also appears unlikely since the meson multiplicity would be too high for a shower of half-width 12.5°, unless we assume many secondary interactions. Thus it seems probable that the target nucleus was carbon, nitrogen, or oxygen,[2] with a central collision involving fairly complete break-up of the incoming and target nuclei. With oxygen as target, about 22 charged particles must have been created and the identifications made indicate that these were mostly pions. Allowing for 50 percent neutral pions gives about 33 pions created or a multiplicity of two per target nucleon. Consideration of all the nucleons and mesons emitted requires a minimum primary energy of about 2 Bev per nucleon. Even assuming that most of the forward particles are nucleons the width of the shower cone indicates that the primary energy is not much in excess of this limit. It would seem that there were many individual collisions (possibly some secondary) each giving a low pion multiplicity on the average.

FIG. 1. Collision of heavy primary nucleus, $Z=17\pm3$, in G5 emulsion with almost complete break-up of incident and target nuclei.

In the shower there were two close pairs of tracks[3] and a triple (marked D, E, F in Fig. 2) appreciably off the forward direction, and the statistical chance for each such grouping, based on the average angular distribution for this event, is about 5×10^{-3}. The pair D comprised two of the identified pions, and the energies and angular separation would give a Q value 6 ± 4 Mev if we assume them to result from the decay of a very short-lived neutral meson.[4]

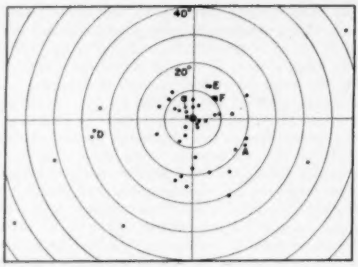

FIG. 2. Projection showing angular distribution of tracks in Fig. 1 relative to direction of the primary, which is perpendicular to the plane of the paper at the origin.

Further measurements will be made for a more detailed analysis of this event. We wish to thank Miss E. Motard for scanning, Mr. H. A. MacDonald for assistance in processing, and Mr. D. W. Rushton for preparing the drawings.

* National Research Council of Canada Fellows.
[1] The emulsions were exposed through a collaborative program of cosmic-ray investigations by the Bartol Research Foundation and the National Research Council of Canada with the cooperation of the ONR project, "Skyhook."
[2] The possibility of sulfur as target nucleus cannot be completely ruled out since it is present in emulsions in the ratio ~1/130 compared with carbon, nitrogen, and oxygen.
[3] J. Y. Mei and E. Pickup, Phys. Rev. **86**, 796 (1952).
[4] Danysz, Lock, and Yekutieli, Nature **169**, 364 (1952); see also reference 3 for the meaning of this result.

A Possible Charged *V*-Particle or Kappa-Meson Event Observed in a Photographic Emulsion

L. VOYVODIC
Physics Division, National Research Council, Ottawa, Canada
(Received April 30, 1952)

ONE of the shower particles in the cosmic-ray disintegration described in the preceding note shows a sudden change in direction through 20°, with no sign of a visible recoil. This resembles the charged *V*-particle tracks observed in cloud-chamber investigations,[1] but which have not been reported so far in emulsion experiments. The shower particle, track *A*, is 11,000 microns long and presents a favorable case for mass determination. The secondary track, *B*, is steep and only 700 microns long before leaving the emulsion.

Figure 1 shows the results of grain density and multiple scattering measurements for particle *A*, for six other long shower particles in the same disintegration, and also for five very long neighboring electron tracks (not associated with this event). The grain density shown for each shower particle is the mean value using two counting conventions, expressed relative to the corresponding mean value for electron tracks over the same region of emulsion depth. Values for $p\beta$ were derived from measured chord-angle mean deflections and the Williams-Molière scattering theory. Similar procedures for fast particle identification were used in a recent series of experiments at Bristol.[2-4] The theoretical ionization loss curves were calculated for silver bromide, the polarization plateau in the extreme relativistic region being normalized to the measured plateau for electrons. These curves were recently shown[2] to be in close agreement with experiment, although the treatment of ionization theory with polarization and Čerenkov radiation effects presents serious difficulties.[5]

It is seen from Fig. 1 that five of the other shower particles may be identified as pi-mesons and one as a proton. For track *A*, the combined grain density and scattering results yield a mass of $1210\pm180m_e$. Track *B* shows a grain density 1.14 ± 0.07 times "plateau," and an observed mean scattering deflection $\bar{D}(90\mu)=0.10$ microns. These combined measurements indicate a mass $>600m_e$.

The above results are consistent with either decay in flight or large angle scattering for shower particle *A*. Kappa-mesons[6] decaying at rest in emulsions have a mass $\sim1200m_e$, but appear to decay to mu-mesons and two neutral particles. A recent analysis[7] has shown that most of the available data on charged *V*-particles can also be similarly explained, although a pi-meson secondary is indicated in some cases.[8] The shower particles with masses $\sim1200m_e$, recently observed at Bristol[3] were also tentatively identified as being the same as kappa-mesons. For the present event a kappa-mu decay appears to be ruled out. A possible interpretation here is that of charged *V*-particle decay into a tau-meson and one or more neutral particles. An alternative interpretation is that of scattering of a kappa-meson, presumably nuclear scattering because of the large angle (20°) and short deBroglie wavelength ($\sim2\times10^{-14}$ cm).

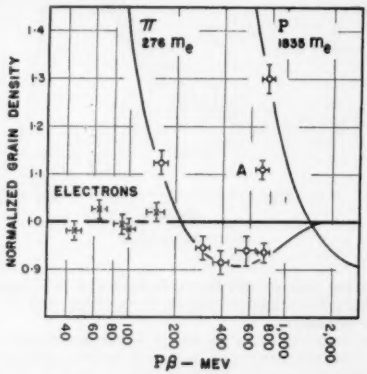

FIG. 1. Grain density, relative to the plateau for high energy electrons, plotted *versus* $p\beta$, the product of momentum and particle velocity. The indicated uncertainties are those derived solely from estimated statistical probable errors in grain counting and multiple scattering measurements. Approximate theoretical ionization loss curves are also shown for pi-mesons and protons.

Further work is in progress for this event, including refinements of measuring techniques, tracing the secondary track *B* into the facing plate, and calibration of mass resolution. One of the particles analyzed for calibration also appears to have a mass of $1330\pm200m_e$.

The author wishes to thank Dr. E. Pickup for discussions on this investigation.

[1] G. D. Rochester and C. C. Butler, Nature **160**, 855 (1947).
[2] L. Voyvodic, Bristol Conference Report (Dec. 1951).
[3] Daniel, Davies, Mulvey, and Perkins, Bristol Conference Report (Dec. 1951).
[4] Danysz, Lock, and Yekutieli, Bristol Conference Report (Dec. 1951).
[5] See M. Schonberg, Nuovo cimento **9**, 210 (1952).
[6] C. O'Ceallaigh, Phil. Mag. **42**, 1032 (1951).
[7] Armenteros, Barker, Butler, Cachon, and York (to be published).
[8] See H. S. Bridge and M. Annis, Phys. Rev. **82**, 445 (1951).

A Magnetic Effect in Magnesium Titanate*

E. K. WEISE AND H. KATZ†
Electrical Engineering Research Laboratory, University of Illinois, Urbana, Illinois
(Received April 23, 1952)

INCREASING attention is being given to the study of the magnetic properties of chemical compounds as a source of knowledge about the relation between electrical conductivity and the structure of some selected semiconductors. The high sensi-

tivity of the magnetic susceptibility for changes of the chemical composition is well known. Taking this into account, measurements were undertaken with the aim of widening the range of weighing for the determination of the number of vacant lattice sites in some titanates which had been slightly reduced for conversion to semiconductors. The three magnesium titanates were made by reaction in solid state and shaped into rods of about 2 mm diameter and 15 mm length. For conductivity measurements, platinum contacts were sintered on the ends. All rods were presintered in oxygen in a platinum furnace at 1450°C. This temperature was never exceeded in either the reduction treatment or the measurements. The rods were reduced in a wolfram furnace in hydrogen at different temperatures from 850°C upward.

The electrical conductivity was measured with an ohmmeter in helium or in toluene, depending on the temperature. The plotting showed the usual straight lines in a $1/T_{abs}$ *vs* log$R$ system. Nothing peculiar was found in these plottings.

The magnetic measurements were made at room temperature with a modified Curie-Chéveneau balance. The calibration was established using nickel chloride solutions with known concentrations. In the plotting of paramagnetic susceptibility *vs* percentage of removed oxygen, the values for two titanates, $MgTiO_3$ and Mg_2TiO_4, increased smoothly with a decrease of the oxygen. However, the third compound, $MgTi_2O_5$, showed a remarkable peak between 0.15 percent and 0.25 percent; as yet it has not been possible to determine the exact value of the peak with the equipment available. The samples with about 0.2 percent were so strongly magnetic that they were remarkably attracted by an ordinary toy magnet.

In order to determine the nature of this phenomenon, the dependence on magnetic field strength was determined. There was no apparent influence using the laboratory electromagnet, which could be varied from zero to about 2000 gauss field strength. This behavior is typical for paramagnetism and eliminates the possibility of a ferromagnetic effect, which was assumed at first because of the size of the observed forces.

Investigations (including other heavy metal titanates) of the dependence on temperature are in progress for a wider range of temperatures.

* Based in part on work done under contract with the USAF.
† A complete paper on this subject will be submitted by H. Katz to the Department of Electrical Engineering of the University of Illinois in partial fulfillment of the requirements for the Ph.D. degree.

Secondary Electron Spectrum of Pr^{142}†

ERLING N. JENSEN, L. JACKSON LASLETT, AND D. J. ZAFFARANO
Institute for Atomic Research and Department of Physics, Iowa State College, Ames, Iowa
(Received April 21, 1952)

IN a previous publication concerning the radiations of Pr^{142}, the authors[1] reported the presence of one gamma-ray, having an energy of 1.57$_6$ Mev, and two beta-groups, with maximum energies of 2.15$_4$ Mev and 0.63$_6$ Mev. Other investigators[2] have reported a number of low energy gamma-rays for Pr^{142}. In the original work of the present authors[1] a search was made for low energy gamma-rays, but none was found. If these gamma-rays existed, however, they would have been observed as photoelectric lines superposed on a broad distribution of electrons which was ascribed to secondary electrons produced by bremsstrahlung.

Dr. Alburger[3] of Brookhaven National Laboratory has suggested that the broad distribution of electrons ascribed to secondary electrons produced by bremsstrahlung, as reported in our original paper,[1] might be due to beta-rays that have passed through part of the Lucite holder and then scattered from another part of the source holder. On repeating the experiment with Sr^{90}—Y^{90} it was found that a substantial fraction, but not all, of the electron distribution attributed to bremsstrahlung was, in fact, due to scattered beta-particles, as suggested.

It seemed worthwhile, therefore, to re-examine the secondary electron spectrum of Pr^{142} in order to make a search for low energy gamma-rays under more favorable circumstances and also to determine the existence or nonexistence of an appreciable number of secondary electrons produced by bremsstrahlung. A sample of spectrographically pure (contaminants of Nd, La, and Ce less than 0.1 percent) Pr_6O_{11} made available through the courtesy of Dr. F. H. Spedding and Mr. T. A. Butler of this laboratory was

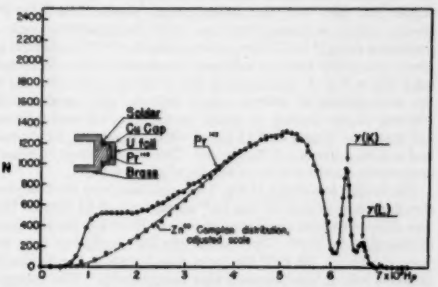

FIG. 1. The solid line, given by the circles, is the secondary electron spectrum of Pr^{142} as obtained with the arrangement shown in the insert. The broken line, given by squares, was obtained from the Compton distribution produced by the Zn^{65} gamma-ray (1.12 Mev) normalized to the Compton distribution from Pr^{142}. N is the number of counts per minute.

irradiated in the Argonne pile and then examined with a thin-lens spectrometer[4] modified to incorporate ring focusing.[5]

The irradiated praseodymium was placed in a brass holder and covered with a copper cap, of surface density 2.92 g/cm^2, on which was fastened a uranium foil of surface density 42 mg/cm^2. The secondary electron spectrum obtained with this source is shown by the solid line in Fig. 1. The insert in Fig. 1 shows a

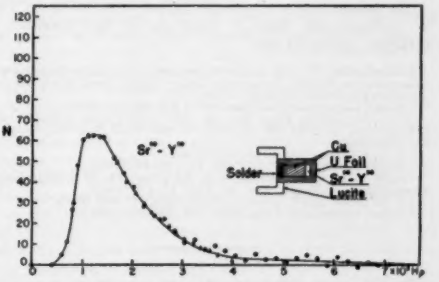

FIG. 2. The curve given by the solid circles is the secondary electron spectrum from the copper capsule and uranium foil, as produced by bremsstrahlung arising in the copper capsule due to the absorption the of beta-particles from Sr^{90}-Y^{90}. The arrangement of source, copper capsule, and uranium foil is shown in the insert. N is the number of counts per minute for this distribution. The triangles were obtained by subtracting the two curves shown in Fig. 1 and multiplying by an appropriate normalizing factor.

scale drawing of the arrangement of the Pr^{142}, brass holder, copper cap, and uranium foil. Spectra were obtained with and without the solder ring on the shoulder of the brass holder and no change in the shape of the spectrum was observed. Only one gamma-ray was observed, having an energy of 1.57$_6$ Mev as reported previously.[1]

Since no low energy gamma-rays were observed and the material surrounding the source was sufficient to absorb completely electrons with an energy greater than 5 Mev, it was concluded that the broad distribution of electrons observed at the low energy

end of the spectrum, in addition to the expected Compton distribution, is due to secondary electrons that are produced in the copper cap and uranium foil by the bremsstrahlung arising in the copper cap as a result of the absorption of the beta-particles.

As a check of the foregoing interpretation for the broad distribution of electrons at the low energy end of the spectrum shown in Fig. 1, a source of $Sr^{90}-Y^{90}$ was placed in a copper capsule to which was fastened the same uranium foil as that used with the Pr^{143} source. This copper capsule had the same diameter as the copper cap used with the praseodymium source. The $Sr^{90}-Y^{90}$ source, which is gamma-free and emits beta-particles with a maximum energy[6] (2.23 Mev) close to that for Pr^{143}, was found to give a secondary electron spectrum as shown by the circles and solid line in Fig. 2. The insert in Fig. 2 shows a scale drawing of the arrangement of source, copper capsule, and uranium foil. The end of the capsule on which the uranium foil was fastened had a surface density of 2.43 g/cm² while the sides of the capsule had a surface density of 2.12 g/cm². This was sufficient to absorb completely electrons with an energy of about 4 Mev.

The broken line shown in Fig. 1 was obtained from the Compton distribution produced by the Zn^{65} gamma-ray (1.12 Mev).[7] This was obtained under conditions similar to those for the Compton distribution for Pr^{143}. The scale of the Zn^{65} curve has been adjusted to match the Pr^{143} Compton distribution at the maximum ordinate and at the Compton high energy "edge." The triangles shown in Fig. 2 were obtained by substracting the two curves shown in Fig. 1 and normalizing the ordinates. It may be seen that the two secondary electron distributions produced by bremmstrahlung are in good agreement. It appears, then, that the broad distribution of electrons at the low energy end of the Pr^{143} spectrum shown in Fig. 1 is due to bremsstrahlung.

The secondary electron spectrum of Pr^{143}, shown in Fig. 1, is therefore regarded as a composite of the photoelectrons and Compton electrons arising from a single gamma-ray, plus the electrons produced by bremsstrahlung. This conclusion, accordingly, in no way alters the final results and conclusions regarding the radiations from Pr^{143} nor the decay scheme reported in the previous publication.[1]

The authors wish to express their appreciation to Messrs. Earl W. McMurry and James T. Jones, Jr. for their assistance in obtaining part of the data.

† Contribution No. 183 from the Institute for Atomic Research and Department of Physics, Iowa State College, Ames, Iowa. Work was performed in the Ames Laboratory of the AEC.

[1] Jensen, Laslett, and Zaffarano, Phys. Rev. **80**, 862 (1950).
[2] C. E. Mandeville, Phys. Rev. **75**, 1287 (1949); Cork, Schreffler, and Fowler, Phys. Rev. **74**, 1657 (1948); E. R. Rae, Proc. Phys. Soc. (London) **63A**, 292 (1950).
[3] D. E. Alburger (private communication).
[4] Jensen, Laslett, and Pratt, Phys. Rev. **75**, 458 (1949).
[5] Pratt, Boley, and Nichols, Rev. Sci. Instr. **22**, 92 (1951); Keller, Koenigsberg, and Paskin, Rev. Sci. Instr. **21**, 713 (1950).
[6] E. N. Jensen and L. J. Laslett, Phys. Rev. **75**, 1949 (1949).
[7] Jensen, Laslett, and Pratt, Phys. Rev. **76**, 430 (1949).

The Nature of Cosmic-Ray Bursts Underground*

C. N. Chou
Department of Physics, University of Chicago, Chicago, Illinois
(Received April 28, 1952)

In a previous publication,[1] size-frequency relations of cosmic-ray bursts observed underground were reported. The apparatus used was a duralumin ionization chamber of wall 1.2 cm thick, filled with argon to a pressure of 88 atmospheres at 20°. It was at least 2 to 4 meters from the wall of a tunnel under 30 meters of clay. It had a collecting volume of about 1.2 liters, and recorded bursts predominantly of sizes 10^6–10^7 ion-pairs, corresponding to about 15–150 minimum-ionizing particles. The integral size-frequency distributions [given originally in Fig. 4(c) of the previous publication] are reproduced in Fig. 1 with added indications of standard deviations. The ordinate gives the observed integral rate of bursts (except curve Pb, which has been adjusted as explained below) in number per hour. The abscissa gives the estimated energy of bursts assuming that they were produced by μ-mesons through the usual processes of knock-on, bremsstrahlung, and pair-production. The scale of the abscissa does not apply to curve *S*, which gives the theoretically estimated contribution of nuclear stars (presumably produced by μ-mesons) inside the chamber, based on observations by George and Evans.[2] Curve *C* indicates the actually observed number of bursts with the chamber unshielded (corrected for the contribution of stars as given by curve *S*), and hence probably produced from the clay of the wall of the tunnel. The energy of the bursts is estimated from the shower development and the geometry. Curve Pb indicates the bursts observed with lead plates of size 20×20 cm² and of average thickness 13 cm placed above the chamber (the correction for stars being negligible in this case). The interception efficiency (with respect to burst size) was estimated to have increased by a factor of 5, and the frequency by a factor of 30 in comparison with the observations for bursts produced from clay. This adjustment seems justified by comparing our results with those obtained recently by Driggers[3] at sea level. The dashed curve *D* represents his results directly. The agreement is satisfactory within experimental uncertainties.

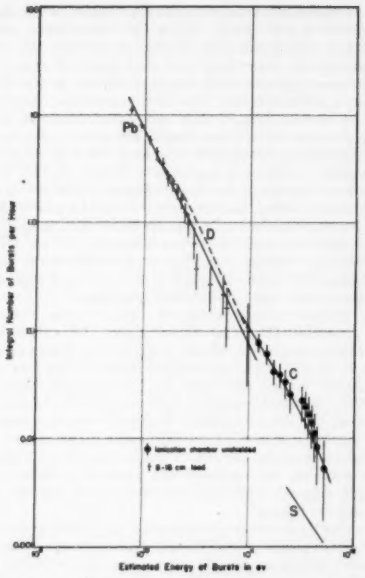

FIG. 1. Integral size—frequency relations of bursts.

The curves Pb and *C* should be compared with the well-known underground intensity *vs* depth relation actually observed.[2] The slope of curve *C* agrees well with the slope of the intensity *vs* depth curve at depth greater than about 200 m water equivalent. Hence if we assume that the conclusion is valid that the efficiency of burst production under similar geometrical conditions remained the same at ground level as underground, our experimental results show that either (a) fewer μ-mesons of energy higher than about 10^{11} ev or/and (b) more μ-mesons of energies in the range 10^{10}–10^{11} ev exist under 60 m water equivalent than at ground level.

Explanation based on alternative (a) has been given independently by Greisen[4] and by Hayakawa[5] in 1948. Due to the relativistic increase of the lifetime of the high-energy π-mesons,

the probability of their undergoing interaction before decay increases, and hence it results in the reduction of the number of μ-mesons of energies greater than about 10^{11} ev. Since the experimental information we possess regarding the number of μ-mesons underground is not too precise, some contribution of the type (b) cannot be ruled out entirely. Recently Hayakawa[6] discussed the possible effects of κ-mesons underground. He assumed that κ^0-mesons should interact in the earth crust according to the scheme

$$\kappa^0+P(N)\rightarrow N(P)+\kappa^+(\kappa^-),$$

and that the mean free path of all κ-mesons should be of the order of several tens of meters of water equivalent. Most of the $\kappa^{\pm}$-mesons[7] of energies more than about 10^{11} ev would survive since their mean life is about 10^{-9} sec. On the other hand, most of those of energies less than about 10^{11} ev should decay possibly into μ-mesons. Hayakawa suggested the following decay scheme:

$$\kappa^{\pm}\rightarrow\kappa^0+\mu^{\pm}+\mu^0.$$

Formerly only processes of type (a) seemed to be responsible for the results observed here; recently, however, the comparatively large abundance of the production of κ-mesons at high energies[8] may mean that the contribution of process (b) is considerable and cannot be neglected in explaining the frequency of bursts underground.

The author is greatly indebted to Professor Marcel Schein for the use of the facilities of the Cosmic-Ray Laboratory and for valuable and stimulating discussions. He also wishes to thank the Department of State for a grant.

[6] Supported in part by the joint program of the ONR and AEC.
[1] C. N. Chou, Phys. Rev. **74**, 1659 (1948).
[2] J. G. Wilson, *Progress in Cosmic-Ray Physics* (North-Holland Publishing Company, Amsterdam, Holland, 1952), p. 395.
[3] F. E. Driggers, private communication to Professor Marcel Schein (1952).
[4] K. I. Greisen, Phys. Rev. **73**, 521 (1948).
[5] S. Hayakawa, Prog. Theor. Phys. (Japan) **3**, 199 (1948).
[6] S. Hayakawa, Proc. Phys. Soc. (London) **A65**, 215 (1952).
[7] C. O'Ceallaigh, Phil. Mag. (London) **42**, 1032 (1951).
[8] Proc. Rochester Conference on Meson Physics (University of Rochester, Rochester, 1952), p. 58.

Double Beta-Decay of Sn^{124}†

R. M. Pearce and E. K. Darby
Department of Physics, University of British Columbia, Vancouver, Canada
(Received April 23, 1952)

SEVERAL attempts have been made to detect the double beta-decay of Sn^{124}.[1-3] Fireman[1] has obtained a positive result from which he concluded that the half-life of the process is 0.4×10^{16} years. Lawson[2] and very recently Kalkstein and Libby[3] came, however, to the conclusion that if the double beta process exists at all, its half-life must be much longer ($>2\times10^{17}$ years).

We have carried out another experiment with the view of detecting the double beta-decay of Sn^{124}. The experiment gave a negative result, thus confirming Lawson's, and Kalkstein and Libby's findings. However, our experiment was quite different in nature from the experiments quoted above, and we feel, should lead to a more reliable identification of the double beta-decay, should it exist.

According to the existing theories, the double beta-decay of a nucleus may, in principle, take place in two different manners, one in which the beta-particles are accompanied by two neutrinos and the other in which only the two beta-particles are emitted.

The predicted half-life from the different theories is rather uncertain; there is, however, no doubt that the half-life should be several orders of magnitude longer for a four-particle process than for a two-particle process. In addition to the predicted difference in half-life, the two-particle process possesses another distinguishing feature: since no neutrinos are emitted the sum of the energies of the two beta-particles must be equal to the total energy carried away and thus must be constant.

It follows from these considerations that if the double beta-decay is observable at all, it will very likely be a two-particle process, so that the sum of the beta energies will be constant. Consequently, we have devised an experiment with Sn^{124} in which the sum of the energies of coincident events in the tin was displayed on a "kicksorter." The energy spectrum of the double beta process recorded with the kicksorter should then consist of the background with a "peak" at an energy corresponding to the sum of the two beta-energies. It is difficult to imagine another process in which such a sharp peak could occur, so a positive identification should be possible.

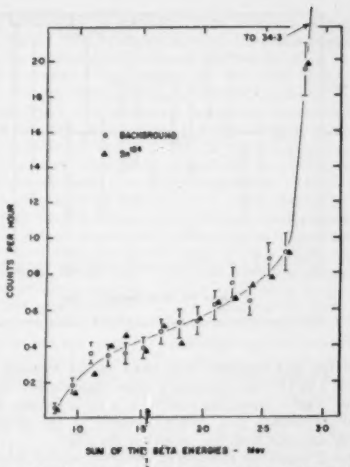

FIG. 1. Coincidence spectra for tin sample and for background as obtained on an 18-channel kicksorter.

A source consisting of a 200-mg tin foil (100 mg/cm^2) containing 95 percent Sn^{124} was placed between two scintillation counters. (The source was made at Oak Ridge National Laboratory and supplied through the cooperation of the Atomic Energy Project, Chalk River.) Coincident beta-particles were detected in the thick anthracene crystals ($1\times1\times\frac{1}{4}$ in.) which were separated by 1 cm. The background rate was obtained by replacing the tin foil with an aluminum foil of equal weight. (An aluminum "dummy" was used because available natural tin foils showed some slight contamination.) The amplitudes of two coincident pulses from the detectors were added electronically. The pulse representing this sum was then displayed on an 18 channel "kicksorter" of Chalk River design. A "gate" controlled by the coincidence mixer allowed the output from the pulse adder to reach the kicksorter only in the case of a coincident event.

Since the amplitudes of the detector pulses are proportional to the energy of the beta-particles,[4] the added pulses from double beta-events were expected to have constant amplitude. This would result in a "peak" on the graph of the number of coincidences *versus* the sum of energies of the two beta-particles. The counters were calibrated and adjusted to have identical graphs of pulse height *versus* energy by using the 2.4 Mev beta-particle group from Sb^{124}.

Figure 1 shows the coincidence spectrum obtained with the Sn^{124} in place, and also the background coincidence spectrum. The data were obtained over a period of 264 hours, the background being taken every second day. The counters were shielded by 16 cm of lead from above and by 8 cm of lead in other directions. The large number of counts in channel 18 (energies >3.0 Mev) is the result of cosmic radiation. A large liquid scintillator placed above the counters and connected in anticoincidence reduced the number of counts in channel 18 by 40

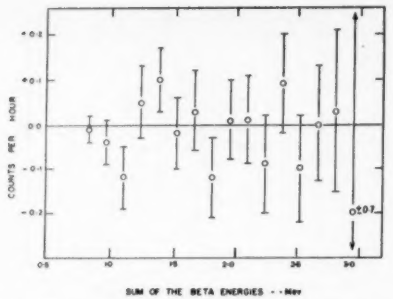

FIG. 2. Difference between tin and background coincidence spectra.

percent but had relatively little effect on the counting rate in channels 1 to 17. The coincidence mixer channels were biased at 0.3 Mev, since a lower bias resulted in a rapid increase in background coincidence rate, owing probably to the detection of particles scattered from one counter to the other.

Figure 2 shows the coincidence spectrum derived from Fig. 1 by subtracting the background. No trace of a peak is found. In order to obtain a lower limit for the half-life of the double beta-decay, the width of the expected peak must be estimated. Although the source weighed 100 mg/cm², the total energy lost by the two beta-particles in traversing it will be nearly constant since both the rate of energy loss above 0.3 Mev and the total path length are practically constant. The peak width would therefore be mainly determined by the energy resolution of the crystals, which is about 10 percent. This corresponds to one, or at the most two channels on the kicksorter. Since the background is about 0.5 count per hour per channel, the effective background is not more than 1.0 count per hour. This compares favorably with that of Fireman[1] (14 per hour) and that of Kalkstein and Libby[2] (80 per hour).

A peak of 0.2 count per hour would just be detectable (see Fig. 2). The geometric efficiency of the counters for coincidence counting is 0.2 and the transmission factor of the foil is estimated to be 0.4 at 1.0 Mev and 0.7 at 3.0 Mev. An estimate of the counting losses incurred by biasing the coincidence mixer at 0.3 Mev is included in the transmission factor. With these assumptions a lower limit of 0.3 to 0.6×10^{17} years is set for the half-life of the double beta-decay of Sn^{124}.[5]

The authors would like to thank Professor W. Opechowski for many helpful discussions.

† This work was sponsored by the Atomic Energy Project, Chalk River, Canada, and supported by the National Research Council of Canada.

[1] E. L. Fireman, Phys. Rev. **75**, 323 (1949).
[2] J. S. Lawson, Phys. Rev. **81**, 299 (1951).
[3] M. I. Kalkstein and W. F. Libby, Phys. Rev. **85**, 368 (1952).
[4] J. I. Hopkins, Phys. Rev. **77**, 406 (1950).
[5] A similar experiment with essentially the same results has just been reported by J. A. McCarthy, Bull. Am. Phys. Soc. **27**, No. 3, 18 (1952).

A Method of Interpreting the Distribution in Multiplicity of Shower Secondaries

JOHN LINSLEY
University of Virginia, Charlottesville, Virginia
(Received April 25, 1952)

A TARGET, either emulsion or cloud-chamber plate, that is carried to high altitude is exposed there to a particle flux which is essentially the primary cosmic-radiation. If interactions in the target with fast charged primaries are selected, those interactions will be mostly proton-induced. The multiplicity n of shower secondaries (ionization $\leqslant 1.5$ times minimum) can be found rather easily, and an integral distribution in n, ψ_n, for the sample can be obtained.

The energy spectrum of the primary radiation has been determined with fair accuracy[1,2] and the distribution in interaction energy for the sample is the same as the distribution in primary energy since the interaction cross section is geometric at the high energies involved.

From ψ_n and the primary spectrum the variation in multiplicity of shower secondaries with energy could be found with ease if the multiplicity did not fluctuate considerably about its average value $\bar{n}$ for a given interaction energy. But the effective "lack of resolution" caused by the fluctuations could be taken into account if the behavior of the fluctuations were known.

The scanty experimental evidence that has been obtained[3] indicates that the fluctuations follow a Poisson distribution. Equation (1) is an integral equation for $\bar{n}(E)$ derived under the assumptions that the primary proton energy spectrum is N/E^{k-1} (E is the total energy in rest mass units) and that fluctuations follow a Poisson distribution.

$$N(k-1)\sum_{j=n}^{\infty}\int_{E_\lambda}^{\infty}[\bar{n}(E)]^j\exp[-\bar{n}(E)]dE/E^k j!=\psi_n. \qquad (1)$$

E_λ is the energy at which the primary spectrum is cut off by the earth's field at latitude λ.

Using for ψ_n-values observed by the Bristol group[3] for stars in emulsion with $N_h \geq 7$, a solution has been obtained which is shown in Fig. 1. Substitution of $\bar{n}(E)$ shown in the figure into (1) gives

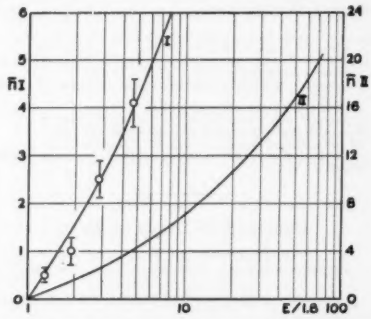

FIG. 1. Variation of average multiplicity of shower secondaries with interaction energy.

calculated ψ_n values that agree with the data within statistical errors for $0 \leqslant n \leqslant 15$. Values of $\bar{n}$ found by direct measurement are shown also.[4] The agreement is somewhat remarkable since the direct measurements of $\bar{n}$ were not consulted in deriving the solid curve, except in determining the threshold energy E_0 which is defined below. The trial function $\bar{n}(E)$ shown is of the form $K(E^s-E_0^s)$. $E_0=1.8$, $s=\frac{1}{4}$, $K=4.8$. Trial functions with $s=\frac{1}{4}$ to $\frac{1}{3}$ and suitably adjusted K values are not much different from the curve shown over the energy range considered, and they give nearly as good agreement with the ψ_n data. They disagree most for small n values, and they do not agree with the direct measurements (which are for low energies) as well as the curve shown.

Since the shower secondaries are mostly mesons,[3] $\bar{n}(E)$ is essentially the average meson multiplicity as a function of energy. Provided that the assumption about fluctuations is reasonably correct, one has here a way of measuring average meson multiplicity as a function of energy with fair accuracy out to energies greater than 100 Bev.

It can be shown that that assumption can be checked by measurement of the latitude effect on the distribution in n, for the integral equation takes into account the latitude cutoff.

The ψ_n data treated above apply to collisions of protons with nuclei of silver and bromine. Data are available for the lighter

nuclei in emulsion and for lead, and corresponding solutions $n(E)$ are being computed in an investigation of the effect of mass number of the target nucleus. It is hoped that a complete account can be published shortly.

[1] Winckler, Stix, Dwight, and Sabin, Phys. Rev. **79**, 656 (1950).
[2] Kaplon, Peters, Reynolds, and Ritson, Phys. Rev. **85**, 295 (1952).
[3] Camerini, Davies, Fowler, Franzinetti, Lock, Perkins, and Yekutieli, Phil. Mag. **42**, 1241 (1951).
[4] Camerini, Davies, Franzinetti, Lock, Perkins, and Yekutieli, Phil. Mag. **42**, 1261 (1951).

Half-Life and Radiations of Tc^{100}

G. E. Boyd, Q. V. Larson, and G. W. Parker
Chemistry Division, Oak Ridge National Laboratory, Oak Ridge, Tennessee
(Received April 24, 1952)

SEVERAL years ago a preliminary report[1] was made on an 80±10-second activity which appeared to follow the chemistry of technetium. Subsequent 14-Mev deuteron and 7-Mev proton bombardments of 90.2 percent Mo^{100} by the present senior author, however, showed the half-life to be 70±2 sec, and the charged particle energy to be 2.1±0.2 Mev. Magnetic deflection measurements, in addition, indicated these particles were positrons. Although positron emission in Tc^{100} was unexpected, the possibility of its occurrence could not be excluded since this radionuclide is isobaric with stable Mo^{100} as well as with Ru^{100}.

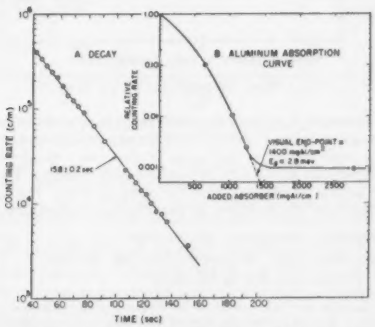

FIG. 1. A. Decay of gamma-radiations from Tc^{100} measured through 1.96 g Pb/cm². B. Aluminum absorption curve for 15.8-sec Tc^{100} constructed from isochrone on decays through varying thicknesses of aluminum.

Additional chemical tests were made, since the half-life and radiations of the ostensible technetium activity were very similar to those reported for F^{17} ($T_{\frac{1}{2}}$=69 sec; 2.1-Mev positrons). The rapid volatility procedure employed earlier to separate Tc from irradiated Mo^{100} metal was modified to include a separation of HF. The 70-second period was then found only in the fluoride fractions. Presumably the 70-sec F^{17} activity previously confused with technetium resulted from $(d, 2n)$ and (d, n) reactions on very small amounts of oxygen remaining in the probe target after the reduction of $Mo^{100}O_3$ to molybdenum metal with hydrogen.

Additional proton and deuteron irradiations of Mo^{100} were then made in a careful search for Tc^{100}. After chemistry no new technetium activities were observed with a Geiger counter, from which it was concluded that the half-life of Tc^{100} was either less than 30 seconds, or greater than several years. Because of the time required for chemistry, it was not possible to decide if a reported[2] 18-second beta-emitting activity produced in natural molybdenum by 7-Mev protons should be assigned to technetium. Recently, however, the preparation of Tc^{100} without the need for ultra-rapid chemical separations has become possible by reason of the availability of fractional gram amounts of long-lived, fission product Tc^{99}. Milligram amounts of purified Tc metal[3] and TcO_2 were irradiated with thermal neutrons for 20 to 30 second periods in the Oak Ridge graphite pile. The decay of the induced activity was measured through varying thicknesses of aluminum and lead using a mica end-window beta-proportional counter as a detector and strip chart recording. A typical decay curve of the gamma radiations is shown in Fig. 1A, while a rough aluminum absorption curve taken from an isochrone is given in Fig. 1B. It has been concluded that Tc^{100} decays with a 15.8±0.2 second half-life and that beta-rays of 2.8±0.2-Mev maximum energy are emitted together with gamma-radiations. Almost certainly the beta- and gamma-spectrum of Tc^{100} is complex.[4] Numerous levels in Ru^{100} have been seen in the decay of 20-hr Rh^{100}, while the logft value for 15.8-sec Tc^{100} is but 4.45 when it is assumed that no other beta-rays than the 2.8-Mev group occur in the decay. Quantitative measurements of the radiations of Tc^{100} are in progress.

A search was also made for a possible long-lived isomeric state of Tc^{100} with negative results. Ten milligrams of technetium metal were irradiated with slow neutrons until an integrated flux, nvt, of 1.8×10^{18} neutrons/cm², was accumulated. The irradiated metal was converted to pertechnetate, and the latter purified by anion exchange chromatography. Sources were prepared and examined within 32 hours after bombardment using a (Tl+Na)I scintillation spectrometer and a krypton-filler beta-proportional spectrometer. No quantum radiations other than those which could be attributed to very small amounts of 92.8-hr Re^{186} and 26.8-hr As^{76} impurity were seen. This finding appears to be consistent with the observed absence of Tc^{100} in mass spectrographically analyzed fission product Tc^{99}.[5]

[1] E. E. Motta and G. E. Boyd, Phys. Rev. **73**, 1470 (1948).
[2] L. A. Dubridge, private communication to G. T. Seaborg, Revs. Modern Phys. **16**, 14 (1944).
[3] Cobble, Nelson, Parker, Smith, Jr., and Boyd, J. Am. Chem. Soc. **74**, 1852 (1952).
[4] House, Colligan, Kundu, and Pool, Phys. Rev. **86**, 654 (1952).
[5] Ingham, Hess, and Hayden, Phys. Rev. **72**, 1269 (1947).

High Energy Photodisintegration of the Deuteron*

Raphael Littauer and James Keck
Cornell University, Ithaca, New York
(Received May 2, 1952)

RECENT experiments[1–9] on the photodisintegration of the deuteron by high energy quanta have indicated that above the meson threshold the cross section for this process rises appreciably over the photoelectric cross section of the phenomenological theory.[4,6] The excitation function and angular distribution in this region are of considerable interest in connection with meson theory and current speculation about an isobaric state of the nucleon. We therefore felt it desirable to extend to higher energy the measurements of Benedict and Woodward[1] who investigated the photodisintegration up to 160 Mev.

Bremsstrahlung from the Cornell 310-Mev electron synchrotron was allowed to strike equivalent targets of H_2O and D_2O. Charged particles emitted at a given laboratory angle were detected in a coincidence-anticoincidence counter telescope which defined their ranges and selected protons by means of their specific ionization. Figure 1 shows the ranges of angle and energy used for the experiment. By subtracting the H_2O count from the D_2O count, one obtains an effect that can be due only to the process $D(\gamma, n)p$, since the contribution from the oxygen cancels out and meson production cannot give recoil protons in the ranges selected. We have so far examined the disintegration produced by quanta of about 180 and 260 Mev in the laboratory, corresponding to 165 and 230 Mev in the center-of-mass system. The gamma flux was measured with an ionization chamber placed behind 1 cm of lead. This had previously been calibrated against a pair spectrometer[6] and by means of a shower curve analysis.[7] The estimated error

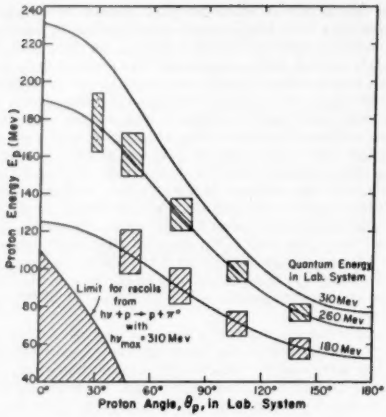
Proton Energy E_p (Mev)
Proton Angle, θ_p, in Lab. System
Quantum Energy in Lab. System
310 Mev
260 Mev
180 Mev
Limit for recoils from $h\nu + p \rightarrow p + \pi^0$ with $h\nu_{max}$ = 310 Mev

FIG. 1. Kinematics of the photodisintegration.

in the beam calibration obtained this way is ±15 percent, which we believe to be the main uncertainty in the absolute scale of cross sections of this experiment.

Figure 2 shows the cross sections for photodisintegration measured at the two energies as a function of proton angle in the c.m. system. For comparison, we have plotted the points obtained by Benedict and Woodward[1] at 160 Mev on the same figure. Except for a point in the back hemisphere, agreement is seen to be good.

The statistical errors make it impossible to determine the angular distributions very well. The points are consistent with an isotropic distribution at both energies, and it would be difficult to accommodate anisotropic terms to more than about 50 percent. For lack of better information, we have computed the total cross sections under the assumption that the angular distributions are isotropic. This contrasts with the treatment of Benedict and Woodward, who fitted a distribution of the form $\sin^2\theta(a+b\cos\theta)+c$ to their experimental points. At 160 Mev, they found $b\sim c\sim 0.4a$, subject to some uncertainty because only three points in the angular distribution were measured.

Figure 3 gives the total cross sections as a function of quantum energy in the c.m. system. We have shown the data of Benedict and Woodward as well as our own, together with a curve taken from the paper by Schiff.[4] The experimental errors shown are

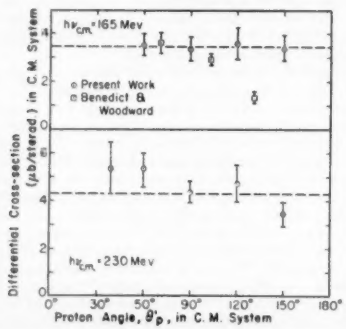
$h\nu_{c.m.}$ = 165 Mev
o Present Work
□ Benedict & Woodward
$h\nu_{c.m.}$ = 230 Mev
Differential Cross-section (μb/steradian) in C.M. System
Proton Angle, θ'_p, in C.M. System

FIG. 2. Differential cross sections in the c.m. system.

statistical; in addition, there is an over-all uncertainty of about ±20 percent in the absolute scale for our data and ±30 percent for that of Benedict and Woodward.[6] Most of the disagreement between the two points at 160 Mev can be traced to the difficulty of angular integration pointed out above and indicates the extent to which the total cross section is uncertain at present.

Our values are considerably lower than those reported by Gilbert and Rose,[2] who, however, allow an error of a factor of two in their absolute cross sections. The recent data of Kikuchi,[3] obtained by multiplying the 90° differential cross section by 4π, agrees with our results, although the stated error is a factor of three. Kikuchi also reports a forward asymmetry of the photoprotons in the c.m. system, for which we have here not found any strong indication.

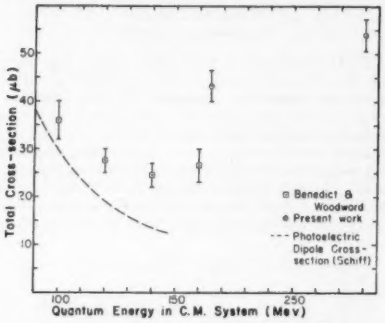
Total Cross-section (μb)
Quantum Energy in C.M. System (Mev)
□ Benedict & Woodward
o Present work
Photoelectric Dipole Cross-section (Schiff)

FIG. 3. Total cross sections in the c.m. system.

In summary, it appears at present that the photodisintegration cross section begins to deviate from the phenomenological electric dipole cross section in the region of the meson threshold, and thereafter rises slowly with increasing quantum energy. The total cross section at 230 Mev is of the order of 50 μb. The angular distribution of the photoprotons shows no very marked anisotropy.

* Work done under contract with the ONR.
[1] T. S. Benedict and W. M. Woodward, Phys. Rev. **85**, 924 (1952).
[2] W. S. Gilbert and J. W. Rose, Phys. Rev. **85**, 766 (1952).
[3] S. Kikuchi, Phys. Rev. **85**, 1062 (1952).
[4] L. I. Schiff, Phys. Rev. **78**, 733 (1950).
[5] J. F. Marshall and E. Guth, Phys. Rev. **78**, 738 (1950).
[6] This calibration was carried out by Professor J. W. DeWire.
[7] Dr. A. M. Perry undertook most of the shower curve measurements.
[8] Since the same beam calibration was used for the two experiments, however, these errors are not entirely independent.

Radiation Loss by Electrons in Large Orbits*

DALE R. CORSON
Cornell University, Ithaca, New York
(Received May 1, 1952)

DOUBT has recently been raised[1] concerning the validity of the classical calculations[2] of radiation loss by electrons moving in large orbits in a uniform magnetic field. Parzen's[1] quantum mechanical calculations indicated a much smaller total energy loss than is given by classical theory.

The radiation loss can be measured by observing how the orbit radius in a synchrotron changes with time when the radio frequency accelerating voltage is removed. We have $E=300H\rho$ and $H=H_0(\rho_0/\rho)^n$, where E is measured in electron volts, H in gauss, and ρ in cm. When both the orbit radius and time are allowed to vary we have

$$\dot{E}/E=(1-n)\dot{\rho}/\rho+\dot{H}/H.$$

Here $\dot{E}$ is the total rate of change of the electron's energy:

$$\dot{E}=\dot{E}_{rf}+\dot{E}_{\beta}+\dot{E}_{rad}+\dot{E}_0,$$

where $\dot{E}_{rf}$ is the rate at which energy is gained from the rf accelerating field, which is zero in these measurements since the electrons are accelerated up to energy E and then the rf voltage is removed. $\dot{E}_\beta$ is the rate at which energy is gained by the betatron effect resulting from changing flux within the orbit. This is measured at each point of the magnetic cycle by placing a turn of wire at the orbit radius (actually above or below the donut) and measuring the peak voltage on a peak-reading vacuum tube voltmeter. The wave form is displayed on an oscilloscope, and the voltage is measured at various points in the cycle by scaling the deflection relative to the peak value. $\dot{E}_{rad}$ is the rate of energy loss by radiation which we are measuring. $\dot{E}_0$ is the rate of energy loss by other means, e.g., by image currents in the conducting walls of the donut. No coherent energy loss, i.e., loss that depends on the number of electrons being accelerated, has been detected.

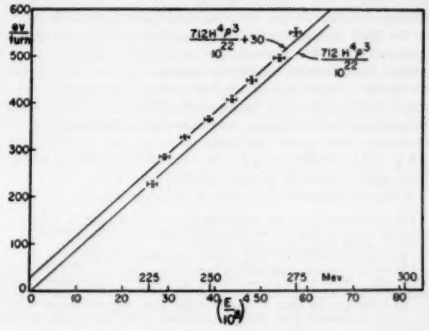

FIG. 1. Radiation loss per turn vs (energy)^4.

The orbit shrink rate ($\dot{\rho}$) is measured by focusing the visible radiation on to a grid placed over a photomultiplier tube. As the orbit shrinks the spot of light moves across the grid producing a modulated output from the photomultiplier. Distances inside the synchrotron donut are calibrated by intercepting the beam at different orbit radii with the synchrotron target. The radial dependence exponent (n) can be determined by comparing the orbit shrink rates at symmetrical points before and after the peak of the magnetic cycle.

The most sensitive measure of the rate of energy loss, and one which is independent of the radial magnetic field dependence, is the determination of the point on the back side of the magnetic cycle where $\dot{\rho}=0$. This point is determined by moving the rf turn-off time later and later in the cycle until the orbit is observed, as indicated by the photomultiplier signal, to move in to smaller radii and then outward again. The time at which $\dot{\rho}=0$ can be precisely determined.

H and $\dot{H}$ are determined throughout the magnetic cycle by measuring the output voltage of a coil that rotates synchronously (30 cycles/sec) with the magnetic field. By varying the phase both H and $\dot{H}$ can be measured at any point in the cycle. The coil is calibrated in a dc magnetic field with a proton magnetic resonance apparatus. H and $\dot{H}$ have also been measured by displaying on an oscilloscope the output of an annular loop of wire placed in the magnet gap.

The results for electron energies (obtained by varying the magnet current) from 225 Mev to 275 Mev are shown in Fig. 1. The engineering formula for classical energy loss, ev/turn $=(712H^4\rho^3)/10^{22}$, is also plotted. More refined measurements will be required to determine whether or not the fixed loss per turn of 30 ev indicated in Fig. 1 is real or only represents a systematic error. The $\dot{\rho}$ measurements up to 318 Mev give results close to the classical result also, but with somewhat larger uncertainties. In any case there can be little doubt of the soundness of the classical calculation for radiated power.

* Supported in part by the ONR.

[1] G. Parzen, Phys. Rev. **84**, 235 (1951). See also the following Letters which appeared after this manuscript was completed: Judd, Lepore, Ruderman, and Wolff, Phys Rev. **86**, 123 (1952); H. Olsen and H. Wergeland, Phys. Rev. **86**, 123 (1952).

[2] J. Schwinger, Phys. Rev. **75**, 1912 (1949).

Angular Distribution of 53-Mev Positive Pions Scattered by Protons*

E. C. FOWLER, W. B. FOWLER, R. P. SHUTT, A. M. THORNDIKE, AND W. L. WHITTEMORE
Brookhaven National Laboratory, Upton, New York
(Received April 23, 1952)

SCATTERING of positive pions with an energy of 53 ± 10 Mev has been observed in the gas of a diffusion cloud chamber filled with 21 atmospheres of hydrogen and methanol vapor, as described previously.[1] The pions were produced by the Columbia University Nevis cyclotron.[2] 8400 photographs were obtained. Pions decaying to muons in the gas in the chamber were counted if the projected angle between pion and muon tracks amounted to more than 4°. From the 967 decay events observed, one calculates that a total pion path length of 1820 g/cm^2 of hydrogen has been scanned. In the calculation a correction of 24 percent has been applied to compensate for the $\pi-\mu$ events with angles $<4°$, many of which may be missed. Furthermore, a pion lifetime of 2.6×10^{-8} sec has been used besides the known average pion energy and gas density. The theoretical angular distribution of $\pi-\mu$ events cuts off abruptly at an angle of 17.5° if the energy of the pions is exactly 53 Mev. The measured distribution slopes off gradually up to angles $>30°$, and one must infer an average uncertainty of the pion energy of ±10 Mev. This uncertainty is partially due to a distribution in energy of the incident pions and partially due to straggling in the wall of the diffusion chamber (5 g/cm^2 of stainless steel).

Twenty-one scattering events were observed, leading to a total cross section of 20 ± 4 millibarns. This value, which is equal to $\frac{1}{4}$ of the geometrical cross section defined by $3.14(\hbar/m_\pi c)$,[3] agrees with the Chicago result[3] of 20 ± 10 mb measured at 56 Mev and probably also agrees with the Columbia result[4] of 27.8 ± 2.5 mb measured at an average energy of 58 Mev. According to the Chicago measurements,[3] the cross section increases rapidly with energy at such energies; therefore, differences or fluctuations in the energy of the incident pions can easily lead to relatively large differences or uncertainties in the experimentally determined cross sections.

The value of 20 mb for the π^+-p cross section should be compared with the very small value of approximately 3 mb found for the π^--p cross section for ordinary scattering.[1] As discussed in reference 3, this big difference is very probably due to the contribution of charge exchange scattering to the total π^--p cross section, not easily observable by the present method, and due to the particularly rapid increase of the π^+-p resonance scattering cross section with energy.

All of the observed events are consistent with the kinematic conditions for elastic π^+-p scattering (coplanarity, consistent angles, and consistent ranges and ionization density wherever possible to determine). The measured angles (θ) between ingoing and outgoing pion tracks have been transformed to the center-of-mass system (θ_0), and the differential cross section $d\sigma/d\omega$(mb/sterad) could has been plotted against θ_0 (Fig. 1). Events with $\theta_0<20°$ could not be counted because of the shortness of the proton recoil track and the resulting confusion with $\pi-\mu$ decays. The isotropic, $\cos^2\theta_0$, and $(1+3\cos^2\theta_0)$ distributions have also been indicated in Fig. 1. Comparison, including a χ^2-test, shows that the isotropic distribution is quite inconsistent with the experimental data, while either one of the other distributions may be consistent.

The present result does not agree with the theory of Ashkin *et al.*,[5] employing the "weak coupling" approximation and pre-

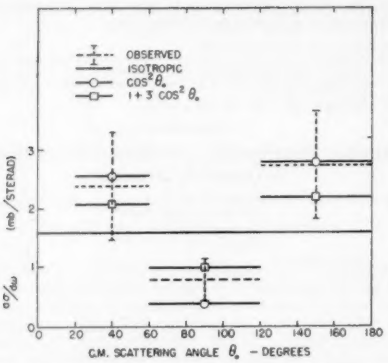

FIG. 1. Experimental π^+-p differential scattering distribution in the center-of-mass system. Distributions of the forms $\cos^2\theta_0$ and $1+3\cos^2\theta_0$ are also indicated besides the isotropic distribution.

dicting a practically isotropic distribution for the low meson energies considered here. The results obtained by the Chicago group[3] have already indicated the validity of a "strong coupling" theory,[4] the characteristic features of which have been pointed out by Brueckner.[7] For pseudoscalar mesons (spin 0) and pseudovector interaction, p-wave scattering must predominate, and the total angular momentum can assume the values $1\pm\frac{1}{2}$. As further pointed out by the Chicago group, the scattering in the angular momentum state $\frac{1}{2}$ should lead to an isotropic distribution, while in the state $\frac{3}{2}$ a distribution of the form $1+3\cos^2\theta_0$ is expected. Furthermore, interference effects can lead to a $\cos\theta_0$ term. Thus, the present result can be tentatively identified as being due to scattering in the angular momentum state $\frac{3}{2}$ alone.

We are indebted to the Nevis cyclotron staff for the opportunity to operate there and for the generous cooperation of members of the staff and operating crew.

* Work done at Brookhaven National Laboratory under the auspices of the AEC.

[1] Shutt, Fowler, Miller, Thorndike, and Fowler, Phys. Rev. **84**, 1247 (1951).
[2] Supported jointly by the ONR and AEC.
[3] Anderson, Fermi, Long, and Nagle, Phys. Rev. **85**, 936 (1952).
[4] Isaacs, Sachs, and Steinberger, Phys. Rev. **85**, 803 (1952).
[5] Ashkin, Simon, and Marshak, Progr. Theoret. Phys. **5**, 634 (1950).
[6] Pauli and Dancoff, Phys. Rev. **62**, 85 (1942).
[7] K. A. Brueckner, Phys. Rev. **86**, 106 (1952).

Photodisintegration of the Deuteron at High Energies

B. BRUNO AND S. DEPKEN
Institute of Mathematical Physics, University of Stockholm, Stockholm, Sweden
(Received May 2, 1952)

RECENT experiments[1,2] on the photodisintegration of the deuteron at high energies give evidence of cross sections exceeding what might be expected on the basis of earlier calculations.[3,4] The discrepancy seems to be appreciable for energies above about 80 Mev.

In previous treatments, which admittedly are not applicable at very high energies, the contributions from charged mesons are only taken into account as giving rise to the exchange interactions and the anomalous magnetic moments for the nucleons.[5] It is, however, conceivable that at sufficiently high energies the meson exchange currents in the deuteron will play the dominant rôle in the photoeffect.

Using ordinary perturbation theory we have, therefore, calculated the contribution to the cross section from processes in which a π-meson is emitted by one of the nucleons, absorbs the photon, and is then absorbed by the other nucleon. The nucleons are treated nonrelativistically and plane waves are used in the intermediate and final states. The ground state of the deuteron is described by a wave function of the Hulthén form. Pseudoscalar meson theory is applied.

It turns out that calculations with pseudovector coupling give total cross sections in reasonable agreement with experiment, while pseudoscalar coupling affords too low values. The result may, therefore, serve as a further argument for the pseudovector coupling form of the pseudoscalar theory.

The predominance at high energies of the process considered by us over the direct absorption of the photon by the nucleons may be understood in the following way. Firstly, the absorption of a photon by a meson instead of by a nucleon is favored by the smaller mass of the meson. Secondly, the cross section for the direct absorption contains a factor giving the probability of finding a nucleon in the deuteron with momentum $\mathbf{p}-\mathbf{k}$, where $\mathbf{p}$ is the final momentum of the absorbing nucleon and $\mathbf{k}$ is the momentum of the photon. For increasing energies the cross section is, therefore, rapidly decreasing. On the other hand, in the indirect process the emission of a meson of momentum $\mathbf{q}$ gives rise to a matrix element, the squared amplitude of which measures the probability of finding a nucleon with momentum $\mathbf{p}+\mathbf{q}$ in the deuteron. Since $\mathbf{q}$ may be chosen so as to give a small value of $\mathbf{p}+\mathbf{q}$, large contributions to the cross section will be obtained from meson momenta roughly satisfying $\mathbf{q}\approx-\mathbf{p}$.

A further account will appear in *Arkiv für Fysik*.

[1] W. S. Gilbert and J. W. Rose, Phys. Rev. **85**, 766 (1952).
[2] T. S. Benedict and W. M. Woodward, Phys. Rev. **86**, 629 (1952).
[3] L. I. Schiff, Phys. Rev. **78**, 733 (1950).
[4] J. F. Marshall and E. Guth, Phys. Rev. **78**, 738 (1950).
[5] Recently, however, calculations have been reported by M. H. Friedman [Phys. Rev. **86**, 625 (1952)] on the dependence of the anomalous magnetic moments of the nucleons upon the frequency of the incident light. According to our estimates the effect of this upon the cross sections should, however, be small compared with the contributions from the meson exchange currents.

Internal Conversion in Cu^{64} and Fe^{59}†

D. BROWER, G. HINMAN, G. LANG, R. LEAMER, AND D. ROSE
Carnegie Institute of Technology, Pittsburgh, Pennsylvania
(Received April 24, 1952)

MEASUREMENTS of the K-conversion coefficients of the 1.34-Mev γ-ray of Cu^{64} and the 1.11-Mev and 1.30-Mev γ-rays of Fe^{59} have been taken, using the β-ray spectroscope ($\rho=50$ cm) recently constructed at Carnegie Institute of Technology. In all cases the coefficient was obtained by measuring the ratio of the number of conversion electrons to the number of β-rays in a component of the continuous spectrum. This value was divided by the number of γ-rays per β-ray as found from a decay scheme.

TABLE I. Observed K-conversion coefficients, α_K.

Original nucleus	Nucleus emitting γ-ray	Energy of γ-ray (Mev)	α_K	Number of sources used
Cu^{64}	Ni^{64}	1.34	$(1.0-1.6)\times10^{-4}$	2
Fe^{59}	Co^{59}	1.11	$(1.45\pm0.05)\times10^{-4}$	1
Fe^{59}	Co^{59}	1.30	$(0.84\pm0.05)\times10^{-4}$	1

To obtain the continuous spectrum below the cut-off point of the counter windows, the Kurie plots for these spectra were extrapolated. It is felt that, for this reason, the α_K value for the Cu^{64} γ-ray was high. The Cu^{64} sources used were rather thick ($\sim$10 mg/cm^2) and this thickness increases the relative number of slow electrons. Using the data of Tyler,[1] a rough estimate was made of the effect of source thickness, and the coefficient given includes this correction.

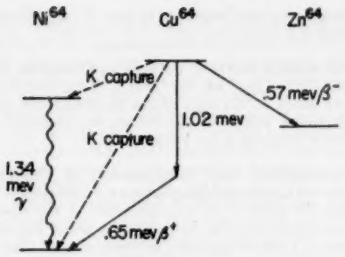

FIG. 1. Decay scheme of Cu^{64}.

The decay schemes used are shown in Figs. 1 and 2 below. The ratio N_γ/N_{β^+} for Cu^{64} is taken to be 0.025.[2] The number of 0.19-Mev γ-rays per disintegration of Fe^{59} is taken as 0.025.[3] The number of 0.27-Mev β-rays was measured to be 0.48 per disintegration; the number of 0.46-Mev β-rays was 0.52 per disintegration.

The measurements yield the values for α_K given in Table I. Further experiments are planned to remeasure these quantities.

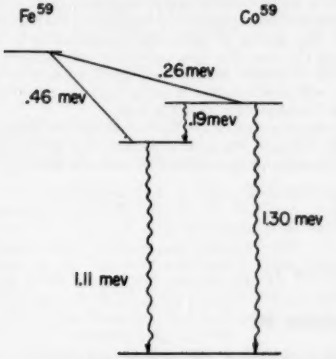

FIG. 2. Decay scheme of Fe^{59}.

The authors would like to thank the staff members at the Argonne and Oak Ridge piles for their cooperation in irradiating copper foils.

† This work was supported by the AEC.

[1] A. W. Tyler, Phys. Rev. **56**, 125 (1939).
[2] M. Deutsch, Phys. Rev. **72**, 729 (1947).
[3] Franz R. Metzger, Phys. Rev. **85**, 727 (1952).

Lattice Imperfections of Diamond

P. G. KLEMENS
Division of Physics, Commonwealth Scientific and Industrial Research Organisation, Sydney, Australia
(Received April 29, 1952)

TO account for dielectric loss and non-uniformities in the electrical properties of diamond, Ahearn[1] has proposed that the lattice imperfections are not uniformly distributed, but form clusters and linear arrays, resulting in "pools of mobile charge" and "conducting channels." Measurements of the thermal conductivity of dielectric solids at low temperatures give information on the spatial grouping of individual imperfections,[2,3] and recent measurements of Berman[4] of the thermal conductivity of a diamond give some support to Ahearn's hypothesis.

At temperatures below 30°K the thermal conductivity is given by

$$\kappa = \tfrac{1}{3}CvL, \tag{1}$$

where C is the specific heat, v the velocity of the transverse elastic waves and L a length of the order of the shortest linear dimension of the specimen. This corresponds to resistance due to the limitation of the phonon free path by the external boundaries. At temperatures above 100°K the conductivity fits

$$\begin{aligned} \kappa &\propto Te^{\theta/3T} \quad \text{for} \quad T \lesssim \theta/6, \\ &\propto 1/T \quad \text{for} \quad T > \theta/6, \end{aligned} \tag{2}$$

where θ, the Debye temperature, is about 1840°K, which suggests that the major contribution to the resistance comes from "Umklapp"—processes, that is from interactions between phonons in which the total wave vector is changed by an inverse lattice vector. Between 30°K and 100°K the interaction varies only weakly with temperature.

It can be shown by using the exact formulas of the general theory of thermal conduction,[3] or by using the "cut-off approximation," that the observed conductivity in this temperature interval cannot be described by a gradual transition from boundary to Umklapp resistance, but that another scattering process predominates at these temperatures. This must be ascribed to structural imperfections, which are in all probability "frozen in" at these low temperatures, so that the temperature dependence of this additional resistance depends only on the variation with phonon-frequency of the scattering cross section.

The additional resistance is more or less independent of temperature, so that the scattering cross section varies as the cube of the frequency for frequencies between $30k/h \sim 6.5\times10^{11}$ and $100k/h \sim 2\times10^{13}$, which correspond to wavelengths between 60 and 20 interatomic distances.

Two interpretations are possible: either the imperfections form linear arrays of length large and diameter small compared with the above wavelengths (these may be dislocations), or they form clusters, whose diameters are of the same order as those wavelengths. The latter case would correspond to Ahearn's "pools of mobile charge." Their concentration would have to be about 10^9 per cm^3 to account for the magnitude of the thermal resistance.

Thus there is some support for Ahearn's hypothesis. It would be interesting to see whether significant differences in the thermal conductivity between 30°K and 100°K would be found if specimens of different dielectric loss and breakdown resistance were studied.

[1] A. J. Ahearn, Phys. Rev. **84**, 798 (1951).
[2] Berman, Klemens, Simon, and Fry, Nature **166**, 277 (1950).
[3] P. G. Klemens, Proc. Roy. Soc. (London) **A208**, 108 (1951).
[4] Berman, Simon, and Wilks, Nature **168**, 277 (1951).

Errata

Nuclear Magnetic Moment and *j-j* Coupling Shell Model, MASATAKA MIZUSHIMA AND MINORU UMEZAWA [Phys. Rev. **85**, 37 (1952)]. In Table III, the value of μ_{calc} for Cl^{35} in the $T=\frac{1}{2}$ state should be 0.26, instead of -0.48. The authors wish to thank Professor M. Goeppert-Mayer for checking our results.

Microwave Spectrum and Molecular Constants of Hydrogen Cyanide, JAMES W. SIMMONS, WALLACE E. ANDERSON, AND WALTER GORDY [Phys. Rev. **77**, 77 (1950)]. In the paper of the above title a mistake of exactly 30 Mc was made in all frequency measurements of $HC^{13}N^{14}$ and of $HC^{13}N^{14}$. This resulted from an incorrect identification of the standard frequency markers. The 30 Mc are to be added to the frequencies. The corrected B_0 value for $HC^{13}N^{14}$ is 43169.83±0.15 Mc.

In the remeasurement a somewhat better accuracy was obtained for the $HC^{13}N^{14}$ lines; the new B_0 value is 44315.97 $\pm$0.10 Mc (with the same D_J value as was used previously). The frequencies for the deuterated isotopic forms are correct as given, but a small numerical error was detected in the structural calculations. With these corrections, the interatomic distances are determined as follows:

Molecular pair used	CH or CD distance (10^{-8} cm)	CN distance (10^{-8} cm)
$DC^{13}N^{14}-DC^{13}N^{15}$	1.0658	1.1555
$HC^{13}N^{14}-HC^{13}N^{15}$	1.0674	1.1557
$DC^{13}N^{14}-HC^{13}N^{14}$	1.0625	1.1566
$DC^{13}N^{14}-HC^{13}N^{15}$	1.0623	1.1567
$HC^{13}N^{14}-DC^{13}N^{15}$	1.0624	1.1563
$HC^{13}N^{14}-DC^{13}N^{15}$	1.0619	1.1568
	Av. 1.0637 $\pm$0.004	1.1563 $\pm$0.001

The average values for the two interatomic distances are very close to the original values quoted. However, the spread in the values obtained with the different isotopic combinations is significantly narrowed. As a result, a much smaller probable error in the determination of the interatomic distances is indicated.

We are indebted to Dr. A. E. Douglas, of the National Research Council of Canada, and to Professor D. H. Rank, of Pennsylvania State College, for calling to our attention the probability of the mistake in frequencies. We are indebted to Dr. Ralph Trambarulo and to Mr. W. C. King for assisting with the remeasurement and the recalculation.

Multiple Events Produced in Hydrogen by Very High Energy Cosmic-Ray Particles at an Altitude of 90,000 Feet, M. L. VIDALE AND MARCEL SCHEIN [Phys. Rev. **84**, 593 (1951)]. The first column of Table I, under the heading "Number of counters activated in tray T" should read **2, 3,** instead of $\geqslant 2, \geqslant 3$.

Thermoelectric Power of Carbons and Graphite, EGON E. LOEBNER [Phys. Rev. **84**, 153 (1951)]. A regrettable mistake has been made in the sign of the thermoelectric power of carbons *versus* platinum. All values are positive and not negative as reported in the letter.

Semiconductivity and Diamagnetism of Polycrystalline Graphite and Condensed Ring Systems, S. MROZOWSKI [Phys. Rev. **85**, 609 (1952)]. As a consequence of the unfortunate mixup in the sign of the thermoelectric power of carbons in the work of Loebner (see the preceding erratum) the general picture of the electronic processes in carbons has to be inverted, that is, all through the paper "excess electrons" should read "excess holes" ("traps" instead of "donors"). Excess holes are created in the filled band by trapping of resonance electrons on surface sites. The nature of these surface traps can be described in the following way (the following should be substituted for lines 15 to 1 from the bottom on p. 617 in the right-hand column): "When the atom attached to the peripheral carbon is removed, the carbon orbital corresponding to the free valence can now accommodate two electrons. A resonance electron jumps into the planar valence orbital, if the activation energy necessary for the change of the configuration happens to be supplied by the heat vibration; due to the pairing of spins this configuration is the more stable of the two. The hole created in the band of resonace electrons is almost free; a very small amount ϵ of kinetic energy will suffice to tear it away from the negative ion left behind. Consequently, this hole will. . . ."

The negative sign of the Hall coefficient for baked carbons does fit well into the general picture; this point will be discussed in subsequent publications from our laboratory.

PHYSICAL REVIEW VOLUME 86, NUMBER 6 JUNE 15, 1952

Author Index to Volume 86

References with (A) are to abstracts of papers presented at meetings of the American Physical Society, and those with (T) designate title only. References with (L) are to Letters to the Editor.

Accardo, C. A. (see Lehovec, K.)—615(A)
Adair, Robert K. Angular distribution of neutrons scattered by He—155
Adams, Edward N., II. Bardeen's theory of superconductivity and the f-sum rule—258(L)
—— Motion of an electron in a perturbed periodic potential—427(L)
Adams, R. V., Dorothy Montgomery Hirshfelder, J. A. Northrop, and N. R. Whetten. Scintillation counter measurements of the cosmic radiation—589(A)
Ahrens, T. and E. Feenberg. First forbidden β-decay matric elements—64
—— **and E. Feenberg.** First forbidden β-transition—609(A)
Alburger, David E. and J. Kraushaar. Decay scheme and angular correlation of Pr^{144}—633(A)
—— (see Motz, Henry T.)—165
Allen, A. J. (see Ely, Ralph, Jr.)—859
—— (see Reilley, E. M.)—857
Allen, Clayton H. Pure fused silica—a new material—816(A)
Allen, James S. (see Rodeback, George W.)—446
Allen, K. W. (see Dewan, J. T.)—416(L)
Allen, N. L., J. Y. Mei, E. Pickup, and L. Voyvodic. Collision of heavy primary cosmic-ray nucleus—1045(L)
Allen, R. A. (see Beghian, L. E.)—1044(L)
Allis, W. P. Progress in gaseous electronics—600(T)
Almqvist, E. (see Dewan, J. T.)—416(L)
—— (see Pepper, T. P.)—630(A)
Anderson, David L. Applications of a small Ra-Be neutron source in the undergraduate laboratory. I. Source characteristics—819(A)
—— (see Manning, Thurston E.)—819(A)
Anderson, H. L. and E. Fermi. Scattering and capture of pions by hydrogen—794(L)
——, **E. Fermi, D. E. Nagle, and G. B. Yodh.** Angular distribution of pions scattered by hydrogen—793(L)
——, **E. Fermi, D. E. Nagle, and G. B. Yodh.** Deuterium total cross sections for positive and negative pions—413(L)
—— (see Lundby, A.)—603(A)
—— (see Martin, R. L.)—604(A)
—— (see Nagle, D. E.)—603(A)
—— (see Yodh, G.)—603(A)
Anderson, James L. Operators and field theories—597(A)
Anderson, P. W. Approximate quantum theory of the antiferromagnetic ground state—694
—— Method of synthesis of the statistical and impact theories of pressure broadening—809(L)

Anderson, Wallace E. (see Simmons, James W.)—1055(L)
Andrew, A., M. R. Jeppson, and H. P. Yockey. Effect of cyclotron irradiation on some thermocouple materials—643(A)
Andrews, R. D. Correlation of dynamic and static measurements on rubber-like materials. II—644(A)
Annis, Martin and H. S. Bridge. Collision mean-free-path of secondary particles from nuclear interaction—589(A)
——, **Herbert S. Bridge, and Stanislaw Olbert.** Application of the multiple scattering theory to cloud-chamber measurements. II—590(A)
Anslow, Gladys A. and Irene S. White. Detection of water-alcohol azeotropes through ultraviolet spectra—587(A)
Anthony, R. L. (see Derenthal, R. J.)—653(A)
Antonoff, George. Thermal expansion of propylalcohol—640(A)
—— Thermal expansion of water—660(A)
——, **A. Yakimac, A. Urmanczy, and R. Madrazo, Jr.** Angular points in liquid *versus* temperature—586(A)
Arfken, G. B., L. C. Biedenharn, and M. E. Rose. Angular correlation of first and third γ-rays—761
——, **L. C. Biedenharn, and M. E. Rose.** One-three γ-γ angular correlation—619(A)
——, **E. D. Klema, and F. K. McGowan.** γ-γ angular correlation in Pd^{106}—413(L)
Arnold, W. R. (see Sawyer, G. A.)—583(A)
Aron, Jack (see Hill, John J.)—615(A)
Arthur, J. S. (see Ely, Ralph, Jr.)—859
—— (see Reilley, E. M.)—857
Atkins, K. R. First and second sound in liquid He—646(T)
Austern, N. (see Bethe, H. A.)—121(L)
Averbach, B. L. (see Flinn, P. A.)—655(A)
—— (see McKeeham, M.)—656(A)
—— (see Rudman, Peter S.)—656(A)
—— (see Warren, B. E.)—656(A)

Bailey, D. K., R. Bateman, L. V. Berkner, H. G. Booker, G. F. Montgomery, E. M. Purcell, W. W. Salisbury, and J. B. Wiesner. New kind of radio propagation at very high frequencies observable over long distances—141
Bainbridge, K. T. Effects of chemical combination and of pressure on the lifetime of a nucleus—582(T)
Bair, Joe Keagy (see Willard, Harvey B.)—259(L); 629(A)
Baldwin, F. P. (see Derenthal, R. J.)—653(A)
Ball, W. P. (see Richardson, R. E.)—29
Ballam, J. Absorption in C of protons in the cosmic radiation at sea level—591(A)
Ballard, Stanley S. (see Combes, Lewis S.)—623(A)
Barber, W. C. and R. H. Helm. Evidence for K-shell ionization accompanying the α-decay of Po^{210}—175
Barbour, Ian. Z-dependence of cross section and energy in cosmic-ray stars—591(A)
Barfield, W. D. (see Gordon, M. M.)—679
Barkas, Walter H., Robert W. Deutsch, F. C. Gilbert, and Charles E. Violet. High energy electron-electron scattering—59
Barnes, B. T. Dynamic characteristics of a low-pressure discharge—351
Barnes, C. A., J. H. Carver, G. H. Stafford, and D. H. Wilkinson. Photodisintegration of the deuteron at intermediate energies. I—359
Baroody, E. M. Wooldridge's theory of secondary emission—915
Barrett, John H. Dielectric constant in perovskite type crystals—118
Barschall, H. H. Regularities in the total cross sections for fast neutrons—431(L)
Bartholomew, G. A. and B. B. Kinsey. Measurements of γ-ray energies with a pair spectrometer—605(A)
Bartnoff, Shepard and Charles R. Mingins. Constriction type of electromechanical filter employing a shear mode—613(A)
Bateman R. (see Bailey, D. K.)—141
Bauss, Herbert and R. F. Boyer. Random noise in dielectrics. II—653(A)
Beach, W. H., W. J. Childs, P. V. C. Hough, J. S. King, and W. C. Parkinson. Radial oscillations in the cyclotron—experimental—582(A)
Beams, J. W. Some recent experiments with high centrifugal fields—610(T)
—— (see Walker, W. E.)—597(A)
Bederson, Benjamin (see Eisinger, Joseph T.)—73
Beeman, W. W. Small-angle scattering of x-rays by solutions of macromolecules—645(T)
Beghian, L. E., R. A. Allen, J. M. Calvert, and H. Halban. Fast neutron spectrometer—1044(L)
Beiser, Arthur. Cosmic-ray neutron production—589(A)
Belinfante, F. J. Electron self-energy—596(A)
Beling, J. K., J. O. Newton, and B. Rose. Soft radiations from Am^{241}—797(L)
Bell, E. E., R. L. Hansler, R. A. Oetjen, and H. E. Schauwecker. Measurements in the far infrared spectrum—819(A)
Bell, R. E. and R. L. Graham. Disintegration scheme of I^{121}—212
Belmont, E. and J. M. Miller. Reactions of 370-Mev protons with Co—630(A)
Bender, R. S. (see Ely, Ralph, Jr.)—859
—— (see Reilley, E. M.)—857
Benedict, T. S. and W. M. Woodward. High energy photodisintegration of the deuteron—629(A)
Bergmann, Peter G. and Ralph Schiller. Time-dependent canonical transformations—621(A)
—— (see Thomson, Robb)—621(A)
Beringer, R. and E. B. Rawson. Lambda-doubling in a microwave spectrum of NO—607(A)
Berkner, L. V. (see Bailey, D. K.)—141
Berko, Stephan. Multiple scattering of μ-mesons in magnetized Fe—598(A)
Berlin, T. H. and M. Kac. Spherical model of a ferromagnet—821
Berman, Alan. Hfs anomalies in the $^2P_{\frac{1}{2}}$ state of Tl^{205} and Tl^{203}—1005
Bernstein, William, R. L. Chase, M. Slavin, J. Garfield, and A. W. Schardt. Photographic gray wedge pulse-height analysis—584(A)
—— (see Rubinson, William)—545
—— (see Schardt, A. W.)—583(A)
Bersohn, R., J. Weneser, and N. M. Kroll. Fourth-order radiative correction to atomic energy levels—596(A)
Betchov, Robert. Experimental model of turbulence—601(A)
Bethe, H. A. and N. Austern. Angular distribution of π^+-production in π-p collisions—121(L)
—— **and F. Rohrlich.** Small angle scattering of light by a Coulomb field—10
Biard, F. K. (see Ting, Yu)—618(A)
Biedenharn, L. C., Keith Boyer, and R. A. Charpie. Angular correlation of the radiations from deuteron stripping reactions—619(A)
—— (see Arfken, G. B.)—619(A); 761
—— (see Blatt, John M.)—399
Biondi, M. A. Ionization and recombination processes in the afterglow—611(T)
Bird, J. R. (see Preston, M. A.)—610(A)
Birks, J. B. Nuclear emulsion and scintillation crystal processes—791(L)
—— Theory of the response of organic scintillation crystals to short-range particles—569(L)
—— (see King, J. W.)—568(L)
Birnbaum, M., M. M. Shapiro, B. Stiller, and F. W. O'Dell. Shape of cosmic-ray star-size distributions in nuclear emulsions—86
Bishop, A. S. (see Steinberger, J.)—171
Biswas, S. and V. D. Hopper. High energy collisions with the production of meson showers—209

Bitondo, D., I. I. Glass, and G. N. Patterson. One-dimensional theory of absorption and amplification of a plane shock wave by a gaseous layer—601(A)
Bitter, Francis (see Brossel, Jean)—308
Blair, J. S. and B. Segall. Scattering of π-mesons by the deuteron—626(A)
Blatt, John M. n-p scattering with spin-orbit coupling; formal theory—610(A)
—— **and L. C. Biedenharn.** n-p scattering with spin-orbit coupling. I. General expressions—399
Bleakney, Walker. Shock waves and their interactions—610(T)
Blewitt, T. H. Radiation effects in Cu single crystals—646(T)
—— (see Coltman, R. R.)—641(A)
—— (see Jamison, R. E.)—641(A)
Block, M. M., W. W. Brown, and G. G. Slaughter. Diffusion cloud-ion chamber for detection of nuclear interactions—583(A)
—— (see Passman, S.)—602(A)
Bloembergen, N. Recent work on magnetic resonance, and relaxation effects in ferromagnetic resonance—639(T)
Bogdonoff, S. M. and A. H. Solarski. Preliminary investigation of a shock wave turbulent boundary layer interaction—601(A)
Bonfiglioli, G., A. Ferro, and G. Montalenti. Comparison of magnetoelastic energy losses and magnetic hysteresis in ferromagnetic materials—959
Bonner, T. W. Disintegrations produced by monoenergetic 14-Mev neutrons—624(T)
—— (see Lillie, A. B.)—630(A)
Booker, H. G. (see Bailey, D. K.)—141
Boorse, H. A. (see Brown, A.)—134(L)
—— (see Brown, A.)—627(A)
Borkowski, C. J. and R. L. Clark. γ-energy resolution with NaI scintillation spectrometer—583(A)
Borowitz, Sidney. Neutron-electron interaction—567(L)
—— **and Walter Kahn.** On the stress tensor of the electron—985
Borsellino, A. Distribution of the total momentum of the electrons in pair production by photons—596(A)
Borst, Lyle B. Dynamics of supernovae—613(A)
Bowen, Dwain. Order-disorder theory—655(A)
Bowen, E. G. Recent advances in radiofrequency astronomy—579(T)
Bowers, R. Heat conductivity of quartz—646(T)
Bowman, Mark, Jr., and H. L. Smith. Work to create fracture surfaces in methyl methacrylate—623(A)
Boyd, G. E. γ-radiations from 36.5-hr Rh^{105g}—578(L)
——, **Q. V. Larson, and G. W. Parker.** Half-life and radiations of Tc^{100}—1051(L)
Boyer, Keith (see Biedenharn, L. C.)—619(A)
Boyer, R. F. New molecular weight distribution technique for polystyrene. II. Experimental results—658(A)
—— (see Bauss, Herbert)—653(A)
Bragg, J. K. (see Crowe, R. W.)—641(A)
Bramson, H. J. (see Seifert, A. M.)—603(A)
Branscomb, Lewis M. Emission of the atmospheric oxygen bands in discharges and afterglows—258(L); 587(A)
Brattain, W. H. Physics of the transistor—579(T)
Breit, G. Spectroscopic isotope shift and nuclear shell structure—254(L)
Bridge, Herbert S. (see Annis, Martin)—589(A); 590(A)
Briggs, H. B. (see Haynes, J. R.)—647(A)
Brill, R. Structure and properties of polyamides—657(A)
Britt, Frances. Absorption bands in the electrical spectrum of a glass and quartz—816(A)
Britten, R. J. (see Shoemaker, F. C.)—582(A)
Brodhun, Carl G. Dielectric breakdown of polymers under prolonged stress—653(A)
Bromley, D. A. and L. M. Goldman. Parities of the ground states of N^{14} and C^{14}—790(L)
Brooks, Franklin C. Convergence of intermolecular force series—92
Brooks, H. Recent calculations on the alkali metals—648(T)
Brosi, A. R. (see Zeldes, H.)—811(L)
Brossel, Jean and Francis Bitter. New "double resonance" method for investigating atomic energy levels, application to Hg $^3P_1$—308
Brower, D., G. Hinman, G. Lang, R. Leamer, and D. Rose. Internal conversion in Cu^{64} and Fe^{59}—1054(L)
Brown, A., M. W. Zemansky, and H. A. Boorse. Behavior of the heat capacity of superconducting Nb below 4.5°K—134(L)
——, **M. W. Zemansky, and H. A. Boorse.** Low temperature heat capacity of Nb—627(A)
Brown, D. E. and W. C. Dunlap, Jr. Comparison of p-n junctions and radioactive tracers for measurement of diffusion—616(A)
—— (see Dunlap, W. C., Jr.)—417(L)
Brown, Fielding, R. Ronald Rau, and George T. Reynolds. Cosmic-ray stars produced in the gas of a cloud-ion chamber—591(A)
Brown, R. J. S. (see Freier, G. D.)—593(A)
Brown, Sanborn C. (see Phelps, Arthur V.)—102
Brown, W. W. (see Block, M. M.)—583(A)
Brueckner, Keith A. Meson-nucleon scattering and nucleon isobars—106; 626(A)
—— **and K. M. Watson.** Phenomenological relationships between photomeson production and meson-nucleon scattering—923
Bruno, B. and S. Depken. Photodisintegration of the deuteron at high energies—1054(L)
Brysk, Henry. Nuclear matrix elements in the theory of β-decay—996
Bueche, F. Self-diffusion and bulk viscosity of high polymers—652(A)
Buechner, W. W. Magnetic-analysis studies of nuclear energy levels—624(T)
—— (see Endt, P. M.)—630(A)
—— (see Van de Graaff, R. J.)—966
—— (see Van Patter, D. M.)—502; 630(A)
Burbury, D. W. P. High latitude north-south asymmetry of cosmic rays—577(L)
Burgess, R. E. Dispersion of permittivity and conductivity of semiconductors—131(L)
Burk, D. and F. Darnell. Specific heat of Hf at 40–190°K—628(A)
—— (see Weertman, J.)—628(A)
Burns, J. S. (see Smith, Charles S.)—655(A)
Burson, S. B. and W. C. Rutledge. Experimental determination of K/L ratios for $_{71}Lu^{175}$ and $_{21}Sc^{46m}$ (20 seconds)—633(A)
—— (see Rutledge, W. C.)—775
Burstein, E., J. J. Oberly, B. W. Henvis, and Margaret White. Color center formation in NaCl containing Ag^+—255(L)
——, **P. L. Smith, and J. W. Davisson.** Color center formation in plastically deformed KCl—615(A)
Burton, R. L. (see Cobbs, W. H., Jr.)—645(T)
Byfield, H., J. Kessler, and L. M. Lederman. Scattering and absorption of π-mesons in C—17

Caianiello, E. R. Argument against the Majorana theory of neutral particles—564(L)
Callen, Herbert B. and Richard F. Greene. Theorem of irreversible thermodynamics—702
—— (see Dank, M.)—622(A)
Callendine, George W., Jr., Virginia C. Ridolfo, and M. L. Pool. Diffusion effects of Co when bombarded with neutrons—642(A)
Calvert, J. M. (see Beghian, L. E.)—1044(L)
Cameron, A. G. W. Emission of deuterons from the nucleus—435(L)

Carlson, B. C. (see Shoemaker, F. C.)—582(A)
Carlson, R. O. (see Fabricand, B. P.)—607(A)
—— (see Lee, C. A.)—607(A)
Carr, W. J. Theory of intrinsic magnetization in alloys—599(A)
Carroll, Thomas J. Radio propagation beyond the horizon and the surface refractive index—614(A)
Carver, J. H. (see Barnes, C. A.)—359
Caswell, Randall S. Average energy of β-ray spectra—82
Chang, L. C. (see Intrater, J.)—598(A)
Chandrasekhar, B. S. He II transfer rates on lucite and perspex surfaces—414(L)
Charpie, R. A. (see Biedenharn, L. C.)—619(A)
Chase, R. L. (see Bernstein, W.)—584(A)
Cheatham, R. G. and Albert G. H. Dietz. Ultrasonic investigation of plasticized polymethyl methacrylate—645(A)
Childs, W. J. (see Beach, W. H.)—582(A)
Chou, C. N. Nature of cosmic-ray bursts underground—1048(L)
Christian, Darleane, Russell F. Mitchell, and Don S. Martin, Jr. Radioactivities of Pt and Ir from photonuclear reactions in Pt—946
Chwalow, Morton L. E. Electron microscopic and diffraction studies of some paraffinic Na soaps—650(A)
Cladis, J. B., J. Hadley, and W. N. Hess. Fast protons from 270-Mev n-d collisions—110
Clark, Donald L. Production of 40-Mev π-mesons by 240-Mev protons in seven elements—602(A)
Clark, J. R. (see Weiss, R. J.)—656(A)
Clark, M. A. Analysis of the hard component of cosmic rays in the upper atmosphere—589(A)
Clark, R. L. (see Borkowski, C. J.)—583(A)
Clarke, R. L. (see Paul, E. B.)—605(A)
Cleland, J. W. (see Crawford, J. H.)—641(A)
Cleland, M. R. and H. W. Koch. Scintillation spectrometer for measuring total energy of x-ray photons—588(A)
Clendenin, W. W. Hfs of $p_{\frac{1}{2}}$ states—810(L)
Closmann, Philip and Richard T. Swim. Co-existence of liquid He I and II—576(L)
Cobbs, W. H., Jr., and R. L. Burton. Studies of rapid crystallization in polymers—645(T)
Cocconi, G. (see Silverman, A.)—602(A)
Cohen, S. G. and A. A. Jaffe. Spectrum of L x-rays from RaD and the possibility of $L_{\mathrm{I}} \rightarrow L_{\mathrm{II}}$ Auger transitions—800(L)
—— (see Jaffe, A. A.)—1041(L)
Cohen, V. W. (see Kikuchi, C.)—608(A)
Cohn, Hans O. (see Karzmark, C. J.)—591(A)
Colligan, R. L. (see House, R. A.)—654(A)
Collins, R. J. and H. Y. Fan. Infrared absorption band in Ge—648(A)
Collins, Thomas L., Alfred O. Nier, and Walter H. Johnson, Jr. Atomic masses from Ti through Zn—408
Coltman, R. R. and T. H. Blewitt. Effect of neutron irradiation on metallic diffusion—641(A)
Combes, Lewis S., Stanley S. Ballard, and Kathryn A. McCarthy. Comparative elastic studies of single crystals of the NaCl type—623(A)
Conforto, Anna Maria and R. D. Sard. Production of neutrons by μ-meson capture in Pb, Mg, and Ca—465
Conklin, G. L. (see Mandeville, C. E.)—631(A); 813(L)
Conner, J. P. (see Lillie, A. B.)—630(A)
Cook, C. Sharp (see Owen, Paul H.)—961
Cook, Thomas B., Jr., and Sherwood K. Haynes. Measurement of the In^{113*} conversion coefficient with a scintillation spectrometer—190
Cooper, H. G. (see Henderson, J. W.)—642(A)
Cooper, John N. (see Russell, Leonard N.)—653(A); 819(A)
—— (see Taylor, Warren E.)—630(A)
Coor, T. (see Hafner, E. M.)—593(A)
Cork, J. M., J. M. LeBlanc, F. B. Stumpf, and W. H. Nester. Radioactive decay of Ru^{103}—575(L)
——, **J. M. LeBlanc, F. B. Stumpf, and W. H. Nester.** Radioactivity in neutron-activated Pt—415(L)
—— (see Rutledge, W. C.)—775
Corliss, L. (see Weiss, R. J.)—656(A)
Corson, Dale R. Radiation loss by electrons in large orbits—1052(L)
Coryell, Charles D. and Hans E. Suess. Empirical evaluation of unpaired spin effects for protons and neutrons—609(A)
Coté, R. E. (see Logan, R. A.)—280
Cowie, D. B., N. P. Heydenburg, G. M. Temmer, and C. A. Little, Jr. Precision α-α scattering at low energies—593(A)
Cox, C. D. (see Johns, M. W.)—632(A)
Cox, Henry L., Jr. Improved "lock-in" amplifier—640(A)
Cramer, William S. and Irving Silver. Acoustic properties of rubber as a function of chemical composition—645(A)
Crandall, Harold F. (see Dunlap, Robert D.)—579(A)
Crawford, J. H., Jr., and J. W. Cleland. Energy levels in Ge produced by nucleon bombardment—641(A)
Creeger, Elva Sterns (see Van Dyke, Karl S.)—579(A)
Crittenden, E. C., Jr., E. H. Layer, and R. W. Hoffman. Effect of thickness of thin metal films on the mean free path of conduction electrons—657(A)
Crocco, L. and L. Lees. Mixing theory for dissipative flows with increasing pressure in the flow direction—584(T)
Croft, G. T., W. F. Love, and F. C. Nix. De Haas-Van Alphen effect in Sn—650(A)
Crosbie, Edwin A. Effect of a singular triplet tensor interaction on p-p scattering below 10 Mev—610(A)
Crowe, M. O'L. and A. Walker. Fluorescence and absorption spectral data and other physical characteristics of xanthopterin-like pigment synthesized by the human tubercle bacillus and isolated by chromatographic and fluorescence analyses—817(A)
Crowe, R. W., A. H. Sharbaugh, and J. K. Bragg. Cathode effects in dielectric breakdown—641(A)

Dabbs, J. W. T. (see Roberts, L. D.)—628(A)
Danforth, W. E. Electrolysis of thorium oxide—416(L)
Dank, M. and H. B. Callen. Calculation of energy bands in solids by the integral iteration method—622(A)
Darby, E. K. (see Pearce, R. M.)—1049(L)
Darling, B. T. and J. A. Weiss. Theory of the ozone molecule—655(A)
Darnell, F. (see Burk, D.)—628(A)
Daunt, J. G. Low temperature properties of He^3—639(T)
—— **and C. V. Heer.** Solubility of He^3 in liquid He^4—205; 627(A)
——, **T. P. Tseng, and C. V. Heer.** Further considerations regarding the theory of Bose-Einstein liquids—627(A); 911
—— (see Heer, C. V.)—649(A)
—— (see Horowitz, M.)—818(A)
—— (see Nicol, J.)—649(A)
—— (see Smith, T. S.)—818(A)
Davidson, Jack P. Magnetic moments of even-odd nuclei—609(A)
Davies, J. M. (see Miller, R. F.)—644(A)
Davis, Marguerite. Irradiation of *B. subtilis* with low voltage electrons—612(A)
Davis, Raymond, Jr. Nuclear recoil following neutrino emission from Be^7—976
Davisson, J. W. (see Burstein, E.)—615(A)
Dean, Christopher. Zeeman effect of the Cl nuclear quadrupole rf resonance—607(A)
Dekker, A. J. and A. van der Ziel. Theory of the production of secondary electrons in solids—755
Demos, P. T., J. D. Fox, I. Halpern, and J. Koch. Angular distribution of fast photoneutrons—605(A)
Dennison, D. M. Survey of the spectrum of water-vapor—658(T)
dePackh, David C. Optical focusing in constant radius accelerators—433(L)

Depken, S. (see Bruno, B.)—1054(L)
Derenthal, R. J., F. P. Baldwin, and R. L. Anthony. Strain-temperature studies of transitions in rubbers—653(A)
der Mateosian, E. (see Thornton, W. A., Jr.)—604(A)
Detwiler, D. P. and Henry A. Fairbank. Thermal conductivity in the intermediate state of pure superconductors—574(L)
Deutsch, Martin. Positronium—579(T)
—— (see Sunyar, A. W.)—1023
Deutsch, Robert W. (see Barkas, Walter H.)—59
Dewan, J. T., T. P. Pepper, K. W. Allen, and E. Almqvist. α-particles from the Li^7+T reactions—416(L)
Dexter, D. L. Scattering of electrons in metals by dislocations—770
—— **and F. Seitz.** Effects of dislocations on mobilities in semiconductors—964
Dharmatti, S. S. and H. E. Weaver, Jr. Magnetic moment of Se^{77}—259(L)
Dienes, G. J. Mechanism for self-diffusion in graphite—651(A)
—— Theoretical estimate of the effect of radiation on the elastic constants of simple metals—228
—— (see Feldman, M.)—623(A)
Dietz, Albert G. H. (see Cheatham, R. G.)—645(A)
Dimond, A. E. (see Pollard, E.)—612(A)
Diven, B. C. (see Martin, H. C.)—565(L)
Dolecek, R. L. Research of the Cryogenics Branch at the Naval Research Laboratory—646(T)
Drenck, K. (see Pepinsky, R.)—793(L)
Dresden, M. Lattice oscillations and superconductivity—627(A)
Duckworth, Henry E. (see Hogg, Benjamin G.)—567(L)
—— (see Stanford, G. S.)—617(A)
Dudziak, Walter F. Measurement of the production cross section of negative mesons in C by 341-Mev protons—602(A)
Duerig, William H. Experimental search for self-trapped electrons in the alkali halides—565(L); 659(A)
Duller, N. M. (see Walker, W. D.)—865
Dunlap, Robert D. and Harold F. Crandall. Energy and volume changes attending the mixing of nonpolar liquids—579(A)
Dunlap, W. C., Jr. Measurement of diffusion in Ge by means of p-n junctions—615(A)
—— **and D. E. Brown.** p-n junction method for measuring diffusion in Ge—417(L)
—— (see Brown, D. E.)—616(A)

Eichholz, G. G. and L. A. Ficko. Half-life of Ta^{182}—794(L)
Eirich, F. R. (see Kamath, P. M.)—657(A)
—— (see Rosen, B.)—657(A)
Eisinger, J. T., B. Bederson, and B. T. Feld. Magnetic moment of K^{40} and the hfs anomaly of the K isotopes—73
Ellis, R. H., Jr., H. H. Rossi, and G. Failla. Stopping power of polystyrene and acetylene for α-particles—562(L)
Ely, Ralph, Jr., A. J. Allen, J. S. Arthur, R. S. Bender, H. J. Hausman, and E. M. Reilley. Inelastic scattering of protons from Ni—859
—— (see Reilley, E. M.)—857
Emerson, W. H. (see Rado, G. T.)—599(A)
Emigh, C. R. Relative pair production cross sections in the energy region 50 to 300 Mev—1028
Emslie, A. G. (see King, Gilbert W.)—586(A)
Endt, P. M., H. A. Enge, J. Haffner, and W. W. Buechner. Excited states of Mg^{25} from the $Al^{27}(d,\alpha)Mg^{25}$ and $Mg^{24}(d,p)Mg^{25}$ reactions—630(A)
——, **J. W. Haffner, and D. M. Van Patter.** Magnetic analysis of the $Mg^{25}(d,p)Mg^{26}$, $Mg^{26}(d,p)Mg^{27}$, and $Mg^{25}(d,\alpha)Na^{23}$ reactions—518
—— (see Van Patter, D. M.)—502; 630(A)
Enge, H. A. (see Endt, P. M.)—630(A)
—— (see Van de Graaff, R. J.)—966
Engel, Olive G. Lower electron energy losses in ZnO—617(A)
Engler, N. and A. E. S. Green. Semi-empirical mass surfaces—654(A)
—— (see Green, A. E. S.)—609(A)
Epstein, Saul T. Theory of the impulse approximation—836
Ewen, H. I. 1420-Mc radiation from interstellar hydrogen—627(T)
—— Radiation of the hfs levels from galactic hydrogen—579(T)
Eyges, L. Interpretation of experiments on the photonuclear effect in heavy elements—325

Fabricand, B. P., R. O. Carlson, C. A. Lee, and I. I. Rabi. Rotational spectrum of KCl—607(A)
—— (see Lee, C. A.)—607(A)
Failla, G. (see Ellis, R. H., Jr.)—562(L)
Fairbank, Henry A. (see Detwiler, D. P.)—574(L)
Falk, C. E. (see Hafner, E. M.)—593(A)
Fan, H. Y. and K. Lark-Horovitz. Optical properties of irradiated semiconductors—646(T)
—— (see Collins, R. J.)—648(A)
—— (see Forster, J. H.)—643(A)
Feenberg, E. (see Ahrens, T.)—64; 609(A)
Feld, B. T. Hfs anomaly and models of nuclear structure—609(A)
—— (see Eisinger, J. T.)—73
Feldman, M., W. Goeddel, and G. J. Dienes. Studies of self-diffusion in graphite using C^{14} tracer—623(A)
Fermi, Enrico. Large-cyclotron research at the University of Chicago—611(T)
—— (see Anderson, H. L.)—413(L); 793(L); 794(L)
—— (see Lundby, A.)—603(A)
—— (see Nagle, D. E.)—603(A)
Ferri, A. Application of linearized characteristic systems to supersonic non-linear problems—584(T)
Ferro, A. (see Bonfiglioli, G.)—959
Ferry, John D. and Edwin R. Fitzgerald. Dynamic mechanical and electrical properties of the system polyvinyl chloride-dimethylthianthrene—645(A)
—— (see Fitzgerald, Edwin R.)—644(A)
—— (see Grandine, Lester D., Jr.)—645(A)
Feshbach, Herman. Scattering of fast electrons by nuclei—582(T)
—— (see Rubinow, S. I.)—610(A)
Ficko, L. A. (see Eichholz, G. G.)—794(L)
Fireman, E. L. and D. Schwarzer. Re-investigation of the double β-decay from Sn^{124}—451
Fisher, John C. Size effect in the strength of NaCl crystals—817(A)
Fisher, L. H. (see Menes, M.)—134(L)
Fishman, Herbert and Alfred Morris Perry, Jr. Stars initiated by high energy protons and neutrons—167
Fitzgerald, Edwin R. and John D. Ferry. Method for determining dynamic mechanical properties of gels and solids at audiofrequencies; comparison of mechanical and electrical properties—644(A)
—— (see Ferry, John D.)—645(A)
—— (see Grandine, Lester D., Jr.)—645(A)
—— (see Miller, R. F.)—644(A)
Flannagan, R. (see Smoluchowski, R.)—598(A)
Flinn, Paul A. and B. L. Averbach. Atomic arrangements in Au-Ni solid solutions—655(A)
—— (see Rudman, Peter S.)—656(A)
Flowers, B. H. jj-coupling in nuclei—254(L)
Foldy, L. L. Pseudoscalar interaction—626(A)
—— Electron-neutron interaction—646(T)
Forster, J. H., H. Y. Fan, and K. Lark-Horovitz. Conductivity of deuteron irradiated Ge and Si—643(A)
Fowler, C. A., Jr., and E. M. Fryer. Magnetic domains on Si iron by the longitudinal Kerr effect—426(L)

Fowler, E. C., W. B. Fowler, R. P. Shutt, A. M. Thorndike, and W. L. Whittemore. Angular distribution of 53-Mev positive pions scattered by protons—1053(L)
Fowler, William A. (see Schardt, Alois)—527
Fowler, W. B. (see Fowler, E. C.)—1053(L)
Fox, J. D. (see Demos, P. T.)—605(A)
Fox, T. G. Effect of diluents on the second-order transition and flow properties of polystyrene—652(A)
Francis, A. E. (see McCue, J. J. G.)—632(A)
Frederikse, H. P. G. Thermoelectric effects in Ge at low temperatures—647(A)
Freedman, Melvin S., F. Wagner, Jr., A. H. Jaffey, and J. May. Radiations of Th^{231}(UY)—633(A)
—— (see Wagner, Frank, Jr.)—631(A)
Freely, John (see Jacobs, Harold)—585(A)
Freier, G. D., W. R. Stratton, R. J. S. Brown, H. D. Holmgren, and J. L. Yarnell. Angular distribution of protons scattered by 1.0 to 3.02-Mev deuterons—593(A)
—— (see Stratton, W. R.)—593(A)
Fried, Burton D. Electron neutron interaction—434(L)
Friedman, M. H. Some meson contributions to the photodisintegration of the deuteron—625(A)
Frisch, D. H. (see Hafner, E. M.)—593(A)
Froehlich, F. E. (see Harth, E. M.)—590(A)
Fry, W. F. Unusual π-μ decays in photographic emulsions—418(L)
Fryer, E. M. (see Fowler, C. A., Jr.)—426(L)
Fuchs, L. (see Primak, W.)—651(A)
Fuller, Calvin S. Diffusion of donor and acceptor elements into Ge—136(L)
Fultz, C. R. (see Zeldes, H.)—811(L)
Fultz, S. C. and M. L. Pool. Radioisotopes of Br—347; 631(A)
—— (see Jones, D. R.)—654(A)
Fumi, Fausto G. Third-order elastic coefficients in trigonal and hexagonal crystals—561(L)

Gage, H. P. Measuring small strains with polarized light (lecture demonstration of the principles of the Friedel eyepiece)—816(A)
Gailar, Norman M. and Earle K. Plyler. $3\nu_3$ bands of CO_2 and CS_2—586(A)
Galt, J. K. and Conyers Herring. Elastic and plastic properties of very small metal specimens—656(A)
Gamow, G. Role of turbulence in the evolution of the universe—251(L)
Gardner, J. W. and H. Messel. Numerical work on the fluctuation problem in cascade shower theory—808(L)
Garfield, J. (see Bernstein, W.)—584(A)
Garfinkel, Boris (see Nielsen, John P.)—624(A)
Garrett, C. G. B. Cooperative effects in paramagnetic crystals having low critical temperatures—658(T)
Garrett, Milan W. New mutual inductance formula—613(A)
Gatha, Kantilal M. and R. J. Riddell, Jr. Investigation into the nuclear scattering of high energy protons—1035
Geib, I. G. and R. E. Grace. Hardness of deuteron irradiated Mo—643(A)
Geiger, J. S. (see Stanford, G. S.)—617(A)
Gelinas, R. W. and S. S. Hanna. Short-range protons from the deuteron bombardment of Li^6—253(L)
George, E. P. Cosmic rays underground—590(T)
Gerber, Eugene H. Multiple scattering of protons in gases—525; 816(A)
Gerhart, J. (see Sherr, R.)—619(A)
Geschwind, Stanley. Determination of nuclear masses from microwave spectra—617(T)
Ghiorso, A. (see Momyer, F. F.)—805(L)
Gilbert, F. C. (see Barkas, Walter H.)—59
Gingrich, N. S. (see Henderson, R. E.)—585(A)
Glass, I. I. (see Bitondo, D.)—601(A)
Glenn, W. E. (see Momyer, F. F.)—805(L)
Gluckstern, R. L. (see Rohrlich, R.)—1
Godfrey, T. N. K. (see Harrison, F. B.)—616(A)
—— (see Keuffel, J. W.)—616(A)
Goeddel, W. (see Feldman, M.)—623(A)
Goertz, Matilda (see Williams, H. J.)—599(A)
Goldberg, Joshua and Ralph Schiller. Equations of motion in a covariant field theory—620(A)
—— (see Schiller, Ralph)—620(A)
Goldberg, M. D. (see Harvey, J. A.)—604(A)
Goldgraber, Howard D. Term values in Mn III—587(A)
Goldhaber, M. (see Sunyar, A. W.)—1023
—— (see Thornton, W. A., Jr.)—604(A)
Goldman, J. E. Collective electron theory of the saturation moment of alloys—599(A)
—— (see Weertman, J.)—628(A)
Goldman, L. M. (see Bromley, D. A.)—790(L)
Goldschmidt, G. H. and D. G. Hurst. Structure of NH_4Cl by neutron diffraction—797(L)
Goldwasser, E. L. (see Hanson, A. O.)—617(A)
Good, R. H., Jr. Interaction term in β-decay theory—620(A)
Goodman, Clark (see McClelland, Clyde L.)—631(A)
—— (see McCue, J. J. G.)—632(A)
—— (see Stelson, P. H.)—629(A)
Gora, E. Lower limits for interaction times in elementary particle processes—597(A)
Gordon, M. M. and W. D. Barfield. Low energy n-d scattering: comparison of experiment with theory—679
Gordy, Walter (see Simmons, James W.)—1055(L)
Gorter, E. W. (see Went, J. J.)—424(L)
Goucher, F. S. (see Prince, M. B.)—647(A)
Gove, H. E. and A. Hedgran. Angular correlation between γ-rays and inelastically scattered protons from Mg^{24}—574(L)
—— **and H. F. Stoddart.** Angular distributions of inelastically scattered protons from C^{13} and Mg^{24}—572(L)
Grace, F. (see Rittner, E. S.)—615(A); 955
Grace, R. E. (see Geib, I. G.)—643(A)
Graham, R. L. (see Bell, R. E.)—212
Grandine, Lester D., Jr., Edwin R. Fitzgerald, Ivo Jordan, and John D. Ferry. Relaxation distribution function in polyisobutylene and polyisobutylene-decalin solutions—645(A)
Graves, G. A. (see Langer, L. M.)—632(A)
Grebenkemper, C. J. and John P. Hagen. High frequency resistance of metals in the normal and superconducting state—673
Green, Alex E. S. Empirical mass surface—654(A)
—— Subtractive bosons in a generalized theory—596(A)
——, **N. Engler, and N. J. Marucci.** Line of β-stability—609(A)
—— (see Engler, N.)—654(A)
—— (see Minogue, R. B.)—654(A)
—— (see Nader, U. S.)—654(A)
Green, David (see Ticho, Harold K.)—422(L)
Green, Melville S. Markoff random processes and the statistical mechanics of time-dependent phenomena—621(A)
Greenberg, J. Mayo. Application of the variational method to scattering by a square well potential—610(A)
—— (see Montroll, Elliott)—889
Greene, Richard F. (see Callen, Herbert B.)—702
Grieco, A. and H. C. Montgomery. Thermal conductivity of Ge—570(L)
Griest, Edward M., Wayne Webb, and Robert W. Schiessler. Influence of specific volume on the viscosity-pressure behavior of some hydrocarbon liquids—612(A)
—— (see Webb, Wayne)—612(T)
Grimeland, Bertel. Measurement of neutron densities with crystals of NaI(Tl)—937
Guderley, G. Flows in the vicinity of Mach-number one—584(T)
Guernsey, Gordon L. Angular distribution of 215-Mev neutrons scattered by protons—594(A)

—— (see Mott, George R.)—594(A)
Guier, W. H. and A. J. F. Siegert. Definition of the integral over paths in Feynman's formulation of nonrelativistic quantum mechanics—596(A)
Guth, E. Polymer research as a branch of solid-state physics—639(T)
—— (see Thie, J. A.)—628(A)

Hadley, J. (see Cladis, J. B.)—110
Haffner, J. W. (see Endt, P. M.)—518; 630(A)
Hafner, E. M., D. H. Frisch, C. E. Falk, T. Coor, and W. F. Hornyak. n-p total cross section—593(A)
Hagen, John P. (see Grebenkemper, C. J.)—673
Halban, H. (see Beghian, L. E.)—1044(L)
Hall, M. B. and R. G. Nester. Zr concentrated-arc infrared source for infrared spectroscopy—653(A)
Hall, R. N. Surface and volume recombination in Ge—600(T)
Halpern, I. (see Demos, P. T.)—605(A)
Halpern, J. (see Rothman, M. A.)—629(A)
Halpern, Otto. Condensation phenomenon of an ideal Einstein-Bose gas—126(L)
Hammel, E. F., H. L. Laquer, S. G. Sydoriak, and W. E. McGee. Investigation of the magnetic properties of liquid He^3—432(L)
Hanna, S. S. (see Gelinas, R. W.)—253(L)
Hansler, R. L. (see Bell, E. E.)—819(A)
Hanson, A. O., E. L. Goldwasser, and F. E. Mills. Energy loss of 15-Mev electrons—617(A)
Hardy, W. A., G. Silvey, and C. H. Townes. Spin and quadrupole moment of Se^{79}—608(A)
Harris, J. C. (see Taylor, Warren E.)—630(A)
Harris, P. M. (see Olsen, C. E.)—651(A)
—— (see Stambaugh, C. K.)—651(A)
—— (see Tsai, Khi-Ruey)—651(A)
Harrison, F. B., J. W. Keuffel, T. N. K. Godfrey, and George T. Reynolds. Capture probabilities of μ-mesons in heavy elements—616(A)
—— (see Keuffel, J. W.)—616(A)
Harrison, R. J. Development of the Korringa method for energy band calculations—651(A)
Harth, E. M., F. E. Froehlich, and K. Sitte. High energy nuclear interactions in Pb—590(A)
Harvey, J. A., M. D. Goldberg, and D. J. Hughes. Reflection and refraction of neutrons from a Be mirror—604(A)
Hastings, J. (see Weiss, R. J.)—656(A)
Hausman, H. J. (see Ely, Ralph, Jr.)—859
—— (see Reilley, E. M.)—857
Havas, Peter. Absorber theory of radiation—974
Havens, W. W., Jr. Production of charged pions by protons—624(T)
—— (see Meservey, E. B.)—605(A)
—— (see Passman, S.)—602(A)
—— (see Seifert, A. M.)—603(A)
Haynes, J. R. and H. B. Briggs. Radiation produced in Ge and Si by electron-hole recombination—647(A)
Haynes, Sherwood K. (see Cook, Thomas B., Jr.)—190
Hayward, Evans. Electron spectra produced by a Co^{60} source in water—493
Hazen, W. E. Production of high energy secondaries by cosmic rays underground—764
——, **R. E. Heineman, and E. S. Lennox.** Application of the Fermi model to cosmic-ray events of primary energy greater than 10^{13} ev—198
Healy, D. W., Jr. Ferromagnetic resonance in $NiOFe_2O_3$ as a function of temperature—1009
Hedgran, A. (see Gove, H. E.)—574(L)
Heer, C. V. and J. G. Daunt. Relativistic quantum statistics of thermal excitations and its application to condensed systems at very low temperatures—649(A)
—— (see Daunt, J. G.)—205; 627(A); 627(A); 911
—— (see Nicol, J.)—649(A)
Heineman, R. E. (see Hazen, W. E.)—198
Heller, W. and W. J. Pangonis. Explicit light-scattering functions for colloidal solutions of spheres—645(T)
Helm, R. H. (see Barber, W. C.)—175
Henderson, J. W., H. G. Cooper, and J. W. Marx. Analysis of the resistivity changes produced by deuteron irradiation of Cu, Ag, and Au—642(A)
Henderson, R. E. and N. S. Gingrich. Diffraction of x-rays by liquid Na-K alloys—585(A)
Henry, Warren E. Spin paramagnetism of Cr^{+++} at liquid He temperatures and high magnetic fields—628(A)
Henvis, B. W. (see Burstein, E.)—255(L)
Hepner, G. (see Herman, R.)—570(L)
Herlin, M. A. Propagation of second sound in liquid He II—579(T)
Herman, L. (see Herman, R.)—570(L)
Herman, R., L. Herman, and G. Hepner. Short duration afterglow of N_2 in the photographic infrared—570(L)
Herring, Conyers (see Galt, J. K.)—656(A)
Herzberg, G. and D. A. Ramsay. Absorption spectrum of free NH_2 radicals—587(A)
Hess, W. N. (see Cladis, J. B.)—110
Heydenburg, N. P. (see Cowie, D. B.)—593(A)
Hibbs, R. F. (see Zeldes, H.)—811(L)
Hidnert, Peter. Relations between thermal expansion and chemical composition of some binary Al alloys—597(A)
Higgins, G. H. and K. Street, Jr. Radiation characteristics of Cm^{240} and Cm^{241}—252(L)
Hill, John J. and Jack Aron. Investigation of the thermoluminescence of CaF_2 colored by x-ray irradiation—615(A)
Hinchey, J. J., P. H. Stelson, and W. M. Preston. Total neutron cross section of N—483
—— (see Preston, W. M.)—594(A)
Hinman, G. (see Brower, D.)—1054(L)
—— (see Rose, D.)—863
Hintz, Norton M. Excitation in high energy nuclear reactions—1042(L)
Hirshfelder, Dorothy Montgomery (see Adams, R. V.)—589(A)
Hoffman, John D. Specific heat and degree of crystallinity of polychlorotrifluoroethylene—657(A)
Hoffman, R. E. Self-diffusion of liquid Hg—585(A)
Hoffman, R. W. (see Crittenden, E. C., Jr.)—657(A)
Hofmann, J. A. and K. Strauch. Angular and energy spectrum of neutrons produced in several elements bombarded with 110-Mev protons. I. Experimental—605(A)
—— (see Strauch, K.)—563(L); 605(A)
Hogg, Benjamin G. and Henry E. Duckworth. Energy available for double β-decay of Sn^{124}—567(L)
—— (see Stanford, G. S.)—617(A)
Holden, A. N. (see Wang, T. C.)—809(L)
Hollis-Hallett, A. C. Experiments with a rotating cylinder viscometer in liquid He II—649(A)
Holmgren, H. D. (see Freier, G. D.)—593(A)
Holt, R. B. (see Thorn, R. N.)—618(A)
—— (see Waniek, R. W.)—619(A)
Honig, A. (see Stitch, M. L.)—607(A); 813(L)
Hopper, V. D. (see Biswas, S.)—209
Hornyak, W. F. (see Hafner, E. M.)—593(A)
Horowitz, M., A. A. Silvidi, S. F. Malaker, and J. G. Daunt. Specific heat of Pb in the temperature range 1.0°K to 75°K—818(A)
Hoshino, Sadao (see Shirane, Gen)—248(L)
Hough, P. V. C. Radial oscillations in the cyclotron—582(A)
—— (see Beach, W. H.)—582(A)
House, R. A., R. L. Colligan, D. N. Kundu, and M. L. Pool. Technetium 98 and 100—654(A)
Houston, W. V. Experiments on supraconducting spheres—653(T)
—— (see Pry, R. H.)—905
Howard, J. N. (see Shaw, J. H.)—654(A)

Howard, Louis N. (see McGuire, T. R.)—599(A)
Howe, Richard H. Some demonstrations of high frequency phenomena—818(A)
Hudson, Donald E. Association of bursts and penetrating showers—453
Hughes, D. J. Measurement of the neutron-electron interaction by mirror reflection—606(T)
—— (see Harvey, J. A.)—604(A)
Hughes, V. W. (see Tucker, G. L.)—618(A)
Hults, M. and S. Mrozowski. Forbidden lines in spectra of Sb I and As I—587(A)
Humphrey, J. N., F. L. Lummis, and W. W. Scanlon. Impedance of semiconducting films—660(A)
Hurst, D. G. (see Goldschmidt, G. H.)—797(L)
Hutchinson, C. A. Paramagnetic resonance absorption in a single crystal of MnF_2—639(T)
Hutchinson, Franklin. Bombardment of biological molecules with slow electrons—612(A)
Hyde, E. K. (see Momyer, F. F.)—805(L)

Inoki, M., T. Yasaki, and Y. Matsukawa. Search for new mesons by means of a cloud chamber—129(L)
Intrater, J., L. C. Chang, and T. A. Read. Influence of stress on the temperature of the diffusionless transformation in Au-Cd single crystals—598(A)
Irwin, G. R. (see Smith, H. L.)—623(A)

Jablonski, F. E., B. Waldman, and W. C. Miller. Energy loss of 2-Mev electrons—617(A)
Jacobs, Donald H. and Seymour Scholnick. Device for converting a shaft rotation to an input for a digital computer—614(A)
Jacobs, Harold and John Freely. Field dependent secondary emission—585(A)
Jacobsohn, B. A. Intrinsic properties of the τ-meson derived from conservation laws—626(A)
Jaffe, A. A. and S. G. Cohen. β-spectrum of RaD—1041(L)
—— (see Cohen, S. G.)—800(L)
Jaffey, A. H. (see Freedman, M. S.)—633(A)
Jamgochian, E. (see Lehovec, K.)—615(A)
Jamison, R. E. and T. H. Blewitt. Slip lines in pile irradiated Cu single crystals—641(A)
Javan, A. and C. H. Townes. Anomalies in the hfs of ICN—608(A)
Jenks, G. H. and F. H. Sweeton. Calorimetric determination of the relationship between the half-life and average β-energy of C^{14}—803(L)
Jensen, Erling N., L. Jackson Laslett, and D. J. Zaffarano. Secondary electron spectrum of Pr^{148}—1047(L)
Jensen, J. H. D. and J. M. Luttinger. Angular momentum distributions in the Thomas-Fermi model—907
Jentschke, W. K. (see Kreger, W. E.)—593(A)
Jepson, M. R. (see Andrew, A.)—643(A)
John G. (see Lin-Sheng, Cheng)—632(A)
Johns, M. W., C. D. Cox, and C. C. McMullen. Spins of the excited states of Cd^{114}—632(A)
Johnson, E. H. Unique form of the Ellicott compensated pendulum—818(A)
Johnson, H. R. and M. W. P. Strandberg. Broadening of microwave absorption lines by collisions with the cell walls—811(L)
Johnson, R. D. and A. B. Martin. Experiments in Ag self-diffusion—642(A)
Johnson, V. A. (see Whitesell, W. J., II)—648(A)
Johnson, Virgil R. Energy levels of C^{11} and C^{13} from photographic plate observation of neutron spectra—302
Johnson, Walter H., Jr. (see Collins, Thomas L.)—408
Johnston, R. W. and D. H. Tomboulian. Absorption by Be in the neighborhood of the K edge—587(A)
Jones, D. R., S. C. Fultz, and M. L. Pool. Radiations of Nb^{98}—654(A)
Jordan, Ivo (see Grandine, Lester D., Jr.)—645(A)
Judd, D. L., J. V. Lepore, M. Ruderman, and P. Wolff. Radiation from an electron in a magnetic field—123(L)
Juretschke, Hellmut J. Electrical properties of the sodium tungsten bronzes—124(L)
Jurney, E. T. and C. W. Zabel. Scattering of fast neutrons—594(A)

Kac, M. (see Berlin, T. H.)—821
Kamath, P. M., B. Rosen, and F. R. Eirich. Relations between viscosity and flow birefringence of polyelectrolytes—657(A)
Kanazawa, Hideo. Saturation property of nuclear forces—428(L)
Kaplan, Harvey. Spin wave treatment of the saturation magnetization of ferrites—121(L)
Kaplon, M. F. (see Lal, D.)—569(L)
Karp, Samuel N. Diffraction by finite and infinite gratings—586(A)
Karplus, Robert and Abraham Klein. Electrodynamic corrections to the fine structure of positronium—257(L)
——, **Abraham Klein, and Julian Schwinger.** Electrodynamic displacement of atomic energy levels. II. Lamb shift—288
Karzmark, C. J., R. W. Thompson, and Hans O. Cohn. Disintegration of V-particles—591(A)
Katz, H. (see Weise, E. K.)—1046(L)
Keating, D. T. and B. E. Warren. Effect of a low absorption coefficient on x-ray spectrometer measurements—656(A)
Keck, James and Raphael Littauer. Production of photomesons from D—602(A)
—— (see Littauer, Raphael)—1051(L)
—— (see Perry, A. M.)—629(A)
Keepin, G. R. (see Stratton, W. R.)—593(A)
Keister, G. L. (see Schmidt, F. H.)—632(A)
Keller, K. J. Formation and annulment of space charges in glass and their influence on electric breakdown—804(L)
Kennedy, J. M. Theory of μ-meson capture—616(A)
Kerman, R. O. (see Kreger, W. E.)—593(A)
Kernohan, Robert H. and Grace M. McCammon. Fading characteristics of γ-induced coloration in high density glass—641(A)
Kessler, J. (see Byfield, H.)—17
Ketelle, B. H. (see Zeldes, H.)—811(L)
Keuffel, J. W., F. B. Harrison, T. N. K. Godfrey, and George T. Reynolds. Improved technique for μ-meson capture measurements—616(A)
—— (see F. B. Harrison)—616(A)
Kies, J. A. (see Smith, H. L.)—623(A)
Kikuchi, C., V. W. Cohen, and John Turkevich. Anistropy in paramagnetic resonance in free radicals—608(A)
Kikuchi, Seishi. Nuclear photodissociation by high energy synchrotron γ-rays—41
—— Photodissociation of the He nucleus by high energy γ-rays—126(L)
Kim, Y. (see Salvini, G.)—592(A)
King, Gilbert W. and A. G. Emslie. Spectroscopy from the point of view of communication theory. III. Line shapes—586(A)
King, J. S. (see Beach, W. H.)—582(A)
King, J. W. and J. B. Birks. Scintillation response of organic crystals to low energy α-particles—568(L)
Kington, J. D. (see Willard, H. B.)—259(L)
Kinsey, B. B. (see Bartholomew, G. A.)—605(A)
Kittel, C. E. Theory of antiferromagnetic resonance—648(T)
—— (see Knight, W. D.)—573(L)
Klein, Abraham (see Karplus, Robert)—257(L); 288
Klein, J. A. (see Nethercot, A. H., Jr.)—798(L)
Klein, Martin J. Isolated and adiabatic susceptibilities—807(L)
Kleinman, David A. Diffuse scattering of neutrons and x-rays—622(A)

Klema, E. D. and G. C. Phillips. Q-values of the $C^{13}(d,p)C^{14}$, $Be^{9}(d,p)Be^{10}$, and $O^{16}(d,p)O^{17}$ reactions—951
—— (see Arfken, G. B.)—413(L)
Klemens, P. G. Lattice imperfections of diamond—1055(L)
Klick, Clifford. Optical and electrical properties of edge emission in CdS—659(A)
Klontz, E. E. and K. Lark-Horovitz. Displacements produced by electron bombardment of Ge—643(A)
Kmetko, Edward A. Structure of graphitized carbon blacks—651(A)
Knight, W. D. and C. Kittel. Nuclear resonance and the electronic structure of transition metals—573(L)
Knowlton, Ansel Alphonse. Opportunities and rewards in physics teaching—611(T)
Knudsen, Arthur W. 498-kev γ-ray of Ru^{102}—571(L)
Koch, H. W. (see Cleland, M. R.)—588(A)
Koch, J. (see Demos, P. T.)—605(A)
Koehler, J. S. Nature of work-hardening—52
—— (see Marx, J.)—643(A)
Kofoed-Hansen, O. and Aage Winther. β-decay of mirror nuclei and the shell model—428(L)
Kohn, Walter (See Borowitz, Sidney)—985
Kojima, Yuzo (see Okamura, Tosihiko)—1040(L)
Korff, S. A. Recent developments in the physics of counters—611(T)
—— (see Soberman, R. K.)—584(A)
—— (see Swetnick, M. J.)—589(A)
Koster, G. F. Effects of configuration interaction on the atomic hfs of Ga—148
Kotani, M. (see Miller, S. L.)—607(A)
Kouts, Herbert J. and Luke C. L. Yuan. Production rate of cosmic ray neutrons and C^{14}—128(L)
Kouvelites, J. S. and L. W. McKeehan. Magnetostrictive vibration of prolate spheroids. Ni-Fe and Ni-Cu alloys—898
Krafft, J. M. Strain rate, temperature, and time effects in the ballistic-speed deformation of mild steel—598(A)
Kraushaar, J. (see Alburger, D. E.)—633(A)
Kraushaar, William L. Mean life of the positive π-meson—513
Kraybill, Henry L. Large air showers at airplane altitudes—590(A)
Kreger, W. E., R. O. Kerman, and W. K. Jentschke. Proton-alpha particle scattering using photographic techniques—593(A)
Krohn, V. E., Jr., and E. F. Shrader. Photodisintegration of the deuteron—391; 629(A)
Kroll, Norman M. and Franklin Pollock. Second order radiative corrections to hfs—876
—— (see Bersohn, R.)—596(A)
Kronig, R. Collective description of electron interactions—795(L)
Krueger, G. C. and C. W. Miller. Study in the dynamics of crystal growth from a supersaturated solution—623(A)
Krzywoblocki, M. Z. v. Boundary layer theory in hypersonic flow in rarefied gases—634(A)
—— Recent development in the turbulence theory in compressible fluids—601(A)
Kubo, Ryogo. Thermal ionization of trapped electrons—929
Kundu, D. N. (see House, R. A.)—654(A)
Kurbatov, J. D. (see Lin-Sheng, Cheng)—632(A)
Kusch, P. Magnetic moment of the electron—611(T)
—— (see Logan, R. A.)—280
—— (see Sherwood, J. E.)—618(A)

Ladenburg, Rudolf. Absorption rate of cosmic-ray neutrons producing C^{14} in the atmosphere—128(L)
Lal, D., Yash Pal, M. F. Kaplon, and B. Peters. Composition and time variation of primary cosmic radiation—569(L)
Lamb, Willis E., Jr., and Robert C. Retherford. Fine structure of the H atom. IV—1014
Landecker, K. Possibility of frequency multiplication and wave amplification by means of some relativistic effects—852
Landon, H. H. and V. L. Sailor. Slow neutron resonances in Cs and Pd—605(A)
Lang, G. (see Brower, D.)—1054(L)
Lang, L. G. (see Rose, D.)—863
Langer, L. M., R. D. Moffat, and G. A. Graves. Decay of the metastable state in In^{116}—632(A)
Langmuir, David B. Technique for self-diffusion measurements—642(A)
Laquer, Henry L. (see Hammel, E. F.)—432(L)
—— (see Schuch, Adam F.)—803(L)
Lark-Horovitz, K. (see Fan, H. Y.)—646(T)
—— (see Forster, J. H.)—643(A)
—— (see Klontz, E. E.)—643(A)
Larson, Q. V. (see Boyd, G. E.)—1051(L)
Laslett, L. Jackson (see Jensen, Erling N.)—1047(L)
—— (see Smith, Warren H.)—523
Lathrop, Arthur L. (see Pry, Robert)—628(A); 905
Latter, A. L. and R. Latter. Phase shift analysis of n-d scattering—727
Latter, R. (see Latter, A. L.)—727
Laughlin, R. D. Electronic instrument for the measurement of crystal anelasticity—623(A)
Lauritsen, Charles C. Some investigations of light nuclei—611(T)
—— (see Schardt, Alois)—527
Lax, Benjamin and J. R. Terrall. Perturbation treatment of electromagnetic problems. II. Applications—595(A)
—— (see Terrall, J. R.)—595(A)
Lax, Melvin. Application of the quantum-mechanical Franck-Condon principle to complex systems—660(A)
—— Multiple scattering of waves. II. Effective field in dense systems—624(A)
—— Semiclassical Franck-Condon principle and its application to complex systems—640(A)
—— (see Rosenberg, R.)—624(A)
Layer, E. H. (see Crittenden, E. C., Jr.)—657(A)
Lazarus, D. (see Slifkin, L.)—656(A)
Leamer, R. (see Brower, D.)—1054(L)
Leavitt, C. P. Absorption of negative π-mesons in He gas—603(A)
LeBlanc, J. M. (see Cork, J. M.)—415(L); 575(L)
Lederman, L. (see Byfield, H.)—17
Lee, C. A., R. O. Carlson, B. P. Fabricand, and I. I. Rabi. Observation of rotational spectra by molecular beam techniques—607(A)
—— (see Fabricand, B. P.)—607(A)
Lees, L. and R. F. Probstein. Hypersonic viscous flow over a flat plate—600(A)
—— (see Crocco, L.)—584(T)
Lehovec, K., C. A. Accardo, and E. Jamgochian. Injected light emission from SiC crystals—615(A)
Leighton, R. B. and S. D. Wanlass. Occurrence of heavy mesons in penetrating showers—426(L)
Leith, C. E., Jr. (see Richardson, R. E.)—29
Lennox, E. S. (see Hazen, W. E.)—198
Lepore, J. V. (see Judd, D. L.)—123(L)
Levinger, J. S. Scattering of gammas by bound electrons—592(A)
Levinstein, Henry (see Sclar, Nathan)—622(A)
—— (see Tiller, Calvin)—657(A)
Levy, Henri A. Phase transitions in the ammonium halides—658(T)
—— **and S. W. Peterson.** Neutron diffraction study of the crystal structure of NH_4Cl—766
Lévy, Maurice M. Non-adiabatic treatment of the relativistic two-body problem—626(A)
—— Symmetrical pseudoscalar meson theory of nuclear forces—806(L)

Levy, S. (see Ying, C. F.)—133(L)
Lewis, H. W. Energy levels of a one-dimensional Bose solid—649(A)
—— Multiple meson production—625(A)
Leyshon, W. E. (see Walchli, H. E.)—618(A)
Lillie, A. B., T. W. Bonner, and J. P. Conner. Disintegration of He^3 by deuterons—630(A)
Lin-Sheng, Cheng, G. John, and J. D. Kurbatov. β-spectra of Ce^{144} and Pr^{144}—632(A)
Linsley, John. Method of interpreting the distribution in multiplicity of shower secondaries—1050(L)
—— **and E. P. Ney.** Multiplicity of mesons produced in Pb—592(A)
Littauer, Raphael and James Keck. High energy photodisintegration of the deuteron—1051(L)
—— **and Darcy Walker.** Charged photomesons from various nuclei—838
—— (see Keck, James)—602(A)
Little, C. A., Jr. (see Cowie, D. B.)—593(A)
Little, R. N., Jr. (see Longley, H. J.)—419(L)
Livingston, Ralph. Pure quadrupole spectra of solid Cl compounds—627(T); 639(T)
Loeb, Leonard B. Mechanism of the Trichel pulses of short time duration in air—256(L)
Loebner, E. E. Thermoelectric power of carbons and graphite, erratum—1056(L)
Loferski, Joseph J. and Park Hays Miller, Jr. Optical polarization in single crystals of Te—652(A)
Logan, John K. Hall effect in Zn crystals at low temperatures—598(A)
Logan, R. A., R. E. Coté, and P. Kusch. Sign of the quadrupole interaction energy in diatomic molecules—280
Lohman, C. (see Serin, B.)—162
Lokajíček, M. (see Votruba, V.)—260(L)
Lomont, J. S. Nonlocal photons—596(A)
Long, E. A. (see Nagle, D. E.)—603(A)
Longley, H. J., R. N. Little, Jr., and J. M. Slye. Polarization of D-D neutrons—419(L)
Lorrain, P. (see Pepper, T. P.)—630(A)
Loshaek, S. Effect of cross linking on the second-order transition temperature of polymethyl methacrylate—652(A)
Love, W. F. Magnetic properties of superconducting Sn-Bi alloys—650(A)
—— (see Croft, G. T.)—650(A)
Lummis, F. L. and R. L. Petritz. Relation between noise and response time in photoconductors. II. Experiment—660(A)
—— (see Humphrey, J. N.)—660(A)
—— (see Scanlon, W. W.)—659(A)
Lundby, A., E. Fermi, H. L. Anderson, D. E. Nagle, and G. Yodh. Scattering of negative pions by H—603(A)
Lutes, O. S., Jr. (see Maxwell, E.)—649(A)
Luttinger, J. M. Pion production and charge independence—571(L)
—— (see Jensen, J. H. D.)—907
Lyons, Harold (see Sherwood, J. E.)—618(A)

MacArthur, J. W. Electron mobility in CdS—615(A)
MacGregor, M. H. and M. L. Wiedenbeck. Decay of Rb^{97}—420(L)
Mack, Rex C., Donald I. Prickett, and M. L. Pool. Europium-148 and 150—633(A)
Madrazo, R., Jr. (see Antonoff, G.)—586(A)
Major, J. K. K-capture and positron emission in Zn^{65}—631(A)
Malaker, S. F. (see Horowitz, M.)—818(A)
Malenka, Bertram J. Nonlinear meson theory for heavy nuclei—68
Malkin, M. S. Electron mobilities in liquid and solid A and liquid He—585(A)
Mandeville, C. E., E. Shapiro, R. I. Mendenhall, E. R. Zucker, and G. L. Conklin. Characteristic radiations of Zr^{97} and Nb^{97}—631(A)
——, **E. Shapiro, R. I. Mendenhall, E. R. Zucker, and G. L. Conklin.** Radiations from Nb^{97}—813(L)
——, **C. P. Swann, and F. J. Seymour.** Scattering of fast neutrons by W— 861
Mann, A. K. (see Rothman, M. A.)—629(A)
Manning, Thurston E. and David L. Anderson. Applications of a small Ra-Be neutron source in the undergraduate laboratory. II. Typical experiments—819(A)
—— Experiments on multiple-beam interferometer—818(A)
Marcus, Paul M. Free energies and phase transition of a cylindrical superconductor—649(A)
Markham, Jordan J. Interpretation of the absence of F' centers in KCl and KBr x-rayed at 4°K—659(A)
—— Second order acoustic fields: Streaming with viscosity and relaxation—497; Relations between density and pressure—710; Energy relations—712
—— Soft and hard F-centers—433(L)
Marquez, Luis. Yield of F^{18} from medium and heavy elements with 420-Mev protons—405
Marshall, John. Čerenkov radiation counting—583(A)
—— Particle counting by Čerenkov radiation—685
—— (see Nedzel, V. A.)—604(A)
Martin, A. B. (see Johnson, R. D.)—642(A)
Martin, Don S., Jr. (see Christian, Darleane)—946
Martin, H. C. and B. C. Diven. Energy dependence of $(n,2n)$ reactions in Ni^{58}, Cu^{63}, and Tl^{203} from 11 to 19 Mev—565(L)
Martin, Jack. New dispenser type cathode—584(A)
Martin, R. L., H. L. Anderson, and G. Yodh. Nuclear cross sections for negative pions of energy 109 and 133 Mev—604(A)
—— (see Nagle, D. E.)—603(A)
Marton, L. Basic principles of an electron interferometer—585(A)
—— Progress in electron physics—600(T)
Marucci, N. J. (see Green, A. E. S.)—609(A)
—— (see Nader, J. S.)—654(A)
Marvin, Robert S. New approximate conversion method for relating stress relaxation and dynamic modulus—644(A)
Marx, J. W., J. Koehler, and C. Wert. Effect of deuteron bombardment on the electrical resistivity of Cu, Ag, and Au—643(A)
—— (see Henderson, J. W.)—642(A)
Mather, Joseph W. Experimental evidence for classical electron radiation at 300 Mev—795(L)
Matsukawa, Y. (see Inoki, M.)—129(L)
Matthews, P. T. and Abdus Salam. Intermediate coupling theory of the pseudoscalar meson-nucleon interaction—715
Matthias, B. T. New supraconducting compounds—653(T)
Maxwell, E. Superconductivity of the isotopes of Sn—235
—— **and O. S. Lutes, Jr.** Superconductivity of Tl isotopes—649(A)
—— (see Williams, W. E., Jr.)—649(A)
May, J. (see Freedman, M. S.)—633(A)
McAfee, K. B., W. Shockley, and M. Sparks. Measurement of diffusion in semiconductors by a capacitance method—137(L)
McCammon, Grace M. (see Kernohan, Robert H.)—641(A)
McCarthy, Kathryn A. (see Combes, Lewis S.)—623(A)
McCarty, C. M. (see Pepinsky, R.)—650(A); 793(L)
McClelland, Clyde L., Clark Goodman, and Paul H. Stelson. Energy levels in Mn^{53} from scintillation studies of $Cr^{50}(p,n\gamma)Mn^{53}$—631(A)
McClure, Gordon W. (see Pomerantz, Martin A.)—536; 588(A)
McCracken, R. H. (see Sherwood, J. E.)—618(A)
McCrackin, Frank L. Total collision cross sections of negative atomic iodine ions in N_2 and A—135(L)
McCue, J. J. G., A. E. Francis, and Clark Goodman. Excitation of metastable Cd^{111} by inelastic scattering of neutrons—632(A)
McDaniel, B. D. (see Weil, J. W.)—582(A)

McFadden, J. A. Approximate analytic solutions in the problem of a spherical blast—600(A)
McGee, W. E. (see Hammel, E. F.)—432(L)
McGowan, F. K. (see Arfken, G. B.)—413(L)
McGuire, Joseph C. (see Sidhu, S. S.)—655(A)
McGuire, T. R., Louis N. Howard, and J. Samuel Smart. Magnetic properties of the chromites—599(A)
McKeeham, M., B. L. Averbach, and B. E. Warren. Effect of cold work on x-ray patterns of Al—656(A)
McKeehan, L. W. (see Kouvelites, J. S.)—898
McMullen, C. C. (see Johns, M. W.)—632(A)
McReynolds, A. W. Inelastic thermal neutron scattering in Pb—594(A)
Mei, J. Y. and E. Pickup. Associated pairs of particles in cosmic ray showers in photographic emulsions—796(L)
—— (see Allen, N. L.)—1045(L)
Melnick, Donald A. and Douglas M. Warschauer. Theory of photoconductivity of ZnO—614(A)
Melvin, M. Avramy. Phenomenological quantum electrodynamics with magnetic poles—640(A)
Mendenhall, R. I. (see Mandeville, C. E.)—631(A); 813(L)
Menes, M. and L. H. Fisher. Formative time lags of positive point corona in air—134(L)
Mengali, O. J. (see Middleton, A. E.)—647(A)
Meservey, E. B., W. W. Havens, Jr., and L. J. Rainwater. Neutron capture cross sections from (n,γ) reactions—605(A)
Messel, H. and R. B. Potts. Solution of the fluctuation problem in electron-photon shower theory—847
—— (see Gardner, J. W.)—808(L)
Messiah, A. M. L. Slow π-meson reactions in He^3—603(A)
—— Tests of charge independence from pion production in nuclear collisions—430(L)
Metzger, Franz R. Spin and parity of the first (603-kev) excited state of Te^{124}—435(L)
Michel, Louis. μ-meson decay and β-radioactivity—814(L)
Michels, A. Influence of pressure on some electron phenomena in solids—658(T)
Middleton, A. E., C. S. Peet, O. J. Mengali, and R. C. Sirrine. High temperature reduced-TiO_2 rectifiers—647(A)
—— (see Peet, C. S.)—647(A)
—— (see Reynolds, D. C.)—659(A)
Mihelich, J. W. (see Sunyar, A. W.)—1023
Miller, C. W. (see Krueger, G. C.)—623(A)
Miller, J. M. (see Belmont, E.)—630(A)
Miller, Park Hays, Jr., and B. R. Russell. Effect of lattice imperfections upon x-ray diffraction and linear dimensions of crystals—650(A)
—— (see Loferski, Joseph J.)—652(A)
Miller, R. F., E. R. Fitzgerald, J. M. Davies, and W. C. Sears. Dielectric properties of liquids, gels, and solids at audio-frequencies. II. Polyvinylchloride plasticized by Di-2-ethylhexylphthalate and dimethylthianthrene—644(A)
Miller, S. L., M. Kotani, and C. H. Townes. Magnetic hfs in the O_2 molecule—607(A)
Miller, W. C. (see Jablonski, F. E.)—617(A)
Miller, William (see Motz, J. W.)—584(A)
Mills, F. E. (see Hanson, A. O.)—617(A)
Mingins, Charles R. (see Bartnoff, Shepard)—613(A)
Minogue, R. B., R. Oppenheim, and A. E. S. Green. Experimental mass surface—654(A)
Mitchell, Allan C. G. (see Smith, Alan B.)—619(A)
Mitchell, Russell F. (see Christian, Darleane)—946
Mizushima, Masataka and Minoru Umezawa. Nuclear magnetic moment and *j-j* coupling shell model, erratum—1055(L)
Mizushima, S. Thermal and electrical conductivities of carbon materials—1040(L)
Moffat, R. D. (see Langer, L. M.)—632(A)
Molmud, Paul. Order of magnitude of the signal radius of the electron—639(A)
Momyer, F. F., E. K. Hyde, A. Ghiorso, and W. E. Glenn. Recent studies of the isotopes of Em, Fr, and Ra—805(L)
Montalenti, G. (see Bonfiglioli, G.)—959
Montgomery, G. F. (see Bailey, D. K.)—141
Montgomery, H. C. (see Grieco, A.)—570(L)
Montroll, Elliott and J. Mayo Greenberg. Scattering of plane waves by soft obstacles. III. Scattering by obstacles with spherical and circular cylindrical symmetry—889
Morrison, P. (see Pine, J.)—606(A)
Mott, George R., Gordon L. Guernsey, and Bruce K. Nelson. Total cross sections of C and H for high energy neutrons—594(A)
Motz, Henry T. and David E. Alburger. β- and γ-radiation of Al^{28}—165
—— (see Thornton, W. A., Jr.)—604(A)
Motz, J. W. γ-ray spectra of the Los Alamos reactors—753
——, **William Miller, and H. O. Wyckoff.** Magnetic Compton spectrometer—584(A)
Moyer, B. J. (see Richardson, R. E.)—29
Mrozowski, S. Anisotropy of thermal expansion and internal stresses in polycrystalline graphite and carbons—622(A)
—— Semiconductivity and diamagnetism of polycrystalline graphite and condensed ring systems, erratum—1056(L)
—— Thermal conductivity of carbons and graphite—251(L)
—— (see Hults, M.)—587(A)
Mullin, C. J. (see Thie, J. A.)—628(A)
Murray, G. T. and W. E. Taylor. Neutron bombardment of a Cu-Be alloy—642(A)

Nabholz, H., P. Stoll, and H. Wäffler. (γ,α) reactions on Li^7 O^{16}, and $Br^{79,81}$—1043(L)
Nader, J. S., N. J. Marucci, and A. E. S. Green. Mass surface and radioactivity—654(A)
Nagle, D. E., H. L. Anderson, E. Fermi, E. A. Long, and R. L. Martin. Total collision cross sections of negative pions on protons—603(A)
—— (see Anderson, H. L.)—413(L); 793(L)
—— (see Lundby, A.)—603(A)
—— (see Yodh, G.)—603(A)
Nakamura, S. (see Tomozawa, Y.)—791(L)
Nedzel, V. A. and John Marshall. Total cross sections for 400-Mev neutrons—604(A)
Nelson, Bruce K. Neutron energy distributions from Be, C, and Pb bombarded by 245-Mev protons—594(A)
—— (see Mott, George R.)—594(A)
Nester, R. G. (see Hall, M. B.)—653(A)
Nester, W. H. (see Cork, J. M.)—415(L); 575(L)
Nethercot, A. H. Jr., J. A. Klein, and C. H. Townes. Microwave spectrum and molecular constants of HCN—798(L)
Neuburg, H. A. C. (see Swetnick, M. J.)—589(A)
Newkirk, Lester L. New technique for the determination of photonuclear cross sections—249(L)
Newton, J. O. (see Beling, J. K.)—797(L)
Ney, E. P. (see Linsley, John)—592(A)
Nicol, J., T. S. Smith, C. V. Heer, and J. G. Daunt. Design and performances of a new type heat interchanger for large He liquefiers—649(A)
Nielsen, H. H. Infrared spectra and molecular structure of pyramidal molecules—658(T)
Nielsen, John P. and Boris Garfinkel. Shape of a two-dimensional crystal minimizing the surface energy—624(A)
Nier, Alfred O. (see Collins, Thomas L.)—408
Nix, F. C. (see Croft, G. T.)—650(A)
Norberg, R. E. Nuclear magnetic resonance in metallic Na—639(T)
—— Nuclear magnetic resonance of hydrogen absorbed into Pd wires—745
Northrop, J. A. (see Adams, R. V.)—589(A)
Novey, T. B. Angular correlation and intensity of inner bremsstrahlung from P^{32} and RaE—619(A)

Nowick, A. S. Activation energy for grain boundary viscosity in metals—597(A)
Noyes, H. P. Stability of neutral scalar heavy mesons—625(A)

Oberly, J. J. Photoconductivity of trapped electrons in KCl crystals between 24°C and −190°C—799(L)
—— (see Burstein, E.)—255(L)
O'Dell, Francis W. (see Birnbaum, M.)—86
Oetjen, R. A. (see Bell, E. E.)—819(A)
—— (see Shaffer, W. H.)—819(A)
Okamura, Tosihiko and Yuzo Kojima. Ferromagnetic resonance in copper ferrite—1040(L)
Olbert, Stanislaw. Application of the multiple scattering theory to cloud-chamber measurements. I—589(A)
—— (see Annis, Martin)—590(A)
Olsen, C. E. and P. M. Harris. Structure of ordered phase of Ag_2HgI_4—651(A)
Olsen, H. and H. Wergeland. Radiation loss of electrons in the synchrotron—123(L)
Oppenheim, R. (see Minogue, R. B.)—654(A)
Osborn, Richard K. Second quantized theory of spin-½ particles in the nonrelativistic limit—340
Osborne, M. F. M. and M. C. Steele. Size effects and diamagnetism in finite systems—247(L)
Overhauser, Albert W. Paramagnetic relaxation in metals—646(A)
Owen, Paul H. and C. Sharp Cook. Hysteresis effect in the transmission of electrons through a thin dielectric foil—961

Paganelli, M. and G. Quareni. Disintegration scheme of K^{40}—423(L)
Pais, A. Some remarks on the V-particles—663
Pake, G. E. Hfs in free-radical paramagnetic resonance—639(T)
Pal, Yash (see Lal, D.)—569(L)
Palevsky, Harry and R. R. Smith. Low energy cross section measurements of Be with the Brookhaven slow neutron chopper—604(A)
Palfrey, T. R., Jr., and R. R. Wilson. Photoproduction of mesons on nuclei—602(A)
Pangonis, W. J. (see Heller, W.)—645(T)
Panofsky, W. K. H., J. N. Steinberger, and J. Steller. Further results on the production of neutral mesons by photons—180
Parker, G. W. (see Boyd, G. E.)—1051(L)
Parkins, W. H. Changes produced by irradiation in the steady-state and the kinetic properties of metals—646(T)
Parkinson, W. C. (see Beach, W. H.)—582(A)
Parmenter, R. H. Electronic energy bands in crystals—552
Passman, S., M. M. Block, and W. W. Havens, Jr. Dependence of charged pion production on incident proton energy—602(A)
Patterson, G. N. (see Bitondo, D.)—601(A)
Paul, E. B. and R. L. Clarke. Fast neutron reaction cross sections—605(A)
Pearce, R. M. and E. K. Darby. Double β-decay of Sn^{124}—1049(L)
Pearson, G. L., W. T. Read, and W. Shockley. Probing the space-charge layer in a p-n junction—647(A)
Peaslee, D. C. Comparative models in nuclear scattering—269
—— V^0-particles and isotopic spin—127(L)
Peet, C. S. and A. E. Middleton. Analysis of high temperature reduced-TiO_2 rectifier characteristics—647(A)
—— (see Middleton, A. E.)—647(A)
—— (see Reynolds, D. C.)—659(A)
Peierls, R. E. Nonlocal field-theory—625(T)
Pepinsky, R., C. M. McCarty, E. Zemyan, and K. Drenck. Ferroelectric ammonium metaphosphate—793(L)
——, **R. Thakur, and C. McCarty.** Low temperature dielectric behavior of $KNbO_3$—650(A)
Pepper, T. P., E. Almqvist, and P. Lorrain. Angular distribution of α-particles from $Li^7(t,\alpha)He^4$—630(A)
—— (see Dewan, J. T.—416(L)
Perls, Thomas A. Stress-induced noise in cables—613(A)
Perry, Alfred Morris, Jr., and J. C. Keck. Excitation functions for photoprotons from C—629(A)
—— (see Fishman, Herbert)—167
Peters, B. (see Lal, D.)—569(L)
Peterson, S. W. (see Levy, Henri A.)—776
Petrie, W. Rotational temperatures of Vegard-Kaplan auroral bands—790(L)
Petritz, Richard L. Relation between noise and response time in photoconductors. I. Theory—660(A)
—— Theory of noise in photoconductors—614(A)
—— (see Lummis, F. L.)—660(A)
—— (see Scanlon, W. W.)—659(A)
Phelps, Arthur V. and Sanborn C. Brown. Positive ions in the afterglow of a low pressure He discharge—102
Philippoff, W. Investigations on plastics in a large range of mechanical frequencies—644(A)
Phillips, G. C. (see Klema, E. D.)—951
Phillips, J. A. (see Sawyer, G. A.)—583(A)
Phillips, M. Perturbations of atomic g values—595(A)
Pickup, E. (see Allen, N. L.)—1045(L)
—— (see Mei, J. Y.)—796(L)
Pine, J. and P. Morrison. Neutron source strength of granitic rock—606(A)
Pines, D. Collective description of electron interactions—648(T)
Pinnick, H. T. X-ray studies of the graphitization process—817(A)
Piper, William W. and Ferd E. Williams. Electrical and optical properties of single crystals of ZnS—659(A)
Pippard, A. B. Supercurrents and mean free paths—653(T)
Pirenne, Jean. Covariant theory of radiation damping—395
Placzek, G. Scattering of neutrons by systems of heavy nuclei—377
—— Scattering of x-rays by atoms—588(A)
Plass, Gilbert N. and Douglas Warner. Pressure broadening of absorption lines—138(L)
Plyler, Earle K. (see Gailar, Norman M.)—586(A)
Polachek, H. and R. J. Seeger. Shock-wave phenomena: aerothermodynamic interaction—601(A)
Pollard, Ernest and A. E. Dimond. Effect of deuteron bombardment on the serology of tobacco mosaic virus—612(A)
—— (see Preiss, J. W.)—612(A)
Pollock, Franklin (see Kroll, Norman M.)—876
Pomerantz, Martin A. and Gordon W. McClure. Primary cosmic radiation at high latitudes—536; 588(A)
Pool, M. L. (see Callendine, George W., Jr.)—642(A)
—— (see Fultz, S. C.)—347; 631(A)
—— (see House, R. A.)—654(A)
—— (see Jones, D. R.)—654(A)
—— (see Mack, Rex C.)—633(A)
Post, R. F. (see Shiren, N. S.)—617(A)
Potts, R. B. (see Messel, H.)—847
Preiss, J. W. and Ernest Pollard. Energy loss of deuterons in hydrocarbons—612(A)
Preston, M. A., J. R. Bird, and J. Shapiro. Nucleon scattering with repulsive core potentials—610(A)
Preston, W. M., P. H. Stelson, and J. J. Hinchey. Total elastic scattering cross section of N for fast neutrons—594(A)
—— (see Hinchey, J. J.)—483
—— (see Stelson, P. H.)—132(L); 629(A); 807(L)
Price, P. J. Radial distribution function in liquid He—495
Prickett, Donald I. (see Mack, Rex C.)—633(A)
Primak, W. and L. Fuchs. Electrical conductivities of natural graphite crystals—651(A)
Prince, M. B. and F. S. Goucher. Test of transistor equations—647(A)
Probstein, R. F. (see Lees, L.)—600(A)

Pry, Robert and Arthur L. Lathrop. Gyromagnetic effect in a superconductor—628(A)
——, **A. L. Lathrop, and W. V. Houston.** Gyromagnetic effect in a superconductor—905
Purcell, E. M. (see Bailey, D. K.)—141

Quareni, G. (see Paganelli, M.)—423(L)

Rabi, I. I. (see Fabricand, B. P.)—607(A)
—— (see Lee, C. A.)—607(A)
Rado, G. T., R. W. Wright, W. H. Emerson, and A. Terris. Temperature dependence of the magnetic spectrum of a ferrite—599(A)
Rainwater, L. J. (see Meservey, E. B.)—605(A)
Ramsay, D. A. (see Herzberg, G.)—587(A)
Ramsey, Norman F. Chemical effects in nuclear magnetic resonance and in diamagnetic susceptibility—243
Rank, D. H., R. P. Ruth, and K. L. Vander Sluis. Velocity of light determined by the band spectrum method—799(L)
Rankin, D. (see Stratton, W. R.)—593(A)
Rathenau, G. W. (see Went, J. J.)—424(L)
Rau, R. Ronald (see Brown, Fielding)—591(A)
Rawson, E. B. (see Beringer, R.)—607(A)
Raychaudhuri, Amalkumar. Condensations in expanding cosmologic models—90
Read, T. A. (see Intrater, J.)—598(A)
Read, W. T. (see Pearson, G. L.)—647(A)
Reilley, E. M., A. J. Allen, J. S. Arthur, R. S. Bender, R. L. Ely, and H. J. Hausman. Nuclear energy levels of Al^{27}—857
—— (see Ely, Ralph, Jr.)—859
Retherford, Robert C. (see Lamb, Willis E., Jr.)—1014
Reynolds, C. A. (see Serin, B.)—162
Reynolds, D. C., C. S. Peet, and A. E. Middleton. Preparation and properties of In_2S_3 phosphors—659(A)
Reynolds, George T. (see Brown, Fielding)—591(A)
—— (see Harrison, F. B.)—616(A)
—— (see Keuffel, J. W.)—616(A)
Rhoderick, E. H. (see Tucker, G. L.)—618(A)
Richardson, J. Reginald (see Schrank, G.)—248(L)
—— (see Ticho, Harold K.)—422(L)
Richardson, John M. Noise and dissipation—613(A)
Richardson, R. E., W. P. Ball, C. E. Leith, Jr., and B. J. Moyer. Nuclear elastic scattering of high energy protons—29
Riddell, R. J., Jr. (see Gatha, Kantilal M.)—1035
Ridolfo, Virginia (see Callendine, George W., Jr.)—642(A)
Ritow, Herman. Dark current in the intermittent glow discharge in H_2—130(L)
Rittner, E. S. and F. Grace. Impedance measurements on PbS photoconductive cells—615(A); 955
Roberts, L. D. and J. W. T. Dabbs. Superconductivity of a Hf-Zr alloy—628(A)
Roche, Arthur F., Jr. Polystyrene molecular weight distribution by turbidity titration and the effect on this distribution of variations in the preparation of the polymers—658(A)
Rodeback, George W. and James S. Allen. Neutrino recoils following the capture of orbital electrons in A^{37}—446
Rogers, John D. and Dudley Williams. Nuclear quadrupole interactions in the microwave spectrum of hydrogen azide—654(A)
Rogosa, George L. (see Schwarz, Guenter)—421(L)
Rohrlich, F. and R. L. Gluckstern. Forward scattering of light by a Coulomb field—1
—— (see Bethe, H. A.)—10
Rose, B. (see Beling, J. K.)—797(L)
Rose, D., G. Hinman, and L. G. Lang. Internal conversion in I^{131}—863
—— (see Brower, D.)—1054(L)
Rose, M. E. and T. A. Welton. Virial theorem for a Dirac particle—432(L)
—— (see Arfken, G. B.)—619(A); 761
Rosen, B. and F. R. Eirich. Sedimentation and diffusion of polyelectrolytes—657(A)
—— (see Kamath, P. M.)—657(A)
Rosenberg, R. and M. Lax. High temperature susceptibility of permanent dipolar lattices—624(A)
Rosenthal, Jenny E. Grid bar mask focusing in a color TV tube—614(A)
Rossi, H. H. (see Ellis, R. H., Jr.)—562(L)
Rothman, M. A., A. K. Mann, and J. Halpern. Angular distributions of photoprotons—629(A)
Rothstein, Jerome. Information, thermodynamics, and life—620(A)
—— Information, thermodynamics, and time—634(A)
—— Phenomenological uncertainty principle—640(A)
—— Theory as organization of observation—634(A)
Ruark, Arthur, E. Theory of discrimination and reliability in crowded situations—620(A)
Rubinow, S. I. Triton binding energy by a randomized net-point method—388
—— **and Herman Feshbach.** Variational principle for $k \cot\delta$—610(A)
Rubinson, William and William Bernstein. Emission of L x-rays of Pb in Po^{210} decay—545
Ruderman, M. (see Judd, D. L.)—123(L)
Rudman, Peter S., Paul A. Flinn, and B. L. Averbach. Short range order diffuse scattering in Al-Zn—656(A)
Russell, B. R. (see Miller, P. H., Jr.)—650(A)
Russell, Leonard N., Warren E. Taylor, and John N. Cooper. γ-rays from excited states of Al^{27}—819(A)
——, **Warren E. Taylor, and John N. Cooper.** Positron activity arising from the proton bombardment of Mg^{25}—653(A)
—— (see Taylor, Warren E.)—630(A)
Ruth, R. P. (see Rank, D. H.)—799(L)
Rutledge, W. C., J. M. Cork, and S. B. Burson. γ-rays associated with selected neutron-induced radioactivities—775
—— (see Burson, S. B.)—633(A)

Sachs, A. (see Steinberger, J.)—624(T)
Sailor, V. L. (see Landon, H. H.)—605(A)
Salam, Abdus. Renormalized S-matrix for scalar electrodynamics—731
—— (see Matthews, P. T.)—715
Salisbury, W. W. (see Bailey, D. K.)—141
Salpeter, E. E. Mass corrections to the fine structure of H and D—595(A)
Salvini, G. and Y. Kim. Production cross section and energy spectrum of the π^0-meson (cosmic-ray measurement)—592(A)
Sard, R. D. (see Conforto, Anna Maria)—465
—— (see Wilkins, H. C.)—591(A)
Savitt, J. (see Starr, L.)—600(A)
Sawyer, G. A., W. R. Arnold, J. A. Phillips, E. J. Stovall, Jr., and J. L. Tuck. SiO films—583(A)
Scanlon, W. W., R. L. Petritz, and F. L. Lummis. Multiple time constants in photoconductivity—659(A)
—— (see Humphrey, J. N.)—660(A)
Schardt, Alois W. and W. Bernstein. Mixed NaI-LiI crystal for a neutron spectrometer—583(A)
——, **William A. Fowler, and Charles C. Lauritsen.** Disintegration of N^{16} by protons—527
—— (see Bernstein, R. L.)—584(A)
Scharff-Goldhaber, G. (see Sunyar, A. W.)—1023
Schauwecker, H. E. (see Bell, E. E.)—819(A)
Schawlow, A. L. (see Wang, T. C.)—809(L)
Schein, Marcel (see Vidale, M. L.)—1056(L)
Scheitlin, F. M. (see Walchli, H. E.)—618(A)
Schiessler, Robert W. (see Griest, Edward M.)—612(A)
—— (see Webb, Wayne)—612(T)

Schiff, L. I. Nonlinear meson theory of nuclear forces. III. Quantization of the neutral scalar case with nonlinear coupling—856
—— Quantization of a nonlinear meson theory—625(A)
Schiller, Ralph and Joshua Goldberg. Super-potentials in covariant theories—620(A)
—— (see Bergmann, Peter G.)—621(A)
—— (see Goldberg, Joshua)—620(A)
Schmidt, F. H. and G. L. Keister. β-spectrum of 2.3-year Cs^{134}—632(A)
Scholnick, Seymour (see Jacobs, Donald H.)—614(A)
Schrank, G. and J. R. Richardson. Radiations from Ne^{19} and Na^{21}—248(L)
Schuch, Adam F. and Henry L. Laquer. Low temperature thermal expansion of U—803(L)
Schwartz, Herman M. Shapes of β-spectra at the low energy end—195
Schwarz, Guenter and George L. Rogosa. Transmission of x-rays through calcite near the Bragg angle—421(L)
Schwarz, Ruth F. Rotational magnetic moments—606(A)
Schwarzer, D. (see Fireman, E. L.)—451
Schweinler, H. C. Ferroelectricity in the ilmenite structure—624(A)
Schwinger, Julian (see Karplus, Robert)—288
Sclar, Nathan and Henry Levinstein. Evidence for a pressure effect in thin films of LiF—622(A)
Scott, W. T. Characteristic functionals in cascade theory—591(A)
Sears, W. C. (see Miller, R. F.)—644(A)
Seeger, R. J. (see Polachek, H.)—601(A)
Seemann, H. E. (see Splettstosser, H. R.)—816(A)
Segall, B. (see Blair, J. S.)—626(A)
Segrè, Emilio. Spontaneous fission—21
Seifert, A. M., H. J. Bramson, and W. W. Havens, Jr. Photographic study of the muon range spectrum from $\pi \rightarrow \mu$ decay—603(A)
Seitz, F. Introduction to irradiation effects in solids—646(T)
—— (see Dexter, D. L.)—964
Senitzky, I. R. Interaction between quantized electromagnetic field and classical electron—595(A)
Serin, B., C. A. Reynolds, and C. Lohman. Isotope effect in superconductivity. II. Sn and Pb—162
Seymour, D. W. and W. F. G. Swann. Redetermination of mesotron mean lifetime as a function of momentum—592(A)
—— (see Swann, W. F. G.)—588(A)
Seymour, F. J. (see Mandeville, C. E.)—861
Shaffer, W. H. and R. A. Oetjen. Some properties of multilayer optical reflection interference filter—819(A)
Shapiro, E. (see Mandeville, C. E.)—631(A); 813(L)
Shapiro, J. (see Preston, M. A.)—610(A)
Shapiro, Maurice M. (see Birnbaum, M.)—86
Sharbaugh, A. H. (see Crowe, R. W.)—641(A)
Shaw, C. H. and Nathan Spielberg. $L\alpha_{1,2}$ and $L\beta_1$ emission lines of Cu and Zn—641(A)
Shaw, J. H. and J. N. Howard. Absorption bands of atmospheric CO—654(A)
Shaw, R. P. Explicit construction of large-amplitude water waves in channels—601(A)
Sherr, R. and J. Gerhart. γ-radiation of C^{10}—619(A)
Sherwood, J. E., Harold Lyons, R. H. McCracken, and P. Kusch. High frequency lines in the hfs spectrum of Cs—618(A)
Shirane, Gen. Ferroelectricity and antiferroelectricity in ceramic $PbZrO_3$ containing Ba or Sr—219
—— **and Sadao Hoshino.** Crystal structure of the ferroelectric phase in $PbZrO_3$ containing Ba or Ti—248(L)
Shiren, N. S. and R. F. Post. Experiment to detect pair-production by electrons—617(A)
Shockley, W. (see McAfee, K. B.)—137(L)
—— (see Pearson, G. L.)—647(A)
Shoemaker, F. C., R. J. Britten, and B. C. Carlson. New method for focusing ion beams—582(A)
Shrader, E. F. (see Krohn, V. E., Jr.)—391; 629(A)
Shull, C. G. Structure of solids by neutron-diffraction—648(T)
—— **and M. K. Wilkinson.** Neutron diffraction studies of various transition elements—599(A)
Shutt, R. P. (see Fowler, E. C.)—1053(L)
—— (see Whittemore, W. L.)—592(A); 940
Sidhu, S. S. and Joseph C. McGuire. Study of the Hf-H system—655(A)
Siegert, A. J. F. Brownian motion theory as a tool in statistical mechanics—621(A)
—— (see Guier, W. H.)—596(A)
Silver, Irving (see Cramer, William S.)—645(A)
Silverman, A. and G. Cocconi. Relative production of neutral mesons by 310-Mev γ-rays in H and D—602(A)
Silvey, G. (see Hardy, W. A.)—608(A)
Silvidi, A. A. (see Horowitz, M.)—818(A)
Simha, R. Viscosity of concentrated macromolecular solutions—652(T)
Simmons, James W., Wallace E. Anderson, and Walter Gordy. Microwave spectrum and molecular constants of HCN, erratum—1055(L)
Simons, Lennart. Internal conversion of the 0.411-Mev γ-ray of Hg^{198}—570(L)
Simpson, J. Arol. Limitations of the electron interferometer—585(A)
Sinton, William M. Detection of mm wave solar radiation—424(L)
Sirrine, R. C. (see Middleton, A. E.)—647(A)
Sitte, K. Ratio of soft to hard particles in air showers—590(A)
—— (see Harth, E. M.)—590(A)
Slater, J. C. Electronic wave functions for magnetism and chemical binding—648(T)
Slater, M. Electron inactivation of enzymes and viruses—612(A)
Slaughter, G. G. (see Block, M. M.)—583(A)
Slavin, M. (see Bernstein, W.)—584(A)
Slifkin, L., D. Lazarus, and T. Tomizuka. Diffusion of Ag and Sb in Ag—656(A)
Slye, J. M. (see Longley, H. J.)—419(L)
Smart, J. Samuel. Molecular field treatment of ferromagnetism and antiferromagnetism—968
—— (see McGuire, T. R.)—599(A)
Smith, Alan B. Nuclear spectrum of Ge^{77}—98; —— and Allan C. G. Mitchell—619(A)
Smith, Charles S. and J. W. Burns. Elastic constants of a Cu-Si alloy—655(A)
Smith, D. F. Microwave spectrum and structure of ClF_3—608(A)
Smith, H. L., J. A. Kies, and G. R. Irwin. Instability criteria for the fracture of solids—623(A)
—— (see Bowman, Mark, Jr.)—623(A)
Smith, P. L. (see Burstein, E.)—615(A)
Smith, R. R. (see Palevsky, Harry)—604(A)
Smith, T. S. and J. G. Daunt. Influence of physical strain on the physical properties of superconductors—818(A)
—— (see Nicol, J.)—649(A)
Smith, Warren H. and L. Jackson Laslett. Cloud chamber identification of photodeuterons from Cu—523
Smoluchowski, R. Critical shear stresses in body-centered cubic lattices—787
—— Kinetics of grain boundary diffusion—656(A)
—— Structure of solid solutions—648(T)
—— **and R. Flannagan.** Grain boundary diffusion of Zn in Cu—598(A)
Snowdon, S. C. Neutrons from the disintegration of P by deuterons—630(A)
Soberman, R. K. and S. A. Korff. Deterioration of BF_3 counters due to rapid counting rates—584(A)
Solarski, A. H. (see Bogdonoff, S. M.)—601(A)

Sorrels, J. D. (see Walker, W. D.)—865
Spangler, R. D. Viscoelastic properties of polymers by phase angle measurements—644(A)
Sparks, M. (see McAfee, K. B.)—137(L)
Sperduto, A. (see Van Patter, D. M.)—502; 630(A)
—— (see Van de Graaf, R. J.)—966
Spielberg, Nathan (see Shaw, C. H.)—641(A)
Splettstosser, H. R. and H. E. Seemann. Application of fluorescence x-rays to metallurgical microradiography—816(A)
Stadler, H. (see Yodh, G.)—603(A)
Stafford, G. H. (see Barnes, C. A.)—359
Stambaugh, C. K. and P. M. Harris. Charge distribution and vibration amplitudes in LiH and LiD—651(A)
Stanford, G. S., H. E. Duckworth, B. G. Hogg, and J. S. Geiger. Masses of Pb^{208}, Th^{228}, U^{234}, and U^{238}—617(A)
Starr, L. and J. Savitt. Spalting produced by detonation of explosives in very heavy walled metal tubes—600(A)
Stearns, M. B. Nuclear scattering of 17-Mev γ-rays—593(A)
Steele, M. C. (see Osborne, M. F. M.)—247(L)
Steffen, Rolf M. Angular correlation of the Pd^{106} γ-rays—632(A)
Steinberger, J. and A. S. Bishop. Production of positive mesons by photons—171
—— **and A. Sachs.** Nuclear interactions of pions of energy near 70 Mev—624(T)
Steinberger, J. N. (see Panofsky, W. K. H.)—180
Steller, J. (see Panofsky, W. K. H.)—180
Stelson, Paul H. and W. M. Preston. Inelastic scattering of fast neutrons from Fe—132(L)
—— **and W. M. Preston.** Neutron groups from protons on Cr^{53}, Co^{59}, and Cl^{37}—807(L)
——, **W. M. Preston, and Clark Goodman.** γ-rays from Na bombarded by protons—629(A)
—— (see Hinchey, J. J.)—483
—— (see McClelland, Clyde L.)—631(A)
—— (see Preston, W. M.)—594(A)
Sterner, John. Interferometric measurements of the hfs of the Hg green line—139(L)
Sternheimer, R. Effect of the atomic core on magnetic hfs—316
—— Magnetic hfs—595(A)
Stiller, B. (see Birnbaum, M.)—86
Stitch, M. L., A. Honig, and C. H. Townes. High temperature microwave spectroscopy-spectrum of KCl, TlCl—607(A)
——, **A. Honig, and C. H. Townes.** Microwave spectroscopy at high temperature—spectra of CsCl and NaCl—813(L)
Stoddart, H. F. (see Gove, H. E.)—572(L)
Stoll, P. (see Nabholz, H.)—1043(L)
Stout, J. W. Meissner effect in alloys—653(T)
Stovall, E. J., Jr. (see Sawyer, G. A.)—583(A)
Strandberg, M. W. P. (see Johnson, H. R.)—811(L)
Stratton, T. F. (see Stratton, W. R.)—593(A)
Stratton, W. R., G. D. Freier, G. R. Keepin, D. Rankin, and T. F. Stratton. Angular distribution of 1.5 to 3.0-Mev deuterons scattered by T nuclei—593(A)
—— (see Freier, G. D.)—593(A)
Strauch, K. and J. A. Hofmann. Angular and energy spectrum of neutrons produced in several elements bombarded with 110-Mev protons. II. Results—605(A)
—— **and J. A. Hofmann.** Scattering of protons by the loosely bound neutron in Be—563(L)
—— (see Hofmann, J. A.)—605(A)
Street, K., Jr. (see Higgins, G. H.)—252(L)
Strickler, Thomas D. and W. G. Wadey. Automatic recording scintillation spectrometer for γ-rays—583(A)
Stump, Robert. β-γ polarization correlation in Sb^{124}—249(L)
Stumpf, F. B. (see Cork, J. M.)—415(L); 575(L)
Suess, Hans E. (see Coryell, Charles D.)—609(A)
Sugarman, Nathan. Meson fission of Hg—604(A)
Suhl, H. and L. R. Walker. Faraday rotation of guided waves—122(L)
Sunyar, A. W., J. W. Mihelich, G. Scharff-Goldhaber, M. Goldhaber, N. S. Wall, and M. Deutsch. Decay of Sr^{85} and Sr^{85m}—1023
Sutherland, G. B. B. M. Infrared analysis of the structure of high polymers: recent developments—645(T)
Suwa, S. Hfs of the spectra of Gd and Zr—247(L)
Swann, C. P. (see Mandeville, C. E.)—861
Swann, W. F. G. and D. W. Seymour. Latitude variation of the vertical cosmic-ray intensity at high altitudes—588(A)
—— (see Seymour, D. W.)—592(A)
Swartz, J. C. and J. W. Trischka. Some molecular constants of Li^6F^{19}—606(A)
Sweeton, F. H. (see Jenks, G. H.)—803(L)
Swenson, C. A. Liquid-solid transformation in He from 1.6° to 4°K—870
Swetnick, M. J., H. A. C. Neuburg, and S. A. Korff. Diurnal effect on cosmic-ray neutrons at high altitudes—589(A)
Swim, Richard T. (see Closmann, Philip)—576(L)
Sydoriak, S. G. (see Hammel, E. F.)—432(L)

Tannenwald, L. M. Nuclear phenomena deducible from μ-pair theory with pseudoscalar coupling—332
Tannenwald, P. Disintegration of He by 90-Mev neutrons—629(A)
Tauber, G. E. and J. W. Weinberg. Thermal equilibrium in general relativity—621(A)
—— (see Weinberg, J. W.)—621(A)
Taylor, Warren E. Comparison of thermally induced lattice defects in Ge and Si with defects produced by nucleon bombardment—642(A)
——, **L. N. Russell, John N. Cooper, and J. C. Harris.** γ-ray resonances in the proton bombardment of Mg^{26}—630(A)
—— (see Murray, G. T.)—642(A)
—— (see Russell, Leonard N.)—653(A); 819(A)
Tchen, C. M. Configuration distribution of a chain molecule with correlations—658(A)
Temmer, G. M. (see Cowie, D. B.)—593(A)
Terrall, J. R. and Benjamin Lax. Perturbation treatment of electromagnetic problems. I. Theory—595(A)
—— (see Lax, Benjamin)—595(A)
Terris, A. (see Rado, G. T.)—599(A)
Tetenbaum, S. J. Microwave spectrum of BrCN at 6 mm—440
Thakur, R. (see Pepinsky, R.)—650(A)
Thie, J. A., C. J. Mullin, and E. Guth. Excitation and disintegration of nuclei by electrons—628(A)
Thomas, L. H. Stability of plane Poiseuille flow—812(L)
Thompson, R. W. (see Karzmark, C. J.)—591(A)
Thomson, Robb and Peter G. Bergmann. General relativity and angular momentum—621(A)
Thorn, R. N., R. W. Waniek, and R. B. Holt. Measurement of short β-decay lifetimes—618(A)
—— (see Waniek, R. W.)—619(A)
Thorndike, A. M. (see Fowler, E. C.)—1053(L)
Thornton, W. A., Jr., E. der Mateosian, H. T. Motz, and M. Goldhaber. Slow neutron capture γ-rays—604(A)
Ticho, Harold K., David Green, and J. Reginald Richardson. γ-radiations from V^{48} and Nb^{92}—422(L)
Tiller, Calvin and Henry Levinstein. Optical properties of evaporated Sb films—657(A)
Ting, Yu, F. K. Biard, and Dudley Williams. Nuclear magnetic moment of In^{115}—618(A)
Tisza, L. Thermodynamics of phase transitions—658(T)
Todd, B. J. Effect of ball milling on the surface area and porosity of silica soot—817(A)
Todd, F. C. (see Wyler, E. N.)—640(A)
Tomboulian, D. H. (see Johnston, R. W.)—587(A)
Tomizuka, T. (see Slifkin, L.)—656(A)
Tomozawa, Y., M. Umezawa, and S. Nakamura. Third forbidden β-spectrum from Rb^{87}—791(L)

Torrey, H. C. Relaxation of nuclear spins by diffusion—639(T)
Townes, C. H. (see Hardy, W. A.)—608(A)
—— (see Javan, A.)—608(A)
—— (see Miller, S. L.)—607(A)
—— (see Nethercot, A. H., Jr.)—798(L)
—— (see Stitch, M. L.)—607(A); 813(L)
—— (see Wang, T. C.)—809(L)
Treiman, S. B. Analysis of the nucleonic component based on neutron latitude variations—917
Trigg, George L. Interpretation of image transitions in β-decay theory—506
Trilling, Leon. Transonic flow past a wedge at zero angle of attack—600(A)
Trischka, J. W. (see Swartz, J. C.)—606(A)
Truell, R. (see Ying, C. F.)—133(L)
Tsai, Khi-Ruey and P. M. Harris. Crystal structure of Cs_2O—651(A)
Tseng, T. S. (see Daunt, J. G.)—627(A); 911
Tuck, J. L. (see Sawyer, G. A.)—583(A)
Tucker, G. L., V. W. Hughes, E. H. Rhoderick, and G. Weinreich. Magnetic moment of He in the metastable $^3S_1$ state by atomic beam method—618(A)
Turkevich, John (see Kikuchi, C.)—608(A)
Turner, T. J. (see Walker, W. E.)—597(A)
Twersky, Vic. Multiple scattered reflection from a striated surface—586(A)
Tyler, W. W. Plastic flow in alkali halide crystals—801(L)
—— Thermal conductivity of non-metals at low temperatures—646(T)

Ubbink, J. Theory of antiferromagnetic resonance in a crystal of rhombic symmetry at the absolute zero—567(L)
Umezawa, Minoru (see Mizushima, Masataka)—1055(L)
—— (see Tomozawa, Y.)—791(L)
Urmanczy, A. (see Antonoff, G.)—586(A)

Van de Graaff, R. J., A. Sperduto, W. W. Buechner, and H. A. Enge. Search for α-particles from the $O^{18}(d,\alpha)N^{14*}$ reaction—966
Vander Sluis, K. L. (see Rank, D. H.)—799(L)
van der Ziel, A. (see Dekker, A. J.)—755
Van Dyke, Karl S. and Elva Sterns Creeger. Rotated piezoelectric, elastic, and dielectric constants of quartz—579(A)
van Oosterhout, G. W. (see Went, J. J.)—424(L)
Van Patter, D. M., P. M. Endt, A. Sperduto, and W. W. Buechner. Excited states of P^{32} from the $P^{31}(d,p)P^{32}$ reaction—502; 630(A)
—— (see Endt, P. M.)—518
Van Vleck, J. H. Significance of microwave spectroscopy for the theory of magnetism—606(T)
Verlet, Loup. Possible influence of κ-mesons on the underground cosmic radiation—792(L)
Vidale, M. L. and Marcel Schein. Multiple events produced in hydrogen by very high energy cosmic-ray particles at an altitude of 90,000 feet, erratum—1056(L)
Villars, Felix. Exchange current effects in the deuteron—476
Violet, Charles E. (see Barkas, Walter H.)—59
Votruba, V. and M. Lokajíček. Unified description of leptons—260(L)
Voyvodic, L. Possible charged V-particle or kappa-meson event observed in a photographic emulsion—1046(L)
—— (see Allen, N. L.)—1045(L)

Wadey, W. G. (see Strickler, Thomas D.)—583(A)
Wäffler, H. (see Nabholz, H.)—1043(L)
Wagner, Frank, Jr., and Melvin S. Freedman. β-spectrum of Tc^{99}—631(A)
—— (see Freedman, M. S.)—633(A)
Walchli, H. E., W. E. Leyshon, and F. M. Scheitlin. Nuclear gyromagnetic ratio of V^{50}—618(A)
Waldman, B. (see Jablonski, F. E.)—617(A)
Walker, A. (see Crowe, M. O'L.)—817(A)
Walker, Darcy (see Littauer, Raphael)—838
Walker, L. R. (see Suhl, H.)—122(L)
Walker, W. D., N. M. Duller, and J. D. Sorrels. Comparison of penetrating showers in light and heavy elements. I—865
Walker, W. E., T. J. Turner, and J. W. Beams. Mechanical properties of thin films of Ag—597(A)
Wall, N. S. (see Sunyar, A. W.)—1023
Wang, T. C., C. H. Townes, A. I. Schawlow, and A. N. Holden. Quadrupole coupling ratio of the Cl isotopes—809(L)
Wangsness, Roald K. Magnetic resonance in a system containing two magnetic sublattices—146; 646(A)
Waniek, R. W., R. N. Thorn, and R. B. Holt. Preliminary results from the measurement of short β-decay lifetimes—619(A)
—— (see Thorn, R. N.)—618(A)
Wanlass, S. D. (see Leighton, R. B.)—426(L)
Wannier, G. H. Progress in computing the statistics of cooperative assemblies—658(T)
Wapstra, A. H. Decay energy of Pb^{202}—562(L)
—— Decay energy of Si^{31}—561(L)
Warner, Douglas (see Plass, Gilbert N.)—138(L)
Warren, B. E. and B. L. Averbach. Separation of cold work distortion and particle size broadening in x-ray patterns—656(A)
—— (see Keating, D. T.)—656(A)
—— (see McKeeham, M.)—656(A)
Warren, Dana T. Altitude effects on cosmic-ray fine structure—588(A)
Warschauer, Douglas M. (see Melnick, Donald A.)—614(A)
Watson, Kenneth M. Applications of the charge independence hypothesis to meson phenomena—625(A)
—— (see Brueckner, K. A.)—923
Way, Katharine and Marion Wood. Nuclear shell interactions—608(A)
Weaver, H. E., Jr. (see Dharmatti, S. S.)—259(L)
Webb, Wayne, Edward M. Griest, and Robert W. Schiessler. Effect of pressure on the viscosity of higher hydrocarbons and their mixtures—612(T)
—— (see Griest, Edward M.)—612(A)
Weertman, J., D. Burk, and J. E. Goldman. Specific heat of Cr below room temperature—628(A)
Weil, J. W. and B. D. McDaniel. Monoenergetic γ-rays from the synchrotron—582(A)
Weinberg, J. W. and G. E. Tauber. Statistical mechanics in general relativity—621(A)
—— (see Tauber, G. E.)—621(A)
Weinreich, G. (see Tucker, G. L.)—618(A)
Weise, E. K. and H. Katz. Magnetic effect in $MgTiO_3$—1046(L)
Weiss, J. A. (see Darling, B. T.)—655(A)
Weiss, R. J. Extinction effects in neutron transmission of polycrystalline media—271; 622(A)
——, **J. R. Clark, J. Hastings, and L. Corliss.** Neutron diffraction studies of cold-worked brass—656(A)
Weisskopf, V. F. Problems of nuclear shell structure —582(T)
Welton, T. A. (see Rose, M. E.)—432(L)
Weneser, J. (see Bersohn, R.)—596(A)
Went, J. J., G. W. Rathenau, E. W. Gorter, and G. W. van Oosterhout. Hexagonal iron-oxide compounds as permanent-magnet materials—424(L)
Wentzel, G. Pion-proton scattering and the strong coupling meson theory—437
—— Pseudoscalar coupling in pseudoscalar meson theory—802(L)
Wergeland, H. (see Olsen, H.)—123(L)
Wert, C. (see Marx, J.)—643(A)
Wessel, Walter. Theory of the electron—639(A)
Westervelt, Donald. Radiation damage in NaCl—643(A)

Weyl, W. A. Structure and mechanical properties of glasses—648(T)
Whetten, N. R. (see Adams, R. V.)—589(A)
White, Irene S. (see Anslow, Gladys A.)—587(A)
White, Margaret (see Burstein, E.)—255(L)
Whitesell, W. J., II, and V. A. Johnson. Calculation of magnetic field effect upon the Hall coefficient of impurity semiconductors—648(A)
Whittemore, W. L. and R. P. Shutt. Momentum spectra of cosmic-ray mesons and protons at sea level and 3.4-km altitude—592(A); 940
—— (see Fowler, E. C.)—1053(L)
Wiedenbeck, M. L. (see MacGregor, M. H.)—420(L)
Wiesner, J. B. (see Bailey, D. K.)—141
Wigner, E. P. Connection between scattering and derivative matrices—609(A)
Wilkins, H. C. and R. D. Sard. Nuclear interaction of fast μ-mesons—591(A)
Wilkinson, D. H. Photodisintegration of the deuteron at intermediate energies. II—373
—— (see Barnes, C. A.)—359
Wilkinson, M. K. (see Shull, C. G.)—599(A)
Willard, Harvey B. and Joe Keagy Bair. (p,n) yields from the light elements—629(A)
——, **J. D. Kington, and J. K. Bair.** Mass difference Mg^{23}-Na^{23}—259(L)
Williams, Dudley (see Rogers, John D.)—654(A)
—— (see Ting, Yu)—618(A)
Williams, Ferd E. (see Piper, William W.)—659(A)
Williams, H. J. and Matilda Goertz. Domain structure of perminvar with a rectangular hysteresis loop—599(A)
Williams, W. E., Jr., and E. Maxwell. NBS liquid level indicator for condensed gases—649(A)
Wilson, Robert R. Monte Carlo study of shower production—261; 590(A)
—— Photodisintegration by meson reabsorption—125(L)
—— (see Palfrey, T. R., Jr.)—602(A)
Winther, Aage (see Kofoed-Hansen, O.)—428(L)
Witmer, Enos E. Integral and rational numbers in the nuclear domain—618(A)
Witt, W. R., Jr. Free-flight determination of the boundary layer transition on cone cylinders—601(A)
Wolff, P. (see Judd, D. L.)—123(L)
Wood, Marion (see Way, Katharine)—608(A)
Woodgate, G. K. Optical hfs by techniques of atomic beams—627(T)
Woodward, W. M. (see Benedict, T. S.)—629(A)
Wright, R. W. (see Rado, G. T.)—599(A)
Wrinch, Dorothy. Fourier transforms and intensities from crystalline proteins—611(A)
Wyckoff, H. O. (see Motz, J. W.)—584(A)
Wyckoff, R. W. G. Big molecules in biological systems—610(T)
Wyler, E. N. and F. C. Todd. Relative variation of dc and pulse emission from mixtures of rare-earth oxides—640(A)

Yadoff, Oleg. Production of electric turbulences in a fluid medium—585(A)
Yakimac, A. (see Antonoff, G.)—586 (A)
Yarnell, J. L. (see Freier, G. D.)—593(A)
Yasaki, T. (see Inoki, M.)—129(L)
Ying, C. F., S. Levy, and R. Truell. Domain patterns on FeSi crystals—133(L)
Yntema, George B. Effect of grain size on magneto-resistance of polycrystalline Cu—598(A)
Yockey, H. P. (see Andrew, A.)—643(A)
Yodh, G. B., H. L. Anderson, D. E. Nagle, and H. Stadler. Difference of H and D total cross sections for charged π-mesons—603(A)
—— (see Anderson, H. L.)—413(L); 604(A); 793(L)
—— (see Lundby, A.)—603(A)
Yuan, Luke C. L. (see Kouts, Herbert J.)—128(L)

Zabel, C. W. (see Jurney, E. T.)—594(A)
Zaffarano, D. J. (see Jensen, Erling N.)—1047(L)
Zeldes, H., B. H. Ketelle, A. R. Brosi, C. R. Fultz, and R. F. Hibbs. Half-life and mass assignment of A^{39}—811(L)
Zemansky, M. W. (see Brown, A.)—134(L); 627(A)
Zemyan, E. (see Pepinsky, R.)—793(L)
Zener, C. Physical basis of ferromagnetism—648(T)
Zilsel, P. R. Darling's theory of fundamental length—620(A)
Zucker, E. R. (see Mandeville, C. E.)—631(A); 813(L)

PHYSICAL REVIEW VOLUME 86, NUMBER 6 JUNE 15, 1952

Analytic Subject Index to Volume 86

References with (A) are to abstracts of papers presented at meetings of the American Physical Society. References with (L) are to Letters to the Editor.

Absorption of radiation (see **Radiation**)
Acoustics
Second-order acoustic fields: streaming with viscosity and relaxation, Jordan J. Markham—497; relations between density and pressure—710; energy relations—712
Adsorption
Effect of ball milling on surface area and porosity of silica soot, B. J. Todd—817(A)
Aerodynamics (see also **Hydrodynamics**)
Boundary layer theory in hypersonic flow in rarefied gases, M. Z. v. Krzywoblocki—634(A)
Afterglow (see **Discharge of electricity in gases**)
Alloys (see **Crystalline states**)
Antiferroelectric phenomena (see **Ferroelectric and antiferroelectric phenomena**)
Antiferromagnetism (see **Magnetic properties**)
Astrophysics
Detection of mm wave solar radiation, William M. Sinton—424(L)
Dynamics of supernovae, Lyle B. Borst—613(A)
Atmosphere (see **Meteorology**)
Atomic and molecular beams
Sign of quadrupole interaction energy in diatomic molecules, R. A. Logan, R. E. Cote, and P. Kusch—280
Atomic mass (see **Isotopes and atomic mass; Mass spectroscopy**)
Aurora
Rotational temperatures of Vegard-Kaplan auroral bands, W. Petrie—790(L)
Biophysics
Bombardment of biological molecules with slow electrons, Franklin Hutchinson—612(A)

Effect of deuteron bombardment on serology of tobacco mosaic virus, E. Pollard and A. E. Dimond—612(A)
Electron inactivation of enzymes and viruses, M. Slater—612(A)
Fluorescence and absorption spectral data and other physical characteristics of xanthopterin-like pigment synthesized by human tubercle bacillus and isolated by chromatographic and fluorescence analyses, M. O'L. Crowe and A. Walker—817(A)
Fourier transforms and intensities from crystalline proteins, Dorothy Wrinch—611(A)
Irradiation of *B. subtilis* with low voltage electrons, Marguerite Davis—612(A)
Boson theory (see **Field theory**)
Bremsstrahlung (see **Radiation**)
Broadening of spectral lines
Broadening of microwave absorption lines by collisions with cell walls, H. R. Johnson and M. W. P. Strandberg—811(L)
Pressure broadening of absorption lines, Gilbert N. Plass and Douglas Warner—138(L)
Synthesis of statistical and impact theories of pressure broadening, P. W. Anderson—809(L)

Cold emission (see **Field currents**)
Conductivity, electrical (see **Electrical conductivity; Discharge of electricity in gases; Semiconductors; Superconductivity**)
Conductivity, thermal (see **Thermal conductivity**)
Constants, physical standards
Darling's theory of fundamental length. P. R. Zilsel—620(A)
Integral and rational numbers in nuclear domain, Enos E. Witmer—618(A)
Velocity of light determined by band spectrum method, D. H. Rank, R. P. Ruth, and K. L. Vander Sluis—799(L)
Cosmic radiation
Absorption in C of protons at sea level, J. Ballam—591(A)
Absorption rate of cosmic-ray neutrons producing C^{14} in atmosphere, Rudolf Ladenburg—128(L)
Altitude effects on cosmic-ray fine structure, Dana T. Warren—588(A)
Analysis of nucleonic component based on neutron latitude variations, S. B. Treiman—917
Application of Fermi model to events of primary energy greater than 10^{13} ev, W. E. Hazen, R. E. Heineman, and E. S. Lennox—198
Application of multiple scattering theory to cloud-chamber measurements. I, Stanislaw Olbert—589(A); II, Martin Annis, Herbert S. Bridge, and Stanislaw Olbert—590(A)
Associated pairs of particles in showers in photographic emulsions, J. Y. Mei and E. Pickup—796(L)
Association of bursts and penetrating showers, Donald E. Hudson—453
Characteristic functionals in cascade theory, W. T. Scott—591(A)
Collision mean-free-path of secondary particles from nuclear interaction, M. Annis and H. S. Bridge—589(A)
Collision of heavy primary nucleus, N. L. Allen, J. Y. Mei, E. Pickup, and L. Voyvodic—1045(L)
Comparison of penetrating showers in light and heavy elements. I, W. D. Walker, N. M. Duller, and J. D. Sorrels—865
Composition and time variation of primary radiation, D. Lal, Yash Pal, M. F. Kaplon, and B. Peters—569(L)
Cosmic-ray neutron production, Arthur Beiser—589(A)
Cosmic-ray stars produced in gas of cloud-ion chamber, Fielding Brown, R. Ronald Rau, and George T. Reynolds—591(A)
Distribution in multiplicity of shower secondaries, John Linsley—1050(L)
Diurnal effect on neutrons at high altitudes, M. J. Swetnick, H. A. C. Neuburg, and S. A. Korff—589(A)
Fluctuation problem in cascade shower theory, J. W. Gardner and H. Messel—808(L)
Hard component in upper atmosphere, M. A. Clark—589(A)
Heavy mesons in penetrating showers, R. B. Leighton and S. D. Wanlass—426(L)
High energy collisions with production of meson showers, S. Biswas and V. D. Hopper—209
High energy nuclear interactions in Pb, E. M. Harth, F. E. Froehlich, and K. Sitte—590(A)
High latitude north-south asymmetry, D. W. P. Burbury—577(L)
Large air showers at airplane altitudes, Henry L. Kraybill—590(A)
Latitude variation of vertical intensity at high altitudes, W. F. G. Swann and D. W. Seymour—588(A)
Mesotron mean lifetime as function of momentum, D. W. Seymour and W. F. G. Swann—592(A)
Momentum spectra of mesons and protons at sea level and 3.4-km altitude, W. L. Whittemore and R. P. Shutt—592(A); 940
Monte Carlo study of shower production, Robert R. Wilson—261; 590(A)
Multiple events produced in hydrogen by very high energy particles at 90,000 feet, erratum, M. L. Vidale and Marcel Schein—1056(L)
Multiplicity of mesons produced in Pb, John Linsley and E. P. Ney—592(A)
Nature of bursts underground, C. N. Chou—1048(L)
Nuclear interaction of fast μ-mesons, H. C. Wilkins and R. D. Sard—591(A)
Possible charged *V*-particle or kappa-meson event in photographic emulsion, L. Voyvodic—1046(L)
Possible influence of κ-mesons on underground cosmic radiation, Loup Verlet—792(L)
Primary radiation at high latitudes, Martin A. Pomerantz and Gordon W. McClure—536; 588(A)
Production cross section and energy spectrum of the π^0-meson (cosmic-ray measurement), G. Salvini and Y. Kim—592(A)
Production of high energy secondaries underground, W. E. Hazen—764
Production of neutrons by μ-meson capture in Pb, Mg, and Ca, Anna Maria Conforto and R. D. Sard—465
Production rate of cosmic-ray neutrons and C^{14}, Herbert J. Kouts and Luke C. L. Yuan—128(L)
Ratio of soft to hard particles in air showers, K. Sitte—590(A)
Scintillation counter measurements, R. V. Adams, Dorothy Montgomery Hirschfelder, J. A. Northrop, and N. R. Whetten—589(A)
Search for new mesons by means of cloud chamber, M. Inoki, T. Yasaki, and Y. Matsukawa—129(L)
Shape of star-size distributions in nuclear emulsions, M. Birnbaum, M. M. Shapiro, B. Stiller, and F. W. O'Dell—86
Solution of fluctuation problem in electron-photon shower theory, H. Messel and R. B. Potts—847
V-particle disintegration, C. J. Karzmark, R. W. Thompson, and Hans O. Cohn—591(A)
V^0-particles and isotopic spin, D. C. Peaslee—127(L)
Z-dependence of cross section and energy in cosmic-ray stars, Ian Barbour—591(A)
Cosmology
Condensations in expanding cosmologic models, Amalkumar Raychaudhuri—90
Role of turbulence in evolution of universe, G. Gamow—251(L)

Cross section, measurements, theory (see also **Scattering of electrons, mesons, neutrons, protons, and ions**)
Deuterium total cross sections for positive and negative pions, H. L. Anderson, E. Fermi, D. E. Nagle, and G. B. Yodh—413(L)
Fast neutron reaction cross sections, E. B. Paul and R. L. Clarke—605(A)
Low energy cross section of Be for neutrons, Harry Palevsky and R. R. Smith—604(A)
Neutron capture cross sections from (n,γ) reactions, E. B. Meservey, W. W. Havens, Jr., and L. J. Rainwater—605(A)
n-p total cross section, E. M. Hafner, D. H. Frisch, C. E. Falk, T. Coor, and W. F. Hornyak—593(A)
Regularities in total cross sections for fast neutrons, H. H. Barschall—431(L)
Slow neutron resonances in Cs and Pd, H. H. Landon and V. L. Sailor—605(A)
Total collision cross sections of negative atomic iodine ions in N_2 and A, Frank L. McCrackin—135(L)
Total cross sections for 400-Mev neutrons, V. A. Nedzel and John Marshall—604(A)
Total cross sections of C and H for high energy neutrons, George R. Mott, Gordon L. Guernsey, and Bruce K. Nelson—594(A)
Total neutron cross section of N, J. J. Hinchey, P. H. Stelson, and W. M. Preston—483
Crystal counters (see **Methods and Instruments**)
Crystal structure
Of NH_4Cl by neutron diffraction, G. H. Goldschmidt and D. G. Hurst—797(L); Henri A. Levy and S. W. Peterson—766
Atomic arrangements in Au-Ni solid solutions, P. A. Flinn and B. L. Averbach—655
Charge distribution and vibration amplitudes in LiH and LiD, C. K. Stambaugh and P. M. Harris—651(A)
Configuration distribution of chain molecule with correlations, C. M. Tchen—658(A)
Ferroelectric ammonium metaphosphate, R. Pepinsky, C. M. McCarty, E. Zemyan, and K. Drenck—793(L)
Of ferroelectric phase in $PbZrO_3$ containing Ba or Ti, Gen Shirane and Sadao Hoshino—248(L)
Fourier transforms and intensities from crystalline proteins, Dorothy Wrinch—611(A)
Of graphitized carbon blacks, Edward A. Kmetko—651(A)
Hf-H system, S. S. Sidhu and Joseph C. McGuire—655(A)
Preparation and properties of In_2S_3 phosphors, D. C. Reynolds, C. S. Peet, and A. E. Middleton—659(A)
Structure of ordered phase of Ag_2HgI_4, C. E. Olsen and P. M. Harris—651(A)
Crystalline state
Activation energy for grain boundary viscosity in metals, A. S. Nowick—597(A)
Anisotropy of thermal expansion and internal stresses in polycrystalline graphite and carbons, S. Mrozowski—622(A)
Atomic arrangements in Au-Ni solid solutions, P. A. Flinn and B. L. Averbach—655(A)
Collective description of electron interactions, R. Kronig—795(L)
Collective electron theory of saturation moment of alloys, J. E. Goldman—599(A)
Color center formation in plastically deformed KCl, E. Burstein, P. L. Smith, and J. W. Davisson—615(A)
Color center formation in NaCl containing Ag^+, E. Burstein, J. J. Oberly, B. W. Henvis, and Margaret White—255(L)
Critical shear stresses in body-centered cubic lattices, R. Smoluchowski—787
Dielectric constant in perovskite type crystals, John H. Barrett—118
Diffusion effects of Co when bombarded with neutrons, George W. Callendine, Jr., Virginia C. Ridolfo, and M. L. Pool—642(A)
Displacements produced by electron bombardment of Ge, E. E. Klontz and K. Lark-Horovitz—643(A)
Domain patterns on FeSi crystals, C. F. Ying, S. Levy, and R. Truell—133(L)
Domain structure of perminvar with rectangular hysteresis loop, H. J. Williams and Maltilda Goertz—599(A)
Dynamics of crystal growth from supersaturated solution, G. C. Krueger and C. W. Miller—623(A)
Effect of cold work on x-ray patterns of Al, M. McKeeham, B. L. Averbach, and B. E. Warren—656(A)
Effect of grain size on magnetoresistance of polycrystalline Cu, George B. Yntema—598(A)
Effect of neutron irradiation on metallic diffusion, R. R. Coltman and T. H. Blewitt—641(A)
Effects of dislocations on mobilities in semiconductors, D. L. Dexter and F. Seitz—964
Elastic and plastic properties of very small metal specimens, J. K. Galt and Conyers Herring—656(A)
Elastic constants of Cu-Si alloy, Charles S. Smith and J. W. Burns—655(A)
Elastic studies of single crystals of NaCl type, Lewis S. Combes, Stanley S. Ballard, and Kathryn A. McCarthy—623(A)
Electrical and optical properties of single crystals of ZnS, William W. Piper and Ferd E. Williams—659(A)
Electrical properties of sodium tungsten bronzes—124(L)
Electrolysis of thorium oxide, W. E. Danforth—416(L)
Electronic energy bands in crystals, R. H. Parmenter—552
Electronic instrument for measurement of crystal anelasticity, R. D. Laughlin—623(A)
Extinction effects in neutron transmission of polycrystalline media, R. J. Weiss—271; 622(A)
Fading characteristics of γ-induced coloration in high density glass, Robert H. Kernohan and Grace M. McCammon—641(A)
Formation and annulment of space charges in glass and their influence on electric breakdown, K. J. Keller—804(L)
Grain boundary diffusion of Zn in Cu, R. Smoluchowski and R. Flannagan—598(A)
Hall effect in Zn crystals at low temperatures, John K. Logan—598(A)
Hardness of deuteron irradiated Mo, I. G. Geib and R. E. Grace—643(A)
High temperature susceptibility of permanent dipolar lattices, R. Rosenberg and M. Lax—624(A)
Influence of stress on temperature of diffusionless transformation in Au-Cd single crystals, J. Intrater, L. C. Chang, and T. A. Read—598(A)
Injected light emission from SiC crystals, K. Lehovec, C. A. Accardo, and E. Jamgochian—615(A)
Interpretation of absence of F' centers in KCl and KBr x-rayed at 4°K, Jordan J. Markham—659(A)
Lattice imperfections of diamond, P. G. Klemens—1055(L)
Lattice oscillations and superconductivity, M. Dresden—627(A)
Magnetic resonance in system containing two magnetic sublattices, Roald K. Wangsness—146; 646(A)
Motion of electron in perturbed periodic potential, Edward N. Adams, II—427(L)
Neutron bombardment of Cu-Be alloy, G. T. Murray and W. E. Taylor—642(A)
Neutron diffraction studies of cold-worked brass, R. J. Weiss, J. R. Clark, J. Hastings, and L. Corliss—656(A)
Nuclear resonance and electronic structure of transition metals, W. D. Knight and C. Kittel—573(L)
Optical and electrical properties of edge emission in CdS, Clifford Klick—659(A)

Order-disorder theory, Dwain Bowen—655(A)
Photoconductivity of trapped electrons in KCl crystals between 24°C and −190°C, J. J. Oberly—799(L)
Plastic flow in alkali halide crystals, W. W. Tyler—801(L)
Radiation damage in NaCl, Donald Westervelt—643(A)
Relations between thermal expansion and chemical composition of some binary Al alloys, Peter Hidnert—597(A)
Self-trapped electrons in alkali halides, William H. Duerig—565(L); 659(A)
Semiconductivity and diamagnetism of polycrystalline graphite and condensed ring systems, erratum, S. Mrozowski—1056(L)
Separation of cold work distortion and particle size broadening in x-ray patterns, B. E. Warren and B. L. Averbach—656(A)
Shape of two-dimensional crystal minimizing surface energy, John P. Nielsen and Boris Garfinkel—624(A)
Short-range order diffuse scattering in Al-Zn, Peter S. Rudman, Paul A. Flinn, and B. L. Averbach—656(A)
Size effect in strength of NaCl crystals, John C. Fisher—817(A)
Slip lines in pile irradiated Cu single crystals, R. E. Jamison and T. H. Blewitt—641(A)
Soft and hard *F*-centers, Jordan J. Markham—433(L)
Spherical model of ferromagnet, T. H. Berlin and M. Kac—821
Spin wave treatment of saturation magnetization of ferrites, Harvey Kaplan—121(L)
Theoretical estimate of effect of radiation on elastic constants of simple metals, G. J. Dienes—228
Thermal ionization of trapped electrons, Ryogo Kubo—929
Work-hardening, J. S. Koehler—52
X-ray studies of graphitization process, H. T. Pinnick—817(A)

Diamagnetism (see **Magnetic properties**)
Dielectrics and dielectric properties
Absorption bands in electrical spectrum of glass and quartz, Frances Britt—816(A)
Cathode effects in dielectric breakdown, R. W. Crowe, A. H. Sharbaugh, and J. K. Bragg—641(A)
Dielectric breakdown of polymers under prolonged stress, Carl G. Brodhun—653(A)
Dielectric constant in perovskite type crystals, John H. Barrett—118
Formation and annulment of space charges in glass and their influence on electric breakdown, K. J. Keller—804(L)
Hysteresis effect in transmission of electrons through thin dielectric foil, Paul H. Owen and C. Sharp Cook—961
Low temperature dielectric behavior of $KNbO_3$, R. Pepinsky, R. Thakur, and C. McCarty—650(A)
Pressure effect in thin films of LiF, Nathan Sclar and Henry Levenstein—622(A)
Pure fused silica, Clayton H. Allen—816(A)
Random noise in dielectrics. II, Herbert Bauss and R. F. Boyer—653(A)
Rotated piezoelectric, elastic, and dielectric constants of quartz, Karl S. Van Dyke and Elva Sterns Creeger—579(A)
Diffraction of electrons (see **Electron diffraction**)
Diffraction of neutrons (see **Neutron diffraction**)
Diffraction of radiation (see **Radiation**)
Diffusion (see also **Thermal diffusion**)
Comparison of *p-n* junctions and radioactive tracers for measurement of diffusion, D. E. Brown and W. C. Dunlap, Jr.—616(A)
Diffusion effects of Co when bombarded with neutrons, George W. Callendine, Jr., Virginia C. Ridolfo, and M. L. Pool—642(A)
Of donor and acceptor elements into Ge, Calvin S. Fuller—136(L)
Effect of neutron irradiation on metallic diffusion, R. R. Coltman and T. H. Blewitt—641(A)
In Ge by *p-n* junction method, W. C. Dunlap, Jr. and D. E. Brown—417(L); W. C. Dunlap, Jr.—615(A)
Grain boundary diffusion of Zn in Cu, R. Smoluchowski and R. Flannagan—598(A)
Kinetics of grain boundary diffusion, R. Smoluchowski—656(A)
Mechanism for self-diffusion in graphite, G. J. Dienes—651(A)
Of polyelectrolytes, B. Rosen and F. R. Eirich—657(A)
Self-diffusion and bulk viscosity of high polymers, F. Bueche—652(A)
Self-diffusion in graphite using C^{14} tracer, M. Feldman, W. Goeddel, and G. J. Dienes—623(A)
Self-diffusion of liquid Hg, R. E. Hoffman—585(A)
In semiconductors, K. B. McAfee, W. Shockley, and M. Sparks—137(L)
Of Ag and Sb in Ag, L. Slifkin, D. Lazarus, and T. Tomizuka—656(A)
Ag self-diffusion, R. D. Johnson and A. B. Martin—642(A)
Technique for self-diffusion measurements, David B. Langmuir—642(A)
Discharge of electricity in gases
Dark current in intermittent glow discharge in H_2, Herman Ritow—130(L)
Dynamic characteristics of a low pressure discharge, B. T. Barnes—351
Emission of atmospheric oxygen bands in discharges and afterglows, Lewis M. Branscomb—258(L); 587(A)
Formative time lags of positive point corona in air, M. Menes and L. H. Fisher—134(L)
Mechanism of trichel pulses of short time duration in air, Leonard B. Loeb—256(L)
Positive ions in afterglow of low pressure He discharge, Arthur V. Phelps and Sanborn C. Brown—102
Short duration afterglow of N_2 in photographic infrared, R. Herman, L. Herman, and G. Hepner—570(L)
Disintegration and excitation of nucleus (see also **Nuclear Spectra; Radioactivity; Photodisintegration**)
α-particles from Li^7+T reactions, J. T. Dewan, T. P. Pepper, K. W. Allen, and E. Almqvist—416(L)
Angular and energy spectrum of neutrons produced in several elements bombarded with 110-Mev protons. I. Experimental, J. A. Hofmann and K. Strauch—605(A); II. Results, K. Strauch and J. A. Hofmann—605(A)
Angular correlation between γ-rays and inelastically scattered protons from Mg^{24}, H. E. Gove and A. Hedgran—574(L)
Angular correlation of radiations from deuteron stripping reactions, L. C. Biedenharn, Keith Boyer, and R. A. Charpie—619(A)
Angular distribution of α-particles from $Li^7(l,\alpha)He^4$, T. P. Pepper, E. Almqvist, and P. Lorrain—630(A)
Angular distributions of inelastically scattered protons from C^{12} and Mg^{24}, H. E. Gove and H. F. Stoddart—572(L)
Deuterium total cross sections for positive and negative pions, H. L. Anderson, E. Fermi, D. E. Nagle, and G. B. Yodh—413(L)
Emission of deuterons from the nucleus, A. G. W. Cameron—435(L)
Energy dependence of $(n,2n)$ reactions in Ni^{58}, Cu^{63}, and Tl^{203} from 11 to 19 Mev, H. C. Martin and B. C. Diven—565(L)
Energy levels in Mn^{53} from scintillation studies of $Cr^{52}(p,n\gamma)Mn^{53}$, Clyde L. McClelland, Clark Goodman, and Paul H. Stelson—631(A)
Energy levels of C^{11} and C^{12} from photographic plate observation of neutron spectra, Virgil R. Johnson—302

Disintegration and excitation of nucleus (continued)
Excitation and disintegration of nuclei by electrons, J. A. Thie, C. J. Mullin, and E. Guth—628(A)
Excitation in high energy nuclear reactions, Norton M. Hintz—1042(L)
Excitation of metastable Cd^{111} by inelastic scattering of neutrons, J. J. G. McCue, A. E. Francis, and Clark Goodman—632(A)
Excited states of Mg^{25} from $Al^{27}(d,\alpha)Mg^{25}$ and $Mg^{24}(d,p)Mg^{25}$, P. M. Endt, H. A. Enge, J. Haffner, and W. W. Buechner—630(A)
Excited states of P^{32} from $P^{31}(d,p)P^{32}$, D. M. Van Patter, P. M. Endt, A. Sperduto, and W. W. Buechner—502; 630(A)
Fast neutron reaction cross sections, E. B. Paul and R. L. Clarke—605(A)
Fast protons from 270-Mev *n-d* collisions, J. B. Cladis, J. Hadley, and W. N. Hess—110
γ-ray resonances in proton bombardment of Mg^{26}, Warren E. Taylor, L. N. Russell, John N. Cooper, and J. C. Harris—630(A)
γ-rays from excited states of Al^{27}, Leonard N. Russell, Warren E. Taylor, and John N. Cooper—819(A)
γ-rays from Na bombarded by protons, P. H. Stelson, W. M. Preston, and Clark Goodman—629(A)
Of He by 90-Mev neutrons, P. Tannenwald—629(A)
Of He^3 by deuterons, A. B. Lillie, T. W. Bonner, and J. P. Conner—630(A)
Inelastic scattering of fast neutrons from Fe, P. H. Stelson and W. M. Preston—132(L)
Inelastic scattering of protons from Ni, Ralph Ely, Jr., A. J. Allen, J. S. Arthur, R. S. Bender, H. J. Hausman, and E. M. Reilley—859
Magnetic analysis of $Mg^{25}(d,p)Mg^{26}$, $Mg^{26}(d,p)Mg^{27}$, and $Mg^{25}(d,\alpha)Na^{23}$, P. M. Endt, J. W. Haffner, and D. M. Van Patter—518
Mass difference $Mg^{23}-Na^{23}$, H. B. Willard, J. D. Kington, and J. K. Bair—259(L)
Neutron capture cross sections from (n,γ) reactions, E. B. Meservey, W. W. Havens, Jr., and L. J. Rainwater—605(A)
Neutron energy distributions from Be, C, and Pb bombarded by 245-Mev protons, B. K. Nelson—594(A)
Neutron groups from protons on Cr^{53}, Co^{59}, and Cl^{37}, P. H. Stelson and W. M. Preston—807(L)
Neutrons from disintegration of P by deuterons, S. C. Snowdon—630(A)
N^{14} and C^{14} ground state parities, D. A. Bromley and L. M. Goldman—790(L)
Of N^{15} by protons, Alois Schardt, William A. Fowler, and Charles C. Lauritsen—527
Nuclear energy levels of Al^{27}, E. M. Reilley, A. J. Allen, J. S. Arthur, R. S. Bender, R. L. Ely, and H. J. Hausman—857
Positron activity arising from proton bombardment of Mg^{25}, Leonard N. Russell, Warren E. Taylor, and John N. Cooper—653(A)
Production of neutrons by μ-meson capture in Pb, Mg, and Ca, Anna Maria Conforto and R. D. Sard—465
(p,n) yields from light elements, Harvey B. Willard and Joe Keagy Bair—629(A)
Q-values of $C^{13}(d,p)C^{14}$, $Be^9(d,p)Be^{10}$, and $O^{16}(d,p)O^{17}$, E. D. Klema and G. C. Phillips—951
Reactions of 370-Mev protons with Co, E. Belmont—630(A)
Scattering of fast neutrons by W, C. E. Mandeville, C. P. Swann, and F. J. Seymour—861
Scattering of protons by loosely bound neutron in Be, K. Strauch and J. A. Hofmann—563(L)
Search for α-particles from $O^{16}(d,\alpha)N^{14*}$, R. J. Van de Graaff, A. Sperduto, W. W. Buechner, and H. A. Enge—966
Short-range protons from $Li^6(d,p)Li^7$, R. W. Gelinas and S. S. Hanna—253(L)
Slow neutron capture γ-rays, W. A. Thornton, Jr., E. der Mateosian, H. T. Motz, and M. Goldhaber—604(A)
Stars initiated by high energy protons and neutrons, Herbert Fishman and Alfred Morris Perry, Jr.—167
Yield of F^{18} from medium and heavy elements with 420-Mev protons, Luis Marquez—405

Elasticity
Anisotropy of thermal expansion and internal stresses in polycrystalline graphite and carbons, S. Mrozowski—622(A)
Critical shear stresses in body-centered cubic lattices, R. Smoluchowski—787
Elastic constants of Cu-Si alloy, Charles S. Smith and J. W. Burns—655(A)
Elastic studies of single crystals of NaCl type, Lewis S. Combes, Stanley S. Ballard, and Kathryn A. McCarthy—623(A)
Electronic instrument for measurement of crystal anelasticity, R. D. Laughlin—623(A)
Instability criteria for fracture of solids, H. L. Smith, J. A. Kies, and G. R. Irwin—623(A)
Measuring small strains with polarized light, H. P. Gage—816(A)
Rotated piezoelectric, elastic, and dielectric constants of quartz, Karl S. Van Dyke and Elva Sterns Creeger—579(A)
Strain rate, temperature, and time effects in ballistic-speed deformation of mild steel, J. M. Krafft—598(A)
Third-order elastic coefficients in trigonal and hexagonal crystals, Fausto G. Fumi—561(L)
Of very small metal specimens, J. K. Galt and Conyers Herring—656(A)
Work to create fracture surfaces in methyl methacrylate, Mark Bowman, Jr., and H. L. Smith—623(A)

Electrical conductivity and resistance (see also **Semiconductors; Superconductivity**)
Of carbon materials, S. Mizushima—1040(L)
Effect of deuteron bombardment on electrical resistivity of Cu, Ag, and Au, J. Marx, J. Koehler, and C. Wert—643(A)
Effect of grain size on magnetoresistance of polycrystalline Cu, George B. Yntema—598(A)
Effect of thickness of thin metal films on mean free path of conduction electrons, E. C. Crittenden, Jr., E. H. Layer, and R. W. Hoffman—657(A)
Electric turbulences in fluid medium, Oleg Yadoff—585(A)
Electrical properties of sodium tungsten bronzes, Hellmut J. Juretschke—124(L)
High frequency resistance of metals in normal and superconducting state, C. J. Grebenkemper and John P. Hagen—673
Impedance measurements on PbS photoconductive cells, E. S. Rittner and F. Grace—615(A); 955
Of natural graphite crystals, W. Primak and L. Fuchs—651(A)
New mutual inductance formula, Milan W. Garrett—613(A)
Resistivity changes produced by deuteron irradiation of Cu, Ag, and Au, J. W. Henderson, H. G. Cooper, and J. W. Marx—642(A)

Electrodynamics (see **Electromagnetic theory and electrodynamics**)

Electrolysis
Of thorium oxide, W. E. Danforth—416(L)

Electromagnetic theory and electrodynamics (see also **Quantum electrodynamics**)
Experimental evidence for classical electron radiation at 300 Mev, Joseph W. Mather—795(L)

Frequency multiplication and wave amplification by means of some relativistic effects, K. Landecker—852
Optical focusing in constant radius accelerators, David D. dePackh—433(L)
Perturbation treatment of electromagnetic problems. I, J. R. Terrall and Benjamin Lax—595(A); II, Benjamin Lax and J. R. Terrall—595(A)
Radiation from electron in magnetic field, D. L. Judd, J. V. Lepore, M. Ruderman, and P. Wolff—123(L)
Radiation loss by electrons in large orbits, Dale R. Corson —1052(L)
Radiation loss of electrons in the synchrotron, H. Olsen and H. Wergeland—123(L)

Electron affinity
Electron microscopic studies of some paraffinic Na soaps, Morton L. E. Chwalow—650(A)

Electron diffraction
Of some paraffinic Na soaps, Morton L. E. Chwalow—650(A)

Electron optics
Electron interferometer, limitations, J. Arol Simpson—585(A); principles, L. Marton—585(A)

Electronic tubes
Grid bar mask focusing in color TV tube, Jenny E. Rosenthal—614(A)

Electrons (see also **Positrons; E/m; Electromagnetic theory and electrodynamics**)
Electron-neutron interaction, Burton D. Fried—434(L); Sidney Borowitz—567(L)
Experimental evidence for classical electron radiation at 300 Mev, Joseph W. Mather—795(L)
Hysteresis effect in transmission of electrons through thin dielectric foil, Paul H. Owen and C. Sharp Cook—961
Order of magnitude of signal radius of electron, Paul Molmud—639(A)
Theory of the electron, Walter Wessel—639(A)

Electrons in metals
Collective description of electron interactions, R. Kronig—795(L)
Nuclear resonance and electronic structure of transition metals, W. D. Knight and C. Kittel—573(L)
Production of secondary electrons in solids, A. J. Dekker and A. van der Ziel—755
Scattering of electrons in metals by dislocations, D. L. Dexter—770

Electrons, positive (see **Positrons**)

Electrons, scattering of
High energy electron-electron scattering, Walter H. Barkas, Robert W. Deutsch, F. C. Gilbert, and Charles E. Violet—59
In metals by dislocations, D. L. Dexter—770

Electrons, secondary
Field dependent secondary emission, Harold Jacobs and John Freely—585(A)
Wooldridge's theory of secondary emission, E. M. Baroody —915

Electrons, thermionic (see **Thermionic emission**)

Elements (see **Isotopes**)

Energy loss of particles (see **Range and energy loss of particles**)

Energy states of atoms (see **Spectra, atomic**)

Energy states of molecules (see **Molecular structure and constants; Spectra, molecular**)

Energy states of nucleus (see **Disintegration and excitation of nucleus; Nuclear spectra; Nuclear structure**)

Errata
Microwave spectrum and molecular constants of HCN, James W. Simmons, Wallace E. Anderson, and Walter Gordy—1055(L)
Multiple events produced in H by very high energy cosmic-ray particles at altitude of 90,000 ft, M. L. Vidale and Marcel Schein—1056(L)
Nuclear magnetic moment and j-j coupling shell model, Masatake Mizushima and Minoru Umezawa—1055(L)
Semiconductivity and diamagnetism of polycrystalline graphite and condensed ring systems, S. Mrozowski—1056(L)
Thermoelectric power of carbons and graphite, E. E. Loebner—1056(L)

Excitation of nuclei (see **Disintegration and exitation of nucleus; Nuclear spectra; Nuclear structure**)

Explosion phenomena (see also **Shock waves**)
Spalling produced by detonation of explosives in very heavy walled metal tubes, L. Starr and J. Savitt—600(A)
Spherical blast, approximate analytic solutions, J. A. McFadden—600(A)

Faraday effect (see **Magneto-optical effects**)

Ferroelectric and antiferroelectric phenomena
In ceramic $PbZrO_3$ containing Ba or Sr, Gen Shirane—219
Crystal structure of the ferroelectric phase in $PbZrO_3$ containing Ba or Ti, Gen Shirane and Sadao Hoshino—248(L)
Ferroelectric ammonium metaphosphate, R. Pepinsky, C. M. McCarty, E. Zemyan, and K. Drenck—793(L)
In the ilmenite structure, H. C. Schweinler—624(A)

Ferromagnetism (see **Magnetic properties**)

Field theory (see also **Quantum electrodynamics**)
Applications of charge independence hypothesis to meson phenomena, Kenneth M. Watson—625(A)
Argument against the Majorana theory of neutral particles, E. R. Caianiello—564(L)
Electron-neutron interaction, Burton D. Fried—434(L); Sidney Borowitz—567(L)
Equations of motion in covariant field theory, Joshua Goldberg and Ralph Schiller—620(A)
Intermediate coupling theory of pseudoscalar meson-nucleon interaction, P. T. Matthews and Abdus Salam—715
Intrinsic properties of τ-meson derived from conservation laws, B. A. Jacobsohn—626(A)
μ-pair theory with pseudoscalar coupling, L. M. Tannenwald—332
Non-adiabatic treatment of relativistic two-body problem, Maurice M. Levy—626(A)
Nonlinear meson theory for heavy nuclei, Bertram J. Malenka—68
Nonlocal photons, J. S. Lomont—596(A)
Phenomenological relationships between photomeson production and meson-nucleon scattering, K. A. Brueckner and K. M. Watson—923
Pion production and charge independence, J. M. Luttinger —571(L)
Pion-proton scattering and strong coupling meson theory, G. Wentzel—437
Pseudoscalar coupling in pseudoscalar meson theory, G. Wentzel—802(L)
Pseudoscalar interaction, L. L. Foldy—626(A)
Quantization of neutral scalar meson theory with nonlinear coupling, L. I. Schiff—856
Quantization of nonlinear meson theory, L. I. Schiff—625(A)
Stability of neutral scalar heavy mesons, H. P. Noyes—625(A)
Subtractive bosons in generalized theory, Alex E. S. Green 596(A)
Super-potentials in covariant theories, Ralph Schiller and Joshua Goldberg—620(A)
Symmetrical pseudoscalar meson theory of nuclear forces, Maurice M. Levy—806(L)
Time-dependent canonical transformations, Peter G. Bergmann and Ralph Schiller—621(A)
Unified description of leptons, V. Votruba and M. Lokajíček —260(L)
V-particles, A. Pais—663

Films, properties of
Effect of thickness of thin metal films on mean free path of conduction electrons, E. C. Crittenden, Jr., E. H. Layer, and R. W. Hoffman—657(A)
Mechanical properties of thin films of Ag, W. E. Walker, T. J. Turner, and J. W. Beams—597(A)
Optical properties of evaporated Sb films, Calvin Tiller and Henry Levinstein—657(A)
Pressure effect in thin films of LiF, Nathan Sclar and Henry Levinstein—622(A)
SiO films, G. A. Sawyer, W. R. Arnold, J. A. Phillips, E. J. Stovall, Jr., and J. L. Tuck—583(A)
Fine structure (see **Spectra, etc.; Hyperfine structure**)
Fission of nucleus (see also **Disintegration and excitation of nucleus**)
γ-ray spectra of Los Alamos reactors, J. W. Motz—753
Meson fission of Hg, Nathan Sugarman—604(A)
Spontaneous fission, Emilio Segrè—21
Fluctuation phenomena
Configuration distribution of chain molecule with correlations, C. M. Tchen—658(A)
Fluctuation problem in cascade shower theory, J. W. Gardner and H. Messel—808(L)
Impedance of semiconducting films, J. N. Humphrey, F. L. Lummis, and W. W. Scanlon—660(A)
Noise and dissipation, John M. Richardson—613(A)
Random Noise in dielectrics. II, Herbert Bauss and R. F. Boyer—653(A)
Relation between noise and response time in photoconductors. I. Theorg, R. L. Petritz—660(A)
Solution of fluctuation problem in electron-photon shower theory, H. Messel and R. B. Potts—847
Stress-induced noise in cables, Thomas A. Perls—613(A)
Theory of noise in photoconductors, Richard L. Petritz—614(A)
Fluid dynamics (see also **Hydrodynamics; Aerodynamics**)
Condensation phenomenon of ideal Einstein-Bose gas, Otto Halpern—126(L)
Experimental model of turbulence, Robert Betchov—601(A)
Explicit construction of large-amplitude water waves in channels, R. P. Shaw—601(A)
Free-flight determination of boundary layer transition on cone cylinders, W. R. Witt, Jr.—601(A)
Hypersonic viscous flow over a flat plate, L. Lees and R. F. Probstein—600(A)
Second-order acoustic fields: streaming with viscosity and relaxation, Jordan J. Markham—497; relations between density and pressure—710; energy relations—712
Shock wave turbulent boundary layer interaction, S. M. Bogdonoff and A. H. Solarski—601(A)
Stability of plane Poiseuille flow, L. H. Thomas—812(L)
Theory of Bose-Einstein liquids, J. G. Daunt, T. P. Tseng, and C. V. Heer—627(A); 911
Transonic flow past a wedge at zero angle of attack, Leon Trilling—600(A)
Turbulence theory in compressible fluids, M. Z. v. Krzywoblocki—601(A)
Fluorescence (see also **Luminescence**)
Metallurgical microradiography with fluorescence x-rays, H. R. Splettstosser and H. E. Seemann—816(A)
Scintillation response of organic crystals to low energy α-particles, J. W. King and J. B. Birks—568(L)
Theory of response of organic scintillation crystals to short-range particles, J. B. Birks—569(L)
Of xanthopterin-like pigment, M. O'L. Crowe and A. Walker—817(A)

Gamma-rays (see also **Disintegration and excitation of nucleus; Nuclear spectra; Radioactivity**)
Electron spectra produced by Co^{60} source in water, Evans Hayward—493
γ-energy resolution with NaI scintillation spectrometer, C. J. Borkowski and R. L. Clark—583(A)
γ-ray energy measurements with pair spectrometer, G. A. Bartholomew and B. B. Kinsey—605(A)
γ-ray spectra of Los Alamos reactors, J. W. Motz—753
Monoenergetic γ-rays from synchrotron, J. W. Weil and B. D. McDaniel—582(A)
Nuclear photodissociation by high energy synchrotron γ-rays, Seishi Kikuchi—41
Nuclear scattering of 17-Mev γ-rays, M. B. Stearns—593(A)
Scattering of gammas by bound electrons, J. S. Levinger—592(A)
Geophysics
Absorption bands of atmospheric CO, J. H. Shaw and J. N. Howard—654(A)
Gyromagnetization (see **Magnetic properties**)

Hall effect
Magnetic field effect upon Hall coefficient of impurity semiconductors, W. J. Whitesell, II and V. A. Johnson—648(A)
In Zn crystals at low temperatures, John K. Logan—598(A)
Heat conduction (see **Thermal conductivity**)
Helium, liquid
Co-existence of liquid He I and II, Philip Closmann and Richard T. Swim—576(L)
Experiments with rotating cylinder viscometer in liquid He II, A. C. Hollis-Hallett—649(A)
He II transfer rates on lucite and perspex surfaces, B. S. Chandrasekhar—414(L)
Liquid-solid transformation in He from 1.6° to 4°K, C. A. Swenson—870
Magnetic properties of liquid He^3, E. F. Hammel, H. L. Laquer, S. G. Sydoriak, and W. E. McGee—432(L)
Radial distribution function in liquid He, P. J. Price—495
Solubility of He^3 in liquid He^4, J. G. Daunt and C. V. Heer—205; 627(A)
Theory of Bose-Einstein liquids, J. G. Daunt, T. P. Tseng, and C. V. Heer—627(A); 911
Hydrodynamics
Explicit construction of large-amplitude water waves in channels, R. P. Shaw—601(A)
Hyperfine structure (see also **Nuclear moments and spin**)
Effect of atomic core on magnetic hfs, R. Sternheimer—316
Effects of configuration interaction on atomic hfs of Ga, G. F. Koster—148
Of Gd and Zr, S. Suwa—247(L)
High frequency lines in hfs spectrum of Cs, J. E. Sherwood, Harold Lyons, R. H. McCracken, and P. Kusch—618(A)
Hfs anomalies in the $^2P_{\frac{1}{2}}$ state of Tl^{205} and Tl^{203}, Alan Berman—1005
Hfs anomalies of ICN, A. Javan and C. H. Townes—608(A)
Hfs anomaly and models of nuclear structure, B. T. Feld—609(A)
Magnetic hfs, R. Sternheimer—595(A)
Magnetic hfs in O_2, S. L. Miller, M. Kotani, and C. H. Townes—607(A)
Magnetic moment of K^{40} and hfs anomaly of K isotopes, J. T. Eisinger, B. Bederson, and B. T. Feld—73
Of Hg green line, John Sterner—139(L)
Of $p_{\frac{1}{2}}$ states, W. W. Clendenin—810(L)
Second-order radiative corrections to hfs, Norman M. Kroll and Franklin Pollock—876

Instruments (see **Methods and instruments**)
Internal conversion (see **Nuclear spectra**)
Ionization
K-shell ionization accompanying α-decay of Po^{210}, W. C. Barber and R. H. Helm—175

Ionosphere
New kind of radio propagation at very high frequencies observable over long distances, D. K. Bailey, R. Bateman, L. V. Berkner, H. G. Booker, G. F. Montgomery, E. M. Purcell, W. W. Salisbury, and J. B. Wiesner—141

Ions
Ion beam focusing, F. C. Shoemaker, R. J. Britten, and B. C. Carlson—582(A)
Total collision cross sections of negative atomic I ions in N_2 and A, Frank L. McCrackin—135(L)

Ions and electrons, mobility
Electron mobilities in liquid and solid A and liquid He, M. S. Malkin—585(A)
Electron mobility in CdS, J. W. MacArthur—615(A)

Isobars
Meson-nucleon scattering and nucleon isobars, Keith A. Brueckner—106, 626(A)

Isomers, nuclear (see also **Nuclear spectra; Radioactivity**)
Decay of Sr^{85}, A. W. Sunyar, J. W. Mihelich, G. Scharff-Goldhaber, M. Goldhaber, N. S. Wall, and M. Deutsch—1023
Decay of metastable state in In^{115}, L. M. Langer, R. D. Moffat, and G. A. Graves—632(A)
Excitation of metastable Cd^{111} by inelastic scattering of neutrons, J. J. G. McCue, A. E. Francis, and Clark Goodman—632(A)
In^{112*} conversion coefficient using scintillation spectrometer, Thomas B. Cook, Jr. and Sherwood K. Haynes—190

Isotopes and atomic mass
Atomic masses from Ti through Zn, Thomas L. Collins, Alfred O. Nier, and Walter H. Johnson, Jr.—408
Empirical mass surface, Alex E. S. Green—654(A)
Experimental mass surface, R. B. Minogue, R. Oppenheim, and A. E. S. Green—654(A)
Mass difference $Mg^{25}-Na^{25}$, H. B. Willard, J. D. Kington, and J. K. Bair—259(L)
Mass surface and radioactivity, J. S. Nader, N. J. Marucci, and A. E. S. Green—654(A)
Masses of Pb^{208}, Th^{228}, U^{234}, and U^{235}, G. S. Stanford, H. E. Duckworth, B. G. Hogg, and J. S. Geiger—617(A)
Radioisotopes of Br, S. C. Fultz and M. L. Pool—347
Semi-empirical mass surfaces, N. Engler and A. E. S. Green—654(A)

Kerr effect (see **Electro-optical effects**)

Liquids (see also **Hydrodynamics**)
Angular points in liquids *versus* temperature, G. Antonoff, A. Yakimac, A. Urmanczy, and R. Madrazo—586(A)
Energy and volume changes attending the mixing of nonpolar liquids, Robert D. Dunlap and Harold F. Crandall—579(A)

Low temperature phenomena (see also **Helium, liquid**)
Low temperature dielectric behavior of $KNbO_3$, R. Pepinsky, R. Thakur, and C. McCarty—650(A)
Low temperature heat capacity of Nb, A. Brown, M. W. Zemansky, and H. A. Boorse—627(A)
Low temperature thermal expansion of U, Adam F. Schuch and Henry L. Laquer—803(L)
Specific heat of Pb in temperature range 1.0°K to 75°K, M. Horowitz, A. A. Silvidi, S. F. Malaker, and J. G. Daunt—818(A)

Luminescence (see also **Fluorescence; Phosphorescence**)
Of edge emission in CdS, Clifford Klick—659(A)
Injected light emission from SiC, K. Lehovec, C. A. Accardo, and E. Jamgochian—615(A)
Of single crystals of ZnS, William W. Piper and Ferd E. Williams—659(A)

Magnetic properties (see also **Nuclear moments and spin; Crystal structure; Magnetic resonance absorption**)
Antiferromagnetic resonance in crystal of rhombic symmetry at absolute zero, J. Ubbink—567(L)
Approximate quantum theory of antiferromagnetic ground state, P. W. Anderson—694
Chemical effects in nuclear magnetic resonance and in diamagnetic susceptibility, Norman F. Ramsey—243
Of chromites, T. R. McGuire, Louis N. Howard, and J. Samuel Smart—599(A)
Collective electron theory of saturation moment of alloys, J. E. Goldman—599(A)
Domain patterns on FeSi crystals, C. F. Ying, S. Levy, and R. Truell—133(L)
Domain structure of perminvar with rectangular hysteresis loop, H. J. Williams and Matilda Goertz—599(A)
Effect of grain size on magnetoresistance of polycrystalline Cu, George B. Yntema—598(A)
Gyromagnetic effect in superconductor, Robert Pry and Arthur L. Lathrop—628(A); R. H. Pry, A. L. Lathrop, and W. V. Houston—905
Hexagonal iron-oxide compounds as permanent-magnet materials, J. J. Went, G. W. Rathenau, E. W. Gorter, and G. W. van Oosterhout—424(L)
High temperature susceptibility of permanent dipolar lattices, R. Rosenberg and M. Lax—624(A)
Intrinsic magnetization in alloys, W. J. Carr—599(A)
Of liquid He^3, E. F. Hammel, H. L. Laquer, S. G. Sydoriak, and W. E. McGee—432(L)
Magnetic domains on Si iron by longitudinal Kerr effect, C. A. Fowler, Jr., and E. M. Fryer—426(L)
Magnetic effect in $MgTiO_3$, E. K. Weise and H. Katz—1046(L)
Magnetoelastic energy losses and magnetic hysteresis in ferromagnetic materials, G. Bonfiglioli, A. Ferro, and G. Montalenti—959
Magnetostrictive vibration of prolate spheroids. Ni-Fe and Ni-Cu alloys, J. S. Kouvelites and L. W. McKeehan—898
Molecular field treatment of ferromagnetism and antiferromagnetism, J. Samuel Smart—968
Neutron diffraction studies of various transition elements, C. G. Shell and M. K. Wilkinson—599(A)
Nuclear resonance and electronic structure of transition metals, W. D. Knight and C. Kittel—573(L)
Semiconductivity and diamagnetism of polycrystalline graphite and condensed ring systems, erratum, S. Mrozowski—1056(L)
Size effects and diamagnetism in finite systems, M. F. M. Osborne and M. C. Steele—247(L)
Spherical model of ferromagnet, T. H. Berlin and M. Kac—821
Spin paramagnetism of Cr^{+++} at liquid He temperatures and high magnetic fields, Warren E. Henry—628(A)
Spin wave treatment of saturation magnetization of ferrites, Harvey Kaplan—121(L)
Temperature dependence of magnetic spectrum of a ferrite, G. T. Redo, R. W. Wright, W. H. Emerson, and A. Terris—599(A)

Magnetic resonance absorption (see also **Nuclear moments and spin**)
Anisotropy in paramagnetic resonance in free radicals, C. Kikuchi, V. W. Cohen, and John Turkevich—608(A)
Antiferromagnetic resonance in crystal of rhombic symmetry at absolute zero, J. Ubbink—567(L)
Chemical effects in nuclear magnetic resonance and in diamagnetic susceptibility, Norman F. Ramsey—243
Double resonance method for investigating atomic energy levels, Hg $^3P_1$, Jean Brossel and Francis Bitter—308

Magnetic resonance absorption (continued)
Ferromagnetic resonance in Cu ferrite, Tosihiko Okamura and Yuzo Kojima—1040(L)
Ferromagnetic resonance in $NiOFe_2O_3$ as function of temperature, D. W. Healy, Jr.—1009
Magnetic resonance in system containing two magnetic sublattices, Roald K. Wangsness—146; 646(A)
Nuclear magnetic resonance of hydrogen absorbed into Pd wires, R. E. Norberg—745
Nuclear resonance and electronic structure of transition metals, W. D. Knight and C. Kittel—573(L)
Paramagnetic relaxation in metals, Albert W. Overhauser—646(A)
Sign of quadrupole interaction energy in diatomic molecules, R. A. Logan, R. E. Cote, and P. Kusch—280
Temperature dependence of magnetic spectrum of a ferrite, G. T. Rado, R. W. Wright, W. H. Emerson, and A. Terris—599(A)
Magneto-optical effects
Faraday rotation of guided waves, H. Suhl and L. R. Walker—122(L)
Magnetic domains on Si iron by longitudinal Kerr effect, C. A. Fowler, Jr., and E. M. Fryer—426(L)
Magnetostriction (see **Magnetic properties**)
Mass spectroscopy
Atomic masses from Ti through Zn, Thomas L. Collins, Alfred O. Nier, and Walter H. Johnson, Jr.—408
Energy available for double β-decay of Sn^{124}, Benjamin G. Hogg and Henry E. Duckworth—567(L)
Masses of Pb^{208}, Th^{232}, U^{234}, and U^{238}, G. S. Stanford, H. E. Duckworth, B. G. Hogg, and J. S. Geiger—617(A)
Measurements (see **Methods and instruments**)
Mechanics, quantum—atomic structure and spectra
Effects of configuration interaction on atomic hfs of Ga, G. F. Koster—148
Fourth-order radiative correction to atomic energy levels, R. Bersohn, J. Weneser, and N. M. Kroll—596
Mass corrections to fine structure of H and D, E. E. Salpeter—595(A)
Perturbations of atomic g-values, M. Phillips—595(A)
Mechanics, quantum—general
Angular momentum distributions in Thomas-Fermi model, J. H. D. Jensen and J. M. Luttinger—907
Application of quantum-mechanical Franck-Condon principle to complex systems, Melvin Lax—660(A)
Application of variational method to scattering by square well potential, J. Mayo Greenberg—610(A)
Darling's theory of fundamental length, P. R. Zilsel—620(A)
Order of magnitude of signal radius of electron, Paul Molmud—639(A)
Quantization of nonlinear meson theory, L. I. Schiff—625(A)
Radiation from electron in magnetic field, D. L. Judd, J. V. Lepore, M. Ruderman, and P. Wolff—123(L)
Radiation loss of electrons in synchrotron, H. Olsen and H. Wergeland—123(L)
Semiclassical Franck-Condon principle and its application to complex systems, Melvin Lax—640(A)
Theory of the electron, Walter Wessel—639(A)
Virial theorem for Dirac particle, M. E. Rose and T. A. Welton—432(L)
Mechanics, quantum—molecular structure and spectra
Convergence of intermolecular force series, Franklin C. Brooks—92
Ozone molecule, theory, B. T. Darling and J. A. Weiss—655(A)
Mechanics, quantum—nuclear
Angular correlation of first and third γ-rays, G. B. Arfken, L. C. Biedenharn, and M. E. Rose—761
Angular correlation of radiations from deuteron stripping reactions, L. C. Biedenharn, Keith Boyer, and R. A. Charpie—619(A)
Angular distribution of π^+-production in n-p collisions, H. A. Bethe and N. Austern—121(L)
Angular momentum distributions in Thomas-Fermi model, J. H. D. Jensen and J. M. Luttinger—907
β-decay of mirror nuclei and shell model, O. Kofoed-Hansen and Aage Winther—428(L)
Comparative models in nuclear scattering, D. C. Peaslee—269
Exchange current effects in deuteron, Felix Villars—476
First forbidden β-decay matrix elements, T. Ahrens and E. Feenberg—64
First forbidden β-transition, T. Ahrens and E. Feenberg—609(A)
Impulse approximation, Saul T. Epstein—836
Interaction term in β-decay theory, R. H. Good, Jr.—620(A)
Interpretation of image transitions in β-decay theory, George L. Trigg—506
jj-coupling in nuclei, B. H. Flowers—254(L)
Magnetic moments of even-odd nuclei, Jack P. Davidson—609(A)
Meson-nucleon scattering and nucleon isobars, Keith A. Brueckner—106, 626
μ-meson decay and β-radioactivity, Louis Michel—814(L)
n-p scattering with spin-orbit coupling. I, John M. Blatt and L. C. Biedenharn—399; John M. Blatt—610(A)
Nonlinear meson theory for heavy nuclei, Bertram J. Malenka—68
Nuclear magnetic moment and j-j coupling shell model, erratum, Masataka Mizushima and Minoru Umezawa—1055(L)
Nuclear matrix elements in theory of β-decay, Henry Brysk—996
One-three γ-γ angular correlation, G. B. Arfken, L. C. Biedenharn, and M. E. Rose—619(A)
Pseudoscalar interaction, L. L. Foldy—626(A)
Saturation property of nuclear forces, Hideo Kanazawa—428(L)
Tests of charge independence from pion production in nuclear collisions, A. M. L. Messiah—430(L)
Third forbidden β-spectrum from Rb^{87}, Y. Tomozawa, M. Umezawa, and S. Nakamura—791(L)
Triton binding energy by a randomized net-point method, S. I. Rubinow—388
Mechanics, quantum—of solid bodies
Approximate quantum theory of antiferromagnetic ground state, P. W. Anderson—694
Bardeen's theory of superconductivity and f-sum rule, Edward N. Adams, II—258(L)
Calculation of energy bands in solids by integral iteration method, M. Dank and H. B. Callen—622(A)
Dielectric constant in perovskite type crystals, John H. Barrett—118
Electronic energy bands in crystals, R. H. Parmenter—552
Intrinsic magnetization in alloys, W. J. Carr—599(A)
Korringa method for energy band calculations, R. J. Harrison—651(A)
Motion of electron in perturbed periodic potential, Edward N. Adams, II—427(L)
Production of secondary electrons in solids, A. J. Dekker and A. van der Ziel—755
Scattering of electrons in metals by dislocations, D. L. Dexter—770
Spin wave treatment of saturation magnetization of ferrites, Harvey Kaplan—121(L)
Thermal ionization of trapped electrons, Ryogo Kubo—929
Mechanics, statistical
Brownian motion theory as tool in statistical mechanics, A. J. F. Siegert—621(A)

Condensation phenomenon of ideal Einstein-Bose gas, Otto Halpern—126(L)
Energy levels of one-dimensional Bose solid, H. W. Lewis—649(A)
In general relativity, J. W. Weinberg and G. E. Tauber—621(A)
Markoff random processes and statistical mechanics of time-dependent phenomena, Melville S. Green—621(A)
Relativistic quantum statistics of thermal excitations and its application to condensed systems at very low temperatures, C. V. Heer and J. G. Daunt—649(A)
Theory as organization of observation, Jerome Rothstein—634(A)
Thermal equilibrium in general relativity, G. E. Tauber and J. W. Weinberg—621(A)

Mesons (see also **Cosmic radiation**)
Absorption of π^--mesons in He gas, C. P. Leavitt—603(A)
Angular distribution of 53-Mev positive pions scattered by protons, E. C. Fowler, W. B. Fowler, R. P. Shutt, A. M. Thorndike, and W. L. Whittemore—1053(L)
Angular distribution of π^+-production in π-p collisions, H. A. Bethe and N. Austern—121(L)
Angular distribution of pions scattered by hydrogen, H. L. Anderson, E. Fermi, D. E. Nagle, and G. B. Yodh—794(L)
Application of Fermi model to cosmic-ray events of primary energy greater than 10^{13} ev, W. E. Hazen, R. E. Heineman, and E. S. Lennox—198
Applications of charge independence hypothesis to meson phenomena, Kenneth M. Watson—625(A)
Associated pairs of particles in cosmic-ray showers in photographic emulsions, J. Y. Mei and E. Pickup—796(L)
Charged photomesons from various nuclei, Raphael Littauer and Darcy Walker—838
Collision of heavy primary cosmic-ray nucleus, N. L. Allen, J. Y. Mei, E. Pickup, and L. Voyvodic—1045(L)
Dependence of charged pion production on incident proton energy, S. Passman, M. M. Block, and W. W. Havens, Jr.—602(A)
Deuterium total cross sections for positive and negative pions, H. L. Anderson, E. Fermi, D. E. Nagle, and G. B. Yodh—413(L)
Difference of H and D total cross sections for charged π-mesons, G. Yodh, H. L. Anderson, D. E. Nagle, and H. Stadler—603(A)
Disintegration of V-particles, C. J. Karzmark, R. W. Thompson, and Hans O. Cohn—591(A)
Heavy mesons in penetrating showers, R. B. Leighton and S. D. Wanlass—426(L)
High energy collisions with production of meson showers, S. Biswas and V. D. Hopper—209
Intrinsic properties of τ-meson derived from conservation laws, B. A. Jacobsohn—626(A)
Mean life of positive π-meson, William L. Kraushaar—513
Meson contributions to photodisintegration of deuteron, M. H. Friedman—625(A)
Meson fission of Hg, Nathan Sugarman—604(A)
Meson-nucleon scattering and nucleon isobars, Keith A. Brueckner—106; 626(A)
Mesotron mean lifetime as function of momentum, D. W. Seymour and W. F. G. Swann—592(A)
μ-meson capture measurements, technique, J. W. Keuffel, F. B. Harrison, T. N. K. Godfrey, and George T. Reynolds—616(A)
μ-meson capture probabilities in heavy elements, F. B. Harrison, J. W. Keuffel, T. N. K. Godfrey, and George T. Reynolds—616(A)
μ-meson capture, theory, J. M. Kennedy—616(A)
μ-meson decay and β-radioactivity, Louis Michel—814(L)
Multiple meson production, H. W. Lewis—625(A)
Multiple scattering of μ-mesons in magnetized Fe, Stephan Berko—598(A)
Multiplicity of mesons produced in Pb, John Linsley and E. P. Ney—592(A)
Muon range spectrum from $\pi \rightarrow \mu$ decay, A. M. Seifert, H. J. Bramson, and W. W. Havens, Jr.—603(A)
Nuclear cross sections for negative pions of energy 109 and 133 Mev, R. L. Martin, H. L. Anderson, and G. Yodh—604(A)
Nuclear interaction of fast μ-mesons, H. C. Wilkins and R. D. Sard—591(A)
Phenomenological relationships between photomeson production and meson-nucleon scattering, K. A. Brueckner and K. M. Watson—923
Photomesons from D, James Keck and Raphael Littauer—602(A)
Photoproduction of mesons on nuclei, T. R. Palfrey, Jr. and R. R. Wilson—602(A)
Pion production and charge independence, J. M. Luttinger, —571(L)
Possible charged V-particle or κ-meson event in a photographic emulsion, L. Voyvodic—1046(L)
Possible influence of κ-mesons on underground cosmic radiation, Loup Verlet—792(L)
Production cross section and energy spectrum of π_0-meson (cosmic-ray measurement), G. Salvini and Y. Kim—592(A)
Production cross section of negative mesons in C by 341-Mev protons, Walter F. Dudziak—602(A)
Production of 40-Mev π-mesons by 240-Mev protons in seven elements, Donald L. Clark—602(A)
Production of neutral mesons by photons, W. K. H. Panofsky, J. N. Steinberger, and J. Steller—180
Production of neutrons by μ-meson capture in Pb, Mg, and Ca, Anna Maria Conforto and R. D. Sard—465
Production of positive mesons by photons, J. Steinberger and A. S. Bishop—171
Relative production of neutral mesons by 310-Mev γ-rays in H and D, A. Silverman and G. Cocconi—602(A)
Scattering and absorption of π-mesons in C, H. Byfield, J. Kessler, and L. M. Lederman—17
Scattering and capture of pions by H, H. L. Anderson and E. Fermi—794(L)
Scattering of negative pions by H, A. Lundby, E. Fermi, H. L. Anderson, D. E. Nagle, and G. Yodh—603(A)
Scattering of π-mesons by deuteron, J. S. Blair and B. Segall—626(A)
Slow π-meson reactions in He^3, A. M. L. Messiah—603(A)
Stability of neutral scalar heavy mesons, H. P. Noyes—625(A)
Tests of charge independence from pion production in nuclear collisions, A. M. L. Messiah—430(L)
Total collision cross sections of negative pions on protons, D. E. Nagle, H. L. Anderson, E. Fermi, E. A. Long, and R. L. Martin—603(A)
Unusual π-μ decays in photographic emulsions, W. F. Fry —418(L)
V-particles, A. Pais—663
V^0-particles and isotopic spin, D. C. Peaslee—127(L)

Meson field theory (see **Field theory**)

Metals (see **Crystalline state**)

Methods and instruments
Automatic recording scintillation spectrometer for γ-rays, Thomas D. Strickler and W. G. Wadey—583(A)
Čerenkov radiation counting, John Marshall—583(A)
Constriction type of electromechanical filter employing a shear mode, Shepard Bartnoff and Charles R. Mingins—613(A)
Conversion method for relating stress relaxation and dynamic modulus, Robert S. Marvin—644(A)

Methods and instruments (continued)
Deterioration of BF_3 counters due to rapid counting rates, R. K. Soberman and S. A. Korff—584(A)
Device for converting shaft rotation to input for digital computer, Donald H. Jacobs and Seymour Scholnick—614(A)
Diffusion cloud-ion chamber, M. M. Block, W. W. Brown, and G. G. Slaughter—583(A)
Electron interferometer, limitations, J. Arol Simpson—585(A); principles, L. Marton—585(A)
Electronic instrument for measurement of crystal anelasticity, R. D. Laughlin—623(A)
Ellicott compensated pendulum, E. H. Johnson—818(A)
Far infrared spectrum measurements, E. E. Bell, R. L. Hansler, R. A. Oetjen, and H. E. Schauwecker—819(A)
Fast neutron spectrometer, L. E. Beghian, R. A. Allen, J. M. Calvert, and H. Halban—1044(L)
Frequency multiplication and wave amplification by relativistic effects, K. Landecker—852
γ-energy resolution with NaI scintillation spectrometer, C. J. Borkowski and R. L. Clark—583(A)
Grid bar mask focusing in color TV tube, Jenny E. Rosenthal—614(A)
Heat interchanger for large He liquefiers, J. Nicol, T. S. Smith, C. V. Heer, and J. G. Daunt—649(A)
High frequency phenomena, demonstration, Richard H. Howe—818(A)
Improved "lock-in" amplifier, Henry L. Cox, Jr.—640(A)
Ion beam focusing, F. C. Shoemaker, R. J. Britten, and B. C. Carlson—582(A)
Magnetic Compton spectrometer, J. W. Motz, William Miller, and H. O. Wyckoff—584(A)
Measurement of neutron densities with crystals of NaI (Tl), Bertel Grimeland—937
Measuring small strains with polarized light, H. P. Gage—816(A)
Method for determining dynamic mechanical properties of gels and solids at audiofrequencies, Edwin R. Fitzgerald and John D. Ferry—644(A)
Mixed NaI–LiI crystal for neutron spectrometer, A. W. Schardt and W. Bernstein—583(A)
Monoenergetic γ-rays from the synchrotron, J. W. Weil and B. D. McDaniel—582(A)
Multi-layer optical reflection interference filter, W. H. Shaffer and R. A. Oetjen—819(A)
Multiple-beam interferometer, Thurston E. Manning—818(A)
μ-meson capture measurements, improved technique, J. W. Keuffel, F. B. Harrison, T. N. K. Godfrey, and George T. Reynolds—616(A)
NBS liquid level indicator for condensed gases, W. E. Williams, Jr. and E. Maxwell—649(A)
New dispenser type cathode, Jack Martin—584(A)
New molecular weight distribution technique for polystyrene, R. F. Boyer—658(A)
New technique for photonuclear cross sections, Lester L. Newkirk—249(L)
Optical focusing in constant radius accelerators, David C. dePackh—433(L)
Particle counting by Čerenkov radiation, John Marshall—685
Photographic gray wedge pulse-height analysis, W. Bernstein, R. L. Chase, M. Slavin, J. Garfield, and A. W. Schardt—594(A)
Radial oscillations in cyclotron, W. H. Beach, W. J. Childs, P. V. C. Hough, J. S. King, and W. C. Parkinson—582(A); P. V. C. Hough—582(A)
Scintillation response of organic crystals to low energy α-particles, J. W. King and J. B. Birks—568(L)
Scintillation spectrometer for measuring total energy of x-ray photons, M. R. Cleland and H. W. Koch—588(A)
Small Ra-Be neutron source for undergraduate laboratory. I, David L. Anderson—819(A); II, Thurston E. Manning and David L. Anderson—819(A)
Technique for self-diffusion measurements, David B. Langmuir—642(A)
Theory of response of organic scintillation crystals to short-range particles, J. B. Birks—569(L)
Zr concentrated-arc infrared source for infrared spectroscopy, M. B. Hall and R. G. Nester—653(A)
Microwaves (see also **Electromagnetic theory; Electronic tubes; Spectra, microwave**)
Faraday rotation of guided waves, H. Suhl and L. R. Walker—122(L)
Mobility of ions and electrons (see **Ions and electrons, mobility**)
Molecular beams (see **Atomic and molecular beams**)
Molecular structure and constants (see also **Spectra, microwave; Spectra, molecular; Raman spectra**)
Of ClF_3, D. F. Smith—608(A)
Of HCN, A. H. Nethercot, Jr., J. A. Klein, and C. H. Townes—798(L)
Of HCN, erratum, James W. Simmons, Wallace E. Anderson, and Walter Gordy—1055(L)
Li^6F^{19} molecular constants, J. C. Swartz and J. W. Trischka—606(A)
Ozone molecule, theory, B. T. Darling and J. A. Weiss—655(A)
Rotational magnetic moments, Ruth F. Schwarz—606(A)

Neutrino (see also **Radioactivity; Scattering of electrons, mesons, neutrons, protons, and ions**)
Neutrino recoils following capture of orbital electrons in A^{37}, George W. Rodeback and James S. Allen—446
Nuclear recoil following neutrino emission from Be^7, Raymond Davis, Jr.—976
Neutron diffraction
Of cold-worked brass, R. J. Weiss, J. R. Clark, J. Hastings, and L. Corliss—656(A)
Structure of NH_4Cl, G. H. Goldschmidt and D. G. Hurst—797(L); Henri A. Levy and S. W. Peterson—766
Of various transition elements, C. G. Shull and M. K. Wilkinson—599(A)
Neutrons
Electron neutron interaction, Burton D. Fried—434(L); Sidney Borowitz—567(L)
Extinction effects in neutron transmission of polycrystalline media, R. J. Weiss—271; 622(A)
Fast neutron reaction cross sections, E. B. Paul and R. L. Clarke—605(A)
Fast neutron spectrometer, L. E. Beghian, R. A. Allen, J. M. Calvert, and H. Halban—1044(L)
Low energy cross section of Be for neutrons, Harry Palevsky and R. R. Smith—604(A)
Measurement of neutron densities with crystals of NaI(Tl), Bertel Grimeland—937
Neutron source strength of granitic rock, J. Pine and P. Morrison—606(A)
Polarization of D–D neutrons, H. J. Longley, R. N. Little, Jr., and J. M. Slye—419(L)
Reflection and refraction of neutrons from Be mirror, J. A. Harvey, M. D. Goldberg, and D. J. Hughes—604(A)
Regularities in total cross sections for fast neutrons, H. H. Barschall—431(L)
Slow neutron resonances in Cs and Pd, H. H. Landon and V. L. Sailor—605(A)
Total cross sections for 400-Mev neutrons, V. A. Nedzel and John Marshall—604(A)
Total neutron cross section of N, J. J. Hinchey, P. H. Stelson, and W. M. Preston—483
Noise (see **Fluctuation phenomena**)

Nuclear induction (see **Magnetic resonance absorption; Nuclear moments and spin**)
Nuclear moments and spin (see also **Hyperfine structure**)
Cd^{114}, spins of the excited states, M. W. Johns, C. D. Cox, and C. C. McMullen—632(A)
Effect of atomic core on magnetic hfs, R. Sternheimer—316
Hfs anomalies in $^2P_{\frac{1}{2}}$ state of Tl^{205} and Tl^{203}, Alan Berman, —1005
Hfs of Gd and Zr, S. Suwa—247(L)
In^{115} magnetic moment, Yu Ting, F. K. Biard, and Dudley Williams—618(A)
Magnetic moment of He in metastable $^3S_1$ state by atomic beam method, G. L. Tucker, V. W. Hughes, E. H. Rhoderick, and G. Weinreich—618(A)
Magnetic moment of K^{40} and hfs anomaly of K isotopes, J. T. Eisinger, B. Bederson, and B. T. Feld—73
Magnetic moments of even-odd nuclei, Jack P. Davidson—609(A)
Nuclear magnetic moment and *j-j* coupling shell model, erratum, Masataka Mizushima and Minoru Umezawa——1055(L)
Quadrupole coupling ratio of Cl isotopes, T. C. Wang, C. H. Townes, A. I. Schawlow, and A. N. Holden—809(L)
Se^{77} magnetic moment, S. S. Dharmatti and H. E. Weaver, Jr.—259(L)
Se^{79} spin and quadrupole moment, W. A. Hardy, G. Silvey, and C. H. Townes—608(A)
Sign of quadrupole interaction energy in diatomic molecules, R. A. Logan, R. E. Cote, and P. Kusch—280
V^{50} nuclear gyromagnetic ratio, H. E. Walchli, W. E. Leyshon, and F. M. Scheitlin—618(A)
Zeeman effect of Cl nuclear quadrupole rf resonance, Christropher Dean—607(A)
Nuclear reactions (see **Disintegration and excitation of nucleus**)
Nuclear spectra (see also **Disintegration and excitation of nucleus**)
Al^{28} β- and γ-radiation, Henry T. Motz and David E. Alburger—165
Am^{241} soft radiations, J. K. Beling, J. O. Newton, and B. Rose—797(L)
Angular correlation and intensity of inner bremsstrahlung from P^{32} and RaE, T. B. Novey—619(A)
Angular correlation of first and third γ-rays, G. B. Arfken, L. C. Biedenharn, and M. E. Rose—761
Angular correlation of radiations from deuteron stripping reactions, L. C. Biedenharn, Keith Boyer, and R. A. Charpie—619(A)
Sb^{124} $\beta-\gamma$ polarization correlation, Robert Stump—249(L)
β-spectrum of 2.3-yr Cs^{134}, F. H. Schmidt and G. L. Keister —632(A)
Br radioisotopes, S. C. Fultz and M. L. Pool—347; 631(A)
Cd^{114}, spins of excited states, M. W. Johns, C. D. Cox, and C. C. McMullen—632(A)
C^{10} γ-radiation, R. Sherr and J. Gerhart—619(A)
Ce^{144} and Pr^{144}, β-spectra, Cheng Lin-Sheng, G. John, and J. D. Kurbatov—632(A)
Cu^{64} and Fe^{59} internal conversion, D. Brower, G. Hinman, G. Lang, R. Leamer, and D. Rose—1054(L)
Em, Fr, and Ra isotopes, F. F. Momyer, E. K. Hyde, A. Ghiorso, and W. E. Glenn—805(L)
Energy levels in Mn^{53} from scintillation studies of Cr^{53}-$(p,n\gamma)Mn^{53}$, Clyde L. McClelland, Clark Goodman, and Paul H. Stelson—631(A)
Energy levels of C^{11} and C^{13} from photographic plate observation of neutron spectra, Virgil R. Johnson—302
Europium-148 and 150, Rex C. Mack, Donald I. Prickett, and M. L. Pool—633(A)
First forbidden β-decay matrix elements, T. Ahrens and E. Feenberg—64
First forbidden β-transition, T. Ahrens and E. Feenberg—609(A)
$\gamma-\gamma$ angular correlation in Pd^{106}, G. B. Arfken, E. D. Klema, and F. K. McGowan—413(L)
γ-ray energies with pair spectrometer, G. A. Bartholomew and B. B. Kinsey—605(A)
γ-rays from excited states of Al^{27}, Leonard N. Russell, Warren E. Taylor, and John N. Cooper—819(A)
γ-rays associated with selected neutron-induced radioactivities, W. C. Rutledge, J. M. Cork, and S. B. Burson —775
γ-rays from Na bombarded by protons, P. H. Stelson, W. M. Preston, and Clark Goodman—629(A)
Of Ge^{77}, Alan B. Smith—98; Alan B. Smith and Allan C. G. Mitchell—619(A)
In^{114*} conversion coefficient using scintillation spectrometer, Thomas B. Cook, Jr. and Sherwood K. Haynes—190
In^{115}, decay of metastable state, L. M. Langer, R. D. Moffat, and G. A. Graves—632(A)
Of I^{131}, R. E. Bell and R. L. Graham—212
I^{131} internal conversion, D. Rose, G. Hinman, and L. G. Lang—863
$_{71}Lu^{175}$ and $_{21}Sc^{46m}$ (20 seconds) K/L ratios, S. B. Burson and W. C. Rutledge—633(A)
Hg^{198}, internal conversion of 0.411-Mev γ-ray, Lennart Simons—570(L)
Of Ne^{19} and Na^{21}, G. Schrank and J. R. Richardson—248(L)
Of Nb^{95}, D. R. Jones, S. C. Fultz, and M. L. Pool—654(A)
Of Nb^{97}, C. E. Mandeville, E. Shapiro, R. I. Mendenhall, E. R. Zucker, and G. L. Conklin—813(L)
Nuclear matrix elements in theory of β-decay, Henry Brysk—996
One-three $\gamma-\gamma$ angular correlation, G. B. Arfken, L. C. Biedenharn, and M. E. Rose—619(A)
Pd^{106} γ-rays, angular correlation, Rolf M. Steffen—632(A)
Of K^{40}, M. Paganelli and G. Quareni—423(L)
Pr^{142} secondary electron spectrum, Erling N. Jensen, L. Jackson Laslett, and D. J. Zaffarano—1047(L)
Pr^{144}, decay scheme and angular correlation, D. E. Alburger and J. Kraushaar—633(A)
Radioactivity in neutron-activated Pt, J. M. Cork, J. M. LeBlanc, F. B. Stumpf, and W. H. Nester—415(L)
RaD β-spectrum, A. A. Jaffe and S. G. Cohen—1041(L)
Rh^{104g} γ-radiations, G. E. Boyd—578(L)
Ru^{103} decay, J. M. Cork, J. M. LeBlanc, F. B. Stumpf, and W. H. Nester—575(L)
Ru^{103} 498-kev γ-ray, Arthur W. Knudsen—571(L)
Shapes of β^--spectra at low energy end, Herman M. Schwartz—195
Slow neutron capture γ-rays, W. A. Thornton, Jr., E. Der Mateosian, H. T. Motz, and M. Goldhaber—604(A)
Sr^{85} and Sr^{85m} decay, A. W. Sunyar, J. W. Mihelich, G. Scharff-Goldhaber, M. Goldhaber, N. S. Wall, and M. Deutsch—1023
Tc^{98} and Tc^{100}, R. A. House, R. L. Colligan, D. N. Kundu, and M. L. Pool—654(A)
Tc^{99} β-spectrum, Frank Wagner, Jr., and Melvin S. Freedman—631(A)
Tc^{100} half-life and radiations, G. E. Boyd, Q. V. Larson, and G. W. Parker—1051(L)
Te^{125}, spin and parity of first (603 kev) excited state, Franz R. Metzger—435(L)
Third forbidden β-spectrum from Rb^{87}, Y. Tomozawa, M. Umezawa, and S. Nakamura—791(L)
Of Th^{231}(UY), M. S. Freedman, F. Wagner, Jr., A. H. Jaffey, and J. May—633(A)
V^{48} and Nb^{98} γ-rays, Harold K. Ticho, David Green, and J. Reginald Richardson—422(L)
Zn^{65}, K-capture and positron emission, J. K. Major—631(A)
Of Zr^{97} and Nb^{97}, C. E. Mandeville, E. Shapiro, R. I. Mendenhall, E. R. Zucker, and G. L. Conklin—631(A)

Nuclear structure (see also **Disintegration and excitation of nucleus; Nuclear spectra; Radioactivity**)
Angular momentum distributions in Thomas-Fermi model, J. H. D. Jensen and J. M. Luttinger—907
Application of Fermi model to cosmic-ray events of primary energy greater than 10^{13} ev, W. E. Hazen, R. E. Heineman, and E. S. Lennox—198
β-decay of mirror nuclei and shell model, O. Kofoed-Hansen and Aage Winther—428(L)
Comparative models in nuclear scattering, D. C. Peaslee—269
Empirical mass surface, Alex E. S. Green—654(A)
Exchange current effects in deuteron, Felix Villars—476
Experimental mass surface, R. B. Minogue, R. Oppenheim, and A. E. S. Green—654(A)
Hfs anomaly and models of nuclear structure, B. T. Feld—609(A)
jj-coupling in nuclei, B. H. Flowers—254(L)
Line of β-stability, A. E. S. Green, N. Engler, and N. J. Marucci—609(A)
Nonlinear meson theory for heavy nuclei, Bertram J. Malenka—68
Nuclear magnetic moment and *j-j* coupling shell model, erratum, Masataka Mizushima and Minoru Umezawa—1055(L)
Nuclear shell interactions, Katharine Way and Marion Wood—608(A)
Saturation property of nuclear forces, Hideo Kanazawa—428(L)
Semi-empirical mass surfaces, N. Engler and A. E. S. Green—654(A)
Spectroscopic isotope shift and nuclear shell structure, G. Breit—254(L)
Triton binding energy by randomized net-point method, S. I. Rubinow—388
Unpaired spin effects for protons and neutrons, Charles D. Coryell and Hans E. Suess—609(A)

Optical constants and properties
Of edge emission in CdS, Clifford Klick—659(A)
Of evaporated Sb films, Calvin Tiller and Henry Levenstein—657(A)
Fading characteristics of γ-induced coloration in high density glass, Robert H. Kernohan and Grace M. McCammon—641(A)
Optical polarization in single crystals of Te, Joseph J. Loferski and Park Hays Miller—652(A)
Of single crystals of ZnS, William W. Piper and Ferd E. Williams—659(A)
Optical instruments (see **Methods and instruments**)

Pair production and annihilation
Distribution of total momentum of electrons in pair production by photons, A. Borsellino—596(A)
Pair production by electrons, N. S. Shiren and R. F. Post—617(A)
Relative pair production cross sections from 50 to 300 Mev, C. R. Emigh—1028
Phosphorescence (see also **Luminescence**)
Preparation and properties of In_2S_3 phosphors, D. C. Reynolds, C. S. Peet, and A. E. Middleton—659(A)
Photoconductivity
Of edge emission in CdS, Clifford Klick—659(A)
Electron mobility in CdS, J. W. MacArthur—615(A)
Impedance measurements on PbS photoconductive cells, E. A. Rittner and F. Grace—615(A); 955
Multiple time constants in photoconductivity, W. W. Scanlon, R. L. Petritz, and F. L. Lummis—659(A)
Relation between noise and response time in photoconductors. I. Theory, R. L. Petritz—660(A); II, Experiment. F. L. Lummis and R. L. Petritz—660(A)
Of single crystals of ZnS, William W. Piper and Ferd E. Williams—659(A)
Soft and hard *F*-centers, Jordan J. Markham—433(L)
Theory of noise in photoconductors, Richard L. Petritz—614(A)
Of trapped electrons in KCl crystals between 24°C and −190°C, J. J. Oberly—799(L)
Of ZnO, theory, Donald A. Melnick and Douglas M. Warschauer—614(A)
Photodisintegration
Angular distribution of fast photoneutrons, P. T. Demos, J. D. Fox, I. Halpern, and J. Koch—605(A)
Angular distributions of photoprotons, M. A. Rothman, A. K. Mann, and J. Halpern—629(A)
Charged photomesons from various nuclei, Raphael Littauer and Darcy Walker—838
Cloud-chamber identification of photodeuterons from Cu, Warren H. Smith and L. Jackson Laslett—523
Of deuteron, V. E. Krohn, Jr., and E. F. Shrader—391; 629(A)
Of deuteron at high energies, B. Bruno and S. Depken—1054(L); Raphael Littauer and James Keck—1051(L)
Of deuteron at intermediate energies, C. A. Barnes, J. H. Carver, G. H. Stafford, and D. H. Wilkinson—359; D. H. Wilkinson—373
Emission of deuterons from the nucleus, A. G. W. Cameron—435(L)
Excitation functions for photoprotons from C, A. M. Perry and J. C. Keck—629(A)
(γ,α) reactions on Li^7, O^{16}, and $Br^{79,81}$, H. Nabholz, P. Stoll, and H. Wäffler—1043(L)
Of He by high energy γ-rays, Seishi Kikuchi—126(L)
High energy photodisintegration of deuteron, T. S. Benedict and W. M. Woodward—629(A)
Meson contributions to photodisintegration of deuteron, M. H. Friedman—625(A)
By meson reabsorption, Robert R. Wilson—125(L)
New technique for photonuclear cross sections, Lester L. Newkirk—249(L)
Nuclear photodissociation by high energy synchrotron γ-rays, Seishi Kikuchi—41
Phenomenological relationships between photomeson production and meson-nucleon scattering, K. A. Brueckner and K. M. Watson—923
Photomesons from D, James Keck and Raphael Littauer—602(A)
Photonuclear effect in heavy elements, interpretation, L. Eyges—325
Photoproduction of mesons on nuclei, T. R. Palfrey, Jr., and R. R. Wilson—602(A)
Production of neutral mesons by photons, W. K. H. Panofsky, J. N. Steinberger, and J. Steller—180
Production of positive mesons by photons, J. Steinberger and A. S. Bishop—171
Relative production of neutral mesons by 310-Mev γ-rays in H and D, A. Silverman and G. Cocconi—602(A)
Photography and photographic emulsions (see also **Methods and instruments**)
Nuclear emulsion and scintillation crystal processes, J. B. Birks—791(L)
Photographic gray wedge pulse-height analysis, W. Bernstein, R. L. Chase, M. Slavin, J. Garfield, and A. W. Schardt—584(A)
Photons (see also **Gamma-rays; Radiation**)
Nonlocal photons, J. S. Lomont—596(A)
Piezoelectric effect
Rotated piezoelectric, elastic, and dielectric constants of quartz, Karl S. Van Dyke and Elva Sterns Creeger—579(A)
Plasticity
Plastic flow in alkali halide crystals, W. W. Tyler—801(L)

Of very small metal specimens, J. K. Galt and Conyers Herring—656(A)

Polymerization, properties of polymers
Acoustic properties of rubber as function of chemical composition, William S. Cramer and Irving Silver—645(A)
Conversion method for relating stress relaxation and dynamic modulus, Robert S. Marvin—644(A)
Correlation of dynamic and static measurements on rubber-like materials. II, R. D. Andrews—644(A)
Dielectric breakdown of polymers under prolonged stress, Carl G. Brodhun—653(A)
Dielectric properties of liquids, gels, and solids at audio-frequencies. II. Polyvinylchloride plasticized by di-2-ethylhexylphthalate and dimethylthianthrene, R. F. Miller, E. R. Fitzgerald, J. M. Davies, and W. C. Sears—644(A)
Dynamic mechanical and electrical properties of system polyvinyl chloride-dimethylthianthrene, John D. Ferry and Edwin R. Fitzgerald—645(A)
Effect of cross linking on second-order transition temperature of polymethyl methacrylate, S. Loshaek—652(A)
Effect of diluents on second-order transition and flow properties of polystyrene, T. G. Fox—652(A)
Investigations on plastics in large range of mechanical frequencies, W. Philippoff—644(A)
Method for determining dynamic mechanical properties of gels and solids at audiofrequencies, Edwin R. Fitzgerald and John D. Ferry—644(A)
New molecular weight distribution technique for polystyrene, R. F. Boyer—658(A)
Polystyrene molecular weight distribution by turbidity titration, Arthur F. Roche, Jr.—658(A)
Random noise in dielectrics. II, Herbert Bauss and R. F. Boyer—653(A)
Relations between viscosity and flow birefringence of polyelectrolytes, P. M. Kamath, B. Rosen, and F. R. Eirich—657(A)
Relaxation distribution function in polyisobutylene and polyisobutylene-decalin solutions, Lester D. Grandine, Jr., Edwin R. Fitzgerald, Ivo Jordan, and John D. Ferry—645(A)
Polychlorotrifluoroethylene, John D. Hoffman—657(A)
Polyelectrolytes, B. Rosen and F. R. Eirich—657(A)
Self-diffusion and bulk viscosity of high polymers, F. Bueche—652(A)
Strain-temperature studies of transitions in rubbers, R. F. Derenthal, F. P. Baldwin, and R. L. Anthony—653(A)
Structure and properties of polyamides, R. Brill—657(A)
Ultrasonic investigation of plasticized polymethyl methacrylate, R. G. Cheatham and Albert G. H. Dietz—645(A)
Viscoelastic properties of polymers by phase angle measurements, R. D. Spangler—644(A)

Positrons
Electrodynamic corrections to fine structure of positronium, Robert Karplus and Abraham Klein—257(L)

Probability
Theory of discrimination and reliability in crowded situations, Arthur E. Ruark—620(A)

Proceedings of the American Physical Society
New England Section Meeting, Hartford, Connecticut, November 3, 1951—579
Annual Meeting at New York City, New York, January 31, 1952 to February 2, 1952 [Bull. Am. Phys. Soc. **27**, No. 1 (1952)]—579
Meeting at Columbus, Ohio, March 20–22, 1952 [Bull. Am. Phys. Soc. **27**, No. 2 (1952)]—637
New York State Section Spring Meeting, Corning, New York, April 18–19, 1952—816.
Ohio State Section Spring Meeting, Kent State University, Kent, Ohio, April 18, 1952—818

Quantum electrodynamics
Absorber theory of radiation, Peter Havas—974
Convariant theory of radiation damping, Jean Pirenne—395
Definition of integral over paths in Feynman's formulation of nonrelativistic quantum mechanics, W. H. Guier and A. J. F. Siegert—596(A)
Electrodynamic corrections to fine structure of positronium, Robert Karplus and Abraham Klein—257(L)
Electrodynamic displacement of atomic energy levels. II. Lamb shift, Robert Karplus, Abraham Klein, and Julian Schwinger—288
Electron self-energy, F. J. Belinfante—596(A)
Foward scattering of light by a Coulomb field, F. Rohrlich and R. L. Gluckstern—1
Fourth-order radiative correction to atomic energy levels, R. Bersohn, J. Weneser, and N. M. Kroll—596(A)
Interaction between quantized electromagnetic field and classical electron, I. R. Senitzky—595(A)
Lower limits for interaction times in elementary particle processes, E. Gora—597(A)
Phenomenological quantum electrodynamics with magnetic poles, M. Avramy Melvin—640(A)
Renormalized S-matrix for scalar electrodynamics, Abdus Salam—731
Nonlocal photons, J. S. Lomont—596(A)
Second order radiative corrections to hfs, Normal M. Kroll and Franklin Pollock—876
Second quantized theory of spin-$\frac{1}{2}$ particles in nonrelativistic limit, Richard K. Osborn—340
Small angle scattering of light by Coulomb field—10
Theory of the electron, Walter Wessel—639(A)

Quantum mechanics (see **Mechanics, quantum**)

Radiation (see also **Thermal radiation; scattering of radiation**)
Angular correlation and intensity of inner bremsstrahlung from P^{32} and RaE, T. B. Novey—619(A)
Detection of mm wave solar radiation, William M. Sinton—424(L)
Diffraction by finite and infinite gratings, Samuel N. Karp—586(A)
From electron in magnetic field, D. L. Judd, J. V. Lepore, M. Ruderman, and P. Wolff—123(L)
Experimental evidence for classical electron radiation at 300 Mev, Joseph W. Mather—795(L)
Multiple scattered reflection from striated surface, Vic Twersky—586(A)
Particle counting by Čerenkov radiation, John Marshall—583(A); 685
Radiation loss by electrons in large orbits, Dale R. Corson—1052(L)
Radiation loss of electrons in synchrotron, H. Olsen and H. Wergeland—123(L)

Radio (see also **Ionosphere; Radiation**)
High frequency phenomena, demonstration, Richard H. Howe—818(A)
New kind of radio propagation at very high frequencies observable over long distances, D. K. Bailey, R. Bateman, L. V. Berkner, H. G. Booker, G. F. Montgomery, E. M. Purcell, W. W. Salisbury, and J. B. Wiesner—141
Radio propagation beyond horizon and surface refractive index, Thomas J. Carroll—614(A)

Radioactivity (see also **Disintegration and excitation of nucleus; Nuclear spectra**)
Am^{241} soft radiations, J. K. Beling, J. O. Newton, and B. Rose—797(L)
A^{39}, half-life and mass assignment, H. Zeldes, B. H. Ketelle, A. R. Brosi, C. R. Fultz, and R. F. Hibbs—811(L)
Average energy of β-spectra, Randall S. Caswell—82

Radioactivity (continued)
β-decay of mirror nuclei and shell model, O. Kofoed-Hansen and Aage Winther—428(L)
Br radioisotopes, S. C. Fultz and M. L. Pool—347; 631(A)
Calorimetric determination of relationship between half-life and average β-energy of C^{14}, G. H. Jenks and F. H. Sweeton—803(L)
Of Cm^{240} and Cm^{241}, G. H. Higgins and K. Street, Jr.—252(L)
Em, Fr, and Ra isotopes, F. F. Momyer, E. K. Hyde, A. Ghiorso, and W. E. Glenn—805(L)
Emission of L x-rays of Pb in Po^{210} decay, William Rubinson and William Bernstein—545
Energy available for double β-decay of Sn^{124}, Benjamin G. Hogg and Henry E. Duckworth—567(L)
Excitation of metastable Cd^{111} by inelastic scattering of neutrons, J. J. G. McCue, A. E. Francis, and Clark Goodman—632(A)
Evidence for K-shell ionization accompanying α-decay of Po^{210}, W. C. Barber and R. H. Helm—175
γ-rays associated with selected neutron-induced radioactivity, W. C. Rutledge, J. M. Cork, and S. B. Burson—775
Image transitions in β-decay theory, George L. Trigg—506
Interaction term in β-decay theory, R. H. Good, Jr.—620(A)
Pb^{209} decay energy, A. H. Wapstra—562(L)
Line of β-stability, A. E. S. Green, N. Engler, and N. J. Marucci—609(A)
Mass surface and radioactivity, J. S. Nader, N. J. Marucci, and A. E. S. Green—654(A)
μ-meson decay and β-radioactivity, Louis Michel—814(L)
In neutron-activated Pt, J. M. Cork, J. M. LeBlanc, F. B. Stumpf, and W. H. Nester—415(L)
Of Pt and Ir from photonuclear reactions in Pt, Darleane Christian, Russell F. Mitchell, and Don S. Martin, Jr.—946
Of Rb^{87}, M. H. MacGregor and M. L. Wiedenbeck—420(L)
Short β-decay lifetimes, R. N. Thorn, R. W. Waniek, and R. B. Holt—618(A); R. W. Waniek, R. N. Thorn, and R. B. Holt—619(A)
Si^{31} decay energy, A. H. Wapstra—561(L)
Spectrum of L x-rays from RaD and possibility of $L_I \rightarrow L_{II}$ Auger transitions, S. G. Cohen and A. A. Jaffe—800(L)
Of Sr^{85} and Sr^{85m}, A. W. Sunyar, J. W. Mihelich, G. Scharff-Goldhaber, M. Goldhaber, N. S. Wall, and M. Deutsch—1023
Ta^{182} half-life, G. G. Eichholz and L. A. Ficko—794(L)
Tc^{98} and Tc^{100}, R. A. House, R. L. Colligan, D. N. Kundu, and M. L. Pool—654(A)
Tc^{100} half-life and radiations, G. E. Boyd, Q. V. Larson, and G. W. Parker—1051(L)
Of Th^{231}(UY), M. S. Freedman, F. Wagner, Jr., A. H. Jaffey, and J. May—633(A)
Sn^{124} double β-decay, E. L. Fireman and D. Schwarzer—451
Zn^{65}, K-capture and positron emission, J. K. Major—631(A)
Of Zr^{97} and Nb^{97}, C. E. Mandeville, E. Shapiro, R. I. Mendenhall, E. R. Zucker, and G. L. Conklin—631(A)

Range and energy loss of particles
Energy loss of deuterons in hydrocarbons, J. W. Preiss and Ernest Pollard—612(A)
Energy loss of 15-Mev electrons, A. O. Hanson, E. L. Goldwasser, and F. E. Mills—617(A)
Energy loss of 2-Mev electrons, F. E. Jablonski, B. Waldman, and W. C. Miller—617(A)
Lower electron energy losses in ZnO, Olive G. Engel—617(A)
Nuclear emulsion and scintillation crystal processes, J. B. Birks—791(L)
Stopping power of polystyrene and acetylene for α-particles, R. H. Ellis, Jr., H. H. Rossi, and G. Failla—562(L)

Rectifier (see **Electrical conductivity and resistance; Semiconductors**)

Relativity
Condensations in expanding cosmologic models, Amalkumar Raychaudhuri—90
Equations of motion in covariant field theory, Joshua Goldberg and Ralph Schiller—620(A)
General relativity and angular momentum, Robb Thomson and Peter G. Bergmann—621(A)
Statistical mechanics in general relativity, J. W. Weinberg and G. E. Tauber—621(A)
Super-potentials in covariant theories, Ralph Schiller and Joshua Goldberg—620(A)
Thermal equilibrium in general relativity, G. E. Tauber and J. W. Weinberg—621(A)

Resistance, electrical (see **Electrical conductivity and resistance**)

Scattering of electrons, mesons, neutrons, protons, deuterons, and ions (see also **Electron diffraction; Cross section, measurements, theory**)
Angular correlation between γ-rays and inelastically scattered protons from Mg^{24}, H. E. Gove and A. Hedgran—574(L)
Angular distribution of 53-Mev positive pions scattered by protons, E. C. Fowler, W. B. Fowler, R. P. Shutt, A. M. Thorndike, and W. L. Whittemore—1053(L)
Angular distribution of neutrons scattered by He, Robert K. Adair—155
Angular distribution of 1.5 to 3.0-Mev deuterons scattered by T nuclei, W. R. Stratton, G. D. Freier, G. R. Keepin, D. Rankin, and T. F. Stratton—593(A)
Angular distribution of π^+-production in $n-p$ collisions, H. A. Bethe and N. Austern—121(L)
Angular distribution of pions scattered by hydrogen, H. L. Anderson, E. Fermi, D. E. Nagle, and G. B. Yodh—793(L)
Angular distribution of protons scattered by 1.0 to 3.02-Mev deuterons, G. D. Freier, W. R. Stratton, R. J. S. Brown, H. D. Holmgren, and J. L. Yarnell—593(A)
Angular distribution of 215-Mev neutrons scattered by protons, G. L. Guernsey—594(A)
Angular distributions of inelastically scattered protons from C^{12} and Mg^{24}, H. E. Gove and H. F. Stoddart—572(L)
Application of multiple scattering theory to cloud-chamber measurements. I, Stanislaw Olbert—589(A); II, Martin Annis, Herbert S. Bridge, and Stanislaw Olbert—590(A)
Application of variational method to scattering by square well potential, J. Mayo Greenberg—610(A)
Comparative models in nuclear scattering, D. C. Peaslee—269
Connection between scattering and derivative matrices, E. P. Wigner—609(A)
Difference of H and D total cross sections for charged π-mesons, G. Yodh, H. L. Anderson, D. E. Nagel, and H. Stadler—603(A)
Diffuse scattering of neutrons and x-rays, David A. Kleinman—622(A)
Effect of singular triplet tensor interaction on $p-p$ scattering below 10 Mev, Edwin A. Crosbie—610(A)
Of electrons in metals by dislocations, D. L. Dexter—770
Of fast neutrons, E. T. Jurney and C. W. Zabel—594(A)
Of fast neutrons by W, C. E. Mandeville, C. P. Swann, and F. J. Seymour—861
High energy electron-electron scattering, Walter H. Barkas, Robert W. Deutsch, F. C. Gilbert, and Charles E. Violet—59
Inelastic scattering of fast neutrons from Fe, P. H. Stelson and W. M. Preston—132(L)
Inelastic scattering of protons from Ni, Ralph Ely, Jr., A. J. Allen, J. S. Arthur, R. S. Bender, H. J. Hausman, and E. M. Reilley—859

Inelastic thermal neutron scattering in Pb, A. W. McReynolds—594(A)
Low energy $n-d$ scattering, M. M. Gordon and W. D. Barfield—679
Meson-nucleon scattering and nucleon isobars, Keith A. Brueckner—106; 626(A)
Multiple scattering of μ-mesons in magnetized Fe, Stephan Berko—598(A)
Multiple scattering of protons in gases, Eugene H. Gerber—525
Multiple scattering of protons in gases, Eugene H. Gerber—816(A)
Of negative pions by H, A. Lundby, E. Fermi, H. L. Anderson, D. E. Nagle, and G. Yodh—603(A)
$n-p$ scattering with spin-orbit coupling, John M. Blatt and L. C. Biedenharn—399; John M. Blatt—610(A)
$n-p$ total cross section, E. M. Hafner, D. H. Frisch, C. E. Falk, T. Coor, and W. F. Hornyak—593(A)
Of neutrons by systems of heavy nuclei, G. Placzek—377
Nuclear elastic scattering of high energy protons, R. E. Richardson, W. P. Ball, C. E. Leith, Jr., and B. J. Moyer—29
Nuclear scattering of high energy protons, Kantilal M. Gatha and R. J. Riddell, Jr.—1035
Nucleon scattering with repulsive core potentials, M. A. Preston, J. R. Bird, and J. Shapiro—610(A)
Phase shift ana ysis of $n-d$ scattering, A. L. Latter and R. Latter—727
Phenomenological relationships between photomeson production and meson-nucleon scattering, K. A. Brueckner and K. M. Watson—923
Of π-mesons by deuteron, J. S. Blair and B. Segall—626(A)
Pion-proton scattering and strong coupling meson theory, G. Wentzel—437
Precision $\alpha-\alpha$ scattering at low energies, D. B. Cowie, N. P. Heydenburg, G. M. Temmer, and C. A. Little, Jr.—593(A)
Proton-α-particle scattering using photographic techniques, W. E. Kreger, R. O. Kerman, and W. K. Jentschke—593(A)
Of protons by loosely bound neutron in Be, K. Strauch and J. A. Hofmann—563(L)
Scattering and absorption of π-mesons in C, H. Byfield, J. Kessler, and L. M. Lederman—17
Scattering and capture of pions by hydrogen, H. L. Anderson and E. Fermi—794(L)
Scattering by obstacles with spherical and circular cylindrical symmetry, Elliott Montroll and J. Mayo Greenberg—889
Theory of impulse approximation, Saul T. Epstein—836
Total collision cross sections of negative pions on protons, D. E. Nagle, H. L. Anderson, E. Fermi, E. A. Long, and R. L. Martin—603(A)
Total cross sections of C and H for high energy neutrons, George R. Mott, Gordon L. Guernsey, and Bruce K. Nelson—594(A)
Total elastic scattering cross section of N for fast neutrons, W. M. Preston, P. H. Stelson, and J. J. Hinchey—594(A)
Variational principle for $k\cot\delta$, S. I. Rubinow and Herman Feshbach—610(A)

Scattering of radiation (see also **Raman spectra**)
Diffuse scattering of neutrons and x-rays, David A. Kleinman—622(A)
Forward scattering of light by Coulomb field, F. Rohrlich and R. L. Gluckstern—1
By obstacles with spherical and circular cylindrical symmetry, Elliott Montroll and J. Mayo Greenberg—889
Multiple scattered reflection from striated surface, Vic Twersky—586(A)
Multiple scattering of waves. II. Effective field in dense systems, M. B. Stearns—624(A)
Nuclear scattering of 17-Mev γ-rays, M. B. Stearns—593(A)
Scattering of gammas by bound electrons, J. S. Levinger—592(A)
Scattering of x-rays by atoms, G. Placzek—588(A)
Small angle scattering of light by Coulomb field, H. A. Bethe and F. Rohrlich—10

Scintillation counters (see **Methods and instruments**)

Secondary electrons (see **Electrons, secondary**)

Semiconductors (see also **Electrical conductivity and resistance**)
Comparison of $p-n$ junctions and radioactive tracers for measurement of diffusion, D. E. Brown and W. C. Dunlap, Jr.—616(A)
Comparison of thermally induced lattice defects in Ge and Si with defects produced by nucleon bombardment, W. E. Taylor—642(A)
Conductivity of deuteron irradiated Ge and Si, J. H. Forster, H. Y. Fan, and K. Lark-Horovitz—643(A)
Diffusion in semiconductors using capacitance method, K. B. McAfee, W. Shockley, and M. Sparks—137(L)
Dispersion of permittivity and conductivity of semiconductors, R. E. Burgess—131(L)
Displacements produced by electron bombardment of Ge, E. E. Klontz and K. Lark-Horovitz—643(A)
Donor and acceptor elements into Ge, Calvin S. Fuller—136(L)
Effects of dislocations on mobilities in semiconductors, D. L. Dexter and F. Seitz—964
Energy levels in Ge produced by nucleon bombardment, J. H. Crawford, Jr. and J. W. Cleland—641(A)
High temperature reduced-TiO_2 rectifiers, A. E. Middleton, C. S. Peet, O. J. Mengali, and R. C. Sirrine—647(A); C. S. Peet and A. E. Middleton—647(A)
Impedance of semiconducting films, J. N. Humphrey, F. L. Lummis, and W. W. Scanlon—660(A)
Infrared absorption band in Ge, R. J. Collins and H. Y. Fan—648(A)
Magnetic field effect upon Hall coefficient of impurity semiconductors, W. J. Whitesell, II, and V. A. Johnson—648(A)
Of polycrystalline graphite and condensed ring systems, erratum, S. Mrozowski—1056(L)
Probing space-charge layer in $p-n$ junction, G. L. Pearson, W. T. Read, and W. Shockley—647(A)
$p-n$ junction method for measuring diffusion in Ge, W. C. Dunlap, Jr., and D. E. Brown—417(L); W. C. Dunlap, Jr.—615(A)
Radiation produced in Ge and Si by electron-hole recombination, J. R. Haynes and H. B. Briggs—647(A)
Test of transistor equations, M. B. Prince and F. S. Goucher—647(A)
Thermoelectric effects in Ge at low temperatures, H. P. G. Frederikse—647(A)

Shock waves (see also **Explosion phenomena**)
One dimensional theory of absorption and amplification of a plane shock wave by a gaseous layer, D. Bitondo, I. I. Glass, and G. N. Patterson—601(A)
Shock-wave phenomena: aerothermodynamic interaction, H. Polachek and R. J. Seeger—601(A)
Shock-wave turbulent boundary layer interaction, S. M. Bogdonoff and A. H. Solarski—601(A)

Solid state (see **Crystalline state; Mechanics, quantum—of solid bodies**)

Specific heat
Of Cr below room temperature, J. Weertman, D. Burk, and J. E. Goldman—628(A)
Of Hf at 40–190°K, D. Burk and F. Darnell—628(A)
Of Pb in temperature range 1.0°K to 75°K, M. Horowitz, A. A. Silvidi, S. F. Malaker, and J. G. Daunt—818(A)
Of polychlorotrifluoroethylene, John D. Hoffman—657(A)

Specific heat (continued)
Of superconducting Nb below 4.5°K, A. Brown, M. W. Zemansky, and H. A. Boorse—134(L); 627(A)
Spectra, absorption (see also **Absorption of radiation; Spectra, general; Spectra, microwave; Spectra, molecular**)
Absorption by Be in neighborhood of K edge, R. W. Johnston and D. H. Tomboulian—587(A)
Of atmospheric CO, J. H. Shaw and J. N. Howard—654(A)
Detection of mm wave solar radiation, William M. Sinton—424(L)
Of free NH_2 radicals, G. Herzberg and D. A. Ramsey—587(A)
Infrared absorption band in Ge, R. J. Collins and H. Y. Fan—648(A)
Pressure broadening of absorption lines, Gilbert N. Plass and Douglas Warner—138(L)
Velocity of light determined by band spectrum method, D. H. Rank, R. P. Ruth, and K. L. Vander Sluis—799(L)
Of xanthopterin-like pigment, M. O'L. Crowe and A. Walker—817(A)
Spectra, atomic
"Double resonance" method for investigating atomic energy levels, Hg $^3P_1$, Jean Brossel and Francis Bitter—308
Electrodynamic displacement of atomic energy levels, Lamb shift, Robert Karplus, Abraham Klein, and Julian Schwinger—288
Fine structure of H atom. IV, Willis E. Lamb, Jr. and Robert C. Retherford—1014
Forbidden lines in spectra of Sb I and As I, M. Hults and S. Mrozowski—587(A)
Term values in Mn III, Howard D. Goldgraber—587(A)
Spectra, general
Detection of water-alcohol azeotropes through ultraviolet spectra, Gladys A. Anslow and Irene S. White—587(A)
γ-ray spectra of Los Alamos reactors, J. W. Motz—753
Short duration afterglow of N_2 in photographic infrared, R. Herman, L. Herman, and G. Hepner—570(L)
Spectroscopy from point of view of communication theory. III. Line shapes, Gilbert W. King and A. G. Emslie—586(A)
Synthesis of statistical and impact theories of pressure broadening, P. W. Anderson—809(L)
Spectra, microwave
Broadening of microwave absorption lines by collisions with cell walls, H. R. Johnson and M. W. P. Strandberg—811(L)
Of BrCN at 6 mm, S. J. Tetenbaum—440
Of CsCl and NaCl at high temperature, M. L. Stitch, A. Honig, and C. H. Townes—813(L)
Of ClF_3, D. F. Smith—608(A)
Of HCN, A. H. Nethercot, Jr., J. A. Klein, and C. H. Townes—798(L)
Of HCN, erratum, James W. Simmons, Wallace E. Anderson, and Walter Gordy—1055(L)
Lambda-doubling in microwave spectrum of NO, R. Beringer and E. B. Rawson—607(A)
Magnetic hfs in O_2, S. L. Miller, M. Kotani, and C. H. Townes—607(A)
Nuclear quadrupole interactions in microwave spectrum of hydrogen azide, John D. Rogers and Dudley Williams—654(A)
KCl, TlCl high temperature spectra, M. L. Stitch, A. Honig, and C. H. Townes—607(A)
Spectra, molecular (see also **Molecular structure and constants**)
Observation of rotational spectra by molecular beam techniques, C. A. Lee, R. O. Carlson, B. P. Fabricand, and I. I. Rabi—607(A)
KCl rotational spectrum, B. P. Fabricand, R. O. Carlson, C. A. Lee, and I. I. Rabi—607(A)
Rotational temperatures of Vegard-Kaplan auroral bands, W. Petrie—790(L)
$3\nu_3$ bands of CO_2 and CS_2, Norman M. Gailar and Earle K. Plyler—586(A)
Spectra, nuclear (see **Nuclear spectra**)
Spectra, rf
Li^6F^{19} molecular constants, J. C. Swartz and J. W. Trischka—606(A)
Zeeman effect of Cl nuclear quadrupole rf resonance, Christopher Dean—607(A)
Spectra, x-ray (see **X-rays, spectra**)
Statistical mechanics (see **Mechanics, statistical**)
Statistical methods
Theory of discrimination and reliability in crowded situations, Arthur E. Ruark—620(A)
Superconductivity (see also **Electrical conductivity and resistance; Low temperature phenomena**)
Bardeen's theory of superconductivity and *f*-sum rule, Edward N. Adams, II—258(L)
De Haas-Van Alphen effect in Sn, G. T. Croft, W. F. Love, and F. C. Nix—650(A)
Free energies and phase transition of cylindrical superconductor, Paul M. Marcus—649(A)
Gyromagnetic effect in superconductor, Robert Pry and Arthur L. Lathrop—628(A); R. H. Pry, A. L. Lathrop, and W. V. Houston—905
Of Hf-Zr alloy, L. D. Roberts and J. W. T. Dabbs—628(A)
Heat capacity of superconducting Nb below 4.5°K, A. Brown, M. W. Zemansky, and H. A. Boorse—134(L)
High frequency resistance of metals in normal and superconducting state, C. J. Grebenkemper and John P. Hagen—673
Influence of physical strain on physical properties of superconductors, T. S. Smith and J. G. Daunt—818(A)
Isotope effect in superconductivity. II. Sn and Pb, B. Serin, C. A. Reynolds and C. Lohman—162
Lattice oscillations and superconductivity, M. Dresden—627(A)
Magnetic properties of superconducting Sn–Bi alloys, W. F. Love—650(A)
Of Tl isotopes, E. Maxwell and O. S. Lutes, Jr.—649(A)
Thermal conductivity in intermediate state of pure superconductors, D. P. Detwiler and Henry A. Fairbank—574(L)
On Sn isotopes, E. Maxwell—235
Thermal conductivity
Of carbon materials, S. Mizushima—1040(L)
Of carbons and graphite, S. Mrozowski—251(L)
Of Ge, A. Grieco and H. C. Montgomery—570(L)
In intermediate state of pure superconductors, D. P. Detwiler and Henry A. Fairbank—574(L)
Thermal expansion
Anisotropy of thermal expansion and internal stresses in polycrystalline graphite and carbons, S. Mrozowski—622(A)
Of propylalcohol, George Antonoff—640(A)
Relations between thermal expansion and chemical composition of some binary Al alloys, Peter Hidnert—597(A)
Of U at low temperatures, Adam Schuch and Henry L. Laquer—803(L)
Of H_2O, George Antonoff—660(A)
Thermionic emission; emitting surfaces
New dispenser type cathode, Jack Martin—584(A)
Relative variation of dc and pulse emission from mixtures of rate-earth oxides, E. N. Wyler and F. C. Todd—640(A)
Thermodynamics
Information, thermodynamics, and life, Jerome Rothstein—620(A)
Information, thermodynamics, and time, Jerome Rothstein—634(A)

Noise and dissipation, John M. Richardson—613(A)
Phenomenological uncertainty principle, Jerome Rothstein—640(A)
Theorem of irreversible thermodynamics, Herbert B. Callen and Richard F. Greene—702
Theory as organization of observation, Jerome Rothstein—634(A)

Thermoelectric effects
Effect of cyclotron irradiation on thermocouple materials, A. Andrew, M. R. Jeppson, and H. P. Yockey—643(A)
In Ge at low temperatures, H. P. G. Frederikse—647(A)
Thermoelectric power of carbons and graphite, erratum, E. E. Loebner—1056(L)

Thermoluminescence
Of CaF_2 colored by x-ray irradiation, John J. Hill and Jack Aron—615(A)

Viscosity
Activation energy for grain boundary viscosity in metals, A. S. Nowick—597(A)
Bulk viscosity of high polymers, F. Bueche—652(A)
Experiments with rotating cylinder viscometer in liquid He II, A. C. Hollis-Hallett—649(A)
Hypersonic viscous flow over flat plate, L. Lees and R. F. Probstein—600(A)
Influence of specific volume on viscosity-pressure behavior of some hydrocarbon liquids, Edward M. Griest, Wayne Webb, and Robert W. Schiessler—612(A)
Relations between viscosity and flow birefringence of polyelectrolytes, P. M. Kamath, B. Rosen, and F. R. Eirich—657(A)

X-rays, absorption, diffraction, scattering, reflection, refraction, and polarization
Atomic arrangements in Au-Ni solid solutions, P. A. Flinn and B. L. Averbach—655(A)
Charge distribution and vibration amplitudes in LiH and LiD, C. K. Stambaugh and P. M. Harris—651(A)
Effect of cold work on x-ray patterns of Al, M. McKeeham, B. L. Averbach, and B. E. Warren—656(A)
Effect of lattice imperfections upon x-ray diffraction and linear dimensions of crystals, P. H. Miller, Jr. and B. R. Russell—650(A)
Scattering of x-rays by atoms, G. Placzek—588(A)
Separation of cold work distortion and particle size broadening in x-ray patterns, B. E. Warren and B. L. Averbach—656(A)
Short-range order diffuse scattering in Al-Zn, Peter S. Rudman, Paul A. Flinn, and B. L. Averbach—656(A)
Transmission of x-rays through calcite near Bragg angle, Guenter Schwarz and George L. Rogosa—421(L)
X-ray diffraction, R. E. Henderson and N. S. Gingrich—585(A)
X-ray studies of graphitization process, H. T. Pinnick—817(A)

X-rays, emission (see also **X-rays, spectra and spectroscopy, etc.**)
Emission of L x-rays of Pb in Po^{210} decay, William Rubinson and William Bernstein—545
K-shell ionization accompanying α-decay of Po^{210}, W. C. Barber and R. H. Helm—175

X-rays, spectra and spectroscopy, wavelength measurements (see also **X-rays, emission**)
Effect of low absorption coefficient on x-ray spectrometer measurements, D. T. Keating and B. E. Warren—656(A)
$L\alpha_{1,2}$ and $L\beta_1$ emission lines of Cu and Zn, C. H. Shaw and Nathan Spielberg—641(A)
Scintillation spectrometer for measuring total energy of x-ray photons, M. R. Cleland and H. W. Koch—588(A)
Spectrum of L x-rays from RaD and possibility of $L_I \rightarrow L_{II}$ Auger transitions, S. G. Cohen and A. A. Jaffe—800(L)

Zeeman effect
Of the Cl nuclear quadrupole rf resonance, Christopher Dean—607(A)